universität wien

MASTERARBEIT / MASTER'S THESIS

Titel der Masterarbeit / Title of the Master's Thesis

"Electroweak Sudakov Logarithms in $e^+e^- \to t\bar{t}$ at Next-to-Leading Order"

verfasst von / submitted by

Daniel Lechner, BSc

angestrebter akademischer Grad / in partial fulfilment of the requirements for the degree of

Master of Science (MSc)

Wien, 2017 / Vienna, 2017

Studienkennzahl lt. Studienblatt / degree programme code as it appears on the student record sheet:	A 066 876
Studienrichtung lt. Studienblatt / degree programme as it appears on the student record sheet:	Masterstudium Physik UG2002
Betreut von / Supervisor:	Univ.-Prof. Dr. André H. Hoang

Abstract

In this work the electroweak radiative corrections to the process $e^+e^- \to t\bar{t}$ up to next-to-leading order (NLO) in the electroweak coupling α are studied. This thesis focuses on the weak corrections, pure QED contributions are not treated. The calculation is done in the continuum region above the top quark pair-production threshold $s = 4m_t^2$, where $\sqrt{s}$ is the partonic center-of-mass energy. Apart from treating the fermions from bottom quark downwards as massless, no simplifying assumptions, like degenerate weak boson masses etc., are made in this thesis. The results are computed analytically (in renormalizable R_ξ-gauge) at the level of the S-matrix element, allowing for strong self-contained checks of various intermediate results. Due to the calculations being relatively involved, computer-based assistance in terms of various `Mathematica`-packages is used heavily. Nevertheless, technical points like renormalization and systematic treatment of Feynman integrals are explicitly covered in detail as well throughout this work. The UV- and gauge-cancellations necessary for obtaining scale- and gauge-independent predictions are discussed. This leads to the natural formation of "building blocks" within the full computation. After completion of the continuum calculation, the results are expanded in the high-energy limit $\sqrt{s} \gg m_t \sim \Lambda_{\text{EW}}$, where $\Lambda_{\text{EW}} \sim 10^2$ GeV is the electroweak scale. Special emphasis is put on the extraction of the high-energy logarithms of the theory (*Sudakov logarithms*), which are of the form $\ln^k(\Lambda_{\text{EW}}^2/s)$, with $k = 1, 2$. Power-suppressed terms $\mathcal{O}(\Lambda_{\text{EW}}^2/s)$ are neglected. In the last chapter the analytic results (both in the continuum and the high-energy limit) of the S-matrix elements are finally turned into cross-sections and studied numerically.

Zusammenfassung

In dieser Arbeit werden die elektroschwachen Strahlungskorrekturen für den Prozess $e^+e^- \to t\bar{t}$ bis zur next-to-leading order (NLO) in der elektroschwachen Kopplungskonstanten α studiert. Der Fokus liegt auf schwachen Korrekturen, reine QED-Beiträge werden nicht untersucht. Die Rechnung wird in der Kontinuumsregion über der Topquark-Paarproduktionsschwelle $s = 4m_t^2$ durchgeführt, wobei $\sqrt{s}$ die partonische Schwerpunktsenergie darstellt. Abgesehen davon, dass von Bottomquark abwärts alle Fermionen als masselos behandelt werden, werden in dieser Arbeit keine weiteren vereinfachenden Annahmen, wie entartete Massen der schwachen Bosonen etc., getroffen. Die Ergebnisse werden analytisch (in renormierbarer R_ξ-Eichung) auf dem Level des S-Matrixelementes berechnet, was aussagekräftige unabhängige Überprüfungen auf Korrektheit einiger Zwischenergebnisse ermöglicht. Da die Rechnungen relativ umfangreich sind, wird intensiv auf Computer-basierte Assistenz in Form einiger `Mathematica`-Packages zurückgegriffen. Nichtsdestotrotz werden im Laufe dieser Arbeit auch technische Punkte wie Renormierung und die systematische Behandlung von Feynman-Integralen explizit im Detail behandelt. Die Aufhebung der UV-Divergenzen sowie der Eichabhängigkeiten, welche notwendig ist, um UV-endliche und eichunabhängige Aussagen tätigen zu können, wird diskutiert. Dies führt auf natürlichem Wege zur Formation von "Bausteinen" innerhalb der gesamten Rechnung. Nach Vollendung der Berechnungen im Kontinuum werden diese Ergebnisse im Hochenergielimes $\sqrt{s} \gg m_t \sim \Lambda_{\text{EW}}$ entwickelt, wobei $\Lambda_{\text{EW}} \sim 10^2$ GeV die elektroschwache Skala bezeichnet. Spezieller Fokus wird auf die Extraktionen der Hochenergielogarithmen der Theorie (*Sudakov-Logarithmen*) gelegt, welche von der Form $\ln^k(\Lambda_{\text{EW}}^2/s)$ mit $k = 1, 2$ sind. Potenzunterdrückte Terme $\mathcal{O}(\Lambda_{\text{EW}}^2/s)$ werden vernachlässigt. Schließlich werden im letzten Kapitel die analytischen Ergebnisse für die S-Matrixelemente (sowohl im Kontinuum als auch im Hochenergielimes) in Wirkungsquerschnitte übergeführt und einer numerischen Studie unterzogen.

Acknowledgements

First I want to thank my thesis supervisor Prof. André Hoang for giving me the opportunity to write this thesis in the very fruitful environment that is the Theoretical Particle Physics Group of the University of Vienna. I would also like to express my gratitude for the excellent introductory lectures, interesting scientific discussions, guidance throughout as well as providing me with the chance to give tutorials and attend summer schools and workshops to present the work done in this thesis.

Special thanks to my (unofficial) co-supervisor Dr. Massimiliano Procura, who, despite his almost inhuman working and traveling schedules, always found time for discussions and provided advice, whether it'd be calculational, motivational or in form of `Mathematica`-packages, papers and feedback. Not to forget the spectacular "inofficial-Particle-Physics-III"-lecture! Thank you!!

I also would like to personally thank Prof. Helmuth Hüffel, for letting me provide tutorials for some of his courses (which was an invaluable experience for me) as well as giving the lecture "Statistical Physics II", my favorite up to now, in very fine style.

Many thanks also to the other members of the particle group in Vienna. The last two years here with you guys have simply been amazing, from serious discussions to seminars and summer schools to light-hearted lunch-breaks, where especially the latter were worth their weight in gold figuratively.

Thanks also to all my colleagues who accompanied me on the way through university up to now. I could think of a thousand stories that could be told, but as space is too limited and there would be too many names unfortunately, I just want to take the chance to say thank you to all of you!

Lastly I want to thank my family. I am deeply indebted especially to my parents for their incredible lifelong support, without whom I would have never come that far. Big thanks also to my girlfriend Beate, who was always there for me and cheered me up when things were not going as smoothly (which happened quite a few times) or when I was complaining about work and life again (which also happened quite a few times).

Contents

Chapter 1

Introduction

With the celebrated discovery of the Higgs boson at the Large Hadron Collider (LHC) in 2012, completing the Standard Model (SM), particle physics ultimately entered a new era. Despite its undeniable impact on the scientific field, the Higgs-discovery put particle physicists at a multiway crossroads and handed them a compass containing a spinning needle. Although there exist some mild tensions for various observables between theoretical predictions of the SM and corresponding experimental observations, at this point in time there is no direct evidence for particles not belonging to the SM spectrum[1].

This unsatisfactory situation has consequences in that much of the current focus of particle physics, theoretically and experimentally, lies on *precision physics*, i.e. trying to improve the accuracy of theoretical SM-predictions and experimental SM-studies as far as possible to either extinguish or solidify the existing tensions within the SM, thereby testing for its (potential) shortcomings. Two of the successor machines of the LHC, the International Linear Collider (ILC) and the Compact Linear Collider (CLIC), are accelerators tailored to such precision measurements. Contrary to the LHC, they will collide leptons (positrons and electrons), which has important advantages experimentally and theoretically (for example better control of the partonic center-of-mass (CM) energies, higher efficiency of beam energy use and cleaner theoretical descriptions due to non-compositeness of the colliding particles etc.). The linear set-up forces concessions in the beam energy however, so the designed partonic CM-energies range from ~ 250 GeV (starting for ILC) to 3 TeV (for final-stage CLIC, after various stages of upgrades).

Besides the Higgs-boson, the most interesting particle of the SM for studies at linear colliders is the top quark. It has unique properties that make it an almost ideal object (both theoretically and experimentally) for BSM searches or precision studies of the SM at these accelerators. For one, its enormous mass of $m_t \sim 173$ GeV (which lead to a relatively late discovery at Tevatron in 1995) results in a very short lifetime of about $5 \times 10^{-25} s$, which corresponds to a total decay width of about 1.4 GeV. This feature of $\Gamma_t > \Lambda_{\text{QCD}}$, where $\Lambda_{\text{QCD}} \sim 300$ MeV is the hadronization scale, leads to the fact that the top quark decays (weakly) before it can hadronize[2]. Secondly its large Yukawa-coupling y_t to the Higgs-field (related to m_t by the vacuum-expectation value (vev) v of the Higgs-field) results in a close connection between these two heaviest SM-particles, and they are believed to be the most sensitive to (hypothetical) new particles and BSM-phyics.

Studying the top parameters like the top quark mass m_t is therefore of high-importance. There are various strategies to access these experimentally. For example measuring cross-sections close to the top-pair production threshold region (threshold-scans) or other observables that are ideally very sensitive to the top mass (for example as in [1], [2], where a reconstruction method was worked out theoretically). Apart from experimental finesses of each of these measurements, there are severe theoretical challenges

[1]The most frequently quoted BSM hint is *Dark Matter* (DM). Despite some constraints from mainly cosmological observables its particle interpretation has not been established yet. At least it is safe to say that DM quanta have escaped any of the detection mechanisms so far. There is also evidence for non-zero neutrino masses, but their precise origin is not known yet.

[2]It does of course participate in strong interactions in the time between production and decay, but with the characteristic scales well above Λ_{QCD} it is possible to treat this time slice with perturbative QCD (pQCD).

that need to be addressed systematically. Starting with the fact that a theoretically well-behaved definition of the top mass parameter is far from trivial, to the fact that the extraction methods frequently lead to kinematic regimes and edges of phase-space where perturbative theory (especially QCD, but also electroweak theory) may encounter validity problems connected to the phenomenon of *large logarithms*. The issue is usually a large separation of (many) scales leading to large-logarithmic enhancement.

One especially important process at linear colliders involving top quarks is the pair-production of top quarks from e^+e^--annihilation. For any such process governed by a hard partonic production scale s the top mass m_t naturally sets up 2 regions that are of specific interest: the threshold region where the tops are produced close to rest, and the continuum region $s > 4m_t^2$, ultimately leading to the highly-boosted regime $s \gg 4m_t^2$. In both regimes, threshold and the highly-boosted, a lot of progress has been made at $\mathcal{O}(\alpha_s)$ and beyond. Up to this point in time (i.e. in the LEP and LHC eras), electroweak effects (EW effects) have been included either only fully inclusively (for example with a constant width of the top quark as in [1], [2]) or at fixed-order, leading to a precision sufficient for those machines. With the new generation of high-precision accelerators on the horizon, this is not the case anymore however, and there is the need for systematic inclusion of electroweak effects, both beyond leading order and in a more differential way.

The aim of this work is therefore to provide a first step towards a more systematic inclusion of electroweak effects in top quark production at e^+e^--colliders. Starting point is the NLO corrections to the production of stable top quarks, and a lot of work has already been done in this respect by various authors, see e.g. [3], [4], [5], [6], [7]. These works were geared towards numerical implementation of these fixed-order results into codes and numerical libraries, but going beyond numerics and discussing things at an analytical level as much as possible has some important advantages. Firstly analytic calculations allow to straightforwardly identify proper subsets of the full calculation (in terms of scale- and gauge-independence) and subsequently clarify their role (conceptually and numerically) within the larger picture. Secondly for the reconstruction of top parameters in kinematic regions as mentioned above, it is necessary to systematize the approach beyond the pure fixed-order calculations, for example by applications of *Effective Field Theories* (EFTs) tailored to the specific situation. For this reason precise knowledge of the underlying structures is necessary, in order to clarify the need and possibility of resumming large logarithms of the theory. Since full higher-order calculations at EW two-loop and beyond are tremendously complicated and often off-limits, resummation might prove useful as it allows to access higher-order effects at a much reduced technical cost.

In this work we will focus on the (highly-)boosted region $s \gg \Lambda_{\mathrm{EW}}^2$. Firstly we derive analytic results for the continuum without any major simplifying assumptions, which are very hard to get across in the existing literature as they are rarely (and always partially) given in explicit form. This thesis aims to fill this gap in the literature, showing explicitly expressions in R_ξ-gauge down to single diagrams, as well as details concerning renormalization schemes and gauge-cancellations. These expressions will be expanded to extract the leading logarithmic structure (including constant terms) in the high-energy limit. Obtaining analytic results enables precise statements about the structure of the calculation, like logarithmic vs. constant vs. power-suppressed terms, discussion of proper subsets of the calculation (in terms of scale- and gauge-independence etc.), and it is also very useful (for later work) for cross-checking and matching procedures of EFTs formulated in this kinematic regime.

This thesis is organized as follows: in chapter 2 we review the QFT of electroweak interactions, GWS-theory (after Glashow, Weinberg, Salam), a spontaneously broken gauge-theory based on the group $SU(2) \times U(1)$. Following [4], [8] we then discuss two variants of the commonly used *on-shell renormalization scheme* (*OS*-scheme), which is necessary to obtain 1-loop-predictions free of ultraviolet (UV) divergences.

The backbone of this thesis is chapter 3, where we extensively treat the calculation of the amplitude $\mathcal{M}(e^+e^- \to t\bar{t})$ in renormalizable R_ξ-gauge in the continuum, i.e. for arbitrary $s > 4m_t^2$. We start by introducing notation (following [5]), kinematics and the tree-level calculations, before moving on to the radiative corrections at one-loop (NLO EW). In this work we focus on weak corrections, excluding the pure QED contributions, which is possible due to the residual $U(1)$-local-gauge-symmetry after spontaneous symmetry breaking (SSB). The results are presented at the level of the S-matrix element in terms of *chirality amplitudes* multiplied by scalar coefficient functions that depend on the invariants of the process.

In chapter 4 the mechanism of UV- and gauge-cancellations is discussed, which unveils interesting and non-trivial interplay of various parts of the calculation. Obtaining UV-finite and gauge-independent quantities in a spontaneously broken gauge theory is a much less straightforward subject than in unbroken theories like QED or QCD. In this thesis, renormalization and gauge parameter cancellation are thoroughly discussed and subtleties are clarified. The UV- and gauge-structure leads to the natural formation of building blocks within the full calculation.

Another core chapter of this work is ch. 5, where we expand the continuum results in the high-energy limit $s \gg \Lambda_{\mathrm{EW}}^2 \sim 10^2$ GeV. All the weak boson masses M_Z, M_W, M_H and the top mass m_t are treated as $\sim \Lambda_{\mathrm{EW}}$, with other fermions assumed to be (effectively) massless. In this thesis we focus on the central scattering region $\theta \sim \pi/2$, which implies $|t|, |u| \gg \Lambda_{\mathrm{EW}}^2$ as well. We give explicit analytic results for the leading logarithmic structures in this regime including constants, neglecting power-suppressed terms. The results, full and expanded, are studied numerically in chapter 6 according to absolute size, relative importance and accuracy of expansion. We summarize and give a short outlook in chapter 7.

Chapter 2

Electroweak theory

The goal of this thesis is to construct the electroweak next-to-leading order (EW NLO) calculation of the process $e^+e^- \to t\bar{t}$ and discuss its behaviour in the regime of boosted top quarks. In contrast to QCD corrections to top pair production, having leptons in the initial state is actually complicating things here, as they are not singlets under the electroweak gauge group $SU(2)_W \times U(1)_Y$. The same is true for the virtual gauge bosons in the s-channel diagrams, namely γ^* and Z^*, which results in a more complicated structure of the amplitude.

This chapter is organized as follows: the QFT of electroweak interactions, GWS-theory, is reviewed in the first section 2.1. At one-loop and higher, the theory shows UV-divergences in loop integrals that have to be treated properly. The following sections 2.2, 2.3 and 2.4 are dedicated to the procedure of renormalization, producing UV-finite answers for observable quantities. This can be done in a scheme-dependent, but process-independent way (due to symmetry relations). In the last section 2.5 we give explicit EW NLO results for the renormalization constants.

2.1 GWS-theory

From experiment it is known that there are 3 massive vector bosons mediating the weak force, while one massless vector boson propagates the electromagnetic force. An elegant field theoretical model explaining this fact was worked out by Glashow, Weinberg and Salam [9], [10], [11], which we quickly review in this section (following conventions used in [8]).

2.1.1 Prior to SSB

Starting point is a gauge theory based on the (non-simple) group $SU(2)_W \times U(1)_Y$, with Yang-Mills Lagrangian

$$\mathcal{L}_{\text{YM}} = -\frac{1}{4} W^a_{\mu\nu} W_a^{\mu\nu} - \frac{1}{4} B_{\mu\nu} B^{\mu\nu} \tag{2.1}$$

where

$$W^a_{\mu\nu} = \partial_\mu W^a_\nu - \partial_\nu W^a_\mu + g\,\varepsilon^{abc} W^b_\mu W^c_\nu, \qquad B_{\mu\nu} = \partial_\mu B_\nu - \partial_\nu B_\mu \tag{2.2}$$

are the field-strengths of the isotriplet W^a_μ ($a = 1, 2, 3$) with generators $\tau^a = \sigma^a/2$ and the isosinglet B_μ with abelian generator Y (*hypercharge*). The covariant derivative reads

$$D_\mu = \partial_\mu - ig\,\tau^a W^a_\mu + ig' Y B_\mu \tag{2.3}$$

Furthermore, a complex scalar $SU(2)_W$-doublet Φ in the fundamental representation of $SU(2)_W$, the *Higgs-doublet*, is introduced

$$\mathcal{L}_{\text{Higgs}} = (D_\mu \Phi)^\dagger (D^\mu \Phi) - V(\Phi) \tag{2.4}$$

with a bounded-from-below, renormalizable potential $V(\Phi)$.

Fermions are incorporated into the theory via Yukawa couplings to the Higgs doublet

$$\begin{aligned}\mathcal{L}_{\text{fer}} = &\sum_i \left[\bar{Q}^i_L i\not{D} Q^i_L + \bar{u}^i_R i\not{D} u^i_R + \bar{d}^i_R i\not{D} d^i_R\right] + \sum_i \left[\bar{L}^i_L i\not{D} L^i_L + \bar{e}^i_R i\not{D} e^i_R + \bar{\nu}^i_R i\not{\partial} \nu^i_R\right] + \\ &- \sum_{ij} \left[\bar{Q}^i_L \Phi\, G^{ij}_d d^j_R + \bar{d}^i_R \Phi^\dagger\, G^{\dagger,ij}_d Q^j_L\right] - \sum_{ij} \left[\bar{Q}^i_L \tilde{\Phi}\, G^{ij}_u u^j_R + \bar{u}^i_R \tilde{\Phi}^\dagger\, G^{\dagger,ij}_u Q^j_L\right] + \\ &- \sum_{ij} \left[\bar{L}^i_L \Phi\, G^{ij}_l e^j_R + \bar{e}^i_R \Phi^\dagger\, G^{\dagger,ij}_l L^j_L\right], \end{aligned} \tag{2.5}$$

where $\tilde{\Phi} \equiv i\sigma^2\Phi^*$ is the charge conjugated Higgs doublet. As experiments show that the theory of weak interactions is chiral, left- and right-handed fermion fields are in different representations of $SU(2)_W$. The left-handed fields form doublets (fundamental rep), while the right-handed pieces are $SU(2)_W$-singlets (trivial rep). The corresponding quantum numbers to be inserted into the various covariant derivatives are listed in table 2.1.

Quantum nr.	$Q = \begin{pmatrix} u_L \\ d_L \end{pmatrix}$	u_R	d_R	$L = \begin{pmatrix} \nu_L \\ e_L \end{pmatrix}$	ν_R	e_R	H	χ	ϕ^+
T_3	$\pm\frac{1}{2}$	0	0	$\pm\frac{1}{2}$	0	0	$-\frac{1}{2}$	$-\frac{1}{2}$	$\frac{1}{2}$
Y	$\frac{1}{6}$	$\frac{2}{3}$	$-\frac{1}{3}$	$-\frac{1}{2}$	0	-1	$\frac{1}{2}$	$\frac{1}{2}$	$\frac{1}{2}$

Table 2.1: Quantum numbers of the fields for the gauge group $SU(2)_W \times U(1)_Y$. $T_3 = \pm 1/2$ indicates transformation in the fundamental rep of $SU(2)_W$, while for $Y = 0, T_3 = 0$ the field is in the trivial rep of the respective group. The hypercharges Y are adjusted to reproduce the electromagnetic charges $Q = T_3 + Y$. Antiparticles have the signs reversed.

2.1.2 After SSB

Since explicit mass terms of the gauge bosons and fermions are forbidden by the gauge symmetry, it needs to be broken with the Higgs-mechanism [12], [13], [14] to allow for the generation of mass terms. Starting from the unbroken gauge theory in the last section, it is now assumed that the vacuum expectation value of the Higgs doublet is non-vanishing: $|\langle\Phi\rangle| \neq 0$. The simplest realization of this is to use a mexican-hat-type potential for $V(\Phi)$,

$$V(\Phi) = -\mu^2\Phi^\dagger\Phi + \frac{\lambda}{4}(\Phi^\dagger\Phi)^2 \qquad (\mu^2 > 0, \lambda > 0). \tag{2.6}$$

A constant shift $\Phi_0 \in \mathbb{C}^2$ in the field value Φ is now necessary to formulate perturbation theory around the correct vacuum. Conventionally one picks $\Phi_0 = (0, v/\sqrt{2})$ with $v \in \mathbb{R}$, so that $|\langle\Phi\rangle|^2 \equiv \frac{v^2}{2} = \frac{2\mu^2}{\lambda} \in \mathbb{R}$, i.e.

$$\Phi(x) = \begin{pmatrix} \phi^+(x) \\ \frac{1}{\sqrt{2}}\left(v + H(x) + i\chi(x)\right) \end{pmatrix} \tag{2.7}$$

so that $|\langle H\rangle| = |\langle\chi\rangle| = |\langle\phi^+\rangle| = 0$, where H, χ are real (pseudo-)scalar fields. Working through eq. (2.1), (2.4) and (2.5) one observes mass terms emerging for all the particles (except the neutrinos)[1]. As these mass terms are not explicit from the start, but generated by the Higgs-mechanism breaking the underlying symmetry, these new couplings that are identified with particle masses share many relations among them and are expressible in terms of the parameters of the unbroken theory. We get[2]

$$M_H = \sqrt{2}\mu, \qquad M_W = \frac{v}{2}g, \qquad M_Z = \frac{v}{2}\sqrt{g^2 + g'^2}, \qquad M_A = 0. \tag{2.8}$$

[1]The Lagrangian for the broken theory is quite lengthy, and we refer the reader to literature and textbooks.

[2]In this work we use capital letters for boson masses, and lower case for fermion masses.

To read off these masses, the gauge boson states have to be transformed to mass eigenstates

$$W_\mu^\pm \equiv \frac{1}{\sqrt{2}}\Big(W_\mu^1 \mp i W_\mu^2\Big), \qquad \begin{pmatrix} Z_\mu \\ A_\mu \end{pmatrix} \equiv \begin{pmatrix} c_W & s_W \\ -s_W & c_W \end{pmatrix} \begin{pmatrix} W_\mu^3 \\ B_\mu \end{pmatrix} \tag{2.9}$$

which defines the Weinberg angle θ_W:

$$\cos(\theta_W) \equiv c_W \equiv \frac{g}{\sqrt{g^2 + g'^2}}, \qquad \sin(\theta_W) \equiv s_W \equiv \sqrt{1 - c_W^2} \tag{2.10}$$

This combined with eq. (2.8) has the extremely important consequence that the weak boson masses are related by

$$M_W = c_W M_Z. \tag{2.11}$$

Another important definition is that of the electric charge e as prefactor of the electromagnetic current $-eQ_i\, J^\mu_{\text{em}} \equiv -eQ_i\, \bar{f}_i \gamma_\mu f_i$, where $Q_i \equiv T_i^3 + Y_i$ (with fermion i, where T_i^3 is its associated $SU(2)$ quantum number):

$$e \equiv \frac{gg'}{\sqrt{g^2 + g'^2}} \tag{2.12}$$

which also implies

$$g = \frac{e}{s_W}, \qquad g' = \frac{e}{c_W}. \tag{2.13}$$

The electric charge is frequently replaced by the fine structure constant α with its usual definition

$$\alpha \equiv \frac{e^2}{4\pi}. \tag{2.14}$$

Lastly, the Higgs mechanism also generates fermion masses via their coupling to the Higgs doublet (cf. eq. (2.5)),

$$m_{f,i} = U_{ik}^{f,L} G_f^{km} U_{mi}^{f,R;\dagger} \tag{2.15}$$

where $U^{f,L/R}$ transform the fermion fields $f_i^{L/R}$ into the mass eigenstates ${f'}_i^{L/R} = U_{ik}^{f,L/R} f_i^{L/R}$. In case of the quarks a final important quantity is constructed from these transformation matrices U_f, the *CKM-matrix*

$$V_{ij} \equiv U_{ik}^{u,L} U_{kj}^{d,L;\dagger}, \tag{2.16}$$

which survives as an additional parameter in the charged-current Lagrangian of left-handed quarks due to an incomplete cancellation the quark field transformation matrices. From experiment it is known that the CKM-matrix is numerically very close to the unit matrix. Many calculations of EW radiative corrections work with the simplification of actually setting it equal to the unit matrix, an approach we shall also adopt in the rest of this work.

2.1.3 Role of the parameters

A central role in SSB is played by the constant v (or alternatively μ^2). For $v = 0$ ($\mu^2 < 0$), the quadratic term would just be a regular mass term for the field Φ, and the underlying symmetry group $SU(2)_W \times U(1)_Y$ would remain unbroken. In that case the theory would be quite similar to QCD, with 4 massless gauge bosons instead of 8. $v \neq 0$ (i.e. $\mu^2 > 0$) however breaks this symmetry spontaneously. v therefore effectively acts as sort of an order parameter, as used frequently in statistical physics, which is able to distinguish two different phases of a physical system, as it is only non-zero in one of them. The regime with $v \neq 0/v = 0$ ($\mu^2 > 0/\mu^2 < 0$) is called *broken/unbroken phase*. In our particle theory $v \neq 0$ and $\mu^2 > 0$ fixed (as μ is related to the mass of the Higgs boson M_H, cf. eq. (2.8)), but it is tempting to borrow some language from statistical physics nevertheless and refer to working with the broken/unbroken theory as being in the broken/unbroken phase. Specifically, if one considers an EW process at a scale $s \gg v^2$, the order parameter is parametrically very close to 0, and one is allowed to work with the unbroken theory to good accuracy. Contrary, for $s \sim v^2$, it is necessary to compute things in the broken phase.

The question of what free tunable parameters to use also has to be addressed. In the unbroken phase these were the the coupling constants g, g', λ, μ^2 and the set of fermion-Higgs Yukawa couplings G_f^{ij}. For convenience, in the broken phase these are replaced by another set, namely the boson and fermion masses, the electric charge e and the CKM-matrix,

$$g,\, g',\, \lambda,\, \mu^2,\, G_{f,ij} \qquad \stackrel{\text{SSB}}{\longrightarrow} \qquad e,\, M_W,\, M_Z,\, M_H,\, m_f,\, V_{ij}. \tag{2.17}$$

This set is not fixed however. While fermion masses, Z- and Higgs mass are mostly used as input, the W-boson mass is often substituted by the Fermi-constant G_F (sometimes denoted G_μ, not to be confused with the fermion-Higgs Yukawa coupling matrices G_f), obtained from a low-energy process like muon decay

$$G_F = \frac{e^2}{2^{5/2} s_W^2 M_W^2}. \tag{2.18}$$

2.1.4 Quantization

Quantization of the theory requires a gauge fixing procedure. Firstly, we introduce gauge fixing functionals into the Lagrangian[3]

$$F^{\pm} = \frac{1}{\sqrt{\xi_W}}\, \partial^\mu W_\mu^{\pm} \mp i\, M_W \sqrt{\xi_W}\, \phi^{\pm}, \tag{2.19}$$

$$F^{Z} = \frac{1}{\sqrt{\xi_Z}}\, \partial^\mu Z_\mu - M_Z \sqrt{\xi_Z}\, \chi, \tag{2.20}$$

$$F^{A} = \frac{1}{\sqrt{\xi_A}}\, \partial^\mu A_\mu, \tag{2.21}$$

leading to the gauge fixing part of $\mathcal{L}$

$$\mathcal{L}_{\text{gauge-fix}} = -\frac{1}{2}\left[(F^A)^2 + (F^Z)^2 + 2F^+F^-\right]. \tag{2.22}$$

This procedure of introducing a 3-parameter family of gauge choices is called R_ξ-gauge. While it is possible to already plug in certain values for ξ_i at the level of the Lagrangian (or equivalently at the level of Feynman rules), it is often advisable to calculate quantities for arbitrary (but finite) values of ξ_i, and only fix ξ_i after completion of the calculation. In this way one is able to check the consistency of a calculation by inspecting cancellations of these gauge parameters, as will happen for any gauge invariant quantity. In EW calculations however, more often than not, the gauge is already chosen at the level of the Lagrangian, because the expressions in R_ξ-gauge written out in full glory tend to be quite lengthy. The default choice for EW calculations (but also in QCD) is Feynman gauge ($\xi_i = 1$).

Another scheme applicable in EW theory is unitary gauge, which formally corresponds to the limit $\xi_i \to \infty$. The important difference to finite choices for ξ_i is that it is **not** possible to compute things in R_ξ-gauge and at the end take $\xi_i \to \infty$. One rather needs to perform the limiting process at the level of Feynman rules. The appeal for unitary gauge lies in the fact that unphysical would-be-Goldstone modes decouple in this limit, and only physical modes propagate. This however comes at the prize that the longitudinal parts of massive gauge boson propagators tend to a constant value in the UV rather than dropping like $\frac{1}{p^2}$ (see the Feynman rules in the appendix G.1), screwing up the naive power counting in the process. This gauge choice is therefore rarely seen in radiative correction computations.

Due to the non-abelian nature of the EW symmetry group, an additional step is necessary in the gauge

[3] This specific choice of gauge fixing functionals, sometimes called *t'Hooft-gauge*, is very convenient as the mixed terms in eq. (2.22) cancel the gauge-Goldstone kinetic mixing terms appearing in $\mathcal{L}_{\text{Higgs}}$. It also introduces non-zero, gauge-dependent masses into the propagators of the formerly massless Goldstones, so that from now on we will sometimes also call them *would-be-Goldstone bosons*.

fixing procedure, namely the introduction of anti-commuting scalars termed *Fadeev-Popov ghosts.* These fields exclusively propagate on internal lines, and their job is to cancel unphysial polarizations of the gauge fields in non-abelian theories. Their Lagrangian reads

$$\mathcal{L}_{\mathrm{FP}} = \bar{u}^{\alpha}(x)\frac{\delta F^{\alpha}}{\delta\theta^{\beta}(x)}u^{\beta}(x) \tag{2.23}$$

where $\delta F^{\alpha}/\delta\theta^{\beta}(x)$ is the infinitesimal form of finite $SU(2)_W \times U(1)_Y$ gauge transformation $\exp\left[i\tau^{\beta}\theta^{\beta}(x)\right]$ of the gauge fixing functionals F^{α}. This Lagrangian (including kinetic parts for $u, \bar{u}$) yields ghost-gauge and ghost-Higgs vertices as well as ghost propagators. It is emphasized that ghost u^{α} and anti-ghost $\bar{u}^{\alpha}$ are not their respective anti-particle, but have to be treated as different particles.

2.2 Renormalization

This section is rather detailed for various reasons. Firstly, because of the flurry of parameters and the quite frequently occurring cancellations characteristic of EW theory, special care is required to avoid missing or overcounting details, so that fully renormalized results can be obtained. Secondly, even within certain schemes such as the on-shell scheme (OS-scheme), there is a considerable amount of freedom as to which extent the symmetries of the initially unbroken theory are used to derive Slavonov-Taylor identities (= relations between renormalization constants) in the broken phase. Additionally, there is also some freedom in fixing the residues of particles, especially those that only propagate on internal lines, as their field-strength renormalization constants will cancel between vertices and propagators.

Within the the *on-shell-scheme* (*OS-scheme*) that we will use (almost) exclusively in this work there are 2 specific variants which we focus on in some detail: the *Denner-scheme* [8] and the *BHS-scheme* [3] (after Böhm, Hollik and Spiesberger[4]):

- **Denner-scheme**: The renormalization (i.e. introduction of renormalization constants) is carried out in the broken phase from the start. On-shell renormalization conditions are imposed on all masses, all residues and the electric charge, i.e. renormalized masses are identified with the OS-masses, residues are fixed to 1 and the electric charge is defined in the Thomson limit. No symmetries are used, with the only exception being the renormalization of the on-shell electric charge, so that it can be completely related to 2-point functions.
- **BHS-scheme**: Renormalization constants are already introduced in the unbroken phase. Through SSB they are related to the renormalization constants in the broken phase, through which a high number of relations between those parameters is obtained. On-shell conditions are imposed in the broken phase: all masses are put on-shell, and the pure-QED parameters (photon residue and electric charge) are also fixed on-shell (as in the Denner-scheme). The rest of the parameters (massive gauge boson residues etc.) are then fixed by Slavnov-Taylor identities. As not all residues are renormalized to 1, the inclusion of non-trivial wave-function factors in the application of the LSZ-formalism might be necessary, depending on the process under consideration.

It is emphasized that if the renormalization procedure is carried out consistently (i.e. including wave-function factors), the above variants of the OS-renormalization scheme are completely identical. Both have advantages and disadvantages, depending on the specific application. In general, the Denner-scheme is more straightforward and intuitive, but has the downside of having a serious amount of redundancy (more renormalization constants need to be calculated separately). The BHS-scheme is more elegant, making use of the symmetries of the unbroken theory and constraining a lot of parameters. Also, some expression are significantly simpler. The disadvantage is that the renormalization constants between unbroken and broken phase need to be related, which makes additional calculations necessary. Also, some residues which are fixed by symmetry do not propagate with value 1, which makes the inclusion of wave-function factors necessary if these fields occur on external lines.

[4]Following [15] concerning terminology for the schemes.

This section is structured as follows: we start with the renormalization of the radiative corrections to the fermionic 2-point functions (*fermionic self-energies*) in sec. 2.3.1, which is the same in Denner- and BHS-scheme. Next up are the corrections to bosonic 2-point functions (*bosonic self-energies*), where besides the gauge boson masses the proper treatment of the 2-dimensional neutral gauge boson space, spanned by Z-boson and photon, is crucial. Closely connected to the bosonic 2-point functions is the renormalization of the electric charge, which can be related to bosonic 2-point renormalization constants by symmetry. We firstly discuss these renormalization in the Denner scheme (sec. 2.3) before turning to the BHS-scheme (sec. 2.4)). We wrap up this chapter by giving explicit results for the BHS-renormalization constants in the last section 2.5. Before we go on we emphasize that in this work we focus on the renormalization of the physical sector, excluding the renormalization of Goldstone and ghost fields as well as gauge-parameters, as it does not influence the calculations of this work. For a detailed treatment of the unphysical sector we refer the reader to [3].

2.3 Denner-scheme

2.3.1 Fermions

In order to write down renormalization conditions, we use the *fermion self-energy* $\Sigma(p^2)$ (= radiative contributions to 1-PI fermion 2-point function), defined to all loop orders by[5]

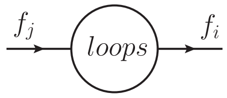

$$\begin{aligned} &= (-i)\Sigma^f_{ij}(p) = \\ &= (-i)\Big[\not{p}\,\omega_-\,\Sigma^f_{ij,L}(p^2) + \not{p}\,\omega_+\,\Sigma^f_{ij,R}(p^2) + (m_{f,i}\,\omega_- + m_{f,j}\,\omega_+)\,\Sigma^f_{ij,S}(p^2)\Big] = \\ &= (-i)\Big[\not{p}\sum_{\rho=\pm}\omega_\rho\,\Sigma^f_{ij,\rho}(p^2) + m_i\sum_{\rho=\pm}\omega_\rho\,\Sigma^f_{ij,\rho}(p^2)\Big] \end{aligned} \tag{2.24}$$

where $i, j = 1, 2, 3$ are generation indices (not Dirac indices), $\rho = \pm$ is a chirality index[6] and $f \in \{u, d, \nu, e\}$. The $\omega_\mp$ are defined below in eq. (2.33). Usually, the self energies only contain 1-particle-irreducible (1-PI) diagrams, but in EW theory we have to extend this rule somewhat. For reasons that will become apparent later, we make the following definition:

In this work, all self-energies (i.e. radiative corrections to 2-point functions of arbitrary external particles) contain, by definition, all 1-PI contributions ***and*** *diagrams that contain* ***Higgs-mediated tadpoles****,*

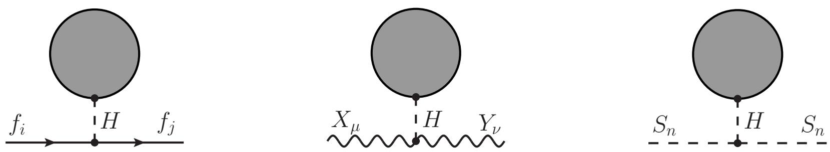

on (internal) lines. Per line, only one of these tadpole attachments is allowed.

The scalar functions $\Sigma_i(p^2)$ have perturbative expansions in α,

$$\Sigma^f_{ij,I}(p^2) = \sum_{k=1}^{\infty}\Sigma^{f,(k)}_{ij,I}(p^2) = \Sigma^{f,(1)}_{ij,I}(p^2) + \mathcal{O}(\alpha^2), \tag{2.25}$$

[5]In the SM with a unit CKM matrix, terms of $\Sigma(p)$ of the form $\sim m_f\,\gamma_5$ are absent to all orders, which is reflected in the way we parametrize (in this case we also always have $m_i = m_j$ for the masses of the external particles). In the (more general) chiral parametrization in the second line of eq. (2.24) this translates into $\Sigma_{ij,-}(p^2) = \Sigma_{ij,+}(p^2)$.

[6]Instead of the index $-$ or $+$ we will sometimes write L or R.

where $I \in \{V, A, S, \pm\}$ and the $\Sigma^{f,(k)}_{ij,I}$ are formally $\mathcal{O}(\alpha^k)$. The renormalized self-energy is obtained by adding necessary counterterms order by order. Diagrammatically we get [7]

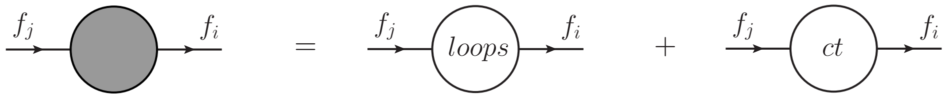

$$
\begin{aligned}
(-i)\hat{\Sigma}^f_{ij}(p) &= (-i)\Big[\not{p}\,\omega_-\,\hat{\Sigma}^f_{ij,L}(p^2) + \not{p}\,\omega_+\,\hat{\Sigma}^f_{ij,R}(p^2) + (m_i\,\omega_- + m_j\,\omega_+)\,\hat{\Sigma}^f_{ij,S}(p^2)\Big] = \\
&= (-i)\Big[\not{p}\sum_{\rho=\pm}\omega_\rho\,\hat{\Sigma}^f_{ij,\rho}(p^2) + m_i\sum_{\rho=\pm}\omega_\rho\,\hat{\Sigma}^f_{ij,\rho}(p^2)\Big]. \qquad (2.26)
\end{aligned}
$$

Quantities with a hat on top will denote renormalized quantities from now on.

In the on-shell scheme, particles should have their poles (assuming stable particles for the moment) at the pole mass, and propagate with residue 1. These requirements are enforced by imposing the following renormalization conditions[8] onto the radiative parts of Σ_{ij}:

$$
\mathrm{Re}\left[\hat{\Sigma}^f_{ij}(p)\right] u^f_j(p)\Big|_{p^2=m^2_{f,j}} = 0, \qquad \bar{u}^f_i(p')\,\mathrm{Re}\left[\hat{\Sigma}^f_{ij}(p')\right]\Big|_{p'^2=m^2_{f,i}} = 0, \qquad (2.27)
$$

$$
\lim_{p^2\to m^2_{f,j}} \frac{\not{p} + m_{f,j}}{p^2 - m^2_{f,j}}\,\mathrm{Re}\left[\hat{\Sigma}^f_{jj}(p)\right] u^f_j(p) = 0, \qquad \lim_{p^2\to m^2_{f,i}} \bar{u}^f_i(p')\,\mathrm{Re}\left[\hat{\Sigma}^f_{ii}(p')\right]\frac{\not{p}' + m_{f,i}}{p'^2 - m^2_{f,i}} = 0. \qquad (2.28)
$$

where u^f are particle spinors, not fields. Taking the real part of Σ is necessary, as the scalar functions $\Sigma_i(p^2)$ might develop imaginary parts (in the top quark case owing to the W-diagrams, see later). Only stable fermions with real masses have poles in their propagators for real p^2, while unstable particles have their poles shifted away from the real axis. In this work we will treat the top quarks as stable fermions, and postpone further treatment of these issues to future work. The conditions in the first row fix renormalization of the masses and CKM-matrix elements. The latter is the unit matrix in our work however, and therefore does not get renormalized (since $\Sigma^f_{i\neq j} = 0$ trivially). The second row contains the residue conditions for determining the field-strength constants. If generation mixing is switched off, the above equations simplify somewhat and we will list these conditions again below for the external particles of the process we consider: electrons and top quarks.

2.3.1.1 Field-strength ambiguity

Some further comments are in order here. Left- and right-handed components as fundamentally different fields are renormalized by separate constants Z_L and Z_R respectively. One complication now comes from the fact that while the right-handed fields are $SU(2)$-singlets where up- and down-type fields get their own Z_R-factor, the left-handed fermionic fields are organized in $SU(2)$-doublets and are renormalized by a common Z_L. For the i-th quark generation, for example, this implies

$$
Q^{i,0}_L = \begin{pmatrix} u^{i,0}_L \\ d^{i,0}_L \end{pmatrix} = \sqrt{Z^i_L} Q^i_l = \sqrt{Z^i_{Q,L}} \begin{pmatrix} u^i_L \\ d^i_L \end{pmatrix}, \qquad (2.29)
$$

$$
u^{i,0}_R = \sqrt{Z^i_{u,R}}\, u^i_R, \qquad d^{i,0}_R = \sqrt{Z^i_{d,R}}\, d^i_R, \qquad (2.30)
$$

Consequently, the residues of the right-handed fields can be fixed independently (for example to 1 in the OS-scheme), while for the left-handed particles even in the OS-scheme either up- or down-type

[7] At 1-loop the counterterm blob just consists of the local 2-point counterterm given below. At higher orders, the structure is more complicated due to nested divergences.

[8] These renormalization conditions hold in the same form if the Σ's include contributions of arbitrary loop level.

necessarily propagates with a residue $\neq 1$. This implies the necessity of wave-function renormalization for those external particles when computing S-matrix elements. An alternative way of dealing with that issue would be to start in the broken phase, forget about the doublet structure altogether and introduce separate renormalization constants for left-handed up- and down-type fields,

$$Q_L^0 = \begin{pmatrix} \sqrt{Z_{u,L}}\, u_L \\ \sqrt{Z_{d,L}}\, d_L \end{pmatrix}. \tag{2.31}$$

This approach is less elegant, but ultimately equivalent when the exclusive aim is to calculate S-matrix elements. For our purpose (i.e. the calculation of the process $e^+e^- \to t\bar{t}$) these subtleties are not of crucial importance actually, since we only have particles of fixed isospin as external particles ($T_3 = -\frac{1}{2}$ in case of the electrons, $T_3 = \frac{1}{2}$ in case of the tops), so we can simply fix the residues of these to 1. In the initial state we fix the residue of the electrons to 1, while in the final state we will use Z_L to fix the up-type residue to 1, not caring about the residues of the respective isospin partners (neutrinos and bottom quarks).

2.3.1.2 Fermionic renormalization constants

The fermion Lagrangian for GWS-theory can be found in eq. (2.5), with mass terms only appearing in the broken phase. The fermion kinetic terms are $SU(2)$-diagonal, so we can break down the renormalization of the top quark to the treatment of a $SU(2)$-singlet Dirac field f of mass m_f, whose dynamics are governed by the free (bare) Dirac Lagrangian

$$\mathcal{L}^0_{\text{Dirac}} = \bar{f}^0_L i\partial\!\!\!/\, f^0_L + \bar{f}^0_R i\partial\!\!\!/\, f^0_R - m^0_f\, \bar{f}^0_R f^0_L - m^0_f\, \bar{f}^0_L f^0_R \tag{2.32}$$

with left-/right-handed fields $f_{L/R} = \omega_\mp f$ obtained with the chiral projectors

$$\omega_\mp = \frac{1 \mp \gamma_5}{2}. \tag{2.33}$$

For the bare quantities we introduce multiplicative renormalization constants

$$Z_i = 1 + \sum_{k=1}^{\infty} \delta Z_i^{(k)} \equiv 1 + \delta Z_i + \mathcal{O}\big(\alpha^2\big), \tag{2.34}$$

where the $\delta Z_i^{(k)} \sim \mathcal{O}(\alpha^k)$. Since we will be working at the one-loop level exclusively, we dropped the superscript indicating the loop number. At $\mathcal{O}(\alpha)$ we have

$$\begin{aligned} f^0_L &\equiv \sqrt{Z_{f,L}}\, f_L = \left(1 + \frac{1}{2}\,\delta Z_{f,L}\right) f_L + \mathcal{O}(\alpha^2), \\ f^0_R &\equiv \sqrt{Z_{f,R}}\, f_R = \left(1 + \frac{1}{2}\,\delta Z_{f,R}\right) f_R + \mathcal{O}(\alpha^2), \\ m^0_t &\equiv Z_{m_f}\, m_f = \big(1 + \delta Z_{m_f}\big)\, m_f + \mathcal{O}(\alpha^2). \end{aligned} \tag{2.35}$$

For massless particles there are no mass renormalization constants of course. Since we assume no generation mixing, we cleaned up our notation in comparison to the preceding section, as generation indices became redundant. Returning to eq. (2.32), plugging in the renormalized quantities of eq. (2.35) gives to one-loop order

$$\mathcal{L}^0_{\text{Dirac}} = \bar{f}\left(i\partial\!\!\!/ - m_f\right) f + \bar{f}\, i\partial\!\!\!/\left(\delta Z_{f,L}\,\omega_- + \delta Z_{f,R}\,\omega_+\right) f - m_f\left(\frac{1}{2}\,\delta Z_{f,L} + \frac{1}{2}\,\delta Z_{f,R} + \delta Z_{m_f}\right)\bar{f}\, f + \mathcal{O}\left(\alpha^2\right), \tag{2.36}$$

where the chiral fields $f_{L/R}$ have been replaced by full fields f, and we used the reality of the field renormalization constants $\delta Z^\dagger_{L/R} = \delta Z_{L/R}$ for a unit CKM-matrix (see below). The above Lagrangian can be turned into Feynman rules for the renormalized propagator and the 2-point fermionic counterterm

$$= \frac{i(p\!\!\!/ + m_f)}{p^2 - m_f^2 + i0^+},$$

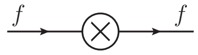

$$= i\not{p}\,(\delta Z_{f,L}\,\omega_- + \delta Z_{f,R}\,\omega_+) - i\,m_f\left(\frac{1}{2}\,\delta Z_{f,L} + \frac{1}{2}\,\delta Z_{f,R} + \delta Z_{m_f}\right). \tag{2.37}$$

The massless cases ($m_f = 0$) for propagator and counterterm are read off straightforwardly. At one-loop, eq. (2.26) in combination with eqs. (2.37) and (2.24) yield for our external particles (also dropping the superscript for $\Sigma^{(k)}$, i.e. $\Sigma^{(1)} \equiv \Sigma$ from now on)

$$\begin{aligned} \hat{\Sigma}_{f,\eta}(p^2) &= \Sigma_{f,\eta}(p^2) - \delta Z_{f,\eta}, \\ \hat{\Sigma}_{f,S}(p^2) &= \Sigma_{f,S}(p^2) + \frac{1}{2}\,\delta Z_{f,L} + \frac{1}{2}\,\delta Z_{f,R} + \delta Z_{m_f}, \end{aligned} \tag{2.38}$$

where we used the chirality index[9] $\eta = \mp$ to clean up notation, a handy convention we will use extensively throughout the rest of this work.

In the on-shell subtraction scheme, the renormalization conditions are chosen such that the renormalized mass is identified with the pole location and the residue is 1 (or i) at every order in perturbation theory. Specifically for the electron and top quark the renormalization conditions are

$$\begin{aligned} &\lim_{p^2\to 0}\frac{\not{p}}{p^2}\,\mathrm{Re}\left[\hat{\Sigma}_e(p)\right] u_e(p) = 0, &&\lim_{p^2\to 0}\bar{u}_e(p)\,\mathrm{Re}\left[\hat{\Sigma}_e(p)\right]\frac{\not{p}}{p^2} = 0, \\ &\lim_{p^2\to m_t^2}\frac{\not{p}+m_t}{p^2-m_t^2}\,\mathrm{Re}\left[\hat{\Sigma}_t(p)\right] u_t(p) = 0, &&\lim_{p^2\to m_t^2}\bar{u}_t(p)\,\mathrm{Re}\left[\hat{\Sigma}_t(p)\right]\frac{\not{p}+m_t}{p^2-m_t^2} = 0, \\ &\mathrm{Re}\left[\hat{\Sigma}_t(p)\right] u_t(p)\Big|_{p^2=m_t^2} = 0, &&\bar{u}_t(p)\,\mathrm{Re}\left[\hat{\Sigma}_t(p)\right]\Big|_{p^2=m_t^2} = 0. \end{aligned} \tag{2.39}$$

These conditions are equivalent row-wise because of the restriction to one generation. By taking the real part of Feynman integrals and setting the CKM-matrix to 1, the renormalization constants are manifestly real. From now on we will suppress the Re and keep it implicit. At one loop we find for electron (treated as massless) and top quark (treated as massive) after some manipulations

$$\begin{aligned} \delta Z_{e,\eta} &= \Sigma_{e,\eta}(0), \\ \delta Z_{t,\eta} &= \Sigma_{t,\eta}(m_t^2) + m_t^2\left[\frac{d\Sigma_{f,L}(p^2)}{dp^2} + \frac{d\Sigma_{t,R}(p^2)}{dp^2} + 2\,\frac{d\Sigma_{t,S}(p^2)}{dp^2}\right]_{p^2=m_t^2}, \\ \delta Z_{m_t} &= -\Sigma_{t,S}(m_t^2) - \frac{1}{2}\left[\Sigma_{t,L}(m_t^2) + \Sigma_{t,R}(m_t^2)\right]. \end{aligned} \tag{2.40}$$

2.3.2 Renormalization of gauge fields

Quite analogous to the fermion self-energy, we introduce the *gauge boson self-energies* [10] $\Pi(p^2)$ (= radiative corrections to 1-PI gauge boson 2-point function), which we use to impose on-shell renormalization conditions for masses and fields. The loop contributions can be cast into the form[11]

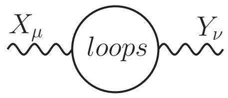

$$= i\,\Pi^{\mu\nu}_{XY}(p^2) = i\left(g^{\mu\nu} - \frac{p^\mu p^\nu}{p^2}\right)\Pi^T_{XY}(p^2) + i\,\frac{p^\mu p^\nu}{p^2}\,\Pi^L_{XY}(p^2), \tag{2.41}$$

Like the fermion self energies, the quantity $\Pi^{\mu\nu}_{XY}$ also contains Higgs-mediated tadpoles besides the usual 1-PI contributions. The $\Pi^T(p^2)$ and $\Pi^L(p^2)$ are the transverse and longitudinal scalar functions of this

[9] Instead of the index $\mp$ we sometimes write L/R on fields and renormalization constants, i.e. $- \equiv L$ and $+ \equiv R$.

[10] The reduced quantity $\frac{\Pi(p^2)}{p^2}$ is often called *vacuum polarization.*

[11] Note: the bosonic self energies are often defined with an additional minus sign analogous to the fermionic case. Our convention has the advantage that positive/negative contributions to Π give positive/negative contributions to the boson mass relative to tree level.

rank-2 tensor object connecting external gauge bosons X and Y. They have a perturbative expansion analogous to eq. (2.25)

$$\Pi^{T/L}_{XY}(p^2) = \sum_{k=1}^{\infty} \Pi^{T/L,(k)}_{XY}(p^2) = \Pi^{T/L,(1)}_{XY}(p^2) + \mathcal{O}(\alpha^2). \tag{2.42}$$

Constructing the renormalized gauge boson self energies

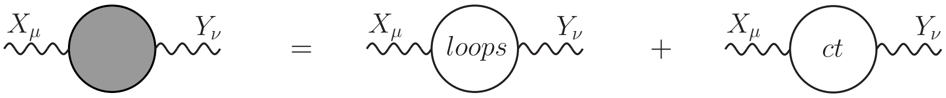

$$i\,\hat{\Pi}^{\mu\nu}_{XY}(p^2) = i\left(g^{\mu\nu} - \frac{p^\mu p^\nu}{p^2}\right)\hat{\Pi}^T_{XY}(p^2) + i\,\frac{p^\mu p^\nu}{p^2}\,\hat{\Pi}^L_{XY}(p^2), \tag{2.43}$$

where the hats once again denote renormalized quantities.

It is now possible to impose on-shell conditions in close analogy to the fermionic ones (with X, Y taking the role of the generation indices i, j). In the Denner-scheme there is an on-shell condition for each boson mass and residue. Also the off-diagonal elements of $\hat{\Pi}_{XY}$ are fixed on the various mass shells. This will not be the case in the BHS-scheme (see sec. 2.4). For now the renormalization conditions (Denner-scheme) read

$$\mathrm{Re}\left[\hat{\Pi}^{\mu\nu}_{XY}(p^2)\right]\varepsilon^\star_\nu(p)\Big|_{p^2=M_X^2} = 0, \qquad \mathrm{Re}\left[\hat{\Pi}^{\mu\nu}_{XY}(p^2)\right]\varepsilon_\nu(p)\Big|_{p^2=M_Y^2} = 0,$$

$$\lim_{p^2\to M_X^2}\frac{1}{p^2-M_X^2}\,\mathrm{Re}\left[\hat{\Pi}^{\mu\nu}_{XY}(p^2)\right]\varepsilon^\star_\nu(p) = 0, \qquad \lim_{p^2\to M_Y^2}\frac{1}{p^2-M_Y^2}\,\mathrm{Re}\left[\hat{\Pi}^{\mu\nu}_{XY}(p^2)\right]\varepsilon_\nu(p) = 0, \tag{2.44}$$

Using the orthogonality of the polarization vectors on-shell, $p^\mu\,\varepsilon^{(\star)}_\mu(p) = 0$ for $p^2 \to M^2$, the renormalization conditions can be brought into the equivalent form

$$\mathrm{Re}\left[\hat{\Pi}^T_{XY}(p^2)\right]\Big|_{p^2=M_X^2} = 0, \qquad \mathrm{Re}\left[\hat{\Pi}^T_{XY}(p^2)\right]\Big|_{p^2=M_Y^2} = 0,$$

$$\lim_{p^2\to M_X^2}\frac{1}{p^2-M_X^2}\,\mathrm{Re}\left[\hat{\Pi}^T_{XY}(p^2)\right] = 0, \qquad \lim_{p^2\to M_Y^2}\frac{1}{p^2-M_Y^2}\,\mathrm{Re}\left[\hat{\Pi}^T_{XY}(p^2)\right] = 0, \tag{2.45}$$

That only the transverse part enters the renormalization prescriptions is sensible, as pole location and residues of longitudinal parts (or rather the $p^\mu p^\nu$-pieces) of the propagators are gauge-dependent and should never contribute to physical observables and predictions. In fact, naively Dyson summing the 1PI-contributions for a propagator of a massive vector boson V_μ

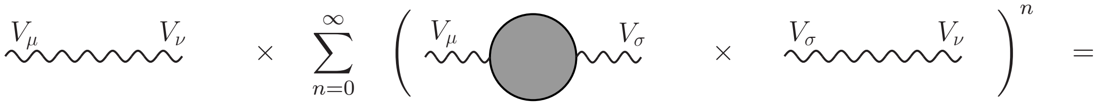

$$= \frac{(-i)}{p^2 - M_V^2 - \hat{\Pi}^T_{VV}(p^2) + i0^+}\left(g^{\mu\nu} - \frac{p^\mu p^\nu}{p^2}\right) + \frac{(-i)\xi_V}{p^2 - \xi_Z(M_V^2 + \hat{\Pi}^L_{VV}(p^2)) + i0^+}\,\frac{p^\mu p^\nu}{p^2}. \tag{2.46}$$

shows that the transverse pieces Π^T_{VV} correct the physical pole, while the longitudinal parts Π^L_{VV} correct the unphysical, gauge dependent pole (often referred to as *Goldstone pole*). It has to be noted that this argument is somewhat heuristic, because in general the Dyson summation is not a useful concept for gauge bosons, since their 2-point functions are usually highly gauge-dependent quantities. Only fermion bubble or bubble-chain contributions allow for this procedure, as they are trivially gauge-independent (cf. sec. 3.4.2). For more details concerning the unphysical parts we again refer to [3].

2.3.2.1 $W^\pm$ renormalization

We start with the charged bosons $W^\pm$, as their field and mass renormalization is somewhat simpler than for the neutral ones. The corresponding free part of the bare Lagrangian including the gauge-fixing part (2.19) (without the Goldstones) reads

$$\mathcal{L}_{\text{free}}^{W,0} = W_\nu^{+,0} \left[g^{\mu\nu} \left(\Box + (M_W^0)^2 \right) - \left(1 - \frac{1}{\xi_W} \right) \partial^\mu \partial^\nu \right] W_\mu^{-,0}. \tag{2.47}$$

Introducing renormalized fields and mass (again supressing the superscript indicating the loop order)

$$W_\mu^{\pm,0} \equiv \sqrt{Z_W}\, W_\mu^\pm = \left(1 + \frac{1}{2}\, \delta Z_W \right) W_\mu^\pm + \mathcal{O}(\alpha^2),$$

$$(M_W^0)^2 \equiv Z_{M_W} M_W^2 = (1 + \delta Z_{M_W})\, M_W^2 + \mathcal{O}(\alpha^2), \tag{2.48}$$

we obtain the decomposition into renormalized and one-loop counterterm Lagrangian

$$\begin{aligned} \mathcal{L}_{\text{free}}^{W,0} = W_\nu^+ &\left[g^{\mu\nu} \left(\Box + M_W^2 \right) - \left(1 - \frac{1}{\xi_W} \right) \partial^\mu \partial^\nu \right] W_\mu^- + \\ &+ \delta Z_W W_\nu^+ \left[g^{\mu\nu} \left(\Box + M_W^2 \right) - \left(1 - \frac{1}{\xi_W} \right) \partial^\mu \partial^\nu \right] W_\mu^- + \delta Z_{M_W} M_W^2\, W_\nu^+ g^{\mu\nu} W_\mu^- + \mathcal{O}\left(\alpha^2\right), \end{aligned} \tag{2.49}$$

yielding the Feynman rules[12]

$$= \frac{(-i)}{p^2 - M_W^2 + i0^+} \left(g^{\mu\nu} - \frac{p^\mu p^\nu}{p^2} \right) + \frac{(-i)\xi_W}{p^2 - \xi_W M_W^2 + i0^+} \frac{p^\mu p^\nu}{p^2},$$

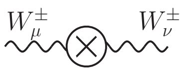

$$= (-i) \left[(p^2 - M_W^2) g^{\mu\nu} - \left(1 - \frac{1}{\xi_W} \right) p^\mu p^\nu \right] \delta Z_W + i\, M_W^2\, g^{\mu\nu}\, \delta Z_{M_W}. \tag{2.50}$$

When combined with $\Pi_{WW}^T(p^2)$, these counterterms form the renormalized W-self-energy

$$\hat{\Pi}_{WW}^T(p^2) = \Pi_{WW}^T(p^2) - (p^2 - M_W^2)\, \delta Z_W + M_W^2 \delta Z_{M_W}. \tag{2.51}$$

The renormalization conditions (2.45) for $W^\pm$ read[13]

$$\hat{\Pi}_{WW}^T(M_W^2) = 0, \qquad \left. \frac{\hat{\Pi}_{WW}^T(p^2)}{dp^2} \right|_{p^2 = M_W^2} = 0. \tag{2.52}$$

They fix M_W- and W-field strength renormalization constants in the on-shell scheme

$$\delta Z_{M_W} = -\frac{\Pi_{WW}^T(M_W^2)}{M_W^2},$$

$$\delta Z_W = \left. \frac{d\Pi_{WW}^T(p^2)}{dp^2} \right|_{p^2 = M_W^2}. \tag{2.53}$$

[12]Note that there exist alternative representations of the W-boson propagator (see appendix G). The one presented here makes it clear that no problems arise in the UV in terms of power counting.

[13]As usual omitting Re(...).

2.3.3 Z/A renormalization

The neutral gauge boson sector is not as straightforward as $W^\pm$ due to radiative mixing between Z-boson and photon. The equations become most transparent when written as matrix equations in this 2-dimensional space spanned by the mass eigenstates Z_0 and A_0. The free bare Lagrangian is diagonal

$$\mathcal{L}_{\text{free}}^{Z/A,0} = \frac{1}{2}\begin{pmatrix} Z_\nu^0 \\ A_\nu^0 \end{pmatrix}^T \begin{pmatrix} g^{\mu\nu}\left(\Box + (M_Z^0)^2\right) - \left(1-\frac{1}{\xi_Z}\right)\partial^\mu\partial^\nu & 0 \\ 0 & g^{\mu\nu}\Box - \left(1-\frac{1}{\xi_A}\right)\partial^\mu\partial^\nu \end{pmatrix}\begin{pmatrix} Z_\mu^0 \\ A_\mu^0 \end{pmatrix} \equiv$$

$$\equiv \frac{1}{2}\begin{pmatrix} Z_\nu^0 \\ A_\nu^0 \end{pmatrix}^T \begin{pmatrix} \Box_{Z,0}^{\mu\nu} & 0 \\ 0 & \Box_A^{\mu\nu} \end{pmatrix}\begin{pmatrix} Z_\mu^0 \\ A_\mu^0 \end{pmatrix}. \tag{2.54}$$

The box-operators can be read off and are also given in the appendix A.1.1, eq. (A.3). The multiplicative renormalization constants for the fields are assembled as 2x2 matrix

$$\begin{pmatrix} Z_\mu^0 \\ A_\mu^0 \end{pmatrix} \equiv \begin{pmatrix} \sqrt{Z_{AA}} & \sqrt{Z_{ZA}} \\ \sqrt{Z_{AZ}} & \sqrt{Z_{ZZ}} \end{pmatrix}\begin{pmatrix} Z_\mu \\ A_\mu \end{pmatrix} = \begin{pmatrix} 1+\frac{1}{2}\,\delta Z_{AA} & \frac{1}{2}\,\delta Z_{ZA} \\ \frac{1}{2}\,\delta Z_{AZ} & 1+\frac{1}{2}\,\delta Z_{ZZ} \end{pmatrix}\begin{pmatrix} Z_\mu \\ A_\mu \end{pmatrix} + \mathcal{O}(\alpha^2), \tag{2.55}$$

The Z-boson mass renormalization is analogous to the $W^\pm$ case,

$$(M_Z^0)^2 = Z_{M_Z} M_Z^2 = (1+\delta Z_{M_Z})\, M_Z^2 + \mathcal{O}(\alpha^2). \tag{2.56}$$

Inserting those into the Lagrangian (2.54) gives

$$\mathcal{L}_{\text{free}}^{Z/A,0} = \frac{1}{2}\begin{pmatrix} Z_\nu \\ A_\nu \end{pmatrix}^T \begin{pmatrix} \sqrt{Z_{AA}} & \sqrt{Z_{ZA}} \\ \sqrt{Z_{AZ}} & \sqrt{Z_{ZZ}} \end{pmatrix}^T \begin{pmatrix} \Box_{Z,0}^{\mu\nu} & 0 \\ 0 & \Box_A^{\mu\nu} \end{pmatrix}\begin{pmatrix} \sqrt{Z_{AA}} & \sqrt{Z_{ZA}} \\ \sqrt{Z_{AZ}} & \sqrt{Z_{ZZ}} \end{pmatrix}\begin{pmatrix} Z_\mu \\ A_\mu \end{pmatrix} =$$

$$= \frac{1}{2}\begin{pmatrix} Z_\nu \\ A_\nu \end{pmatrix}^T \begin{pmatrix} Z_{ZZ}\Box_{Z,0}^{\mu\nu} + Z_{AZ}\Box_A^{\mu\nu} & \sqrt{Z_{ZZ}}\sqrt{Z_{ZA}}\,\Box_{Z,0}^{\mu\nu} + \sqrt{Z_{AZ}}\sqrt{Z_{AA}}\,\Box_A^{\mu\nu} \\ \sqrt{Z_{ZZ}}\,\sqrt{Z_{ZA}}\,\Box_{Z,0}^{\mu\nu} + \sqrt{Z_{AZ}}\sqrt{Z_{AA}}\,\Box_A^{\mu\nu} & Z_{ZA}\Box_{Z,0}^{\mu\nu} + Z_{AA}\Box_A^{\mu\nu} \end{pmatrix}\begin{pmatrix} Z_\mu \\ A_\mu \end{pmatrix}. \tag{2.57}$$

When expanding this expression to first order, one needs to pay attention to the fact that both Z_{ZA} and Z_{AZ} are $\sim \mathcal{O}(\alpha)$, and to the mass renormalization factor contained in $\Box_{Z,0}^{\mu\nu}$. We find

$$\mathcal{L}_{\text{free}}^{Z/A,0} = \frac{1}{2}\begin{pmatrix} Z_\nu \\ A_\nu \end{pmatrix}^T \begin{pmatrix} (1+\delta Z_{ZZ})\,\Box_Z^{\mu\nu} + g^{\mu\nu}\delta Z_{M_Z} M_Z^2 & \frac{1}{2}\,\delta Z_{ZA}\Box_Z^{\mu\nu} + \frac{1}{2}\,\delta Z_{AZ}\Box_A^{\mu\nu} \\ \frac{1}{2}\,\delta Z_{ZA}\Box_Z^{\mu\nu} + \frac{1}{2}\,\delta Z_{AZ}\Box_A^{\mu\nu} & (1+\delta Z_{AA})\,\Box_A^{\mu\nu} \end{pmatrix}\begin{pmatrix} Z_\mu \\ A_\mu \end{pmatrix} + \mathcal{O}\left(\alpha^2\right) \tag{2.58}$$

This Lagrangian turns into the Feynman rules

$$= \frac{(-i)\left(g^{\mu\nu} - (1-\xi_A)\frac{p^\mu p^\nu}{p^2})\right)}{p^2 + i0^+}, \tag{2.59}$$

$$= \frac{(-i)}{p^2 - M_Z^2 + i0^+}\left(g^{\mu\nu} - \frac{p^\mu p^\nu}{p^2}\right) + \frac{(-i)\xi_Z}{p^2 - \xi_Z M_Z^2 + i0^+}\frac{p^\mu p^\nu}{p^2} =$$

$$= (-i)\left[(p^2 - M_Z^2)g^{\mu\nu} - \left(1-\frac{1}{\xi_Z}\right)p^\mu p^\nu\right]\delta Z_{ZZ} + i\, M_Z^2\, g^{\mu\nu}\delta Z_{M_Z}, \tag{2.60}$$

$$= (-i)\left[p^2 g^{\mu\nu} - \left(1-\frac{1}{\xi_A}\right)p^\mu p^\nu\right]\delta Z_{AA}, \tag{2.61}$$

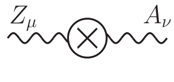

$$= \frac{(-i)}{2}\left[\left(p^2 - M_Z^2\right)\delta Z_{ZA} + p^2\delta Z_{AZ}\right]g^{\mu\nu} +$$

$$-\frac{(-i)}{2}\left[\left(1-\frac{1}{\xi_Z}\right)\delta Z_{ZA}+\left(1-\frac{1}{\xi_A}\right)\delta Z_{AZ}\right]p^\mu p^\nu. \tag{2.62}$$

To one-loop order, the renormalized transverse pieces read

$$\begin{aligned}
\hat{\Pi}^T_{AA}(p^2) &= \Pi^T_{AA}(p^2) - p^2\delta Z_{AA},\\
\hat{\Pi}^T_{ZZ}(p^2) &= \Pi^T_{ZZ}(p^2) - (p^2-M_Z^2)\delta Z_{ZZ} + M_Z^2\delta Z_{M_Z},\\
\hat{\Pi}^T_{AZ}(p^2) &= \Pi^T_{AZ}(p^2) - \frac{1}{2}p^2\delta Z_{AZ} - \frac{1}{2}(p^2-M_Z^2)\,\delta Z_{ZA}.
\end{aligned} \tag{2.63}$$

The two off-diagonal field strength renormalization constants δZ_{AZ} and δZ_{ZA} will be extracted by taking different on-shell limits: $p^2 \to 0$ and $p^2 \to M_Z^2$ (cf. eq. (2.45)), the rest is analogous to $W^{\pm}$[14]. Restating (2.45) for the case at hand[15]

$$\left.\frac{d\hat{\Pi}^T_{ZZ}(p^2)}{dp^2}\right|_{p^2=M_Z^2} = 0, \qquad \left.\frac{d\hat{\Pi}^T_{AA}(p^2)}{dp^2}\right|_{p^2=0} = 0,$$

$$\hat{\Pi}^T_{ZA}(0) = 0, \qquad \hat{\Pi}^T_{ZA}(M_Z^2) = 0, \tag{2.64}$$

as well as

$$\hat{\Pi}^T_{ZZ}(M_Z^2) = 0, \tag{2.65}$$

yields the residue counterterms

$$\delta Z_{ZZ} = \left.\frac{d\Pi^T_{ZZ}(p^2)}{dp^2}\right|_{p^2=M_Z^2}, \qquad \delta Z_{AA} = \left.\frac{d\Pi^T_{AA}(p^2)}{dp^2}\right|_{p^2=0},$$

$$\delta Z_{ZA} = -2\,\frac{\Pi^T_{AZ}(0)}{M_Z^2}, \qquad \delta Z_{AZ} = 2\,\frac{\Pi^T_{AZ}(M_Z^2)}{M_Z^2}, \tag{2.66}$$

and the Z-mass constant

$$\delta Z_{M_Z} = -\frac{\Pi^T_{ZZ}(M_Z^2)}{M_Z^2}. \tag{2.67}$$

This completes the one-loop renormalization of the various 2-point functions. Next we turn to the other parameters of the theory.

2.3.4 Charge renormalization

A central parameter in EW theory is the electric charge e. In QFT it is defined to be the coupling constant multiplying the EM current $-ieQ_f\bar{\psi}_f(x)\gamma^\mu\psi_f(x)$ in units Q_f. There exist two main options for defining its renormalization scheme: $\overline{\text{MS}}$- and OS-scheme. The $\overline{\text{MS}}$-scheme is the almost exclusive choice in QCD (for the QCD-coupling g_s or α_s), and often used in pure QED, as its associated RG-evolution is able to resum leading logarithmic contributions to all orders. Another benefit is that computing the $\overline{\text{MS}}$-counterterms is simpler than in other schemes, as only the $\frac{1}{\epsilon}$-pieces are needed. In EW theory the usefulness of the $\overline{\text{MS}}$-scheme is significantly reduced because of the would-be-Goldstone modes, that have to be added order by order. Summing to all orders by running parameters is a very delicate subject. The reason is that this usually implies treating different subprocesses (for example vertex and propagator corrections) at different orders, which spells disaster if they are intrinsically connected by gauge dependence and/or renormalization. Quantities like masses and couplings are therefore usually defined in the OS-scheme. Since the bosons and fermions are not confined from the EW point of view, the pole

[14]The "mass" condition eq. (2.45) for the photon part $\hat{\Pi}^T_{AA}$ is automatically fulfilled due to a Ward identity, which we confirm by explicit computation later on.

[15]We again suppress the Re indicating that for the renormalization constants only the real part of the self energies (if it is nonzero) must be taken.

mass is a more useful scheme than quark pole masses in QCD[16]. We will therefore stick to this logic and define the electric charge in the OS-scheme incorporating all EW contributions. There exists a hybrid system that is frequently used, where the fermionic pure QED corrections (i.e. fermionic loops in the photon 2-point function) are treated in $\overline{\text{MS}}$, with subsequent running of α. This treatment is referred to as the *QED-improved Born approximation*, which we discuss in sec. 3.4.2.

Returning to the OS-scheme, the charge definition is chosen such that at large distances (i.e. momentum transfer $q \to 0$, the *Thomson limit*) it coincides with the electric charge defintion of classical electrodynamics: the interaction strength of the Coulomb potential between 2 point charges like electrons. Translated to QFT, this means that the renormalization of the electric charge e is given by the Thomson limit of the electromagnetic electron-electron vertex with all external particles on-shell.

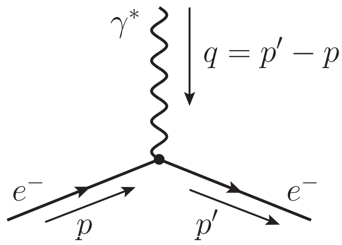

Figure 2.1: Momentum conventions of electromagnetic vertex

In figure 2.1 the notation of momenta can be read off. Quantitatively the Thomson limit means that the S-matrix element must obey

$$i\,\varepsilon_\mu(q)\mathcal{M}^\mu(e^-\gamma^* \to e^-) \overset{q^2=0}{=} i\,e\,\varepsilon_\mu(0)\,\bar{u}(p)\gamma^\mu u(p), \tag{2.68}$$

for zero momentum transfer, i.e. $q = p' - p = 0$. Actually, it is not important to take electrons as external particles, any other fermion will also do the job. Since we chose on-shell renormalization conditions for the fermion and gauge fields, we do not need to take into account additional residue corrections when computing the S-matrix element. This means we can focus on the (renormalized) amputated one-loop vertex function of an off-shell current (dropping the polarization vector), which we can decompose in terms of form factors as (for an arbitrary fermion f)

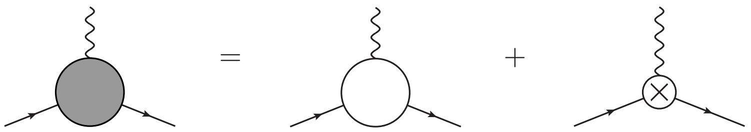

$$\equiv \quad ie\,\bar{u}_e(p')\hat{\Lambda}^\mu_{Aff}(q^2)u_e(p),$$

$$\hat{\Lambda}^\mu_{Aff}(q^2) = \gamma^\mu\,\hat{F}_1^V(q^2) + \gamma^\mu\gamma_5\,\hat{F}_1^A(q^2) + \frac{(p'+p)^\mu}{2m_f}\,\hat{F}_2^V(q^2) + \frac{(p'-p)^\mu}{2m_f}\gamma_5\,\hat{F}_3^A(q^2), \tag{2.69}$$

where the white empty blob denotes all 1-PI loop contributions. Therefore all this form factors incorporate only loop contributions (pure loops + counterterms), the tree-level result is treated separately. For the bare loop contributions $\Lambda^\mu_{Aff}(q^2)$ the same decomposition is possible, but with hats omitted above the form factors. The notation for the form factors is standard, the two remaining ones are 0 because of vector current conservation ($F_3^V(q^2) = 0$) and by explicit calculation at one loop ($F_2^A(q^2) = 0$). This also holds for the Z-vertex, and we will come back to this in chapter 3.5.2.

We focus on the QED interaction of a generic Dirac fermion f, which is described by a quantum field ψ with the chiral field renormalization constants

$$\psi^0_{L/R} = \sqrt{Z_{L/R}}\,\psi_{L/R} = \left(1 + \frac{1}{2}\,\delta Z_{L/R}\right)\psi_{L/R} + \mathcal{O}(\alpha^2), \tag{2.70}$$

[16]There is however the subtlety that most of these particles are unstable, which turns asymptotic states and the pole mass into problematic concepts once again. We will not treat this issue any further in this work however, and refer the reader to the literature and planned future work on that subject.

with a photon field A_μ (see eq. (2.55)). Furthermore electric charge is renormalized by

$$e_0 = Z_e\, e = (1+\delta Z_e)\, e + \mathcal{O}(\alpha^2). \tag{2.71}$$

To derive the counterterms we start with the the bare interaction Lagrangian

$$\begin{aligned}\mathcal{L}^0_{Aff} &= -Q_f\, e_0\, \bar\psi^0\gamma^\mu A^0_\mu\psi^0 = -Q_f\, e_0\, \bar\psi^0_L\gamma^\mu A^0_\mu\psi^0_L - Q_f\, e_0\, \bar\psi^0_R\gamma^\mu A^0_\mu\psi^0_R = \\ &= -Q_f\, e\,\bar\psi\gamma^\mu A_\mu\psi - Q_f\, e\,\bar\psi\gamma^\mu A_\mu \left(\delta Z_e + \omega_-\delta Z_L + \omega_+\delta Z_R + \frac{1}{2}\,\delta Z_{AA}\right)\psi + \\ &\quad - Q_f\, e\,\frac{1}{2}\,\delta Z_{AZ}\,\bar\psi\gamma^\mu Z_\mu\psi + \mathcal{O}\left(\alpha^2\right).\end{aligned} \tag{2.72}$$

This last term with the $\bar\psi \not{Z}\psi$ coupling actually does not contribute to the Aff-vertex counterterm, but rather to the renormalization of the Zff-vertex and can be dropped for the analysis in this chapter. Conversely however, in $\mathcal{L}^0_{Zff}$ there should hide a corresponding term that contributes to the photon vertex. Below we extract this piece quickly by only introducing renormalization constants for the Z_μ-field (eq. (2.55)). The full analysis for the Z-vertex can be found in section 3.5. We get:

$$\begin{aligned}\mathcal{L}^0_{Zff} &\approxeq e\,\bar\psi\gamma^\mu\left(v_f - a_f\gamma_5\right) Z^0_\mu\psi = \\ &= e\,\bar\psi\gamma^\mu\left(v_f - a_f\gamma_5\right)\left[\left(1+\frac{1}{2}\,\delta Z_{ZZ}\right) Z_\mu + \frac{1}{2}\,\delta Z_{ZA} A_\mu\right]\psi + \mathcal{O}\left(\alpha^2\right) = \\ &= \ldots + e\,\frac{1}{2}\,\delta Z_{ZA}\bar\psi\gamma^\mu\left(v_f - a_f\gamma_5\right) A_\mu\psi.\end{aligned} \tag{2.73}$$

v_f and a_f are the vector and axial-vector couplings of the fermion to the Z boson (see appendix G.1). The relevant counterterm Lagrangian for the Aff-vertex is therefore

$$\begin{aligned}\mathcal{L}^{\mathrm{ct}}_{Aff} = e&\left[-Q_f\left(\delta Z_e + \frac{1}{2}\left(\delta Z_L + \delta Z_R\right) + \frac{1}{2}\,\delta Z_{AA}\right) + v_f\,\frac{1}{2}\,\delta Z_{ZA}\right]\bar\psi\gamma^\mu A_\mu\psi + \\ &+ e\left[Q_f\,\frac{1}{2}\left(\delta Z_L - \delta Z_R\right) - a_f\,\frac{1}{2}\,\delta Z_{ZA}\right]\bar\psi\gamma^\mu\gamma_5 A_\mu\psi.\end{aligned} \tag{2.74}$$

We have expressed things in terms of γ^μ and $\gamma^\mu\gamma_5$ to make contact with the form factor decomposition. This gives the one-loop counterterm Feynman rule

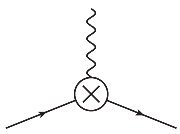

$$\begin{aligned}&= ie\gamma^\mu\left[-Q_f\left(\delta Z_e + \frac{1}{2}\left(\delta Z_L + \delta Z_R\right) + \frac{1}{2}\,\delta Z_{AA}\right) + \frac{1}{2}\,v_f\,\delta Z_{ZA} + \right. \\ &\qquad\left. + \gamma_5\left[Q_f\,\frac{1}{2}\left(\delta Z_L - \delta Z_R\right) - \frac{1}{2}\,a_f\,\delta Z_{ZA}\right]\right].\end{aligned} \tag{2.75}$$

For the loops we write

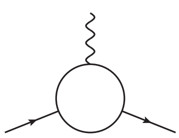

$$= ie\left[\gamma^\mu\, F^V_1(q^2) + \gamma^\mu\gamma_5\, F^A_1(q^2) + \frac{(p'+p)^\mu}{2m_f}\, F^V_2(q^2) + \frac{(p'-p)^\mu}{2m_f}\gamma_5\, F^A_3(q^2)\right]. \tag{2.76}$$

Combining the two contributions we get the renormalized one-loop vertex function

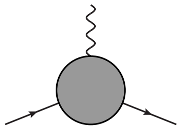

$$\begin{aligned}&= ie\gamma^\mu\left[F^V_1(q^2) - Q_f\left(\delta Z_e + \frac{1}{2}\left(\delta Z_L + \delta Z_R\right) + \frac{1}{2}\,\delta Z_{AA}\right) + v_f\,\frac{1}{2}\,\delta Z_{ZA}\right] + \\ &\quad + ie\gamma^\mu\gamma_5\left[F^A_1(q^2) + Q_f\,\frac{1}{2}\left(\delta Z_L - \delta Z_R\right) - \frac{1}{2}\,a_f\,\delta Z_{ZA}\right] +\end{aligned}$$

$$+ \frac{(p'+p)^\mu}{2m_f} F_2^V(q^2) + \frac{(p'-p)^\mu}{2m_f}\gamma_5 F_3^A(q^2). \tag{2.77}$$

Taking the Thomson limit means $q = p' - p \to 0$, i.e. $p' \to p$. The F_3^A-term vanishes in this limit, but F_2^V will contribute. To see how we use a Gordon identity

$$\bar{u}(p') \left[\frac{(p'+p)^\mu}{2m_f} + \frac{i\sigma^{\mu\nu}}{2m_f}(p'-p)_\nu \right] u(p) = \bar{u}(p')\gamma^\mu u(p). \tag{2.78}$$

The $\sigma^{\mu\nu}$-term obviously vanishes in the Thomson limit, allowing us (in this limit) to replace the scalar structure by a γ^μ. To fulfill the on-shell condition (2.68) we have to set the renormalized 1-PI one-loop vertex correction to zero at the kinematic point $q = 0$. The rest is straightforward leading to

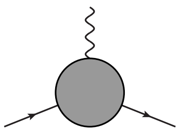

$$\Bigg|_{q=0} = ie\gamma^\mu \left[F_1^V(0) + F_2^V(0) - Q_f \left(\delta Z_e + \frac{1}{2}(\delta Z_L + \delta Z_R) + \frac{1}{2}\delta Z_{AA} \right) + v_f \frac{1}{2}\delta Z_{ZA} \right] +$$

$$+ ie\gamma^\mu\gamma_5 \left[F_1^A(0) + Q_f \frac{1}{2}(\delta Z_L - \delta Z_R) - \frac{1}{2} a_f \delta Z_{ZA} \right] \overset{!}{=} 0. \tag{2.79}$$

Because of the independence of γ^μ and $\gamma^\mu\gamma_5$ this actually gives two conditions as both prefactors have to vanish. The second one derived from the axial part is automatically fulfilled due to a Ward identity[17] (cf. [8])

$$F_1^A(0) + Q_f \frac{1}{2}(\delta Z_{f,L} - \delta Z_{f,R}) - \frac{1}{2} a_f \delta Z_{ZA} \overset{\text{Ward identity}}{=} 0. \tag{2.80}$$

The same Ward identity also implies

$$F_1^V(0) + F_2^V(0) - Q_f \frac{1}{2}(\delta Z_L + \delta Z_R) + a_f \frac{1}{2}\delta Z_{ZA} \overset{\text{Ward identity}}{=} 0, \tag{2.81}$$

allowing to eliminate the fermion field strength renormalization constants and the form factors for the vector part, which leaves a pretty simple equation

$$0 = -Q_f \left(\delta Z_e + \frac{1}{2}\delta Z_{AA} \right) + \frac{1}{2}(v_f - a_f)\delta Z_{ZA} = -Q_f \left(\delta Z_e + \frac{1}{2}\delta Z_{AA} \right) - Q_f \frac{1}{2}\frac{s_W}{c_W}\delta Z_{ZA}. \tag{2.82}$$

Note that all remnants of the involved fermion f (i.e. form factors, fermion field strengths and quantum numbers) have been eliminated, which reflects charge universality [8]. Electric charge renormalization is therefore given by

$$\delta Z_e = -\frac{1}{2}\delta Z_{AA} - \frac{1}{2}\frac{s_W}{c_W}\delta Z_{ZA}. \tag{2.83}$$

2.3.5 $\cos(\theta_W)$ and $\sin(\theta_W)$

Since we pick M_Z and M_W to be physical parameters of the theory, the Weinberg angle θ_W and the two associated trigonometric functions will be treated as derived quantities, given by

$$\cos(\theta_W) \equiv c_W = \frac{M_W}{M_Z}, \qquad \sin(\theta_W) \equiv s_W = \sqrt{1 - \frac{M_W^2}{M_Z^2}}. \tag{2.84}$$

Its renormalization constants will therefore be expressible via mass renormalization constants of the massive gauge bosons. We start by defining

$$c_W^0 = Z_c\, c_W = (1 + \delta Z_c)\, c_W, \qquad s_W^0 = Z_s\, s_W = (1 + \delta Z_s)\, s_W, \tag{2.85}$$

[17]The Ward identity is a non-perturbative statement, but to keep things consistent we also needed to expand the form factors to the corresponding order of counterterm insertions.

which allows to write both sides of equation 2.84

$$
\begin{aligned}
\text{lhs}: \quad & (c_W^0)^2 = (1+\delta Z_c)^2\, c_W^2 = (1+2\,\delta Z_c)\, c_W^2 + \mathcal{O}\left(\alpha^2\right), \\
\text{rhs}: \quad & (c_W^0)^2 = \frac{(M_W^0)^2}{(M_Z^0)^2} = \frac{1+\delta Z_{M_W}}{1+\delta Z_{M_Z}} \frac{M_W^2}{M_Z^2} = (1+\delta Z_{M_W} - \delta Z_{M_Z})\, \frac{M_W^2}{M_Z^2} + \mathcal{O}\left(\alpha^2\right).
\end{aligned} \tag{2.86}
$$

Comparing both sides one can read off

$$
\delta Z_c = \frac{1}{2}\,(\delta Z_{M_W} - \delta Z_{M_Z})\,. \tag{2.87}
$$

For s_W we note that $s_W^2 = 1 - c_W^2$, so that

$$
\begin{aligned}
\text{lhs}: \quad & (s_W^0)^2 = (1+\delta Z_s)^2 s_W^2 = (1+2\,\delta Z_s)\, s_W^2 + \mathcal{O}\left(\alpha^2\right), \\
\text{rhs}: \quad & 1-(c_W^0)^2 = 1-(1+\delta Z_c)^2\, c_W^2 = 1-(1+2\,\delta Z_c)\, c_W^2 + \mathcal{O}\left(\alpha^2\right).
\end{aligned} \tag{2.88}
$$

Again comparing both sides yields

$$
\delta Z_s = -\frac{c_W^2}{s_W^2}\,\delta Z_c = -\frac{1}{2}\frac{c_W^2}{s_W^2}\,(\delta Z_{M_W} - \delta Z_{M_Z})\,. \tag{2.89}
$$

2.4 BHS-scheme

In contrast to the approach adapted in the last section, where we exclusively worked in the broken phase and derived all renormalization constants there, it is also possible to start in the unbroken phase and make use of the symmetries of the theory (which will translate into Slavnov-Taylor identities). The parameters now available for renormalization are the ones on the lhs of eq. (2.17) and the field content. The renormalization of fermions is completely analogous to the Denner-scheme, so we skip it here. This means we can ignore the Yukawa couplings $G_{f,ij}$, but for the rest we introduce the following multiplicative renormalization constants (following [4] concerning notation):

$$
\begin{aligned}
g^0 &\equiv Z_g g \equiv Z_1^W \left(Z_2^W\right)^{-3/2} g, \\
g'^0 &\equiv Z_{g'} g' \equiv Z_1^B \left(Z_2^B\right)^{-3/2} g', \\
W_\mu^{a,0} &\equiv Z_2^W W_\mu^a, \\
B_\mu^0 &\equiv Z_2^B B_\mu, \\
\left(M_Z^0\right)^2 &\equiv Z_{M_Z} M_Z^2, \\
\left(M_W^0\right)^2 &\equiv Z_{M_W} M_W^2,
\end{aligned} \tag{2.90}
$$

The mass renormalization constants are defined as in the Denner-scheme, and since the on-shell conditions are chosen identical (cf. eq. (2.113)) the renormalization constants Z_{M_W} and Z_{M_Z} are exactly the same as those defined in eq. (2.48) and (2.56). The definition of the renormalization constants of the couplings is a matter of taste, but we try to follow [4] closely to facilitate comparison. An important difference to the broken phase is that the gauge triplet W_μ^a only gets one common field renormalization constant. In the broken phase just the $W_\mu^\pm$ shared such a factor, while for the two neutral bosons we even had 4 different δZ's. Since the theory´s renormalizability is not destroyed by SSB this implies that there is in fact quite some redundancy involved with the approach we adopted so far. While this chapter will not lead to new techniques or details necessary for the overall calculation, the main aim is to explore these symmetry details and constraints not visible in the scheme choice of the previous section.

In the following we will focus on the gauge bosons. The parameters for the renormalization of the

Higgs fields are μ^2 (fixed by imposing OS-conditions for the H-mass, cf. eq. (2.8)) and the Higgs quartic coupling λ (fixed by the Higgs pole mass and demanding that the the vev renormalization δv sucks up Higgs tadpoles). Since we will not need any of these renormalization constants related to the Higgs field in this work, so we will not explore the scalar sector any further here. A reference dealing with renormalization of scalars in a more general context is [16].

2.4.1 Gauge couplings

The task is to transport the renormalization constants given above over to the broken phase, i.e. to express the renormalization constants of the new parameter set (rhs of eq. (2.17)) in terms of the old (lhs of eq. (2.17)). We start with the gauge couplings g, g', whose renormalization constants read according to eq. (2.13)

$$\left.\begin{aligned} \delta Z_g &= \delta Z_e + \tfrac{c_W^2}{s_W^2}\,\delta Z_c \\ \delta Z_{g'} &= \delta Z_e - \delta Z_c \end{aligned}\right\} \quad \Longleftrightarrow \quad \left\{\begin{aligned} \delta Z_e &= s_W^2 \delta Z_g + c_W^2 \delta Z_{g'} \\ \delta Z_c &= s_W^2\left(\delta Z_g - \delta Z_{g'}\right) \end{aligned}\right. \tag{2.91}$$

From eq. (2.90) we get at $\mathcal{O}(\alpha)$

$$\delta Z_g = \delta Z_1^W - \frac{3}{2}\,\delta Z_2^W, \qquad \delta Z_{g'} = \delta Z_1^B - \frac{3}{2}\,\delta Z_2^B, \tag{2.92}$$

so that

$$\delta Z_e = s_W^2 \delta Z_1^W + c_W^2 \delta Z_1^B - \frac{3}{2}\left[s_W^2 \delta Z_2^W + c_W^2 \delta Z_2^B\right], \tag{2.93}$$

$$\delta Z_c = s_W^2\left(\delta Z_1^W - \delta Z_1^B - \frac{3}{2}\left[\delta Z_2^W - \delta Z_2^B\right]\right). \tag{2.94}$$

For reasons that become more transparent later, it is convenient to define certain linear combinations of the renormalization constants

$$\begin{pmatrix} \delta Z_i^Z \\ \delta Z_i^\gamma \end{pmatrix} = \begin{pmatrix} c_W^2 & s_W^2 \\ s_W^2 & c_W^2 \end{pmatrix} \begin{pmatrix} \delta Z_i^W \\ \delta Z_i^B \end{pmatrix} \quad \Longleftrightarrow \quad \begin{pmatrix} \delta Z_i^W \\ \delta Z_i^B \end{pmatrix} = \frac{1}{c_W^2 - s_W^2}\begin{pmatrix} c_W^2 & -s_W^2 \\ -s_W^2 & c_W^2 \end{pmatrix}\begin{pmatrix} \delta Z_i^Z \\ \delta Z_i^\gamma \end{pmatrix}, \tag{2.95}$$

as well as

$$\delta Z_i^{\gamma Z} = \frac{c_W s_W}{c_W^2 - s_W^2}\left(\delta Z_i^Z - \delta Z_i^\gamma\right) \tag{2.96}$$

In terms of these new renormalization constants we get

$$\begin{aligned} \delta Z_e &= \delta Z_1^\gamma - \frac{3}{2}\,\delta Z_2^\gamma, \\ \delta Z_c &= \frac{1}{2}\frac{s_W}{c_W}\left(2\delta Z_1^{\gamma Z} - 3\delta Z_2^{\gamma Z}\right). \end{aligned} \tag{2.97}$$

We have to use this form in the following section.

2.4.2 Gauge bosons

The renormalization of the bare gauge fields Z_μ^0 and A_μ^0 of the broken phase can be related to the unbroken gauge fields $W_\mu^{3,0}$ and B_μ^0 according to

$$\begin{pmatrix} Z_\mu^0 \\ A_\mu^0 \end{pmatrix} = \begin{pmatrix} c_W^0 & s_W^0 \\ -s_W^0 & c_W^0 \end{pmatrix}\begin{pmatrix} W_\mu^{3,0} \\ B_\mu^0 \end{pmatrix} \equiv \boldsymbol{\Omega}^0 \begin{pmatrix} W_\mu^{3,0} \\ B_\mu^0 \end{pmatrix}. \tag{2.98}$$

The renormalization of $W_\mu^{3,0}$ and B_μ^0 is diagonal

$$\begin{pmatrix} W_\mu^{3,0} \\ B_\mu^0 \end{pmatrix} = \begin{pmatrix} Z_2^W & 0 \\ 0 & Z_2^B \end{pmatrix}\begin{pmatrix} W_\mu^3 \\ B_\mu \end{pmatrix} \equiv \boldsymbol{Z}_2 \begin{pmatrix} W_\mu^{3,0} \\ B_\mu^0 \end{pmatrix}. \tag{2.99}$$

Using eq. (2.85) and expanding $\boldsymbol{Z}_2$ we find

$$\boldsymbol{\Omega}^0 = \begin{pmatrix} c_W & s_W \\ -s_W & c_W \end{pmatrix} + \begin{pmatrix} c_W \delta Z_c & s_W \delta Z_s \\ -s_W \delta Z_s & c_W \delta Z_c \end{pmatrix} + \mathcal{O}(\alpha^2) \equiv \boldsymbol{\Omega} + \boldsymbol{\delta\Omega} + \mathcal{O}(\alpha^2), \tag{2.100}$$

$$\boldsymbol{Z}_2 = \begin{pmatrix} 1 & 0 \\ 0 & 1 \end{pmatrix} + \frac{1}{2} \begin{pmatrix} \delta Z_2^W & 0 \\ 0 & \delta Z_2^B \end{pmatrix} + \mathcal{O}(\alpha^2) \equiv \mathbf{1} + \frac{1}{2} \boldsymbol{\delta Z}_2 + \mathcal{O}(\alpha^2). \tag{2.101}$$

Plugging into eq. (2.98) we get

$$\begin{pmatrix} Z_\mu^0 \\ A_\mu^0 \end{pmatrix} = \left(\mathbf{1} + \boldsymbol{\delta\Omega}\, \boldsymbol{\Omega}^T + \frac{1}{2} \boldsymbol{\Omega}\, \boldsymbol{\delta Z}_2\, \boldsymbol{\Omega}^T \right) \begin{pmatrix} Z_\mu \\ A_\mu \end{pmatrix} + \mathcal{O}(\alpha^2). \tag{2.102}$$

Making use of eq. (2.89) the first correction simplifies

$$\boldsymbol{\delta\Omega}\, \boldsymbol{\Omega}^T = \frac{c_W}{s_W} \delta Z_c \begin{pmatrix} 0 & -1 \\ 1 & 0 \end{pmatrix}, \tag{2.103}$$

while the second reads (cf. eqs. (2.95) and (2.96))

$$\boldsymbol{\Omega}\, \boldsymbol{\delta Z}_2\, \boldsymbol{\Omega}^T = \begin{pmatrix} \delta Z_2^Z & -\delta Z_2^{\gamma Z} \\ -\delta Z_2^{\gamma Z} & \delta Z_2^\gamma \end{pmatrix}. \tag{2.104}$$

Using eq. (2.97) we obtain for the bare $Z\mu$ and A_μ fields

$$\begin{pmatrix} Z_\mu^0 \\ A_\mu^0 \end{pmatrix} = \begin{pmatrix} 1 + \frac{1}{2} \delta Z_2^Z & -\delta Z_1^{\gamma Z} + \delta Z_2^{\gamma Z} \\ \delta Z_1^{\gamma Z} - 2\delta Z_2^{\gamma Z} & 1 + \frac{1}{2} \delta Z_2^\gamma \end{pmatrix} \begin{pmatrix} Z_\mu \\ A_\mu \end{pmatrix} \tag{2.105}$$

2.4.3 Counterterm Lagrangian

With the definitions of the last two sections, the counterterm Lagrangian and Feynman rules can be derived. Going back to the bare ZA-Lagrangian eq. (2.54), plugging in the bare fields as well as the Z-mass renormalization (which is the same as in eq. (2.56)) and expanding to $\mathcal{O}(\alpha)$ we obtain

$$\mathcal{L}_{\text{free}}^{Z/A,0} =$$

$$= \frac{1}{2} \begin{pmatrix} Z_\nu \\ A_\nu \end{pmatrix}^T \begin{pmatrix} \left(1 + \delta Z_2^Z\right) \Box_Z^{\mu\nu} + g^{\mu\nu} \delta Z_{M_Z} M_Z^2 & -\left(\delta Z_1^{\gamma Z} - \delta Z_2^{\gamma Z}\right) \left(\Box_Z^{\mu\nu} - \Box_A^{\mu\nu}\right) - \delta Z_2^\gamma \Box_A^{\mu\nu} \\ -\left(\delta Z_1^{\gamma Z} - \delta Z_2^{\gamma Z}\right) \left(\Box_Z^{\mu\nu} - \Box_A^{\mu\nu}\right) - \delta Z_2^\gamma \Box_A^{\mu\nu} & \left(1 + \delta Z_{AA}\right) \Box_A^{\mu\nu} \end{pmatrix} \times$$

$$\times \begin{pmatrix} Z_\mu \\ A_\mu \end{pmatrix} + \mathcal{O}\left(\alpha^2\right) \tag{2.106}$$

The OS-conditions are once again imposed on the $g^{\mu\nu}$-pieces, so we ignore the $\partial^\mu \partial^\nu$-parts of the $\Box_{Z/A}^{\mu\nu}$, which simplifies $\mathcal{L}_{\text{free}}^{Z/A,0}$ to

$$\begin{aligned} \mathcal{L}_{\text{free}}^{Z/A,0} \sim\ & \frac{1}{2} \left(1 + \delta Z_2^Z\right) g^{\mu\nu} Z_\nu \left(\Box + M_Z^2\right) Z_\mu + \frac{1}{2} M_Z^2\, g^{\mu\nu} Z_\nu Z_\mu + \frac{1}{2} \left(1 + \delta Z_2^\gamma\right) g^{\mu\nu} A_\nu \Box A_\mu + \\ & - \delta Z_2^{\gamma Z} g^{\mu\nu} A_\nu \Box Z_\mu - M_Z^2 \left(\delta Z_1^{\gamma Z} - \delta Z_2^{\gamma Z}\right) g^{\mu\nu} Z_\mu A_\nu + \partial^\mu \partial^\nu - \text{pieces} + \mathcal{O}(\alpha^2). \end{aligned} \tag{2.107}$$

The free bare $W^\pm$-Lagrangian is eq. (2.49) with the replacement $\delta Z_W \to \delta Z_2^W$. The corresponding transverse counterterm Feynman rules are

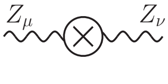

$$= (-i)\, g^{\mu\nu} \left[(p^2 - M_Z^2)\, \delta Z_2^Z - M_Z^2\, \delta Z_{M_Z} \right],$$

$$= (-i)\, g^{\mu\nu} p^2\, \delta Z_2^\gamma,$$

$$= i\, g^{\mu\nu} \left[p^2\, \delta Z_2^{\gamma Z} - M_Z^2 \left(\delta Z_1^{\gamma Z} - \delta Z_2^{\gamma Z} \right) \right],$$

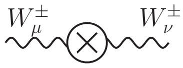

$$= (-i)\, g^{\mu\nu} \left[(p^2 - M_W^2)\, \delta Z_2^W - M_W^2\, \delta Z_{M_W} \right], \tag{2.108}$$

which allow to build renormalized gauge boson self energies (transverse parts only):

$$\begin{aligned}
\hat{\Pi}_{ZZ}^T(p^2) &= \Pi_{ZZ}^T(p^2) - (p^2 - M_Z^2)\, \delta Z_2^Z + M_Z^2\, \delta Z_{M_Z}, \\
\hat{\Pi}_{AA}^T(p^2) &= \Pi_{AA}^T(p^2) - p^2\, \delta Z_2^\gamma, \\
\hat{\Pi}_{ZA}^T(p^2) &= \Pi_{ZA}^T(p^2) + p^2\, \delta Z_2^{\gamma Z} - M_Z^2 \left(\delta Z_1^{\gamma Z} - \delta Z_2^{\gamma Z} \right), \\
\hat{\Pi}_{WW}^T(p^2) &= \Pi_{WW}^T(p^2) - (p^2 - M_W^2)\, \delta Z_2^W + M_W^2\, \delta Z_{M_W},
\end{aligned} \tag{2.109}$$

where the various renormalization constants are related by eqs. (2.95) and (2.96).

2.4.4 Ward identity

Before putting those Feynman rules to use, we pause for a moment to derive another important ingredient for the OS renormalization constants. We start by observing that in the unbroken phase the $U(1)_Y$ Ward identity implies a relation analogous to $Z_1 = Z_2$ in pure QED[18], which holds in the OS- and $\overline{\text{MS}}$-scheme. Translated to our notation, we have

$$Z_1^B = Z_2^B. \tag{2.110}$$

Using eq. (2.95) this relation can be rephrased as

$$\delta Z_1^Z - \delta Z_2^Z = \frac{c_W^2}{s_W^2} \left(\delta Z_1^\gamma - \delta Z_2^\gamma \right) \tag{2.111}$$

We will refer to this equation as "Ward identity", although strictly speaking it is only a Slavnov-Taylor identity that follows from the $U(1)_Y$ Ward identity. By using eq. (2.96) we also get

$$\delta Z_1^{\gamma Z} - \delta Z_2^{\gamma Z} = \frac{c_W}{s_W} \left(\delta Z_1^\gamma - \delta Z_2^\gamma \right) = \frac{s_W}{c_W} \left(\delta Z_1^Z - \delta Z_2^Z \right). \tag{2.112}$$

2.4.5 On-shell renormalization conditions in the BHS-scheme

The preparatory tasks have been completed, so it is time to write down the renormalization conditions. As before, we use the pole-mass scheme for the massive gauge bosons $W_\mu^\pm$ and Z_μ (cf. eqs. (2.52) and (2.65)),

$$\hat{\Pi}_{WW}^T(M_W^2) = 0, \qquad \hat{\Pi}_{ZZ}^T(M_Z^2) = 0. \tag{2.113}$$

This has the important consequence that the renormalization of c_W is exactly the same as before, eq. (2.87).

Again the photon mass does not receive radiative corrections, so we do not need to impose a renormalization condition on its pole location. However, in order to produce renormalized quantities as closely related to pure QED as possible (cf. [4]) we fix its residue to be exactly 1 by the familiar condition[19]

$$\left. \frac{d\hat{\Pi}_{AA}^T(p^2)}{dp^2} \right|_{p^2=0} = 0. \tag{2.114}$$

[18]Note: the notation in pure QED is a bit different than here: Z_2 and Z_3 are the fermionic and photonic renormalization constants, while $Z_1 = Z_e Z_2 Z_3^{1/2}$ is the photon-fermion vertex renormalization constant.

[19]This choice facilitates the treatment of real photonic emission diagrams, which are mandatory to cancel IR-divergences. The LSZ-wavefunction-factor is $R_A = 1$ in this case.

If furthermore the ZA-mixing is renormalized to 0 on the photon mass shell, i.e.

$$\hat{\Pi}^T_{ZA}(0) = 0, \tag{2.115}$$

then the $U(1)_Y$ Ward identity of the last section ensures that the electric charge is properly OS-renormalized as in pure QED, that is the OS-condition eq. (2.68) is fulfilled. In contrast to the Denner-scheme, we now do not impose any constraints onto $\hat{\Pi}^T_{ZA}$ on the Z-boson mass shell, $p^2 = M_Z^2$.

In summary we get 4 OS-conditions that can be used to fix 4 renormalization constants in the gauge boson sector. The rest is constrained by the gauge symmetry. Starting with the second and third rows of eq. (2.109) and imposing eqs. (2.114) and (2.115) we get

$$\begin{aligned} \delta Z_2^\gamma &= \left.\frac{d\Pi^T_{AA}(p^2)}{dp^2}\right|_{p^2=0}, \\ \delta Z_1^{\gamma Z} - \delta Z_2^{\gamma Z} &= \frac{\Pi^T_{ZA}(0)}{M_Z^2}. \end{aligned} \tag{2.116}$$

The combination $\delta Z_1^{\gamma Z} - \delta Z_2^{\gamma Z}$ can be used to express δZ_1^γ by virtue of the relation eq. (2.96). The other constants $\delta Z_1^Z, \delta Z_2^Z$ and δZ_2^W are already fixed. They can be expressed by using eqs. (2.95), (2.96) and, importantly, (2.97). They read

$$\begin{aligned} \delta Z_1^Z &= \delta Z_2^\gamma + \frac{3c_W^2 - 2s_W^2}{c_W s_W}\left(\delta Z_1^{\gamma Z} - \delta Z_2^{\gamma Z}\right) - 2\,\frac{c_W^2 - s_W^2}{s_W^2}\,\delta Z_c, \\ \delta Z_2^Z &= \delta Z_2^\gamma + 2\,\frac{c_W^2 - s_W^2}{c_W s_W}\left(\delta Z_1^{\gamma Z} - \delta Z_2^{\gamma Z} - \frac{c_W}{s_W}\,\delta Z_c\right), \\ \delta Z_2^W &= \delta Z_2^\gamma + 2\,\frac{c_W}{s_W}\left(\delta Z_1^{\gamma Z} - \delta Z_2^{\gamma Z}\right) - 2\,\frac{c_W^2}{s_W^2}\,\delta Z_c. \end{aligned} \tag{2.117}$$

2.4.6 Collection of BHS-renormalization constants

Below we give all the counterterms in the BHS-scheme in terms of unrenormalized bosonic self energies:

$$\begin{aligned} \delta Z_{M_Z} &= -\frac{\Pi^T_{ZZ}(M_Z^2)}{M_Z^2}, \\ \delta Z_{M_W} &= -\frac{\Pi^T_{WW}(M_W^2)}{M_W^2}, \\ \delta Z_1^\gamma &= \left.\frac{d\Pi^T_{AA}(p^2)}{dp^2}\right|_{p^2=0} + \frac{s_W}{c_W}\,\frac{\Pi^T_{ZA}(0)}{M_Z^2}, \\ \delta Z_2^\gamma &= \left.\frac{d\Pi^T_{AA}(p^2)}{dp^2}\right|_{p^2=0}, \\ \delta Z_1^Z &= \left.\frac{d\Pi^T_{AA}(p^2)}{dp^2}\right|_{p^2=0} + \frac{3c_W^2 - 2s_W^2}{c_W s_W}\,\frac{\Pi^T_{ZA}(0)}{M_Z^2} + \frac{c_W^2 - s_W^2}{s_W^2}\left(\frac{\Pi^T_{WW}(M_W^2)}{M_W^2} - \frac{\Pi^T_{ZZ}(M_Z^2)}{M_Z^2}\right), \\ \delta Z_2^Z &= \left.\frac{d\Pi^T_{AA}(p^2)}{dp^2}\right|_{p^2=0} + \frac{c_W^2 - s_W^2}{c_W s_W}\left(2\,\frac{\Pi^T_{ZA}(0)}{M_Z^2} + \frac{c_W}{s_W}\left[\frac{\Pi^T_{WW}(M_W^2)}{M_W^2} - \frac{\Pi^T_{ZZ}(M_Z^2)}{M_Z^2}\right]\right), \\ \delta Z_2^W &= \left.\frac{d\Pi^T_{AA}(p^2)}{dp^2}\right|_{p^2=0} + 2\,\frac{c_W}{s_W}\,\frac{\Pi^T_{ZA}(0)}{M_Z^2} + \frac{c_W^2}{s_W^2}\left(\frac{\Pi^T_{WW}(M_W^2)}{M_W^2} - \frac{\Pi^T_{ZZ}(M_Z^2)}{M_Z^2}\right). \end{aligned} \tag{2.118}$$

It is now obvious that only the four renormalization constants $\delta Z_{M_Z}, \delta Z_{M_W}, \delta Z_1^{\gamma}, \delta Z_2^{\gamma}$ are independent, and it is interesting to compare the two schemes when amputated vertex corrections or propagators are renormalized (see sec. 3.5).

2.5 Explicit expressions for renormalization constants in the BHS-scheme

In this section we give explicit expressions for the renormalization constants in the BHS-scheme. They are mainly derived from bosonic XY-transitions, and the complete diagram sets for the weak contributions are shown in the appendix G.2. To facilitate checks for UV-finitness in later chapters, we split off the $\frac{1}{\epsilon}$-parts of the PV-functions (defined in app. B), and denote the UV-finite functions with a hat on top. For example

$$B_0(p^2; m_0, m_1) = \frac{1}{\epsilon} + \hat{B}_0(p^2; m_0, m_1) \tag{2.119}$$

and so forth. We emphasize once more that for the construction of renormalization constants the real parts of the PV-functions need to be taken. We assume this implicitly in the expressions given below.

2.5.1 Fermionic renormalization constants

For the renormalization of our process, only the field-strength renormalization constants of the top quark and the electron are necessary. Top mass renormalization constants are not needed in this work. Besides the subscripts t, e indicating the external particle, we will also add superscripts. For reasons concerning gauge independence (discussed in more detail in sec. 4.3) it is advantageous to *cluster* (i.e. add) diagrams with the same type of particle content, i.e. the same gauge parameter dependence. The fermionic field strengths can be unambiguously grouped into Z $(= Z, \chi)$, W $(= W, \phi)$ and H-cluster, denoted by the corresponding superscript. For the electron there are no scalar diagrams and consequently no H-cluster. Using

$$y_t \equiv \frac{m_t}{2 s_W M_W}, \tag{2.120}$$

we find

$$\begin{aligned} \delta Z^H_{t,\eta} = -\frac{\alpha}{4\pi}\frac{y_t^2}{2}\bigg\{ & \frac{1}{\epsilon} - \frac{1}{m_t^2}\hat{A}_0(M_H) + \frac{1}{m_t^2}\hat{A}_0(m_t) + \frac{M_H^2}{m_t^2}\hat{B}_0\left(m_t^2; M_H, m_t\right) + \\ & - \left(8m_t^2 - 2M_H^2\right)\Big[B_0^{\langle 1,2\rangle}\left(m_t^2; M_H, m_t\right) + B_1^{\langle 1,2\rangle}\left(m_t^2; M_H, m_t\right)\Big]\bigg\}, \end{aligned} \tag{2.121}$$

$$\begin{aligned} \delta Z^Z_{t,\eta} = \frac{\alpha}{4\pi}\bigg\{ & -\left(\xi_Z (v_t - \eta\, a_t)^2 + \frac{y_t^2}{2}\right)\frac{1}{\epsilon} + (v_t - \eta\, a_t)^2 - \left((v_t + \eta\, a_t)^2 + \frac{y_t^2}{2}\right)\frac{1}{m_t^2}\hat{A}_0(m_t) + \\ & + \left((v_t + \eta\, a_t)^2 + (v_t^2 + a_t^2)\frac{m_t^2}{M_Z^2}\right)\frac{1}{m_t^2}\hat{A}_0(M_Z) + \\ & + \left(\frac{y_t^2}{2} - (v_t^2 + a_t^2)\frac{m_t^2}{M_Z^2}\right)\frac{1}{m_t^2}\hat{A}_0\left(M_Z\sqrt{\xi_Z}\right) + \\ & - \left((v_t + \eta\, a_t)^2\frac{M_Z^2}{m_t^2} - 2\eta\, v_t a_t\right)\hat{B}_0\left(m_t^2; M_Z, m_t\right) + \\ & + 2\left(\eta\, v_t a_t - a_t^2\right)\xi_Z\,\hat{B}_0\left(m_t^2; M_Z\sqrt{\xi_Z}, m_t\right) + \\ & - 2\Big(v_t^2\left(2m_t^2 + M_Z^2\right) - a_t^2\left(4m_t^2 - M_Z^2\right)\Big)\Big[B_0^{\langle 1,2\rangle}\left(m_t^2; M_Z, m_t\right) + B_1^{\langle 1,2\rangle}\left(m_t^2; M_Z, m_t\right)\Big]\bigg\}, \end{aligned} \tag{2.122}$$

$$\delta Z^W_{t,\eta} = \frac{\alpha}{4\pi}\frac{\delta_{\eta,-1}}{2s_W^2}\Bigg\{ -\frac{\xi_W}{\epsilon} + 1 + \frac{1}{2M_W^2}\,\hat{A}_0(M_W) - \left(\frac{m_t^2}{M_W^2} + \frac{1}{2}\right)\hat{B}_0\left(m_t^2; M_W, 0\right) +$$
$$+ \left(\frac{m_t^2}{M_W^2} - \xi_W\right)\hat{B}_0\left(m_t^2; M_W\sqrt{\xi_W}, 0\right) +$$
$$+ \frac{m_t^4 + m_t^2 M_W^2 - 2M_W^4}{2M_W^2}\left[\hat{B}_0^{\langle 1,2\rangle}\left(m_t^2; M_W, 0\right) + B_1^{\langle 1,2\rangle}\left(m_t^2; M_W, 0\right)\right]\Bigg\} +$$
$$+ \frac{\alpha}{4\pi}\frac{\delta_{\eta,1}}{2s_W^2}\Bigg\{ -\frac{m_t^2}{2M_W^2\epsilon} + \frac{1}{m_t^2}\,\hat{A}_0(M_W) - \frac{m_t^4 + 2M_W^4}{2m_t^2 M_W^2}\,\hat{B}_0\left(m_t^2; M_W, 0\right) +$$
$$+ \frac{m_t^4 + m_t^2 M_W^2 - 2M_W^4}{2M_W^2}\left[B_0^{\langle 1,2\rangle}\left(m_t^2; M_W, 0\right) + B_1^{\langle 1,2\rangle}\left(m_t^2; M_W, 0\right)\right]\Bigg\}, \qquad (2.123)$$

$$\delta Z^Z_{e,\eta} = -\frac{\alpha}{4\pi}(v_e - \eta\, a_e)^2\left\{\xi_Z\left[\frac{1}{\epsilon} + \ln\left(\frac{\mu^2}{M_Z^2}\right) + 1 - \ln(\xi_Z)\right] - \frac{3}{2}\right\}, \qquad (2.124)$$

$$\delta Z^W_{e,\eta} = -\frac{\alpha}{4\pi}\frac{\delta_{\eta,-1}}{2s_W^2}\left\{\xi_W\left[\frac{1}{\epsilon} + \ln\left(\frac{\mu^2}{M_W^2}\right) + 1 - \ln(\xi_W)\right] - \frac{3}{2}\right\}, \qquad (2.125)$$

We point out that the quantities $B_0^{\langle 1,2\rangle}\left(m_t^2; M_W, 0\right)$ and $B_1^{\langle 1,2\rangle}\left(m_t^2; M_W, 0\right)$, despite being UV-finite, have $\frac{1}{\epsilon}$-poles corresponding to fake IR-divergences. In the sum $B_0^{\langle 1,2\rangle}\left(m_t^2; M_W, 0\right) + B_1^{\langle 1,2\rangle}\left(m_t^2; M_W, 0\right)$ these poles indeed cancel (cf. app. B), so we do not need to write them with hats on top.

2.5.2 Bosonic renormalization constants

Next up are the bosonic renormalization constants: mass shifts, residues, charge and Weinberg-angle renormalization. Since the (left-handed) fermions form doublets, which influences the renormalization procedure (sometimes UV-divergences etc. only cancel if a full doublet is taken into account), we quote the results in terms of contributions per doublet. We will consider *light doublets* D_{lf} where both isospin constituents are light (and treated as massless in this work), and the top-bottom doublet, where only the top is treated with a non-zero mass. Let $n_l = 3$ denote the number of light charged leptons (to be used again for the QED running, sec. 3.4.2) and $n_q = 5$ the number of light quarks. We then get $n_l + \frac{n_q-1}{2}$ light doublets plus the top-bottom doublet and split every renormalization constant δZ_i into bosonic, light doublet (D_{lf}) and top-bottom doublet (D_{tb}) contributions:

$$\delta Z_i = \left(\delta Z_i\right)_{\mathrm{bos}} + \left(\delta Z_i\right)_{D_{\mathrm{lf}}} + \left(\delta Z_i\right)_{D_{tb}}. \qquad (2.126)$$

The light-fermion diagrams result in technical difficulties for the renormalization constant δZ_{AA} and δZ_2^γ, as there the light-fermion loops of the AA-transition need to be evaluated at $p^2 = 0$. We postpone their treatment to sec. 3.4.2, where we include them in a fashion convenient for our purposes.

We start with the boson mass renormalization constants. They are the same in both Denner- and BHS-scheme. From these it is straightforward to construct δZ_c and δZ_s from eqs. (2.87), (2.89). Note that some fermionic contributions, although organised in doublets, can be written as a sum of 2 independent isospin parts. We present those in a suggestive form to enable a quick reading-off of the single isospin parts.

$$\left(\delta Z_{M_Z}\right)_{\mathrm{bos}} = \frac{\alpha}{4\pi}\Bigg\{\frac{1}{2s_W^2\epsilon}\left(\frac{-84c_W^4 + 14c_W^2 + 11}{6c_W^2} - \frac{3\left(2c_W^4 + 1\right)M_W^2}{c_W^4 M_H^2} - \frac{3M_H^2}{2M_W^2}\right) +$$
$$+ \frac{1}{s_W^2}\left(\frac{\left(2c_W^4 + 1\right)M_W^2}{c_W^4 M_H^2} - \frac{72c_W^6 - 24c_W^4 + 10c_W^2 + 1}{18c_W^2} - \frac{M_H^2}{6M_W^2}\right) +$$

$$
\begin{aligned}
&- \frac{1}{2s_W^2 M_W^2}\left(\frac{c_W^2 M_H^2}{6M_W^2}+1\right)\hat{A}_0(M_H)+\\
&- \frac{1}{s_W^2 M_W^2}\left(\frac{-24c_W^4+8c_W^2+1}{6}+\frac{3M_W^2}{M_H^2}\right)\hat{A}_0(M_W)+\\
&+ \frac{1}{2s_W^2 M_W^2}\left(\frac{c_W^2 M_H^2}{6M_W^2}-\frac{3M_W^2}{c_W^2 M_H^2}-\frac{1}{3}\right)\hat{A}_0\left(M_Z\right)+\\
&+ \frac{-48c_W^6-68c_W^4+16c_W^2+1}{12c_W^2 s_W^2}\hat{B}_0\left(M_Z^2;M_W,M_W\right)+\\
&+ \frac{1}{s_W^2}\left(\frac{c_W^2 M_H^4}{12M_W^4}+\frac{1}{c_W^2}-\frac{M_H^2}{3M_W^2}\right)\hat{B}_0\left(M_Z^2;M_Z,M_H\right)\Bigg\},
\end{aligned}
\tag{2.127}
$$

$$
\left(\delta Z_{M_Z}\right)_{D_{\rm lf}} = \frac{\alpha}{4\pi}\frac{4}{3}N_{c,D_{\rm lf}}\sum_{f\in D_{\rm lf}}\left(v_f^2+a_f^2\right)\left(\frac{1}{\epsilon}+\hat{B}_0\left(M_Z^2;0,0\right)-\frac{1}{3}\right),
\tag{2.128}
$$

$$
\begin{aligned}
\left(\delta Z_{M_Z}\right)_{D_{tb}} = \frac{\alpha}{4\pi}N_c\Bigg\{&\left(\frac{4}{3}\left(v_t^2+a_t^2\right)-a_t^2\frac{8m_t^2}{M_Z^2}\right)\frac{1}{\epsilon}+\\
&- \frac{4\left(v_t^2+a_t^2\right)\left(M_Z^2-6m_t^2\right)}{9M_Z^2}-\frac{8\left(v_t^2+a_t^2\right)}{3M_Z^2}\hat{A}_0(m_t)+\\
&+ \frac{4\left(v_t^2+a_t^2\right)M_Z^2+8(v_t^2-2a_t^2)m_t^2}{3M_Z^2}\hat{B}_0\left(M_Z^2;m_t,m_t\right)+\\
&+ \frac{4}{3}\left(v_b^2+a_b^2\right)\left(\frac{1}{\epsilon}+\hat{B}_0\left(M_Z^2;0,0\right)-\frac{1}{3}\right)+\\
&+ \frac{2m_t^4}{s_W^2 M_H^2 M_W^2}\left(\frac{1}{\epsilon}+\frac{1}{m_t^2}\hat{A}_0(m_t)\right)\Bigg\},
\end{aligned}
\tag{2.129}
$$

$$
\begin{aligned}
\left(\delta Z_{M_W}\right)_{\rm bos} = \frac{\alpha}{4\pi}\Bigg\{&\frac{1}{2s_W^2\epsilon}\left(\frac{9-68c_W^2}{6c_W^2}-\frac{3\left(2c_W^4+1\right)M_W^2}{c_W^4 M_H^2}-\frac{3M_H^2}{2M_W^2}\right)+\\
&+ \frac{1}{s_W^2}\left(\frac{\left(2c_W^4+1\right)M_W^2}{c_W^4 M_H^2}-\frac{56c_W^2+3}{18c_W^2}-\frac{M_H^2}{6M_W^2}\right)+\\
&- \frac{1}{2M_W^2 s_W^2}\left(\frac{M_H^2}{6M_W^2}+1\right)\hat{A}_0(M_H)+\\
&+ \frac{1}{s_W^2 M_W^2}\left(\frac{12c_W^2+1}{12c_W^2}+\frac{M_H^2}{12M_W^2}-\frac{3M_W^2}{M_H^2}\right)\hat{A}_0(M_W)+\\
&- \frac{1}{2c_W^2 s_W^2 M_W^2}\left(\frac{3M_W^2}{M_H^2}+\frac{-24c_W^4+8c_W^2+1}{6}\right)\hat{A}_0\left(M_Z\right)-4\hat{B}_0\left(M_W^2;M_W,0\right)+\\
&+ \frac{1}{s_W^2}\left(\frac{M_H^4}{12M_W^4}-\frac{M_H^2}{3M_W^2}+1\right)\hat{B}_0\left(M_W^2;M_W,M_H\right)+\\
&+ \frac{-48c_W^6-68c_W^4+16c_W^2+1}{12c_W^4 s_W^2}\hat{B}_0\left(M_W^2;M_W,M_Z\right)\Bigg\},
\end{aligned}
\tag{2.130}
$$

$$\left(\delta Z_{M_W}\right)_{D_{\rm lf}} = \frac{\alpha}{4\pi}\frac{1}{3s_W^2}\,N_{c,D_{\rm lf}}\left(\frac{1}{\epsilon}+\hat{B}_0\left(M_W^2;0,0\right)-\frac{1}{3}\right), \tag{2.131}$$

$$\begin{aligned}\left(\delta Z_{M_W}\right)_{D_{tb}} = \frac{\alpha}{4\pi}\frac{1}{3s_W^2}\,N_c\Bigg\{&\frac{2M_W^2-3m_t^2}{2M_W^2\epsilon}-\frac{M_W^2-3m_t^2}{3M_W^2}+\frac{m_t^2-2M_W^2}{2M_W^4}\,\hat{A}_0(m_t)+\\ &-\frac{m_t^4+m_t^2M_W^2-2M_W^4}{2M_W^4}\,\hat{B}_0\left(M_W^2;m_t,0\right)+\\ &+\frac{6m_t^4}{M_H^2M_W^2}\left(\frac{1}{\epsilon}+\frac{1}{m_t^2}\,\hat{A}_0(m_t)\right)\Bigg\},\end{aligned} \tag{2.132}$$

where $N_{c,D}$ is the colour factor of doublet D, with the general colour factor of fermion f being defined as

$$N_{c,f} \equiv \begin{cases} 1 & \text{if } f \text{ is a lepton,} \\ N_c = 3 & \text{if } f \text{ is a quark.}\end{cases} \tag{2.133}$$

It is once again emphasized that we also included the Higgs-tadpoles to the self-energies (see sec. 3.3.2). This procedure renders both $\left(\delta Z_{M_Z}\right)_{\rm bos}$ and $\left(\delta Z_{M_W}\right)_{\rm bos}$ gauge-independent. For the fermionic corrections only the top tapdole is non-vanishing (the other fermions are treated as massless), and we group this tadole with the top doublet. In these fermionic expressions we have arranged the results such that the Higgs-tapdole contribution can be read off easily (last line respectively).

For the field-strenghts we give δZ_1^γ and δZ_2^γ. The rest can be obtained straightforwardly by applying eqs. (2.112), (2.117). The bosonic contributions read

$$\begin{aligned}\left(\delta Z_1^\gamma\right)_{\rm bos} = \frac{\alpha}{4\pi}\Bigg\{&\frac{5-3\xi_W}{2\epsilon}-\frac{16}{3}+\xi_W+\\ &+\frac{1}{2M_W^2(\xi_W-1)}\left[(13\xi_W-5)\hat{A}_0(M_W)-(3\xi_W+5)\hat{A}_0\left(M_W\sqrt{\xi_W}\right)\right]+\\ &+\frac{(\xi_W-1)^2}{2}\,M_W^2\left[B_0^{\langle 1,2\rangle}(0;M_W\sqrt{\xi_W},M_W)+B_1^{\langle 1,2\rangle}(0;M_W\sqrt{\xi_W},M_W)\right]\Bigg\},\end{aligned} \tag{2.134}$$

$$\begin{aligned}\left(\delta Z_2^\gamma\right)_{\rm bos} = \frac{\alpha}{4\pi}\Bigg\{&\frac{4-\xi_W}{\epsilon}+\frac{2\xi_W-17}{3}+\\ &+\frac{1}{3M_W^2(\xi_W-1)}\left[4(5\xi_W-3)\hat{A}_0(M_W)-(3\xi_W+5)\hat{A}_0\left(M_W\sqrt{\xi_W}\right)\right]+\\ &+\frac{(\xi_W-1)^2}{3}\,M_W^2\left[B_0^{\langle 1,2\rangle}(0;M_W\sqrt{\xi_W},M_W)+B_1^{\langle 1,2\rangle}(0;M_W\sqrt{\xi_W},M_W)\right]\Bigg\},\end{aligned} \tag{2.135}$$

The fermionic corrections are again split into light (lf) and massive (top) contributions. Since $\Pi_{ZA}^T(0)$ does not get any corrections from fermion loops, we have $\delta Z_1^\gamma = \delta Z_2^\gamma$ for the fermionic contributions. The light fermion loops are somewhat problematic for δZ_1^γ and δZ_2^γ, as the on-shell limit $p^2 \to 0$ for massless loops is not defined (see secs. B and E in the appendix). As will be outlined in sec. 3.4.2, either the on-shell counterterms with small but non-zero fermion masses or the $\overline{\rm MS}$-scheme with subsequent running of α can be used. Below we give just the former version, the $\overline{\rm MS}$-counterterm can be read off easily. Some more details on fermion loops can be found in sec. 3.4.2 and in the appendix F.

$$\left(\delta Z_1^\gamma\right)_{D_{\rm lf}} = \left(\delta Z_2^\gamma\right)_{D_{\rm lf}} = -\frac{\alpha}{4\pi}\frac{4}{3}\,N_{c,D_{\rm lf}}\sum_{f\in D_{\rm lf}} Q_f^2\left(\frac{1}{\epsilon}+\ln\left(\frac{\mu^2}{m_f^2}\right)+\frac{5}{3}\right), \tag{2.136}$$

$$\left(\delta Z_1^\gamma\right)_{D_{tb}} = \left(\delta Z_2^\gamma\right)_{D_{tb}} = -\frac{\alpha}{4\pi}\frac{4}{3}\,N_c\sum_{f\in\{t,b\}} Q_f^2\left(\frac{1}{\epsilon}+\ln\left(\frac{\mu^2}{m_f^2}\right)+\frac{5}{3}\right), \tag{2.137}$$

Chapter 3

Weak radiative corrections to $e^+e^- \to t\bar{t}$

Having discussed the necessary prerequisites, it is now time to focus on a specific EW-process: $e^+e^- \to t\bar{t}$. The amplitude $\mathcal{M}$ can be written perturbatively as

$$\mathcal{M}(e^+e^- \to t\bar{t}) = \sum_{i=0}^{\infty} \mathcal{M}^{(i)} = \underbrace{\mathcal{M}^{(0)}}_{\mathcal{O}(\alpha)} + \underbrace{\mathcal{M}^{(1)}}_{\mathcal{O}(\alpha^2)} + \mathcal{O}(\alpha^3), \tag{3.1}$$

and one of the goals of this thesis is to compute the EW corrections at $\mathcal{O}(\alpha^2)$[1] (i.e. $\mathcal{M}^{(1)}$). As pointed out earlier, the one-loop computation in EW theory is significantly more involved than computing QCD-corrections to this process, where one is able to focus on the coloured final-state top quarks. However, the EW radiative corrections to the amplitude at 1-loop can be split into smaller bits of calculation, as shown schematically below in eq. (3.20).

Before delving deeper, we point out again that the calculation of (heavy) fermion-pair production from e^+e^--annihilation at EW NLO in the continuum has been worked out by various authors (for example [4], [5], [6], [7]) at different stages of complexity (massless fermions $\to$ massive fermions, Feynman gauge $\to$ R_ξ-gauge, ...), which have also given rise to various numerical codes. Parts of this work (especially the next two chapters) aim at reviewing this calculation in a general setup (massive fermions, R_ξ-gauge), while keeping notation/conventions close to the respective sources (as referenced in the text) to facilitate comparisons etc.

The structure of this chapter is as follows: in the first section 3.1 we quickly go over the calculation of the tree-level amplitude and Born-cross-section, a necessary prerequisite for the numerics later on. This will also give us the opportunity to introduce some basic notation and conventions used throughout the rest of this work, like the amplitude basis etc. Sec. 3.3 will be dedicated to the Higgs tadpoles and the way they do (or do not) contribute. Sec. 3.4 will focus on the oblique corrections and the determination of width and higher-order effects. The initial-state and final-state vertex corrections are discussed in sec. 3.5, before we turn to the computation of the box diagrams in sec. 3.6. Results for the various diagrams will be given in the respective section, with explicit expressions for generic diagrams listed in appendix E.

3.1 Tree-level amplitude and Born-level cross-section

In EW theory at tree-level there are two s-channel diagrams with photon and Z-exchange[2] contributing to $\mathcal{M}^{(0)}$ (fig. 3.1, for momentum flow notation see fig. 3.5).
Note that in this work we treat the initial-state leptons as massless, which is why there is no diagram with a Higgs-boson H in the s-channel. Its coupling to the electrons is proportional to $m_e = 0$.

[1] The order in the perturbative expansion given in this thesis is to be interpreted at the level of the S-matrix element. $\mathcal{O}(\alpha^2)$ for the amplitude means including corrections of $\mathcal{O}(\alpha^3)$ at the level of cross-sections.

[2] Since we have $s > 4m_t^2 > M_Z^2$.

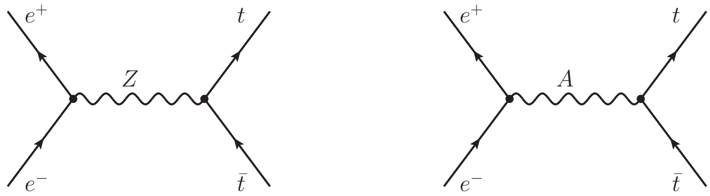

Figure 3.1: Tree level diagrams of the process $e^+e^- \to t\bar{t}$.

For the tree-level matrix element we get

$$i\mathcal{M}^{(0)}(e^+e^- \to t\bar{t}) = i\,\frac{4\pi\alpha}{s}\Big\{\Big(Q_tQ_e + v_tv_e\,\chi^{(0)}(s)\Big)\,\gamma^\mu\otimes\gamma_\mu + $$
$$+\,\chi(s)\left(a_ta_e\,\gamma^\mu\gamma_5\otimes\gamma_\mu\gamma_5 - a_tv_e\,\gamma^\mu\gamma_5\otimes\gamma_\mu - v_ta_e\,\gamma^\mu\otimes\gamma_\mu\gamma_5\right)\Big\}, \qquad (3.2)$$

where we introduced a handy shortcut for Dirac structures Γ_1, Γ_2 sandwiched between electron and top spinors (spin indices implicit)

$$\Gamma_1\otimes\Gamma_2 \equiv \bar{u}_t(q_1)\Gamma_1\,v_t(q_2)\,\bar{v}_e(l_2)\Gamma_2\,u_e(l_1). \qquad (3.3)$$

The symbol $\otimes$ is frequently used in HEP-calculations (and especially in EFT-language) to indicate convolution, but in this work it will be used in the above context exclusively. $\chi^{(0)}(s)$ is the lowest-order Z-propagator ratio, defined below in eq. (3.41). The Mandelstam invariants s, t, u are defined as

$$\begin{aligned} s &\equiv (l_1+l_2)^2 = (q_1+q_2)^2, \\ t &\equiv (l_1-q_1)^2 = (l_2-q_2)^2, \\ u &\equiv (l_1-q_2)^2 = (l_2-q_1)^2, \end{aligned} \qquad (3.4)$$

which satisfy

$$s+t+u = 2m_t^2. \qquad (3.5)$$

For the specific scattering kinematics under consideration the Mandelstam invariants t and u can be expressed as

$$\begin{aligned} t &= m_t^2 - \frac{s}{2}\left[1-\beta\cos(\theta)\right], \\ u &= m_t^2 - \frac{s}{2}\left[1+\beta\cos(\theta)\right], \end{aligned} \qquad (3.6)$$

where $\beta = \sqrt{1-4\,\frac{m_t^2}{s}}$ is the quark velocity and θ is the scattering angle between the incoming positron (l_2) and the outgoing top (q_1).

Before we square and spin-sum the tree-level matrix element, we make one more formal step. We introduce a basis of amplitudes labeled by final- and initial-state chirality ρ and κ (following the notation of ref. [5]). A brute-force computation allows the reduction[3] to the basis

$$\begin{aligned} M_1^{\rho\kappa} &\equiv \left[\bar{u}_t(q_1)\,\gamma^\mu\omega_\rho\,v_t(q_2)\right]\left[\bar{v}_e(l_2)\,\gamma_\mu\omega_\kappa\,u_e(l_1)\right] = \gamma^\mu\omega_\rho\otimes\gamma_\mu\omega_\kappa \\ M_2^{\rho\kappa} &\equiv \left[\bar{u}_t(q_1)\,\not{l}_2\,\omega_\rho\,v_t(q_2)\right]\left[\bar{v}_e(l_2)\,\frac{(\not{q}_1-\not{q}_2)}{2}\,u_e(l_1)\right] = \not{l}_2\,\omega_\rho\otimes\frac{\not{p}}{2}\,\omega_\kappa \\ M_3^{\rho\kappa} &\equiv \left[\bar{u}_t(q_1)\,\omega_\rho\,v_t(q_2)\right]\left[\bar{v}_e(l_2)\,\frac{(\not{q}_1-\not{q}_2)}{2}\,u_e(l_1)\right] = \omega_\rho\otimes\frac{\not{p}}{2}\,\omega_\kappa \end{aligned}$$

[3]For all diagrams but the boxes, it is actually possible to directly reduce to the minimal basis in eq. (3.8).

$$M_4^{\rho\kappa} \equiv \left[\bar{u}_t(q_1)\,\gamma^\mu \not{l}_2\,\omega_\rho\, v_t(q_2)\right]\left[\bar{v}_e(l_2)\,\gamma_\mu\omega_\kappa\, u_e(l_1)\right] = \gamma^\mu \not{l}_2\,\omega_\rho \otimes \gamma_\mu\omega_\kappa, \tag{3.7}$$

where $p \equiv q_1 - q_2$ and the $\omega_\mp$ are chiral projectors defined in eq. (2.33). This basis, which we will call *Beenakker-basis* (cf. [5]), is overcomplete and not ideal for comparison between oblique, vertex and box corrections to check for gauge independence etc. The minimal basis best suited to this is given by (cf. [6])

$$\begin{aligned}
\bar{M}_1^{\rho\kappa} &\equiv \left[\bar{u}_t(q_1)\,\gamma^\mu\omega_\rho\, v_t(q_2)\right]\left[\bar{v}_e(l_2)\,\gamma_\mu\omega_\kappa\, u_e(l_1)\right] = \gamma^\mu\omega_\rho \otimes \gamma_\mu\omega_\kappa \\
\bar{M}_2^{\rho\kappa} &\equiv \left[\bar{u}_t(q_1)\,\omega_\rho\, v_t(q_2)\right]\left[\bar{v}_e(l_2)\,\frac{(\not{q}_1 - \not{q}_2)}{m_t}\,u_e(l_1)\right] = \omega_\rho \otimes \frac{\not{p}}{m_t}\,\omega_\kappa,
\end{aligned} \tag{3.8}$$

where the factors m_t are inserted for convenience. We indicate the amplitudes of the minimal basis with a bar on top. The larger amplitude basis can be rewritten in terms of the minimal one by using the replacements

$$\begin{aligned}
M_1^{\rho\kappa} &= \bar{M}_1^{\rho\kappa}, \\
M_2^{\rho\kappa} &= \frac{1}{2}\left(\left(t\,\delta^{\rho,\kappa} - u\,\delta^{-\rho,\kappa}\right)\bar{M}_1^{\rho,\kappa} + m_t^2\left(\delta^{\rho,\kappa} - \delta^{-\rho,\kappa}\right)\bar{M}_1^{-\rho\kappa} + m_t^2\left(\delta^{-\rho,\kappa}\bar{M}_2^{\rho\kappa} - \delta^{\rho,\kappa}\bar{M}_2^{-\rho\kappa}\right)\right), \\
M_3^{\rho\kappa} &= \frac{m_t}{2}\,\bar{M}_2^{\rho\kappa}, \\
M_4^{\rho\kappa} &= -m_t\,\delta^{-\rho,\kappa}\left(\bar{M}_1^{\rho\kappa} + \bar{M}_1^{-\rho\kappa} - \bar{M}_2^{\rho\kappa}\right).
\end{aligned} \tag{3.9}$$

The preference of chiral amplitudes over a VA-basis is a matter of taste, but this basis becomes more useful the more difficult the computations are. For example it facilitates writing expressions in a very compact form and will therefore be especially convenient for the calculation of the box diagrams (see sec. 3.6).

The matrix element (for arbitrary chiralities of the initial-state leptons) can be written in terms of these basis amplitudes in a very compact form,

$$\mathcal{M}_\kappa(e^+e^- \to t\bar{t}) = \sum_{i=1}^{4}\sum_{\rho=\pm} c_i^{\rho\kappa} M_i^{\rho\kappa} = \sum_{i=1}^{2}\sum_{\rho=\pm} \bar{c}_i^{\rho\kappa}\bar{M}_i^{\rho\kappa}, \tag{3.10}$$

where the $\bar{c}_i^{\rho\kappa}$ (and the $c_i^{\rho\kappa}$) can be expanded perturbatively

$$\bar{c}_i^{\rho\kappa} \equiv \frac{\alpha}{s}\sum_{k=0}^{\infty}\bar{c}_i^{(k),\rho\kappa} \tag{3.11}$$

The $\bar{c}_i^{(k),\rho\kappa}$ are then formally $\mathcal{O}(\alpha^k)$. The normalization chosen in eq. 3.11 is convenient as it keeps the $\bar{c}_i^{(1),\rho\kappa}$ dimensionless. For the massless initial-state lepton pair the chirality κ equals helicity, so we do not need a sum over κ[4], while the finite final-state quark mass induces a non-zero admixture of different chiralities for fixed helicity.

The tree level matrix element is entirely composed of $\bar{M}_1^{\rho\kappa} = M_1^{\rho\kappa}$,

$$\mathcal{M}_\kappa^{(0)}(e^+e^- \to t\bar{t}) = \frac{4\pi\alpha}{s}\sum_{\rho=\pm 1}\left(Q_tQ_e + \chi^{(0)}(s)\left[v_t - \rho\,a_t\right]\left[v_e - \kappa\,a_e\right]\right)\bar{M}_1^{\rho\kappa}, \tag{3.12}$$

[4] There would be no harm in doing so however, as the formalism takes care of this automatically. The matrix element in lepton chirality/helicity space is diagonal, which can be seen from the $\delta^{\kappa}_{\kappa'}$ when spins are summed over (see below).

i.e.

$$\frac{1}{4\pi}\,\bar{c}_i^{(0),\rho\kappa} = Q_t Q_e + \chi^{(0)}(s)\,[v_t - \rho a_t]\,[v_e - \kappa a_e]\,,$$
$$\frac{1}{4\pi}\,\bar{c}_i^{(0),\rho\kappa} = 0. \tag{3.13}$$

To obtain the cross section for (un-)polarized incoming and outgoing fermions, the matrix element is squared and spin-summed. Since we restrict ourselves up to one-loop corrections, it suffices to compute the interferences of the $\bar{M}_i^{\rho\kappa}$ only with $\left(\bar{M}_1^{\rho\kappa}\right)^*$, i.e.

$$\sum_{\sigma_e,\sigma_t} \bar{M}_i^{\rho\kappa}\left(\bar{M}_1^{\rho'\kappa'}\right)^*, \qquad\qquad (i \in 1,2,3,4). \tag{3.14}$$

Carrying out the traces we obtain[5]

$$\sum_{\sigma_e,\sigma_t} \bar{M}_1^{\rho\kappa}\left(\bar{M}_1^{\rho'\kappa'}\right)^* = 4\,\delta^{\kappa}_{\kappa'}\left\{\delta^{\rho}_{\rho'}\left[\delta^{\rho,\kappa}\left(u-m_t^2\right)^2 + \delta^{-\rho,\kappa}\left(t-m_t^2\right)^2\right] + \delta^{\rho}_{-\rho'}\,s\,m_t^2\right\},$$

$$\sum_{\sigma_e,\sigma_t} \bar{M}_2^{\rho\kappa}\left(\bar{M}_1^{\rho'\kappa'}\right)^* = -4\,\delta^{\kappa}_{\kappa'}\left(t\,u - m_t^4\right). \tag{3.15}$$

For the Beenakker-basis we obtain

$$\sum_{\sigma_e,\sigma_t} M_1^{\rho\kappa}\left(M_1^{\rho'\kappa'}\right)^* = 4\,\delta^{\kappa}_{\kappa'}\left\{\delta^{\rho}_{\rho'}\left[\delta^{\rho,\kappa}\left(u-m_t^2\right)^2 + \delta^{-\rho,\kappa}\left(t-m_t^2\right)^2\right] + \delta^{\rho}_{-\rho'}\,s\,m_t^2\right\},$$

$$\sum_{\sigma_e,\sigma_t} M_2^{\rho\kappa}\left(M_1^{\rho'\kappa'}\right)^* = 2\,\delta^{\kappa}_{\kappa'}\delta^{\rho}_{\rho'}\left(t\,u - m_t^4\right)\left\{\delta^{\rho,\kappa}\left(u-m_t^2\right) - \delta^{-\rho,\kappa}\left(t-m_t^2\right)\right\},$$

$$\sum_{\sigma_e,\sigma_t} M_3^{\rho\kappa}\left(M_1^{\rho'\kappa'}\right)^* = -2\,\delta^{\kappa}_{\kappa'}m_t\left(t\,u - m_t^4\right),$$

$$\sum_{\sigma_e,\sigma_t} M_4^{\rho\kappa}\left(M_1^{\rho'\kappa'}\right)^* = 4\,\delta^{\kappa}_{\kappa'}\delta^{-\rho,\kappa}s\,m_t\left\{\delta^{\rho}_{\rho'}\left(t-m_t^2\right) + \delta^{\rho}_{-\rho'}\left(u-m_t^2\right)\right\}. \tag{3.16}$$

By using eqs. (3.9) it is straightforward to show that eqs. (3.8) and (3.7) are consistent.

The initial-state chirality feature discussed above is manifest here as $\delta^{\kappa}_{\kappa'}$[6]. The Born matrix element eq. (3.12) can now be squared and spin summed. Replacing the Mandelstam invariant t by the scattering angle θ (eq. (3.6)) we obtain (cf. [5])

$$\left(\frac{d\sigma}{d\Omega}\right)^{(0)}_{\kappa} = \frac{1}{(4\pi)^2}\frac{N_c\beta}{4s}\sum_{\sigma_e,\sigma_t}\left|\mathcal{M}^{(0)}_{\kappa}\right|^2 = \frac{\alpha^2 N_c\beta}{4s}\Big\{2\big(T_1(s)-\kappa K_1(s)\big)\left[1+\cos^2(\theta)\right] +$$
$$+\,2\big(T_2(s)-\kappa K_2(s)\big)\left(1-\beta^2\right)\sin^2(\theta) +$$
$$+\,2\big(T_3(s)-\kappa K_3(s)\big)\,\beta\,\cos(\theta)\Big\}. \tag{3.17}$$

for the polarized differential cross section, where the helicity of the lepton pair is labeled by $\kappa = \pm$. The auxillary functions $A_i(s)$ are given by

$$T_1(s) = Q_t^2 Q_e^2 + 2\,Q_t Q_e v_t v_e\,\mathrm{Re}\left[\chi^{(0)}(s)\right] + \left(v_t^2 + \beta\,a_t^2\right)\left(v_e^2 + a_e^2\right)\left|\chi^{(0)}(s)\right|^2,$$

[5] No summation over repeated indices. Mixed type of indices for δ only for better readability.

[6] This ensures that the answer one gets when either computing the amplitude inclusively for lepton chiralities with subsequent squaring and spin-summing is the same as when the processes are computed for fixed initial-state chiralities and only then added incoherently. For the massive final-state however, the different chiralities do talk to each other, so they need to be included inclusively at the level of the amplitude to ensure that the spin-summation leads to the correct result.

$$T_2(s) = Q_t^2 Q_e^2 + 2\,Q_t Q_e v_t v_e \,\mathrm{Re}\left[\chi^{(0)}(s)\right] + v_t^2\left(v_e^2 + a_e^2\right)\left|\chi^{(0)}(s)\right|^2,$$

$$T_3(s) = 4\,Q_t Q_e a_t a_e \,\mathrm{Re}\left[\chi^{(0)}(s)\right] + 8\,v_t v_e a_t a_e\,\left|\chi^{(0)}(s)\right|^2,$$

$$K_1(s) = 2\,Q_t Q_e v_t a_e \,\mathrm{Re}\left[\chi^{(0)}(s)\right] + 2 v_e a_e\left(v_t^2 + \beta\, a_t^2\right)\left|\chi^{(0)}(s)\right|^2,$$

$$K_2(s) = 2\,Q_t Q_e v_t a_e \,\mathrm{Re}\left[\chi^{(0)}(s)\right] + 2 v_e a_e v_t^2\left|\chi^{(0)}(s)\right|^2,$$

$$K_3(s) = 4\,Q_t Q_e a_t v_e \,\mathrm{Re}\left[\chi^{(0)}(s)\right] + 4\,v_t a_t\left(v_e^2 + a_e^2\right)\,\left|\chi^{(0)}(s)\right|^2. \tag{3.18}$$

The unpolarized case is the average of $\kappa = \pm$, and the terms linear in κ in eq. (3.17) drop out to give

$$\left(\frac{d\sigma}{d\Omega}\right)^{(0)} \equiv \frac{1}{4}\left\{\left(\frac{d\sigma}{d\Omega}\right)^{(0)}_{-} + \left(\frac{d\sigma}{d\Omega}\right)^{(0)}_{+}\right\} =$$
$$= \frac{\alpha^2 N_c \beta}{4s}\Big\{T_1(s)\,\left[1+\cos^2(\theta)\right] + T_2(s)\,\left(1-\beta^2\right)\sin^2(\theta) + T_3(s)\,\beta\,\cos(\theta)\Big\}. \tag{3.19}$$

This completes the discussion of the amplitude basis and the tree-level contributions. In the next sections we give the contributions of the radiative corrections to the matrix element and (differential) cross sections.

3.2 Overview of radiative corrections

As outlined in the introduction to this chapter, the radiative corrections $\mathcal{M}^{(1)}$ to the S-matrix element $\mathcal{M}$ of the process $e^+e^- \to t\bar{t}$ consist of various types of corrections, schematically shown in eq. (3.20).

$$i\,\mathcal{M}^{(1)}(e^+e^- \to t\bar{t}) =$$

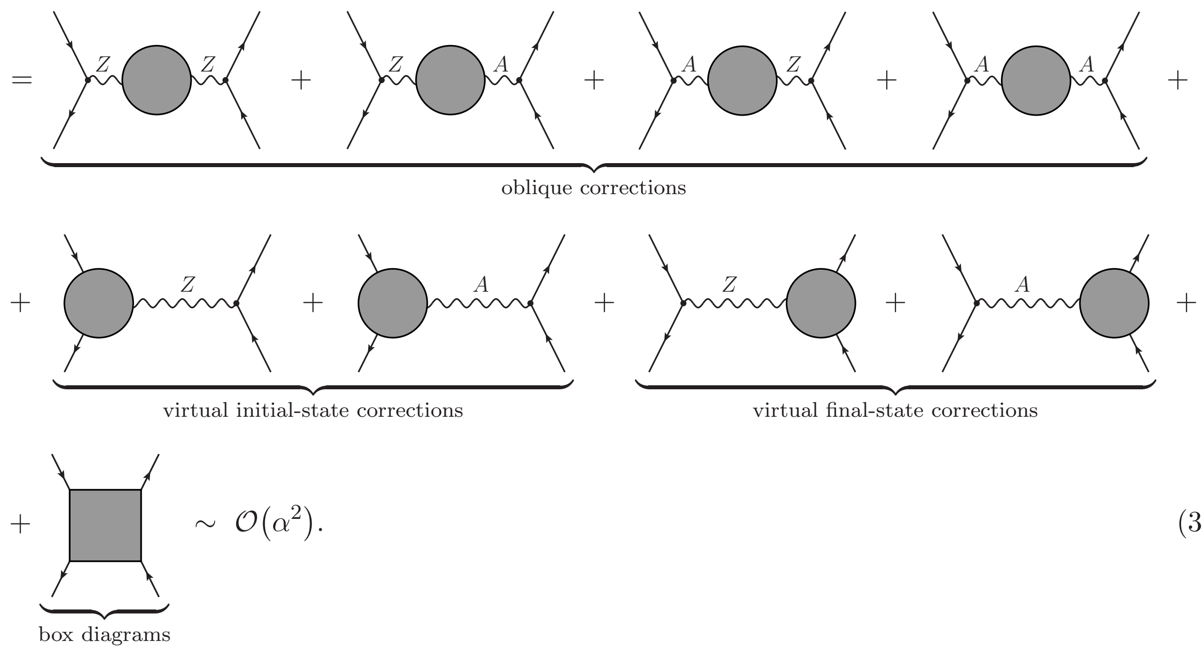

$$\sim\; \mathcal{O}\big(\alpha^2\big). \tag{3.20}$$

The tree-level s-channel exchange diagrams receive radiative corrections at the initial- and final-state gauge-fermion vertices and at the s-channel gauge boson propagators. If added up they comprise what we refer to as the *s-channel* or *reducible corrections*. In addition, there are also box diagrams, i.e. 1-PI contributions to $\mathcal{M}^{(1)}$. Focusing on the reducible contributions for the moment, we can write it as a matrix equation in the 2-dimensional space of the neutral gauge bosons $\{Z, A\}$ that mediate these type of radiative corrections to one-loop order as (summation over $X, Y \in \{Z, A\}$ implied)

$$
\begin{aligned}
i\mathcal{M}^{(0)+(1)}_{\text{reducible}} &= \left[\left(V^{(0)}_{t,X}\right)^{\alpha} + \left(V^{(1)}_{t,X}\right)^{\alpha}\right] \times \left[\left(D^{(0)}_{XY}\right)_{\alpha\beta} + \left(D^{(1)}_{XY}\right)_{\alpha\beta}\right] \times \left[\left(V^{(0)}_{e,Y}\right)^{\beta} + \left(V^{(1)}_{e,Y}\right)^{\beta}\right] + O(\alpha^3) = \\
&= \underbrace{\left(V^{(0)}_{t,Z}\right)^{\alpha} D^{(0)}_{ZZ} \left(V^{(0)}_{e,Z}\right)_{\alpha} + \left(V^{(0)}_{t,A}\right)^{\alpha} D^{(0)}_{AA} \left(V^{(0)}_{e,A}\right)_{\alpha}}_{\text{tree-level } \mathcal{O}(\alpha)} + \\
&+ \underbrace{\left(V^{(0)}_{t,Z}\right)^{\alpha} D^{(1)}_{ZZ} \left(V^{(0)}_{e,Z}\right)_{\alpha} + \left(V^{(0)}_{t,A}\right)^{\alpha} D^{(1)}_{AA} \left(V^{(0)}_{e,A}\right)_{\alpha} + \left(V^{(0)}_{t,Z}\right)^{\alpha} D^{(1)}_{ZA} \left(V^{(0)}_{e,A}\right)_{\alpha} + \left(V^{(0)}_{t,A}\right)^{\alpha} D^{(1)}_{AZ} \left(V^{(0)}_{e,Z}\right)_{\alpha}}_{\text{oblique corrections } \mathcal{O}(\alpha^2)} + \\
&+ \underbrace{\left(V^{(1)}_{t,Z}\right)^{\alpha} D^{(0)}_{ZZ} \left(V^{(0)}_{e,Z}\right)_{\alpha} + \left(V^{(1)}_{t,A}\right)^{\alpha} D^{(0)}_{AA} \left(V^{(0)}_{e,A}\right)_{\alpha}}_{\text{initial state corrections } \mathcal{O}(\alpha^2)} + \underbrace{\left(V^{(0)}_{t,Z}\right)^{\alpha} D^{(0)}_{ZZ} \left(V^{(1)}_{e,Z}\right)_{\alpha} + \left(V^{(0)}_{t,A}\right)_{\alpha} D^{(0)}_{AA} \left(V^{(1)}_{e,A}\right)_{\alpha}}_{\text{final state corrections } \mathcal{O}(\alpha^2)},
\end{aligned}
\tag{3.21}
$$

where we assumed $\left(D^{(i)}_{XY}\right)_{\alpha\beta} = g_{\alpha\beta} D^{(i)}_{XY}$ for reasons outlined in sec. 3.5. The superscripts indicate the loop order. The task is now to parametrize the 1-loop propagator function $D^{(1)}_{\alpha\beta}$ and both vertex functions $V^{(1)}$, as well as the box diagrams. In terms of Feynman diagrams we encounter the following types that are contributing to the radiative corrections (in ascending order of technical complexity):

- **(Higgs-)tadpoles**: the tadpoles can contribute at many stages, but because of their reducible nature they can be treated in a factorized manner. The technical task is to compute one-point functions of the scalar field H.
- **Oblique corrections**: corrections to the s-channel gauge-boson propagators, i.e. Z and photon. The technical task is to evaluate renormalized, off-shell gauge-boson self-energies.
- **Amputated vertex corrections**: corrections to the e^+e^-Z/e^+e^-A (initial-state) and $t\bar{t}Z/t\bar{t}A$ vertices. The technical task is to compute renormalized, off-shell 3-point functions to the respective vertices.
- **Boxes**: 1-PI contributions to the amplitude. The technical task is to compute 4-point functions.

IMPORTANT: In this work we only treat **weak radiative corrections**, i.e. we do not consider pure QED contributions (i.e. diagrams with photons in the loop[7]). This class of diagrams (QED-vertices and -boxes) is infrared divergent, and the proper treatment requires additional machinery both conceptually (inclusion of real-radiation contributions to cancel IR-divergences at the level of the cross-section) and from a technical point of view (a few of the formulae used in this work are only applicable in IR-finite cases). Fortunately, due to the residual unbroken $U(1)_Q$-symmetry of the theory these pure-QED contributions can be treated completely separated from the weak corrections this thesis is focusing on. However it should be kept in mind that in order to connect to experiment (i.e. to compute realistic distributions etc.), the QED corrections must be included at some point. At this point we refer the reader to future planned work or to the existing literature (for example [6], [7], [17]). The weak contributions are all IR-finite, as the divergences have been explicitly regulated by non-zero masses of the weak gauge-bosons. The Sudakov-logarithms we will extract in the later stages of this thesis can in fact be viewed as the infrared logarithms of the theory.

We will deal with each of above mentioned "building blocks" of the total calculation in the following sections. Once the amplitude coefficients $\bar{c}^{(1),\rho\kappa}$ for $\mathcal{M}^{(1)}_{\kappa}$ are computed, we can obtain the 1-loop

[7] There is one minor exception for the WW-self-energy (see diagrams in app. G.2), where we include the diagrams with virtual photons since they do not lead to IR-divergences.

contribution to the cross section with unpolarized tops analogous to the Born-section by summing over spins[8]

$$\left(\frac{d\sigma}{d\Omega}\right)^{(1)}_{\kappa} = \frac{1}{(4\pi)^2}\frac{N_c\beta}{4s}\sum_{\sigma_e,\sigma_t} 2\,\mathrm{Re}\left[\mathcal{M}^{(1)}_{\kappa}\big(\mathcal{M}^{(0)}_{\kappa}\big)^*\right] =$$
$$= \frac{\alpha^2}{(4\pi)^2}\frac{N_c\beta}{2s^3}\sum_{\sigma_e,\sigma_t}\sum_{\rho,\rho'}\mathrm{Re}\left[\left(\bar{c}_1^{(1),\rho\kappa}\bar{M}_1^{\rho\kappa} + \bar{c}_2^{(1),\rho\kappa}\bar{M}_2^{\rho\kappa}\right)\big(\bar{c}_1^{(0),\rho'\kappa}\big)^*\big(\bar{M}_1^{\rho'\kappa}\big)^*\right] =$$
$$= \frac{\alpha^2 N_c\beta}{8\pi s}\sum_{\rho}\Bigg\{Q_eQ_t\Bigg[\frac{1}{2}\mathrm{Re}\big[\bar{c}_1^{(1),\rho\kappa}\big]\Big(\beta^2\big(\cos(2\theta)-1\big)+4\big(\kappa\rho\beta\cos(\theta)+1\big)\Big)+$$
$$-2\,\mathrm{Re}\big[\bar{c}_2^{(1),\rho\kappa}\big]\beta^2\sin^2(\theta)\Bigg]+$$
$$+(v_e-\kappa a_e)\big[\chi^{(0)}(s)\big]^*\Bigg[\mathrm{Re}\big[\bar{c}_1^{(1),\rho\kappa}\big]\Big((v_t-\rho a_t)\big(\beta^2(1+\cos^2(\theta))+2\rho\kappa\beta\cos\theta\big)+$$
$$+2v_t(1-\beta^2)\Big)-2\mathrm{Re}\big[\bar{c}_2^{(1),\rho\kappa}\big]\beta^2 v_t\sin^2(\theta)\Bigg]\Bigg\}. \tag{3.22}$$

The unpolarized (differential) cross section can be obtained by simply averaging the expressions for $\kappa=\pm$ as in eq. (3.19). The expression (3.22) can be analyzed further according to the angular structure like in eq. (3.17), but since this is not the focus of this thesis (we focus on the structure of the one-loop amplitude $\mathcal{M}^{(1),\rho\kappa}$) we do not further simplify or reorder this expression. The form given above is sufficient for our purposes in terms of numerical discussions. In the following we will split the 1-loop-coefficients $c_i^{(1),\rho\kappa}$ according to the various contributions to $\mathcal{M}^{(1)}$

$$\bar{c}_i^{(1),\rho\kappa} \equiv \big(\bar{c}_i^{(1),\rho\kappa}\big)_{\text{oblique}} + \big(\bar{c}_i^{(1),\rho\kappa}\big)_{\text{vertex}} + \big(\bar{c}_i^{(1),\rho\kappa}\big)_{\text{box}}. \tag{3.23}$$

3.3 Higgs-tadpoles

3.3.1 Tadpoles in the SM

The simplest radiative building blocks to consider are tadpoles, i.e. loop contributions with only one loop propagator. In EW theory there exist 2 tadpole topologies sitting on some "external line", shown schematically in fig. 3.2. The first one, which we call the 4-tadpole, exists due to 4-couplings in the

Figure 3.2: Two types of tadpole topologies that can appear as correction to some propagator: 4-tadpole (left) and Higgs-mediated tadpole (right).

theory, and despite having all the mathematical properties your average tadpole contributions possesses, its the latter type of tadpole diagrams that really contributes in interesting ways. There are 3 main reasons for this:

- Despite not being 1-PI in the strict sense (as the mediator propagator connecting the loop with the external line can be cut), it is 1-PI with respect to the external line it couples to (cutting the

[8] We set $\kappa'=\kappa$ from the start because of the expected $\delta^{\kappa}_{\kappa'}$ as in the tree-level calculation.

mediator propagator gives a one-point (at 1-loop) and a 3-point function (at tree-level), but not two 2-point functions). This type of diagram shows up frequently in the calculation, as the particle in the propagator (in EW theory the field H) only needs a 3-coupling to the external fields, while the 4-tadpoles need 4-couplings.

- Consequently, this type of tadpole also couples to fermions, i.e. fermions may appear on the external line and in the loop, while neither is the case for 4-tadpoles. This is a very important fact, as fermionic loop contributions are trivially gauge-independent and might (as is the case for the top quark) be parametrically large ($y_t \sim 1$).

- In the SM the only mediator can be the Higgs boson H (see discussion below), which is why from now on these tadpoles are referred to as *Higgs-mediated-tadpoles*, or shortly *Higgs-tadpoles*. Because of their reducibility they are related (by a prefactor depending on the coupling of the Higgs to the external fields) to the Higgs-one-point function $\langle 0|H|0\rangle$, which in turn is related to the vev v, the most crucial parameter of GWS-theory.

Understanding the role of this type of tadpole (not just on a calculational, but a conceptual level) is therefore mandatory. Before going into further detail, lets first spend a second on figuring out which

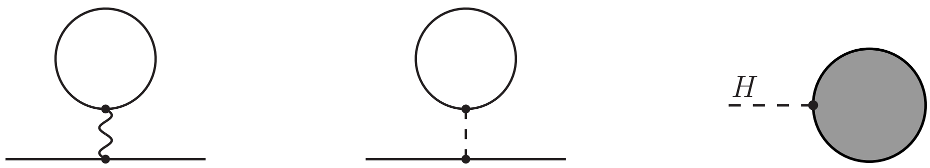

Figure 3.3: The tadpoles could (in principle) be mediated by vectors (left) or scalars (middle), but only Higgs-mediated tadpoles are non-zero, which allows focusing on the Higgs one-point function (right).

particles of the SM can mediate this tadpole type. Lets first start with a vector particle (massive or massless). In the massless case, we give it an infinitesimal mass λ to regulate the otherwise ill-defined mediator propagator (due to momentum conservation on the external vertex, the momentum flowing through this propagator is 0). Depending on the particle in the loop it can have 2 types of interactions: derivative coupling p^μ (to bosons) or $\gamma^\mu \omega_\rho$ (to fermions). Since the propagator of the mediator feeds in 0 momentum, the derivative coupling is necessarily proportional to the loop momentum k^μ. As the bosonic loop-propagators are all symmetric in $k \to -k$, the full loop expression now vanishes by the "even-times odd-argument"

$$\int d^d k \; k^\mu \times (\text{even in } k) = 0. \tag{3.24}$$

The argument for fermions in the loop is somewhat different, as there is no derivative coupling. The loop is a trace over the fermion propagator $\not{k} + m_f$ and $\gamma^\mu \omega_\rho$. The $\not{k}$-part vanishes again by the even-times-odd argument, while the mass part gives 0 because of $\mathrm{Tr}(\gamma^\mu \omega_\rho) = 0$. Afterwards the regulator can be removed $\lambda \to 0$.

For scalars things are not that clear, and a lot depends on the actual theory at hand. Cubic scalar couplings or couplings of scalars to 2 vectors are not proportional to the loop momentum, and the integrals consequently do not vanish. Also the fermionic traces for the mass part of the fermion propagator do only vanish for the γ_5-part of the coupling, i.e. pseudoscalars (like χ) give no contributions, while scalars (like H) do. Tadpoles mediated by scalars with massive fermions in the loop are non-vanishing. In addition charge conservation has to be respected, which forbids charged scalars in the mediator propagator. Tadpoles with bosons in the loop can both be mediated by scalar and pseudoscalars, and it then depends on the specific theory at hand what diagrams are non-vanishing. In GWS-theory there are only couplings of the form HXX, but none of the form χXX for any boson X (cf. app. G.1). We conclude that in the SM the only particle that can mediate non-zero tadpoles of this type is therefore the physical Higgs-boson H.

3.3.2 Higgs-mediated tadpoles in $e^+e^- \to t\bar{t}$

Before listing explicit results for the Higgs-tadpoles, we take a look where they appear in our calculation of $e^+e^- \to t\bar{t}$. As is obvious from fig. 3.2 they will contribute to the 2-point functions of all particles (vectors, scalars, massive fermions) the Higgs couples to. For our purposes they contribute to 3 transitions of interest, shown below. The momentum-independence allows to write the expression in a factorized form

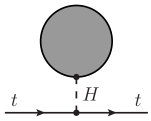

$$= -\frac{i\alpha}{4\pi}\frac{m_t}{2s_W M_W M_H^2}\mathcal{T} \equiv \mathcal{T}_{tt}\, g_{\mu\nu},$$

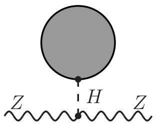

$$= \frac{i\alpha}{4\pi}\frac{M_W}{c_W^2 s_W M_H^2}\, g_{\mu\nu}\mathcal{T} \equiv \mathcal{T}_{ZZ}\, g_{\mu\nu},$$

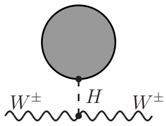

$$= \frac{i\alpha}{4\pi}\frac{M_W}{s_W M_H^2}\, g_{\mu\nu}\mathcal{T} \equiv \mathcal{T}_{WW}\, g_{\mu\nu},, \tag{3.25}$$

where $\mathcal{T}$ is the tadpole parameter, related to the amputated Higgs one-point function

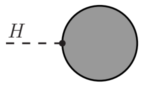

$$= \frac{ie}{(4\pi)^2}\mathcal{T}. \tag{3.26}$$

The EW-corrections to the Higgs one-point function are given in the following subsection. The Higgs-tadpoles will appear in the renormalization constants derived from bosonic 2-point functions, but not in the field strength renormalization constants as those are obtained by taking a derivative in the external invariant p^2, but the tadpoles are independent of momentum p. Apart from counterterms the Higgs-tadpoles also appear explicitly on the ZZ-transition of the s-channel diagram. They are however immediately cancelled by the renormalization procedure, as will be shown below. There are 2 further tadpole insertions that do not need to be taken into account, shown schematically in fig. 3.4. The

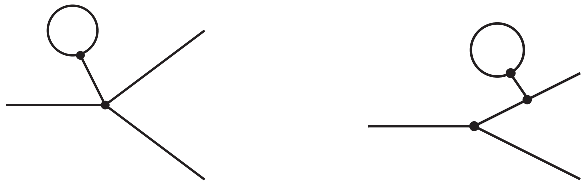

Figure 3.4: Two examples of Higgs-tadpole topologies not relevant for the calculation in this work due to different reasons outlined in the text.

first one does not exist for our SM-process of $e^+e^- \to t\bar{t}$ (but might appear in other processes like ZH-production). The latter topology is amputated by the LSZ-formalism, but the tadpoles also do not contribute to the wavefunction factors R (essentially the finite remnants of the field-strengths that have not been included in the renormalization constants $\delta Z_{L/R}$, in the OS-scheme we have $R = 1$).

The question is now: do the tadpoles contribute to the renormalized self-energies etc. at 1-loop? Take for example the ZZ-transition for an arbitrary external invariant and construct the renormalized quantity $\hat{\Pi}^T_{ZZ}$ in the Denner-scheme for simplicity[9] according to eq. (2.63). δZ_{ZZ} is free of tadpole contributions as discussed before, since it is a field-strength renormalization constant. For the rest we get

$$\left(\hat{\Pi}^T_{ZZ}(p^2)\right)_{\text{tadpole}} = \left(\Pi^T_{ZZ}(p^2)\right)_{\text{tadpole}} + M_Z^2\left(\delta Z_{M_Z}\right)_{\text{tadpole}} = \left(\Pi^T_{ZZ}(p^2)\right)_{\text{tadpole}} - \left(\Pi^T_{ZZ}(M_Z^2)\right)_{\text{tadpole}} = 0, \tag{3.27}$$

[9]The BHS-scheme is completely analogous though, as δZ_2^Z is also free of tadpole contributions.

as the tadpole contributions are independent of the off-shellness p^2 (cf. eq. (3.25)). In the on-shell scheme the tadpoles therefore completely drop out of the renormalized quantities. However, the inclusion of Higgs-tadpoles is **necessary to obtain gauge-independence of bare self-energies on the mass-shell**. For example $\Pi^T_{ZZ}(M_Z^2)$ is only manifestly free of gauge-parameters if the Higgs-tadpoles are included via eq. (3.25). Bare self-energies evaluated on the mass-shell correspond to on-shell mass-renormalization constants that connect gauge-invariant quantities (bare mass and pole-mass or physical mass[10]), so a proper inclusion of the Higgs-tadpoles is necessary. Our simple scheme of just including them into the self-energies is shown to be consistent (and equivalent to other proper schemes) in a recent review by Denner et al [18]. The inclusion of tadpoles into the mass renormalization constants can be a numerical problem however. For example the Higgs-tadpole with the top quark in the loop is quite a dangerous customer in that respect, with its contribution to the top mass shift[11], i.e. the difference between OS- and $\overline{\text{MS}}$-scheme, being

$$\left(\delta Z_{m_t}\right)_{\text{OS}} - \left(\delta Z_{m_t}\right)_{\overline{\text{MS}}} = \frac{\alpha(m_t)}{4\pi} N_c \frac{m_t^5}{s_W^2 M_W^2 M_H^2} \sim 13.1 \text{ GeV}, \tag{3.28}$$

where the fine-structure constant has been run from the non-relativistic value $\alpha(m_e) = 137^{-1}$ to $\alpha(m_t) \equiv \alpha^{3,5}(m_t) \sim 125.6^{-1}$ by means of the light-fermion loops (see sec. 3.4.2). 13.1 GeV is a huge shift, basically cancelling the QCD-corrections to this difference (cf. [19])

$$\left(\delta Z_{m_t}\right)_{\text{OS}} - \left(\delta Z_{m_t}\right)_{\overline{\text{MS}}} \sim -10.4 \text{ GeV} \qquad \text{at } \mathcal{O}(\alpha_s). \tag{3.29}$$

As this example shows, usage of mass definitions in EW theory that have reduced sensitivity to or are even completely free of tadpole contributions is desirable. We refer the reader to [19], which apart from being a nice read on this topic contains suggestions for mass definitions in this direction.

Lastly we point out that in the renormalization constant δZ_c the Higgs-tadpoles cancel completely, as it is related to the difference

$$\delta Z_c \sim \frac{\Pi^T_{WW}(M_W^2)}{M_W^2} - \frac{\Pi^T_{ZZ}(M_Z^2)}{M_Z^2} \overset{(3.25)}{=} \frac{\alpha}{4\pi} \frac{M_W}{s_W M_H^2} \left(\frac{1}{M_W^2} - \frac{1}{c_W^2 M_Z^2}\right) \mathcal{T} \overset{(2.11)}{=} 0. \tag{3.30}$$

δZ_c is actually already gauge-independent without the inclusion of Higgs-tadpoles.

3.3.3 EW corrections to the amputated Higgs one-point function

Assuming all fermions except the top quark to be massless, we get 8 distinct EW contributions to the Higgs one-point function, shown in eq. 3.32. If other fermions are treated as massive, their inclusion would be straightforward by simply replacing $m_t \to m_f$ in the top contribution. For the vector tadpoles we define an auxillary function $T^\xi(M)$ by

$$T^\xi(M) = d\left[A_0(M) + \frac{A_{00}\left(M\sqrt{\xi}\right) - A_{00}(M)}{M^2}\right] = -2M^2 + 4A_0(M) + \left[\xi A_0\left(M\sqrt{\xi}\right) - A_0(M)\right], \tag{3.31}$$

where we arranged things such that the expression in Feynman gauge can be read off quickly.

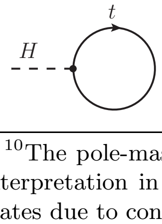

$= \frac{ie}{(4\pi)^2} N_c \frac{2m_t^2}{s_W M_W} A_0(m_t)$

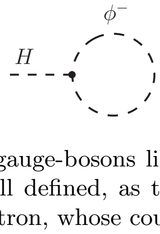

$= \frac{ie}{(4\pi)^2} \frac{M_H^2}{4 s_W M_W} A_0(M_W\sqrt{\xi_W})$

[10]The pole-mass for coloured objects (quarks) as well as weak gauge-bosons like W, Z is a perturbative concept whose interpretation in terms of a physical mass is theoretically not well defined, as those fields cannot appear as asymptotic states due to confinement and/or instability. However, for the electron, whose coupling to the Higgs is small but non-zero, this concept is more straightforward.

[11]In this work we do not give further explicit results for δZ_{m_t}.

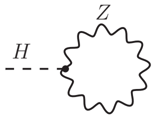

$$= \frac{ie}{(4\pi)^2} \frac{M_W}{2c_W^2 s_W} T^{\xi_Z}(M_Z)$$

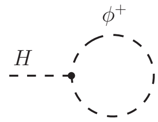

$$= \frac{ie}{(4\pi)^2} \frac{M_H^2}{4s_W M_W} A_0(M_W\sqrt{\xi_W})$$

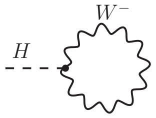

$$= \frac{ie}{(4\pi)^2} \frac{M_W}{2s_W} T^{\xi_W}(M_W)$$

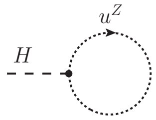

$$= -\frac{ie}{(4\pi)^2} \frac{M_W \xi_Z}{2c_W^2 s_W} A_0(M_Z\sqrt{\xi_Z})$$

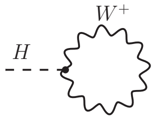

$$= \frac{ie}{(4\pi)^2} \frac{M_W}{2s_W} T^{\xi_W}(M_W)$$

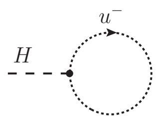

$$= -\frac{ie}{(4\pi)^2} \frac{M_W \xi_W}{2s_W} A_0(M_W\sqrt{\xi_W})$$

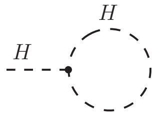

$$= \frac{ie}{(4\pi)^2} \frac{3M_H^2}{4s_W M_W} A_0(M_H)$$

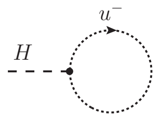

$$= -\frac{ie}{(4\pi)^2} \frac{M_W \xi_W}{2s_W} A_0(M_W\sqrt{\xi_W})$$

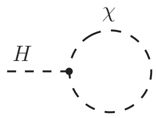

$$= \frac{ie}{(4\pi)^2} \frac{M_H^2}{4s_W M_W} A_0(M_Z\sqrt{\xi_Z}), \tag{3.32}$$

Some caution in interpreting these results is required, as the tadpole topology introduces a symmetry factor of $S = \frac{1}{2}$ per diagram. We included this factor explicitly in the above expressions. We furthermore point out that fermion and ghost loops do not have the symmetry factor $S = \frac{1}{2}$ but rather $S = 1$ effectively, as for these particles the fields and anti-fields have to be treated as separate entities, giving another factor of 2, which removes the symmetry factor of the tadpole topology. In the above expressions this factor 2 has been explicitly included already for fermions and ghosts, and we consequently do not have to take into account anti-ghost or anti-fermion diagrams etc.

3.4 Oblique corrections

The virtual gauge bosons also receive weak corrections at one-loop. For historical reasons these are termed *oblique corrections*. Because of the mixing of the neutral gauge bosons, the oblique part of the rhs of eq. (3.22) actually reads in matrix notation in this two-dimensional space of neutral gauge bosons

$$i\mathcal{M}_{\text{rad}}^{\text{oblique}} = \begin{pmatrix} \left(\hat{V}_{t,Z}^{(0)}\right)^{\alpha} \\ \left(\hat{V}_{t,A}^{(0)}\right)^{\alpha} \end{pmatrix}^{T} \begin{pmatrix} \left(\hat{D}_{ZZ}^{(1)}\right)_{\alpha\beta} & \left(\hat{D}_{ZA}^{(1)}\right)_{\alpha\beta} \\ \left(\hat{D}_{AZ}^{(1)}\right)_{\alpha\beta} & \left(\hat{D}_{AA}^{(1)}\right)_{\alpha\beta} \end{pmatrix} \begin{pmatrix} \left(\hat{V}_{e,Z}^{(0)}\right)^{\beta} \\ \left(\hat{V}_{e,A}^{(0)}\right)^{\beta} \end{pmatrix}, \tag{3.33}$$

and the upcoming sections 3.4.1, 3.4.2 will be devoted to the computation and renormalization of the corrections $D_{XY}^{(1)}$. The diagrammatic contributions are listed in sec. 3.4.4. According to the particle species in the loop we will make a distinction between *fermionic oblique corrections* (FOC) and *bosonic oblique corrections* (BOC).

3.4.1 Renormalized propagator corrections

The renormalized propagator matrix $D_{\alpha\beta}$ can be determined by inversion of the proper 2-point function $\Gamma_2^{\alpha\beta}$ via $D_{\alpha\beta} = i\left(\Gamma_2^{\alpha\beta}\right)^{-1}$, which reads

$$i\,\Gamma_2^{\alpha\beta} = (-i)\begin{pmatrix} q^2 - M_Z^2 - \hat{\Pi}_{ZZ}^T & -\hat{\Pi}_{AZ}^T \\ -\hat{\Pi}_{ZA}^T & q^2 - \hat{\Pi}_{AA}^T \end{pmatrix} g^{\alpha\beta} + (q^\alpha q^\beta - \text{terms}). \tag{3.34}$$

The $q^\alpha q^\beta$-terms do not need to be taken into account for reasons outlined in section 3.5. The $\hat{\Pi}^T_{XY}$ denote renormalized one-loop corrections to the corresponding two-point functions, cf. eqs. (2.63), (2.109). We remind that $\Pi^T_{ZA}(q^2) = \Pi^T_{AZ}(q^2)$.

Dropping the $q^\alpha q^\beta$-terms a straightforward inversion of this 2x2 matrix yields

$$i\left(\Gamma_2^{\alpha\beta}\right)^{-1} = \frac{(-i)}{\left(q^2 - M_Z^2 - \hat{\Pi}^T_{ZZ}\right)\left(q^2 - \hat{\Pi}^T_{AA}\right) - \left(\hat{\Pi}^T_{AZ}\right)^2} \begin{pmatrix} q^2 - \hat{\Pi}^T_{AA} & \hat{\Pi}^T_{AZ} \\ \hat{\Pi}^T_{ZA} & q^2 - M_Z^2 - \hat{\Pi}^T_{ZZ} \end{pmatrix} g_{\alpha\beta}. \tag{3.35}$$

This result incorporates corrections to all orders, but has to be expanded to the corresponding order in perturbation theory one is working at, to make sure it is compatible with the vertex corrections at the same order[12]. We only consider $O(\alpha)$ corrections, so as a first step the squared off-diagonal term in the denominator is dropped because $\left(\hat{\Pi}^T_{AZ}\right)^2 \sim O(\alpha^2)$. Since the off-diagonal elements without the prefactor are already $O(\alpha)$ to $D_{\alpha\beta}$, corrections in the denominator can be neglected altogether there,

$$(-i)\left(\Gamma_2^{\alpha\beta}\right)^{-1} = (-i)\begin{pmatrix} \frac{1}{q^2 - M_Z^2 - \hat{\Pi}^T_{ZZ}} & \frac{\hat{\Pi}^T_{AZ}}{q^2\left(q^2 - M_Z^2 - \hat{\Pi}^T_{ZZ}\right)} \\ \frac{\hat{\Pi}^T_{AZ}}{q^2\left(q^2 - M_Z^2 - \hat{\Pi}^T_{ZZ}\right)} & \frac{1}{q^2 - \hat{\Pi}^T_{AA}} \end{pmatrix} g_{\alpha\beta} + O(\alpha^2). \tag{3.36}$$

We now focus on the ZZ-piece in the denominators. Firstly we split[13] $\hat{\Pi}^T_{ZZ}(q^2) = \mathrm{Re}\left[\hat{\Pi}^T_{ZZ}(q^2)\right] + i\,\mathrm{Im}\left[\Pi^T_{ZZ}(q^2)\right]$ in the denominator and use the optical theorem to write

$$\mathrm{Im}\left[\mathcal{M}(Z \to Z)\right] = M_Z\,\Gamma_Z^{\mathrm{tot}}, \tag{3.37}$$

where Γ_Z^{tot} is the total decay width of the Z-boson. The 1-loop forward scattering amplitude is related to the Z-self energy according to

$$\mathcal{M}(Z \to Z) = \varepsilon^*_\mu(q)\,\varepsilon_\nu(q)\left(g^{\mu\nu}\hat{\Pi}^T_{ZZ}(q^2) + q^\mu q^\nu - \text{pieces}\right) \overset{q^2 = M_Z^2}{=} -\hat{\Pi}^T_{ZZ}(M_Z^2), \tag{3.38}$$

where $q \cdot \varepsilon(q) = 0$ for on-shell particles and the conventional normalization of the polarization vectors $\varepsilon^*(q)\cdot\varepsilon(q) = -1$ was used. At $\mathcal{O}(\alpha)$ this allows the approximate replacement $\mathrm{Im}\left[\hat{\Pi}^T_{ZZ}(q^2)\right] \to -M_Z\,\Gamma_Z^{\mathrm{tot}}$ close to the Z-peak, i.e. $q^2 \sim M_Z^2$ (for our top pair production case see discussion below),

$$(-i)\left(\Gamma_2^{\alpha\beta}\right)^{-1} = (-i)\begin{pmatrix} \frac{1}{q^2 - M_Z^2 + i\,M_Z\,\Gamma_Z^{(0)} - \mathrm{Re}\left[\hat{\Pi}^T_{ZZ}\right]} & \frac{\hat{\Pi}^T_{AZ}}{q^2\left(q^2 - M_Z^2 + i\,M_Z\,\Gamma_Z^{(0)} - \mathrm{Re}\left[\hat{\Pi}^T_{ZZ}\right]\right)} \\ \frac{\hat{\Pi}^T_{AZ}}{q^2\left(q^2 - M_Z^2 + i\,M_Z\,\Gamma_Z^{(0)} - \mathrm{Re}\left[\hat{\Pi}^T_{ZZ}\right]\right)} & \frac{1}{q^2 - \hat{\Pi}^T_{AA}} \end{pmatrix} g_{\alpha\beta} + O(\alpha^2). \tag{3.39}$$

Finally expanding the terms in terms of the real parts straightforwardly yields the virtual propagator including $O(\alpha)$-corrections:

$$D_{\alpha\beta}(q^2) = \frac{(-i)}{q^2}\begin{pmatrix} \chi^{(0)}(q^2)\left(1 + \chi^{(0)}(q^2)\frac{\hat{\Pi}^T_{ZZ}}{q^2}\right) & \chi^{(0)}(q^2)\frac{\hat{\Pi}^T_{AZ}}{q^2} \\ \chi^{(0)}(q^2)\frac{\hat{\Pi}^T_{AZ}}{q^2} & 1 + \frac{\hat{\Pi}^T_{AA}}{q^2} \end{pmatrix} g_{\alpha\beta} + O(\alpha^2) =$$

$$, = \underbrace{\frac{(-i)}{q^2}\begin{pmatrix} \chi^{(0)}(q^2) & 0 \\ 0 & 1 \end{pmatrix} g_{\alpha\beta}}_{D^{(0)}} + \underbrace{\frac{(-i)}{q^2}\begin{pmatrix} \left[\chi^{(0)}(q^2)\right]^2\frac{\hat{\Pi}^T_{ZZ}}{q^2} & \chi^{(0)}(q^2)\frac{\hat{\Pi}^T_{AZ}}{q^2} \\ \chi^{(0)}(q^2)\frac{\hat{\Pi}^T_{AZ}}{q^2} & \frac{\hat{\Pi}^T_{AA}}{q^2} \end{pmatrix}}_{D^{(1)}} g_{\alpha\beta} + O(\alpha^2) =$$

[12]We deal with an exception in sec. 3.4.2.

[13]Note that we omit the hat symbol for the imaginary part, as it is free of UV-divergences and there are no counterterms (see also the renormalization conditions, where only Re is taken).

$$= \left(D^{(0)} + D^{(1)}\right) g_{\alpha\beta} + O(\alpha^2), \tag{3.40}$$

where as in ch. 2 we keep the Re implicit in front of $\hat{\Pi}^T_{XY}$ and we introduced the lowest-order dimensionless Z-propagator ratio

$$\chi^{(0)}(q^2) = \frac{q^2}{q^2 - M_Z^2 + iM_Z\Gamma_Z^{(0)}}, \tag{3.41}$$

which has feature that $\chi(q^2) \to 1$ if $q^2 \to \infty$. $\Gamma_Z^{(0)}$ is the tree-level total decay width of the Z-boson. We point out that since we will be working in the regime (far) above the top production threshold, i.e. $q^2 = s > 4m_t^2$, and consequently far above the Z-peak, $q^2 = s \gg M_Z^2$, the above expansions are all valid with no need to worry about resonance enhancement effects. Close to the Z-peak, which is never the case for on-shell or close-to-on-shell top production, the inclusion of higher-order effects would be necessary, i.e. a careful perturbative expansion of eq. (3.35) including two-loop order if $\mathcal{O}(\alpha)$-accuracy is needed and so forth. For a brief discussion see for example [5]. For our purposes of working (far) above the top pair production threshold, keeping a non-zero Z-width results only in very small numerical shifts, so from now on we will set $\Gamma_Z^{\text{tot}} = 0$ in $\chi^{(0)}(s)$, also for the numerics in ch. 6.

The renormalization of the bosonic self-energies Π^T_{XY} is carried out with the results from chapter 2, specifically eqs. (2.63) and (2.109). In this work we will use the BHS-scheme, as the resulting expressions are a bit simpler, i.e. here we use eq. (2.109). The only exception are the (light-)fermion contributions to the AA-transition and consequently to the electric charge renormalization, which will receive a different treatment outlined in the next section.

3.4.2 Light fermion loops - the QED-improved Born approximation

The bosonic self-energies Π_{XY} not only receive contributions from the top quark and the weak bosons living at the scale Λ_{EW}, but also contain loops of light fermions (lf), i.e. leptons and quarks up to (and including) the bottom quark. The logarithms appearing in these loops are quite large, e.g. for $\sqrt{s} = 1$ TeV

$$\alpha \ln\left(\frac{s}{m_e^2}\right) = 137^{-1} \ln\left(\frac{(1\,\text{TeV})^2}{(511\,\text{keV})^2}\right) \sim 0.2, \tag{3.42}$$

and therefore need to be resummed. Fortunately, this is possible without much of an effort. The features of this section are most easily discussed in the BHS-scheme, as one can focus on the corrections to the s-channel boson propagators and ignore the renormalization of the vertices. The reason is that in the BHS-scheme the local 3-point counterterms only consist of the mixing self-energy $\Pi^T_{ZA}(0)$ (cf. eq. 3.76), which does not get contributions from fermion loops.

A quick inspection of the self-energies shows that the light-fermion loops are only problematic in the diagonal parts of the inverse propagator matrix, and more specifically in the terms related to charge renormalization. If on-shell subtraction is applied in conjunction with the renormalization condition 2.114 the counterterm contribution to $\delta Z_2^\gamma = \delta Z_{AA}$ from a light-fermion loop is

$$(\delta Z_2^\gamma)^{\text{OS}}_{\text{lf}} = -\frac{\alpha}{3\pi} N_{c,f}\left[\frac{1}{\epsilon} + \ln\left(\frac{\mu^2}{m_f^2}\right)\right], \tag{3.43}$$

where $N_{c,f}$ is defined in eq. (2.133). When combined with the light-fermion contribution according to eq. (2.109) to form the renormalized AA-self-energy evaluated at a scale $s \gg m_f^2$, we obtain

$$\frac{1}{s}(\hat{\Pi}^T_{AA})^{\text{OS}}_{\text{lf}}(s) = -\frac{\alpha}{3\pi} N_f\left[\frac{5}{3} + \ln\left(\frac{m_f^2}{-s - i0^+}\right)\right] + \mathcal{O}\left(\frac{m_f^2}{s}\right). \tag{3.44}$$

This result is singular in the limit $m_i^2 \to 0$, while for finite but small masses the hierachy inside the log is large. A significant reduction of the dependence on these small fermion masses can be achieved by using $\overline{\text{MS}}$-subtraction for light-fermion contributions to Π_{AA} and by running α from the non-relativistic regime, where it was defined in the on-shell scheme, up to the scale $\Lambda_{\rm EW}$ or $\sqrt{s}$[14]. At one-loop, the running of α for n_l active light (charged) leptons and n_q active light quarks takes the form (see sec. F.3, cf. [15])

$$\alpha^{n_l,n_q}(\mu) = \frac{\alpha_0}{1 - \frac{\alpha_0}{3\pi}\sum_{l=1}^{n_l} Q_l^2 \ln\left(\frac{\mu^2}{m_l^2}\right) - \frac{\alpha_0}{3\pi} N_c \sum_{q=1}^{n_q} Q_q^2 \ln\left(\frac{\mu^2}{m_q^2}\right)}, \tag{3.45}$$

where α_0 is the value determined at the mass of the lightest fermion in eq. (3.45), which we take to be the fine structure constant in the Thomson limit: $\alpha_0 \equiv \alpha^{0,0}(m_e) = 137^{-1}$. This scheme amounts to minimally subtracting the UV-divergences from the light-fermion loops[15] in Π^T_{AA}, i.e. using

$$(\delta Z_2^\gamma)^{\overline{\rm MS}}_{\rm lf} = -\frac{\alpha}{3\pi}\, N_{c,f}\, \frac{1}{\epsilon}, \tag{3.46}$$

and replacing α by $\alpha^{n_l,n_q}(\mu)$ everywhere in the calculation. Note that due to the minimal subtraction we also get explicit $\mu-$dependence in the renormalized transitions. Since we are interested in processes with $s \gg m_t^2$, we will also sum the top contributions into eq. 3.45, although the resulting logarithms would be of the order $\sim \log\left(\frac{\Lambda^2_{\rm EW}}{s}\right)$ which are kept in the rest of the calculation[16]. To avoid writing $\mu-$dependence all the time, in the rest of this work (unless explicitly stated otherwise) we understand α as being run up to the scale $\sqrt{s}$ by including all fermion loops into the RG-evolution of $\alpha = \alpha^{n_l,n_q}(\mu)$. With this convention, the renormalized (light-)fermion contributions read

$$\frac{1}{s}(\hat\Pi^T_{AA})_{\rm lf}(s) = -\frac{\alpha}{3\pi}\sum_{\text{light } f} N_{c,f}\, Q_f^2 \left(\frac{5}{3} + \ln\left(\frac{\mu^2}{-s - i0^+}\right)\right),$$

$$\frac{1}{s}(\hat\Pi^T_{ZA})_{\rm lf}(s) = \frac{\alpha}{3\pi}\, s \sum_{\text{light } f} N_{c,f}\left\{Q_f\, v_f \ln\left(\frac{M_W^2}{-s - i0^+}\right) + \frac{c_W}{s_W}\left(v_f^2 + a_f^2\right) \ln\left(\frac{M_W^2}{M_Z^2}\right)\right\},$$

$$\frac{1}{s}(\hat\Pi^T_{ZZ})_{\rm lf}(s) = -\frac{\alpha}{3\pi}\sum_{\text{light } f} N_{c,f}\left\{\left(v_f^2 + a_f^2\right)\left[s \ln\left(\frac{M_Z^2}{-s - i0^+}\right) + \frac{c_W^2}{s_W^2}\left(s - M_Z^2\right) \ln\left(\frac{M_W^2}{M_Z^2}\right)\right] + \right.$$

$$\left. + Q_f^2(s - M_Z^2)\left[\ln\left(\frac{\mu^2}{M_W^2}\right) + \frac{5}{3}\right]\right\}. \tag{3.47}$$

We emphasize once again that we only minimally subtract for δZ_2^γ. The light-fermion contributions to the rest of the renormalization constants (δZ_2^Z etc.) are treated as in sec. 2. Some more details on the fermion loops can be found in the appendix F.

3.4.3 Connecting with chiral amplitude basis

To enable comparison of the propagator corrections with the amputated vertices and the boxes, we write them down in the amplitude basis of eq. (3.8). From the above expressions its clear that the diagonal oblique corrections (i.e. those without $D^{(1)}_{ZA}$ or $D^{(1)}_{AZ}$) are proportional to the tree-level structures of the Dirac bilinears. We find

$$\left(\mathcal{M}^{(1)}_\kappa\right)_{\rm oblique} = \frac{4\pi\,\alpha}{s}\sum_{\rho=\pm}\left\{\left[\chi^{(0)}(s)\right]^2 \frac{\hat\Pi^T_{ZZ}(s)}{s}\,(v_t - \rho\, a_t)\,(v_e - \kappa\, a_e) + \frac{\hat\Pi^T_{AA}(s)}{s}\, Q_t Q_e + \right.$$

$$\left. + \chi^{(0)}(s)\,\frac{\hat\Pi^T_{ZA}(s)}{s}\Big[(v_t - \rho\, a_t)(-Q_e) + (-Q_t)(v_e - \kappa\, a_e)\Big]\right\} \bar M_1^{\rho\kappa}, \tag{3.48}$$

[14]Either way logarithms of $\Lambda^2_{\rm EW}/s$ remain, as theses also originate from the hierachy of the scales $\Lambda^2_{\rm EW}$ (where the $Z-$contributions were renormalized in the OS-scheme) and the hard scale s of the process.

[15]The bosonic loops are still treated in the OS-scheme!

[16]The unresummed top contributions are lengthy, at least for $\hat\Pi_{ZZ}$. They can be derived straightforwardly by means of the generic diagrams given in the appendix and the counterterms given in sec. (2.5).

which implies

$$\frac{1}{4\pi}\left(\bar{c}_1^{(1),\rho\kappa}\right)_{\text{oblique}} = \left[\chi^{(0)}(s)\right]^2 (v_t - \rho\, a_t)\,(v_e - \kappa\, a_e)\,\frac{\hat{\Pi}^T_{ZZ}(s)}{s} + Q_t Q_e \frac{\hat{\Pi}^T_{AA}(s)}{s} +$$
$$+\,\chi^{(0)}(s)\Big[(v_t - \rho\, a_t)(-Q_e) + (-Q_t)(v_e - \kappa\, a_e)\Big]\frac{\hat{\Pi}^T_{ZA}(s)}{s},$$
$$\frac{1}{4\pi}\left(\bar{c}_2^{(1),\rho\kappa}\right)_{\text{oblique}} = 0. \tag{3.49}$$

We remark that because only $\bar{M}_1^{\rho\kappa}$ appears, the diagonal parts with $\hat{\Pi}^T_{ZZ}(s)$ and $\hat{\Pi}^T_{AA}(s)$ could be grouped with the tree-level expressions [17] We will however refrain from more notational gymnastics and keep things as they are. The above formula concludes the symbolic treatment of propagator corrections at one-loop.

3.4.4 EW corrections to bosonic transitions

The complete sets of diagrams contributing to the ZZ-, ZA- and AA-transitions can be found in the appendix G.2. The analytic expressions are obtained by using the generic expressions for bosonic 2-point functions also given in the appendix E, and plugging in the parameters listed in tab. 3.1. The ingredients for the Higgs-tadpole contributions can be found in secs. 3.3.2 and 3.3.3 . The sum $\hat{\Pi}^T_{XY}$ of renormalized diagrams are then to be inserted into eq. (3.48).

The generic diagrams given in the appendix E were derived with help of projection operators (listed in app. D). We point out that for the calculation we made heavy use of computer assistance in the form of special `Mathematica`-Packages tailored to Feynman diagrammatic calculations. Especially version 2 of the relatively recent program `Package-X` [20], [21], was extensively used for this work. It provides analytical and numerical tools (like built-in projection operators, PV-reductions, numerical implementation of scalar PV-functions) for one-loop calculations up to 4-point diagrams while impressing with spectacular user-friendliness. Other packages used in this work for cross-checking include `FeynArts` ([22], diagram + amplitude generation), `FeynCalc` ([23], algebraic manipulations) and `LoopTools` ([24], numerical library of PV-tensor coefficient).

We give a quick example on how to read tabs. 3.1 - 3.4. Say we want to know the contribution $\left(\Pi^T_{ZZ}\right)_{H\chi}$ of the $H\chi$-diagram to the transverse ZZ-transition Π^T_{ZZ}. For bosonic self-energies we start with eq. (E.9) of sec. E.2 in app. E. The $\boldsymbol{\mathcal{S}}$-column in tab. 3.1 states that the symmetry factor for this diagram is $\mathcal{S} = 1$ in eq. (E.9). For the transverse part we focus on G^T. Now the entry SS in the **type**-column in tab. 3.1 tells us to look in the *scalar-scalar* subsection E.2.5 of sec. E.2. Note that the letters in the **type**-column are abbreviations for the virtual particle type, so $V =$ "vector", $A =$ "massless vector", $S =$ "scalar", $U =$ "ghost", $f =$ "fermion", and need not be confused with the letter $\mathcal{S}$ for the symmetry factor given above or V for "vertex", as used in other parts of this work. Now the function G^T_{SS} (eq. (E.19)) reads

$$G^T_{SS} = 4 g_X g_Y\, B_{00}\left(p^2; M_1, M_2\right). \tag{3.50}$$

Consulting the other entries of the $H\chi$-row in tab. 3.1 tells us to identify[18]

$$g_X = -\frac{i}{2c_W s_W}, \qquad g_Y = \frac{i}{2c_W s_W}, \qquad M_1 = M_H, \qquad M_2 = M_Z\sqrt{\xi_Z}. \tag{3.51}$$

The $-$-entries mean that this specific parameter is absent for this type of diagram, so for our $H\chi$-diagram the last two entries mean that there are no further explicit gauge-parameters appearing (only in the mass

[17] This approach is adopted in [5] and the resulting contribution to the total amplitude is called *dressed Born matrix element.*

[18] Note that the bosonic transitions are always symmetric: $\Pi^{T,L}_{XY} = \Pi^{T,L}_{YX}$, so it does not matter which coupling given in the table we identify with g_X and which with g_Y.

of the Goldstone, but this has already been specified in the mass-column). It may also confuse at first sight that the top row entries contain more than one parameter, like $\{\boldsymbol{M}, \boldsymbol{M_1}, \boldsymbol{M_V}, \boldsymbol{m_1}\}$. However, the expression for a *certain* generic diagram will only contain one of those parameters, which the entry then represents (in our case we had M_1 appearing, but not M, M_V or m_1). Plugging in we are finished, so not forgetting about the rest of the factors in eq. (E.9) and the precise definition of Π^T_{ZZ} in eq. (2.41) (with the i factored out) we have

$$\left(\Pi^T_{ZZ}\right)_{H\chi} = \frac{\alpha}{4\pi}\frac{1}{c_W^2 s_W^2}\, B_{00}\left(p^2; M_H, M_Z\sqrt{\xi_Z}\right). \tag{3.52}$$

The PV-tensor coefficient can then be scalarized by the results given in sec. B.

The rest of the diagrams are obtained analogously. Note that fermionic couplings have chirality indices as superscripts, e.g. g_X^η, where $\eta = \pm$.

$\boldsymbol{ZZ}$	**type**	$\boldsymbol{\mathcal{S}}$	$\boldsymbol{g_X, g_{XY}}$	$\boldsymbol{g_Y}$	$\boldsymbol{M, M_1, M_V, m_1}$	$\boldsymbol{M_2, M_S, m_2}$	$\boldsymbol{\xi, \xi_1}$	$\boldsymbol{\xi_2}$
ff	ff	$N_{c,f}$	$v_f - \eta\, a_f$	$v_f - \eta\, a_f$	m_f	m_f	–	–
$W^\pm W^\mp$	VV	1	$-\frac{c_W}{s_W}$	$-\frac{c_W}{s_W}$	M_W	M_W	ξ_W	ξ_W
$W^-\phi^+$	VS	1	$-\frac{s_W}{c_W}M_W$	$-\frac{s_W}{c_W}M_W$	M_W	$M_W\sqrt{M_W}$	ξ_W	–
$W^+\phi^-$	VS	1	$-\frac{s_W}{c_W}M_W$	$-\frac{s_W}{c_W}M_W$	M_W	$M_W\sqrt{M_W}$	ξ_W	–
ZH	VS	1	$\frac{1}{c_W^2 s_W}M_W$	$\frac{1}{c_W^2 s_W}M_W$	M_Z	M_H	ξ_Z	–
$\phi^\pm\phi^\mp$	SS	1	$\frac{c_W^2 - s_W^2}{2c_W s_W}$	$\frac{c_W^2 - s_W^2}{2c_W s_W}$	$M_W\sqrt{M_W}$	$M_W\sqrt{M_W}$	–	–
$H\chi$	SS	1	$-\frac{i}{2c_W s_W}$	$\frac{i}{2c_W s_W}$	M_H	$M_Z\sqrt{M_Z}$	–	–
$u^-\bar{u}^-$	UU	1	$\frac{c_W}{s_W}$	$\frac{c_W}{s_W}$	$M_W\sqrt{M_W}$	$M_W\sqrt{M_W}$	–	–
$u^+\bar{u}^+$	UU	1	$-\frac{c_W}{s_W}$	$-\frac{c_W}{s_W}$	$M_W\sqrt{M_W}$	$M_W\sqrt{M_W}$	–	–
W^-	T_V	$\frac{1}{2}$	$-\frac{c_W^2}{s_W^2}$	–	M_W	–	ξ_W	–
W^+	T_V	$\frac{1}{2}$	$-\frac{c_W^2}{s_W^2}$	–	M_W	–	ξ_W	–
ϕ^-	T_S	$\frac{1}{2}$	$\frac{(c_W^2 - s_W^2)^2}{2c_W^2 s_W^2}$	–	$M_W\sqrt{\xi_W}$	–	–	–
ϕ^+	T_S	$\frac{1}{2}$	$\frac{(c_W^2 - s_W^2)^2}{2c_W^2 s_W^2}$	–	$M_W\sqrt{\xi_W}$	–	–	–
H	T_S	$\frac{1}{2}$	$\frac{1}{2c_W^2 s_W^2}$	–	M_H	–	–	–
χ	T_S	$\frac{1}{2}$	$\frac{1}{2c_W^2 s_W^2}$	–	$M_Z\sqrt{\xi_Z}$	–	–	–

Table 3.1: ZZ-transition: the virtual particle content is shown in the leftmost column. **type** refers to type in sec. E. All expressions are evaluated at $p^2 = s$. The Higgs-tadpole contributions are given by $\mathcal{T}_{ZZ}$, eq. 3.25. There are $2\,n_l = 6$ light lepton loops ($m_f = 0, v_f = v_e, a_f = a_e$), $n_q = 5$ light quark loops ($m_f = 0, v_f = v_q, a_f = a_q$) and the top loop ($m_f = m_t, v_f = v_t, a_f = a_t$).

$\boldsymbol{ZA}$	type	$\boldsymbol{\mathcal{S}}$	$\boldsymbol{g_X, g_{XY}}$	$\boldsymbol{g_Y}$	$\boldsymbol{M, M_1, M_V, m_1}$	$\boldsymbol{M_2, M_S, m_2}$	$\boldsymbol{\xi, \xi_1}$	$\boldsymbol{\xi_2}$
ff	ff	$N_{c,f}$	$v_f - \eta\, a_f$	$-Q_f$	m_f	m_f	–	–
$W^{\pm}W^{\mp}$	VV	1	$-\frac{c_W}{s_W}$	1	M_W	M_W	ξ_W	ξ_W
$W^{-}\phi^{+}$	VS	1	$-\frac{s_W}{c_W} M_W$	$-M_W$	M_W	$M_W\sqrt{M_W}$	ξ_W	–
$W^{+}\phi^{-}$	VS	1	$-\frac{s_W}{c_W} M_W$	$-M_W$	M_W	$M_W\sqrt{M_W}$	ξ_W	–
$\phi^{\pm}\phi^{\mp}$	SS	1	$\frac{c_W^2 - s_W^2}{2 c_W s_W}$	-1	$M_W\sqrt{M_W}$	$M_W\sqrt{M_W}$	–	–
$u^{-}\bar{u}^{-}$	UU	1	$\frac{c_W}{s_W}$	-1	$M_W\sqrt{M_W}$	$M_W\sqrt{M_W}$	–	–
$u^{+}\bar{u}^{+}$	UU	1	$-\frac{c_W}{s_W}$	1	$M_W\sqrt{M_W}$	$M_W\sqrt{M_W}$	–	–
W^{-}	T_V	$\frac{1}{2}$	$\frac{c_W}{s_W}$	–	M_W	–	ξ_W	–
W^{+}	T_V	$\frac{1}{2}$	$\frac{c_W}{s_W}$	–	M_W	–	ξ_W	–
ϕ^{-}	T_S	$\frac{1}{2}$	$-\frac{c_W^2 - s_W^2}{c_W s_W}$	–	$M_W\sqrt{\xi_W}$	–	–	–
ϕ^{+}	T_S	$\frac{1}{2}$	$-\frac{c_W^2 - s_W^2}{c_W s_W}$	–	$M_W\sqrt{\xi_W}$	–	–	–

Table 3.2: ZA-transition: the virtual particle content is shown in the leftmost column. **type** refers to type in sec. E. All expressions are evaluated at $p^2 = s$. There are no Higgs-tadpole contributions. There are $n_l = 3$ light lepton loops ($m_f = 0, Q_f = Q_e, v_f = v_e, a_f = a_e$), $n_q = 5$ light quark loops ($m_f = 0, Q_f = Q_q, v_f = v_q, a_f = a_q$) and the top loop ($m_f = m_t, Q_f = Q_t, v_f = v_t, a_f = a_t$).

$\boldsymbol{AA}$	type	$\boldsymbol{\mathcal{S}}$	$\boldsymbol{g_X, g_{XY}}$	$\boldsymbol{g_Y}$	$\boldsymbol{M, M_1, M_V, m_1}$	$\boldsymbol{M_2, M_S, m_2}$	$\boldsymbol{\xi, \xi_1}$	$\boldsymbol{\xi_2}$
ff	ff	$N_{c,f}$	$-Q_f$	$-Q_f$	m_f	m_f	–	–
$W^{\pm}W^{\mp}$	VV	1	1	1	M_W	M_W	ξ_W	ξ_W
$W^{-}\phi^{+}$	VS	1	$-M_W$	$-M_W$	M_W	$M_W\sqrt{M_W}$	ξ_W	–
$W^{+}\phi^{-}$	VS	1	$-M_W$	$-M_W$	M_W	$M_W\sqrt{M_W}$	ξ_W	–
$\phi^{\pm}\phi^{\mp}$	SS	1	-1	-1	$M_W\sqrt{M_W}$	$M_W\sqrt{M_W}$	–	–
$u^{-}\bar{u}^{-}$	UU	1	-1	-1	$M_W\sqrt{M_W}$	$M_W\sqrt{M_W}$	–	–
$u^{+}\bar{u}^{+}$	UU	1	1	1	$M_W\sqrt{M_W}$	$M_W\sqrt{M_W}$	–	–
W^{-}	T_V	$\frac{1}{2}$	-1	–	M_W	–	ξ_W	–
W^{+}	T_V	$\frac{1}{2}$	-1	–	M_W	–	ξ_W	–
ϕ^{-}	T_S	$\frac{1}{2}$	2	–	$M_W\sqrt{\xi_W}$	–	–	–
ϕ^{+}	T_S	$\frac{1}{2}$	2	–	$M_W\sqrt{\xi_W}$	–	–	–

Table 3.3: AA-transition: the virtual particle content is shown in the leftmost column. **type** refers to type in sec. E. All expressions are evaluated at $p^2 = s$. There are no Higgs-tadpole contributions. There are $n_l = 3$ light lepton loops ($m_f = 0, Q_f = Q_e$), $n_q = 5$ light quark loops ($m_f = 0, Q_f = Q_q$) and the top loop ($m_f = m_t, Q_f = Q_t$).

$W^\pm W^\pm$	type	$\mathcal{S}$	g_X, g_{XY}	g_Y	M, M_1, M_V, m_1	M_2, M_S, m_2	ξ, ξ_1	ξ_2
tb	ff	N_c	$\frac{1}{\sqrt{2}s_W}\,\delta_{\eta,-1}$	$\frac{1}{\sqrt{2}s_W}\,\delta_{\eta,-1}$	m_t	0	–	–
light doublet	ff	$N_{c,f}$	$\frac{1}{\sqrt{2}s_W}\,\delta_{\eta,-1}$	$\frac{1}{\sqrt{2}s_W}\,\delta_{\eta,-1}$	0	0	–	–
$W^\pm Z$	VV	1	$-\frac{c_W}{s_W}$	$-\frac{c_W}{s_W}$	M_W	M_Z	ξ_W	ξ_Z
$W^\pm A$	VA	1	1	1	M_W	–	ξ_W	–
$W^\pm H$	VS	1	$\frac{1}{s_W}\,M_W$	$\frac{1}{s_W}\,M_W$	M_W	M_H	ξ_W	–
$Z\phi^\pm$	VS	1	$-\frac{s_W}{c_W}\,M_W$	$-\frac{s_W}{c_W}\,M_W$	M_Z	$M_W\sqrt{M_W}$	ξ_Z	–
$A\phi^\pm$	SA	1	$-M_W$	$-M_W$	$M_W\sqrt{M_W}$	–	–	–
$\phi^\pm H$	SS	1	$-\frac{1}{2s_W}$	$\frac{1}{2s_W}$	$M_W\sqrt{M_W}$	M_H	–	–
$\phi^\pm\chi$	SS	1	$-\frac{i}{2s_W}$	$\frac{i}{2s_W}$	$M_W\sqrt{M_W}$	$M_Z\sqrt{\xi_Z}$	–	–
$u^\pm\bar{u}^Z$	UU	1	$\frac{c_W}{s_W}$	$\frac{c_W}{s_W}$	$M_W\sqrt{M_W}$	$M_Z\sqrt{M_Z}$	–	–
$u^\pm\bar{u}^A$	UU	1	-1	-1	$M_W\sqrt{M_W}$	0	–	–
$u^Z\bar{u}^\mp$	UU	1	$-\frac{c_W}{s_W}$	$-\frac{c_W}{s_W}$	$M_Z\sqrt{M_Z}$	$M_W\sqrt{M_W}$	–	–
$u^A\bar{u}^\mp$	UU	1	1	1	0	$M_W\sqrt{M_W}$	–	–
$W^\mp$	T_V	$\frac{1}{2}$	$-\frac{1}{s_W^2}$	–	M_W	–	ξ_W	–
Z	T_V	$\frac{1}{2}$	$-\frac{c_W^2}{s_W^2}$	–	M_Z	–	ξ_Z	–
ϕ^-	T_S	$\frac{1}{2}$	$\frac{1}{2s_W^2}$	–	$M_W\sqrt{\xi_W}$	–	–	–
ϕ^+	T_S	$\frac{1}{2}$	$\frac{1}{2s_W^2}$	–	$M_W\sqrt{\xi_W}$	–	–	–
H	T_S	$\frac{1}{2}$	$\frac{1}{2s_W^2}$	–	M_H	–	–	–
χ	T_S	$\frac{1}{2}$	$\frac{1}{2s_W^2}$	–	$M_Z\sqrt{\xi_Z}$	–	–	–

Table 3.4: WW-transition: the virtual particle content is shown in the leftmost column. **type** refers to type in sec. E. All expressions are evaluated at $p^2 = s$. The Higgs-tadpole contributions are given by $\mathcal{T}_{WW}$, eq. 3.25. The 4-tadpole with the photon is scaleless. In addition to the top-bottom (tb) contribution there are $n_l = 3$ light lepton doublets and $\frac{n_q-1}{2} = 2$ light quark doublets.

3.5 Amputated vertex corrections

In this section we focus on the one-loop contributions to the amputated vertex functions, i.e. $V^{(1)}_{e/t}$ in eq. (3.21): its decomposition into *form factors* according to Lorentz- and Dirac-structure is discussed in secs. 3.5.1, 3.5.2, while the renormalization is dealt with in sec. 3.5.3. The EW diagram contributions are listed in sec. 3.5.5.

3.5.1 Form factor decomposition

Since all external particles are considered on-shell, the (renormalized or unrenormalized) amputated vertex functions V_e and V_t can be written as irreducible vertex functions Λ^β and Ξ^α sandwiched between Dirac spinors of the external particles.

$$(V_e)^\beta\,(q^2) \equiv ie\,\bar{v}_e(l_2)\,\Lambda^\beta(q^2)\,u_e(l_1) = ie\,\bar{v}_e(l_2)\left[\Lambda^\beta_{\text{tree}}(q^2) + \Lambda^\beta_{\text{rad}}(q^2)\right]\,u_e(l_1)$$

$$(V_t)^\alpha\,(q^2) \equiv ie\,\bar{u}_t(q_1)\,\Xi^\alpha(q^2)\,v_t(q_2) = ie\,\bar{u}_t(q_1)\left[\Xi^\alpha_{\text{tree}}(q^2) + \Xi^\alpha_{\text{rad}}(q^2)\right]\,v_t(q_2). \tag{3.53}$$

where $l_1(l_2)$ is the momentum of the incoming electron (positron) and $q_1(q_2)$ the momentum of the outgoing top (antitop). The kinematics are shown in fig. 3.5. We split off the tree-level contributions,

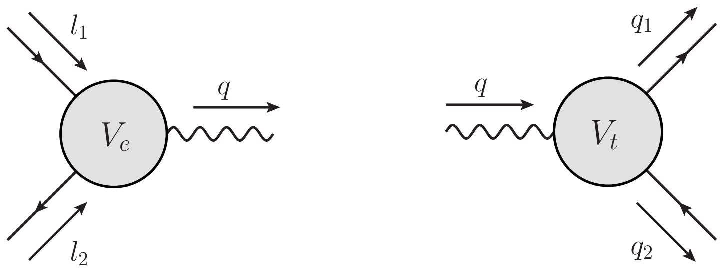

Figure 3.5: Kinematic situations for amputated vertex functions.

which can be easily obtained by the corresponding Feynman rules. The 1-PI radiative corrections to the vertices are contained in $\Lambda^\beta_{\text{rad}}$ and Ξ^α_{rad}, which can be parametrized by 6 form factors (= scalar functions) f_i and F_i respectively:

$$\Lambda^\beta_{\text{rad}}(q^2) = \sum_{\kappa=\pm}\Big\{f^\kappa_1(q^2)\,\gamma^\beta\omega_\kappa + f^\kappa_2(q^2)(l_1-l_2)^\beta\omega_\kappa + f^\kappa_3(q^2)(l_1+l_2)^\beta\omega_\kappa\Big\}, \tag{3.54}$$

$$\Xi^\alpha_{\text{rad}}(q^2) = \sum_{\kappa=\pm}\Big\{F^\rho_1(q^2)\,\gamma^\alpha\omega_\rho + F^\rho_2(q^2)\frac{(q_1-q_2)^\alpha}{m_t}\,\omega_\rho + F^\rho_3(q^2)\frac{(q_1+q_2)^\alpha}{m_t}\,\omega_\rho\Big\}. \tag{3.55}$$

The additional factors of $\frac{1}{m_t}$ in the quark case have been inserted for later convenience. There exist alternative parametrizations of course, but this one is quite practical in the sense that it facilitates reducing the number of nonzero form factors in the case of massless initial-state leptons, as done in the following. Swapping the scalar structures for tensor structures involving $\sigma_{\mu\nu} = \frac{i}{2}\left[\gamma_\mu,\gamma_\nu\right]$ is possible by applying Gordon identities (see appendix A.2), which are useful to switch between various parametrizations. Frequently it is convenient to rewrite and express things in the VA-basis, which for this parametrization is given by

$$\begin{aligned}\Lambda^\beta_{\text{rad}}(q^2) =& \gamma^\beta\left[f^V_1(q^2) + f^A_1(q^2)\,\gamma_5\right] + (l_1-l_2)^\beta\left[f^V_2(q^2) + f^A_2(q^2)\,\gamma_5\right] +\\ &+ (l_1+l_2)^\beta\left[f^V_3(q^2) + f^A_3(q^2)\,\gamma_5\right],\end{aligned} \tag{3.56}$$

$$\Xi^\alpha_{\text{rad}}(q^2) =\gamma^\beta\left[F^V_1(q^2) + F^A_1(q^2)\,\gamma_5\right] + \frac{(q_1-q_2)^\alpha}{m_t}\left[F^V_2(q^2) + F^A_2(q^2)\,\gamma_5\right] +$$

$$+\frac{(q_1+q_2)^\alpha}{m_t}\Big[F_3^V(q^2)+F_3^A(q^2)\,\gamma_5\Big]. \tag{3.57}$$

Since the s-channel mediator can be either photon or Z-boson, each form factor consists of two contributions, which in our notation is arranged as a 2-dim. vector

$$F_i(q^2)=\begin{pmatrix}F_i^{Ztt}(q^2)\\ F_i^{Att}(q^2)\end{pmatrix}, \tag{3.58}$$

and similar for the lepton form factors f_i. The superscript denotes the respective vertex. Since we split off the tree-level contributions (cf. eq. (3.53)), all form factors formally start at $\mathcal{O}(\alpha)$. The form factor decomposition parametrizes the vertex functions to all orders, but since we are only interested in $\mathcal{O}(\alpha)$ contributions, we will omit any further indices and only keep the one-loop contributions to F_i, f_i, unless stated otherwise.

3.5.2 Form factor elimination

In the context of this work, the initial-state leptons are treated as massless ($m_e=0$). In this limit, both vector and axial vector current are conserved exactly, which constrains the lepton vertex function

$$q_\beta\,\bar v_e(l_2)\,\Lambda^\beta(q^2)\,u_e(l_1)\stackrel{!}{=}0. \tag{3.59}$$

Contracting (3.54) with q_β and using on-shellness (and masslessness) of the leptons results in the condition

$$f_3^+(q^2)=f_3^-(q^2)=0,\qquad\text{or}\qquad f_3^V(q^2)=f_3^A(q^2)=0 \tag{3.60}$$

The chiral symmetry present in the massless case immediately kills the remaining (pseudo-)scalar structures with f_2, if these structures are sandwiched between massless spinors. One ends up with

$$\Lambda^\beta_{\text{rad}}(q^2)\approxeq\sum_{\kappa=\pm}f_1^\kappa(q^2)\gamma^\beta=\gamma^\beta\left[f_1^V(q^2)+\gamma_5\,f_1^A(q^2)\right]. \tag{3.61}$$

The transverse property of this expression when sandwiched between the massless lepton spinors (cf. eq. 3.59) has the convenient side effect that for the virtual gauge boson propagator only the $g_{\alpha\beta}$-part gives a non-vanishing contribution, allowing us to ignore the gauge dependent $q_\alpha\,q_\beta$-terms if working in R_ξ-gauge (in Feynman-gauge these pieces are anyway absent).

In case of the top quark vertex, only the vector current is conserved exactly because the tops have to be treated as massive. Contracting the vector part of $\Xi^\alpha(q^2)$ with q_α and using vector current conservation only eliminates one form factor (in the VA-basis) or a linear combination in the chiral basis:

$$F_3^V(q^2)=0,\qquad\text{or}\qquad F_3^-(q^2)+F_3^+(q^2)=0 \tag{3.62}$$

However, because of the transverse $\Lambda^\beta(q^2)$ and the simplified virtual gauge boson propagator

$$F_3^A(q^2)\,\frac{(q_1+q_2)^\alpha}{m_q}\,g_{\alpha\beta}\,\Lambda^\beta(q^2)=F_3^A(q^2)\,\frac{q_\alpha}{m_q}\,\Lambda^\alpha(q^2)=0, \tag{3.63}$$

by eq. 3.59, so the form factor $F_3^A(q^2)$, even if non-vanishing by itself, does not need to be computed.

Note that because of the non-zero masses, the chiral symmetry is not present for the final state, and it is not possible to discard the (pseudo-)scalar structures of F_2 by the same reasoning as above. However, a further simplification is possible for the specific process under consideration in this work. While the above statements are true at arbitrary loop level, CP-invariance dictates the absence of electric dipole moments at the 1-loop level, i.e.

$$F_2^A(q^2)=0,\qquad\text{or}\qquad F_2^+(q^2)-F_2^-(q^2)=0 \tag{3.64}$$

We checked this explicitly for our EW diagrams, and consequently do not give generic expressions for this form factor in this work. The effective top quark vertex parametrization that gives a non-vanishing contribution is therefore given by

$$\Xi^{\alpha}_{\mathrm{rad}}(q^2) \approxeq \sum_{\rho=\pm}\left[F_1^{\rho}(q^2)\gamma^{\alpha}\omega_{\rho}\right] + F_2^V(q^2)\frac{(q_1-q_2)^{\alpha}}{m_t} =$$

$$= \gamma^{\alpha}\left[F_1^V(q^2) + \gamma_5\, F_1^A(q^2)\right] + F_2^V(q^2)\frac{(q_1-q_2)^{\alpha}}{m_t}, \tag{3.65}$$

where $F_2^V = \frac{1}{2}\big(F_2^- + F_2^+\big)$.

3.5.3 Renormalization of gauge - fermion vertices

The form factors defined above will in general show UV-divergences, which have to be renormalized away. Looking at the tree-level Lagrangian, it is clear that at 1-loop it is not possible to write down counterterms for the scalar structure. Since the theory is renormalizable, the form factors multiplying these structures (in our case we only need to consider F_2 from the quark vertex) must therefore be UV-finite. This feature can be used as a first rough check of the consistency of the calculation.

3.5.3.1 Denner-scheme

In this section we therefore give the counterterms for the form factors f_1/F_1, starting with the Denner-scheme. As in the section about electric charge renormalization, we keep the fermion field ψ arbitrary (field renormalization eq. (2.70)), which allows to derive counterterms for lepton and quark vertices simultaneously. The bare vector and axial-vector couplings of the Z-boson to fermions are

$$v_f^0 = v_f + \delta v_f = v_f + \left(\frac{c_W^2 - s_W^2}{s_W^2}\, v_f + 2\,\frac{c_W}{s_W}\, Q_f\right)\delta Z_c + \mathcal{O}\left(\alpha^2\right),$$

$$a_f^0 = a_f + \delta a_f = a_f + a_f\,\frac{c_W^2 - s_W^2}{s_W^2}\,\delta Z_c + \mathcal{O}\left(\alpha^2\right). \tag{3.66}$$

The bare Lagrangian for the local Zff-interaction reads

$$\mathcal{L}^0_{Zff} = e_0 \bar{\psi}^0 Z^0_{\mu}\gamma^{\mu}(v_f^0 - a_f^0\gamma_5)\psi^0 = e_0(v_f^0 + a_f^0)\,\bar{\psi}^0_L Z^0_{\mu}\gamma^{\mu}\psi^0_L + e_0(v_f^0 - a_f^0)\,\bar{\psi}^0_R Z^0_{\mu}\gamma^{\mu}\psi^0_R. \tag{3.67}$$

Quite analogous to the mechanism seen in sec. 2.3.4, the ZA-mixing (eq. (2.55)) introduces an additional A-term into the Lagrangian

$$\delta\mathcal{L}^0_{Zff\to Aff} = e\,\frac{1}{2}\,\delta Z_{ZA}\left[(v_f + a_f)\,\bar{\psi}_L A_{\mu}\gamma^{\mu}\psi_L + (v_f - a_f)\,\bar{\psi}_R A_{\mu}\gamma^{\mu}\psi_R\right]. \tag{3.68}$$

For the renormalization of the Zff-vertex this term is not relevant (it will be needed for the Aff-vertex). Conversely there is a Zff-term coming from mixing in $\mathcal{L}^0_{Aff}$ (see eq. (2.72)). Including that term and expanding the renormalization constants we obtain the counterterm Lagrangian relevant for one-loop renormalization of the Zff-vertex,

$$\mathcal{L}^{\mathrm{ct}}_{Zff} = e\sum_{\eta=\pm}\left\{(v_f - \eta\, a_f)\Big(\delta Z_{\eta} + \delta Z_e + \frac{1}{2}\,\delta Z_{ZZ}\Big) + \delta v_f - \eta\,\delta a_f - Q_f\,\frac{1}{2}\,\delta Z_{AZ}\right\}\bar{\psi}\, Z_{\mu}\gamma^{\mu}\omega_{\eta}\psi, \tag{3.69}$$

with $\delta Z_- = \delta Z_L$ and $\delta Z_+ = \delta Z_R$. We replaced the chiral fields by the full Dirac fields by using the chiral projectors. For the Aff-vertex, applying the same strategy as above leads to the relevant counterterm Lagrangian (using eqs. (2.72), (3.68)),

$$\mathcal{L}^{\mathrm{ct}}_{Aff} = e\sum_{\eta=\pm}\left\{-Q_f\Big(\delta Z_{\eta} + \delta Z_e + \frac{1}{2}\,\delta Z_{AA}\Big) + (v_f - \eta\, a_f)\frac{1}{2}\,\delta Z_{ZA}\right\}\bar{\psi}\, A_{\mu}\gamma^{\mu}\omega_{\eta}\psi. \tag{3.70}$$

These Lagrangians turn into the counterterm Feynman rule

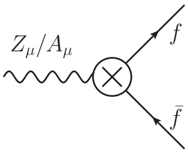

$$= ie\gamma^\mu \sum_{\eta=\pm} \delta F_1^{Zff/Aff,\eta}\, \omega_\eta, \tag{3.71}$$

with

$$\begin{aligned}
\delta F_1^{Zff,\eta} &= (v_f - \eta\, a_f)\left(\delta Z_\eta + \delta Z_e + \frac{1}{2}\,\delta Z_{ZZ} + \frac{c_W^2 - s_W^2}{s_W^2}\,\delta Z_c\right) - Q_f\left(\frac{1}{2}\,\delta Z_{AZ} - 2\,\frac{c_W}{s_W}\,\delta Z_c\right)\\
\delta F_1^{Aff,\eta} &= -Q_f\left(\delta Z_\eta + \delta Z_e + \frac{1}{2}\,\delta Z_{AA}\right) + (v_f - \eta\, a_f)\frac{1}{2}\,\delta Z_{ZA},
\end{aligned} \tag{3.72}$$

where we used eq. (3.66) to replace δv_f and δa_f. The counterterms in the VA-basis can be easily derived from the chiral expressions. In our notation, renormalized chiral form factors are obtained according to

$$\begin{aligned}
\hat{F}_1^{Zff,\eta}(q^2) &= F_1^{Zff,\eta}(q^2) + \delta F_1^{Zff,\eta},\\
\hat{F}_1^{Aff,\eta}(q^2) &= F_1^{Aff,\eta}(q^2) + \delta F_1^{Aff,\eta}.
\end{aligned} \tag{3.73}$$

3.5.3.2 BHS-scheme

In the BHS-scheme the vertex-counterterms show some small differences to the ones presented above. Using the renormalization constants including eq. (3.66) and expanding to one-loop order, we derive the relevant counterterm Lagrangians for the neutral current vertices

$$\begin{aligned}
\mathcal{L}_{Zff}^{\text{ct}} = e\sum_\eta \Big\{&(v_f - \eta\, a_f)\Big(\delta Z_\eta + \delta Z_e + \frac{1}{2}\,\delta Z_2^Z\Big) + \delta v_f - \eta\,\delta a_f - Q_f\left(\delta Z_1^{\gamma Z} - 2\,\delta Z_2^{\gamma Z}\right)\Big\} \times\\
&\times \bar{\psi}\, Z_\mu \gamma^\mu \omega_\eta \psi
\end{aligned} \tag{3.74}$$

$$\begin{aligned}
\mathcal{L}_{Aff}^{\text{ct}} = e\sum_\eta \Big\{&-Q_f\Big(\delta Z_\eta + \delta Z_e + \frac{1}{2}\,\delta Z_2^\gamma\Big) - (v_f - \eta\, a_f)\left(\delta Z_1^{\gamma Z} - \delta Z_2^{\gamma Z}\right)\Big\} \times\\
&\times \bar{\psi}\, A_\mu \gamma^\mu \omega_\eta \psi,
\end{aligned} \tag{3.75}$$

where $\delta Z_e, \delta Z_c$ are given by eq. (2.97). By comparing with eq. (3.69) we see that (since $\delta Z_{ZZ} \neq \delta Z_2^Z$ and $\frac{1}{2}\,\delta Z_{AZ} \neq \delta Z_1^{\gamma Z} - 2\delta Z_2^{\gamma Z}$) the counterterms will differ in finite parts, and that this difference will carry over to the renormalized Zff-vertex form factors. Contrary to this, comparison with eq. (3.70) shows that the counterterms for the Aff-vertices are the same in both schemes (using eqs. (2.116), (2.97)). This is not surprising of course, as the renormalization conditions for the photon residue and electric charge were chosen identical.

After simplifying the bosonic parts (the fermionic parts are the same as in the Denner-scheme) the BHS-counterterms read

$$\begin{aligned}
\delta F_1^{Zff,\eta} &= (v_f - \eta\, a_f)\Big[\delta Z_\eta + \Big(\delta Z_1^Z - \delta Z_2^Z\Big)\Big] + Q_f\Big(\delta Z_1^{\gamma Z} - \delta Z_2^{\gamma Z}\Big),\\
\delta F_1^{Aff,\eta} &= -Q_f\Big[\delta Z_\eta + \Big(\delta Z_1^\gamma - \delta Z_2^\gamma\Big)\Big] - (v_f - \eta\, a_f)\Big(\delta Z_1^{\gamma Z} - \delta Z_2^{\gamma Z}\Big).
\end{aligned} \tag{3.76}$$

The notation concerning the counterterm Feynman rule and the relation to the form factors is the same as in the Denner-scheme (eqs. (3.71), (3.73)). With eq. (2.118) it can be seen that the combinations $\delta Z_1^X - \delta Z_2^X \equiv (\delta Z_1 - \delta Z_2)^X$ take a very simple form:

$$\Big(\delta Z_1 - \delta Z_2\Big)^{\{\gamma,\gamma Z,Z\}} = \left\{\frac{s_W}{c_W}, 1, \frac{c_W}{s_W}\right\} \frac{\Pi_{ZA}^T(0)}{M_Z^2}, \tag{3.77}$$

where $\Pi^T_{ZA}(0)$ itself is a very simple expression

$$\frac{\Pi^T_{ZA}(0)}{M_Z^2} = -\frac{c_W}{2s_W}\left\{(\xi_W+3)\left(\frac{1}{\epsilon}+\ln\left(\frac{\mu^2}{M_W^2}\right)\right)+\frac{1}{2}(\xi_W+5)-\frac{\xi_W(\xi_W+2)}{\xi_W-1}\ln(\xi_W)\right\} = -\frac{1}{2}\,\delta Z_{ZA}. \quad (3.78)$$

Eq. (3.78) has the very convenient feature that it contains no fermion contributions at all (irrespective of the fermions mass or couplings), as can be seen from the generic expression (app. E) when evaluated[19] for $p^2 = 0$. This allows for very transparent bookkeeping, as the discussion of fermionic loops can be shifted to the oblique corrections entirely (cf. sec. 3.4).

Apart from this specific detail the more general point also applying to the bosonic loops is that most of the renormalization constants needed to renormalize a specific building block like amputated vertices or oblique corrections will cancel between those when they are added up to form the total amplitude. The BHS-scheme has the convenient advantage to make this feature manifest from the start, resulting in much simpler local counterterm expressions than the Denner-scheme, which greatly benefits our analytic approach. If one is just interested in numerics, the Denner-scheme might be the better choice as its renormalization constants are obtained in a more naive, but at the same time much more straightforward fashion. In ch. 4 we will take a look at the minimal amount of renormalization constants needed to renormalize the complete amplitude $\mathcal{M}(e^+e^- \to t\bar{t})$ at EW 1-loop. In that chapter we will also explore how the UV-cancellations work within the building blocks in more detail.

3.5.4 Connecting to chiral amplitude basis

The one-loop contributions of the vertices to the amplitude $\mathcal{M}^\kappa$ are constructed straightforwardly

$$\begin{aligned}
\big(\mathcal{M}_\kappa^{(1)}\big)_{\text{vertex}} = \frac{4\pi\alpha}{s}\sum_{\rho=\pm}\Bigg\{\Bigg[&\Big(\hat{F}_1^{Ztt,\rho}(s)\big(v_e-\kappa\, a_e\big)+\big(v_t-\rho\, a_t\big)\hat{f}_1^{Zee,\kappa}(s)\Big)\,\chi^{(0)}(s)+\\
&+\hat{F}_1^{Att,\rho}(s)(-Q_e)+(-Q_t)\hat{f}_1^{Aee,\kappa}(s)\Bigg]\,\bar{M}_1^{\rho\kappa}+\\
&+\Bigg[\hat{F}_2^{Ztt,\rho}(s)\,(v_e-\kappa\, a_e)\,\chi^{(0)}(s)+\hat{F}_2^{Att,\rho}(s)(-Q_e)\Bigg]\,\bar{M}_2^{\rho\kappa},
\end{aligned} \quad (3.79)$$

so by reading off

$$\begin{aligned}
\frac{1}{4\pi}\,\big(\bar{c}_1^{(1),\rho\kappa}\big)_{\text{vertex}} &= \Big(\hat{F}_1^{Ztt,\rho}(s)\big(v_e-\kappa\, a_e\big)+\big(v_t-\rho\, a_t\big)\hat{f}_1^{Zee,\kappa}(s)\Big)\,\chi^{(0)}(s)+\\
&\quad+\hat{F}_1^{Att,\rho}(s)(-Q_e)+(-Q_t)\hat{f}_1^{Aee,\kappa}(s),\\
\frac{1}{4\pi}\,\big(\bar{c}_2^{(1),\rho\kappa}\big)_{\text{vertex}} &= \hat{F}_2^{Ztt,\rho}(s)\,(v_e-\kappa\, a_e)\,\chi^{(0)}(s)+\hat{F}_2^{Att,\rho}(s)(-Q_e).
\end{aligned} \quad (3.80)$$

If the amplitude is decomposed into the VA-basis, its easiest to translate the (renormalized) form factors, i.e.

$$\begin{aligned}
\hat{\Xi}^\alpha_{\text{rad}}(q^2) &= \gamma^\alpha\Big(\big[\hat{F}_1^V(q^2)-\hat{F}_1^A(q^2)\big]\,\omega_-+\big[\hat{F}_1^V(q^2)+\hat{F}_1^A(q^2)\big]\,\omega_+\Big)+F_2^V(q^2)\frac{(q_1-q_2)^\alpha}{m_t}(\omega_-+\omega_+),\\
\hat{\Lambda}^\beta_{\text{rad}}(q^2) &= \gamma^\beta\Big(\big[\hat{f}_1^V(q^2)-\hat{f}_1^A(q^2)\big]\omega_-+\big[\hat{f}_1^V(q^2)+\hat{f}_1^A(q^2)\big]\omega_+\Big),
\end{aligned} \quad (3.81)$$

when the vertex contribution is written as

$$\big(\mathcal{M}_\kappa^{(1)}\big)_{\text{vertex}} =$$

[19]Note that for the photon residue the quantity $\Pi^T_{AA}(p^2)$, which would also vanish for $p^2 = 0$, needs to be divided by p^2 first before taking the on-shell limit. $\Pi^T_{AA}(0) = 0$ is the Ward identity mentioned in chapter 2, keeping the photon mass $m_A = 0$.

$$= \frac{4\pi\alpha}{s} \sum_{\rho=\pm} \Bigg\{ \Bigg[\Big(\big[\hat{F}_1^{Ztt,V}(s) + \rho\, \hat{G}_1^{Ztt,A}(s)\big] \big(v_e - \kappa\, a_e\big) + \big(v_t - \rho\, a_t\big) \big[\hat{f}_1^{Zee,V}(s) + \kappa\, \hat{f}_1^{Zee,A}(s)\big] \Big)\, \chi^{(0)}(s) +$$

$$+ \big[\hat{F}_1^{Att,V}(s) + \rho\, \hat{F}_1^{Att,A}(s)\big](-Q_e) + (-Q_t)\big[\hat{f}_1^{Aee,V}(s) + \kappa\, \hat{f}_1^{Aee,A}(s)\big] \Bigg] \bar{M}_1^{\rho\kappa} +$$

$$+ \Bigg[\hat{F}_2^{Ztt,V}(s)\,(v_e - \kappa\, a_e)\; \chi^{(0)}(s) + \hat{F}_2^{Att,V}(s)(-Q_e) \Bigg] \bar{M}_2^{\rho\kappa}. \tag{3.82}$$

Again the $\left(\bar{c}_i^{\rho\kappa}\right)_{\text{vertex}}$ can be read off straightforwardly.

3.5.5 EW-contributions to vertex corrections

The (unrenormalized) loop corrections to both final- and initial-state vertices with amputated gauge boson (Z or A) are shown in the tables 3.5-3.8. The diagram sets can be found in the appendix G. The tables are read in complete analogy to the bosonic transitions in sec. 3.4.4, a crash-course on how to interpret the entries is found there as well. The only novelty is that the **type**-entry now has a subscript: c for *charged* diagram (indicating that the virtual fermion is a bottom quark of mass 0) or n for *neutral* diagram (indicating that the virtual fermion is a top quark of mass m_t). For the initial-state diagrams there is no need to distinguish, as all fermions are massless, so there is no additional subscript.

$Zt\bar{t}$	type	g_X	g_f	$g_{\bar{f}}$	M, M_1, M_V	M_2, M_S	ξ
ttZ	$(ffV)_n$	$v_t - \eta\, a_t$	$v_t - \eta\, a_t$	$v_t - \eta\, a_t$	M_Z	$-$	ξ_Z
bbW	$(ffV)_c$	$v_b - \eta\, a_b$	$\frac{1}{\sqrt{2}s_W}\,\delta_{\eta,-1}$	$\frac{1}{\sqrt{2}s_W}\,\delta_{\eta,-1}$	M_W	$-$	ξ_W
ttH	$(ffS)_n$	$v_t - \eta\, a_t$	$-\frac{m_t}{2s_W M_W}$	$-\frac{m_t}{2s_W M_W}$	M_H	$-$	$-$
$tt\chi$	$(ffS)_n$	$v_t - \eta\, a_t$	$\eta\frac{i\,m_t}{2s_W M_W}$	$\eta\frac{i\,m_t}{2s_W M_W}$	$M_Z\sqrt{\xi_Z}$	$-$	$-$
$bb\phi$	$(ffS)_c$	$v_b - \eta\, a_b$	$\frac{m_t}{\sqrt{2}s_W M_W}\,\delta_{\eta,-1}$	$\frac{m_t}{\sqrt{2}s_W M_W}\,\delta_{\eta,1}$	$M_W\sqrt{\xi_W}$	$-$	$-$
bWW	$(fVV)_c$	$-\frac{c_W}{s_W}$	$\frac{1}{\sqrt{2}s_W}\,\delta_{\eta,-1}$	$\frac{1}{\sqrt{2}s_W}\,\delta_{\eta,-1}$	M_W	$-$	ξ_W
tZH	$(fVS)_n$	$\frac{1}{c_W^2 s_W}\,M_W$	$v_t - \eta\, a_t$	$-\frac{m_t}{2s_W M_W}$	M_Z	M_H	ξ_Z
tHZ	$(fSV)_n$	$\frac{1}{c_W^2 s_W}\,M_W$	$-\frac{m_t}{2s_W M_W}$	$v_t - \eta\, a_t$	M_Z	M_H	ξ_Z
$bW\phi$	$(fVS)_c$	$-\frac{s_W}{c_W}\,M_W$	$\frac{1}{\sqrt{2}s_W}\,\delta_{\eta,-1}$	$\frac{m_t}{\sqrt{2}s_W M_W}\,\delta_{\eta,1}$	M_W	$M_W\sqrt{\xi_W}$	ξ_W
$b\phi W$	$(fSV)_c$	$-\frac{s_W}{c_W}\,M_W$	$\frac{m_t}{\sqrt{2}s_W M_W}\,\delta_{\eta,-1}$	$\frac{1}{\sqrt{2}s_W}\,\delta_{\eta,-1}$	M_W	$M_W\sqrt{\xi_W}$	ξ_W
$tH\chi$	$(fSS)_n$	$-\frac{i}{2c_W s_W}$	$-\frac{m_t}{2s_W M_W}$	$\eta\frac{i\,m_t}{2s_W M_W}$	M_H	$M_Z\sqrt{\xi_Z}$	$-$
$t\chi H$	$(fSS)_n$	$\frac{i}{2c_W s_W}$	$\eta\frac{i\,m_t}{2s_W M_W}$	$-\frac{m_t}{2s_W M_W}$	$M_Z\sqrt{\xi_Z}$	M_H	$-$
$b\phi\phi$	$(fSS)_c$	$\frac{c_W^2 - s_W^2}{2c_W s_W}$	$\frac{m_t}{2s_W M_W}\,\delta_{\eta,-1}$	$\frac{m_t}{2s_W M_W}\,\delta_{\eta,1}$	$M_W\sqrt{\xi_W}$	$M_W\sqrt{\xi_W}$	$-$

Table 3.5: $Zt\bar{t}$-vertex: the virtual particle content is shown in the leftmost column. **type** refers to type in sec. E, with the subscript denoting charged or neutral diagram. η is the chirality index placeholder, and $m = m_t$.

$At\bar{t}$	**type**	g_X	g_f	$g_{\bar{f}}$	M, M_1, M_V	M_2, M_S	ξ
ttZ	$(ffV)_n$	$-Q_t$	$v_t - \eta\, a_t$	$v_t - \eta\, a_t$	M_Z	$-$	ξ_Z
bbW	$(ffV)_c$	$-Q_b$	$\frac{1}{\sqrt{2}s_W}\,\delta_{\eta,-1}$	$\frac{1}{\sqrt{2}s_W}\,\delta_{\eta,-1}$	M_W	$-$	ξ_W
ttH	$(ffS)_n$	$-Q_t$	$-\frac{m_t}{2s_W M_W}$	$-\frac{m_t}{2s_W M_W}$	M_H	$-$	$-$
$tt\chi$	$(ffS)_n$	$-Q_t$	$\eta\frac{i\,m_t}{2s_W M_W}$	$\eta\frac{i\,m_t}{2s_W M_W}$	$M_Z\sqrt{\xi_Z}$	$-$	$-$
$bb\phi$	$(ffS)_c$	$-Q_b$	$\frac{m_t}{\sqrt{2}s_W M_W}\,\delta_{\eta,-1}$	$\frac{m_t}{\sqrt{2}s_W M_W}\,\delta_{\eta,1}$	$M_W\sqrt{\xi_W}$	$-$	$-$
bWW	$(fVV)_c$	1	$\frac{1}{\sqrt{2}s_W}\,\delta_{\eta,-1}$	$\frac{1}{\sqrt{2}s_W}\,\delta_{\eta,-1}$	M_W	$-$	ξ_W
$bW\phi$	$(fVS)_c$	$-M_W$	$\frac{1}{\sqrt{2}s_W}\,\delta_{\eta,-1}$	$\frac{m_t}{\sqrt{2}s_W M_W}\,\delta_{\eta,1}$	M_W	$M_W\sqrt{\xi_W}$	ξ_W
$b\phi W$	$(fSV)_c$	$-M_W$	$\frac{m_t}{\sqrt{2}s_W M_W}\,\delta_{\eta,-1}$	$\frac{1}{\sqrt{2}s_W}\,\delta_{\eta,-1}$	M_W	$M_W\sqrt{\xi_W}$	ξ_W
$b\phi\phi$	$(fSS)_c$	-1	$\frac{m_t}{2s_W M_W}\,\delta_{\eta,-1}$	$\frac{m_t}{2s_W M_W}\,\delta_{\eta,1}$	$M_W\sqrt{\xi_W}$	$M_W\sqrt{\xi_W}$	$-$

Table 3.6: $At\bar{t}$-vertex: the virtual particle content is shown in the leftmost column. **type** refers to type in sec. E, with the subscript denoting charged or neutral diagram. η is the chirality index placeholder, and $m = m_t$.

$Ze\bar{e}$	**type**	g_X	g_f	$g_{\bar{f}}$	M, M_1, M_V	M_2, M_S	ξ
eeZ	llV	$v_e - \eta\, a_e$	$v_e - \eta\, a_e$	$v_e - \eta\, a_e$	M_Z	$-$	ξ_Z
$\nu\nu W$	llV	$v_\nu - \eta\, a_\nu$	$\frac{1}{\sqrt{2}s_W}\,\delta_{\eta,-1}$	$\frac{1}{\sqrt{2}s_W}\,\delta_{\eta,-1}$	M_W	$-$	ξ_W
νWW	lVV	$-\frac{c_W}{s_W}$	$\frac{1}{\sqrt{2}s_W}\,\delta_{\eta,-1}$	$\frac{1}{\sqrt{2}s_W}\,\delta_{\eta,-1}$	M_W	$-$	ξ_W

Table 3.7: $Ze\bar{e}$-vertex: the virtual particle content is shown in the leftmost column. **type** refers to type in sec. E. η is the chirality index placeholder.

$Ae\bar{e}$	**type**	g_X	g_f	$g_{\bar{f}}$	M, M_1, M_V	M_2, M_S	ξ
eeZ	llV	$-Q_e$	$v_e - \eta\, a_e$	$v_e - \eta\, a_e$	M_Z	$-$	ξ_Z
νWW	lVV	1	$\frac{1}{\sqrt{2}s_W}\,\delta_{\eta,-1}$	$\frac{1}{\sqrt{2}s_W}\,\delta_{\eta,-1}$	M_W	$-$	ξ_W

Table 3.8: $Ae\bar{e}$-vertex: the virtual particle content is shown in the leftmost column. **type** refers to type in sec. E. η is the chirality index placeholder.

3.6 Boxes

Finally we turn to box diagrams. They are advantageous in the sense that they are free of UV-divergences, so no renormalization has to be performed here. This comes at the price of increased technical challenge when computing them, but fortunately there are two simplifications that ease the task somewhat:

- Since we neglect the initial-state lepton masses, we need not consider any boxes with virtual scalar particles, as they are Yukawa-suppressed due to the initial-state scalar-fermion couplings.
- We will restrict ourselves to weak box diagrams and neglect the QED boxes with internal photon lines (this especially includes the ZA-boxes). This way we avoid having to calculate 3-body final state contributions to cancel IR-divergences. The reason that neglecting this type of diagrams is that they form gauge-invariant subsets (cf. sec. 4.3).

There are 2 ways we will compute the box diagrams. Firstly there are projection operators available that can be traced into the numerator structure to project out the form factors. This procedure is straightforward, and we give the results in sec. 3.6.3 with the help of the generic expressions in the appendix E. The second way relies on a brute-force reduction of the Dirac- and Lorentz-structure in combination with successive PV-reduction. A downside of this procedure is that the calculation ends up in the Beenakker-basis eq. (3.7), while the projection operators are designed so that one immediately targets the minimal basis eq. (3.8). For completeness, we nevertheless explicitly show the brute-force calculation (in Feynman gauge) in some detail in the following sections.

3.6.1 Notational setup

The box contributions can be decomposed into form factors at the level of the amplitude that contribute 1:1 to the $c^{\rho\kappa}$ in eq. (3.10). We write

$$\left(\mathcal{M}_\kappa^{(1)}\right)_{\text{box}} = \frac{\alpha}{s} \sum_{i=1}^{4} \sum_{\rho=\pm} \left(\bar{c}_i^{(1),\rho\kappa}\right)_{\text{box}} \bar{M}_i^{\rho\kappa} \tag{3.83}$$

We point out that although we sum over the initial-state chirality κ in the calculation below, due to the chiral symmetry of the initial-state the final expressions will be also valid for fixed chirality (helicity) κ. To obtain those simply drop the corresponding sum. There exist two topologies for one-loop box diagrams with two (massive) virtual s-channel gauge bosons: *direct* and *crossed* diagrams, shown in fig. 3.6. We do not introduce any further parametrization, but compute both direct and crossed box in a

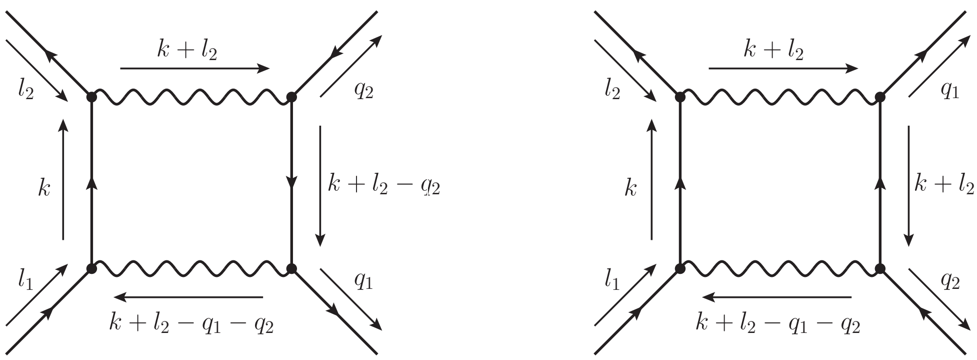

Figure 3.6: Momentum flow conventions for direct and crossed box type.

brute-force manner. Since we will be interested in both WW- and ZZ-boxes, we keep the s-channel bosons as well as the fermion-boson couplings generic, where

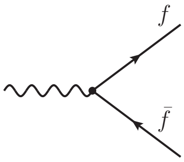

$$= ie\,\gamma^\mu \left(g_f^- \,\omega_- + g_f^+ \,\omega_+\right) = ie\,\gamma^\mu \sum_{\eta=\pm} g_f^\eta \,\omega_\eta. \tag{3.84}$$

Below we will distinguish the couplings according to the external fermion type, and denote incoming/outgoing antifermion couplings with a bar on top of f: $g^{\eta}_{\bar{f}}$.

It is also advisable to switch to generic momentum notation (see fig. 3.7). Conventionally identify-

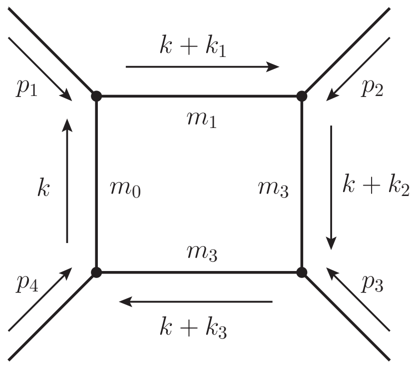

Figure 3.7: Momentum flow and internal mass conventions for generic 4-point diagrams.

ing $p_1 \equiv l_2$, these momenta are then related according to

$$\begin{aligned} k_1 &= p_1 = l_2, \\ k_2 &= p_1 + p_2 = l_2 + \begin{cases} -q_1 & \text{(crossed)} \\ -q_2 & \text{(direct)} \end{cases}, \\ k_3 &= p_1 + p_2 + p_3 = l_2 - q_1 - q_2. \end{aligned} \tag{3.85}$$

It is also useful to construct generic Mandelstam invariants defined by

$$\begin{aligned} \bar{s} &\equiv (p_1+p_2)^2 = (p_3+p_4)^2, \\ \bar{t} &\equiv (p_1+p_3)^2 = (p_2+p_4)^2, \\ \bar{u} &\equiv (p_1+p_4)^2 = (p_2+p_3)^2, \end{aligned} \tag{3.86}$$

Depending on whether the integral in eq. (3.96) is used for the crossed or direct box, the generic Mandelstam invariants correspond to different "real" Mandelstam invariants, as the generic momentum p_2 is different for the two cases[20] (see tab. 3.9).

	$\bar{s}$	$\bar{t}$	$\bar{u}$
crossed	u	t	s
direct	t	u	s

Table 3.9: Mandelstam invariants used in this chapter for the calculation of both box types.

3.6.2 Explicit calculation of crossed and direct boxes

Applying the usual Feynman rules and multiplying out the full expression (assuming massless initial state leptons and final state fermions of mass m_f) both type of boxes read[21]

$$i\mathcal{M}^{\text{crossed}}_{\text{VV-box}} = \alpha^2 \left\{ - \int \frac{d^4k}{i\pi^2} \frac{k_{\beta_2}(k+k_2)_{\alpha_2}}{N^c_0 N^c_2} \left(\gamma^{\alpha_1} \left[g^-_f\, \omega_- + g^+_f\, \omega_+ \right] \gamma^{\alpha_2}\gamma^{\alpha_3} \left[g^-_{\bar{f}}\, \omega_- + g^+_{\bar{f}}\, \omega_+ \right] \right) \otimes \right.$$

[20]For both types, the square of p_2 is the same in our case however, since $p_2^2 = q_1^2 = q_2^2 = m_t^2$, as we have a top pair in the final state.

[21]Note the different conventions for the k_i depending on the box type.

$$
\Big(\gamma^{\beta_1}\left[g_{\bar{l}}^{-}\,\omega_- + g_{\bar{l}}^{+}\,\omega_+\right]\gamma^{\beta_2}\gamma^{\beta_3}\left[g_l^{-}\,\omega_- + g_l^{+}\,\omega_+\right]\Big)+
$$

$$
+\int\frac{d^4k}{i\pi^2}\,\frac{m_2\,k_{\beta_2}}{N_0^cN_2^c}\Big(\gamma^{\alpha_1}\left[g_f^{-}\,\omega_- + g_f^{+}\,\omega_+\right]\gamma^{\alpha_3}\left[g_{\bar{f}}^{-}\,\omega_- + g_{\bar{f}}^{+}\,\omega_+\right]\Big)\otimes
$$

$$
\Big(\gamma^{\beta_1}\left[g_{\bar{l}}^{-}\,\omega_- + g_{\bar{l}}^{+}\,\omega_+\right]\gamma^{\beta_2}\gamma^{\beta_3}\left[g_l^{-}\,\omega_- + g_l^{+}\,\omega_+\right]\Big)\Big\}\times,
$$

$$
\times\left[\frac{1}{N_1^c}\,g_{\alpha_1\beta_1}+\left(\frac{1}{\tilde{N}_1^c}-\frac{1}{N_1^c}\right)\frac{(k+k_1)_{\alpha_1}(k+k_1)_{\beta_1}}{m_1^2}\right]\times,
$$

$$
\times\left[\frac{1}{N_3^c}\,g_{\alpha_3\beta_3}+\left(\frac{1}{\tilde{N}_3^c}-\frac{1}{N_3^c}\right)\frac{(k+k_3)_{\alpha_3}(k+k_3)_{\beta_3}}{m_3^2}\right],
$$

$$
i\mathcal{M}_{\text{VV-box}}^{\text{direct}} = \alpha^2\Big\{\int\frac{d^4k}{i\pi^2}\,\frac{k_{\beta_2}(k+k_2)_{\alpha_2}}{N_0^dN_2^d}\Big(\gamma^{\alpha_3}\left[g_f^{-}\,\omega_- + g_f^{+}\,\omega_+\right]\gamma^{\alpha_2}\gamma^{\alpha_1}\left[g_{\bar{f}}^{-}\,\omega_- + g_{\bar{f}}^{+}\,\omega_+\right]\Big)\otimes
$$

$$
\Big(\gamma^{\beta_1}\left[g_{\bar{l}}^{-}\,\omega_- + g_{\bar{l}}^{+}\,\omega_+\right]\gamma^{\beta_2}\gamma^{\beta_3}\left[g_l^{-}\,\omega_- + g_l^{+}\,\omega_+\right]\Big)+
$$

$$
+\int\frac{d^4k}{i\pi^2}\,\frac{m_2\,k_{\beta_2}}{N_0^dN_2^d}\Big(\gamma^{\alpha_3}\left[g_f^{-}\,\omega_- + g_f^{+}\,\omega_+\right]\gamma^{\alpha_1}\left[g_{\bar{f}}^{-}\,\omega_- + g_{\bar{f}}^{+}\,\omega_+\right]\Big)\otimes
$$

$$
\Big(\gamma^{\beta_1}\left[g_{\bar{l}}^{-}\,\omega_- + g_{\bar{l}}^{+}\,\omega_+\right]\gamma^{\beta_2}\gamma^{\beta_3}\left[g_l^{-}\,\omega_- + g_l^{+}\,\omega_+\right]\Big)\Big\}\times,
$$

$$
\times\left[\frac{1}{N_1^d}\,g_{\alpha_1\beta_1}+\left(\frac{1}{\tilde{N}_1^d}-\frac{1}{N_1^d}\right)\frac{(k+k_1)_{\alpha_1}(k+k_1)_{\beta_1}}{m_1^2}\right]\times,
$$

$$
\times\left[\frac{1}{N_3^d}\,g_{\alpha_3\beta_3}+\left(\frac{1}{\tilde{N}_3^d}-\frac{1}{N_3^d}\right)\frac{(k+k_3)_{\alpha_3}(k+k_3)_{\beta_3}}{m_3^2}\right], \tag{3.87}
$$

where again we adopted the shorthand notation of eq. (3.3), and the momentum convention of fig. 3.6, and

$$
\begin{aligned}
N_0^{c,d} &= k^2 - m_0^2 + i0^+, & & \\
N_1^{c,d} &= (k+k_1)^2 - m_1^2 + i0^+, & \tilde{N}_1^{c,d} &= (k+k_1)^2 - \xi_1 m_1^2 + i0^+, \\
N_2^{c,d} &= (k+k_2)^2 - m_2^2 + i0^+, & & \\
N_3^{c,d} &= (k+k_3)^2 - m_3^2 + i0^+, & \tilde{N}_3^{c,d} &= (k+k_3)^2 - \xi_3 m_3^2 + i0^+.
\end{aligned} \tag{3.88}
$$

For the respective box type, the correct expressions for the momenta k_i according to eq. (3.85) have to be inserted. Using anticommutators we note

$$
\begin{aligned}
\gamma^{\alpha_1}\left[g_f^{-}\,\omega_- + \gamma_f^{+}\,\omega_+\right]\gamma^{\alpha_2}\gamma^{\alpha_3}\left[g_{\bar{f}}^{-}\,\omega_- + g_{\bar{f}}^{+}\,\omega_+\right] &= \gamma^{\alpha_1}\gamma^{\alpha_2}\gamma^{\alpha_3}\sum_{\rho=\pm} g_f^{\rho}\,g_{\bar{f}}^{\rho}\,\omega_\rho, \\
\gamma^{\alpha_1}\left[g_f^{-}\,\omega_- + g_f^{+}\,\omega_+\right]\gamma^{\alpha_3}\left[g_{\bar{f}}^{-}\,\omega_- + g_{\bar{f}}^{+}\,\omega_+\right] &= \gamma^{\alpha_1}\gamma^{\alpha_3}\sum_{\rho=\pm} g_f^{-\rho}\,g_{\bar{f}}^{\rho}\,\omega_\rho,
\end{aligned} \tag{3.89}
$$

with analogous relations for the lepton part and the terms of the direct box. The integrals simplify to

$$
i\mathcal{M}_{\text{VV-box}}^{\text{crossed}} = \alpha^2\Big\{-\int\frac{d^4k}{i\pi^2}\,\frac{k_{\beta_2}(k+k_2)_{\alpha_2}}{N_0^cN_2^c}\sum_{\rho,\kappa=\pm} g_l^{\kappa}\,g_{\bar{l}}^{\kappa}\,g_f^{\rho}\,g_{\bar{f}}^{\rho}\Big[\gamma^{\alpha_1}\gamma^{\alpha_2}\gamma^{\alpha_3}\omega_\rho\otimes\gamma^{\beta_1}\gamma^{\beta_2}\gamma^{\beta_3}\,\omega_\kappa\Big]+
$$

$$
+\,m_2\int\frac{d^4k}{i\pi^2}\,\frac{k_{\beta_2}}{N_0^cN_2^c}\sum_{\rho,\kappa=\pm} g_l^{\kappa}\,g_{\bar{l}}^{\kappa}\,g_f^{-\rho}\,g_{\bar{f}}^{\rho}\Big[\gamma^{\alpha_1}\gamma^{\alpha_3}\omega_\rho\otimes\gamma^{\beta_1}\gamma^{\beta_2}\gamma^{\beta_3}\,\omega_\kappa\Big]\Big\}\times,
$$

$$\times\left[\frac{1}{N_1^c}\,g_{\alpha_1\beta_1}+\left(\frac{1}{\tilde{N}_1^c}-\frac{1}{N_1^c}\right)\frac{(k+k_1)_{\alpha_1}(k+k_1)_{\beta_1}}{m_1^2}\right]\times,$$
$$\times\left[\frac{1}{N_3^c}\,g_{\alpha_3\beta_3}+\left(\frac{1}{\tilde{N}_3^c}-\frac{1}{N_3^c}\right)\frac{(k+k_3)_{\alpha_3}(k+k_3)_{\beta_3}}{m_3^2}\right],$$

$$\begin{aligned}
i\mathcal{M}^{\text{direct}}_{\text{VV-box}} = \alpha^2\Bigg\{&\int\frac{d^4k}{i\pi^2}\,\frac{k_{\beta_2}(k+k_2)_{\alpha_2}}{N_0^dN_2^d}\sum_{\rho,\kappa=\pm} g_l^\kappa\,g_{\bar{l}}^\kappa g_f^\rho\,g_{\bar{f}}^\rho\Big[\gamma^{\alpha_3}\gamma^{\alpha_2}\gamma^{\alpha_1}\omega_\rho\otimes\gamma^{\beta_1}\gamma^{\beta_2}\gamma^{\beta_3}\,\omega_\kappa\Big]+\\
&+m_2\int\frac{d^4k}{i\pi^2}\,\frac{k_{\beta_2}}{N_0^dN_2^d}\sum_{\rho,\kappa=\pm} g_l^\kappa\,g_{\bar{l}}^\kappa g_f^{-\rho}\,g_{\bar{f}}^\rho\Big[\gamma^{\alpha_3}\gamma^{\alpha_1}\omega_\rho\otimes\gamma^{\beta_1}\gamma^{\beta_2}\gamma^{\beta_3}\,\omega_\kappa\Big]\Bigg\}\times,\\
&\times\left[\frac{1}{N_1^d}\,g_{\alpha_1\beta_1}+\left(\frac{1}{\tilde{N}_1^d}-\frac{1}{N_1^d}\right)\frac{(k+k_1)_{\alpha_1}(k+k_1)_{\beta_1}}{m_1^2}\right]\times,\\
&\times\left[\frac{1}{N_3^d}\,g_{\alpha_3\beta_3}+\left(\frac{1}{\tilde{N}_3^d}-\frac{1}{N_3^d}\right)\frac{(k+k_3)_{\alpha_3}(k+k_3)_{\beta_3}}{m_3^2}\right].
\end{aligned}\tag{3.90}$$

By using the important relation

$$\gamma^\mu\gamma^\alpha\gamma^\nu = g^{\mu\alpha}\gamma^\nu+\gamma^{\alpha\nu}\gamma^\mu-\gamma^{\mu\nu}\gamma^\alpha+i\varepsilon^{\mu\alpha\nu\sigma}\gamma_\sigma\gamma_5,\tag{3.91}$$

we find[22]

$$\begin{aligned}
\gamma^\mu\gamma^\alpha\gamma^\nu\omega_\rho\otimes\gamma_\mu\gamma_\beta\gamma_\nu\,\omega_\kappa &= 4\Big(\delta^\rho_\kappa\,\delta^\alpha_\beta\,\gamma^\mu\omega_\rho\otimes\gamma_\mu\,\omega_\kappa+\delta^\rho_{-\kappa}\,\gamma_\beta\,\omega_\rho\otimes\gamma^\alpha\omega_\kappa\Big)\\
\gamma^\nu\gamma^\alpha\gamma^\mu\omega_\rho\otimes\gamma_\mu\gamma_\beta\gamma_\nu\,\omega_\kappa &= 4\Big(\delta^\rho_{-\kappa}\,\delta^\alpha_\beta\,\gamma^\mu\omega_\rho\otimes\gamma_\mu\,\omega_\kappa+\delta^\rho_{\kappa}\,\gamma_\beta\,\omega_\rho\otimes\gamma^\alpha\omega_\kappa\Big)\\
\gamma^\mu\gamma^\nu\omega_\rho\otimes\gamma_\mu\gamma_\beta\gamma_\nu\,\omega_\kappa &= -2\,\omega_\rho\otimes\gamma_\beta\,\omega_\kappa-\rho\,\kappa\,(-2i)\,\sigma_{\beta\mu}\omega_\rho\otimes\gamma^\mu\omega_\kappa,\\
\gamma^\nu\gamma^\mu\omega_\rho\otimes\gamma_\mu\gamma_\beta\gamma_\nu\,\omega_\kappa &= -2\,\omega_\rho\otimes\gamma_\beta\,\omega_\kappa+\rho\,\kappa\,(-2i)\,\sigma_{\beta\mu}\omega_\rho\otimes\gamma^\mu\omega_\kappa,
\end{aligned}\tag{3.92}$$

where we used $\gamma^\mu\gamma^\nu=\frac{1}{2}\left[2g^{\mu\nu}+(-2i)\sigma^{\mu\nu}\right]$, and $\sigma_{\mu\nu}\gamma_5=\frac{i}{2}\,\varepsilon_{\mu\nu\alpha\beta}\,\sigma^{\alpha\beta}$. In the last two expression we also made use of the identity $\gamma_5\omega_\eta=\eta\,\omega_\eta$. Plugging in these simplifications and adopting shortcuts for the 4-point tensor integrals[23]

$$\begin{aligned}
(D^{c,d})^\beta_\alpha &= \int\frac{d^4k}{i\pi^2}\,\frac{k_\alpha k^\beta}{N_1^{c,d}N_2^{c,d}N_3^{c,d}N_4^{c,d}},\\
(D^{c,d})^\beta &= \int\frac{d^4k}{i\pi^2}\,\frac{k^\beta}{N_1^{c,d}N_2^{c,d}N_3^{c,d}N_4^{c,d}},
\end{aligned}\tag{3.93}$$

where the superscript c,d denotes crossed/direct box respectively, we are left with

$$\begin{aligned}
&i\mathcal{M}^{\text{crossed/direct}}_{\text{VV-box}} =\\
&= i\alpha^2\Bigg\{\mp 4\left[(D^{c,d})^\beta_\alpha+k_{2,\alpha}(D^{c,d})^\beta\right]\sum_{\rho,\kappa=\pm1} g_l^\kappa\,g_{\bar{l}}^\kappa\,g_f^\rho\,g_{\bar{f}}^\rho\Big(\delta^\rho_{\pm\kappa}\,\delta^\alpha_\beta\,\gamma^\mu\omega_\rho\otimes\gamma_\mu\,\omega_\kappa+\delta^\rho_{\mp\kappa}\,\gamma_\beta\,\omega_\rho\otimes\gamma^\alpha\omega_\kappa\Big)+\\
&\qquad -m_2\,(D^c)^\beta\sum_{\rho,\kappa=\pm1} g_l^\kappa\,g_{\bar{l}}^\kappa\,g_f^{-\rho}\,g_{\bar{f}}^\rho\Big(2\,\omega_\rho\otimes\gamma_\beta\,\omega_\kappa\mp\rho\,\kappa\,(-2i)\,\sigma_{\mu\beta}\omega_\rho\otimes\gamma^\mu\omega_\kappa\Big)\Bigg\}.
\end{aligned}\tag{3.94}$$

To make notation as compact as possible, we combined the two types into one symbolic expression. Upper/lower signs correspond to the crossed/direct box respectively.

[22] Mixed type of indices for chirality again only for better readability.

[23] Note that these integrals (including prefactors) are usually defined in $d=4-2\varepsilon$ dimensions, but as we do not encounter any UV- or IR-divergences here that need regularization, we simplify to $d=4$ immediately.

Now things get serious, as we have to plug in the PV-decompositions for $(D^{c,d})^\beta$ and $(D^{c,d})^\beta_\alpha$. These decompositions are usually done in terms of the virtual momenta k_i (see fig. 3.7), that is (cf. appendix B)

$$\begin{aligned}
(D^{c,d})^\mu &= k_1^\mu D_1^{c,d} + k_2^\mu D_2^{c,d} + k_3^\mu D_3^{c,d}, \\
(D^{c,d})^{\mu\nu} &= g^{\mu\nu} D_{00}^{c,d} + k_1^\mu k_1^\nu D_{11}^{c,d} + k_2^\mu k_2^\nu D_{22}^{c,d} + k_3^\mu k_3^\nu D_{33}^{c,d} + \\
&\quad + (k_1^\mu k_2^\nu + k_1^\nu k_2^\mu) D_{12}^{c,d} + (k_1^\mu k_3^\nu + k_1^\nu k_3^\mu) D_{13}^{c,d} + (k_2^\mu k_3^\nu + k_2^\nu k_3^\mu) D_{23}^{c,d}.
\end{aligned} \tag{3.95}$$

All these coefficients implicitly carry a set of arguments: $D_{ij}^{c,d} = D_{ij}^{c,d}\left(p_1^2, p_2^2, p_3^2, p_4^2, \bar{s}, \bar{u}; m_0, m_1, m_2, m_3\right)$. This argument ordering is conventional, but quite standard.

The δ^α_β-piece can be simplified without plugging in the PV-coefficients. Instead we find by reducing the numerator

$$\begin{aligned}
\delta^\beta_\alpha (D^{c,d})^\beta_\alpha &= \delta^\alpha_\beta \int \frac{d^4k}{(2\pi)^4} \frac{k^\beta (k+k_2)_\alpha}{N_1^{c,d} N_2^{c,d} N_3^{c,d} N_4^{c,d}} = \\
&= \frac{1}{2} \int \frac{d^4k}{(2\pi)^4} \left[\frac{1}{N_2^{c,d} N_3^{c,d} N_4^{c,d}} + \frac{1}{N_1^{c,d} N_2^{c,d} N_4^{c,d}} + (m_0^2 + m_2^2 - k_2^2) \frac{1}{N_1^{c,d} N_2^{c,d} N_3^{c,d} N_4^{c,d}} \right] = \\
&= \frac{1}{2} \Big\{ C_0(p_1^2, \bar{u}, p_4^2; m_0, m_1, m_3) + C_0(p_2^2, p_3^2, \bar{u}; m_1, m_2, m_3) + \left(m_0^2 + m_2^2 - \bar{s}\right) D_0^{c,d} \Big\},
\end{aligned} \tag{3.96}$$

where $D_0^{c,d}$ carries the same set of arguments as the tensor coefficients in eq. (3.95). Furthermore we can again set $m_0 =$ at this stage. For the respective Mandelstam invariants see tab. 3.9.

For the rest of the calculation the tedious part of plugging in the PV-decomposition and simplifying by e.g. applying on-shellness cannot be spared. The aim is to target the amplitude basis eq. (3.7), so we use the following spinor sandwich simplifications

$$\begin{aligned}
\bar{v}_e(l_2) \not{k}_1 \, \omega_\kappa u_e(l_1) &= \bar{v}_e(l_2) \not{k}_3 \, \omega_\kappa u_e(l_1) = 0, \\
\bar{v}_e(l_2) \not{k}_2 \, \omega_\kappa u_e(l_1) &= \mp \bar{v}_e(l_2) \frac{\not{p}}{2} \, \omega_\kappa u_e(l_1), \\
\bar{u}_t(q_1) \not{k}_1 \, \omega_\rho v_t(q_2) &= \bar{u}_t(q_1) \not{l}_2 \, \omega_\rho v_t(q_2), \\
\bar{u}_t(q_1) \not{k}_2 \, \omega_\rho v_t(q_2) &= \bar{u}_t(q_1) \not{l}_2 \, \omega_\rho v_t(q_2) \mp m_t \bar{u}_t(q_1) \, \omega_{\pm\rho} v_t(q_2), \\
\bar{u}_t(q_1) \not{k}_3 \, \omega_\rho v_t(q_2) &= \bar{u}_t(q_1) \not{l}_2 \, \omega_\rho v_t(q_2) - m_t \big[\bar{u}_t(q_1) \, \omega_\rho v_t(q_2) - \bar{u}_t(q_1) \, \omega_{-\rho} v_t(q_2) \big], \\
\bar{u}_t(q_1)(-2i) \sigma_{\mu\beta} k_1^\beta \, \omega_\rho v_t(q_2) &\simeq 2 \, \bar{u}_t(q_1) \gamma_\mu \not{l}_2 \, \omega_\rho v_t(q_2), \\
\bar{u}_t(q_1)(-2i) \sigma_{\mu\beta} k_2^\beta \, \omega_\rho v_t(p_2) &\simeq 2 \, \bar{u}_t(q_1) \gamma_\mu \not{l}_2 \, \omega_\rho v_t(q_2) + 2 m_t \bar{u}_t(q_1) \gamma_\mu \, \omega_{\pm\rho} v_t(q_2) + p_\mu \bar{u}_t(q_1) \, \omega_\rho v_t(q_2), \\
\bar{u}_t(q_1)(-2i) \sigma_{\mu\beta} k_3^\beta \, \omega_\rho v_t(q_2) &\simeq 2 \, \bar{u}_t(q_1) \gamma_\mu \not{l}_2 \, \omega_\rho v_t(q_2) + 2 m_t \bar{u}_t(q_1) \gamma_\mu \, (\omega_\rho + \omega_{-\rho}) \, v_t(q_2) + 2 p_\mu \bar{u}_t(q_1) \, \omega_\rho v_t(q_2),
\end{aligned} \tag{3.97}$$

where the upper/lower sign corresponds to the crossed/direct box. In the last three relations we made use of the fact that terms like $q_\mu, l_{2,\mu}$ will get contracted with γ^μ on the lepton side, and vanish due to masslessness of the initial state leptons. We therefore dropped these terms (indicated by $\simeq$ instead of $=$). This allows to rewrite the rest of eq. (3.94) as

$$\left[(D^{c,d})^\beta_\alpha + k_{2,\alpha} (D^{c,d})^\beta \right] \gamma_\beta \, \omega_\rho \otimes \gamma^\alpha \omega_\kappa =$$

$$
\begin{aligned}
&= D_{00}^{c,d} M_1^{\rho\kappa} \mp \left(D_1^{c,d} + D_2^{c,d} + D_3^{c,d} + D_{12}^{c,d} + D_{22}^{c,d} + D_{23}^{c,d}\right) M_2^{\rho\kappa} + \\
&\quad + m_t \left(D_2^{c,d} + D_3^{c,d} + D_{22}^{c,d} + D_{23}^{c,d}\right) M_3^{\pm\rho\kappa} - m_t \left(D_3^{c,d} + D_{23}^{c,d}\right) M_3^{\mp\rho\kappa}, \\
&(D^{c,d})^\beta \omega_\rho \otimes \gamma_\beta \, \omega_\kappa = \mp D_3^{c,d} M_3^{\rho\kappa}, \\
&(D^{c,d})^\beta (-2i)\, \sigma_{\beta\sigma} \omega_\rho \otimes \gamma^\sigma \omega_\kappa = 2m_t \left\{ \big(D_2^{c,d} + D_3^{c,d}\big) M_1^{\pm\rho\kappa} + D_3^{c,d} M_1^{\mp\rho\kappa} \right\} + \\
&\quad - \big(D_2^{c,d} + D_3^{c,d}\big) M_3^{\rho\kappa} + \big(D_1^{c,d} + D_2^{c,d} + D_3^{c,d}\big) M_4^{\rho\kappa}.
\end{aligned} \tag{3.98}
$$

To make contact with eq. (3.83) some summation index renaming has to be performed. When the dust settles we find for the form factors $\big(c_i^{\rho\kappa}\big)_{\text{box}}$:

$$
\begin{aligned}
\big(c_1^{(1),\rho\kappa}\big)_{\text{box}}^{c,d} &= \alpha g_l^\kappa \, g_{\bar{l}}^\kappa \times \\
&\times \Big\{ \mp 2 g_f^\rho \, g_{\bar{f}}^\rho \, \delta_{\pm\kappa}^\rho \Big(C_0(p_1^2, \bar{u}, p_4^2; 0, m_1, m_3) + C_0(p_2^2, p_3^2, \bar{u}; m_1, m_2, m_3) + (m_2^2 - \bar{s}) D_0^{c,d} \Big) + \\
&\quad \mp 4 g_f^\rho \, g_{\bar{f}}^\rho \, \delta_{\mp\kappa}^\rho D_{00}^{c,d} + 2 m_f m_2 \Big(\delta_\kappa^\rho - \delta_{-\kappa}^\rho \Big) \Big(g_f^{\mp\rho} \, g_{\bar{f}}^{\pm\rho} \Big[D_2^{c,d} + D_3^{c,d} \Big] - g_f^{\pm\rho} \, g_{\bar{f}}^{\mp\rho} D_3^{c,d} \Big) \Big\}, \\
\big(c_2^{(1),\rho\kappa}\big)_{\text{box}}^{c,d} &= 4\alpha g_l^\kappa \, g_{\bar{l}}^\kappa \, g_f^\rho \, g_{\bar{f}}^\rho \, \delta_{\mp\kappa}^\rho \Big(D_1^{c,d} + D_2^{c,d} + D_3^{c,d} + D_{12}^{c,d} + D_{22}^{c,d} + D_{23}^{c,d} \Big), \\
\big(c_3^{(1),\rho\kappa}\big)_{\text{box}}^{c,d} &= \pm 4\alpha g_l^\kappa \, g_{\bar{l}}^\kappa \times \\
&\times \Big\{ - m_f \, g_f^{\pm\rho} \, g_{\bar{f}}^{\pm\rho} \, \delta_{-\kappa}^\rho \Big(D_2^{c,d} + D_3^{c,d} + D_{22}^{c,d} + D_{23}^{c,d} \Big) + m_f \, g_f^{\mp\rho} \, g_{\bar{f}}^{\mp\rho} \, \delta_\kappa^\rho \Big(D_3^{c,d} + D_{23}^{c,d} \Big) + \\
&\quad + m_2 \, g_f^{-\rho} g_{\bar{f}}^\rho \Big(\delta_{-\kappa}^\rho \Big[D_2^{c,d} + D_3^{c,d} \Big] - \delta_\kappa^\rho D_3^{c,d} \Big) \Big\}, \\
\big(c_4^{(1),\rho\kappa}\big)_{\text{box}}^{c,d} &= \pm 2\alpha m_2 \, g_l^\kappa \, g_{\bar{l}}^\kappa \, g_f^{-\rho} \, g_{\bar{g}}^\rho \Big(\delta_\kappa^\rho - \delta_{-\kappa}^\rho \Big) \Big(D_1^{c,d} + D_2^{c,d} + D_3^{c,d} \Big),
\end{aligned} \tag{3.99}
$$

The reduction in arbitrary R_ξ-gauge now basically proceeds along the exact same lines, but as the expressions are quite involved we (hopefully understandably) refrain from giving those results explicitly. Instead we use `Mathematica`-code to carry out the PV-reduction and symbolic manipulations, with help of the HEP-package `FeynCalc` [23]. As pointed out in the beginning of the section the reduction will only end up in the Beenakker-basis, so eq. (3.99) is the end of the line for the moment. These results for the Beenakker-basis can however be transferred to the minimal one by making use of the substitutions given in eq. 3.9. We will not give any further results however as the projection operator results are somewhat easier to obtain, but note that this brute-force procedure allows a nice non-trivial cross-check of the former technique. To evaluate the tensor coefficients in eq. (3.99) and the R_ξ-expressions, we use the numerical PV-library `LoopTools` [24] to vary from our standard choice of `Package-X` [20]. In summary we have 2 ways of box computation that allow for cross-checks of the results:

- Brute-force PV-reduction (assisted by `FeynCalc` + `LoopTools`)
- Projection operator technique (assisted by `Package-X`)

3.6.3 EW box corrections

As we are focusing on pure weak contributions with massless initial-state leptons, there are just 3 box diagrams contributing (cf. app. G.2). Tab. 3.10 shows the parameters to be plugged into eq. (3.99). The generic results obtained with projection operators (app. D) can be found in the appendix E, and the respective parameters are given in tab. 3.11.

box	**topology**	$g_f = g_{\bar{f}}$	$g_l = g_{\bar{l}}$	$m_1 = m_3$	m_2	$\xi_1 = \xi_3$	$\bar{u}$	$\bar{s}$
WW	crossed	$\frac{1}{\sqrt{2}s_W}\,\delta_{\eta,-1}$	$\frac{1}{\sqrt{2}s_W}\,\delta_{\lambda,-1}$	M_W	0	ξ_W	s	u
ZZ	crossed	$v_t - \eta\, a_t$	$v_e - \lambda\, a_e$	M_Z	m_t	ξ_Z	s	u
ZZ	direct	$v_t - \eta\, a_t$	$v_e - \lambda\, a_e$	M_Z	m_t	ξ_Z	s	t

Table 3.10: Weak boxes (brute-force calculation): the virtual particle content is shown in the leftmost column. The corresponding topology has to be selected (crossed = c, direct = d) in eq. (3.99). η and λ are the final- and initial-state chirality index placeholders.

box	**type**	**topology**	$g_f = g_{\bar{f}}$	$g_l = g_{\bar{l}}$	M	ξ
WW	charged	crossed	$\frac{1}{\sqrt{2}s_W}\,\delta_{\eta,-1}$	$\frac{1}{\sqrt{2}s_W}\,\delta_{\lambda,-1}$	M_W	ξ_W
ZZ	neutral	crossed	$v_t - \eta\, a_t$	$v_e - \lambda\, a_e$	M_Z	ξ_Z
ZZ	neutral	direct	$v_t - \eta\, a_t$	$v_e - \lambda\, a_e$	M_Z	ξ_Z

Table 3.11: Weak boxes (projection operator calculation): the virtual particle content is shown in the leftmost column. **type** refers to type in sec. E. η and λ are the final- and initial-state chirality index placeholders. The invariants s, t, u used in the the generic diagrams are the same as in the actual diagrams.

Chapter 4

UV- and gauge-cancellations

If all the building blocks presented in the last chapter are properly renormalized and added up to form the one-loop contribution $\mathcal{M}^{(1)}$ (with or without chirality index κ), both the UV-divergences and the gauge parameter dependence will cancel, enabling the computation of the 1-loop cross-section and doing numerics. This work is interested in the analytic structure however, so it will pay off to take a closer look at how these cancellations take place within the computation. This information might turn out to be very useful for constructing effective field theories or attempting higher-order calculations.

This chapter is structured in 3 parts: the first section 4.1 will (ad hoc) introduce the concept of *clustering* for vertices and fermionic 2-point functions, i.e. formation of subsets of diagrams that are convenient for discussing the UV- and/or gauge structure. Sec. 4.2 will focus on the UV-divergences within these clusters and how the cancellation with counterterms is working. The final section 4.3 will be investigating the gauge cancellations, which is surprisingly tangled up already at the 1-loop-level. We note that this chapter will not contain many analytic results, as the expressions tend to be quite involved. While the UV-divergences are bite-sized, the gauge-cancellations are entirely studied numerically. We postpone the presentation of explicit results (e.g. for clusters) to the next chapter on the high-energy expansion, as the results simplify enormously in this limit.

4.1 Clustering

Since we did not assume that the weak gauge-bosons were mass-degenerate, $M_Z \neq M_W$, it was sensible to also give them different gauge-parameters ξ_Z, ξ_W (and ξ_A), which need not be chosen identically (although that would be possible of course). Some diagrams, namely the vertex and fermionic 2-point corrections, only have one type of weak boson in the loop and consequently only show dependence on one of the gauge parameters. At the 1-loop-level we can now straightforwardly partition these diagrams into subsets according to the type of weak virtual boson. We start with the amputated vertex corrections, including the fermionic field-strength contributions to the respective local 3-point counterterms. We form the following subsets which we refer to as *clusters* (following [6]):

- ***W*-cluster**: all diagrams of a given vertex (Ztt, Att, Zee, Aee), incl. fermionic field-strength contributions to the local 3-point counterterm, that contain at least one virtual W- or ϕ-line

- ***Z*-cluster**: all diagrams of a given vertex (Ztt, Att, Zee, Aee), incl. fermionic field-strength contributions to the local 3-point counterterm, that contain at least one virtual Z- or χ-line

- ***H*-cluster**: Higgs-exchange diagrams of a given vertex (Ztt, Att, Zee, Aee) and corresponding Higgs-exchange fermionic field-strength contribution to the local 3-point counterterm

The clusters are shown in figs. 4.1t to 4.8. We will investigate initial-state and final state vertices and diagram sets with Z or photon separately.

The H-cluster for both Ztt- and Att-vertex is small, but trivially gauge-independent. As will be shown in sec. 4.2 it is closely tied to the final-state Z-cluster respectively. Also there are Higgs-bosons

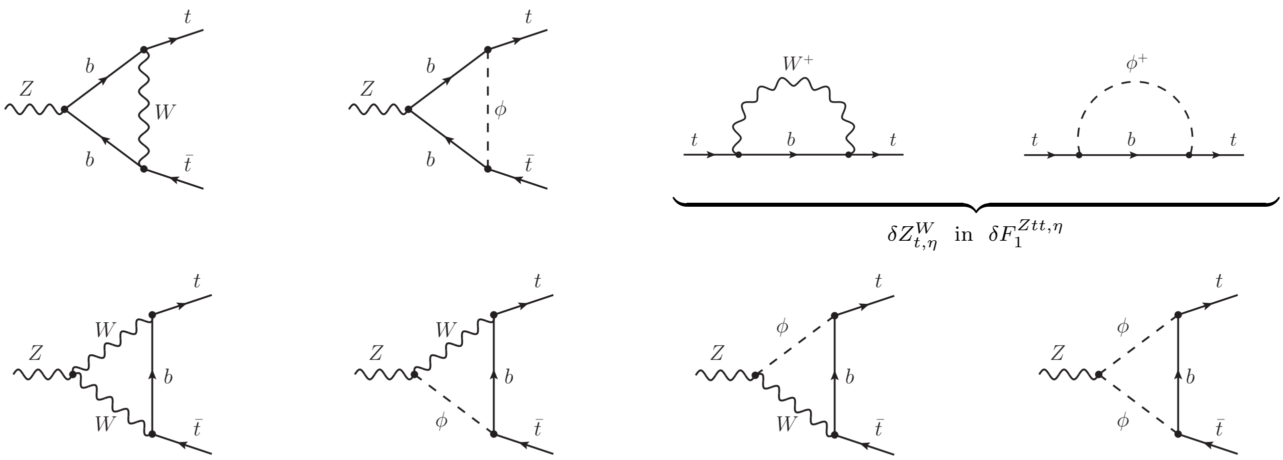

Figure 4.1: W-cluster of Ztt-vertex. A further split into abelian (upper row) and non-abelian W-cluster (lower row) is possible.

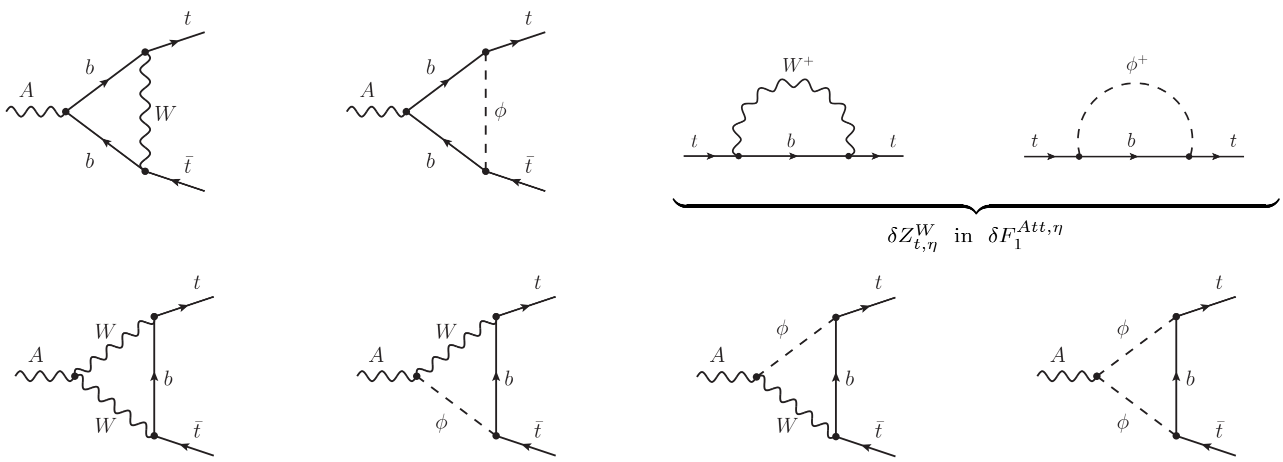

Figure 4.2: W-cluster of Att-vertex. A further split into abelian (upper row) and non-abelian W-cluster (lower row) is possible.

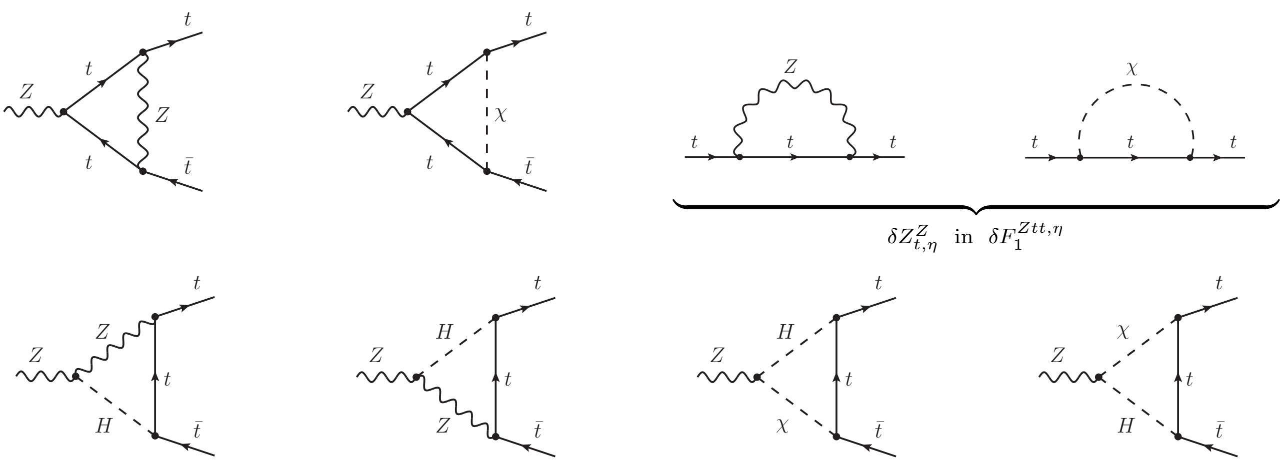

Figure 4.3: Z-cluster of Ztt-vertex. A further split into abelian (upper row) and non-abelian Z-cluster (lower row) is possible.

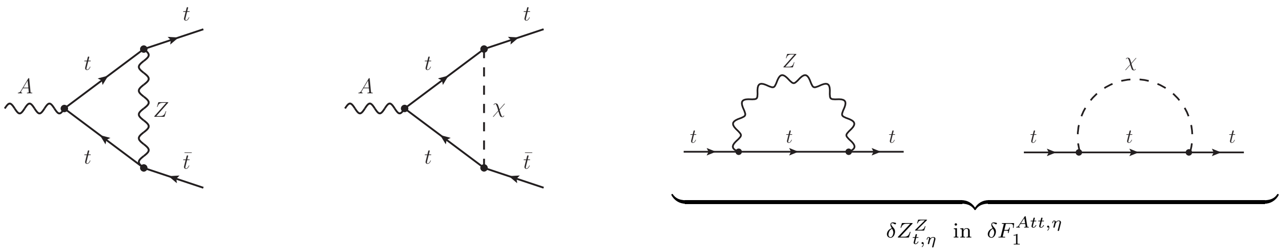

Figure 4.4: Z-cluster of Att-vertex. In contrast to the Ztt-vertex there are no non-abelian diagrams, so we only get the abelian cluster here.

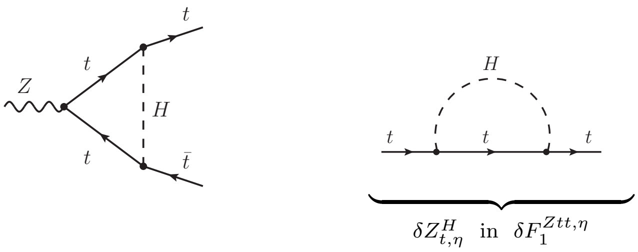

Figure 4.5: H-cluster of Ztt-vertex.

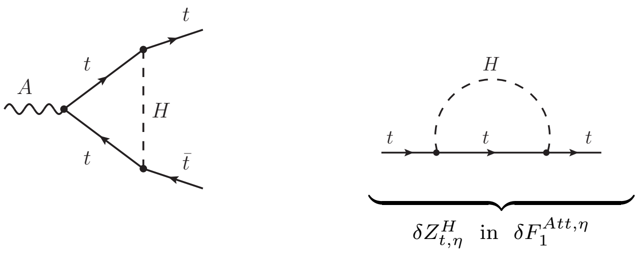

Figure 4.6: H-cluster of Att-vertex.

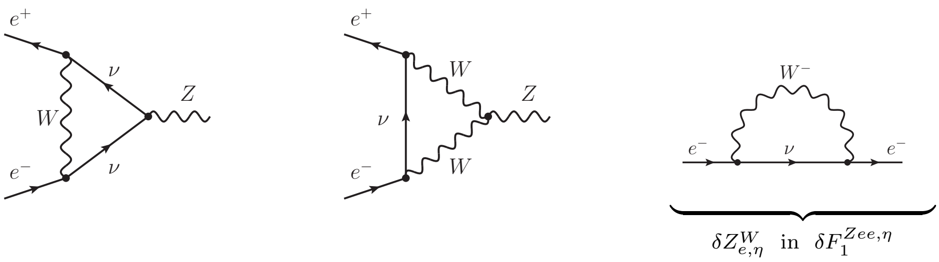

Figure 4.7: W-cluster of Zee-vertex.

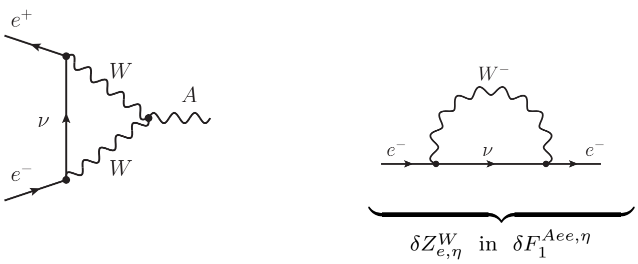

Figure 4.8: W-cluster of Aee-vertex.

in the non-abelian part of the Z-clusters, which motivates alternative clustering according to the charge of the virtual bosons:

- **Charged cluster**: all diagrams of a given vertex (Ztt, Att, Zee, Aee), incl. fermionic field-strength contributions that contain virtual charged bosons **and** bosonic contributions (charge, Weinberg angle, weak field-strengths) to the local 3-point counterterm
- **Neutral cluster**: all diagrams of a given vertex (Ztt, Att, Zee, Aee), incl. fermionic field-strength contributions to the local 3-point counterterm that contain virtual neutral bosons

Effectively this merges Z- and H-cluster into the neutral cluster. It turns out that in the BHS-scheme the bosonic contributions to the 3-point counterterms (i.e. the bosonic loops contributing to charge, Weinberg angle and weak field-strength renormalization constants) are only dependent on ξ_W (cf. eqs. (3.77), (3.78)), and grouping them with the W-clusters therefore does not invalidate the clustering procedure. We show below that they are necessary to complete the UV-cancellations in the charged clusters.

The weak box diagrams also have just one boson species in the loop and could in principle be grouped with the corresponding vertex clusters. They are however not reducible, and live at the level of the amplitude, which makes comparison with the amputated vertices a bit more involved. In addition they are UV-finite and therefore do not influence the renormalization procedure (sec. 4.2). In sec. 4.3 we will see how they have to be combined with the other building blocks to achieve gauge-independence.

Last up are the oblique corrections, especially the bosonic oblique corrections (BOC), as those are not gauge-independent by themselves (the fermionic oblique corrections are trivially gauge-independent). We will explore their connections to the clusters as defined above in the next sections.

4.2 UV-cancellations

In this section we take a closer look at how UV-divergences cancel by the renormalization procedure. We will focus on the amputated vertex corrections (the oblique corrections have been dealt with extensively in chapters 2 and 3 already). We will see that the UV-cancellations are actually not that straightforward in the sense that some UV-poles survive the renormalization of some of the building blocks, and only cancel when certain blocks are combined.

Let us start with some logic that would apply if we were to calculate 1-loop QCD instead of EW corrections to the process $e^+e^- \to t\bar{t}$. In that case the initial-state as well as the EW gauge-boson in the s-channel propagator would be gauge singlets, resulting in a (trivial) factorization of the complete amplitude where only the final-state top-quark current would receive radiative corrections at $\mathcal{O}(\alpha_s)$, shown in fig. 4.9. Due to the vector nature of the gluon the tree-level current $J = \bar{u}(q_1)\Gamma v(q_2)$ (where

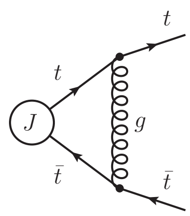

Figure 4.9: The QCD-1-loop correction to the process $e^+e^- \to t\bar{t}$ basically reduces to a matrix element of the current $\mathcal{J} = \bar{t}\gamma^\mu\omega_\pm t$, where $\bar{t}, t$ are in the (anti-)fundamental rep of $SU(3)_c$.

$\Gamma = \gamma^\mu\omega_\pm$ or $\Gamma = \gamma^\mu$ or $\Gamma = \gamma^\mu\gamma_5$) factors out for the UV-divergent parts of the loop-integration (cf. [2]). The 1-loop form factor $F_1(q^2)$ multiplying this structure can therefore be entirely renormalized by the field-strength contributions $\delta Z^g_{t,\eta}$ of the external top quarks, which would enter by $ig_s\delta Z^g_{t,\eta}\bar{u}(q_1)\Gamma_\eta v(q_2)$ i.e.

$$ig_s\left[F_1^{g,\eta}(q^2) + \delta Z^g_{t,\eta}\right]\bar{u}(q_1)\Gamma_\eta v(q_2) = \text{UV-finite}, \tag{4.1}$$

irrespective of the scheme for $\delta Z^{g}_{t,\eta}$ of course[1].

It is now very tempting to ask whether for the EW vertex corrections, or at least parts of them, the same procedure of current + fermionic field strength is sufficient to render the expressions UV-finite. The major difference to QCD now comes from the fact that the EW symmetry is broken, i.e. that left-handed currents (for the quark vertex of the form $Q_L \Gamma Q_L$) and right-handed currents (for the quark vertex of the form $q_R \Gamma q_R$) transform differently under the gauge group. We will start our investigation with the abelian diagrams.

4.2.1 Mechanism of UV-cancellation for vertices

Note: to keep notation transparent in this chapter we set the global factors of $\frac{\alpha}{4\pi} \equiv 1$ (only in this chapter!), and use the abbreviation

$$y_f \equiv \frac{m_f}{2 s_W M_W} \tag{4.2}$$

for the Yukawa-coupling[2]. Diagrams shown are to be understood as representing their respective form factors, i.e. without the additional factor of ie in front (cf. (3.53)).

Let us start with the abelian diagrams of the Ztt-vertex, i.e. the upper rows of figs. 4.1, 4.3 and the Higgs diagram eq. 4.5. In eqs. (4.3) we give the UV-divergences of the form factors $\{F_1^{Ztt,-}, F_1^{Ztt,+}\}$ of the abelian diagrams:

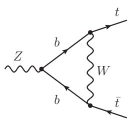

$$\Big|_{\mathrm{UV}} = \left\{ \frac{(v_b + a_b)\,\xi_W}{2 s_W^2 \epsilon}, 0 \right\},$$

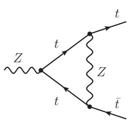

$$\Big|_{\mathrm{UV}} = \left\{ \frac{(v_t + a_t)^3\,\xi_Z}{\epsilon}, \frac{(v_t - a_t)^3\,\xi_Z}{\epsilon} \right\},$$

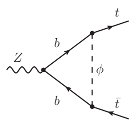

$$\Big|_{\mathrm{UV}} = \left\{ 0, \frac{(v_b + a_b) y_t^2}{\epsilon} \right\},$$

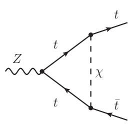

$$\Big|_{\mathrm{UV}} =$$

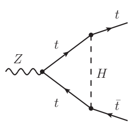

$$\Big|_{\mathrm{UV}} = \left\{ \frac{(v_t - a_t)\,y_t^2}{2\epsilon}, \frac{(v_t + a_t)\,y_t^2}{2\epsilon} \right\}. \tag{4.3}$$

The UV-parts of the fermionic cluster renormalization constant contributions to $\delta F_1^{Ztt,\eta}$ of eq. (2.125), read (we indicate the specific diagram below)

$$\left\{ (v_t + a_t)\,\delta Z^{W}_{t,L}, (v_t - a_t)\,\delta Z^{W}_{t,A} \right\}\Big|_{\mathrm{UV}} = \Big\{ \underbrace{-\frac{(v_t + a_t)\,\xi_W}{2 s_W^2 \epsilon}}_{W}, \underbrace{-\frac{(v_t - a_t) y_t^2}{\epsilon}}_{\phi} \Big\},$$

$$\left\{ (v_t + a_t)\,\delta Z^{Z}_{t,L}, (v_t - a_t)\,\delta Z^{Z}_{t,R} \right\}\Big|_{\mathrm{UV}} = \Big\{ \underbrace{-\frac{(v_t + a_t)^3\,\xi_Z}{\epsilon}}_{Z} \underbrace{-\frac{(v_t + a_t)\,y_t^2}{2\epsilon}}_{\chi}, \underbrace{-\frac{(v_t - a_t)^3\,\xi_Z}{\epsilon}}_{Z} \underbrace{-\frac{(v_t - a_t)\,y_t^2}{2\epsilon}}_{\chi} \Big\},$$

[1] On a fundamental level the fact that the fermionic field-strength is sufficient to renormalize the vertex is a result of the operator $\mathcal{J}$ at the vertex being gauge-invariant under $SU(3)_c$.

[2] Usually a factor e is included into the definition of y_t, i.e. $y_t \equiv \frac{e\,m_t}{2 s_W M_W}$.

$$\Big\{(v_t + a_t)\, \delta Z^H_{t,L}, (v_t - a_t)\, \delta Z^H_{t,R}\Big\}\Big|_{\mathrm{UV}} = \Big\{ -\frac{(v_t + a_t)\, y_t^2}{2\epsilon}, -\frac{(v_t - a_t)\, y_t^2}{2\epsilon}\Big\}. \tag{4.4}$$

Focusing on the neutral clusters first, we observe that the Z-exchange diagram is completely renormalized analogous to the QCD-case by just adding the Z-contribution of the fermionic field-strength to the vertex diagram. For the neutral scalar diagrams, i.e. both χ- and H-exchange, the counterterms have the wrong chirality to cancel the $\frac{1}{\epsilon}$-terms in the respective vertex diagrams. The reason is that scalar interactions flip chirality, so by loops involving scalar exchanges a tree-level current operator J_η gets radiative corrections of the form

$$J_\eta \overset{\text{loops}}{\to} J_\eta + F_1^\eta \times J_{-\eta} + (F_2\text{-terms} + \text{add. loops}), \tag{4.5}$$

while the local vertex counterterms have the form $\delta F_1 \times J_\eta$. Switching to the VA-basis this implies in our case that the vector-form-factor $F_1^{Ztt,V}$ is fully renormalized by the fermionic contributions, but the axial-vector part shows residual UV-divergences. These remaining divergences for the scalar diagrams are cancelled when the neutral non-abelian diagrams, given in eq. (4.6) are added:

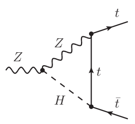

$\Big|_{\mathrm{UV}} +$
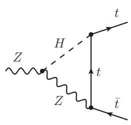

$\Big|_{\mathrm{UV}} = \{0, 0\}\,,$

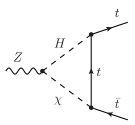

$\Big|_{\mathrm{UV}} +$
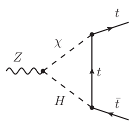

$$\Big|_{\mathrm{UV}} = \Big\{\frac{y_t^2}{2c_W s_W \epsilon}, -\frac{y_t^2}{2c_W s_W \epsilon}\Big\}. \tag{4.6}$$

The cancellation is complete when using $a_t = \frac{T_t}{2c_W s_W}$ and $T_t = \frac{1}{2}$ for the isospin quantum number of the top quark. This feature ties together the Z- with the H-cluster, and in order to avoid scale-dependencies it is basically not possible to consider these cluster as separate entities (as far as the axial-vector current is concerned), which is why we introduced the neutral cluster in the previous section.

Things are even less straightforward in the W-cluster. There the interactions are not only (partly) chirality-changing, but also isospin-changing. It is therefore natural to assume that these corrections will show crucial and non-trivial dependence on the group structure. Comparing eqs. (4.3) and (4.4) we obtain

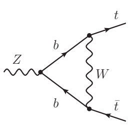

$\Big|_{\mathrm{UV}} +$
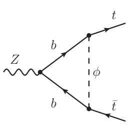

$\Big|_{\mathrm{UV}} + \Big\{(v_t - a_t)\, \delta Z^W_{t,L}, (v_t + a_t)\, \delta Z^W_{t,A}\Big\} =$

$$= \Big\{\frac{(v_b + a_b - v_t - a_t)\, \xi_W}{2s_W^2 \epsilon}, \frac{(v_b + a_b - v_t + a_t)\, y_t^2}{\epsilon}\Big\} = \Big\{-\frac{c_W\, \xi_W}{2s_W^3 \epsilon}, -\frac{(c_W^2 - s_W^2)\, y_t^2}{2c_W s_W \epsilon}\Big\}, \tag{4.7}$$

where we used $v_b + a_b - v_t - a_t = -\frac{c_W}{s_W}$ and $v_b + a_b - v_t + a_t = -\frac{c_W^2 - s_W^2}{2c_W s_W}$. Note that the incomplete cancellation between the W-exchange diagram and the W-contribution to the fermionic field-strength is a consequence of not being inclusive enough in the final-state to meet the requirements of full EW gauge-invariance (not just gauge-independence). If we had also taken into account the W-exchange diagram with bottom quarks in the final state (and tops as virtual particles), the UV-contribution of this renormalized diagram to the left-handed form factor F_1^- would be the same as in eq. (4.7) with the replacement $v_b + a_b - v_t - a_t \to v_t + a_t - v_b - a_b$ (replacing the Ztt-vertex by a Zbb-vertex), as the UV-divergences to not depend on the virtual masses or external invariants (also the UV-parts of the fermionic counterterm $\delta Z^W_{b,\eta}$ would be the same). Summing both contributions would then lead to a complete UV-cancellation for the abelian W-exchange diagrams without the need for any further renormalization constant. The reason for this is that by taking into account external bottom quarks as well one actually calculates the matrix element of the gauge-invariant current $\mathcal{J}_L^Q$ (for UV-discussion of the W-diagrams only the left-handed current is interesting, as the right-handed one gives no UV-contribution at 1-loop) involving the quark doublet Q_L,

$$\mathcal{J}_L^Q \equiv \bar{Q}_L \Gamma\, Q_L = \begin{pmatrix} \bar{t}_L \\ \bar{b}_L \end{pmatrix} \Gamma \begin{pmatrix} t_L \\ b_L \end{pmatrix}, \tag{4.8}$$

while restriction to (left-handed) top quarks (as is the case for our process) we only calculate the matrix element of the current $\mathcal{J}_L^t = \bar{t}_L \Gamma\, t_L$, which obviously is not a gauge-singlet. We will see similar features in the section on gauge-independence.

In the more exclusive case of just top quarks in the final state the remaining UV-divergences must cancel in another way. The non-abelian diagrams of the W-cluster

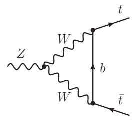

$$\Bigg|_{\text{UV}} = \left\{ \frac{3c_W(1+\xi_W)}{4s_W^3}, 0 \right\},$$

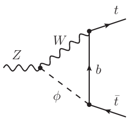

$$\Bigg|_{\text{UV}} +$$

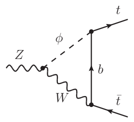

$$\Bigg|_{\text{UV}} = \{0, 0\},$$

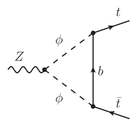

$$\Bigg|_{\text{UV}} = \left\{ 0, \frac{(c_W^2 - s_W^2)\, y_t^2}{2c_W s_W \epsilon} \right\}, \tag{4.9}$$

are only sufficient to cancel the UV-divergences of the scalar diagrams (the same mechanism as in the neutral cluster). So summing up all the contributions from the W-cluster completely renormalizes the right-handed form factor $F_1^{Ztt,+}$, but leaves a residual $\frac{1}{\epsilon}$-dependence in the left-handed form factor $F_1^{Ztt,-}$,

$$F_1^{Ztt,-}\Big|_{\text{UV}} + \left(\delta F_1^{Ztt,-}\right)_{\text{fer}}\Big|_{\text{UV}} = \frac{c_W(3+\xi_W)}{4s_W^3 \epsilon} = \frac{c_W(3+\xi_W)}{4s_W^3 \epsilon}. \tag{4.10}$$

To cancel this divergence the bosonic contributions (charge, Weinberg-angle and bosonic field strength renormalization) to $\delta F_1^{Ztt,\eta}$ (cf. eq. (3.76)) need to be taken into account. Using eqs. (3.77) and (3.78) we get

$$\begin{aligned}
&\left\{ \left(\delta F_1^{Ztt,-}\right)_{\text{bos}}, \left(\delta F_1^{Ztt,+}\right)_{\text{bos}} \right\}\Big|_{\text{UV}} = \\
&\quad = \left\{ -\frac{c_W\left[c_W(v_t + a_t) + s_W Q_t\right](3+\xi_W)}{2s_W^2 \epsilon}, -\frac{c_W\left[c_W(v_t - a_t) + s_W Q_t\right](3+\xi_W)}{2s_W^2 \epsilon} \right\} = \\
&\quad = \left\{ -\frac{c_W(3+\xi_W)}{4s_W^3 \epsilon}, 0 \right\},
\end{aligned} \tag{4.11}$$

where again the quantum numbers $T_t = \frac{1}{2}$ and $Q_t = \frac{2}{3}$ had to be used. We see that adding eq. (4.11) to eq. (4.10) cancels the last UV-divergences.

The UV-cancellation mechanism for the other vertices is basically identical to the one we have shown for the Ztt-vertex. The renormalization of the neutral cluster of the Att-vertex is a bit simpler as for the Ztt-vertex, as the QED-current is vectorlike (no $\gamma^\mu\gamma_5$-term), so the feature of the non-renormalizability of the axial-vector form factor including the scalar particles is absent in this case. Also there are no non-abelian diagrams in the neutral cluster. For the massless initial-state vertices scalar diagrams are absent altogether. The renormalization of the clusters with Z- and W-diagrams works analogous to the Ztt-vertex.

We conclude this section by pointing out that the renormalization of the oblique corrections is straightforward (see ch. 2), and there is not much to be learned by taking a closer look (apart from the fact that fermion loops can always be treated separately from the boson loops, a feature we have discussed already). Box diagrams are UV-finite and need no renormalization procedure. Before turning to gauge cancellations, we briefly discuss the minimal set of necessary renormalization constants in the following section.

4.2.2 Minimal set of renormalization constants

As mentioned earlier, splitting the calculation into building blocks is convenient but might give rise to the inclusion of superfluous renormalization constants that might anyway cancel if the building blocks are added. This is especially obvious in the case of the Denner scheme. Taking all counterterm contributions to the amplitude for this scheme and adding them up (tedious but straightforward) it can be shown that adding the following counterterm expression renders the bare amplitude (with bare vertices and bare oblique corrections) UV-finite

$$\begin{aligned}\delta M^{\kappa}_{\rm ct} = \frac{ie^2}{s}\sum_{\rho=\pm}\Big\{&\Big(\chi^{(0)}(s)(v_e-\kappa\, a_e)(v_t-\rho\, a_t)+Q_tQ_e\Big)\Big(\delta Z_{t,\rho}+\delta Z_{e,\kappa}\Big)+\\ &+\chi^{(0)}(s)(v_e-\kappa\, a_e)(v_t-\rho\, a_t)\Big(2\delta Z_e+2\frac{c_W^2-s_W^2}{s_W^2}\,\delta Z_c+\frac{M_Z^2}{s-M_Z^2}\,\delta Z_{M_Z}\Big)+\\ &-2\chi^{(0)}(s)\Big((-Q_e)(v_t-\rho\, a_t)+(ve-\kappa\, a_e)(-Q_t)\Big)\frac{c_W}{s_W}\,\delta Z_c+2Q_tQ_e\delta Z_e\Big\}\bar{M}_1^{\rho\kappa}. \end{aligned}\tag{4.12}$$

Note especially that the field-strength renormalization constants of the virtual s-channel bosons, i.e. δZ_{ZZ} etc, have cancelled! With this result it is now straightforward (since the renormalization constants in (4.12) are the same by definition in both schemes) to show that the BHS- and Denner-scheme give exactly the same counterterm contributions to the S-matrix element of the process $e^+e^-\to t\bar{t}$.

Now consider the bare tree-level amplitude and expand the bare quantities according to ch. 2 (in any of the two schemes presented there). We obtain after some manipulations

$$\begin{aligned}\mathcal{M}_0^{(0)} &= \frac{i(e^0)^2}{s}\sum_{\rho=\pm}\Big\{\Big(\chi^{(0),0}(s)(v_e^0-\kappa\, a_e^0)(v_t^0-\rho\, a_t^0)+Q_tQ_e\Big)\,\bar{u}_t^0(q_1)\gamma^\mu\omega_\rho v_t^0(q_2)\otimes\bar{v}_e^0(l_2)\gamma_\mu\omega_\kappa u_e^0(l_1)\Big\} =\\ &=\frac{ie^2}{s}\sum_{\rho=\pm}\Big\{\Big(\chi^{(0)}(s)(v_e-\kappa\, a_e)(v_t-\rho\, a_t)+Q_tQ_e\Big)+\\ &+\Big(\chi^{(0)}(s)(v_e-\kappa\, a_e)(v_t-\rho\, a_t)+Q_tQ_e\Big)\Big(\delta Z_{t,\rho}+\delta Z_{e,\kappa}\Big)+\\ &+\chi^{(0)}(s)(v_e-\kappa\, a_e)(v_t-\rho\, a_t)\Big(2\delta Z_e+2\frac{c_W^2-s_W^2}{s_W^2}\,\delta Z_c+\frac{M_Z^2}{s-M_Z^2}\,\delta Z_{M_Z}\Big)+\\ &-2\chi^{(0)}(s)\Big((-Q_e)(v_t-\rho\, a_t)+(ve-\kappa\, a_e)(-Q_t)\Big)\frac{c_W}{s_W}\,\delta Z_c+2Q_tQ_e\delta Z_e\Big\}\bar{M}_1^{\rho\kappa}+\mathcal{O}(\alpha^2), \end{aligned}\tag{4.13}$$

where the second line is the renormalized tree-level amplitude. Comparing with eq. (4.12) we find the same expressions. However, the complexity of the calculation makes the usage and systematic renormalization of building blocks the superior choice over taking the “fast lane” by only renormalizing the full amplitude, as the former route allows for strong cross-checks along the way like in the UV-section 4.2.1 or the upcoming one.

4.3 Gauge cancellations

The second mandatory property of a properly constructed S-matrix element, besides UV-finitness, is gauge-independence. This means that all the dependence on the gauge-parameters ξ_i must cancel. It is clear that gauge-dependences of quantities have to be treated carefully, to avoid making gauge-dependent statements (like plotting quantities with residual gauge-parameter dependence). Some building blocks are trivially gauge-independent, like the fermion-loop-contributions to the oblique corrections. We will see that, similar to the UV-divergences, the gauge-dependences tie together some sets of diagrams that need to be combined for gauge-independence. The clustering for the vertex corrections done in sec. 4.1 was the first obvious step in this direction.

The major complication relative to the UV-divergences now comes from the fact that gauge-dependence is much more complicated than the UV-parts. Usually the gauge-parameters are also contained in the (usually complicated) C- and D-functions, i.e. inside logarithms and Dilogarithms (see for example the generic diagram expressions in the appendix E). Trying to access them and observe the gauge-cancellations analytically is incredibly tedious in the continuum, so in this section we will only check for gauge-independence numerically. In the boosted regime (sec. 5) the expressions simplify greatly, and we will make another attempt there.

We will start with the neutral cluster and the neutral box diagrams, as for these gauge-independence is obtained simpler than for the charged cluster, which will be treated in the section after.

4.3.1 Neutral cluster and ZZ-boxes

The neutral clusters for each of the vertices, i.e. the corrections to the form factors F_i^ρ, f_i^κ including the respective fermionic field-strength contributions to the local 3-point counterterms, form a gauge-indpendent subset individually, with no need to add further diagrams. This behaviour was somewhat expected after the observations made in the UV-section. The neutral clusters are, by construction, independent of the other gauge parameters ξ_W, ξ_A. The H-cluster is trivially independent of any ξ_i and could be considered a separate entity for gauge-discussions (but is of course tied to the neutral sector via UV-dependence).

Consequently the rest of the building blocks should be gauge-independent with respect to ξ_Z as well. The bosonic contributions to 3-point counterterms and the bosonic oblique corrections (BOC) turn out to be ξ_Z-independent individually. This leads to the fact that the ZZ-box-diagrams should also form a gauge-indpendent subset[3]. This is confirmed by numerical evaluation of the coefficients $(c_i^{(1),\rho\kappa})_{\text{box}}$ in fig. 4.10. In fig. 4.10 it can be seen that while each box type separately is not gauge-independent, the sum of them actually is. This feature is far from obvious by looking at the Feynman integral representations for both boxes individually. Besides the CM-energy s each box (and especially the D-functions appearing in the PV-reduction, cf. app. E) depends on a second Mandelstam invariant: the crossed box on u and the direct type on t. For a cancellation as above to happen the gauge parts need to have a very peculiar dependence on the Mandelstam invariants s, t, u, which can be seen in the generic box expressions given in the appendix E. There the additional parts $\Delta F_i^{\rho\kappa}$, which are absent in Feynman gauge, are *independent of t and u* altogether.

We will reencounter this feature of cancellations between both box topologies in the high-energy section, and this property of box diagrams has immediate and interesting consequences for the WW-box (see next section).

[3]Actually, there are also ZA-boxes contributing to the amplitude. We do not give results for them as they are IR-divergent and are therefore treated as part of the pure QED corrections. A priori it is not obvious at all that these boxes form a ξ_Z-independent set instead of interfering with the ZZ-boxes in terms of gauge-dependence, but the ZZ-boxes will form a gauge-independent subset themselves (cf. fig. 4.10)

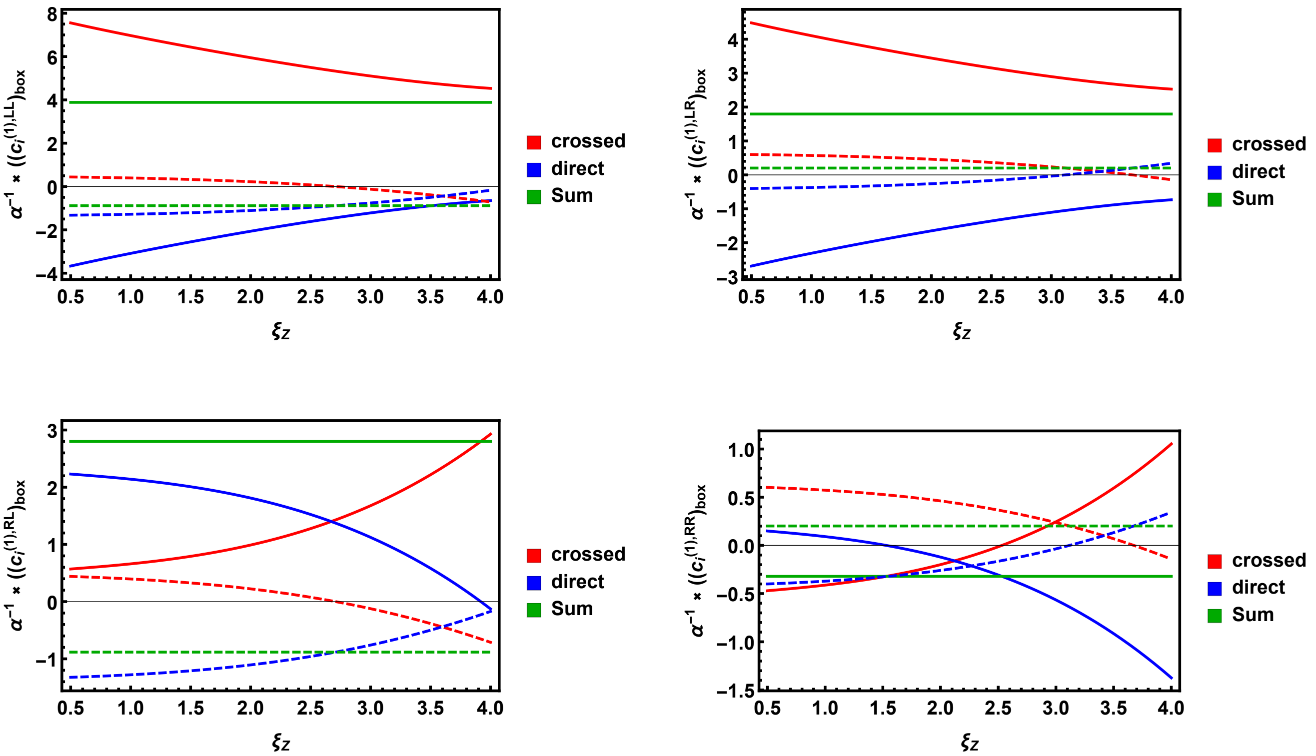

Figure 4.10: Exemplary gauge plots for box form factors of the ZZ-boxes ($\bar{c}_1^{(1),\rho\kappa}$ = solid, $\bar{c}_2^{(1),\rho\kappa}$ = dashed) multiplied by α^{-1} for both ZZ-box topologies as well as their sum. The parameter set given in sec. 6 was used, with $\sqrt{s} = 500$ GeV. Upper-left = LL, upper-right = LR, lower-left = RL, lower-right = RR.

4.3.2 Charged clusters, BOC and WW-box

As we saw in sec. 4.2 the bosonic contributions have to be included into the local counterterms (cf. eq. (3.76)) to render the W-clusters UV-finite. As discussed before, these bosonic contributions do only depend on ξ_W, but not on ξ_Z or ξ_A and thus do not invalidate the clustering procedure. However in contrast to the neutral cluster the W-clusters are (still) gauge-dependent after the renormalization procedure. The same is true for the BOC. To analyze them we can focus on the renormalized boson self-energies $\hat{\Pi}^T_{XY}$. As for the amputated vertices the ξ_Z-dependence is not problematic here as well. By taking a look at the diagram sets (app. G.2) for $ZA-$ and AA-transition we see that they are trivially independent of ξ_Z, as there simply are no diagrams containing a Z- or χ-boson. For the ZZ-transition the independence of ξ_Z is not clear a priori, but analogous to the bosonic contributions to the 3-point counterterms it turns out that $\hat{\Pi}^T_{ZZ}$ is only dependend on ξ_W, but not on ξ_Z. Lastly there is the WW-box diagram. There are no cancellations between various box topologies as in the ZZ-case, since only the crossed box type exists in this case, due to the restriction to top quarks in the final-state.

The building blocks mentioned above are not independent of the gauge-parameter ξ_W, but when the amplitude is constructed and these corrections are added at the level of the matrix element, that is when $c_i^{(1),\rho\kappa}$ is constructed according to eq. (3.23), all the gauge-dependences cancel, as can be seen in fig. 4.11. Note that unless a contribution of some building block vanishes (like the WW-box for $\kappa = +1$, i.e. right-handed electrons) all ingredients are needed to make the gauge-cancellations of ξ_W manifest. This is a nice example of the mechanism of spontaneously broken gauge theories, but at the same time a very strong cross-check of the calculation, as it requires highly-non-trivial interplay of various n-point functions. For example, it requires that the gauge-dependent parts of the WW-box are independent of t, u, since the reducible contributions (oblique and vertex corrections) can only produce dependence[4] on s. As mentioned already this feature is indeed observed (see the gauge parts $\Delta F_i^{\rho\kappa,\xi}$ in app. E).

[4]There is implicit dependence on t, u (or alternatively the scattering angle) in the external fermion spinors $\bar{u}_t, u_t, \bar{v}_e, v_e$, but the parametrization eq. (3.10) basically forces gauge-independence for the $c_i^{(1),\rho\kappa}$.

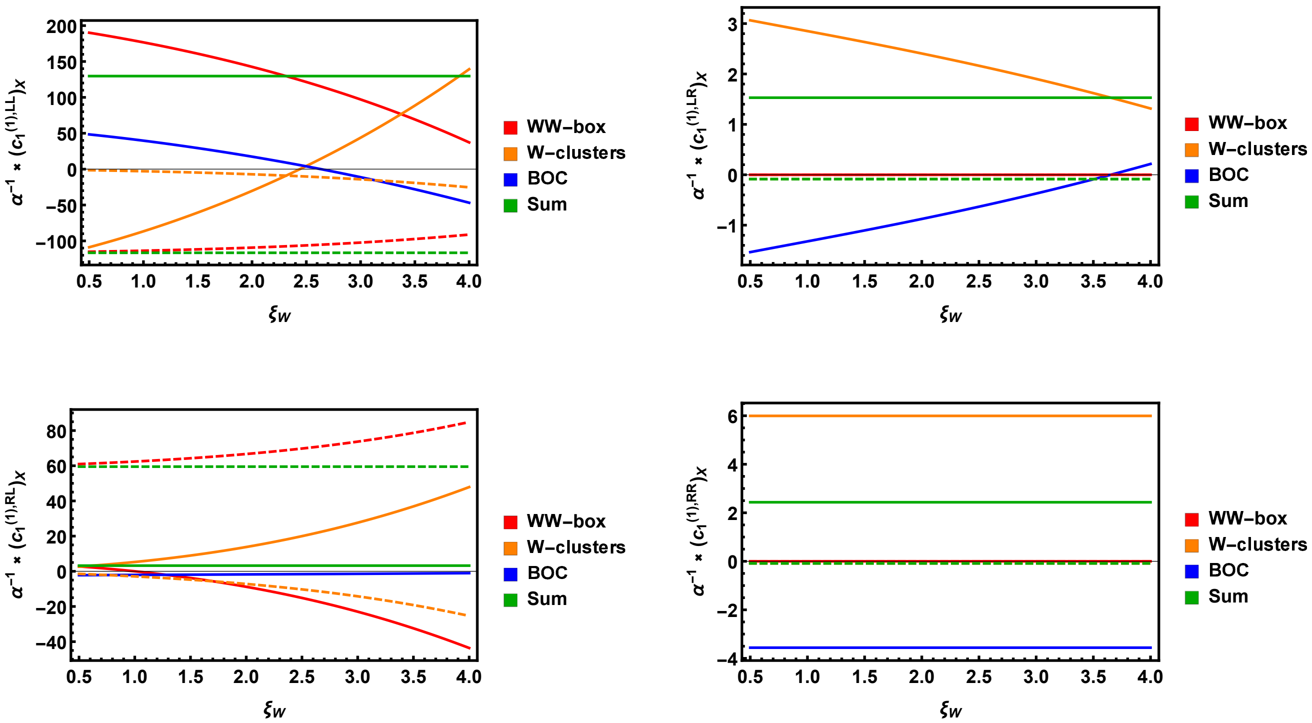

Figure 4.11: Exemplary gauge plots for form factors of the charged sector ($\bar{c}_1^{(1),\rho\kappa}$ = solid, $\bar{c}_2^{(1),\rho\kappa}$ = dashed), consisting of WW-box, W-clusters and bosonic oblique corrections (BOC). The BOC do not give a contribution to $\bar{c}_2^{(1),\rho\kappa}$. The parameter set given in sec. 6 was used, with $\sqrt{s} = 500$ GeV. Again a global factor of α was divided out. Upper-left = LL, upper-right = LR, lower-left = RL, lower-right = RR.

4.4 Summary

Summing up we find the following UV-finite and gauge-independent building blocks:

- **Neutral clusters**: i.e. sets of Z-, χ- and H-diagrams of amputated vertices (Ztt, Att, Zee, Aee), grouped with their respective fermionic field-strength renormalization constants, are each UV-finite and gauge-independent individually.
- ***ZZ*-boxes**: crossed and direct ZZ-box are not independent from ξ_Z individually, but become gauge-independent when added (cf. fig. 4.10).
- **Fermionic oblique corrections (FOC)**: this type of diagram is trivially gauge-independent, and only requires the inclusion of fermionic loops into local counterterms for renormalization.
- **Charged clusters + BOC + *WW*-box ≡ charged sector**: the charged clusters, i.e. sets of W- and ϕ-diagrams of amputated vertices (Ztt, Att, Zee, Aee), and the bosonic oblique corrections are UV-finite individually if renormalized properly. Each of the mentioned contributions is dependend on ξ_W individually (apart from a few form factors), but become gauge-independent when added (cf. fig. 4.11).

Analogously to the charged sector, it is also possible to group the neutral clusters with the ZZ-boxes to form the **neutral sector**. The UV-finite and gauge-independent building blocks shown above will be referred to as *proper building blocks* from now on. They are suitable for numerical evaluation, as there is no scale- or gauge-dependence left[5]. Numerics can be found in ch. 6.

[5] Apart from the explicit μ-dependence from $\overline{\text{MS}}$-subtraction for light-fermion loops for the FOC, which is compensated by running of $\alpha = \alpha(\mu)$.

Chapter 5

High-energy expansions

In the last sections we presented all the necessary ingredients for the computation of the weak NLO corrections to the amplitude $\mathcal{M}(e^+e^- \to t\bar{t})$, assuming stable top quarks. These results are valid above the top production threshold, i.e. $s > 4m_t^2$. The expressions are quite involved, so we do not give them explicitly. For numerical studies we refer the reader to the next chapter 6. In this section we will examine the high-energy limit of the radiative corrections, i.e. take $s \gg 4m_t^2 \sim \Lambda_{\mathrm{EW}}^2$. This phase-space region is often referred to as *boosted regime*, as large boosts are necessary to go from the CM-frame to either of the quark rest frames. We will see that in this limit the expressions simplify enormously, allowing for explicit presentation and discussion of the results. However, there is not only theoretical appeal that encourages detailed studies of the boosted regime. Future linear colliders like CLIC have designed partonic CM-energies $\sqrt{s}$ of up to 3 TeV in their respective final upgrade versions, which, as we will see, give excellent prospects for the successful application of EFTs and other advanced theoretical tools to obatin high-precision predictions in this kinematic region. Another limit that is theoretically appealing is the threshold region $s \sim 4m_t^2$, where detailed experimental studies are planned at early stages of the linear colliders (top-pair threshold scans etc.). In this limit the calculations also simplify drastically, but resummation- and EFT-methods (Green‘s function, NRQCD) are necessary to deal with Coulomb-singularities etc. Also finite-lifetime effects for the top quarks need to be included. Although the continuum results could be expanded around threshold, i.e. $\beta = \sqrt{1 - \frac{4m_t^2}{s}} \sim 0$, this is not the limit we are interested in. We refer the reader to other work in those directions [15].

This chapter is organized as follows: in the first section 5.1 we give a short motivation including an example for the importance of high-energy logarithmic structures, and then introduce some basics like notation, goals and the power-counting we apply. In the following sections we give the explicit high-energy expanded results for the various building blocks, starting with the fermionic oblique corrections in sec. 5.2.1. We then turn to the charged sector (charged clusters, WW-box and the bosonic oblique corrections) in sec. 5.2.2 before turning to the neutral clusters (sec. 5.2.3) and the ZZ-boxes (5.2.4). The last section includes a wrap-up of the results and concludes with a brief discussion of these results, especially the Sudakov logarithms.

5.1 Prerequisites and notations

5.1.1 Z- vs. H-exchange - a short motivation

The natural question to ask first is: why bother with expanding and taking a closer look at the (quite messy) full results at all if they can be simply evaluated numerically? The reason is that the structure of the expressions, especially the logarithms, contain valuable information that is both important for a proper understanding the fixed-order calculations (e.g. for setting up higher order computations), as well as for the application of effective field theories and related tools. Let us take a look at a simple example to motivate the importance of the logarithmic structure a bit further. We consider the vector form factor $F_1^{Ztt,V}$ of the Ztt-vertex, namely the H- and Z-exchange contributions (including the Goldstone χ

contribution for the Z)[1], renormalized with their respective fermionic field-strength counterterms. The reason we investigate these specific quantities as an example is that they are relatively simple yet UV-finite and gauge-indpependent. We could not use the axial-vector form factor, as the Higgs contribution alone was not UV-finite (which forces interplay with the χ-exchange as well as the non-abelian diagrams, see sec. 4.2). The naive expectation is now that the Higgs diagram is numerically larger due to Yukawa-enhancement[2]: $e\, y_t \sim 1$. However fig. 5.1 shows that the validity of this conjecture depends on the CM-energy $\sqrt{s}$. In the lower energy regime the Higgs-exchange is indeed numerically larger, but for

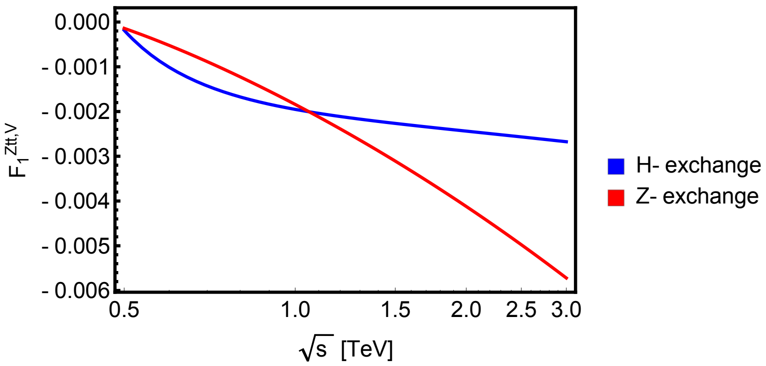

Figure 5.1: H-exchange $\equiv$ abelian H-diagram + fermionic H-counterterm, Z-exchange $\equiv$ abelian Z- + χ-diagrams + fermionic Z- + χ-counterterms. The parameter set given in ch. 6 was used. Note the logarithmic $\sqrt{s}$-axis.

energies above $\sim$ 1 TeV the situation is reversed and the Z-contribution starts to dominate. Due to the logarithmic $\sqrt{s}$-axis the origin is easily deduced: while the H-curve approaches a constant slope in the high-energy regime, signaling linear leading logarithmic dependence on s, the Z-contribution takes a parabolic shape indicating that the leading term in the high-energy regime is a quadratic logarithm of s. The bottom line of this simple example is that the logarithmic structure of various building blocks might differ significantly in the high-energy regime, and knowledge of these logs might be helpful to prove or disprove conjectures like the one mentioned above concerning the importance of Yukawa-enhanced contributions in a systematic way. In the following sections we firstly make the definition of the high-energy limit more precise before targeting the main goal of this thesis: the extraction of these high-energy logarithms.

5.1.2 Power-counting

Returning to the boosted regime we have to make a bit more precise the definition of this limit and how we present the results in the following. We assume all the weak boson masses M_W, M_Z, M_H and the top mass m_t to live around a scale $\Lambda_{\mathrm{EW}} \sim 10^2$ GeV, set by the vev $v \sim 246$ GeV[3]. The partonic CM-energy $\sqrt{s}$ is now taken to be much larger than any of the masses, i.e. $s \gg \Lambda_{\mathrm{EW}}^2$, which implies that both tops produced in the e^+e^--annihilation have large energies compared to their rest masses. Consequently their momenta are close to the light-cone and the fraction

$$\frac{\Lambda_{\mathrm{EW}}^2}{s} \tag{5.1}$$

should be a good expansion parameter for this boosted regime. Organizing the calculation around the expansion in this parameter is known as setting up a *power counting*, a concept lying at the heart of every EFT. s (or $\sqrt{s}$) is often referred to as the *hard scale* of the process. Note that although we do not

[1]We do not give the full explicit results for these two contributions in this work, but it is straightforward to derive those from the generic diagrams given in the appendix E.

[2]This statement could be questioned from the get-go, as the χ-diagram is also Yukawa-enhanced. Since it is a Goldstone however, its contribution is highly gauge-dependent and one would expect significant cancellations against the longitudinal parts of the Z-diagram

[3]We remind that we treat the bottom quark and all the other fermions as massless in this work.

treat the masses as identical, at the same time we assume that they are so close to each other that their fractions

$$r_W = \frac{M_W^2}{m_t^2}, \qquad r_Z = \frac{M_Z^2}{m_t^2}, \qquad r_H = \frac{M_H^2}{m_t^2}, \tag{5.2}$$

can be treated as $\mathcal{O}(1)$ in the power counting defined above.

Besides s the amplitude also depends on the other 2 Mandelstam invariants t and u (explicitly through the box diagrams and implicitly through the external particle spinors), which effectively is a dependence on the scattering angle through eq. (3.6). One of these 3 invariants can be expressed by the other 2 through eq. (3.5), but the third one is independent of s, so the question arises how to assign the power counting to these other invariants. In this work we make the most straightforward (and theoretically convenient) choice and operate under the assumption that the absolute values[4] $|s|, |t|, |u|$ are of the same order (i.e. all are hard scales). In summary we assume the hierachy

$$\{|s|, |t|, |u|\} \gg \{m_t^2, M_W^2, M_Z^2, M_H^2\} \sim \Lambda_{\mathrm{EW}}^2. \tag{5.3}$$

s, t, u being very large simultaneously corresponds to the kinematic situation that the top quarks are being produced with a very high CM-energy $\sqrt{s}$ at a scattering angle θ (= angle between incoming positron and outgoing top) around $\sim \pi/2$. Another way to phrase this would be to demand the scattering angle be very different from 0 or π, so $0 \ll \theta \ll \pi$. The kinematic situation of $\theta = \frac{\pi}{2}$ is called *central scattering*, and the angular neighbourhood around this central value is often referred to a *central region* (see fig. 5.2). Fortunately the central region is not only theoretically convenient, but also the simplest to access

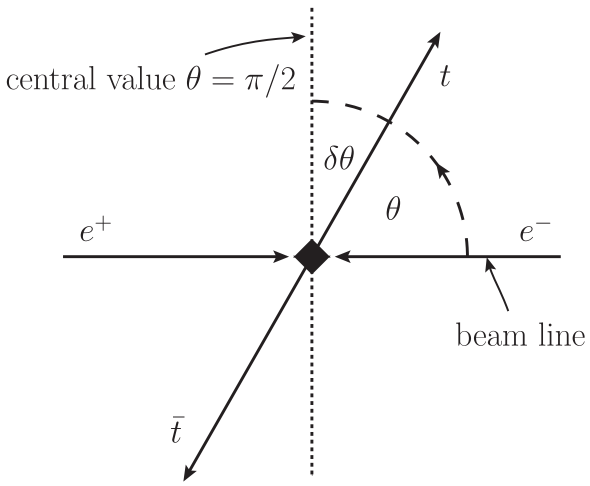

Figure 5.2: Schematic picture of the partonic process. The region around $\theta = \pi/2$ is the central region on which the high-energy expansion is focused.

experimentally, as the detectors are usually placed at large angles away from the beam line.

5.1.3 Sudakov logarithms

Before we turn to concrete results we spent a minute on the structure of the expressions that is expected to emerge in the high-energy regime. Firstly we observe that the theory with massive gauge bosons is IR-finite, where the masses regulate the potential IR-divergences. In a theory like pQCD the IR-divergences, when treated with dimensional regularization, show up as $\frac{1}{\epsilon^k}$-poles, with $k \leq 2n$ at n-th order of perturbation theory. Consequently in n-th order of perturbative EW theory, where besides Λ_{EW} we assume the existence of a hard scale Λ_{hard} with $\Lambda_{\mathrm{hard}} \gg \Lambda_{\mathrm{EW}}$, we expect the appearance of logarithms of the form

$$\alpha^n \ln^k \left(\frac{\Lambda_{\mathrm{EW}}^2}{\Lambda_{\mathrm{hard}}^2} \right), \qquad (0 \leq k \leq 2n). \tag{5.4}$$

[4]For our timelike process $s > 0, t < 0, u < 0$

In our process we actually have 3 hard scales s, t, u. Large logarithms of the form eq. (5.4) due to large hierachies of scales are called *Sudakov logarithms*. They are usually grouped with the coupling of the theory to keep the log-counting transparent. If these logs get large so that $\alpha^n \ln^{2n-k} \sim \mathcal{O}(1)$ down to some k, the perturbative expansion breaks down and resummation of these logs up to N^{k}LL-accuracy is mandatory. We will later see that while in contrast to QCD resummation is not mandatory for EW theory (at least for collider energies that could be reached in the foreseeable future), it could become necessary anyway (at least for the LL-series) for precision physics measurements at linear colliders like ILC or CLIC (we continue this discussion a bit in sec. 5.3).

In this work we only calculate up to EW NLO. Some observable O can then be schematically written as (tree-level couplings absorbed into $O^{(k)}$)

$$O = O^{(0)} + \alpha\, O^{(1)} + \mathcal{O}(\alpha^2). \tag{5.5}$$

Since we assume the large hierachy in eq. (5.3), according to eq. (5.4) the NLO corrections $O^{(1)}$ will be of the form

$$O^{(1)} \sim a_2 \ln^2\left(\frac{\Lambda_{\mathrm{EW}}^2}{s}\right) + a_1 \ln\left(\frac{\Lambda_{\mathrm{EW}}^2}{s}\right) + a_0 + \mathcal{O}\left(\frac{\Lambda_{\mathrm{EW}}^2}{s}\right) \tag{5.6}$$

where we used s as a representative for any of the Mandelstam invariants. The task of this work is to extract these Sudakov logarithms as well as the constant terms a_0, while neglecting the power-suppressed terms $\mathcal{O}\left(\frac{\Lambda_{\mathrm{EW}}^2}{s}\right)$. Note that since we have more than one hard scale, there might be terms in a_1 and a_0 like

$$\ln\left(\frac{-t - i0^+}{-s - i0^+}\right), \quad \ln\left(\frac{-u - i0^+}{-s - i0^+}\right), \tag{5.7}$$

that are not true constants, but are neither of Sudakov-logarithmic form nor suppressed according to our power-counting in eq. (5.3). In the plots of the constant terms a_0 in ch. 6 we will see a mild dependence on s for moderate energies that flats out towards a constant value for higher CM-energies, which can be attributed to terms like the ones in eq. (5.7).

5.1.4 High-energy limit for amplitude basis

In the high-energy limit the amplitude basis also simplifies somewhat. To leading order in the expansion parameters $\frac{m_t^2}{s,t,u}$ the top spinors $\bar{u}_t(q_1)$ and $v_t(q_2)$ are massless (the electron spinors were treated as massless from the start), which results in a restoration of the chiral symmetry also for the final-state. This results in the fact that the amplitude $\bar{M}_2^{\rho\kappa}$ given in eq. (3.8) will be 0 at leading order, effectively reducing the decomposition in eq. (5.8) to

$$\mathcal{M}_\kappa(e^+e^- \to t\bar{t}) = \sum_{\rho=\pm} \left(\bar{c}_1^{\rho\kappa}\right)^{\mathrm{HE}} \left(\bar{M}_1^{\rho\kappa}\right)^{\mathrm{HE}} + \mathcal{O}\Big(\frac{m_t^2}{s,t,u}\Big), \tag{5.8}$$

where $\left(\bar{M}_1^{\rho\kappa}\right)^{\mathrm{HE}}$ has all spinors massless (the precise use of the superscript HE is defined below in eq. (5.9)) and the coefficients $\left(\bar{c}_1^{\rho\kappa}\right)^{\mathrm{HE}}$ are defined in analogy to eq. (3.11) in sec. 3.1. In fact quite analogous to κ the two chirality amplitudes for $\rho = \pm$ also decouple completely in this limit (at leading order), so it is possible to drop the sum over ρ and quote results for $\mathcal{M}_{\rho\kappa}(e^+e^- \to t\bar{t})$ etc.

Besides the suppression for the amplitude $\bar{M}_2^{\rho\kappa}$ we will see that in the boosted regime the coefficients $\bar{c}_2^{(1),\rho\kappa}$ are power-suppressed as well. The statements made above now equally apply to the Beenakker basis eq. (3.7), where the amplitudes $M_3^{\rho\kappa}$ and $M_4^{\rho\kappa}$ will be power-suppressed. This can be either seen directly or from eq. (3.9). That only the structure $\bar{M}_1^{\rho\kappa}$ is not power-suppressed in the high-energy limit has important consequences for the construction of EFTs in this regime. It tells that the operator needed to match the full theory to the EFT at leading order is a four-fermion current-current contact operator. For further discussions and details on this subject we refer the reader to [25], [26] and future work in that direction.

5.2 Explicit results

Having set up the power counting we are ready to enter the boosted regime. In terms of calculational tools we make use of the high-energy expanded PV-functions (especially the scalar ones) worked out in [27], [28], and which are listed in the appendix B.2. Although we will only plot the properly combined gauge-independent building blocks, there are some curiosities concerning the Sudakov-logarithmic and high-energy structure of single diagrams, as can be seen in the generic expressions given in E. We find:

- 2-point diagrams (oblique corrections) only show linear Sudakov-logarithmic dependence
- Vector-exchange triangles and box diagrams contain both linear (*single*) and quadratic (*double*) Sudakov logs
- Non-abelian vector-scalar diagrams are power-suppressed in the boosted regime due to their non-abelian coupling having mass dimension +1 and scaling as $\sim M_W \sim \Lambda_{\rm EW}$
- Scalar exchange and non-abelian scalar-scalar triangles only show single Sudakov logs

Presumably most of these different high-energy behaviours have their origins in the different distributions of the fields on the light-cone (i.e. the decomposition into the light-cone basis), as the logs are basically the regulated IR-divergences of the theory. We postpone a clarification of these features to future work on that subject.

In the following all quantities that are given the superscript HE are understood to be expanded up to power-corrections in the high-energy limit, i.e. for some quantity X

$$X \equiv X^{\rm HE} + \mathcal{O}\left(\frac{\Lambda_{\rm EW}^2}{s,t,u}\right) \tag{5.9}$$

All results given in the following are quote in the BHS-renormalization-scheme (see sec. 2.4).

5.2.1 Fermionic oblique corrections (FOC)

Essentially the high-energy results for FOC are equivalent to the massless fermion results given in the section about QED-improved-Born approximation (sec. 3.4.2) and the appendix (F). The top then also needs to be treated as a light- or massless fermion for the bare contribution, but its counterterm contributions (e.g. to δZ_c) remain as calculated in the continuum. This is an important difference between doing an expansion of the continuum results and calculating with massless fermions from the start. The top counterterm contributions to the bosonic renormalization constants contain terms (logarithmic and non-logarithmic) that depend on the fraction $\frac{m_t^2}{\Lambda_{\rm EW}^2}$, which is $\mathcal{O}(1)$ in our power-counting. These contributions have sizable impact on the numerics, as will be discussed in the next chapter 6. For this reason we have to treat the top separately again, and since it is tied to the bottom we have to exclude the bottom quark from the light-contributions as well and group it with the top. Similar to sec. 2.5.2 we make a split into light-fermion doublet contributions ($D_{\rm lf}$) and the top-bottom doublet D_{tb},

$$\left(\hat{\Pi}_{XY}^T\right)_{\rm fer} \equiv \left[\sum_{D_{\rm lf}} \left(\hat{\Pi}_{XY}^T\right)_{D_{\rm lf}}\right] + \left(\hat{\Pi}_{XY}^T\right)_{D_{\rm tb}}, \tag{5.10}$$

where the sum over $D_{\rm lf}$ extends over all light-doublets of the SM. Apart from this only the consequence for the light-doublet contributions is that the various explicit prefactors of M_Z^2 in the renormalized ZZ-transition $\left(\hat{\Pi}_{ZZ}^T\right)_{\rm fer}$ need to be set to 0 as they are power-suppressed in the boosted regime. We find for the various renormalized transitions

$$\frac{1}{s}\left(\hat{\Pi}_{AA}^T\right)_{D_{\rm lf}}^{\rm HE}(s) = -\frac{\alpha}{3\pi}\sum_{f\in D_{\rm lf}}\left(N_{c,f}\,Q_f^2\right)\left[\ln\left(\frac{\mu^2}{-s-i0^+}\right)+\frac{5}{3}\right],$$

$$\frac{1}{s}\left(\hat{\Pi}^T_{ZA}\right)^{\text{HE}}_{D_{\text{lf}}}(s) = \frac{\alpha}{3\pi}\left\{\Big(\sum_{f\in D_{\text{lf}}} N_{c,f}\, Q_f\, v_f\Big)\ln\left(\frac{M_W^2}{-s-i0^+}\right) + \frac{c_W}{s_W}\Big(\sum_{f\in D_{\text{lf}}} N_{c,f}\big(v_f^2+a_f^2\big)\Big)\ln\left(c_W^2\right)\right\},$$

$$\frac{1}{s}\left(\hat{\Pi}^T_{ZZ}\right)^{\text{HE}}_{D_{\text{lf}}}(s) = -\frac{\alpha}{3\pi}\left\{\Big(\sum_{f\in D_{\text{lf}}} \big(v_f^2+a_f^2\big)\Big)\left[\ln\left(\frac{M_Z^2}{-s-i0^+}\right) + \frac{c_W^2}{s_W^2}\ln\left(c_W^2\right)\right]+\right.$$
$$\left. + \Big(\sum_{f\in D_{\text{lf}}} Q_f^2\Big)\left[\ln\left(\frac{s}{M_W^2}\right)+\frac{5}{3}\right]\right\}, \qquad (5.11)$$

where we remind that $\alpha \equiv \alpha(\sqrt{s})$ is understood. These expressions can then be inserted into the formal contribution to the high-energy matrix element in eq. (5.8)

$$\frac{1}{4\pi}\left(\bar{c}_1^{(1),\rho\kappa}\right)^{\text{HE}}_{\text{FOC}} = (v_t-\rho\, a_t)\,(v_e-\kappa\, a_e)\,\frac{\left(\hat{\Pi}^T_{ZZ}\right)^{\text{HE}}_{\text{fer}}(s)}{s} + Q_tQ_e\frac{\left(\hat{\Pi}^T_{AA}\right)^{\text{HE}}_{\text{fer}}(s)}{s}+$$
$$+\Big[(v_t-\rho\, a_t)(-Q_e)+(-Q_t)(v_e-\kappa\, a_e)\Big]\frac{\left(\hat{\Pi}^T_{ZA}\right)^{\text{HE}}_{\text{fer}}(s)}{s}, \qquad (5.12)$$

$$\frac{1}{4\pi}\left(\bar{c}_2^{(1),\rho\kappa}\right)^{\text{HE}}_{\text{FOC}} = 0. \qquad (5.13)$$

where $\chi^{(0)}(s)\to 1$ in the boosted regime has been used.

5.2.2 Bosonic oblique corrections (BOC), charged cluster and $\boldsymbol{WW}$-box

As we saw in ch. 4 there are 3 major components necessary to achieve complete UV- and gauge-cancellations in the charged sector: the bosonic oblique corrections (BOC), the charged clusters (where the bosonic contributions to the local vertex counterterms are included) and the WW-box.

We start with the bosonic contributions. Like for the FOC the bare diagrams for the transitions are super simple and independent of the boson masses in the high-energy limit, as can be seen from the generic diagrams in the appendix (E.5). The counterterms, namely δZ_{M_W} and δZ_{M_Z}, give relatively involved expressions that are however not really interesting, as they only depend on the quantities $\sim \Lambda_{\text{EW}}$ and ratios thereof, and therefore contribute to the constant term a_0 in eq. (5.6). To make UV-cancellations manifest, we write

$$\left(\delta Z_{M_Z}\right)_{\text{bos}} = \frac{\alpha}{4\pi}\frac{1}{2s_W^2\epsilon}\left(\frac{-84c_W^4+14c_W^2+11}{6c_W^2} - \frac{3\left(2c_W^4+1\right)M_W^2}{c_W^4 M_H^2} - \frac{3M_H^2}{2M_W^2}\right) + \left(\delta\hat{Z}_{M_Z}\right)_{\text{bos}},$$

$$\left(\delta Z_{M_W}\right)_{\text{bos}} = \frac{\alpha}{4\pi}\frac{1}{2s_W^2\epsilon}\left(\frac{9-68c_W^2}{6c_W^2} - \frac{3\left(2c_W^4+1\right)M_W^2}{c_W^4 M_H^2} - \frac{3M_H^2}{2M_W^2}\right) + \left(\delta\hat{Z}_{M_W}\right)_{\text{bos}}, \qquad (5.14)$$

where the hatted quantities are the UV-finite and gauge-independent parts of the renormalization constants[5]. They can be read off from eqs. (2.127) and (2.130) in sec. 2.5.2. Note that the terms with the Higgs-mass appearing come from the Higgs-tadpole contributions to the mass counterterms. The are exactly equal for $\left(\delta Z_{M_Z}\right)_{\text{bos}}$ and $\left(\delta Z_{M_W}\right)_{\text{bos}}$ and cancel in the expressions for the renormalized transitions (cf. sec. 3.3.2). We find for the renormalized transitions

$$\frac{1}{s}\left(\hat{\Pi}^T_{AA}\right)^{\text{HE}}_{\text{bos}}(s) = \frac{\alpha}{4\pi}\left\{-(\xi_W-4)\ln\left(\frac{M_W^2}{-s-i0^+}\right) + \frac{3\xi_W^2+9\xi_W+38}{6} - \frac{\xi_W(\xi_W+2)}{\xi_W-1}\ln(\xi_W)\right\},$$

$$\frac{1}{s}\left(\hat{\Pi}^T_{ZA}\right)^{\text{HE}}_{\text{bos}}(s) = \frac{\alpha}{4\pi}\frac{c_W}{s_W}\left\{\left(\frac{6\xi_W-25}{6} - \frac{s_W^2}{6c_W^2}\right)\ln\left(\frac{M_W^2}{-s-i0^+}\right)+\right.$$

[5]Note that they are dependent on the renormalization scale μ though!

$$
-\frac{9\xi_W^2+27\xi_W+134}{18}-\frac{4s_W^2}{9c_W^2}+\frac{\xi_W(\xi_W+2)}{\xi_W-1}\ln(\xi_W)+
$$
$$
-\frac{1+42c_W^2}{6c_W^2}\ln\left(\frac{\mu^2}{M_W^2}\right)+\left(\delta\hat{Z}_{M_Z}\right)_{\text{bos}}-\left(\delta\hat{Z}_{M_W}\right)_{\text{bos}}\Bigg\}, \tag{5.15}
$$

$$
\frac{1}{s}\left(\hat{\Pi}^T_{ZZ}\right)^{\text{HE}}_{\text{bos}}(s)=\frac{\alpha}{4\pi}\frac{1}{s_W^2}\Bigg\{-\frac{6c_W^4(\xi_W-4)-c_W^2+s_W^2}{6c_W^2}\ln\left(\frac{M_W^2}{-s-i0^+}\right)+
$$
$$
+\frac{3c_W^4\left(3\xi_W^2+9\xi_W+46\right)+4c_W^2-8}{18c_W^2}-\frac{c_W^2\xi_W(\xi_W+2)}{\xi_W-1}\ln(\xi_W)+
$$
$$
-\frac{-84c_W^4+40c_W^2+1}{6c_W^2}\ln\left(\frac{\mu^2}{M_W^2}\right)-(c_W^2-s_W^2)\Big[\left(\delta\hat{Z}_{M_Z}\right)_{\text{bos}}-\left(\delta\hat{Z}_{M_W}\right)_{\text{bos}}\Big]\Bigg\}, \tag{5.16}
$$

We point out that we do not need to set $\mu=\sqrt{s}$ in these expressions since the bosonic contributions are always renormalized on-shell, and the apparent explicit μ-dependence in the respective last lines of the equations is actually cancelling against the μ-dependence in the finite parts of the renormalization constants $\left(\delta Z_{M_Z}\right)_{\text{bos}}$ and $\left(\delta Z_{M_W}\right)_{\text{bos}}$ (cf. eqs. (2.127) and (2.130)). However we emphasize again that $\alpha\equiv\alpha(\sqrt{s})$. The BOC can now be constructed in complete analogy to the FOC in the last section, i.e.

$$
\frac{1}{4\pi}\left(\bar{c}_1^{(1),\rho\kappa}\right)^{\text{HE}}_{\text{BOC}}=(v_t-\rho\,a_t)\,(v_e-\kappa\,a_e)\,\frac{\left(\hat{\Pi}^T_{ZZ}\right)^{\text{HE}}_{\text{bos}}(s)}{s}+Q_tQ_e\frac{\left(\hat{\Pi}^T_{AA}\right)^{\text{HE}}_{\text{bos}}(s)}{s}+
$$
$$
+\Big[(v_t-\rho\,a_t)(-Q_e)+(-Q_t)(v_e-\kappa\,a_e)\Big]\frac{\left(\hat{\Pi}^T_{ZA}\right)^{\text{HE}}_{\text{bos}}(s)}{s}, \tag{5.17}
$$

$$
\frac{1}{4\pi}\left(\bar{c}_2^{(1),\rho\kappa}\right)^{\text{HE}}_{\text{BOC}}=0. \tag{5.18}
$$

Next up are the charged clusters. In contrast to the oblique corrections they contain Sudakov double-logs and the constant parts a_0 show significant dependence on the mass ratio $\frac{M_W^2}{m_t^2+i0^+}\equiv r_W-i0^+$. For the form factors $(F_1)^{\text{HE}}_{\text{CC}}$ (where CC stands for charged cluster) we find

$$
(F_1^{Ztt,-})^{\text{HE}}_{\text{CC}}=\frac{\alpha}{4\pi}\frac{1}{12c_Ws_W^3}\Bigg\{\left(2c_W^2+1\right)\ln^2\left(\frac{M_W^2}{-s-i0^+}\right)+3\left(3c_W^2(\xi_W-1)+1\right)\ln\left(\frac{M_W^2}{-s-i0^+}\right)+
$$
$$
+\left(1-4c_W^2\right)r_W+\frac{4c_W^2-1}{2r_W}+\frac{c_W^2(67-3\xi_W(2\xi_W+5))}{2}+1+
$$
$$
-\left(4c_W^2+2\right)\ln^2(-r_W+i0^+)+\left(\frac{9c_W^2\xi_W^2}{\xi_W-1}-\frac{12c_W^2}{r_W}\right)\ln(\xi_W)+
$$
$$
+\left(\left(4c_W^2-1\right)r_W^2-\frac{12c_W^2}{r_W}+\left(3-12c_W^2\right)r_W+20c_W^2-2\right)\times
$$
$$
\times\ln\left(\frac{r_W}{r_W-1-i0^+}\right)+
$$
$$
+12c_W^2\left(\frac{1}{r_W}-\xi_W\right)\ln\left(\frac{r_W\xi_W}{r_W\xi_W-1-i0^+}\right)+
$$
$$
-4\left(2c_W^2+1\right)\text{Li}_2(r_W-i0^+)\Bigg\},
$$

$$
(F_1^{Ztt,+})^{\text{HE}}_{\text{CC}}=\frac{\alpha}{4\pi}\frac{1}{6c_Ws_W}\Bigg\{-\frac{1}{r_W}\ln\left(\frac{M_W^2}{-s-i0^+}\right)+\frac{3\left(c_W^2-s_W^2\right)}{2s_W^2r_W}+4r_W-1+
$$

$$+\left(-4r_W^2+3r_W+\frac{1}{r_W}\right)\ln\left(\frac{r_W}{r_W-1-i0^+}\right)\Bigg\}, \tag{5.19}$$

$$(F_1^{Att,-})^{\rm HE}_{\rm CC}=\frac{\alpha}{4\pi}\frac{1}{6s_W^2}\Bigg\{-\ln^2\left(\frac{M_W^2}{-s-i0^+}\right)-\frac{9}{2}(\xi_W-1)\ln\left(\frac{M_W^2}{-s-i0^+}\right)+$$
$$+2r_W-\frac{1}{r_W}+\frac{6\xi_W^2+15\xi_W-67}{4}+2\ln^2(-r_W+i0^+)+$$
$$+\left(\frac{6}{r_W}-\frac{9\xi_W^2}{2(\xi_W-1)}\right)\ln(\xi_W)+$$
$$+\left(-2r_W^2+6r_W+\frac{6}{r_W}-10\right)\ln\left(\frac{r_W}{r_W-1-i0^+}\right)+$$
$$+6\left(\xi_W-\frac{1}{r_W}\right)\ln\left(\frac{r_W\xi_W}{r_W\xi_W-1-i0^+}\right)+4\,{\rm Li}_2(r_W-i0^+)\Bigg\}$$

$$(F_1^{Att,+})^{\rm HE}_{\rm CC}=\frac{\alpha}{4\pi}\frac{1}{6s_W^2}\Bigg\{-\frac{1}{r_W}\ln\left(\frac{M_W^2}{-s-i0^+}\right)+4r_W-\frac{3}{r_W}-1+$$
$$+\left(-4r_W^2+3r_W+\frac{1}{r_W}\right)\ln\left(\frac{r_W}{r_W-1-i0^+}\right)\Bigg\}, \tag{5.20}$$

$$(F_1^{Zee,-})^{\rm HE}_{\rm CC}=\frac{\alpha}{4\pi}\frac{1}{4c_Ws_W^3}\Bigg\{-\ln^2\left(\frac{M_W^2}{-s-i0^+}\right)+\left(c_W^2(5-3\xi_W)-3\right)\ln\left(\frac{M_W^2}{-s-i0^+}\right)+$$
$$+\frac{3c_W^2\left(2\xi_W^2+5\xi_W-11\right)-4\pi^2-21}{6}-\frac{3c_W^2\xi_W^2}{\xi_W-1}\ln(\xi_W)\Bigg\},$$

$$(F_1^{Zee,+})^{\rm HE}_{\rm CC}=0, \tag{5.21}$$

$$(F_1^{Aee,-})^{\rm HE}_{\rm CC}=\frac{\alpha}{4\pi}\frac{1}{4s_W^2}\Bigg\{-(5-3\xi_W)\ln\left(\frac{M_W^2}{-s-i0^+}\right)-\frac{2\xi_W^2+5\xi_W-11}{2}+\frac{3\xi_W^2}{\xi_W-1}\ln(\xi_W)\Bigg\}$$

$$(F_1^{Aee,+})^{\rm HE}_{\rm CC}=0. \tag{5.22}$$

The form factors given above allow to construct the high-energy coefficients $\left(\bar{c}_i^{(1),\rho\kappa}\right)^{\rm HE}_{\rm CC}$,

$$\frac{1}{4\pi}\left(\bar{c}_1^{(1),\rho\kappa}\right)^{\rm HE}_{\rm CC}=\left(v_e-\kappa\,a_e\right)\left(\hat{F}_1^{Ztt,\rho}\right)^{\rm HE}(s)+\left(v_t-\rho\,a_t\right)\left(\hat{f}_1^{Zee,\kappa}\right)^{\rm HE}(s)+$$
$$+(-Q_e)\left(\hat{F}_1^{Att,\rho}\right)^{\rm HE}(s)+(-Q_t)\left(\hat{f}_1^{Aee,\kappa}\right)^{\rm HE}(s),$$

$$\frac{1}{4\pi}\left(\bar{c}_2^{(1),\rho\kappa}\right)^{\rm HE}_{\rm CC}=0. \tag{5.23}$$

The WW-box is a relatively simple expression. For the high-energy box coefficients $\left(\bar{c}_1^{(1),\rho\kappa}\right)^{\rm HE}_{WW-{\rm box}}$ we obtain

$$(\bar{c}_1^{(1),\rho\kappa})^{\rm HE}_{WW-{\rm box}}=\frac{\alpha}{2s_W^4}\,\delta^\rho_{-1}\delta^\kappa_{-1}\Bigg\{\ln^2\left(\frac{M_W^2}{-s-i0^+}\right)+\left[\xi_W-1-2\ln\left(\frac{-u-i0^+}{-s-i0^+}\right)\right]\ln\left(\frac{M_W^2}{-s-i0^+}\right)+$$
$$-\frac{\xi^2+2\xi-3}{4}-\frac{2\pi^2}{3}-\ln^2(-r_W+i0^+)-2\,{\rm Li}_2(r_W-i0^+)+$$

$$-\left(\frac{1}{r_W}-1\right)\ln\left(\frac{r_W}{r_W-1-i0^+}\right)+\left(\frac{1}{r_W}-\xi_W\right)\ln\left(\frac{r_W}{\xi_W r_W-1-i0^+}\right)\Bigg\},$$

$$(\bar{c}_2^{(1),\rho\kappa})^{\rm HE}_{WW-{\rm box}}=0. \tag{5.24}$$

Combining the high-energy coefficients to form the UV-finite and gauge-independent building block which we call charged sector (C-sector), consisting of BOC, charged clusters and the WW-box,

$$(\bar{c}_1^{(1),\rho\kappa})^{\rm HE}_{\text{C-sector}}\equiv(\bar{c}_1^{(1),\rho\kappa})^{\rm HE}_{\rm CC}+(\bar{c}_1^{(1),\rho\kappa})^{\rm HE}_{\rm BOC}+(\bar{c}_1^{(1),\rho\kappa})^{\rm HE}_{WW-{\rm box}}, \tag{5.25}$$

we obtain the following expressions

$$\begin{aligned}(\bar{c}_1^{(1),LL})^{\rm HE}_{\text{C-sector}}=\frac{\alpha}{12s_W^4}\Bigg\{&\left(\frac{1}{c_W^2}+2\right)\ln^2\left(\frac{M_W^2}{-s-i0^+}\right)+\frac{\pi^2}{3}\left(\frac{1}{c_W^2}-16\right)+\\&+\left[\frac{1}{6}\left(\frac{1}{c_W^4}+\frac{16}{c_W^2}-92\right)-12\ln\left(\frac{-u-i0^+}{-s-i0^+}\right)\right]\ln\left(\frac{M_W^2}{-s-i0^+}\right)+\\&+\frac{-48c_W^6-1790c_W^4+73c_W^2+16}{36c_W^4}-\frac{2c_W^2+1}{4c_W^2r_W}+\frac{1}{2}\left(\frac{1}{c_W^2}+2\right)r_W+\\&+\left[-\frac{\left(2c_W^2+1\right)r_W^2}{2c_W^2}+\frac{3}{2}\left(\frac{1}{c_W^2}+2\right)r_W-\frac{1}{c_W^2}-2\right]\ln\left(\frac{r_W}{r_W-1-i0^+}\right)+\\&-\left(\frac{1}{c_W^2}+2\right)\ln^2(-r_W+i0^+)-2\left(\frac{1}{c_W^2}+2\right)\mathrm{Li}_2(r_W-i0^+)+\\&+\frac{\left(-84c_W^6-86c_W^4+40c_W^2+1\right)}{6c_W^4}\ln\left(\frac{\mu^2}{M_W^2}\right)+\\&+\left(-2c_W^2+\frac{1}{c_W^2}-2\right)\left[\left(\delta\hat{Z}_{M_W}\right)_{\rm bos}-\left(\delta\hat{Z}_{M_Z}\right)_{\rm bos}\right]\Bigg\},\end{aligned}$$

$$\begin{aligned}(\bar{c}_1^{(1),LR})^{\rm HE}_{\text{C-sector}}=\frac{\alpha}{6c_W^2s_W^2}\Bigg\{&\frac{1}{2}\ln^2\left(\frac{M_W^2}{-s-i0^+}\right)+\frac{1}{6}\left(\frac{1}{c_W^2}+8\right)\ln\left(\frac{M_W^2}{-s-i0^+}\right)+\\&+\frac{1}{36}\left(-24c_W^2+\frac{16}{c_W^2}+18r_W-\frac{9}{r_W}+26\right)+\\&+\frac{1}{2}\left(-r_W^2+3r_W-2\right)\ln\left(\frac{r_W}{r_W-1-i0^+}\right)+\\&-\ln^2(-r_W+i0^+)-2\mathrm{Li}_2(r_W-i0^+)+\\&+\frac{1}{6}\left(-42c_W^2+\frac{1}{c_W^2}+41\right)\ln\left(\frac{\mu^2}{M_W^2}\right)+s_W^2\left[\left(\delta\hat{Z}_{M_W}\right)_{\rm bos}-\left(\delta\hat{Z}_{M_Z}\right)_{\rm bos}\right]\Bigg\},\end{aligned}$$

$$\begin{aligned}(\bar{c}_1^{(1),RL})^{\rm HE}_{\text{C-sector}}=\frac{\alpha}{3c_W^2s_W^2}\Bigg\{&\frac{1}{2}\ln^2\left(\frac{M_W^2}{-s-i0^+}\right)-\frac{1}{4r_W}\ln\left(\frac{M_W^2}{-s-i0^+}\right)+\frac{\pi^2}{3}+\\&+\frac{1}{18}\left(-12c_W^2+\frac{8}{c_W^2}+31\right)+r_W+\\&+\left(-r_W^2+\frac{3r_W}{4}+\frac{1}{4r_W}\right)\ln\left(\frac{r_W}{r_W-1-i0^+}\right)+\\&+\frac{1}{6}\left(-42c_W^2+\frac{1}{c_W^2}+41\right)\ln\left(\frac{\mu^2}{M_W^2}\right)+s_W^2\left[\left(\delta Z_{M_W}\right)_{\rm bos}-\left(\delta Z_{M_Z}\right)_{\rm bos}\right]\Bigg\},\end{aligned}$$

$$(\bar{c}_1^{(1),RR})^{\text{HE}}_{\text{C-sector}} = \frac{2\alpha}{3c_W^2 s_W^2}\Bigg\{ \left[\frac{1}{6}\left(\frac{1}{c_W^2}-1\right) - \frac{1}{4r_W}\right]\ln\left(\frac{M_W^2}{-s-i0^+}\right) +$$
$$-\frac{2c_W^2}{3} + \frac{4}{9c_W^2} + r_W - \frac{3}{8r_W} - \frac{1}{36} +$$
$$+\left(-r_W^2 + \frac{3r_W}{4} + \frac{1}{4r_W}\right)\ln\left(\frac{r_W}{r_W-1-i0^+}\right) +$$
$$+\frac{1}{6}\left(-42c_W^2 + \frac{1}{c_W^2} + 41\right)\ln\left(\frac{\mu^2}{M_W^2}\right) + s_W^2\Big[\left(\delta\hat{Z}_{M_W}\right)_{\text{bos}} - \left(\delta\hat{Z}_{M_Z}\right)_{\text{bos}}\Big]\Bigg\}, \tag{5.26}$$

where the quantum numbers of the fermions (electrons and top quarks) have been used and the explicit μ-dependence cancels against the implicit μ-dependence in $\left(\delta Z_{M_W}\right)_{\text{bos}}$ and $\left(\delta Z_{M_Z}\right)_{\text{bos}}$ as for the BOC. The coefficients $(\bar{c}_2^{(1),\rho\kappa})^{\text{HE}}_{\text{C-sector}}$ are all 0 and therefore not given. The results in eq. (5.26) still look involved, but they have in fact simplified enormously compared to the general continuum case. The sceptical reader may want to compare to the average generic diagrams in the continuum given in the appendix E. A further discussion on the final results is found at the end of this chapter.

5.2.3 Neutral clusters

The neutral cluster of each vertex (Ztt, Att, Zee, Aee) forms a UV-finite and gauge-independent set of its own. The constants parts of the expressions (dependent on the ratios $r_Z = \frac{M_Z^2}{m_t^2+i0^+}$ and $r_H = \frac{M_H^2}{m_t^2+i0^+}$) are somewhat involved (at least for the massive final-state vertices), once again mainly due to the finite counterterm contributions. Readers only interested in the Sudakov logs might want to skip ahead to sec. 5.3.3, where we give the Sudakov logs separately. In contrast to the charged sector where some interactions were maximally chiral, for the presentation of the the neutral clusters we go back to arbitrary chirality indices ρ, κ. For the form factors $(F_1)^{\text{HE}}_{\text{NC}}$ (where NC stands for neutral cluster) we obtain

$$(F_1^{Ztt,\rho})^{\text{HE}}_{\text{NC}} = -\frac{\alpha}{4\pi}(v_t - \rho\, a_t)\times$$
$$\times\Bigg\{(v_t-\rho\, a_t)^2\Bigg[\ln^2\left(\frac{M_Z^2}{-s-i0^+}\right) + 3\ln\left(\frac{m_t^2}{-s-i0^+}\right) - 4\,\Lambda\left(1;1,\sqrt{r_Z}\right) +$$
$$+4\,\mathrm{Li}_2\left(\frac{2}{r_Z+\sqrt{r_Z(r_Z-4)}}\right) + 4\,\mathrm{Li}_2\left(\frac{2}{r_Z-\sqrt{r_Z(r_Z-4)}}\right)\Bigg] +$$
$$-(v_t-\rho\, a_t)\Big[(\xi_Z-1)(v_t-3\rho\, a_t) + 2\rho\, a_t\Big(\Lambda\left(1;1,\sqrt{r_Z}\right) - \xi_Z\Lambda\left(1;1,\sqrt{r_Z}\sqrt{\xi_Z}\right)\Big)\Big] +$$
$$+2\rho\, v_t\, a_t\big(r_Z - 2\xi_Z\big) + v_t^2(\xi_Z+3+3r_Z) - 3a_t^2(\xi_Z+3-r_Z) +$$
$$-\frac{1}{2}\Bigg(v_t^2\left(3r_Z^2-4r_Z-4\right) + a_t^2\left(8\xi_Z+3r_Z^2-2\left(3\xi_Z^2+7\right)r_Z+4\right) + 2\rho\, v_t\, a_t\, r_Z^2 +$$
$$-\frac{\xi_Z(4-3\xi_Z r_Z)}{8c_W^2 s_W^2}\Bigg)\ln(r_Z) +$$
$$+\frac{3v_t^2\left(r_Z^2-2r_Z-4\right) + 3a_t^2\left(r_Z^2-6r_Z+8\right) + 2\rho\, v_t\, a_t\left(r_Z^2-5r_Z+4\right)}{r_Z-4}\times$$
$$\times\Lambda\left(1;1,\sqrt{r_Z}\right) +$$
$$-\frac{32a_t^2 c_W^2 s_W^2(\xi_Z r_Z-3) + 16\rho\, v_t\, a_t c_W^2 s_W^2(\xi_Z r_Z-4) - 3\xi_Z r_Z + 10}{8c_W^2 s_W^2(\xi_Z r_Z-4)}\times$$

$$\times\,\xi_Z\,\Lambda\left(1;1,\sqrt{r_Z}\sqrt{\xi_Z}\right)+$$

$$+\left(a_t^2-\frac{1}{16c_W^2s_W^2}\right)(3r_Z\xi_Z-4)\xi_Z\,\ln(\xi_Z)+$$

$$+\frac{3}{8c_W^2s_W^2r_Z}\Big(r_H-2+r_Z\xi_Z+(r_H-2)\,\Lambda\,(1;1,\sqrt{r_H})-\frac{8-12r_H+3r_H^2}{6}\,\ln\left(r_H\right)\Big)+$$

$$-\frac{1}{4c_W^2s_W^2r_Z}\left[\ln\left(\frac{m_t^2}{-s-i0^+}\right)+1\right]\Bigg\}-\frac{\alpha}{4\pi}\frac{\rho\,a_t}{c_W^2s_W^2r_Z},\tag{5.27}$$

$$(F_2^{Ztt,\rho})^{\rm HE}_{\rm NC}=0,\tag{5.28}$$

$$(F_1^{Att,\rho})^{\rm HE}_{\rm NC}=\frac{\alpha}{4\pi}\,Q_t\times$$

$$\times\Bigg\{(v_t-\rho\,a_t)^2\left[\ln^2\left(\frac{M_Z^2}{-s-i0^+}\right)+3\ln\left(\frac{m_t^2}{-s-i0^+}\right)-4\,\Lambda\,(1;1,\sqrt{r_Z})+\right.$$

$$\left.+4\,\mathrm{Li}_2\left(\frac{2}{r_Z+\sqrt{r_Z\,(r_Z-4)}}\right)+4\,\mathrm{Li}_2\left(\frac{2}{r_Z-\sqrt{r_Z\,(r_Z-4)}}\right)\right]+$$

$$-(v_t-\rho\,a_t)\Big[(\xi_Z-1)(v_t-3\rho\,a_t)+2\rho\,a_t\Big(\Lambda\,(1;1,\sqrt{r_Z})-\xi_Z\Lambda\left(1;1,\sqrt{r_Z}\sqrt{\xi_Z}\right)\Big)\Big]+$$

$$+2\rho\,v_t\,a_t\big(r_Z-2\xi_Z\big)+v_t^2(\xi_Z+3+3r_Z)-3a_t^2(\xi_Z+3-r_Z)+$$

$$-\frac{1}{2}\Big(v_t^2\left(3r_Z^2-4r_Z-4\right)+a_t^2\left(8\xi_Z+3r_Z^2-2\left(3\xi_Z^2+7\right)r_Z+4\right)+2\rho\,v_t\,a_t\,r_Z^2+$$

$$-\frac{\xi_Z(4-3\xi_Zr_Z)}{8c_W^2s_W^2}\Big)\ln(r_Z)+$$

$$+\frac{3v_t^2\left(r_Z^2-2r_Z-4\right)+3a_t^2\left(r_Z^2-6r_Z+8\right)+2\rho\,v_t\,a_t\left(r_Z^2-5r_Z+4\right)}{r_Z-4}\times$$

$$\times\,\Lambda\,(1;1,\sqrt{r_Z})+$$

$$-\frac{32a_t^2c_W^2s_W^2(\xi_Zr_Z-3)+16\rho\,v_t\,a_tc_W^2s_W^2(\xi_Zr_Z-4)-3\xi_Zr_Z+10}{8c_W^2s_W^2(\xi_Zr_Z-4)}\times$$

$$\times\,\xi_Z\,\Lambda\left(1;1,\sqrt{r_Z}\sqrt{\xi_Z}\right)+$$

$$+\left(a_t^2-\frac{1}{16c_W^2s_W^2}\right)(3r_Z\xi_Z-4)\xi_Z\,\ln(\xi_Z)+$$

$$+\frac{3}{8c_W^2s_W^2r_Z}\Big(r_H-\frac{8}{3}+r_Z\xi_Z+(r_H-2)\,\Lambda\,(1;1,\sqrt{r_H})-\frac{8-12r_H+3r_H^2}{6}\,\ln\left(r_H\right)\Big)+$$

$$-\frac{1}{4c_W^2s_W^2r_Z}\,\ln\left(\frac{m_t^2}{-s-i0^+}\right)\Bigg\},\tag{5.29}$$

$$(F_2^{Att,\rho})^{\rm HE}_{\rm NC}=0,\tag{5.30}$$

$$(F_1^{Zee,\rho})^{\rm HE}_{\rm NC} = -\frac{\alpha}{4\pi}\,(ve-\kappa\,a_e)^3\bigg\{\ln^2\left(\frac{M_Z^2}{-s-i0^+}\right)+3\ln\left(\frac{M_Z^2}{-s-i0^+}\right)+\frac{2\pi^2}{3}+\frac{7}{2}\bigg\},$$

$$(F_2^{Zee,\rho})^{\rm HE}_{\rm NC} = 0, \tag{5.31}$$

$$(F_1^{Aee,\rho})^{\rm HE}_{\rm NC} = \frac{\alpha}{4\pi}\,Q_e\,(ve-\kappa\,a_e)^2\bigg\{\ln^2\left(\frac{M_Z^2}{-s-i0^+}\right)+3\ln\left(\frac{M_Z^2}{-s-i0^+}\right)+\frac{2\pi^2}{3}+\frac{7}{2}\bigg\},$$

$$(F_2^{Aee,\rho})^{\rm HE}_{\rm NC} = 0. \tag{5.32}$$

With these form factors the contributions of the neutral clusters to the coefficients $\left(\bar{c}_1^{(1),\rho\kappa}\right)^{\rm HE}$ can be constructed analogously to the charged clusters in eq. (5.23).

5.2.4 ZZ-boxes

As we saw in ch. 4 the ZZ-boxes become gauge-independent when both topologies are added, thus forming a proper building block. However there is another interesting feature appearing in the high-energy limit. In eq. (5.24) it can be seen that single box diagrams have double and single Sudakov logs (this can also be seen in the high-energy expansions of the generic box diagrams given in the appendix E.5). Now the high-energy result for the sum of the ZZ-boxes reads

$$\begin{aligned}
(\bar{c}_1^{(1),\rho\kappa})^{\rm HE}_{ZZ-\rm boxes} &= \alpha\,(v_t-\rho\,a_t)^2(ve-\kappa\,a_e)^2\times\\
&\times\bigg\{4\ln\left(\frac{-t-i0^+}{-u-i0^+}\right)\ln\left(\frac{M_Z^2}{-s-i0^+}\right)+\\
&+\delta_\kappa^{-\rho}\left(\frac{2s}{t}\ln\left(\frac{-u-i0^+}{-s-i0^+}\right)+\frac{t^2+u^2}{t^2}\ln^2\left(\frac{-u-i0^+}{-s-i0^+}\right)\right)+\\
&-\delta_\kappa^{\rho}\left(\frac{2s}{u}\ln\left(\frac{-t-i0^+}{-s-i0^+}\right)+\frac{u^2+t^2}{u^2}\ln^2\left(\frac{-t-i0^+}{-s-i0^+}\right)\right)\bigg\}
\end{aligned}$$

$$(\bar{c}_2^{(1),\rho\kappa})^{\rm HE}_{ZZ-\rm boxes} = 0. \tag{5.33}$$

We infer from this result that when both box topologies (crossed and direct) are added, not only the gauge-dependence, but also the double-log as well as the constant terms independent of the Mandelstam invariants cancel between them. This is obviously a universal feature, i.e. independent of the specific couplings of the gauge-bosons to the fermions. We also find that although a linear Sudakov log survives, it is multiplied by $\ln\left(\frac{-t-i0^+}{-u-i0^+}\right)$, which is a small log according to our hierachy in eq. (5.3), since we take t and u to be of the same order. In fact, at the central point $u=t$ (corresponding to a scattering angle $\theta=\frac{\pi}{2}$) the cancellation is complete including the constant terms, and there is no contribution from the ZZ-boxes at all. This statement is generally true in the continuum (i.e. not only in the boosted regime).

5.3 Discussion and summary

The most interesting terms of the calculation in the boosted regime are the high-energy logarithms (eq. (5.4)) of the theory. If the energy scale s of the process gets large enough these logs might even invalidate the perturbative expansion at some point. Fortunately the fine-structure constant $\alpha\sim10^{-2}$ is relatively small, even when its running is taken into account, as the Landau pole is located far above any conceivable energy scale colliders in the foreseeable future could reach. The largest contribution comes from the double-logs, and plugging in some representative numbers we get

$$\frac{\alpha(\sqrt{s})}{4\pi s_W^2}\ln^2\left(\frac{s}{M_W}\right)\sim 0.1, \tag{5.34}$$

for $\sqrt{s} = 3$ TeV, $s_W = 0.23, M_W = 80$ GeV and $\alpha \sim 121^{-1}$ was run up from $137^{-}1$ at $\mu = m_e$ by including the fermionic contributions (following sec. 3.4.2). We see that the Sudakov double-logs, while nowhere near as large as in QCD (where they become really dangerous really quickly), lead to a substantial enhancement of EW NLO corrections by a full order of magnitude for energies that are already envisioned for future lepton colliders like CLIC. We chose the specific prefactor of $\frac{1}{s_W^2}$ as the largest contributions will come from the charged sector, especially from the W-diagrams (vertices and box, see numerics chapter6).

5.3.1 Logarithmic structure

In summary we (analytically) found the following interesting features concerning the logarithmic structure in the boosted regime of the weak NLO corrections:

- **Universal logarithmic structure**: as can be seen from the results for the clusters, boxes and oblique corrections (especially for the neutral clusters in eq. (5.38) below, since we did not plug in the fermionic quantum numbers yet), the Sudakov logs are independent of the structure of the fermion currents (and hence of their chiralities) and factorize. Also the Sudakov logs only depend on the gauge-boson masses, not on the top mass (some of the linear logs in our results need to be rewritten to make this feature manifest).

- **Effective local high-energy operator**: closely connected to the universal log structure is the fact that the scalar structures parametrized by $\bar{c}_2$ are power-suppressed in the boosted regime. The leading-order high-energy contributions are therefore of the form $\bar{c_1}^{\rho\kappa}\bar{M}_1^{\rho\kappa}$, which implies that the effective operator governing the leading-order behaviour in the boosted regime is a four fermion contact operator $\mathcal{O}_{\text{eff}}^{\rho\kappa}$ which is of *current-current-type*, i.e.

$$\mathcal{O}_{\text{eff}}^{\rho\kappa}(x) = \bar{t}(x)\gamma^\mu\omega^\rho t(x)\, \bar{e}(x)\gamma_\mu\omega_\kappa e(x) \tag{5.35}$$

  While we effectively checked the gauge-*independence* of the S-matrix element of this operator by our high-energy expansions of the gauge-independent full results explicitly, $\mathcal{O}_{\text{eff}}^{\rho\kappa}$ is obviously not gauge-*invariant* under the EW gauge group. We postpone further discussions on this subject to future work, or refer the reader to [25], [26] and the references therein for the moment.

- **Cancellations of ZZ-boxes**: a glimpse of what might happen in a manifestly gauge-invariant formulation of the process was provided by the sum of the crossed and direct ZZ-box types. Not only did the gauge-dependence cancel, but also the leading (= quadratic) Sudakov logs. The surviving linear log was multiplied by a log that was suppressed in the central regime, as defined in sec. 5.1.2. In contrast a lot of these features were absent in the charged sector: Sudakov logs remained uncancelled and a complicated adding procedure of various contributions was necessary to obtain gauge-indpendence. The reason is that the processes with the isospin partners of electrons and tops on the external lines were not taken into account, but they would be required by full EW gauge-invariance.

5.3.2 Constant terms

Although the results in the high-energy limit simplify drastically with respect to the continuum, the expressions are still relatively involved thanks to the constant terms coming mainly from finite parts of on-shell counterterms. Keeping those constants in the expansion is important however for various reasons. Firstly they might be numerically significant, especially in the regime with moderate CM-energies $\sqrt{s}$. We will take a look at this in more detail in the upcoming chapter with the numerical analysis. Apart from numerics however there are also conceptual reasons why a precise knowledge of these constant terms is very valuable. On the one hand they are needed for calculations and consistency checks when working with effective field theories, e.g. for matching procedures. Furthermore by knowing the size and origin of the constant terms one can estimate the reliability of conducting higher-order calculations under some simplifying assumptions. Given the constants be sufficiently small compared to the log-terms above a certain energy, it could become possible to capture most of the higher-order corrections by just computing the higher-order contributions to the anomalous dimensions of some leading operators, which is a much easier task than doing a full multi-loop calculation[6]. If they are not small but their origin is known, it might be possible to work out specific renormalization schemes to treat these corrections in a systematic and efficient way.

5.3.3 Final results (without constant terms)

The numerical significance of the Sudakov logs, also relative to the constant and power-suppressed terms, will be demonstrated in the next chapter covering the numerical evaluation and analysis. To summarize we restate the high-energy results given in the last section, this time leaving out the constant terms and restricting ourselves to the high-energy logarithms to clear up the results somewhat. For the light-fermion contributions we note that we evaluate them at $\mu = \sqrt{s}$, effectively introducing new Sudakov logs into the renormalized ZZ-transition because of the explicit μ-dependence. The top can also be treated as a light fermion to leading order in that limit.

- **FOC**:

$$\begin{aligned}\left(\bar{c}_1^{(1),\rho\kappa}\right)^{\text{HE}}_{\text{FOC}} = -\frac{4\alpha}{3}\sum_{\text{fermions}} N_{c,f}\Big\{&(v_t-\rho\,a_t)\,(v_e-\kappa\,a_e)\times\\ &\times\Big[\left(v_f^2+a_f^2\right)\ln\left(\frac{M_Z^2}{-s-i0^+}\right)+Q_f^2\ln\left(\frac{s}{M_W^2}\right)\Big]+\\ &+\Big[(v_t-\rho\,a_t)(-Q_e)+(-Q_t)(v_e-\kappa\,a_e)\Big]Q_f\,v_f\ln\left(\frac{M_W^2}{-s-i0^+}\right)\Big\}+\\ &+\text{const.}\end{aligned} \tag{5.36}$$

- **Charged sector**:

$$\begin{aligned}(\bar{c}_1^{(1),LL})^{\text{HE}}_{\text{C-sector}} = \frac{\alpha}{12s_W^4}\Big\{&\left(\frac{1}{c_W^2}+2\right)\ln^2\left(\frac{M_W^2}{-s-i0^+}\right)+\\ &+\left[\frac{1}{6}\left(\frac{1}{c_W^4}+\frac{16}{c_W^2}-92\right)-12\ln\left(\frac{-u-i0^+}{-s-i0^+}\right)\right]\ln\left(\frac{M_W^2}{-s-i0^+}\right)\Big\}+\\ &+\text{const.},\end{aligned}$$

$$(\bar{c}_1^{(1),LR})^{\text{HE}}_{\text{C-sector}} = \frac{\alpha}{6c_W^2 s_W^2}\left\{\frac{1}{2}\ln^2\left(\frac{M_W^2}{-s-i0^+}\right)+\frac{1}{6}\left(\frac{1}{c_W^2}+8\right)\ln\left(\frac{M_W^2}{-s-i0^+}\right)\right\}+\text{const.},$$

$$(\bar{c}_1^{(1),RL})^{\text{HE}}_{\text{C-sector}} = \frac{\alpha}{3c_W^2 s_W^2}\left\{\frac{1}{2}\ln^2\left(\frac{M_W^2}{-s-i0^+}\right)-\frac{1}{4r_W}\ln\left(\frac{M_W^2}{-s-i0^+}\right)\right\}+\text{const.},$$

$$(\bar{c}_1^{(1),RR})^{\text{HE}}_{\text{C-sector}} = \frac{2\alpha}{3c_W^2 s_W^2}\left\{\left[\frac{1}{6}\left(\frac{1}{c_W^2}-1\right)-\frac{1}{4r_W}\right]\ln\left(\frac{M_W^2}{-s-i0^+}\right)\right\}+\text{const.}, \tag{5.37}$$

- **Neutral clusters**:

$$\begin{aligned}\left(\bar{c}_1^{(1),\rho\kappa}\right)^{\text{HE}}_{\text{NC}} = -\alpha\Big[&(v_t-\rho\,a_t)\big(v_e-\kappa\,a_e\big)+Q_t\,Q_e\Big]\times\\ &\times\Big\{\Big[(v_t-\rho\,a_t)^2+(ve-\kappa\,a_e)^2\Big]\Big[\ln^2\left(\frac{M_Z^2}{-s-i0^+}\right)+3\ln\left(\frac{M_Z^2}{-s-i0^+}\right)\Big]+\end{aligned}$$

[6] The EW NNLO results are not known yet, only for very specific processes (e.g. threshold results for mass-corrections) and often derived under simplifying assumptions, like degenerate weak boson masses or the so-called *gaugeless limit*, where all the gauge couplings are set to 0, effectively extracting the Yukawa-enhanced terms.

$$- \frac{1}{4c_W^2 s_W^2 r_Z} \ln\left(\frac{m_t^2}{-s-i0^+}\right) \Bigg\} + \text{const.}, \tag{5.38}$$

- ***ZZ*-boxes**:

$$(\bar{c}_1^{(1),\rho\kappa})^{\text{HE}}_{ZZ-\text{boxes}} = 4\alpha\,(v_t - \rho\, a_t)^2 (ve - \kappa\, a_e)^2 \ln\left(\frac{-t-i0^+}{-u-i0^+}\right) \ln\left(\frac{M_Z^2}{-s-i0^+}\right) + \text{const.}, \tag{5.39}$$

Chapter 6

Numerical analysis

For numerical evaluations we use the following set of masses (in units of GeV):

$$m_t = 173,1 \qquad M_Z = 91.2, \qquad M_W = 80.4, \qquad M_H = 125.1. \tag{6.1}$$

c_W and s_W are then derived from these masses according to eq. (2.84) and the fine-structure constant is treated as QED-improved, i.e. run up to the scale $\mu = \sqrt{s}$ by means of the light-fermion contributions (sec. 3.4.2). The energy range chosen for numerical evaluation and presentation is

$$500 \text{ GeV} \leq \sqrt{s} \leq 3 \text{ TeV}, \tag{6.2}$$

as this corresponds to the regimes the future linear colliders will probe (in their various stages of upgrades). Note that in this work our aim is not (yet) to get precision predictions, but rather to perform some exemplary numerics and obtain some representative plots of the various proper building blocks and their respective high-energy expanded versions, which is why we do not plot any errorbars or errorbands. Although we derived the NLO corrections for the S-matrix element in terms of the $\bar{c}_i^{\rho\kappa}$, we will actually use eq. (3.22) to compute the differential helicity cross-sections and subsequently the helicity-averaged NLO contribution to the differential cross-section $\frac{d\sigma^{(1)}}{d\theta}$. The reason the cross-section is preferred over the amplitude for the numerical analysis is that it is the former that is physically relevant. Numerical statements made for the amplitude need not necessarily carry over to the (differential) cross-section, as the interferences with the tree-level amplitude and the insertion of the quantum numbers might result in significant shifts of relative numerical importance.

The gauge plots have been already shown in chapter 4 on gauge-cancellations. In this chapter we therefore primarily focus on the s-dependence of the proper building blocks and their high-energy expanded versions. The t- and u-dependence of the full and expanded results is shown in terms of plots against the scattering angle θ (cf. eq. (3.6)). We proceed as follows: in the first section 6.1 we show the plots for the single building blocks and compare with the expanded results plotted against $\sqrt{s}$ and the scattering angle θ, while the following one 6.2 is dedicated to the complete NLO contributions vs. the tree-level results. Sec. 6.3 investigates the relative numerical importance of the log-terms vs. the constant terms of the full and expanded results, followed up by a short summary in sec. 6.4

6.1 Numerics of proper building blocks

To avoid scale- and/or gauge-dependent statements the smallest sets that can be meaningfully evaluated numerically are the proper building blocks defined in ch. 4. Although it might be possible to dig in further and find some single UV- and gauge-independent form factors for certain smaller diagram sets (as for example the vector form factor for Z- and H-exchanges, as shown in sec. 5.1.1), we will stick to the former method of presentation.

The quantity we will plot in this section for both full and expanded results is the NLO contribution to the differential cross-section over the corresponding tree-level expression[1], i.e.

$$\delta\sigma_i^\kappa(s,\theta) \equiv \left(\frac{d\sigma^{(1)}}{d\theta}\right)_i^\kappa \Big/ \left(\frac{d\sigma^{(0)}}{d\theta}\right)_i^\kappa . \tag{6.3}$$

The index i denotes the building block. The helicity-averaged quantity is obtained by

$$\delta\sigma_i(s,\theta) \equiv \frac{\left(\frac{d\sigma^{(1)}}{d\theta}\right)_i^- + \left(\frac{d\sigma^{(1)}}{d\theta}\right)_i^+}{\left(\frac{d\sigma^{(0)}}{d\theta}\right)_i^- + \left(\frac{d\sigma^{(0)}}{d\theta}\right)_i^+} . \tag{6.4}$$

The prefactor $\frac{1}{4}$ usually applied for averaging drops out. To obtain the total NLO contribution to the respective cross-section, a sum over building blocks i has to be applied to either (6.3) or (6.4).

6.1.1 Plots against $\sqrt{s}$

We start by fixing θ (see plot inserts for concrete values) and plot against the CM-energy $\sqrt{s}$. In fig. 6.1 the helicity-averaged 1-loop contributions per building block over the averaged tree-level contribution (eq. (6.4)) are shown, for 3 representative values of θ. Some important features are already visible:

- The weak NLO corrections are (mostly) negative, which is why we plot the ratio of the 1-loop corrections over the tree-level [2] and not over tree-level + 1-loop, as this would inflate this fraction $\delta\sigma$ by quite some amount. Even so, the NLO contributions are quite sizable, and range up to 30% and beyond (depending on the scattering kinematics) relative to tree-level.
- In the energy regime above $\sim$ 1 TeV the contributions with (double-) Sudakov logs, i.e. the W-sector and the neutral clusters, are numerically the most important, overtaking the FOC and ZZ-boxes that have (at most) linear Sudakov logs.
- The W-sector is numerically by far the most prominent contribution (to be discussed further below).
- The expansion quality depends rather strongly on s, but also on θ (a more detailed discussion is found below).
- There is a large forward-backward-asymmetry. The NLO contributions are much larger for $\theta \to 0$ than for $\theta \to \pi$ (see also the angular plots in sec. 6.1.2). This is a feature not attributed to the logarithmic structure, but rather to the chiral nature of the theory

Some of these observations demand further discussion. Generally speaking the accuracy of the expansions near the central value $\theta = \pi/2$ and for energies of $\sim$ 1 TeV and above is quite good. The dominance of the W-sector over the neutral and fermionic contributions strikes the eye. There are 2 reasons for this. Firstly, we have some significant parametric enhancement for diagrams with virtual W-bosons coupling to fermions. For example, the ratio of the leading logarithmic behaviour of W-exchange diagrams over the Z-exchange diagrams for for left-handed contributions of final-state vertices is basically given by the ratio of the couplings to the external top-quarks (after factoring out the Sudakov log), which numerically estimates as

$$\frac{\left(\frac{1}{\sqrt{2}s_W}\right)^2}{(v_t + a_t)^2} \sim \frac{2.2}{0.7} \sim 3. \tag{6.5}$$

Of course this has to be taken with a grain of salt, as this parametric enhancement only appears in the left-handed contributions. In fig. 6.2 we plot the left- and right-handed differential cross-sections (in the ratios given by eq. (6.3)) separately for a central value $\theta = \pi/2$, and it indeed turns out that while the W-sector dominates the left-handed part, it is comparable to (actually a bit smaller than) the neutral cluster for the right-handed one.

[1] This has the advantage that a normalization to the total tree-level cross section by dividing through σ_0 is obsolete here, as any global normalization cancels out of this fraction.

[2] The tree-level contributions are manifestly positive, as it is basically the absolute value squared of $\mathcal{M}^{(0)}$.

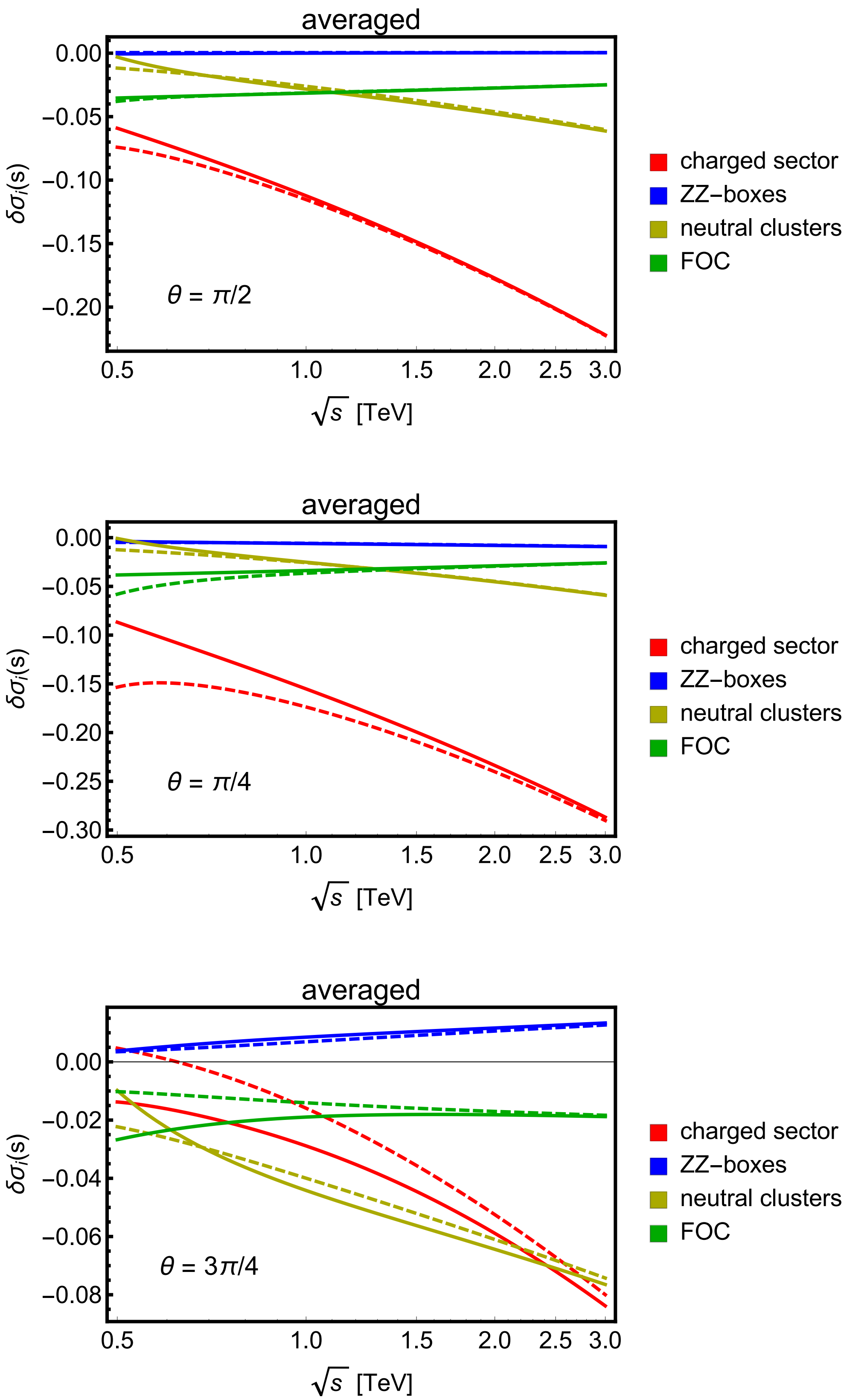

Figure 6.1: Full vs. expanded results per proper building block (helicity-averaged). Solid = full, dashed = expanded. Note the logarithmic $\sqrt{s}$-axes and the variable scalings of the y-axes.

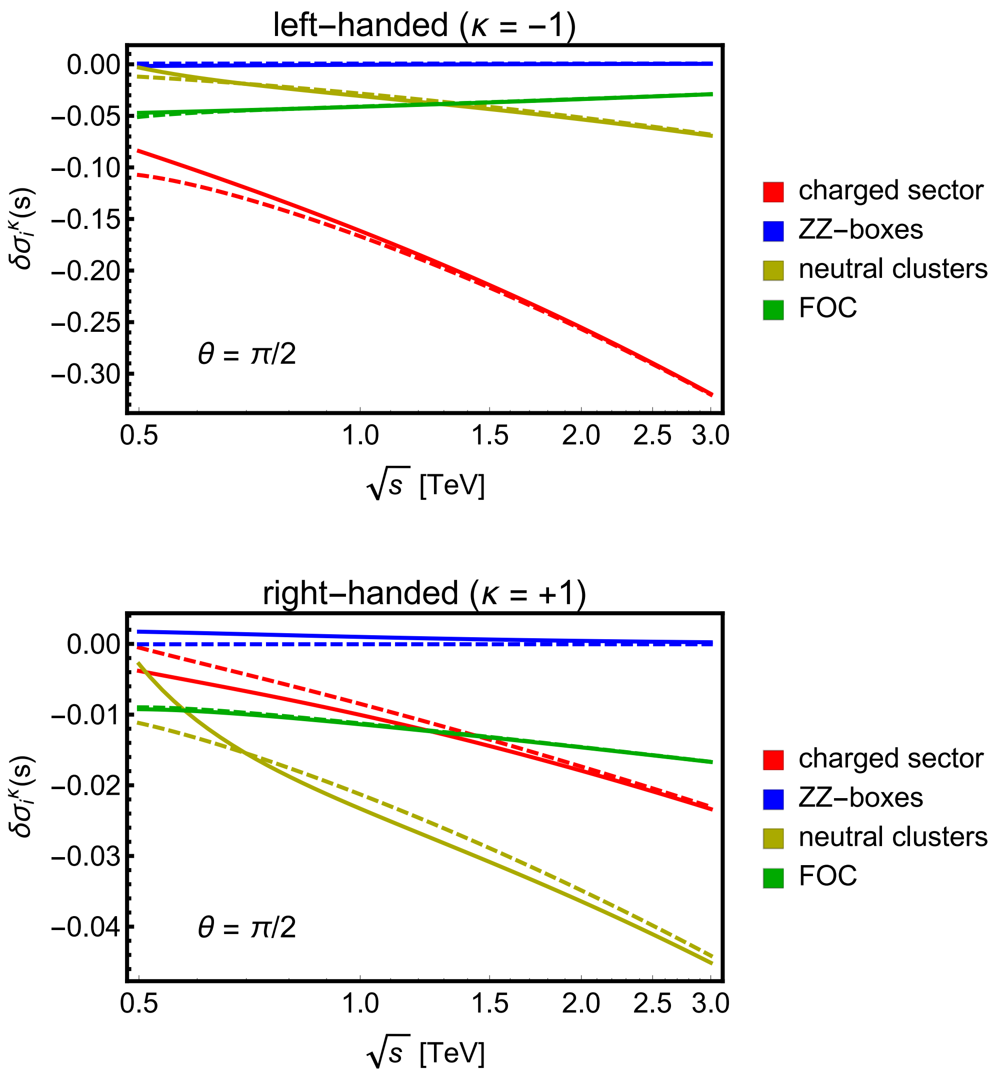

Figure 6.2: Full vs. expanded results per proper building block and helicity. Solid = full, dashed = expanded. Please note the variable scalings of the y-axes.

6.1.2 Angular plots

Now we fix s and vary the scattering angle θ. In fig. 6.3 the various building blocks are numerically evaluated for 3 representative values of the CM-energy $\sqrt{s}$. Note that those are polar plots, hence the somewhat strange-looking axes. The region of $\pm\pi/16$ around the beam axis has been left out for technical reasons, as some contributions (the ZZ-boxes) get numerically unstable in the extreme forward and backward regions.

The forward-backward asymmetry mentioned above is clearly visible here. This feature is especially stringent in the case of the W-sector. Also the accuracy of the expansion depends rather strongly on the scattering angle. Especially for lower energies it deteriorates quickly away from the central value $\theta = \pi/2$, which indicates that the power-corrections $\frac{\Lambda_{\mathrm{EW}}^2}{t,u}$ start to grow in size as the values $\theta \to 0$ or $\theta \to \pi$ are approached. The total cancellation of the ZZ-boxes exactly at the central value $\theta = \pi/2$ can also be observed explicitly.

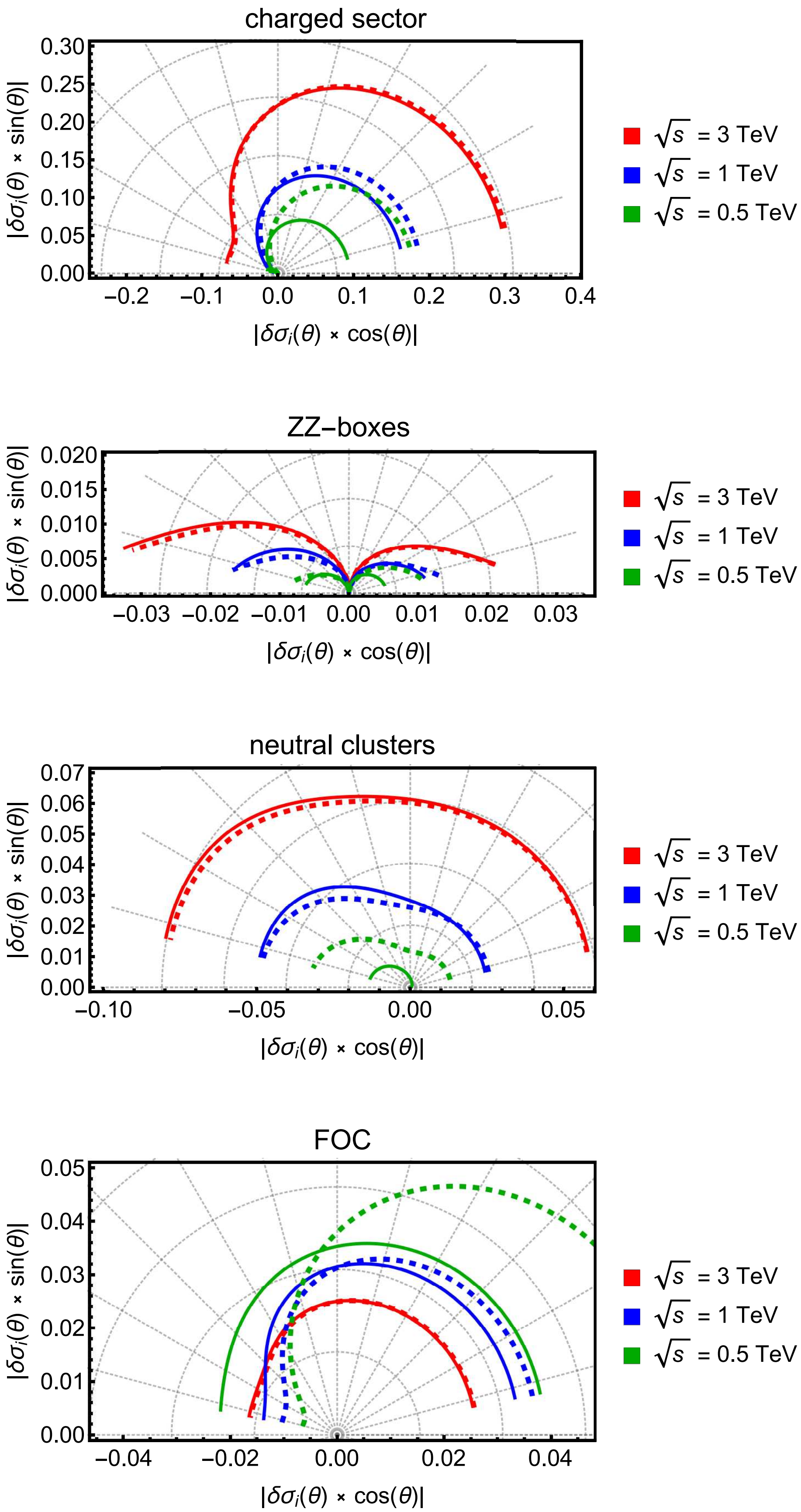

Figure 6.3: Full vs. expanded results per proper building block (all helicity-averaged). Solid = full, dashed = expanded. Note that these are polar plots (radial distance = magnitude) as well as the variable scalings of the axes.

6.2 Total NLO contributions

6.2.1 Plots vs. $\sqrt{s}$

Adding up all the building blocks gives the total weak NLO corrections to the cross-sections. The overall picture is very similar to the case of single building blocks. In fig. 6.4 we show the ratio

$$\sum_i \delta\sigma_i(s,\theta) \equiv \delta\sigma(s,\theta), \tag{6.6}$$

for both helicities as well as the helicity-averaged case for 3 different scattering angles θ.

Focusing on the absolute values of the full results for a moment, we see that the NLO corrections are actually quite large (although the precise statement is s- and θ-dependent, as can be clearly seen in fig. 6.4). For example, the averaged NLO cross-section for a central value $\theta \sim \pi/2$ ranges from about 10% at $\sqrt{s} \sim 500$ GeV to about 30% of the tree-level result at $\sqrt{s} \sim 3$ TeV, which is a very substantial amount given the smallness of the coupling α. It can even exceed these values depending on helicity and scattering angle. Although there are other ingredients for this phenomenon like the parametric enhancement of W-contributions the tree-level misses (cf. eq. (6.5)), the influence of logarithmic enhancement should not be underestimated. The growth of this fraction from eq. (6.4) in energy visible in fig. 6.4 is due to the Sudakov logs that are absent for the tree-level calculation. We discuss their contributions in more detail in sec. 6.3 below.

6.2.2 Accuracy

As a measure for the accuracy of the high-energy expansion, we plot the relative differences of full and expanded (exp) differential cross-sections for each helicity

$$A^\kappa(s,\theta) \equiv 1 - \frac{\left| \left(\frac{d\sigma^{(1)}}{d\theta}\right)^\kappa_{\text{full}} - \left(\frac{d\sigma^{(1)}}{d\theta}\right)^\kappa_{\text{exp}} \right|}{\left| \left(\frac{d\sigma^{(1)}}{d\theta}\right)^\kappa_{\text{full}} \right|}, \tag{6.7}$$

and for the averaged case

$$A(s,\theta) \equiv 1 - \frac{\left| \left(\frac{d\sigma^{(1)}}{d\theta}\right)^-_{\text{full}} + \left(\frac{d\sigma^{(1)}}{d\theta}\right)^+_{\text{full}} - \left(\frac{d\sigma^{(1)}}{d\theta}\right)^-_{\text{exp}} - \left(\frac{d\sigma^{(1)}}{d\theta}\right)^+_{\text{exp}} \right|}{\left| \left(\frac{d\sigma^{(1)}}{d\theta}\right)^-_{\text{full}} + \left(\frac{d\sigma^{(1)}}{d\theta}\right)^+_{\text{full}} \right|}. \tag{6.8}$$

For the angular numerics we define the opening angle $\delta\theta$ around the central values as

$$\theta \equiv \frac{\pi}{2} + \delta\theta. \tag{6.9}$$

The plots vs. the CM-energy can be found in fig. 6.5, and the ones for the angular dependence in fig. 6.6. There are some differences between the different helicities and the averaged case, but overall we find the expected behaviour that either a high CM-energy $\sqrt{s}$ or an angle close to the central value $\theta = \pi/2$ results in a good expansion and a higher tolerance for the respective other parameter differing from its ideal value. Note that the kinks are just artifacts ("overshoots"), the degree of convergence is only to be taken seriously again after the monotony of the curves $A(...)$ has been restored.

For energies below 1 TeV the opening angle around the central value should be rather small, in any case ideally $|\delta\theta| \ll \pi/4$, to get accuracies of about 80%. The regime above 1 TeV already allows for an opening angle of $|\delta\theta| \sim \pi/4$ without dropping far below 80% accuracy in the worst case. This region seems to be the best trade-off in terms of expansion accuracy. From a theoretical point of view, the energy regime above 1 TeV, up to 3 TeV and beyond, would be ideal. The expansions are excellent and very stable over a large range of values for $\delta\theta$. Unfortunately those partonic energies are hard to realize experimentally. Linear colliders like CLIC are envisioned to reach up to 3 TeV, but only in their final versions a few decades down the line. We will come back to the optimal energy range in the next section on Sudakov logarithmic contributions.

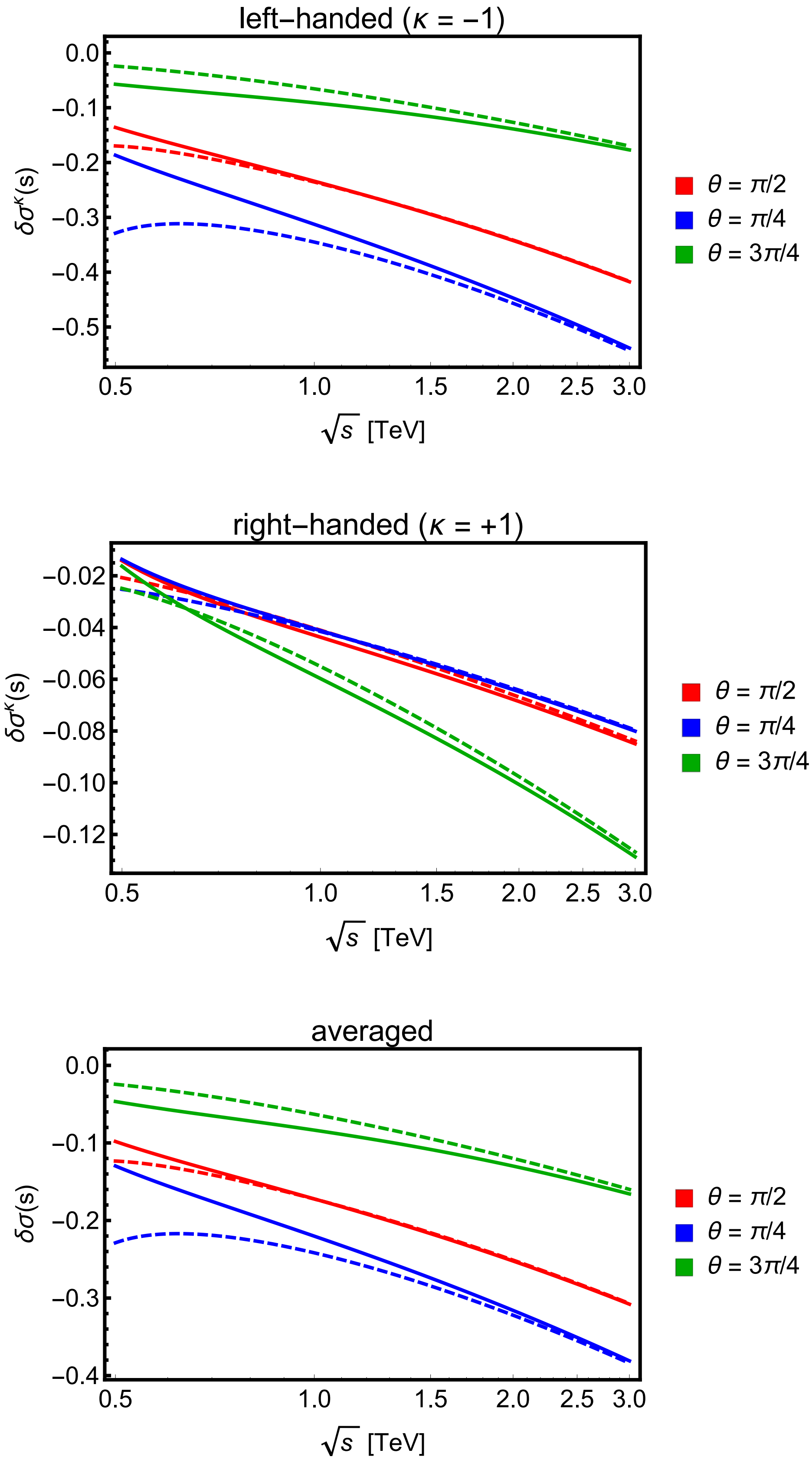

Figure 6.4: Total weak NLO results (full vs. expanded) for each helicity and spin-averaged. Solid = full, dashed = expanded. Note the variable scalings of the axes.

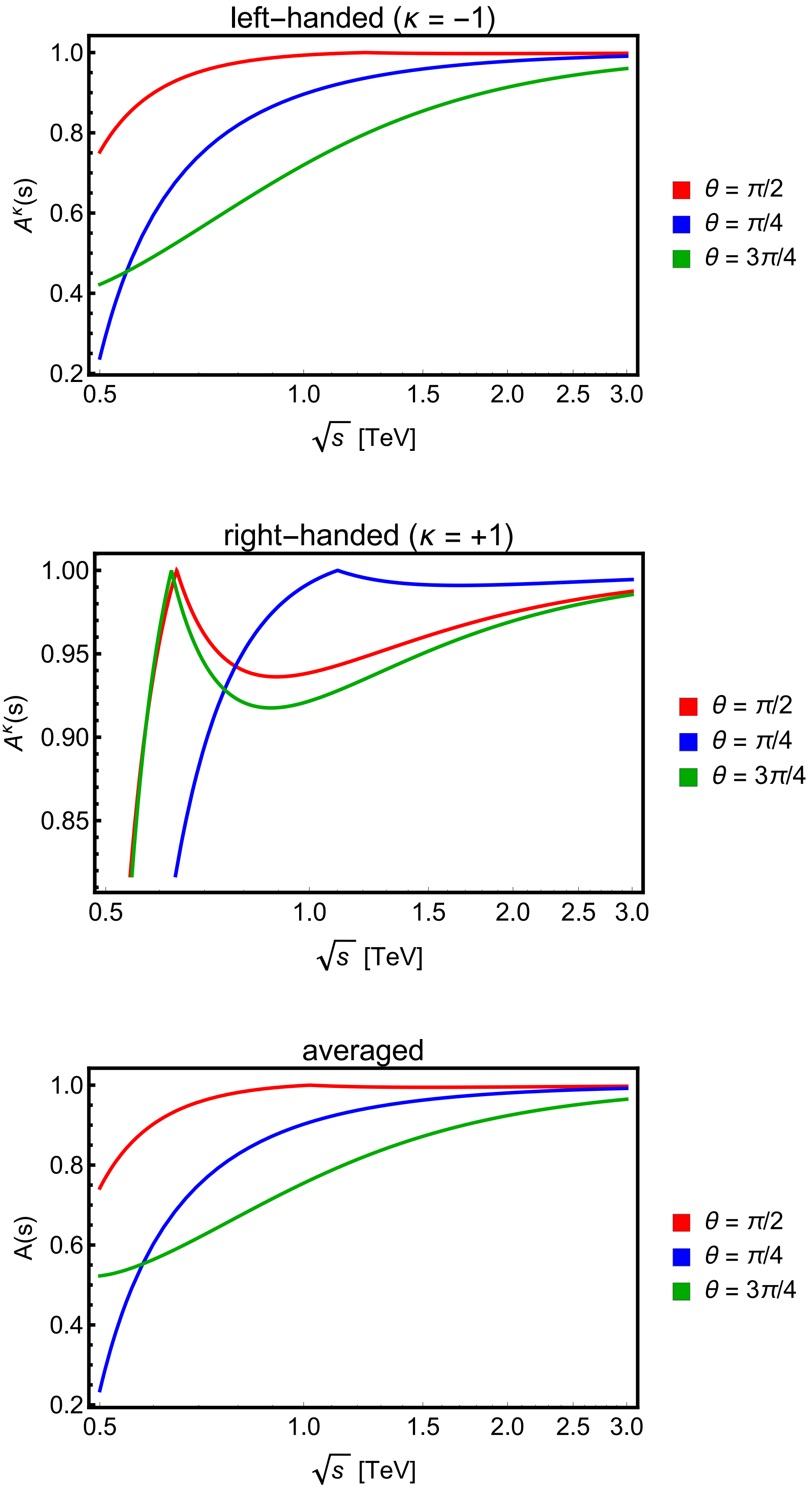

Figure 6.5: Plots of the accuracy measure $A(s)$ with fixed θ. The kinks are due to sign changes of the difference full - expanded.

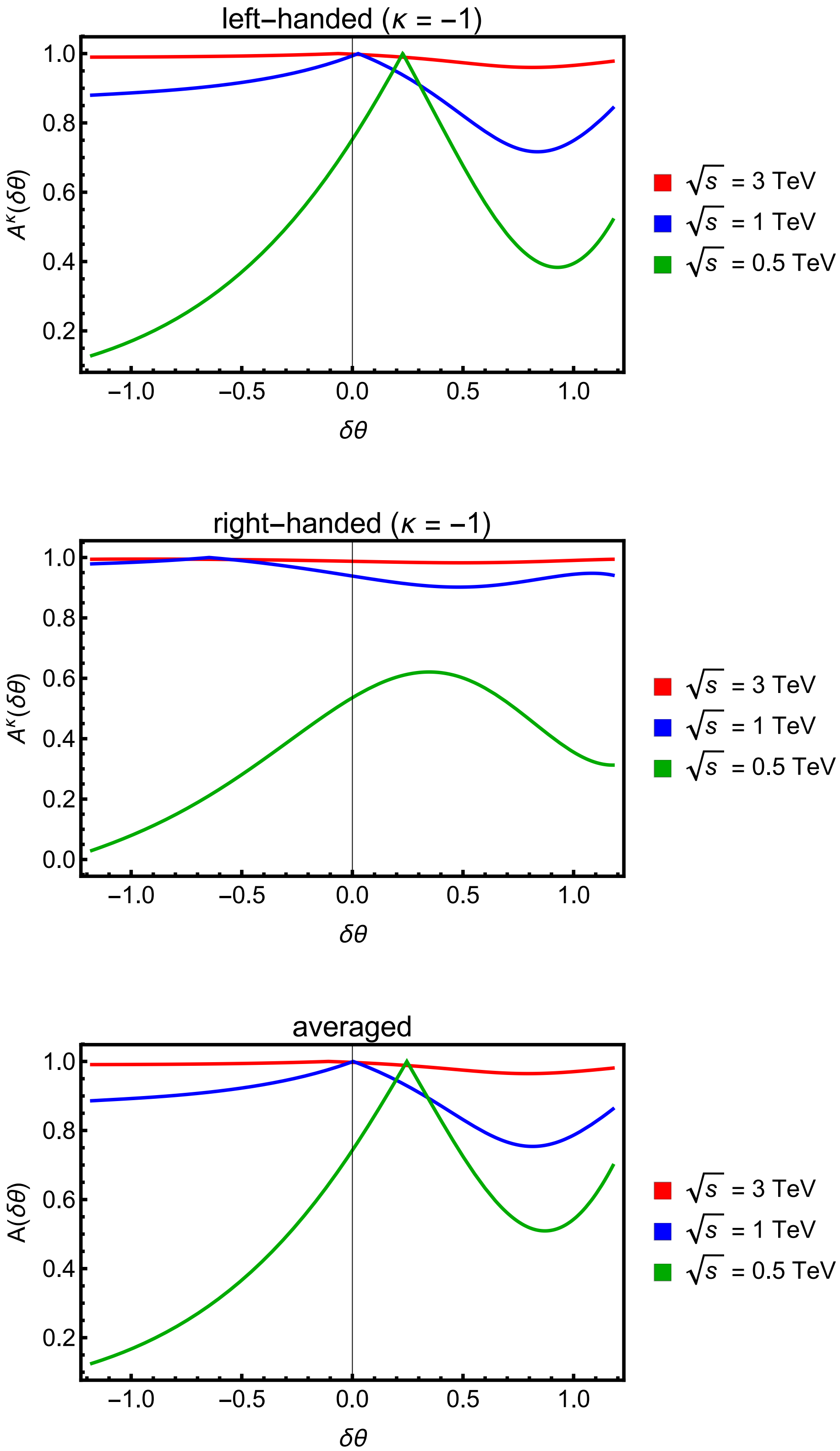

Figure 6.6: Plots of the accuracy measure $A(\pi/2 \pm \delta\theta)$ with fixed s. The kinks are due to sign changes of the difference full - expanded.

6.3 Sudakov logarithms vs. constant terms

Up to now we always compared the full NLO results with the corresponding high-energy expanded versions. The latter can be split again into 3 contributions: Sudakov double-logs, Sudakov single-logs and the constant terms (cf. eq. (5.6)). The naive expectation is that the logarithmic terms constitute the largest parts in the high-energy regime. Fig. 6.7, where the split-up of the high-energy expanded contributions (this time only for the averaged case) is shown, confirms that the Sudakov double-logs of the form $\ln^2(\Lambda^2_{\mathrm{EW}}/s)$ are clearly the largest contribution, at least if the energy exceeds 1 TeV. The single logs are actually in the same ballpark as the constant terms, even for energies well above 1 TeV.

We point out once more that the "constants" shown in fig. 6.7 are not true constants. For one, they contain terms like $\ln\left(\frac{t,u}{s}\right)$ as well as s-dependence in the running of $\alpha = \alpha(\sqrt{s})$ (cf. eq. (3.45)). Due to the former the curves show significant differences from the true constant value in the lower energy regimes, but flat out rather quickly as $\sqrt{s}$ increases. The running coupling is a global factor for each of the contributions shown in fig. 6.7, which is why we kept it nevertheless. Contrary to the $\ln\left(\frac{t,u}{s}\right)$-terms, its "radius of significance" is not confined to the moderate energy regime. Due to the resummed expression of eq. (3.45) its influence is very small numerically however.

The main message from these plots is that in regions were the logs are not dominant by a large margin no resummation has to be performed. Putting all the above statements together one concludes that in the energy regime around 500 GeV, i.e. below 1 TeV but certainly below 750 GeV, usual perturbation theory is still very reliable, as the logarithmic enhancement is not severe enough. For energies around 1 TeV and higher things get more interesting. For precision calculations resummation, at least of the leading logs, could become necessary, depending on the specific scattering kinematics once again.

Another striking feature visible in fig. 6.7 concerns the FOC. They only contribute linear Sudakov logs and constant terms. The dotted curves now show the respective contributions (single-logs and constants) when the FOC are taken out. We observe that this has especially dramatic effect for the constant terms, as their contribution is very small after the FOC have been subtracted. This is extremely interesting and potentially valuable information for higher-order calculations. Having small constants relative to the logarithms allows to focus on the anomalous dimensions of the higher loop integrals, since the perturbative series for the constants is expected to converge well. This would result in a major technical simplification, as the full multi-loop calculations are especially hard in EW theory due to the many diagrams and scales (masses). The FOCs cannot be subtracted ad hoc of course, but due to their nature their contributions are separated (for example concerning gauge-dependence) from the rest of the Sudakov logarithmic structure coming from vertices etc. A suitable renormalization scheme can almost certainly be found that deals with these contributions systematically and effectively removes them. We postpone further details and discussions on that subject to future work.

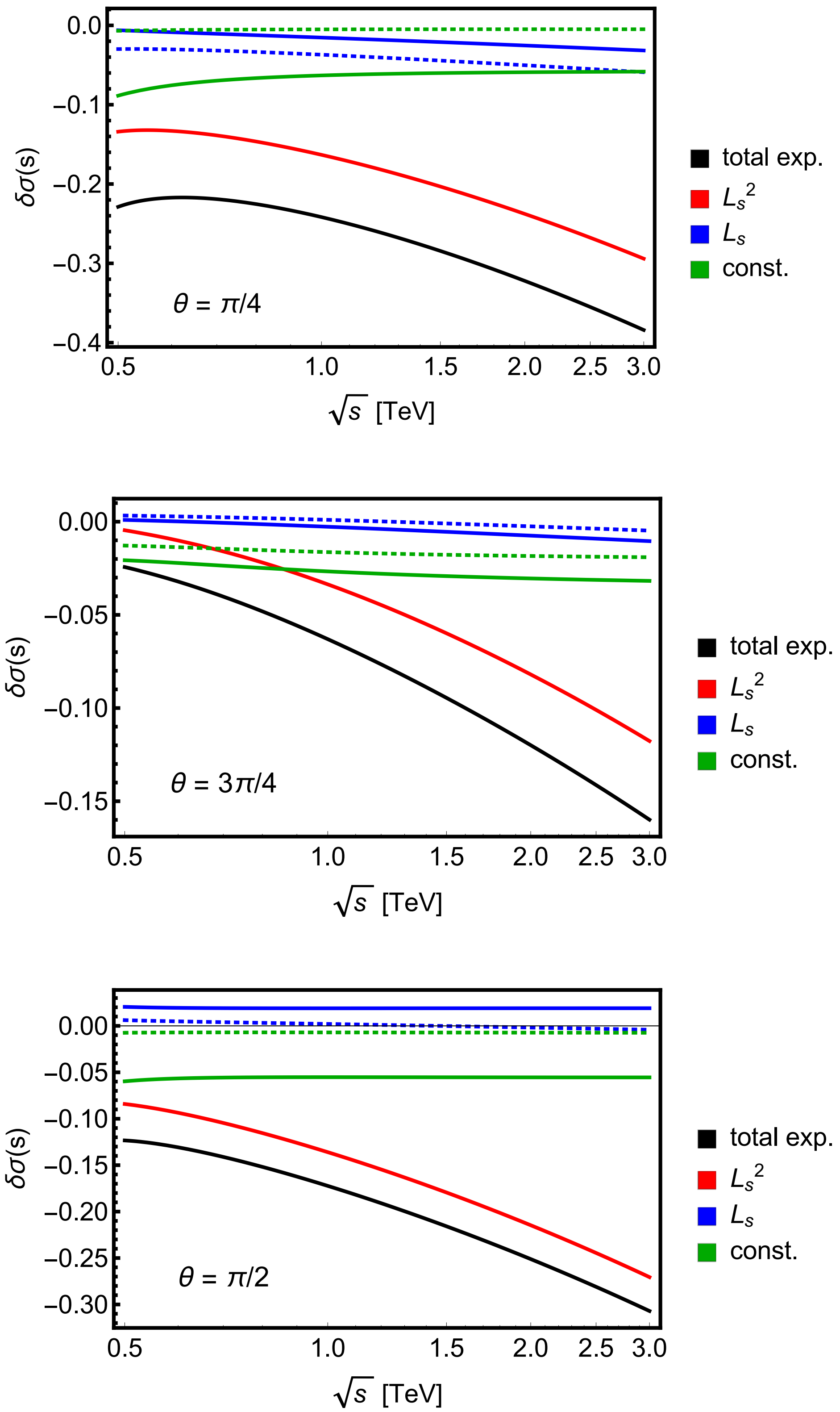

Figure 6.7: Split of the high-energy-expanded NLO cross-section contributions (black) into Sudakov double-log ($= L_s^2$, red), Sudakov single-log ($= L_s$, blue) and constant contributions (= const., green). The dotted curves are the single-log and constant terms with the FOC excluded (see text). Please note the (slight) s-dependence for the constant terms due to $\ln(t, u/s)$-terms (especially in the low-energy region) and the running coupling α as e.g. visible in the higher energy regime of the plot with $\theta = 3\pi/4$.

6.4 Summary

The numerics and plots in this chapter were done to illustrate the high-energy behaviour and the quality of the expansions. For concrete statements about the accuracy of the expansions in the boosted regime one needs to make precise the level of accuracy one desires, or fix the kinematic situation in terms of CM-energy and scattering angle. We emphasize that being able to carry out this type of analysis is another great benefit of having the analytic expressions (i.e. down to the explicit logarithms) instead of only numeric results (at the level of tensor coefficients that are evaluated with a numerical library like `LoopTools`), as precise statements concerning the logarithmic structure are possible.

Keeping in mind that the first few stages of the future linear colliders will not run above 500 GeV, the above analysis suggests that the application of high-energy tools has to be viewed conservatively in that regime, as the peak accuracy is about 60% only. Usage of full conventional perturbation theory, keeping terms of $\mathcal{O}(\Lambda_{\rm EW}^2/s)$ instead of discarding them, is the superior choice in this energy region. Also the log-contributions are not really exceeding the constant contributions by much, as can be seen in fig. 6.7. In the region above 750 GeV the expansions are more accurate, but we argue that only above 1 TeV it leads to very good and stable performances with reliable results of the expansion for scattering angles down to $\theta \sim \pi/2 \pm \pi/4$. In this regime the leading logarithmic structure clearly dominates the constants and power-suppressed terms, such that resummation of these high-energy logarithms is necessary for precision physics.

Chapter 7

Summary and outlook

In this thesis the weak NLO corrections to the process of stable top-production from e^+e^--annihilation were studied. We adopted an analytical approach, using a decomposition of the weak NLO matrix element into an amplitude basis as used in [6], which reduces the problem to the determination of the coefficient scalar functions depending on the external invariants and virtual masses of the process. Earlier works on that subject [4], [5], [6], [7], despite sketching mechanism of renormalization and gauge-cancellations, usually give explicit expressions only very scarcely and have a strong focus towards setting up codes for numerical implementations. With this work we provide a complete self-contained collection of analytic weak NLO results down to single diagrams, allowing for a high degree of flexibility and detail in understanding and discussion of UV-, gauge- and high-energy structure.

Aside from setting the masses of the bottom quark and the lighter fermions to 0, no assumptions, like degenerate boson masses or the gaugeless limit, were used in this text. The scalar functions were derived in the continuum in covariant R_ξ-gauge by means of projection operators as well as brute-force reduction for triangle- and box-diagrams to check for consistency. To allow for program-independent cross checks two different ways of computation were chosen: the `Mathematica`-Package `Package-X` [20], [21] was used extensively in combination with the projection operator technique, while the brute-force PV-reduction method was carried out by `FeynCalc` [23] down to the tensor coefficients, which were then evaluated using the numerical library `LoopTools` [24]. The UV-divergences were cancelled analytically, while the gauge-dependence cancellations were checked numerically in the continuum. The choice of external states of certain isospin forced us to form subsets of diagrams to obtain UV-finite and gauge-indpendent results. Especially the gauge-structure with its complicated cancellation mechanism provides a strong non-trivial cross-check of the calculation. The results are relatively involved, the only exception being the light-fermion loops, which have been discussed in sec. 3.4.2. Explicit results are given in the form of generic expressions for single diagrams in the appendix. Concerning the Feynman gauge expressions of certain building blocks we found agreement with the corresponding results given in [5], [6], [8]. The UV- and gauge-cancellation mechanism as outlined in [6] was shown explicitly by our calculations.

The main task of this thesis was to obtain the analytic leading high-energy expanded results (up to and including the constant terms) for the amplitude. Expansions were carried out for large CM-energies $\sqrt{s}$ and scattering kinematics around the central value $\theta = \pi/2$ for the scattering angle θ, which results in the hierachy $\{|s|, |t|, |u|\} \gg \{M_Z^2, M_W^2, M_H^2, m_t^2\} \sim \Lambda_{\text{EW}}^2$. The high-energy expanded PV-functions given in [27], [28] were used. The expressions simplified enormously in this regime, allowing to redo the checks for gauge-indpendence analytically. Explicit expressions were given in ch. 5. Interesting features inferred from these results were the emergence of a four-fermion current-current operator as the leading effective operators in this regime, closely connected to the universality of the Sudakov logarithms as observed in the results in sec. 5.3.3, as well as the cancellation mechanisms like the one for the leading logarithms in the ZZ-box sum.

The complete analytic continuum and high-energy results allowed for a numerical analysis of the logarithmic structure and the various building blocks, as was carried out in ch. 6. Expansion accuracies were estimated both for the CM-energy as well as the angular variable. Depending on the desired accuracy the cuts on the angular variable generally have to be chosen very small for CM-energies around 500 GeV, with certain observables only reaching a peak accuracy of 60%. The critical energy value seems to be around 1 TeV, when the accuracy becomes relatively stable and does not drop far below $\sim 90\%$ for opening angles down to $\theta \sim \pi/2 \pm \pi/4$. We conclude that resummation of the leading logarithmic series is necessary in this regime to improve convergence for precision predictions. For energies (well) below 1 TeV, conventional fixed-order perturbation theory works fine, and resummation is not necessary.

The results derived analytically in this thesis should form an important first stepping stone for the construction of effective field theories like SCET in the high-energy regime, as they can be used both as a cross-check for the singular structure as well as for non-singular matching procedures since the constants were kept as well in the expansion. We point out that these constants differ when the computations are carried out under simplifying assumptions like unbroken phase or degenerate boson masses, like in [25], [26].

We finish by pointing out that there are still some things to be done in various respects. QED corrections need to be included to derive realistic distributions, and although their dependence on experimental cuts makes the inclusion of real radiation calculations necessary and therefore technically a bit more involved, they should form no conceptual obstacle. The more complicated but equally more interesting part conceptually is to go beyond stable top quarks and narrow-width approximations and include finite-lifetime effects into the calculation. The systematic inclusion of top decay and clarification of how full EW gauge-invariance will be related to this (presumably studied in the high-energy regime) will be crucial for proper formulations of EW EFTs, and provide interesting challenges for the future.

Appendix A

Conventions, notations and calculational tricks

A.1 Conventions

A.1.1 Lorentz algebra

In this work we use the standard metric for special relativity and particle physics with minus signs in the spatial components,

$$g \equiv \mathrm{diag}\{1,-1,-1,-1\}, \tag{A.1}$$

with the property (in d space-time dimensions)

$$g^{\mu\nu}g_{\mu\nu} = d. \tag{A.2}$$

In chapter 2, secs. 2.3.3 and 2.4.3, we use the following notation including the D'Alembertian $\Box \equiv \partial^\mu\partial_\mu$,

$$\begin{aligned}\Box_A^{\mu\nu} &\equiv g^{\mu\nu}\Box - \left(1-\frac{1}{\xi_A}\right)\partial^\mu\partial^\nu,\\ \Box_Z^{\mu\nu} &\equiv g^{\mu\nu}\Big(\Box + M_Z^2\Big) - \left(1-\frac{1}{\xi_Z}\right)\partial^\mu\partial^\nu.\end{aligned} \tag{A.3}$$

$\Box_{Z,0}^{\mu\nu}$ denotes the bare operator, where the replacement $M_Z^2 \to \left(M_Z^0\right)^2$ needs to be made in eq. (A.3).

A derivative $\frac{d}{d(p^2)}$ onto an expression that depends on p, but not manifestly on p^2 (say $k\cdot p$) can be interpreted by the relation

$$\frac{d}{d(p^2)} = \frac{p^\mu}{2p^2}\frac{d}{dp^\mu}. \tag{A.4}$$

A.1.2 Dirac algebra

In chiral theories and high-energy processes (with massless or close-to-massless) fermions the use of the Weyl-basis for the γ-matrices,

$$\gamma^\mu = \begin{pmatrix} 0 & \sigma^\mu \\ \bar\sigma^\mu & 0\end{pmatrix} \tag{A.5}$$

is useful, where $\sigma \equiv (1,\vec\sigma)$ and $\bar\sigma \equiv (1,-\vec\sigma)$. γ_5 is then given by

$$\gamma_5 = \begin{pmatrix} -1 & 0 \\ 0 & 1\end{pmatrix}. \tag{A.6}$$

By means of γ_5 the chiral projectors, as defined in eq. (2.33), can be constructed. Another useful object built out of the commutator of γ-matrices is the tensor structure

$$\sigma^{\mu\nu} \equiv \frac{i}{2}\big[\gamma^\mu,\gamma^\nu\big]. \tag{A.7}$$

The γ-matrices satisfy the Clifford algebra

$$\{\gamma^\mu, \gamma^\nu\} = 2g^{\mu\nu}, \tag{A.8}$$

and allow to write the Dirac equations for on-shell (anti-)particle spinors ($v_s(p)$) $u_s(p,m)$

$$(\not{p} - m)u_s(p) = (\not{p} + m)v_s(p) = 0, \qquad (p^2 = m^2), \tag{A.9}$$

and the completeness relations

$$\begin{aligned} \sum_\sigma u_\sigma(p)\bar{u}_\sigma(p) &= \not{p} + m, \\ \sum_\sigma v_\sigma(p)\bar{v}_\sigma(p) &= \not{p} - m. \end{aligned} \tag{A.10}$$

The relations in eq. (A.10) are essential for deriving and applying projection operators for Feynman diagrams involving external fermions (cf. sec. D). An explicit realization of the spinors in the Weyl-basis reads

$$u_\sigma(p) = \begin{pmatrix} \sqrt{p\cdot\sigma}\,\xi_\sigma \\ \sqrt{p\cdot\bar{\sigma}}\,\xi_\sigma \end{pmatrix}, \qquad v_\sigma(p) = \begin{pmatrix} \sqrt{p\cdot\sigma}\,\eta_\sigma \\ -\sqrt{p\cdot\bar{\sigma}}\,\eta_\sigma \end{pmatrix}, \tag{A.11}$$

where ξ_σ, η_σ are 2-component spinors and σ is the spin quantum number. In this work we will not make use of the explicit realizations of the spinors, the formal expressions in eqs. (A.9) and (A.10) will suffice for our purposes. For more details concerning spinor solutions to the Dirac equation we refer the reader to textbooks on QFT (for example [29]).

The frequently occuring heuristic notation $\frac{d}{d\not{p}}$ is to be interpreted in the sense

$$\frac{d}{d\not{p}} = \frac{1}{d}\gamma^\mu \frac{d}{dp^\mu} = \not{p}\,\frac{p^\mu}{p^2}\frac{d}{dp^\mu} = 2\not{p}\,\frac{d}{d(p^2)}. \tag{A.12}$$

Lastly, due to its importance for reducing numerator structures in Feynman diagrams, we restate a key relation involving 3 Dirac matrices, as already used in the text (eq. (3.91))

$$\gamma^\mu\gamma^\alpha\gamma^\nu = g^{\mu\alpha}\gamma^\nu + \gamma^{\alpha\nu}\gamma^\mu - \gamma^{\mu\nu}\gamma^\alpha + i\varepsilon^{\mu\alpha\nu\sigma}\gamma_\sigma\gamma_5. \tag{A.13}$$

There exists a plethora of similiar relations, and we refer to textbooks on QFT once again.

A.2 Gordon identities

Another useful tool for the form factor approach to Feynman diagrams are Gordon identites, which can be derived by appliciation of the Clifford-algebra eq. (A.8) and the Dirac equations eq. (A.9) as well as the definition of $\sigma^{\mu\nu}$ in eq. (A.7). In this work we make use of the ones given below (we suppress the spin index σ).

$$\begin{aligned} \bar{u}(p_1)\left[\frac{(p_1-p_2)^\mu}{2m} + \frac{i\,\sigma^{\mu\nu}}{2m}\,(p_1+p_2)_\nu\right] v(p_2) &= \bar{u}(p_1)\,\gamma^\mu\,v(p_2), \\ \bar{u}(p_1)\left[\frac{(p_1-p_2)^\mu}{2m}\gamma_5 + \frac{i\,\sigma^{\mu\nu}}{2m}\gamma_5\,(p_1+p_2)_\nu\right] v(p_2) &= 0, \\ \bar{u}(p_1)\left[\frac{(p_1+p_2)^\mu}{2m}\gamma_5 + \frac{i\,\sigma^{\mu\nu}}{2m}\gamma_5\,(p_1-p_2)_\nu\right] v(p_2) &= \bar{u}(p_1)\,\gamma^\mu\gamma_5\,v(p_2), \\ \bar{u}(p_1)\left[\frac{(p_1+p_2)^\mu}{2m} + \frac{i\,\sigma^{\mu\nu}}{2m}\,(p_1-p_2)_\nu\right] u(p_2) &= \bar{u}(p_1)\,\gamma^\mu\,u(p_2), \end{aligned} \tag{A.14}$$

A.3 Non-analytic functions

In loop-calculations one frequently encounters logarithms and Dilogarithms (special cases of Polylogarithms). When considered over the complex numbers $\mathbb{C}$ both show non-analyticities in form of branch-cuts. The logarithm has a cut along the negative real axis, starting at the branch point $z = 0$. Logarithms with negative real arguments need to be given a prescription onto which Riemann-sheet they will be analytically continued. In this work we use the convention (for $x \in \mathbb{R}, x > 0$)

$$\ln(-x \pm i0^+) \equiv \lim_{\epsilon \downarrow 0} \ln\big(-x \pm i\epsilon\big) = \ln\big(x\big) \pm i\pi. \tag{A.15}$$

Also note the generalized addidivity for the complex logarithm [30],

$$\ln(a\,b) = \ln(a) + \ln(b) + \eta(a,b), \tag{A.16}$$

for $a, b \in \mathbb{C}$, with

$$\eta(a,b) \equiv 2\pi i\Big\{\theta\left(\mathrm{Im}[-a]\right)\theta\left(\mathrm{Im}[-b]\right)\theta\left(\mathrm{Im}[a\,b]\right) - \theta\left(\mathrm{Im}[a]\right)\theta\left(\mathrm{Im}[b]\right)\theta\left(\mathrm{Im}[-a\,b]\right)\Big\} \tag{A.17}$$

As a shortcut one can remember:

- $\ln(a\,b) = \ln(a) + \ln(b)$ if $\mathrm{Im}[a], \mathrm{Im}[b]$ have different sign
- $\ln\left(\frac{a}{b}\right) = \ln(a) - \ln(b)$ if $\mathrm{Im}[a], \mathrm{Im}[b]$ have the same sign

Otherwise the η-function gives additional pieces of $2\pi i$, whose sign needs to be determined by eq. (A.17).

The Dilogarithm (also called *Spence's function*), given by its integral repesentation

$$\mathrm{Li}_2(z) \equiv -\int_0^z \frac{\ln(t)}{1-t}\,dt. \tag{A.18}$$

It has a branch cut along the positive real axis, starting at the branch point $z = 1$. For real arguments $x > 1$ a prescription analogous to eq. (A.15) is necessary. There are 2 useful relations for $z \in \mathbb{C}$

$$\begin{aligned} \mathrm{Li}_2(z) &= -\mathrm{Li}_2(1-z) + \frac{\pi^2}{6} - \ln(z)\ln(1-z), \\ \mathrm{Li}_2(z) &= -\mathrm{Li}_2\left(\frac{1}{z}\right) - \frac{\pi^2}{6} - \frac{1}{2}\ln^2(-z). \end{aligned} \tag{A.19}$$

If there is a prescription like in eq. (A.15) for the logarithm, then the Dilog can be analytically continued with the help of eq. (A.19). Another important fact for this work is that the imaginary part of the sum of Dilogs with complex conjugated arguments vanishes. Suppose $z = x + iy$ with $x, y \in \mathbb{R}$, then for $y \neq 0$

$$\mathrm{Im}\left[\mathrm{Li}_2(x+iy) + \mathrm{Li}_2(x-iy)\right] = 0. \tag{A.20}$$

If $y = 0$, then the single Dilogs are manifestly real for $x < 1$. For $x \geq 1$ the careful limiting procedure $y \to 0$ using eqs. (A.15) and (A.19) again confirms eq. (A.20). Some more information (e.g. expansions) concerning the Dilogarithm can be found in [30].

Appendix B

Feynman integrals and Passarino-Veltman reduction

B.1 Systematic treatment of Feynman integrals

B.1.1 Tensor integral reduction

The Feynman integrals are of the generic form

$$T_{N,\mu_1\mu_2\ldots\mu_p}^{\langle w_0,w_1,\ldots w_{N-1}\rangle} := \frac{(2\pi\tilde{\mu})^{4-d}}{i\pi^2}\int\frac{d^dk}{(2\pi)^d}\frac{k_{\mu_1}k_{\mu_2}\ldots k_{\mu_p}}{[k^2-m_0^2]^{w_0}[(k+k_1)^2-m_1^2]^{w_1}\ldots[(k+k_{N-1})^2-m_{N-1}^2]^{w_{N-1}}} \tag{B.1}$$

and are usually referred to as *tensor integrals*. The denominator convention in eq. B.1 corresponds to the diagrammatic situation shown in figs. B.1 and B.2. The k_i are just sums of the $N-1$ external momenta p_i,

$$k_n = \sum_{j=1}^{n} p_j, \quad \text{with overall momentum conservation} \quad \sum_{j=1}^{N-1} p_j = 0. \tag{B.2}$$

By Lorentz covariance it is now possible to express these integrals as linear combinations of the external momenta p_i, or alternatively by the momenta k_i, with the latter being the most frequent choice (e.g. `LoopTools` [24], `Package-X 2.0` [21]). The expansion coefficients can be entirely expressed by the so-called *scalar integrals* of the form

$$T_{N,0}^{\langle w_0,w_1,\ldots w_{N-1}\rangle} := \frac{(2\pi\tilde{\mu})^{4-d}}{i\pi^2}\int\frac{d^dk}{(2\pi)^d}\frac{1}{[k^2-m_0^2]^{w_0}[(k+k_1)^2-m_1^2]^{w_1}\ldots[(k+k_{N-1})^2-m_{N-1}^2]^{w_{N-1}}} \tag{B.3}$$

The natural numbers w_i are called *weights*. To avoid cluttering notation too much, we will only show them explicitly if the set differs from $\langle 1,1,...,1\rangle$. In this work we will need integrals up to 4 denominators, with the usual abreviations

$$\begin{aligned}
A_{\{0,\mu,\mu\nu,\ldots\}}^{\langle w_0\rangle} &:= \frac{(2\pi\tilde{\mu})^{4-d}}{i\pi^2}\int\frac{d^dk}{(2\pi)^d}\frac{\{1,k_\mu,k_\mu k_\nu,...\}}{[k^2-m_0^2]},\\
B_{\{0,\mu,\mu\nu,\ldots\}}^{\langle w_0,w_1\rangle} &:= \frac{(2\pi\mu)^{4-d}}{i\pi^2}\int\frac{d^dk}{(2\pi)^d}\frac{\{1,k_\mu,k_\mu k_\nu,...\}}{[k^2-m_0^2][(k+k_1)^2-m_1^2]},\\
C_{\{0,\mu,\mu\nu,\ldots\}}^{\langle w_0,w_1,w_2\rangle} &:= \frac{(2\pi\mu)^{4-d}}{i\pi^2}\int\frac{d^dk}{(2\pi)^d}\frac{\{1,k_\mu,k_\mu k_\nu,...\}}{[k^2-m_0^2][(k+k_1)^2-m_1^2][(k+k_2)^2-m_2^2]},\\
D_{\{0,\mu,\mu\nu,\ldots\}}^{\langle w_0,w_1,w_2,w_3\rangle} &:= \frac{(2\pi\mu)^{4-d}}{i\pi^2}\int\frac{d^dk}{(2\pi)^d}\frac{\{1,k_\mu,k_\mu k_\nu,...\}}{[k^2-m_0^2]^{w_0}[(k+k_1)^2-m_1^2]^{w_1}[(k+k_2)^2-m_2^2]^{w_2}[(k+k_3)^2-m_3^2]^{w_4}}.
\end{aligned} \tag{B.4}$$

The tensor decomposition up to rank 3 in terms of the momenta k_i read explicitly (supressing weights[1])

$$
\begin{aligned}
A_\mu &= 0, \qquad \text{(by symmetry } k \leftrightarrow -k\text{)}\\
A_{\mu\nu} &= g_{\mu\nu} A_{00},\\
A_{\mu\nu\rho} &= 0, \qquad \text{(by symmetry } k \leftrightarrow -k\text{)}\\
B_\mu &= k_{1\mu} B_1,\\
B_{\mu\nu} &= g_{\mu\nu} B_{00} + k_{1\mu}k_{1\nu} B_{11},\\
B_{\mu\nu\rho} &= \{g, k_1\}_{\mu\nu\rho} B_{001} + k_{1\mu}k_{1\nu}k_{1\rho} B_{111},\\
C_\mu &= k_{1\mu} C_1 + k_{2\mu} C_2,\\
C_{\mu\nu} &= g_{\mu\nu} C_{00} + k_{1\mu}k_{1\nu} C_{11} + k_{2\mu}k_{2\nu} C_{22} + \{k_1, k_2\}_{\mu\nu} C_{12},\\
C_{\mu\nu\rho} &= \{g, k_1\}_{\mu\nu\rho} C_{001} + \{g, k_2\}_{\mu\nu\rho} C_{002} + k_{1\mu}k_{1\nu}k_{1\rho} C_{111} + k_{2\mu}k_{2\nu}k_{2\rho} C_{222} +\\
&\qquad + \{k_1, k_1, k_2\}_{\mu\nu\rho} C_{112} + \{k_1, k_2, k_2\}_{\mu\nu} C_{122},\\
D_\mu &= k_{1\mu} D_1 + k_{2\mu} D_2 + k_{3\mu} D_3,\\
D_{\mu\nu} &= g_{\mu\nu} D_{00} + k_{1\mu}k_{1\nu} D_{11} + k_{2\mu}k_{2\nu} D_{22} + k_{3\mu}k_{3\nu} D_{33} +\\
&\qquad + \{k_1, k_2\}_{\mu\nu} D_{12} + \{k_2, k_3\}_{\mu\nu} D_{23} + \{k_1, k_3\}_{\mu\nu} D_{13},\\
D_{\mu\nu\rho} &= \{g, k_1\}_{\mu\nu\rho} D_{001} + \{g, k_2\}_{\mu\nu\rho} D_{002} + \{g, k_3\}_{\mu\nu\rho} D_{003} +\\
&\qquad + k_{1\mu}k_{1\nu}k_{1\rho} D_{111} + k_{2\mu}k_{2\nu}k_{2\rho} D_{222} + k_{3\mu}k_{3\nu}k_{3\rho} D_{333} +\\
&\qquad + \{k_1, k_1, k_2\}_{\mu\nu\rho} D_{112} + \{k_1, k_1, k_3\}_{\mu\nu\rho} D_{113} + \{k_1, k_2, k_3\}_{\mu\nu\rho} D_{123} +\\
&\qquad + \{k_1, k_2, k_2\}_{\mu\nu\rho} D_{122} + \{k_1, k_3, k_3\}_{\mu\nu\rho} D_{133} +\\
&\qquad + \{k_2, k_2, k_3\}_{\mu\nu\rho} D_{223} + \{k_2, k_3, k_3\}_{\mu\nu\rho} D_{233}.
\end{aligned} \tag{B.5}
$$

The momenta and metric tensors in curly brackets denote sums over all permuation of Lorentz indices, i.e. $\{p_1, p_2\}_{\mu\nu} = p_{1\mu}p_{2\nu} + p_{1\nu}p_{2\mu}$ etc.
The tensor coefficients (as well as the scalar integrals) depend on a set of parameters, namely the internal masses and the external invariants (external four-momenta squared and Mandelstam invariants). More specifically we use the following conventions:

$$
\begin{aligned}
A &= A\left(m_0\right),\\
B &= B\left(p_1^2; m_0, m_1\right),\\
C &= C\left(p_1^2, p_2^2, (p_1+p_2)^2; m_0, m_1, m_2\right),\\
D &= D\left(p_1^2, p_2^2, p_3^2, p_4^2, (p_1+p_2)^2, (p_2+p_3)^2; m_0, m_1, m_2, m_3\right),
\end{aligned} \tag{B.6}
$$

for any index or weight set.

To effectively deal with various topologies (for box diagrams) it is convenient to introduce generalized Mandelstam invariants (denoted with a bar on top)

$$
\begin{aligned}
\bar{s} &\equiv (p_1 + \bar{p}_2)^2 = (p_3 + p_4)^2,\\
\bar{t} &\equiv (p_1 + \bar{p}_3)^2 = (p_2 + p_4)^2,
\end{aligned}
$$

[1] The tensor coefficients carry weight indices according to the original integral. Again, we only write them out explicitly for cases different from $\langle w_0, w_1, ... w_{N-1}\rangle = \langle 1, 1, ..., 1\rangle$.

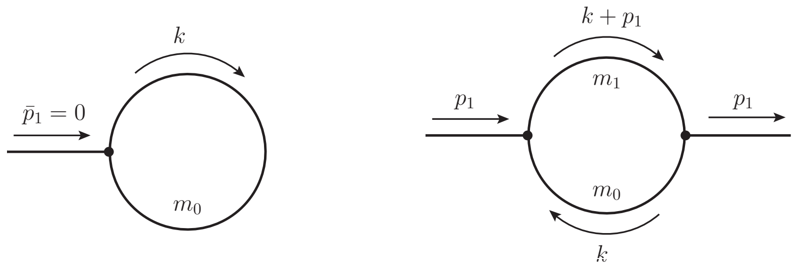

Figure B.1: Momentum flow and internal mass conventions for generic 1- and 2-point diagrams.

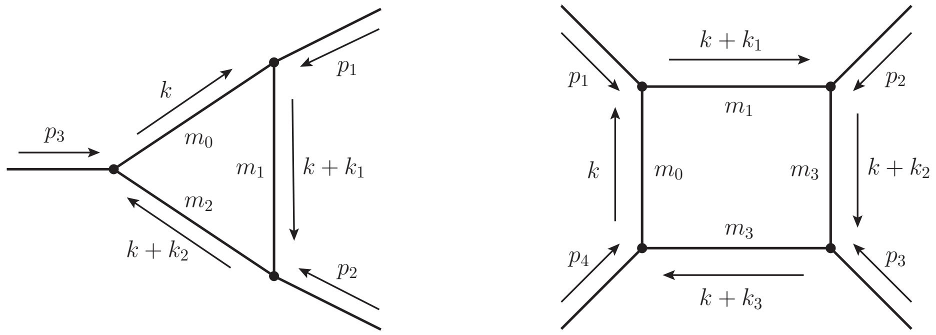

Figure B.2: Momentum flow and internal mass conventions for generic 3- and 4-point diagrams.

$$\bar{u} \equiv (p_1 + p_4)^2 = (p_2 + p_3)^2. \tag{B.7}$$

Note that those need not be equivalent to the usual Mandelstam invariants, i.e. not necessarily $\bar{s} = s$ etc. The exact identification will depend on the box topology, and can be looked up in the corresponding chapter. For divergent parts we use

$$d = 4 - 2\epsilon, \tag{B.8}$$

as well as the usual $\overline{\mathrm{MS}}-$replacement of the the t‘Hooft-scale

$$\tilde{\mu}^2 = \mu^2 \frac{e^{\gamma_E}}{4\pi}, \tag{B.9}$$

where $\gamma_E \equiv -\Gamma'(1)$ is the Euler-Mascheroni constant.

B.1.2 1-point functions

A_0 and A_{00} read explicitly:

$$\begin{aligned} A_0\left(m_0\right) &= m^2 \left(\frac{1}{\epsilon} + \ln\left(\frac{\mu^2}{m_0^2}\right) + 1\right), \\ A_{00}\left(m_0\right) &= \frac{m^4}{4} \left(\frac{1}{\epsilon} + \ln\left(\frac{\mu^2}{m_0^2}\right) + \frac{3}{2}\right). \end{aligned} \tag{B.10}$$

The limiting procedure $m_0 \to 0$ is straightforward and yields

$$A_0(0) = A_{00}(0) = 0. \tag{B.11}$$

B.1.3 Scalar 2-point function

2-point functions depend on the external invariant p^2 and the internal masses m_0, m_1. The scalar function B_0 reads explicitly:

$$B_0\left(p^2; m_0, m_1\right) = \frac{1}{\epsilon} + \ln\left(\frac{\mu^2}{m_1^2}\right) - \frac{p^2 + m_0^2 - m_1^2}{2p^2} \ln\left(\frac{m_0^2}{m_1^2}\right) + 2 + \Lambda\left(p^2; m_0, m_1\right), \tag{B.12}$$

where $\Lambda\left(p^2; m_0, m_1\right)$ is the logarithmic discontinuity of the PV-B_0-function,

$$\Lambda\left(p^2; m_0, m_1\right) \equiv \frac{\lambda^{1/2}(p^2, m_0^2, m_1^2)}{p^2} \ln\left(\frac{-(p^2+i0^+) + m_0^2 + m_1^2 + \lambda^{1/2}(p^2+i0^+, m_0^2, m_1^2)}{2m_0 m_1}\right), \tag{B.13}$$

and $\lambda(a,b,c)$ is the Källen kinematic function,

$$\lambda(a,b,c) \equiv a^2 + b^2 + c^2 - 2(ab + ac + bc). \tag{B.14}$$

$B_0(p^2; m_0, m_1)$ is symmetric under the interchange of masses $m_0 \leftrightarrow m_1$

$$B_0(p^2; m_0, m_1) = B_0(p^2; m_1, m_0). \tag{B.15}$$

This remains true if one of the masses vanishes. Depending on the hierachy of the scales p^2, m_0^2, m_1^2, there are 3 kinematic regions to distinguish:

- $\mathbf{p^2 \leq (m_0 - m_1)^2}$: $\lambda(p^2; m_0, m_1)$ and the argument of the logarithm are both > 0, $\Lambda(p^2; m_0, m_1)$ is therefore manifestly real.

- $\mathbf{(m_0 - m_1)^2 < p^2 \leq (m_0 + m_1)^2}$: $\lambda(p^2; m_0, m_1) < 0$, so the square-root of the Kallen-function needs to be analytically continued as $\sqrt{\lambda(a,b,c)} \to i\sqrt{|\lambda(a,b,c)|}$. $\Lambda(p^2; m_0, m_1)$ can be rewritten in terms of inverse trigonometric functions

$$\Lambda(p^2; m_0, m_1) = -\frac{\sqrt{4m_0^2 m_1^2 - \left(-p^2 + m_0^2 + m_1^2\right)^2}}{p^2} \,\mathrm{ArcCos}\left(\frac{-p^2 + m_0^2 + m_1^2}{2m_0 m_1}\right), \tag{B.16}$$

  and is still manifestly real.

- $\mathbf{p^2 \geq (m_0 + m_1)^2}$: $\lambda(p^2; m_0, m_1) > 0$ again, but now the argument of the logarithm is < 0. To ensure picking the physical branch of the logarithm, the arguments have to be equipped with the usual infinitesimal imaginary parts[2]. $B_0(p^2; m_0, m_1)$ now obtains a non-vanishing imaginary part, which is given by the imaginary part of $\Lambda(p^2; m_0, m_1)$ (cf. eq. B.12). In this kinematic regime we get:

$$\mathrm{Im}\left[B_0(p^2; m_0, m_1)\right] = \pi\, \frac{\lambda^{1/2}(p^2, m_0^2, m_1^2)}{p^2}, \tag{B.17}$$

  a result which can also be obtained by cutting the (4-dimensional) integral expression of B_0 (for details see Sec. C).

  Below we give the scalar B_0-function for some vanishing arguments, as these limits have to be taken before integration.

$$B_0\left(0; m_0, m_1\right) = \frac{1}{\epsilon} + \ln\left(\frac{\mu^2}{m_1^2}\right) - \frac{m_0^2}{m_0^2 - m_1^2} \ln\left(\frac{m_0^2}{m_1^2}\right) + 1,$$

$$B_0\left(0; m, m\right) = \frac{1}{\epsilon} + \ln\left(\frac{\mu^2}{m^2}\right),$$

$$B_0\left(0; 0, m\right) = \frac{1}{\epsilon} + \ln\left(\frac{\mu^2}{m^2}\right) + 1 = B_0\left(0; m, 0\right),$$

$$B_0\left(p^2; 0, m\right) = \frac{1}{\epsilon} + \ln\left(\frac{\mu^2}{m^2}\right) + \frac{m^2 - p^2}{p^2} \ln\left(\frac{m^2 - p^2}{m^2}\right) + 2 = B_0\left(p^2; m, 0\right),$$

$$B_0\left(m^2; 0, m\right) = \frac{1}{\epsilon} + \ln\left(\frac{\mu^2}{m^2}\right) + 2 = B_0\left(m^2; m, 0\right),$$

[2]for masses and external (timelike) invariants: $m_i^2 \to m_i^2 - i0^+, p^2 \to p^2 + i0^+$

$$B_0\left(p^2;0,0\right) = \frac{1}{\epsilon} + \ln\left(-\frac{\mu^2}{p^2}\right) + 2,$$

$$B_0\left(0;0,0\right) = \frac{1}{\epsilon_{\mathrm{UV}}} - \frac{1}{\epsilon_{\mathrm{IR}}} \overset{\epsilon_{\mathrm{UV}}=\epsilon_{\mathrm{IR}}}{=} 0. \tag{B.18}$$

The last integral $B_0(0;0,0)$ is formally scaleless, but contrary to A_0 its 4-dimensional integral expression is dimensionless. The simple limit of $p^2 \neq 0, m_0 = m_1 = m$ can be taken straightforwardly.

B.1.4 2-point tensor coefficients

Below we give the tensor coefficients up to rank 3 in terms of the scalar functions A_0 and B_0. Note that they are in general not symmetric under interchange of masses $m_0 \leftrightarrow m_1$ (except for the coefficients whose indices only contain 0, i.e. $B_{00}, B_{0000}, ...$).

$$\begin{aligned}
B_1(p^2;m_0,m_1) &= \frac{1}{2p^2}\Big\{A_0\left(m_0\right) - A_0\left(m_1\right) - \left(p^2 + m_0^2 - m_1^2\right) B_0(p^2;m_0,m_1)\Big\},\\
B_{00}(p^2;m_0,m_1) &= \frac{1}{12p^2}\Big\{\frac{2}{3}p^2\Big(3(m_0^2+m_1^2)-p^2\Big) + (m_0^2-m_1^2)\big(A_0\left(m_0\right) - A_0\left(m_1\right)\big) +\\
&\quad + p^2\big(A_0\left(m_0\right) + A_0\left(m_1\right)\big) - \lambda(p^2,m_0^2,m_1^2)\, B_0(p^2;m_0,m_1)\Big\},\\
B_{11}(p^2;m_0,m_1) &= -\frac{1}{3p^4}\Big\{\frac{1}{6}p^2\Big(3(m_0^2+m_1^2)-p^2\Big) + (p^2+m_0^2-m_1^2)\,\big(A_0\left(m_0\right) - A_0\left(m_1\right)\big) +\\
&\quad - p^2\, A_0\left(m_1\right) + \Big(\lambda(p^2,m_0^2,m_1^2) + 3m_0^2p^2\Big) B_0(p^2;m_0,m_1),\\
B_{001}(p^2;m_0,m_1) &= \frac{1}{24p^4}\Big\{-\frac{1}{6}p^2\Big(3(m_0^4-m_1^4) + 4p^2(2m_0^2+4m_1^2-p^2)\Big) +\\
&\quad - \Big(\lambda(p^2,m_0^2,m_1^2) + m_0^2p^2\Big)\,\big(A_0\left(m_0\right) - A_0\left(m_1\right)\big) - p^2(2p^2-m_0^2+m_1^2)A_0(m_1) +\\
&\quad + (p^2+m_0^2-m_1^2)\,\lambda(p^2,m_0^2,m_1^2)\, B_0(p^2;m_0,m_1),\\
B_{111}(p^2;m_0,m_1) &= \frac{1}{4p^6}\Big\{\frac{1}{6}p^2\big(3(m_0^4-m_1^4) + 2p^2(2m_0^2+4m_1^2-p^2)\big) +\\
&\quad + \Big(\lambda(p^2,m_0^2,m_1^2) + 3m_0^2p^2\Big)\,\big(A_0\left(m_0\right) - A_0\left(m_1\right)\big) - p^2(2p^2+m_0^2-m_1^2)A_0(m_1) +\\
&\quad - (p^2+m_0^2-m_1^2)\,\Big(\lambda(p^2,m_0^2,m_1^2) + 2m_0^2p^2\Big) B_0(p^2;m_0,m_1).
\end{aligned} \tag{B.19}$$

The UV-divergences of the 2-point functions are

$$\begin{aligned}
B_0^{\mathrm{UV}}(p^2;m_0,m_1) &= \frac{1}{\epsilon},\\
B_1^{\mathrm{UV}}(p^2;m_0,m_1) &= -\frac{1}{2\epsilon},\\
B_{00}^{\mathrm{UV}}(p^2;m_0,m_1) &= \frac{3(m_0^2+m_1^2)-p^2}{12\epsilon},\\
B_{11}^{\mathrm{UV}}(p^2;m_0,m_1) &= \frac{1}{3\epsilon},\\
B_{001}^{\mathrm{UV}}(p^2;m_0,m_1) &= -\frac{2m_0^2+4m_1^2-p^2}{24\epsilon},
\end{aligned}$$

$$B^{\mathrm{UV}}_{111}(p^2; m_0, m_1) = -\frac{1}{4\epsilon}. \tag{B.20}$$

To make UV-cancellations manifest, we will often times write out the ϵ-parts explicitly, and therefore choose the notation

$$B_{\dots}(p^2; m_0, m_1) = B^{\mathrm{UV}}_{\dots}(p^2; m_0, m_1) + \hat{B}_{\dots}(p^2; m_0, m_1), \tag{B.21}$$

indicating the UV-finite parts with a hat on top.

Expressions for vanishing or equal masses can be obtained by using the results of eq. B.18. In case of vanishing ($p^2 = 0$) or on-shell ($p^2 = m_i^2$) external invariant the limiting procedure is not as straightforward. We get:

- $\mathbf{B_1}$

$$\begin{aligned}
B_1\left(0; m_0, m_1\right) &= -\frac{1}{2}\left(\frac{1}{\epsilon} + \ln\left(\frac{\mu^2}{m_1^2}\right)\right) + \frac{m_0^4}{2\left(m_0^2 - m_1^2\right)^2}\ln\left(\frac{m_0^2}{m_1^2}\right) - \frac{3m_0^2 - m_1^2}{4\left(m_0^2 - m_1^2\right)},\\
B_1\left(0; m, m\right) &= -\frac{1}{2}\left(\frac{1}{\epsilon} + \ln\left(\frac{\mu^2}{m^2}\right)\right),\\
B_1\left(0; 0, m_1\right) &= -\frac{1}{2}\left(\frac{1}{\epsilon} + \ln\left(\frac{\mu^2}{m_1^2}\right) + \frac{1}{2}\right),\\
B_1\left(0; m_0, 0\right) &= -\frac{1}{2}\left(\frac{1}{\epsilon} + \ln\left(\frac{\mu^2}{m_0^2}\right) + \frac{3}{2}\right),\\
B_1\left(p^2; 0, m_1\right) &= -\frac{1}{2}\left(\frac{1}{\epsilon} + \ln\left(\frac{\mu^2}{m_1^2}\right)\right) + \frac{\left(m_1^2 - p^2\right)^2}{2p^4}\ln\left(\frac{m_1^2 - p^2}{m_1^2}\right) + \frac{m_1^2 - 2p^2}{2p^2},\\
B_1\left(m_1^2; 0, m_1\right) &= -\frac{1}{2}\left(\frac{1}{\epsilon} + \ln\left(\frac{\mu^2}{m_1^2}\right) + 1\right),\\
B_1\left(p^2; m_0, 0\right) &= -\frac{1}{2}\left(\frac{1}{\epsilon} + \ln\left(\frac{\mu^2}{m_0^2}\right)\right) - \frac{m_0^4 - p^4}{2p^4}\ln\left(\frac{m_0^2 - p^2}{m_0^2}\right) - \frac{m_0^2 + 2p^2}{2p^2},\\
B_1\left(m_0^2; m_0, 0\right) &= -\frac{1}{2}\left(\frac{1}{\epsilon} + \ln\left(\frac{\mu^2}{m_0^2}\right) + 3\right),\\
B_1\left(p^2; 0, 0\right) &= -\frac{1}{2}\left(\frac{1}{\epsilon} + \ln\left(-\frac{\mu^2}{p^2}\right) + 2\right).
\end{aligned} \tag{B.22}$$

- $\mathbf{B_{00}}$

$$\begin{aligned}
B_{00}\left(0; m_0, m_1\right) &= \frac{m_0^2 + m_1^2}{4}\left(\frac{1}{\epsilon} + \ln\left(\frac{\mu^2}{m_1^2}\right)\right) - \frac{m_0^4}{4\left(m_0^2 - m_1^2\right)}\ln\left(\frac{m_0^2}{m_1^2}\right) + \frac{3\left(m_0^2 + m_1^2\right)}{8},\\
B_{00}\left(0; m, m\right) &= \frac{m^2}{2}\left(\frac{1}{\epsilon} + \ln\left(\frac{\mu^2}{m^2}\right) + 1\right),\\
B_{00}\left(0; 0, m\right) &= \frac{m^2}{4}\left(\frac{1}{\epsilon} + \ln\left(\frac{\mu^2}{m^2}\right) + \frac{3}{2}\right) = B_{00}\left(0; m, 0\right).
\end{aligned} \tag{B.23}$$

- $\mathbf{B_{11}}$

$$B_{11}\left(0; m_0, m_1\right) = \frac{1}{3}\left(\frac{1}{\epsilon} + \ln\left(\frac{\mu^2}{m_1^2}\right)\right) - \frac{m_0^6}{3\left(m_0^2 - m_1^2\right)^3}\ln\left(\frac{m_0^2}{m_1^2}\right) + \frac{11m_0^4 - 7m_0^2 m_1^2 + 2m_1^4}{18\left(m_0^2 - m_1^2\right)^2},$$

$$B_{11}\left(0;m,m\right)=\frac{1}{3}\left(\frac{1}{\epsilon}+\ln\left(\frac{\mu^2}{m^2}\right)\right),$$

$$B_{11}\left(0;0,m_1\right)=\frac{1}{3}\left(\frac{1}{\epsilon}+\ln\left(\frac{\mu^2}{m_1^2}\right)+\frac{1}{3}\right),$$

$$B_{11}\left(0;m_0,0\right)=\frac{1}{3}\left(\frac{1}{\epsilon}+\ln\left(\frac{\mu^2}{m_0^2}\right)+\frac{11}{6}\right). \tag{B.24}$$

- $\mathbf{B_{001}}$

$$B_{001}\left(0;m_0,m_1\right)=-\frac{m_0^2+2m_1^2}{12}\left(\frac{1}{\epsilon}+\ln\left(\frac{\mu^2}{m_1^2}\right)\right)+\frac{m_0^6}{12\left(m_0^2-m_1^2\right)^2}\ln\left(\frac{m_0^2}{m_1^2}\right)-\frac{11m_0^2(m_0^2+m_1^2)-16m_1^4}{72\left(m_0^2-m_1^2\right)},$$

$$B_{001}\left(0;m,m\right)=-\frac{m^2}{4}\left(\frac{1}{\epsilon}+\ln\left(\frac{\mu^2}{m^2}\right)+1\right),$$

$$B_{001}\left(0;0,m_1\right)=-\frac{m_1^2}{6}\left(\frac{1}{\epsilon}+\ln\left(\frac{\mu^2}{m_1^2}\right)+\frac{4}{3}\right),$$

$$B_{001}\left(0;m_0,0\right)=-\frac{m_0^2}{12}\left(\frac{1}{\epsilon}+\ln\left(\frac{\mu^2}{m_0^2}\right)+\frac{11}{6}\right). \tag{B.25}$$

- $\mathbf{B_{111}}$

$$B_{111}\left(0;m_0,m_1\right)=-\frac{1}{4}\left(\frac{1}{\epsilon}+\ln\left(\frac{\mu^2}{m_1^2}\right)\right)+\frac{m_0^8}{4\left(m_0^2-m_1^2\right)^4}\ln\left(\frac{m_0^2}{m_1^2}\right)+$$
$$-\frac{25m_0^6-23m_0^4m_1^2+13m_0^2m_1^4-3m_1^4)-16m_1^6}{48\left(m_0^2-m_1^2\right)^3},$$

$$B_{111}\left(0;m,m\right)=-\frac{1}{4}\left(\frac{1}{\epsilon}+\ln\left(\frac{\mu^2}{m^2}\right)\right),$$

$$B_{111}\left(0;0,m_1\right)=-\frac{1}{4}\left(\frac{1}{\epsilon}+\ln\left(\frac{\mu^2}{m_1^2}\right)+\frac{1}{4}\right),$$

$$B_{111}\left(0;m_0,0\right)=-\frac{1}{4}\left(\frac{1}{\epsilon}+\ln\left(\frac{\mu^2}{m_0^2}\right)+\frac{25}{12}\right). \tag{B.26}$$

B.1.5 Derivative of B_0 and higher weights

The computation of field strength renormalization constants includes taking derivatives of 2-point functions. To avoid calculating derivatives of all tensor coefficients, we scalarize the results with help of eq. B.19, B.22, B.23, B.24, B.25, B.26 and only then take the derivative with respect to the external invariant p^2. In this way we only have to give the quantity $B_0'(p^2;m_0,m_1)\equiv\frac{d}{dp^2}B_0(p^2;m_0,m_1)$. By using the replacements of appendix A.1.1 it is straightforward to show that (by differentiating the integral expression)

$$B_0'(p^2;m_0,m_1)=-B_0^{\langle 1,2\rangle}(p^2;m_0,m_1)-B_1^{\langle 1,2\rangle}(p^2;m_0,m_1) \tag{B.27}$$

The scalar functions A_0 and B_0 for weights $\langle 2\rangle$ and $\langle 1,2\rangle$ read

$$A_0^{\langle 2\rangle}(m_0)=\frac{1}{\epsilon}+\ln\left(\frac{\mu^2}{m_0^2}\right)=B_0(0;m_0,m_0),$$

$$B_0^{\langle 1,2\rangle}(p^2;m_0,m_1)=\frac{1}{2p^2}\ln\left(\frac{m_0^2}{m_1^2}\right)-\frac{p^2+m_0^2-m_1^2}{\lambda(p^2,m_0^2,m_1^2)}\Lambda(p^2;m_0,m_1). \tag{B.28}$$

The tensor coefficients up to rank-3 are

$$B_1^{\langle 1,2\rangle}(p^2;m_0,m_1) = \frac{1}{2p^2}\left\{B_0\left(p^2;m_0,m_1\right) - A_0^{\langle 2\rangle}\left(m_1\right) - \left(p^2+m_0^2-m_1^2\right)\, B_0^{\langle 1,2\rangle}(p^2;m_0,m_1)\right\},$$

$$B_{00}^{\langle 1,2\rangle}(p^2;m_0,m_1) = \frac{1}{12p^2}\Big\{2p^2 - A_0(m_0) + A_0(m_1) + \left(p^2-m_0^2+m_1^2\right) A_0^{\langle 2\rangle}\left(m_1\right) +$$
$$+\,2\left(p^2+m_0^2-m_1^2\right)\, B_0\left(p^2,m_0,m_1\right) - \lambda(p^2,m_0^2,m_1^2)\, B_0^{\langle 1,2\rangle}(p^2;m_0,m_1)\Big\},$$

$$B_{11}^{\langle 1,2\rangle}(p^2;m_0,m_1) = \frac{1}{3p^4}\Big\{-\frac{p^2}{2} + A_0(m_0) - A_0(m_1) + \left(2p^2+m_0^2-m_1^2\right) A_0^{\langle 2\rangle}\left(m_1\right) +$$
$$-\,2\left(p^2+m_0^2-m_1^2\right) B_0\left(p^2,m_0,m_1\right) + \Big(\lambda(p^2,m_0^2,m_1^2) + 2m_0^2p^2\Big)\, B_0^{\langle 1,2\rangle}(p^2;m_0,m_1)\Big\},$$

$$B_{001}^{\langle 1,2\rangle}(p^2;m_0,m_1) = \frac{1}{24p^4}\Big\{-\frac{8p^4}{3} + m_1^2p^2 + 2(p^2+m_0^2-m_1^2)\big(A_0(m_0) - A_0(m_1)\big) - p^2\, A_0(m_1) +$$
$$+\Big(\lambda(p^2,m_0^2,m_1^2) - p^2\left(2p^2-2m_0^2+m_1^2\right)\Big) A_0^{\langle 2\rangle}\left(m_1\right) +$$
$$-\Big(\lambda(p^2,m_0^2,m_1^2) + 2\left(p^2+m_0^2-m_1^2\right)^2\Big) B_0\left(p^2,m_0,m_1\right) +$$
$$+\left(p^2+m_0^2-m_1^2\right)\lambda(p^2,m_0^2,m_1^2)\, B_0^{\langle 1,2\rangle}(p^2;m_0,m_1)\Big\},$$

$$B_{111}^{\langle 1,2\rangle}(p^2;m_0,m_1) = -\frac{1}{4p^6}\Big\{-\frac{4p^4}{3} + m_1^2p^2 + 2(p^2+m_0^2-m_1^2)\big(A_0(m_0) - A_0(m_1)\big) - p^2\, A_0(m_1) +$$
$$+\Big(\lambda(p^2,m_0^2,m_1^2) + p^2\left(2p^2+4m_0^2-m_1^2\right)\Big) A_0^{\langle 2\rangle}\left(m_1\right) +$$
$$-\Big(3\,\lambda(p^2,m_0^2,m_1^2) + 10m_0^2p^2\Big) B_0\left(p^2,m_0,m_1\right) +$$
$$+\left(p^2+m_0^2-m_1^2\right)\Big(\lambda(p^2,m_0^2,m_1^2) + 2m_0^2p^2\Big) B_0^{\langle 1,2\rangle}(p^2;m_0,m_1)\Big\}. \qquad \text{(B.29)}$$

Evaluating for specific kinematic situations is intricate because of the possibility of IR-divergences. We have:[3]

- $\mathbf{B_0^{\langle 1,2\rangle}}$

$$B_0^{\langle 1,2\rangle}\left(p^2;0,m_1\right) = \frac{1}{p^2}\ln\left(\frac{m_1^2-p^2}{m_1^2}\right),$$

$$B_0^{\langle 1,2\rangle}\left(m_1^2;0,m_1\right) = \frac{1}{2m_1^2}\left(\frac{1}{\epsilon} + \ln\left(\frac{\mu^2}{m_1^2}\right)\right),$$

$$B_0^{\langle 1,2\rangle}\left(p^2;m_0,0\right) = \frac{1}{m_0^2-p^2}\left(\frac{1}{\epsilon} + \ln\left(\frac{\mu^2}{m_0^2-p^2}\right) - \frac{m_0^2}{p^2}\ln\left(\frac{m_0^2-p^2}{m_0^2}\right)\right),$$

$$B_0^{\langle 1,2\rangle}\left(m_0^2;m_0,0\right) = \frac{1}{2m_0^2}\left(\frac{1}{\epsilon} + \ln\left(\frac{\mu^2}{m_0^2}\right) + 2\right),$$

[3] The integrals $B_0^{\{1,2\}}(m_0^2;m_0,0)$ and $B_1^{\{1,2\}}(m_0^2;m_0,0)$ (as well as on-shell integrals $B_0^{\{2,1\}}(m_1^2;0,m_1)$ and $B_0^{\{2,1\}}(m_1^2;0,m_1)$, which are not presented here) show IR power-divergences, and need to be regularized by either going off-threshold or analytically continuing to suffecently large values of ϵ. The results presented here use the latter method, which however questions the expansions around $d=4$. In the real calculation these power-IR-divergences always cancel or do not show up at all if the calculation is properly reorganized.

$$B_0^{\langle 1,2\rangle}(0;m_0,m_1) = \frac{1}{m_0^2-m_1^2}\left(-\frac{m_0^2}{m_0^2-m_1^2}\ln\left(\frac{m_0^2}{m_1^2}\right)+1\right),$$
$$B_0^{\langle 1,2\rangle}(0;m,m) = -\frac{1}{2m^2},$$
$$B_0^{\langle 1,2\rangle}(0;0,m_1) = -\frac{1}{m_1^2},$$
$$B_0^{\langle 1,2\rangle}(0;m_0,0) = \frac{1}{m_0^2}\left(\frac{1}{\epsilon}+\ln\left(\frac{\mu^2}{m_0^2}\right)+1\right). \tag{B.30}$$

- $\mathbf{B_1^{\langle 1,2\rangle}}$

$$B_1^{\langle 1,2\rangle}\left(p^2;0,m_1\right) = \frac{1}{p^2}\left(\frac{m_1^2-p^2}{p^2}\ln\left(\frac{m_1^2-p^2}{m_1^2}\right)+1\right),$$
$$B_1^{\langle 1,2\rangle}\left(m_1^2;0,m_1\right) = \frac{1}{m_1^2},$$
$$B_1^{\langle 1,2\rangle}\left(p^2;m_0,0\right) = -\frac{1}{m_0^2-p^2}\left(\frac{1}{\epsilon}+\ln\left(\frac{\mu^2}{m_0^2-p^2}\right)-\frac{m_0^4}{p^4}\ln\left(\frac{m_0^2-p^2}{m_0^2}\right)\right)+\frac{1}{p^2},$$
$$B_1^{\langle 1,2\rangle}\left(m_0^2;m_0,0\right) = \frac{1}{m_0^2}\left(\frac{1}{\epsilon}+\ln\left(\frac{\mu^2}{m_0^2}\right)\right),$$
$$B_1^{\langle 1,2\rangle}(0;m_0,m_1) = \frac{1}{m_0^2-m_1^2}\left(\frac{m_0^4}{(m_0^2-m_1^2)^2}\ln\left(\frac{m_0^2}{m_1^2}\right)-\frac{3}{2}\right),$$
$$B_1^{\langle 1,2\rangle}(0;m,m) = \frac{1}{3m^2},$$
$$B_1^{\langle 1,2\rangle}(0;0,m_1) = \frac{1}{2m_1^2},$$
$$B_1^{\langle 1,2\rangle}(0;m_0,0) = -\frac{1}{m_0^2}\left(\frac{1}{\epsilon}+\ln\left(\frac{\mu^2}{m_0^2}\right)+\frac{3}{2}\right). \tag{B.31}$$

- $\mathbf{B_{00}^{\langle 1,2\rangle}}$

$$B_{00}^{\langle 1,2\rangle}\left(p^2;0,m_1\right) = \frac{1}{4}\left\{\frac{1}{\epsilon}+\ln\left(\frac{\mu^2}{m_1^2}\right)-\frac{(m_1^2-p^2)^2}{p^4}\ln\left(\frac{m_1^2-p^2}{m_1^2}\right)+\frac{2p^2-m_1^2}{p^2}\right\},$$
$$B_{00}^{\langle 1,2\rangle}\left(m_1^2;0,m_1\right) = \frac{1}{4}\left\{\frac{1}{\epsilon}+\ln\left(\frac{\mu^2}{m_1^2}\right)+1\right\},$$
$$B_{00}^{\langle 1,2\rangle}\left(p^2;m_0,0\right) = \frac{1}{4}\left\{\frac{1}{\epsilon}+\ln\left(\frac{\mu^2}{m_0^2}\right)+\frac{m_0^4-p^4}{p^4}\ln\left(\frac{m_0^2-p^2}{m_0^2}\right)+\frac{2p^2+m_0^2}{p^2}\right\},$$
$$B_{00}^{\langle 1,2\rangle}\left(m_0^2;m_0,0\right) = \frac{1}{4}\left\{\frac{1}{\epsilon}+\ln\left(\frac{\mu^2}{m_1^2}\right)+3\right\},$$
$$B_{00}^{\langle 1,2\rangle}(0;m_0,m_1) = \frac{1}{4}\left\{\frac{1}{\epsilon}+\ln\left(\frac{\mu^2}{m_1^2}\right)-\frac{m_0^4}{(m_0^2-m_1^2)^2}\ln\left(\frac{m_0^2}{m_1^2}\right)+\frac{3m_0^2-m_1^2}{2(m_0^2-m_1^2)}\right\},$$
$$B_{00}^{\langle 1,2\rangle}(0;m,m) = \frac{1}{4}\left\{\frac{1}{\epsilon}+\ln\left(\frac{\mu^2}{m^2}\right)\right\},$$

$$B_{00}^{\langle 1,2\rangle}(0;0,m_1) = \frac{1}{4}\left\{\frac{1}{\epsilon} + \ln\left(\frac{\mu^2}{m_1^2}\right) + \frac{1}{2}\right\},$$

$$B_{00}^{\langle 1,2\rangle}(0;m_0,0) = \frac{1}{4}\left\{\frac{1}{\epsilon} + \ln\left(\frac{\mu^2}{m_0^2}\right) + \frac{3}{2}\right\},$$

$$B_{00}^{\langle 1,2\rangle}\left(p^2;0,0\right) = \frac{1}{4}\left\{\frac{1}{\epsilon} + \ln\left(-\frac{\mu^2}{p^2}\right) + 2\right\}. \tag{B.32}$$

- $\mathbf{B_{11}^{\langle 1,2\rangle}}$

$$B_{11}^{\langle 1,2\rangle}\left(p^2;0,m_1\right) = \frac{1}{p^4}\left\{\frac{(m_1^2-p^2)^2}{p^2}\ln\left(\frac{m_1^2-p^2}{m_1^2}\right) + \frac{2m_1^2-3p^2}{2}\right\},$$

$$B_{11}^{\langle 1,2\rangle}\left(m_1^2;0,m_1\right) = -\frac{1}{2m_1^2},$$

$$B_{11}^{\langle 1,2\rangle}\left(p^2;m_0,0\right) = \frac{1}{m_0^2-p^2}\left\{\frac{1}{\epsilon} + \ln\left(\frac{\mu^2}{m_0^2-p^2}\right) - \frac{m_0^6}{p^6}\ln\left(\frac{m_0^2-p^2}{m_0^2}\right) - \frac{(m_0^2-p^2)(2m_0^2+3p^2)}{2p^4}\right\},$$

$$B_{11}^{\langle 1,2\rangle}\left(m_0^2;m_0,0\right) = -\frac{3}{2m_0^2}\left\{\frac{1}{\epsilon} + \ln\left(\frac{\mu^2}{m_0^2}\right) + 1\right\},$$

$$B_{11}^{\langle 1,2\rangle}(0;m_0,m_1) = \frac{1}{m_0^2-m_1^2}\left\{-\frac{m_0^6}{(m_0^2-m_1^2)^3}\ln\left(\frac{m_0^2}{m_1^2}\right) + \frac{11m_0^4-7m_0^2m_1^2+2m_1^4}{(m_0^2-m_1^2)^2}\right\},$$

$$B_{11}^{\langle 1,2\rangle}(0;m,m) = -\frac{1}{4m^2},$$

$$B_{11}^{\langle 1,2\rangle}(0;0,m_1) = -\frac{1}{3m_1^2},$$

$$B_{11}^{\langle 1,2\rangle}(0;m_0,0) = \frac{1}{m_0^2}\left\{\frac{1}{\epsilon} + \ln\left(\frac{\mu^2}{m_0^2}\right) + \frac{11}{6}\right\},$$

$$B_{11}^{\langle 1,2\rangle}\left(p^2;0,0\right) = \frac{1}{p^2}\left\{\frac{1}{\epsilon} + \ln\left(-\frac{\mu^2}{p^2}\right) - \frac{3}{2}\right\}. \tag{B.33}$$

It is pointed out that the $\frac{1}{\epsilon}$-terms in eqs. B.30 and B.31 are IR-divergences, although there is no distinction due to analytic continuation.

B.1.6 Scalar 3- and 4-point functions

The scalar 3- and 4-point functions are much more involved than the 2-point functions, and presentation for arbitrary arguments becomes unviable. For a complete discussion including arbitrary arguments see the classic paper [30] or [8]. Except for very specific kinematic argument sets the explicit expressions for scalar functions C_0 and D_0 are relatively lengthy and consist of a sum or Dilogarithms. Since we will not need explicit expression to cancel IR-divergences etc., we keep the C_0 and D_0-functions implicit in this work to avoid getting the notation too involved. The same goes for 3- and 4-point tensor coefficients. Their reduction, albeit straightforward, usually results in quite some lengthy expressions if there are many different scales (internal masses, external invariants) involved, such as in our case. Instead we make heavy use of the `Mathematica` package `Package-X 2.0` [21], which allows the tensor decomposition and subsequent scalarization[4] of Feynman one-loop integrals.

[4]scalarization = replacements of all PV-coefficients by their expressions in terms of scalar functions. The package actually does also substitute A_0, B_0 explicitly, as well as C_0 and D_0 if their set of arguments allows a representation much simpler than the full expression.

A convenient feature for symbolic calculation is the high degree of symmetry in the arguments, characteristic of scalar n-point functions. Specifically, for C_0 and D_0 we have:

$C_0(s_1, s_2, s_3; m_0, m_1, m_2)$ is symmetric w.r.t. the following permutations:

- cyclic, $\{s_1 \to s_2 \to s_3, m_0 \to m_1 \to m_2\}$
- order reversal, $\{s_2 \leftrightarrow s_3, m_0 \leftrightarrow m_1\}$ or $\{s_2 \leftrightarrow s_1, m_0 \leftrightarrow m_3\}$ or $\{s_1 \leftrightarrow s_3, m_2 \leftrightarrow m_1\}$

$D_0(s_1, s_2, s_3, s_4, \bar{s}, \bar{u}; m_0, m_1, m_2, m_3)$ is symmetric w.r.t. the following permutations:

- cyclic, $\{s_1 \to s_2 \to s_3 \to s_4, \bar{s} \leftrightarrow \bar{u}, m_0 \to m_1 \to m_2 \to m_3\}$
- order reversal, $\{s_1 \leftrightarrow s_4, s_2 \leftrightarrow s_3, m_1 \leftrightarrow m_3\}$
- transposition, $\{s_1 \leftrightarrow \bar{s}, s_3 \leftrightarrow \bar{u}, m_1 \leftrightarrow m_2\}$ or $\{s_2 \leftrightarrow \bar{u}, s_4 \leftrightarrow \bar{s}, m_2 \leftrightarrow m_3\}$

B.2 High-energy expansions of scalar n-point functions

For the extraction of the high-energy behaviour of the Passarino-Veltman coefficients we assume the hierachy

$$\{|\bar{s}|, |\bar{t}|, |\bar{u}|\} \gg \{m_i^2, M_V^2, M_S^2\} \sim \Lambda_{\mathrm{EW}}^2. \tag{B.34}$$

We refer to $\bar{s}, \bar{u}, \bar{u} \sim \Lambda_{\mathrm{hard}}^2$ as the hard scales. In the following we only give the expansions of the scalar n-point integrals, as we will adopt the recipe of first scalarizing the diagrams and then use the high-energy expansions for the scalar integrals (followed by another expansion to account for the respective prefactors). The scalarization procedure can be carried out analytically by `Package-X`.

The one-point function A_0 is independent of external invariants, and there is no expansion in the high-energy regime. The higher n-point functions show logarithmic dependence on the ratio $\lambda \equiv \Lambda_{\mathrm{EW}}/\Lambda_{\mathrm{hard}}$, and we will give the expansion up to (and including) $\mathcal{O}\left(\left(\frac{\Lambda_{\mathrm{EW}}}{\Lambda_{\mathrm{hard}}}\right)^0\right)$, with the exception of B_0, where we need to take into account higher-order contributions (see below). The results are drawn from ref. [27], [28][5].

B.2.1 2-point coefficients

The 2-point coefficients show at most linear logarithmic dependence on λ if $p^2 = \bar{s} \gg \Lambda_{\mathrm{EW}}^2$. For the scalar function we find

$$\begin{aligned} B_0(\bar{s}; m_0, m_1) = {} & \frac{1}{\epsilon} + 2 - \ln\left(\frac{\mu^2}{-\bar{s} - i0^+}\right) + \frac{m_0^2 + m_1^2}{\bar{s}}\left[1 + \ln\left(\frac{m_0\, m_1}{-\bar{s} - i0^+}\right)\right] + \\ & - \frac{m_0^4 + m_1^4}{2\bar{s}^2} - \frac{2m_0^2 m_1^2}{\bar{s}^2} \ln\left(\frac{m_0 m_1}{-\bar{s} - i0^+}\right) + \mathcal{O}(\lambda^3). \end{aligned} \tag{B.35}$$

The log-terms have their origin in the logarithmic discontinuity $\Lambda(\bar{s}; m_0, m_1)$, whose expansion reads

$$\begin{aligned} \Lambda(\bar{s}; m_0, m_1) = {} & \ln\left(\frac{m_0\, m_1}{-\bar{s} - i0^+}\right) + \frac{m_0^2 + m_1^2}{\bar{s}}\left[1 + \ln\left(\frac{m_0\, m_1}{-\bar{s} - i0^+}\right)\right] + \\ & - \frac{m_0^4 + m_1^4}{2\bar{s}^2} - \frac{2m_0^2 m_1^2}{\bar{s}^2} \ln\left(\frac{m_0 m_1}{-\bar{s} - i0^+}\right) + \mathcal{O}(\lambda^3). \end{aligned} \tag{B.36}$$

We do the expansion up to (including) $\mathcal{O}(\lambda^2)$ as we will need these higher-order terms for the longitudinal parts of gauge boson diagrams (vertices and boxes).

[5] Note however the different notation for internal masses, using $\{m_0, m_1, m_2, m_3\}$ instead of $\{m_1, m_2, m_3, m_4\}$ in [28]. Futhermore, the ordering of the external invariants in C_0 in [27] is different than the standard one, and a permutation $s_{21} \leftrightarrow s_2$ has to be performed to make contact with the usual cyclic ordering

B.2.2 3-point coefficients

The 3-point coefficients can show both quadratic and linear logarithmic dependence on λ. Following [28] we use the abbreviation

$$L_{abc} \equiv L\left(p_a; m_b, m_c\right) \equiv \mathrm{Li}_2\left(\frac{2p_a^2 + i0^+}{m_b^2 - m_c^2 + p_a^2 + i0^+ + \sqrt{\lambda(p_a^2 + i0^+, m_b^2, m_c^2)}}\right) + \\ + \mathrm{Li}_2\left(\frac{2p_a^2 + i0^+}{m_b^2 - m_c^2 + p_a^2 + i0^+ - \sqrt{\lambda(p_a^2 + i0^+, m_b^2, m_c^2)}}\right). \tag{B.37}$$

For the scalar PV-triangle coefficients we need to distinguish wheter the mass m_1 adjacent to the high-energy external invariant $\bar{s}$ is zero or non-zero[6].

- $m_1 \neq 0$, p_1^2, p_2^2 arbitrary:

$$C_0^{\mathrm{HE}}\left(p_1^2, p_2^2, \bar{s}; m_0, m_1, m_2\right) = \frac{1}{s}\left\{\frac{1}{2}\ln^2\left(\frac{m_1^2}{-\bar{s} - i0^+}\right) + L_{212} + L_{110}\right\}, \tag{B.38}$$

- $m_1 = 0, p_1^2 \neq m_0^2, p_2^2 \neq m_2^2$:

$$C_0^{\mathrm{HE}}\left(p_1^2, p_2^2, \bar{s}; m_0, 0, m_2\right) = \frac{1}{\bar{s}}\left\{\ln\left(\frac{m_0^2 - p_1^2}{-\bar{s} - i0^+}\right)\ln\left(\frac{m_2^2 - p_2^2}{-\bar{s} - i0^+}\right) + \right. \\ \left. + \mathrm{Li}_2\left(\frac{p_1^2 + i0^+}{-m_0^2 + p_1^2 + i0^+}\right) + \mathrm{Li}_2\left(\frac{p_2^2 + i0^+}{-m_2^2 + p_2^2 + i0^+}\right)\right\}, \tag{B.39}$$

- $p_1^2 = m_0^2 = 0, p_2^2 \neq m_2^2$:

$$C_0^{\mathrm{HE}}\left(0, p_2^2, \bar{s}; 0, m_1, m_2\right) = \frac{1}{\bar{s}}\left\{\frac{1}{2}\ln^2\left(\frac{m_1^2}{-\bar{s} - i0^+}\right) + L_{212} + \frac{\pi^2}{6}\right\}, \tag{B.40}$$

The extraction of the imaginary parts from the Dilogs in eqs. B.38 and B.39 via the Dilog-identities A.19 demands some care to take the correct branch. The results for the imaginary parts agree with the ones derived from the Cutkosky-rules (app. C if those are expanded in the high-energy limit.

For reference below we give the explicit expressions for C_0-functions specifically used in this work:

$$C_0^{\mathrm{HE}}\left(0, 0, \bar{s}; 0, M, 0\right) = \frac{1}{\bar{s}}\left\{\ln\left(\frac{M^2}{-\bar{s} - i0^+}\right) + \frac{\pi^2}{3}\right\} \tag{B.41}$$

$$C_0^{\mathrm{HE}}\left(0, 0, \bar{s}; M_1, 0, M_2\right) = \frac{1}{\bar{s}}\ln\left(\frac{M_1^2}{-\bar{s} - i0^+}\right)\ln\left(\frac{M_2^2}{-\bar{s} - i0^+}\right) \tag{B.42}$$

$$C_0^{\mathrm{HE}}\left(m^2, m^2, \bar{s}; 0, M, 0\right) = \frac{1}{\bar{s}}\left\{\frac{1}{2}\ln^2\left(-\frac{M^2}{\bar{s}}\right) + 2\,\mathrm{Li}_2\left(\frac{m^2}{M^2}\right) + \frac{\pi^2}{3}\right\}, \tag{B.43}$$

$$C_0^{\mathrm{HE}}\left(m^2, m^2, \bar{s}; m, M, m\right) = \frac{1}{\bar{s}}\left\{\frac{1}{2}\ln^2\left(-\frac{M^2}{\bar{s}}\right) + 2\mathrm{Li}_2\left(\frac{2m^2}{M^2 + \sqrt{M^2\left(M^2 - 4m^2\right)}}\right) + \right. \\ \left. + 2\mathrm{Li}_2\left(\frac{2m^2}{M^2 - \sqrt{M^2\left(M^2 - 4m^2\right)}}\right)\right\}, \tag{B.44}$$

[6]Because of possible IR-divergences when the other legs go on-shell ($p_1^2 = m_0^2, p_2^2 = m_2^2$) in the case of $m_1 = 0$.

$$C_0^{\mathrm{HE}}\left(m^2, m^2, \bar{s}; M_1, 0, M_2\right) = \frac{1}{\bar{s}}\Bigg\{ \ln\left(\frac{M_1^2 - m^2}{-\bar{s} - i0^+}\right) \ln\left(\frac{M_2^2 - m^2}{-\bar{s} - i0^+}\right) + + \mathrm{Li}_2\left(\frac{m^2 + i0^+}{-M_1^2 + m^2 + i0^+}\right) + \mathrm{Li}_2\left(\frac{m^2 + i0^+}{-M_2^2 + m^2 + i0^+}\right)\Bigg\} \tag{B.45}$$

$$C_0^{\mathrm{HE}}\left(m^2, m^2, \bar{s}; M_1, m, M_2\right) = \frac{1}{\bar{s}}\Bigg\{\frac{1}{2}\ln^2\left(\frac{m_1^2}{-\bar{s} - i0^+}\right) + \mathrm{Li}_2\left(\frac{2m^2}{2m^2 - M_1^2 + \sqrt{M_1^2(M_1^2 - 4m^2)}}\right) + + \mathrm{Li}_2\left(\frac{2m^2}{2m^2 - M_1^2 - \sqrt{M_1^2(M_1^2 - 4m^2)}}\right) + + \mathrm{Li}_2\left(\frac{2m^2}{2m^2 - M_2^2 + \sqrt{M_2^2(M_2^2 - 4m^2)}}\right) + + \mathrm{Li}_2\left(\frac{2m^2}{2m^2 - M_2^2 - \sqrt{M_2^2(M_2^2 - 4m^2)}}\right)\Bigg\}, \tag{B.46}$$

$$C_0^{\mathrm{HE}}\left(0, m^2, \bar{u}; 0, M, m\right) = \frac{1}{\bar{u}}\Bigg\{\frac{1}{2}\ln^2\left(\frac{M^2}{-\bar{u} - i0^+}\right) + \mathrm{Li}_2\left(\frac{2m^2}{M^2 + \sqrt{M^2(M^2 - 4m^2)}}\right) + + \mathrm{Li}_2\left(\frac{2m^2}{M^2 - \sqrt{M^2(M^2 - 4m^2)}}\right) + \frac{\pi^2}{6}\Bigg\}, \tag{B.47}$$

B.2.3 4-point coefficients

The scalar 4-point function in the high-energy regime can be reduced to a linear combination of high-energy expanded versions of scalar 3-point functions. The central result [27] is

$$D_0^{\mathrm{HE}}\left(p_1^2, p_2^2, p_3^2, p_4^2, \bar{s}, \bar{u}; m_0, m_1, m_2, m_3\right) = = -\frac{1}{\bar{s}\bar{u}}\left\{\ln\left(\frac{-\bar{s} - i0^+}{-\bar{u} - i0^+} + \pi^2\right)\right\} + \frac{1}{\bar{u}}\Big\{C_0^{\mathrm{HE}}\left(p_1^2, p_2^2, \bar{s}; m_0, m_1, m_2\right) + C_0^{\mathrm{HE}}\left(p_3^2, p_3^2, \bar{s}; m_2, m_3, m_0\right)\Big\} + + \frac{1}{\bar{s}}\Big\{C_0^{\mathrm{HE}}\left(p_2^2, p_3^2, \bar{u}; m_1, m_2, m_3\right) + C_0^{\mathrm{HE}}\left(p_4^2, p_1^2, \bar{u}; m_3, m_0, m_1\right)\Big\} \tag{B.48}$$

which is also valid if some internal masses vanish, i.e. if the corresponding high-energy expansions of C_0 can be plugged in. Consequently, this formula does not hold for IR-divergent cases.

The two specific expressions used in this work are given below:

$$D_0^{\mathrm{HE}}\left(0, 0, m^2, m^2, \bar{s}, \bar{u}; M_1, 0, M_2, 0\right) = = \frac{1}{\bar{s}\bar{u}}\Bigg\{\ln\left(\frac{M_1^2}{-\bar{s} - i0^+}\right)\ln\left(\frac{M_2^2}{-\bar{s} - i0^+}\right) + \ln\left(\frac{m^2 - M_1^2}{-\bar{s} - i0^+}\right)\ln\left(\frac{m^2 - \mathrm{M2}^2}{-\bar{s} - i0^+}\right) + + \frac{1}{2}\ln^2\left(\frac{M_1^2}{-\bar{u} - i0^+}\right) + \frac{1}{2}\ln^2\left(\frac{M_2^2}{-\bar{u} - i0^+}\right) - \ln^2\left(\frac{-\bar{u} - i0^+}{-\bar{s} - i0^+}\right) - \frac{\pi^2}{3} + + \mathrm{Li}_2\left(\frac{m^2 + i0^+}{M_1^2}\right) + \mathrm{Li}_2\left(\frac{m^2 + i0^+}{M_2^2}\right) + \mathrm{Li}_2\left(\frac{m^2 + i0^+}{-M_1^2 + m^2 + i0^+}\right) + \mathrm{Li}_2\left(\frac{m^2 + i0^+}{-M_2^2 + m^2 + i0^+}\right)\Bigg\}, \tag{B.49}$$

$$
\begin{aligned}
&D_0^{\mathrm{HE}}\left(0,0,m^2,m^2,\bar{s},\bar{u};M_1,0,M_2,m\right)=\\
&=\frac{1}{\bar{s}\bar{u}}\Bigg\{\ln\left(\frac{M_1^2}{-\bar{s}-i0^+}\right)\ln\left(\frac{M_2^2}{-\bar{s}-i0^+}\right)+\frac{1}{2}\ln^2\left(\frac{m^2}{-\bar{s}-i0^+}\right)+\frac{1}{2}\ln^2\left(\frac{M_1^2}{-\bar{u}-i0^+}\right)+\\
&\qquad+\frac{1}{2}\ln^2\left(\frac{M_2^2}{-\bar{u}-i0^+}\right)-\ln^2\left(\frac{-\bar{u}-i0^+}{-\bar{s}-i0^+}\right)-\frac{2\pi^2}{3}+\\
&\qquad+\mathrm{Li}_2\left(\frac{2m^2}{M_1^2+\sqrt{M_1^2\left(M_1^2-4m^2\right)}}\right)+\mathrm{Li}_2\left(\frac{2m^2}{M_1^2-\sqrt{M_1^2\left(M_1^2-4m^2\right)}}\right)+\\
&\qquad+\mathrm{Li}_2\left(\frac{2m^2}{M_2^2+\sqrt{M_2^2\left(M_2^2-4m^2\right)}}\right)+\mathrm{Li}_2\left(\frac{2m^2}{M_2^2-\sqrt{M_2^2\left(M_2^2-4m^2\right)}}\right)+\\
&\qquad+\mathrm{Li}_2\left(\frac{2m^2}{2m^2-M_1^2+\sqrt{M_1^2\left(M_1^2-4m^2\right)}}\right)+\mathrm{Li}_2\left(\frac{2m^2}{2m^2-M_1^2-\sqrt{M_1^2\left(M_1^2-4m^2\right)}}\right)+\\
&\qquad+\mathrm{Li}_2\left(\frac{2m^2}{2m^2-M_2^2+\sqrt{M_2^2\left(M_2^2-4m^2\right)}}\right)+\mathrm{Li}_2\left(\frac{2m^2}{2m^2-M_2^2-\sqrt{M_2^2\left(M_2^2-4m^2\right)}}\right)\Bigg\}.
\end{aligned}
\tag{B.50}
$$

Appendix C

Imaginary parts

C.1 Imaginary parts of scalar PV-functions

For timelike processes (pair creation, annihilation) the non-analytic functions (i.e. logs and Dilogs) can obtain branch cut singularities that lead to non-zero imaginary parts when these functions are analytically continued according to the $i0^+$-prescription. For $s > 0$ we typically have

$$\ln\left(\frac{-s - i0^+}{\mu^2}\right) = \ln\left(\frac{s}{\mu^2}\right) - i\pi, \tag{C.1}$$

and similiar continuations for the Dilogs. In principle it is possible to (analytically) extract the imaginary parts by calculating the full diagrams/amplitude and use the $i0^+$-prescription as above. However, this procedure is quite involved as the expressions tend to be very lengthy. A more systematic and therefore better way is to determine the imaginary part independently from the (usually very involved) real part computation. The most elegant way is to firstly calculate the discontinuity and subsequently the imaginary part of a diagram/amplitude $\mathcal{M} = \mathcal{M}(s)$ by the relation

$$\mathrm{Disc}\left[i\mathcal{M}(s)\right] = i\mathcal{M}(s + i0^+) - i\mathcal{M}(s - i0^+) = -2\,\mathrm{Im}\left[\mathcal{M}(s)\right]. \tag{C.2}$$

The discontinuity of a diagram/amplitude is given by applying Cutkosky´s rules [1] ([31]), which effectively turn the loop integration into an integration over the Lorentz-invariant 2-body-phase-space of the 2 cut loop propagators that are put on their mass shell[2].

To obtain the discontinuity of a diagram/amplitude, the following manipulations need to be carried out (**Cutkosky rules**):

- Cut through 2 propagators so that energy-momentum conservation is maintained if both propagators are put on their mass shell.
- Replace each cut propagator by

$$\frac{1}{p^2 - m^2 + i0^+} \to (-2\pi i)\theta(\pm p^0)\delta(p^2 - m^2) \tag{C.3}$$

  The sign in $\theta(\pm k^0)$ is determined by the direction the momentum k passes the cut. The choice of direction has to be kept to ensure consistency.

- Carry out the integrations.
- Sum over all possible cuts of the diagram.

[1] This procedure is also frequently referred to as "cutting the diagram".

[2] The application of the cutting rules is essentially equivalent to going back from covariant perturbation theory to old-fashioned time-ordered perturbation theory. It is also closely connected to the optical theorem, but as we will not make use of this, we do not give further details but instead refer the reader to textbooks and reviews on this subject.

- The result is the discontinuity of the amplitude, see eq. C.2.

These rules can be applied to the Feynman diagrams directly including potential non-trivial numerator structures (such as $k \cdot p$). However due to the number of diagrams it is more convenient to first scalarize the expressions and only cut the scalar PV-functions, which we will do in the following. The downside of this procedure is that single cuts of the initial diagrams might not be uniquely resolved anymore. It is emphasized that only IR-finite cases are treated in the following.

C.1.1 Generic cut through 2 propagators

The cutting of the propagators and part of the integration can actually be done without knowledge of the (possibly) more involved structure of the diagram one is interested in cutting. Since we will only treat one-loop diagrams, cuts will always slice and replace 2 propagators according to eq. C.3. Without loss of generality, we can assume that the propagators we want to cut have the form[3]

$$T_0 = \frac{1}{i\pi^2} \int d^4k \left[k^2 - \bar{m}_0^2\right]^{-1} \left[(k+l)^2 - \bar{m}_1^2\right]^{-1} \ldots \tag{C.4}$$

where the dots represent possible additional propagators (or structure) like for C_0 or D_0. Application of eq. C.3 yields

$$\text{Disc}\left[i\,T_0\right] = \frac{(-2\pi i)^2}{\pi^2} \int d^4k\ \theta(\pm k^0)\,\delta(k^2 - \bar{m}_0^2)\,\theta(\mp(k^0 + l^0))\,\delta((k+l)^2 - \bar{m}_1^2)\ldots . \tag{C.5}$$

Note the signs inside the θ-functions. With our choice of momentum routing, the momenta flow through the cut in opposite directions, and hence their time components are equipped with opposite sign. We now make use of the well-known Dirac delta identity[4]

$$\delta\left(f(x)\right) = \sum_i \frac{\delta(x - x_i)}{|f'(x_i)|}, \qquad (f(x_i) = 0 \quad \forall i)\,, \tag{C.7}$$

to write $\theta(\pm p^0)\delta(p^2 - m^2) = (2E_{\vec{p}})^{-1}\delta(p^0 \mp E_{\vec{p}})$ with $E_{\vec{p}} = \sqrt{\vec{p}^2 + m^2}$. Focusing on the integrals for the moment we get

$$\begin{aligned}
&\int d^4k\ \theta(\pm k^0)\,\delta(k^2 - \bar{m}_0^2)\,\theta(\mp(k^0 + l^0))\,\delta((k+l)^2 - \bar{m}_1^2) = \\
&= \int d^4k\ \frac{\theta\left(\sqrt{\vec{k}^2 + \bar{m}_0^2}\right)}{2\sqrt{\vec{k}^2 + \bar{m}_0^2}}\,\frac{\theta\left(\sqrt{(\vec{k}+\vec{l})^2 + \bar{m}_1^2}\right)}{2\sqrt{(\vec{k}+\vec{l})^2 + \bar{m}_1^2}}\,\delta\left(k^0 \mp \sqrt{\vec{k}^2 + \bar{m}_0^2}\right)\,\delta\left(k^0 + l^0 \pm \sqrt{(\vec{k}+\vec{l})^2 + \bar{m}_1^2}\right) = \\
&= \int d^3k\ \frac{1}{4\sqrt{\vec{k}^2 + \bar{m}_0^2}\sqrt{(\vec{k}+\vec{l})^2 + \bar{m}_1^2}}\,\delta\left(l^0 \pm \sqrt{\vec{k}^2 + \bar{m}_0^2} \pm \sqrt{(\vec{k}+\vec{l})^2 + \bar{m}_1^2}\right).
\end{aligned} \tag{C.8}$$

From the δ-functions in eq. C.8 it is clear that (with the chosen momentum routing) k^0 and l^0 must have different sign to ensure consistency of the procedure. Since for a given convention of momentum flow the sign of l^0 is fixed, the proper sign of k^0 can be read off accordingly. In this sense the cut is

[3] If the first one also has a non-trivial momentum within the square, say $\left[(k+l_1)^2 - \bar{m}_0^2\right]\left[(k+l_2)^2 - \bar{m}_1^2\right]$, we can shift momentum $k \to k - l_1$ to achieve the form C.4. When dealing with scalar PV-functions, this shift is for free. If the numerator structure is non-trivial or if there are additional propagators, the shift has to be taken into account there as well.

[4] Since we have a product of 2 δ-fcts. and will use them to carry out integrations over k^0 and $|\vec{k}|$, a quicker treatment would be to use the 2-dimensional generalization of eq. C.5

$$\delta\left(f(x,y)\right)\delta\left(g(x,y)\right) = \sum_i \frac{\delta(x - x_i)\delta(y - y_i)}{\left|\frac{\partial f}{\partial x}\frac{\partial g}{\partial y} - \frac{\partial f}{\partial y}\frac{\partial g}{\partial x}\right|_{x_i,y_i}}, \qquad (f(x_i) = 0,\ g(y_i) = g(y(x_i)) = 0, \quad \forall i). \tag{C.6}$$

The subsequent treatment of both δ's in the text is equivalent however, and somewhat more transparent.

directional. Furthermore the invariant l^2 involved in the cut must be timelike ($l^2 > 0$) to give a non-vanishing contribution to the discontinuity, as in the case of spacelike behaviour ($l^2 < 0$) there is a frame where $l^0 = 0$ and the integrand has no support (cf. arguments of the θ-functions).

Making use of the Lorentz-invariance of the phase-space integration, the above integral is now easiest evaluated in the frame where $\vec{l} = \vec{0}$. In this frame the argument of the δ-function has the roots (taking the positive one as $|\vec{k}| > 0$)

$$f(|\vec{k}|) = l^0 \pm \sqrt{\vec{k}^2 + \bar{m}_0^2} \pm \sqrt{\vec{k}^2 + \bar{m}_1^2} \stackrel{!}{=} 0 \quad \Rightarrow \quad |\vec{k}| = \frac{\lambda^{1/2}\left((l^0)^2, \bar{m}_0^2, \bar{m}_1^2\right)}{2|l^0|},$$

$$f'(|\vec{k}|) = \pm\frac{|\vec{k}|}{\sqrt{\vec{k}^2 + \bar{m}_0^2}} \pm \frac{|\vec{k}|}{\sqrt{\vec{k}^2 + \bar{m}_1^2}} = -\frac{|\vec{k}|\, l^0}{\sqrt{\vec{k}^2 + \bar{m}_0^2}\sqrt{\vec{k}^2 + \bar{m}_0^2}}, \tag{C.9}$$

where in the last line we used $f(|\vec{k}|) = 0$ in the numerator. Using eq. C.5 we obtain

$$\cdots = \int d\Omega_{\vec{k}} \int_0^\infty d|\vec{k}||\vec{k}|^2 \frac{1}{4|\vec{k}||l^0|}\, \theta\Big(\lambda^{1/2}\left((l^0)^2, \bar{m}_0^2, \bar{m}_1^2\right)\Big)\, \theta(|l^0| - \bar{m}_0 - \bar{m}_1)\, \theta\big(l^2\big)\, \delta\Big(|\vec{k}| - \frac{\lambda^{1/2}\left((l^0)^2, \bar{m}_0^2, \bar{m}_1^2\right)}{2|l^0|}\Big). \tag{C.10}$$

Note the θ-functions in eq. C.10. The first one ensures $|\vec{k}| > 0$, but since the Kallen-function $\lambda(a, b, c)$ is symmetric in its arguments, it not only defines the physical threshold ($(l^0)^2 > (\bar{m}_0 + \bar{m}_1)^2$), but also the situations where one of the internal masses is larger than the other two arguments. The second θ-functions avoids the latter case[5], and it has its origins in eq. C.9 (first row). In the following we drop the first one as it is superfluous in presence of the second one (for $m_0, m_1 > 0$). The last one implements the nesessity for timelike invariant $l^2 > 0$.

The integral over $|\vec{k}|$ can now be carried out straightforwardly. We calculated in the rest frame of l ($\vec{l} = \vec{0}$), but the covariant result can be obtained straigthforwardly[6] by replacing $|l^0| \to \sqrt{|l^2|} = \sqrt{l^2}$. Collecting everything we obtain the intermediate result

$$\mathrm{Im}[T^0] = -\frac{1}{2}\,\mathrm{Disc}[i\,T_0] = \underbrace{\frac{\lambda^{1/2}(l^2, \bar{m}_0^2, \bar{m}_1^2)}{4l^2}}_{\frac{|\vec{k}|}{2\sqrt{l^2}}}\, \theta(\sqrt{l^2} - \bar{m}_0 - \bar{m}_1)\, \theta\big(l^2\big) \int d\Omega_{\vec{k}}\ \ldots, \tag{C.11}$$

with

$$k^0 = -\mathrm{sign}(l^0)\sqrt{\vec{k}^2 + \bar{m}_0^2} = -\frac{\mathrm{sign}(l^0)}{2\sqrt{l^2}}\left|l^2 + \bar{m}_0^2 - \bar{m}_1^2\right|,$$

$$|\vec{k}| = \frac{1}{2\sqrt{l^2}}\,\lambda^{1/2}(l^2, \bar{m}_0^1, \bar{m}_1^2) \tag{C.12}$$

where the dots indicate potential additional propagators/structure. The remaining integral over the solid angle has to be interpreted in the principal-value sense, i.e. with the $i0^+$ dropped for additional loop propagators, and needs to be evaluated in the rest-frame of l for consistency. Eq. C.11 will be our starting point for the discussion of B_0, C_0 and D_0 in the upcoming sections.

C.1.2 Scalar 2-point function B_0

Reminder[7]:

$$B_0[p^2; m_0, m_1] = \frac{1}{i\pi^2}\int d^4k\, \frac{1}{\left[k^2 - m_0^2 + i0^+\right]\left[(k+p)^2 - m_1^2 + i0^+\right]} \tag{C.13}$$

[5] Note also that we always have $m_i > 0$

[6] Knowing that the cut can be formulated in a covariant way, this is the only consistent possibility as in this frame we have $(l^0)^2 = l^2$. This trick of reexpressing variables in a certain frame by Lorentz-invariant objects to quote the covariant result will be crucial also in the next sections.

[7] For the determination of the imaginary part it is sufficient to cut the 4-dimensional integral expression rather than the d-dimensional version

The imaginary part of the scalar 2-point function is trivially derived from eq. C.11, as there is no more loop propagators or structure to consider. The angular integral over the full solid angle contributes a factor of 4π. Also, there is only one cut to consider. We get:

$$\mathrm{Im}\big[B_0(s;m_0,m_1)\big] = \pi\,\frac{\lambda^{1/2}(s,m_0^2,m_1^2)}{s}\,\theta(s)\,\theta\big(\sqrt{s}-\bar{m}_0-\bar{m}_1\big) \tag{C.14}$$

C.1.3 Scalar 3-point function C_0

Reminder:

$$C_0[k_1^2,(k_2-k_1)^2,k_2^2;m_0,m_1,m_2] = \frac{1}{i\pi^2}\int d^4k\,\frac{1}{\big[k^2-m_0^2+i0^+\big]\big[(k+k_1)^2-m_1^2+i0^+\big]\big[(k+k_2)^2-m_2^2+i0^+\big]} \tag{C.15}$$

The 3-point case is more involved, as in total there are 3 cuts that (potentially) contribute to the discontinuity of C_0, and there is another propagator in the loop that makes the angualar integration non-trivial. Generically the integral has the form

$$2\pi I_C \equiv \int d\Omega_{\vec{k}}\,\frac{1}{(k+p)^2-\bar{m}_2^2} = 2\pi\int_{-1}^{+1}\frac{dz}{k^2+p^2-\bar{m}_2^2+2k^0p^0-2|\vec{k}||\vec{p}|z} =, \tag{C.16}$$

where the trivial azimuthal integration gave a factor 2π and w.l.o.g. the coordinate system was chosen so that $\vec{p}\,||\,\hat{e}_3$ (and $z\equiv\cos(\theta)$). The remaining integral gives a single logarithm,

$$I_C = -\frac{1}{2|\vec{k}||\vec{p}|}\int_{-1}^{+1}\frac{dz}{z-z_0} \overset{|\mathrm{Re}[z_0]|>1}{=} \frac{1}{2|\vec{k}||\vec{p}|}\ln\left(\frac{z_0+1}{z_0-1}\right), \qquad z_0 = \frac{\bar{m}_0^2-\bar{m}_2^2+p^2+2k^0p^0}{2|\vec{k}||\vec{p}|}. \tag{C.17}$$

To be more specific, consider the cut where in the expression C.15 the first two propagators are cut, i.e. we identify $l=k_1=p_1$ and $p=k_2=p_1+p_2=-p_3$, where the p_i denote the external momenta (all incoming) and we assume the external invariants to be timelike,

$$p_i^2 = s_i > 0. \tag{C.18}$$

The task is to express the momenta in the rest-frame of $l=p_1$ in terms of the Lorentz-invariants s_i. We find:

$$\begin{aligned} p_1 &= \begin{pmatrix}\sigma\sqrt{s_1}\\ \vec{0}\end{pmatrix},\\ p_2 &= \frac{1}{2\sqrt{s_1}}\begin{pmatrix}\sigma(-s_1-s_2+s_3)\\ \lambda^{1/2}(s_1,s_2,s_3)\,\vec{n}_p\end{pmatrix},\\ p_3 &= \frac{1}{2\sqrt{s_1}}\begin{pmatrix}\sigma(-s_1+s_2-s_3)\\ -\lambda^{1/2}(s_1,s_2,s_3)\,\vec{n}_p\end{pmatrix}, \end{aligned} \tag{C.19}$$

where $\sigma=\mathrm{sign}(l^0)$ is indicating whether the momentum is incoming/outgoing. Plugging these expressions into eq. C.17 we get

$$\begin{aligned} I_C^{s_1} &= \frac{\sqrt{s_1}}{|\vec{k}|\lambda^{1/2}(s_1,s_2,s_3)}\times\\ &\times\ln\left(\frac{m_0^2-m_2^2+s_3-\frac{1}{2s_1}\left\{(s_1+m_0^2-m_1^2)(s_1-s_2+s_3)-\lambda^{1/2}(s_1,m_0^2,m_1^2)\lambda^{1/2}(s_1,m_0^2,m_1^2)\right\}}{m_0^2-m_2^2+s_3-\frac{1}{2s_1}\left\{(s_1+m_0^2-m_1^2)(s_1-s_2+s_3)+\lambda^{1/2}(s_1,m_0^2,m_1^2)\lambda^{1/2}(s_1,m_0^2,m_1^2)\right\}}\right). \end{aligned} \tag{C.20}$$

We did not plug in $|\vec{k}|$ as this factor will cancel in eq. C.11, as will the factor $\sqrt{s_1}$ against $\sqrt{|l^2|}$ in the denominator. The other cuts can be treated analogously (or using symmetry relations), and give the same result as eq. C.20 modulo cyclic permutations of the s_i and m_j. Defining a cut-function F^C_{cut},

$$F^C_{\mathrm{cut}}(\bar{s}_1,\bar{s}_2,\bar{s}_3;\bar{m}_0,\bar{m}_1,\bar{m}_2) := \theta(s_1)\,\theta\big(\sqrt{s_1}-\bar{m}_0-\bar{m}_1\big)\times$$

$$\times \ln\left(\frac{\bar m_0^2-\bar m_2^2+\bar s_3-\frac{1}{2\bar s_1}\left\{(\bar s_1+\bar m_0^2-\bar m_1^2)(\bar s_1-\bar s_2+\bar s_3)-\lambda^{1/2}(\bar s_1,\bar m_0^2,\bar m_1^2)\lambda^{1/2}(\bar s_1,\bar m_0^2,\bar m_1^2)\right\}}{\bar m_0^2-\bar m_2^2+\bar s_3-\frac{1}{2\bar s_1}\left\{(\bar s_1+\bar m_0^2-\bar m_1^2)(\bar s_1-\bar s_2+\bar s_3)+\lambda^{1/2}(\bar s_1,\bar m_0^2,\bar m_1^2)\lambda^{1/2}(\bar s_1,\bar m_0^2,\bar m_1^2)\right\}}\right), \tag{C.21}$$

the imaginary part of C_0 can be written as

$$\mathrm{Im}\big[C_0(s_1,s_2,s_3;m_0,m_1,m_2)\big] =$$
$$= \frac{\pi}{\lambda^{1/2}(s_1,s_2,s_3)}\Big\{F^C_{\mathrm{cut}}(s_1,s_2,s_3;m_0,m_1,m_2)+F^C_{\mathrm{cut}}(s_3,s_1,s_2;m_2,m_0,m_1)+F^C_{\mathrm{cut}}(s_2,s_3,s_1;m_1,m_2,m_0)\Big\} \tag{C.22}$$

C.1.4 Scalar 4-point function D_0

Reminder:

$$D_0[k_1^2,(k_2-k_1)^2,(k_3-k_2)^2,k_3^2,k_2^2,(k_3-k_1)^2;m_0,m_1,m_2,m_3] =$$
$$= \frac{1}{i\pi^2}\int d^4k\,\frac{1}{\big[k^2-m_0^2+i0^+\big]\big[(k+k_1)^2-m_1^2+i0^+\big]\big[(k+k_2)^2-m_2^2+i0^+\big]\big[(k+k_3)^2-m_3^2+i0^+\big]} \tag{C.23}$$

The scalar 4-point function D_0 has 6 independent invariants and therefore 6 different cuts contributing to its discontinuity: 4 cuts along the corners plus the $\bar s$- and $\bar u$-channel cuts. The angular integral now has 2 uncut loop propagators, but as in the triangle case the integration can be done symbolically without specifying the cut channel. We start by combining the uncut propagators with Feynman parameters and afterwards perform the angular integrations:

$$2\pi I_D = \int d\Omega_{\vec k}\,\frac{1}{\big[(k+p)^2-\bar m_2^2\big]\big[(k+q)^2-\bar m_3^2\big]} = \int d\Omega_{\vec k}\int_0^1 dx\,\frac{1}{\big[x((k+p)^2-\bar m_2^2)+(1-x)((k+q)^2-\bar m_3^2)\big]^2} =$$
$$= \int d\Omega_{\vec k}\int_0^1 dx\,\frac{1}{\big[A(x)+2k\cdot Q(x)\big]^2} = \frac{2\pi}{4|\vec k|^2|\vec Q(x)|^2}\int_0^1 dx\int_{-1}^{+1}dz\,\frac{1}{\Big[z-\underbrace{\frac{A(x)+2k^0Q^0(x)}{2|\vec k||\vec Q(x)|}}_{\equiv z_0}\Big]^2} =$$
$$= \frac{2\pi}{4|\vec k|^2|\vec Q(x)|^2}\int_0^1 dx\,\frac{2}{z_0^2-1} = 4\pi\int_0^1 dx\,\frac{1}{\big(A(x)+2k^0Q^0(x)\big)^2-4|\vec k|^2|\vec Q(x)|^2}, \tag{C.24}$$

where

$$A(x) = k^2+x(p^2-\bar m_2^2)+(1-x)(q^2-\bar m_3^2),$$
$$Q(x) = xp+(1-x)q. \tag{C.25}$$

The denominator $N(x)$ is now a polynomial of 2nd order in the Feynman parameter x, and can be written as

$$N(x) = ax^2+bx+c = a(x-x_1)(x-x_2), \qquad x_{1,2} = \frac{-b\pm\sqrt{b^2-4ac}}{2a}. \tag{C.26}$$

After partial fraction the integral can be carried out. It yields

$$I_D = \frac{2}{a}\int_0^1 dx\,\frac{1}{(x-x_1)(x-x_2)} = \frac{2}{a(x_1-x_2)}\left\{\ln\left(\frac{x_1-1}{x_1}\right)+\ln\left(\frac{x_2}{x_2-1}\right)\right\} =$$
$$= \frac{2}{a(x_1-x_2)}\left\{\ln\left(\frac{(x_1-1)x_2}{(x_2-1)x_1}\right)-\eta\left(\frac{x_1-1}{x_1},\frac{x_2}{x_2-1}\right)\right\}, \tag{C.27}$$

where the η-function is defined in sec. A, eq. (A.17). Observing

$$a(x_1 - x_2) = \sqrt{b^2 - 4ac}, \qquad x_1 x_2 = \frac{c}{a}, \qquad \frac{(x_1-1)x_2}{(x_2-1)x_1} = \frac{b+2c+\sqrt{b^2-4ac}}{b+2c-\sqrt{b^2-4ac}}, \tag{C.28}$$

the final result for I_D reads

$$I_D = \frac{2}{\sqrt{b^2-4ac}} \left\{ \ln\left(\frac{b+2c+\sqrt{b^2-4ac}}{b+2c-\sqrt{b^2-4ac}} \right) - \eta\left(\frac{x_1-1}{x_1}, \frac{x_2}{x_2-1} \right) \right\}. \tag{C.29}$$

Since the integral was interpreted in the principal-value sense (without $i0^+$), the imaginary parts of this expression are controlled by the behaviour of the discriminant $b^2 - 4ac$. We have

$$\begin{aligned}
\mathrm{Im}\left[\frac{x_1-1}{x_1}\right] &= \theta(4ac-b^2)\,\frac{\sqrt{4ac-b^2}}{2c}, \\
\mathrm{Im}\left[\frac{x_2}{x_2-1}\right] &= \theta(4ac-b^2)\,\frac{2c\sqrt{4ac-b^2}}{(b+2c)^2+4ac-b^2}, \\
\mathrm{Im}\left[\frac{(x_1-1)x_2}{x_1(x_2-1)}\right] &= \theta(4ac-b^2)\,\frac{2c\sqrt{4ac-b^2}}{(b+2c)^2+4ac-b^2}.
\end{aligned} \tag{C.30}$$

Observing that $4ac - b^2 > 0$ in the regime with non-zero imaginary parts, we get for the sign of the imaginary parts:

$$\begin{aligned}
\mathrm{sign}\left(\mathrm{Im}\left[\frac{x_1-1}{x_1}\right]\right) &= \theta(4ac-b^2)\,\mathrm{sign}(c), \\
\mathrm{sign}\left(\mathrm{Im}\left[\frac{x_2}{x_2-1}\right]\right) &= \theta(4ac-b^2)\,\mathrm{sign}(c), \\
\mathrm{sign}\left(\mathrm{Im}\left[\frac{(x_1-1)x_2}{x_1(x_2-1)}\right]\right) &= \theta(4ac-b^2)\,\mathrm{sign}\big(b+2c\big),
\end{aligned} \tag{C.31}$$

so the relevant η-function is

$$\eta\Big(\frac{x_1-1}{x_1}, \frac{x_2}{x_2-1}\Big) = 2\pi i\,\theta(4ac-b^2)\Big(\theta(-c)\,\theta(b+2c) - \theta(c)\,\theta(-b-2c)\Big) \equiv \tilde{\eta}(a,b,c). \tag{C.32}$$

Now let us turn to a specific cut, for example the "corner cut" with s_1 incoming. For this cut we make the identifications

$$l = p_1, \qquad p = p_1 + p_2 = -p_3 - p_4, \qquad q = p_1 + p_2 + p_3 = -p_4. \tag{C.33}$$

In the rest-frame of l we have explicitly

$$\begin{aligned}
p_1 &= \begin{pmatrix} \sigma\sqrt{s_1} \\ \vec{0} \end{pmatrix}, \\
p_2 &= \frac{1}{2\sqrt{s_1}} \begin{pmatrix} \sigma(\bar{s}-s_1-s_2) \\ \lambda^{1/2}(\bar{s},s_1,s_2)\,\vec{n}_p \end{pmatrix}, \\
p_3 &= \frac{1}{2\sqrt{s_1}} \begin{pmatrix} \sigma(\bar{t}-s_1-s_3) \\ \lambda^{1/2}(\bar{t},s_1,s_3)\,\vec{n}_{p'} \end{pmatrix} = \frac{1}{2\sqrt{s_1}} \begin{pmatrix} \sigma(-\bar{s}-\bar{u}+s_2+s_4) \\ \sqrt{(-\bar{s}-\bar{u}+s_2+s_4)^2 - 4s_1s_3}\,\vec{n}_{p'} \end{pmatrix}, \\
p_4 &= \frac{1}{2\sqrt{s_1}} \begin{pmatrix} \sigma(\bar{u}-s_1-s_2) \\ \lambda^{1/2}(\bar{u},s_1,s_4)\,\vec{n}_{p''} \end{pmatrix}.
\end{aligned} \tag{C.34}$$

We rewrote the $\bar{t}$-dependence of p_3 as it is conventional to quote $\bar{u}$ instead of $\bar{t}$ in the list of arguments of the scalar 4-point function D_0. With $Q(x) = -p_4 - xp_3$ and

$$Q^2 = \left(Q^0\right)^2 - |\vec{Q}(x)|^2 = s_4 + x^2 s_3 + x(\bar{s} - s_3 - s_4), \tag{C.35}$$

we are in a position to quote all the necessary ingredients to determine the input parameters of eq. C.29:

$$\begin{aligned}
k^0 &= -\frac{\sigma}{2\sqrt{s_1}}\left(s_1 + \bar{m}_0^2 - \bar{m}_1^2\right), \\
|\vec{k}|^2 &= \frac{\sigma}{4s_1}\,\lambda(s_1, \bar{m}_0^2, \bar{m}_1^2), \\
A(x) &= m_0^2 + x(\bar{s} - \bar{m}_2^2) + (1-x)(s_4 - \bar{m}_3^2), \\
Q^0 &= \frac{\sigma}{2\sqrt{s_1}}\left(-\bar{u} + s_1 + s_4 + x\left[\bar{s} + \bar{u} - s_2 - s_4\right]\right), \\
|\vec{Q}(x)|^2 &= \left(Q^0\right)^2 - \left(s_4 + x^2 x_3 + x\left[\bar{s} - s_3 - s_4\right]\right).
\end{aligned} \tag{C.36}$$

Unfortunately, the expressions for completely generic arguments are quite lengthy, which makes them not well suited for presentation. The rest of the cuts can be obtained from the above results by using the symmetries of the D_0-function and simply reordering the parameters. Again defining a cut function F^D_{cut}

$$\begin{aligned}
&F^D_{\text{cut}}(s_1, s_2, s_3, s_4, \bar{s}, \bar{u}; \bar{m}_0, \bar{m}_1, \bar{m}_2, \bar{m}_3) = \theta(\sqrt{s_1} - \bar{m}_0 - \bar{m}_1)\,\theta\big(s_1\big)\times \\
&\quad\times \frac{\lambda^{1/2}(s_1, \bar{m}_0^2, \bar{m}_1^2)}{s_1\sqrt{b^2 - 4ac}}\left\{\ln\left(\frac{b + 2c + \sqrt{b^2 - 4ac}}{b + 2c - \sqrt{b^2 - 4ac}}\right) - 2\pi i\,\theta(4ac - b^2)\Big(\theta(-c)\,\theta(b+2c) - \theta(c)\,\theta(-b-2c)\Big)\right\},
\end{aligned} \tag{C.37}$$

with the coefficients a, b, c given by the solutions C.26 of the quadratic equation and the parameters eq. C.36, we can write the imaginary part of D_0 (using the symmetry relations) as

$$\begin{aligned}
&\text{Im}\big[D_0(s_1, s_2, s_3, s_4, \bar{s}, \bar{u}; \bar{m}_0, \bar{m}_1, \bar{m}_2, \bar{m}_3)\big] = \\
&\qquad = \pi\Big\{F^D_{\text{cut}}(s_1, s_2, s_3, s_4, \bar{s}, \bar{u}; \bar{m}_0, \bar{m}_1, \bar{m}_2, \bar{m}_3) + F^D_{\text{cut}}(s_4, s_1, s_2, s_3, \bar{u}, \bar{s}; \bar{m}_3, \bar{m}_0, \bar{m}_1, \bar{m}_2) \\
&\qquad\quad + F^D_{\text{cut}}(s_3, s_4, s_1, s_2, \bar{s}, \bar{u}; \bar{m}_2, \bar{m}_3, \bar{m}_0, \bar{m}_1) + F^D_{\text{cut}}(s_2, s_3, s_4, s_1, \bar{u}, \bar{s}; \bar{m}_1, \bar{m}_2, \bar{m}_3, \bar{m}_0) \\
&\qquad\quad + F^D_{\text{cut}}(\bar{s}, s_2, \bar{u}, s_4, s_1, s_3; \bar{m}_0, \bar{m}_2, \bar{m}_1, \bar{m}_3) + F^D_{\text{cut}}(s_1, \bar{u}, s_3, \bar{s}, s_4, s_2; \bar{m}_0, \bar{m}_1, \bar{m}_3, \bar{m}_2)\Big\}.
\end{aligned} \tag{C.38}$$

C.2 Imaginary parts of specific scalar PV-functions

The expressions of the imaginary parts of C_0 and D_0 for generic masses are quite involved (especially eq. C.37 and C.38). Since we will only use these results for very specific kinematics and internal masses, we focus on them and give explicit results in the following. We skip the scalar 2-point function B_0 as its imaginary part is very straightforward (see eq. C.14).

C.2.1 3-point functions

The 3-point functions have a non-trivial imaginary part. In our calculation there appear 6 types of generic triangles (note: $m_b = 0$):

- Massless abelian $C_0(0, 0, \bar{s}; 0, M, 0)$

- Massless non-abelian $C_0(0,0,\bar{s};M_1,0,M_2)$
- Massive charged abelian $C_0(m^2,m^2,\bar{s};0,M,0)$
- Massive charged non-abelian $C_0(m^2,m^2,\bar{s};M_1,0,M_2)$
- Massive neutral abelian $C_0(m^2,m^2,\bar{s};m,M,m)$
- Massive neutral non-abelian $C_0(m^2,m^2,\bar{s};M_1,m,M_2)$

Using the abbreviation $\beta=\sqrt{1-\frac{4m^2}{\bar{s}}}$ we obtain (for the regime $\bar{s}>4m^2>0$)[8]

$$
\begin{aligned}
\mathrm{Im}\big[C_0(0,0,\bar{s};0,M,0)\big] &= \frac{\pi}{\bar{s}}\,\theta(\bar{s})\,\ln\left(\frac{M^2}{\bar{s}+M^2}\right),\\
\mathrm{Im}\big[C_0(0,0,\bar{s};M_1,0,M_2)\big] &= \frac{\pi}{\bar{s}}\,\theta\big(\bar{s}-(M_1+M_2)^2\big)\,\ln\left(\frac{\bar{s}-M_1^2-M_2^2-\lambda^{1/2}(\bar{s},M_1^2,M_2^2)}{\bar{s}-M_1^2-M_2^2+\lambda^{1/2}(\bar{s},M_1^2,M_2^2)}\right),\\
\mathrm{Im}\big[C_0(m^2,m^2,\bar{s};0,M,0)\big] &= \frac{\pi}{\bar{s}\beta}\left\{\theta(\bar{s})\,\ln\left(\frac{\bar{s}(1-\beta)-2(m^2-M^2)}{\bar{s}(1+\beta)-2(m^2-M^2)}\right)+\right.\\
&\qquad\left.+\,2\,\theta\big(m^2-M^2\big)\,\ln\left(\frac{m^2+M^2+\beta(m^2-M^2)}{m^2+M^2-\beta(m^2-M^2)}\right)\right\},\\
\mathrm{Im}\big[C_0(m^2,m^2,\bar{s};M_1,0,M_2)\big] &= \frac{\pi}{\bar{s}\beta}\left\{\theta\big(\bar{s}-(M_1+M_2)^2\big)\,\ln\left(\frac{\bar{s}-2m^2-M_1^2-M_2^2-\beta\,\lambda^{1/2}(\bar{s},M_1^2,M_2^2)}{\bar{s}-2m^2-M_1^2-M_2^2+\beta\,\lambda^{1/2}(\bar{s},M_1^2,M_2^2)}\right)+\right.\\
&\qquad+\,\theta\big(m^2-M_1^2\big)\,\ln\left(\frac{\bar{s}(1+\beta)(m^2-M_1^2)+2m^2(M_1^2-M_2^2)}{\bar{s}(1-\beta)(m^2-M_1^2)+2m^2(M_1^2-M_2^2)}\right)+\\
&\qquad\left.+\,\theta\big(m^2-M_2^2\big)\,\ln\left(\frac{\bar{s}(1+\beta)(m^2-M_2^2)+2m^2(M_2^2-M_1^2)}{\bar{s}(1-\beta)(m^2-M_2^2)+2m^2(M_2^2-M_1^2)}\right)\right\}\\
\mathrm{Im}\big[C_0(m^2,m^2,\bar{s};m,M,m)\big] &= \frac{\pi}{\bar{s}\beta}\,\theta\big(\bar{s}-4m^2\big)\,\ln\left(\frac{M^2}{\bar{s}\beta^2+M^2}\right),\\
\mathrm{Im}\big[C_0(m^2,m^2,\bar{s};M_1,m,M_2)\big] &= \frac{\pi}{\bar{s}\beta}\,\theta\big(\bar{s}-(M_1+M_2)^2\big)\,\ln\left(\frac{\bar{s}-M_1^2-M_2^2-\beta\,\lambda^{1/2}(\bar{s},M_1^2,M_2^2)}{\bar{s}-M_1^2-M_2^2+\beta\,\lambda^{1/2}(\bar{s},M_1^2,M_2^2)}\right).
\end{aligned}
\tag{C.39}
$$

C.2.2 4-point functions

The imaginary parts of 4-point functions are more involved than in the 3-point case, but also only consist of single logarithms. A major simplification (or rather compactification) of the results comes from the fact that the external invariants are symmetric ($p_1^2=p_2^2=0, p_3^2=p_4^2=m^2$) and that $m_1=0$ (virtual lepton propagator), which makes results reasonably compact to allow for presentation. Since we focus on weak contributions (and therefore do not treat the ZA-boxes), there are only 2 types of generic boxes necessary for the computation:

- Massive charged s-channel $D_0(0,0,m^2,m^2,\bar{s},\bar{u};M_1,0,M_2,0)$
- Massive neutral s-channel $D_0(0,0,m^2,m^2,\bar{s},\bar{u};M_1,0,M_2,m)$

[8]Some of the θ-functions involving $\bar{s}$ are redundant with this assumption, but we kept them explicit for completeness, as some of these imaginary parts are non-zero even below the threshold $\bar{s}=4m^2$. In these regimes one would need to analytically continue the quark velocity $\beta\to i\sqrt{\beta^2}$. Since this region is anyway not accessible kinematically, we do not go into further detail.

The various topologies (direct/crossed) are obtained by plugging in t/u for $\bar{u}$. Again defining auxillary functions (supressing kinematics and masses as arguments)

$$
\begin{aligned}
h_c(M_1, M_2) &= \lambda\big(-\bar{s}\bar{u}, (m^2-\bar{u})M_1^2, (m^2-\bar{u})M_2^2\big) - 4\bar{s}\bar{u}M_1^2M_2^2, \\
h_n(M_1, M_2) &= (m^2-\bar{u})^2\lambda\big(\bar{s}, M_1^2, M_2^2\big) - 4\bar{s}\bar{u}M_1^2M_2^2, \\
f_c^{\pm}(M_1, M_2) &= (m^2-\bar{u})\,\lambda\big(\bar{s}, M_1^2, M_2^2\big) - \bar{s}\big(m^2[\bar{s}-(M_1^2+M_2^2)] - 2M_1^2M_2^2\big) + \\
&\qquad \pm\sqrt{\lambda(\bar{s}, M_1^2, M_2^2)\,h_c(M_1, M_2)}, \\
g_c^{\pm}(M_1, M_2) &= \bar{s}\,\bar{u}(m^2-M_1^2) + (M_1^2-M_2^2)\big(-m^2(m^2-M_1^2) + \bar{u}(m^2+M_1^2)\big) + \\
&\qquad \pm(m^2-M_1^2)\sqrt{h_c(M_1, M_2)}, \\
f_n^{\pm}(M_1, M_2) &= (m^2-\bar{u})\,\lambda\big(\bar{s}, M_1^2, M_2^2\big) + 2\bar{s}M_1^2M_2^2 \pm \sqrt{\lambda(\bar{s}, M_1^2, M_2^2)\,h_n(M_1, M_2)},
\end{aligned}
\tag{C.40}
$$

we obtain for the imaginary part of the charged and neutral box

$$
\begin{aligned}
&\mathrm{Im}\big[D_0(0,0,m^2,m^2,\bar{s},\bar{u};M_1,0,M_2,0)\big] = \\
&= \frac{\pi}{\sqrt{h_c(M_1, M_2)}}\Bigg\{\theta\big(\bar{s}-\big(M_1+M_2\big)^2\big)\left[\ln\left(\frac{f_c^+(M_1, M_2)}{f_c^-(M_1, M_2)}\right) - \tilde{\eta}\big(a_{c,0}, b_{c,0}, c_{c,0}\big)\right] + \\
&\qquad + \theta\big(m^2-M_2^2\big)\left[\ln\left(\frac{g_c^+(M_2, M_1)}{g_c^-(M_2, M_1)}\right) - \tilde{\eta}\big(a_{c,1}, b_{c,1}, c_{c,1}\big)\right] + \\
&\qquad + \theta\big(m^2-M_1^2\big)\left[\ln\left(\frac{g_c^+(M_1, M_2)}{g_c^-(M_1, M_2)}\right) - \tilde{\eta}\big(a_{c,2}, b_{c,2}, c_{c,2}\big)\right]\Bigg\},
\end{aligned}
\tag{C.41}
$$

$$
\begin{aligned}
&\mathrm{Im}\big[D_0(0,0,m^2,m^2,\bar{s},\bar{u};M_1,0,M_2,m)\big] = \\
&= \frac{\pi}{\sqrt{h_n(M_1, M_2)}}\Bigg\{\theta\big(\bar{s}-\big(M_1+M_2\big)^2\big)\left[\ln\left(\frac{f_n^+(M_1, M_2)}{f_n^-(M_1, M_2)}\right) - \tilde{\eta}\big(a_n, b_n, c_n\big)\right]\Bigg\}.
\end{aligned}
\tag{C.42}
$$

The arguments of the η-functions are somewhat involved expressions, and are given below for completeness. Only if one (or both) of the ξ_i get large enough are the additional pieces of $2\pi i$ necessary, while in Feynman-gauge (and in properly combined gauge-independent sets) they are absent. We emphasize once again that the expressions given above are only valid above the physical thresholds, i.e. for $\bar{s} > (M_1+M_2)^2$ etc. The proper treatment of the unphysical regions is tricky and beyond the scope of this work.

$$
\begin{aligned}
a_{c,0} &= m^4 + \frac{\bar{u}}{\bar{s}}\,\lambda\big(\bar{s}, M_1^2, M_2^2\big), \\
a_{c,1} &= -\frac{1}{m^2}\Big\{(m^2-\bar{u}-M_1^2)\big(M_2^2(\bar{s}+\bar{u}) - m^2[\bar{s}-(M_1^2-M_2^2)]\big)\Big\}, \\
a_{c,2} &= -\frac{1}{m^2}\Big\{\big(M_1^2(\bar{s}+\bar{u}) - m^2[\bar{s}+M_1^2-M_2^2]\big)\big(m^2-\bar{u}-M_2^2\big)\Big\}, \\
b_{c,0} &= \frac{1}{\bar{s}}\Big\{\bar{s}m^2\big(\bar{s}-2m^2-M_1^2-M_2^2\big) - (m^2+\bar{u})\,\lambda\big(\bar{s}, M_1^2, M_2^2\big)\Big\}, \\
b_{c,1} &= \frac{1}{m^2}\Big\{m^4(M_1^2-M_2^2) - \bar{u}M_2^2\big(\bar{s}+2\bar{u}+M_1^2+M_2^2\big) + m^2\big(\bar{s}\bar{u} - \bar{u}(M_1^2-3M_2^2) - (M_1^2-M_2^2)M_2^2\big)\Big\},
\end{aligned}
$$

$$
\begin{aligned}
b_{c,2} &= \frac{1}{m^2}\Big\{m^4\big(-2\bar{s}-(M_1^2-M_2^2)\big)+M_1^2\big(\bar{u}(M_1^2-M_2^2)-\bar{s}(\bar{u}+2M_2^2)\big)+\\
&\qquad +m^2\big([\bar{u}-(M_1^2-2M_2^2)](M_1^2-M_2^2)+\bar{s}[\bar{u}+2(M_1^2+M_2^2)]\big)\Big\},\\
c_{c,0} &= \frac{1}{4\bar{s}}\Big\{\bar{s}\big(\bar{s}-2m^2-(M_1^2+M_2^2)\big)^2-(\bar{s}-4m^2)\,\lambda\big(\bar{s},M_1^2,M_2^2\big)\Big\},\\
c_{c,1} &= -\frac{\bar{u}M_2^2}{m^2}\Big\{m^2-\bar{u}-M_2^2\Big\},\\
c_{c,2} &= \frac{1}{m^2}\Big\{\bar{s}\big(m^4+M_1^2M_2^2\big)+m^2M^2\big((M_1^2-M_2^2)^2-\bar{s}(M_1^2+M_2^2)\big)\Big\},\\
a_n &= \frac{\bar{u}}{\bar{s}}\,\lambda\big(\bar{s},M_1^2,M_2^2\big),\\
b_n &= -\frac{m^2+\bar{u}}{\bar{s}}\,\lambda\big(\bar{s},M_1^2,M_2^2\big),\\
c_n &= \frac{1}{4\bar{s}}\,\Big\{\bar{s}\big(\bar{s}-(M_1^2+M_2^2)\big)^2-(\bar{s}-4m^2)\,\lambda\big(\bar{s},M_1^2,M_2^2\big)\Big\}.
\end{aligned}
\tag{C.43}
$$

Appendix D

Projection operators

The treatment of Feynman diagrams is tremendously simplified by deconstructing them according to their Lorentz and Dirac structure. The scalar coefficient functions depend on the internal masses, gauge parameters as well as external invariants, and can be projected out by contraction and taking Dirac traces with projection operators. In the following we give those necessary for the diagrams that we encounter in this work. $\mu, \nu \in \{0, 1, 2, 3\}$ will denote Lorentz indices, $\rho, \sigma, \kappa, \lambda = \pm$ will denote chirality indices.

D.1 Bosonic 2-point function

A Lorentz tensor $\mathcal{T}$ of rank-2 that is built out of the metric and one four-vector p^μ (like the bosonic 2-point function) has the generic decomposition into transverse and longitudinal parts

$$\mathcal{T}_{\mu\nu} = \left(g_{\mu\nu} - \frac{p_\mu p_\nu}{p^2}\right) T^T(p^2) + \frac{p_\mu p_\nu}{p^2} T^L(p^2) \tag{D.1}$$

The scalar functions $T^X(p^2)$ (where $X \in \{T, L\}$) can be extracted by contracting with projection operators $\mathcal{O}^{\mu\nu}$

$$\mathcal{O}_{\mu\nu}(T^X) = \left(g_{\mu\nu} - \frac{p_\mu p_\nu}{p^2}\right) \mathcal{P}_T(T^X) + \frac{p_\mu p_\nu}{p^2} \mathcal{P}_L(T^X), \tag{D.2}$$

$$T^X(p^2) = \mathcal{T}^{\mu\nu}\mathcal{O}_{\mu\nu}(T^X), \tag{D.3}$$

where

$$\left\{\mathcal{P}_T(T^T), \mathcal{P}_L(T^T)\right\} = \left\{\frac{1}{d-1}, 0\right\}, \tag{D.4}$$

$$\left\{\mathcal{P}_T(T^L), \mathcal{P}_L(T^L)\right\} = \{0, 1\}\,. \tag{D.5}$$

D.2 Fermionic 2-point function

The fermionic 2-point function allows for a decomposition in terms of 4 Dirac structures: 2 vector structures with $\not{p}$ and 2 scalar structures and 2 scalar structures (these are absent for vanishing fermion mass)[1],

$$\Sigma(\not{p}) = \not{p} \sum_{\rho=\pm} \omega_\rho A_\rho(p^2) + m \sum_{\rho=\pm} \omega_\rho B_\rho(p^2). \tag{D.6}$$

m is inserted for convenience, to keep the scalar functions dimensionless, and it does not necessarily need to be the fermion mass (although it mostly is chosen that way). The projection operators are now also

[1] In the SM we always have $B_+ = B_-$, which is equivalent to the absence of $m\,\gamma_5$ terms.

matrices in Dirac space, and projection of the scalar functions A_ρ, B_ρ is done by taking the Dirac trace with the projection operators $\mathcal{O}$ of the form ($f_\sigma \in \{A_\sigma, B_\sigma\}$)

$$\mathcal{O}(f_\sigma) = \not{p} \sum_{\rho=\pm} \omega_\rho \mathcal{A}_\rho(f_\sigma) + m \sum_{\rho=\pm} \omega_\rho \mathcal{B}_\rho(f_\sigma) \tag{D.7}$$

i.e. summing over spins and using the completeness relation eq. (A.10),

$$f_\sigma = \mathrm{Tr}\left[\Sigma(\not{p})\left(\not{p}+m\right)\mathcal{O}(f_\sigma)\right]. \tag{D.8}$$

For the coefficients $\mathcal{A}(f_\sigma)$ and $\mathcal{B}(f_\sigma)$ we find

$$\begin{aligned}
\Big\{\mathcal{A}_\rho(A_\sigma), \mathcal{B}(A_\sigma)\Big\} &= \left\{-\frac{m}{2p^2(p^2-m^2)}\,\delta_{-\rho,\sigma}, \frac{m}{2m^2(p^2-m^2)}\,\delta_{-\rho,\sigma}\right\}, \\
\Big\{\mathcal{A}_\rho(B_\sigma), \mathcal{B}(B_\sigma)\Big\} &= \left\{\frac{m}{2m^2(p^2-m^2)}\,\delta_{\rho,\sigma}, -\frac{m}{2m^2(p^2-m^2)}\,\delta_{\rho,\sigma}\right\}.
\end{aligned} \tag{D.9}$$

D.3 Amputated gauge-fermion-fermion 3-point vertex

For the pair-production of fermions (mass m and outgoing on-shell four-vectors p_1, p_2 with $p_1^2 = p_2^2 = m^2$) by an off-shell gauge boson of virtuality $s = (p_1+p_2)^2$ the amputated vertex function $\bar{u}(p_1)\Gamma^\mu(q^2)v(p_2)$ can be parametrized by 6 structures and respective scalar functions (usually referred to as *form factors*) due to Lorentz covariance and on-shellness of the fermions. The chiral form reads

$$\bar{u}(p_1)\Gamma^\mu(q^2)v(p_2) = \bar{u}(p_1)\Big\{\gamma^\mu \sum_{\rho=\pm} \omega_\rho\, F_1^\rho(q^2) + \frac{p^\mu}{m} \sum_{\rho=\pm} \omega_\rho\, F_2^\rho(q^2) + \frac{q^\mu}{m} \sum_{\rho=\pm} \omega_\rho\, F_3^\rho(q^2)\Big\}v(p_2), \tag{D.10}$$

where $p = p_1 - p_2$ and $q = p_1 + p_2$. Spin indices on the spinors are implicit. The projection operators have the form,

$$\bar{v}(p_2)\mathcal{O}_\mu(F_i^\sigma)u(p_2) = \bar{v}(p_2)\Big\{\gamma_\mu \sum_{\rho=\pm} \omega_\rho\, \mathcal{C}_1^\rho(F_i^\sigma) + \frac{p_\mu}{m} \sum_{\rho=\pm} \omega_\rho\, \mathcal{C}_2^\rho(F_i^\sigma) + \frac{q_\mu}{m} \sum_{\rho=\pm} \omega_\rho\, \mathcal{C}_3^\rho(F_i^\sigma)\Big\}u(p_1), \tag{D.11}$$

and the form factors $F_i^\sigma(q^2)$ can be extracted by again summing over spins, turning the contraction into the following trace by using the completeness relations eq. (A.10),

$$F_i^\sigma(q^2) = \mathrm{Tr}\left[(\not{p}_1+m)\Gamma^\mu(\not{p}_2-m)\mathcal{O}_\mu(F_i^\sigma)\right]. \tag{D.12}$$

We get

$$\begin{aligned}
\Big\{\mathcal{C}_1^\rho(F_1^\sigma), \mathcal{C}_2^\rho(F_1^\sigma), \mathcal{C}_3^\rho(F_1^\sigma)\Big\} &= \frac{m^2}{(d-2)s(s-4m^2)}\left\{2-\frac{s}{m^2}\,\delta^{\rho,\sigma}, -1, 1-2\delta^{\rho,\sigma}\right\}, \\
\Big\{\mathcal{C}_1^\rho(F_2^\sigma), \mathcal{C}_2^\rho(F_2^\sigma), \mathcal{C}_3^\rho(F_2^\sigma)\Big\} &= \frac{m^2}{(d-2)s(s-4m^2)}\left\{-1, -\frac{2(d-1)m^2}{s-4m^2}\,\delta^{\rho,\sigma} + \frac{2(d-3)m^2-(d-2)s}{s-4m^2}\,\delta^{-\rho,\sigma}, 0\right\}, \\
\Big\{\mathcal{C}_3^\rho(F_3^\sigma), \mathcal{C}_2^\rho(F_3^\sigma), \mathcal{C}_3^\rho(F_3^\sigma)\Big\} &= \frac{m^2}{(d-2)s(s-4m^2)}\Bigg\{-1+2\delta^{\rho,\sigma}, 0, \\
&\qquad \frac{2(d-1)m^2}{s}\,\delta^{\rho,\sigma} - \frac{2(d-1)m^2-(d-2)s}{s}\,\delta^{-\rho,\sigma}\Bigg\}.
\end{aligned} \tag{D.13}$$

In the massless case the vertex consists only of structures $\sim \gamma^\mu\omega_\rho$,

$$\bar{v}(l_2)\Lambda^\mu(q^2)u(l_1) = \bar{v}(l_2)\Big\{\gamma^\mu \sum_{\rho=\pm} \omega_\rho\, f_1^\rho(q^2)\Big\}u(l_1), \tag{D.14}$$

where $q = l_1 + l_2$. Therefore also the projection operator ansatz

$$\bar{u}(l_1)\mathcal{O}_\mu(f_i^\sigma)v(l_2) = \bar{u}(l_1)\Big\{\gamma_\mu \sum_{\rho=\pm} \omega_\rho \, \mathcal{C}_1^\rho(f_i^\sigma)\Big\}v(l_2), \tag{D.15}$$

and the trace

$$f_i^\sigma(q^2) = \mathrm{Tr}\left[\not{l}_2 \Lambda^\mu \not{l}_1 \mathcal{O}_\mu(f_i^\sigma)\right]. \tag{D.16}$$

simplify, and we get (by a limiting process from eq. D.13)

$$\mathcal{C}_1^\rho(f_1^\sigma) = \frac{-\delta^{\rho,\sigma}}{(d-2)s}. \tag{D.17}$$

D.4 Four-fermion s-channel boxes

Matrix element contributions from four-fermion box diagrams can be decomposed in terms of form factors F_i multiplying *chirality amplitudes* M_i (products of spinor sandwiches, so called *fermion chains*, of final and initial state),

$$\mathcal{M}_{\mathrm{box}} = \sum_i \sum_{\rho,\kappa=\pm} F_i^{\rho\kappa} M_i^{\rho\kappa} \tag{D.18}$$

For generic massive external particles, the number of structures is quite large. In our case the massless initial state simplifies things greatly, so that the decomposition reduces to just 2 chirality amplitudes

$$\begin{aligned}
\mathcal{M}_{\mathrm{box}} &= \sum_{\rho,\kappa=\pm} \Big\{F_1^{\rho\kappa}\, \bar{u}_t(p_1)\gamma^\mu\omega_\rho v_t(p_2)\, \bar{v}_e(l_2)\gamma_\mu\omega_\kappa u_e(l_1) + F_2^{\rho\kappa}\, \bar{u}_t(p_1)\omega_\rho v_t(p_2)\, \bar{v}_e(l_2)\frac{\not{p}}{m}\,\omega_\kappa u_e(l_1)\Big\} = \\
&= \sum_{\rho,\kappa=\pm} \Big\{F_1^{\rho\kappa}\bar{M}_1^{\rho\kappa} + F_2^{\rho\kappa}\bar{M}_2^{\rho\kappa}\Big\},
\end{aligned} \tag{D.19}$$

where we denote this minimal-basis amplitudes defined in eq. (3.8) by a bar on top and the subscript t denotes a massive fermion (top) with mass m, while e represents a massless fermion (electron). The external kinematics are

$$\begin{aligned}
p_1^2 = p_2^2 = m^2, &\quad l_1^2 = l_2^2 = 0, \\
s &= (p_1+p_2)^2 = (l_1+l_2)^2, \\
t &= (p_1-l_1)^2 = (p_2-l_2)^2, \\
u &= (p_1+l_2)^2 = (p_2-l_1)^2.
\end{aligned} \tag{D.20}$$

It is now possible to construct a set of "projection operators" that allow to reduce the box integral representation to the form of eq. D.19. The ansatz reads

$$\begin{aligned}
&\mathcal{O}(F_i^{\rho\kappa}) = \\
&= \sum_{\sigma,\lambda=\pm 1} \Big\{\mathcal{C}_1^{\sigma\lambda}(F_i^{\rho\kappa})\, \bar{v}_t(p_2)\, \gamma^\mu\omega_\sigma u_t(p_1)\, \bar{u}_e(l_1)\, \gamma_\mu\omega_\lambda v_e(l_2) + \mathcal{C}_2^{\sigma\lambda}(F_i^{\rho\kappa})\, \bar{v}_t(p_2)\, \omega_\sigma u_t(p_1)\, \bar{u}_e(l_1)\, \frac{\not{p}}{m}\, \omega_\lambda v_e(l_2)\Big\} \equiv \\
&\equiv \sum_{\sigma,\lambda=\pm} \Big\{\mathcal{C}_1^{\sigma\lambda}(F_i^{\rho\kappa})\, (\bar{M}^\dagger)_1^{\rho\kappa} + \mathcal{C}_2^{\sigma\lambda}(F_i^{\rho\kappa})\, (\bar{M}^\dagger)_2^{\rho\kappa}\Big\},
\end{aligned} \tag{D.21}$$

where the coefficients $\mathcal{C}_k^{\sigma\lambda}$ depend on the form factor $F_i^{\rho\kappa}$ that will be projected out. Note that we made a slight abuse of notation here as $\left(\bar{M}_2^{\sigma\lambda}\right)^\dagger = (\bar{M}^\dagger)_2^{(-\sigma)\lambda}$. The results for the other notation can be achieved easily by replacing $\sigma \to -\sigma$ at the appropriate spots in $\mathcal{C}_2^{\sigma\lambda}$ in the equations below. As some amplitude can now be factored (at least formally) into initial- and final-state fermion chains,

$$\mathcal{M} = \sum_n \sum_{\sigma,\lambda=\pm} G_n^{\sigma\lambda}\, \bar{u}_t(p_1)\Gamma_n^\sigma v_t(p_2)\, \bar{v}_e(l_2)\Lambda_n^\lambda u_e(l_1), \tag{D.22}$$

and similarly for the chirality amplitudes $(\bar{M}^\dagger)_n^{\sigma\lambda}$,

$$(\bar{M}^\dagger)_n^{\sigma\lambda} \equiv \bar{v}_t(p_2)(\Gamma_M^\dagger)_n^\sigma u_t(p_1)\,\bar{u}_e(l_1)(\Lambda_M^\dagger)_n^\lambda v_e(l_2) \tag{D.23}$$

a generic product of Dirac bilinears of this type can be reduced to form factor representation by

$$\begin{aligned} F_i^{\rho,\kappa} &= \sum_{\text{spins}} \mathcal{M}\,\mathcal{O}(F_i^{\rho\kappa}) = \\ &= \sum_{n',n''}\sum_{\sigma',\lambda'}\sum_{\sigma'',\lambda''} G_{n'}^{\sigma'\lambda'}\mathcal{C}_{n''}^{\sigma''\lambda''}(F_i^{\rho\kappa})\ \mathrm{Tr}\left[(\not{p}_1+m)\Gamma_{n'}^{\sigma'}(\not{p}_2-m)(\Gamma_M^\dagger)_{n''}^{\sigma''}\right]\mathrm{Tr}\left[\not{l}_2\,\Lambda_{n'}^{\lambda'}\,\not{l}_1\,(\Lambda_M^\dagger)_{n''}^{\lambda''}\right]. \end{aligned} \tag{D.24}$$

It is emphasized that the brute-force reduction only yields a decomposition into a basis M_i that is larger (see calculation of Feynman gauge, sec. 3.6), but the reduction to the minimal basis $\bar{M}_i$ eq. D.19 is very convenient in that it allows to make contact with 2- and 3-point contributions to the 1-loop amplitude and to check for gauge parameter cancellations. This procedure is not really a projection as the spinor sandwiches are completely contracted (they give a number), but rather an effective replacement that gives the same results when spin-summed against the chirality amplitudes in the minimal basis $\bar{M}_i$. Taking the spin sums of eqs. D.19 and D.21 results in a system of equations. Solving for the coefficients yields

$$\begin{aligned} \mathcal{C}_1^{\sigma\lambda}(F_1^{\rho\kappa}) &= \frac{\delta^{\kappa,\lambda}}{4s(m^4-t\,u)^2}\Big\{m^2(2m^4-t^2-u^2)\delta^{-\rho,\sigma}+ \\ &\quad + \Big[\big(m^4(3t-u)-t^2(t+u)\big)\,\delta^{\rho,\kappa}+\big(m^4(3u-t)-u^2(t+u)\big)\,\delta^{-\rho,\kappa}\Big]\delta^{\rho,\sigma}\Big\}, \\ \mathcal{C}_2^{\sigma\lambda}(F_1^{\rho\kappa}) &= \frac{\delta^{\kappa,\lambda}\,m^2}{4s(m^4-t\,u)^2}\Big\{\Big[t^2-m^2(t-u)-m^4\Big]\delta^{\rho,\kappa}+\Big[u^2-m^2(u-t)-m^4\Big]\delta^{-\rho,\kappa}\Big\}, \\ \mathcal{C}_1^{\sigma\lambda}(F_2^{\rho\kappa}) &= \frac{\delta^{\kappa,\lambda}\,m^2}{4s(m^4-t\,u)^2}\Big\{\Big[t^2-m^2(t-u)-m^4\Big]\big(\delta^{\rho,\sigma}\delta^{\rho,\kappa}+\delta^{-\rho,\sigma}\delta^{-\rho,\kappa}\big)+ \\ &\quad + \Big[u^2-m^2(u-t)-m^4\Big]\big(\delta^{-\rho,\sigma}\delta^{\rho,\kappa}+\delta^{\rho,\sigma}\delta^{-\rho,\kappa}\big)\Big\}, \\ \mathcal{C}_2^{\sigma\lambda}(F_2^{\rho\kappa}) &= \frac{\delta^{\kappa,\lambda}\,m^2}{4s(m^4-t\,u)^2}\Big\{m^2 s\;\delta^{\rho,\sigma}+(t-m^2)(u-m^2)\,\delta^{-\rho,\sigma}\Big\}. \end{aligned} \tag{D.25}$$

Appendix E

Generic diagrams

E.1 Fermionic self-energy diagrams

For the convention used for the couplings see section G.1. The mass content of the virtual particles determines the corresponding gauge parameter ξ_i. Concerning notation we quote the scalar functions $\mathcal{A}$ and $\mathcal{B}$ according to the convention

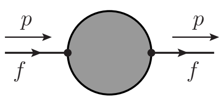

$$= \frac{i\alpha}{4\pi}\,\bar{u}(p,m)\left\{\not{p}\sum_{\eta=\pm}\mathcal{A}^{\eta}\,\omega_\eta + m\sum_{\eta=\pm}\mathcal{B}^{\eta}\,\omega_\eta\right\}u(p,m). \tag{E.1}$$

We did not drop the the spinors only to show the external particle's mass. If the particle is massless, there are no functions $\mathcal{B}$ to determine. For the vector diagarms we split the scalar functions $\mathcal{A},\mathcal{B}$ into Feynman gauge ($\xi = 1$) and additional pieces

$$\begin{aligned}\mathcal{A}^{\eta} &= A^{\eta,\xi=1} + \Delta\mathcal{A}^{\eta,\xi},\\ \mathcal{B}^{\eta} &= B^{\eta,\xi=1} + \Delta\mathcal{B}^{\eta,\xi}.\end{aligned} \tag{E.2}$$

E.1.1 Scalar (fS)

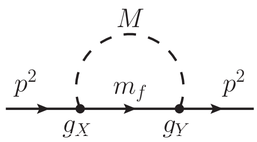

$$\mathcal{A}^{\eta}_{fS} = \frac{g_X^{-\eta}g_Y^{\eta}}{2p^2}\Big\{\left(p^2+m_f^2-M^2\right)B_0\left(p^2;M,m_f\right)+A_0(M)-A_0(m_f)\Big\}, \tag{E.3}$$

$$\mathcal{B}^{\eta}_{fS} = g_X^{\eta}g_Y^{\eta}\frac{m_f}{m}\,B_0\left(p^2;M,m_f\right). \tag{E.4}$$

E.1.2 Vector (fV)

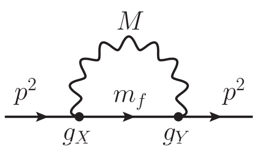

$$\mathcal{A}^{\eta,\xi=1}_{fV} = \frac{g_X^{\eta}g_Y^{\eta}}{p^2}\Big\{p^2+A_0(m_f)-A_0(M)-\left(p^2+m_f^2-M^2\right)B_0\left(p^2;M,m_f\right)\Big\}, \tag{E.5}$$

$$\mathcal{B}^{\eta,\xi=1}_{fV} = 2g_X^{-\eta}g_Y^{\eta}\frac{m_f}{m}\Big\{-1+2\,B_0\left(p^2;M,m_f\right)\Big\}, \tag{E.6}$$

$$\Delta\mathcal{A}^{\eta;\xi}_{fV} = \frac{g^{\eta}_{X} g^{\eta}_{Y}}{2p^2 M^2}\Big\{(p^2 - m_f^2)\Big[A_0\left(M\right) - A_0\left(M\sqrt{\xi}\right)\Big] +$$
$$- \Big[(p^2 - m_f^2)^2 - (p^2 + m_f^2)M^2\Big] B_0\left(p^2; M, m_f\right) +$$
$$+ \Big[(p^2 - m_f^2)^2 - (p^2 + m_f^2)M^2\xi\Big] B_0\left(p^2; M\sqrt{\xi}, m_f\right)\Big\}, \tag{E.7}$$

$$\Delta\mathcal{B}^{\eta;\xi}_{fV} = g^{-\eta}_{X} g^{\eta}_{Y} \frac{m_f}{m}\Big\{\xi\, B_0\left(p^2; M\sqrt{\xi}, m_f\right) - B_0\left(p^2; M, m_f\right)\Big\} \tag{E.8}$$

E.2 Bosonic self-energy diagrams

For the convention used for the couplings see section G.1. The mass content of the virtual particles determines the corresponding gauge parameter ξ_i. For identical particles in the loops the corresponding symmetry factors S have to be applied to the expressions below (we set the symmetry factor of each topology to 1). Concerning notation we quote the scalar functions G^T, G^L and H according to the convention

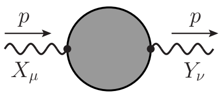

$$= \frac{i\alpha}{4\pi}\,\mathcal{S}\left\{\left(g_{\mu\nu} - \frac{p_\mu p_\nu}{p^2}\right) G^T + \frac{p_\mu p_\nu}{p^2}\, G^L\right\}, \tag{E.9}$$

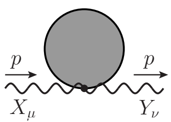

$$= \frac{i\alpha}{4\pi}\,\mathcal{S}\; g_{\mu\nu} H, \tag{E.10}$$

$\mathcal{S}$ is the symmetry factor of the diagram. In contrast to the other sections, we do not split the expressions into Feynman-gauge + rest, as there might be different gauge parameters in the loop. Feynman gauge results are obtained straightforwardly. We also do not fully scalarize the results, as then the limiting process $p^2 \to 0$ might not be taken easily. With the results given below, this limiting procedure can be carried out by applying the results of sec. B for the PV-tensor-coeffcients.

Despite not treating pure-QED contributions, there are QED-diagrams appearing in the WW-transition, which demands evaluating some expressions with one virtual mass vanishing. Revisiting the massive results, it is clear that the reduction still works perfectly fine if the massless particle is a fermion, scalar or ghost. The massless diagrams are obtained by simply setting the corresponding masses to 0 in the massive results. The vector propagator on the other hand differs in the massless case (cf. app. G.1). The double pole for the longitudinal part requires PV-decomposition in terms of higher-weight PV-coefficients. For this reason below we also give separate results for diagrams with one massless internal vector particle (ξ_A denotes the gauge fixing parameter of the massless field)[1].

E.2.1 Massive vector-vector (VV)

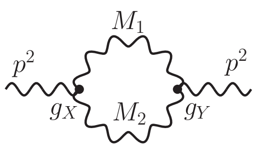

$$\frac{1}{g_X g_Y}\, G^T_{VV}(p^2; M_1, M_2) =$$

[1]For our purposes we do not need diagrams with 2 internal massless gauge bosons, so we omit the presentation here. The scalar functions can be obtained by applying the projection operators of sec. D

$$
\begin{aligned}
&= \frac{-3M_1^2\left(\xi_1^2+15\right)-4M_2^2\left(\xi_2^2+11\right)+16(3\xi_1-2)p^2}{24}+ \\
&- \frac{3}{4}\,A_0(M_1)+\left(\frac{p^2-M_1^2}{M_2^2}-\xi_1+\frac{4}{3}\right)A_0(M_2)+ \\
&+\left(-\frac{p^2-M_1^2}{M_2^2}+\frac{2\xi_2}{3}\right)A_0\left(M_2\sqrt{\xi_2}\right)+\frac{7}{4}\,\xi_1\,A_0\left(M_1\sqrt{\xi_1}\right)+ \\
&+\frac{1}{3M_2^2}\left[A_{00}\left(M_2\sqrt{\xi_2}\right)-A_{00}(M_2)\right]-\frac{\lambda(p^2,M_1^2,M_2^2)}{M_2^2}\,B_0\left(p^2,M_1,M_2\right)+ \\
&+\xi_1\left(-M_1^2\xi_1+2M_2^2+2p^2\right)B_0\left(p^2;M_1\sqrt{\xi_1},M_2\right)+\frac{\left(p^2-M_1^2\right)^2}{M_2^2}\,B_0\left(p^2;M_1,M_2\sqrt{\xi_2}\right)+ \\
&+\frac{\lambda\left(p^2,M_1^2,M_2^2\right)+12\left(p^2+M_1^2\right)M_2^2}{M_1^2M_2^2}\,B_{00}\left(p^2;M_1,M_2\right)+\frac{p^4}{M_1^2M_2^2}\,B_{00}\left(p^2;M_1\sqrt{\xi_1},M_2\sqrt{\xi_2}\right)+ \\
&-\frac{M_2^4+10M_2^2p^2+p^4}{M_1^2M_2^2}\,B_{00}\left(p^2;M_1\sqrt{\xi_1},M_2\right)-\frac{\left(p^2-M_1^2\right)^2}{M_1^2M_2^2}\,B_{00}\left(p^2;M_1,M_2\sqrt{\xi_2}\right),
\end{aligned}
\tag{E.11}
$$

$$
\begin{aligned}
&\frac{1}{g_Xg_Y}\,G^L_{VV}(p^2;M_1,M_2)= \\
&\quad= \frac{-3\left(M_1^2\left(\xi_1^2+4\xi_2-29\right)+4M_2^2(\xi_1-7)\right)-40p^2}{24}+ \\
&\quad+\frac{21}{4}\,A_0(M_1)+5A_0(M_2)+\frac{3\xi_1}{4}\,A_0\left(M_1\sqrt{\xi_1}\right)+\xi_2A_0\left(M_2\sqrt{\xi_2}\right)+ \\
&\quad+\frac{1}{M_2^2}\left[A_{00}(M_2)-A_{00}\left(M_2\sqrt{\xi_2}\right)\right]+\left(6\left(M_1^2+M_2^2\right)-3p^2\right)B_0\left(p^2;M_1,M_2\right) \\
&\quad-3\left(\frac{M_1^2}{M_2^2}+\frac{M_2^2}{M_1^2}+10\right)B_{00}\left(p^2;M_1,M_2\right)+ \\
&\quad+\frac{3M_2^2}{M_1^2}\,B_{00}\left(p^2;M_1\sqrt{\xi_1},M_2\right)+\frac{3M_1^2}{M_2^2}\,B_{00}\left(p^2;M_1,M_2\sqrt{\xi_2}\right)
\end{aligned}
\tag{E.12}
$$

E.2.2 Massless vector-vector (VA)

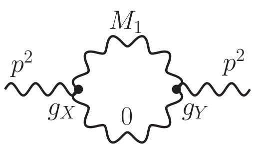

$$
\begin{aligned}
&\frac{1}{g_Xg_Y}\,G^T_{VA}(p^2;M)= \\
&\quad= \frac{8(3\xi-2)p^2-3M^2\left(3\xi^2+5\right)}{72}-\frac{1}{12}\left[A_0(M)-\xi\,A_0\left(M\sqrt{\xi}\right)\right]+ \\
&\quad+\frac{\xi\left(2M^2\xi+p^2\right)}{3}\,B_0\left(p^2;M\sqrt{\xi},0\right)+\frac{14\left(M^2+p^2\right)}{3}\,B_0\left(p^2;M,0\right)+ \\
&\quad+\left(\frac{5p^4}{3M^2}+\frac{5M^2}{3}+2p^2\right)B_1\left(p^2;M,0\right)-\frac{5p^2\left(p^2-M^2\xi\right)}{3M^2}\,B_1\left(p^2;M\sqrt{\xi},0\right)+
\end{aligned}
$$

$$+\,(\xi_A-1)\left\{\left(p^2-M^2\right)^2 B_0^{\langle 1,2\rangle}\left(p^2;M,0\right)-\frac{\left(p^2-M^2\right)^2}{M^2}B_{00}^{\langle 1,2\rangle}\left(p^2;M,0\right)+\right.$$

$$\left.+\,\frac{p^4}{M^2}B_{00}^{\langle 1,2\rangle}\left(p^2;M\sqrt{\xi},0\right)\right\}, \tag{E.13}$$

$$\frac{1}{g_X g_Y}\,G^L_{VA}(p^2;M)=$$

$$=-\frac{M^2\left(\xi^2+15\right)}{8}+\frac{1}{4}\left[A_0(M)-\xi\,A_0\left(M\sqrt{\xi}\right)\right]+$$

$$+\left(M^2+2p^2\right)B_0\left(p^2;M,0\right)+\xi\left(M^2\xi+p^2\right)B_0\left(p^2;M\sqrt{\xi},0\right)+$$

$$+\,5\left(p^2-M^2\right)B_1\left(p^2;M,0\right)+2\,\xi p^2 B_1\left(p^2;M\sqrt{\xi},0\right)$$

$$+\,M^2(\xi_A-1)\left[-\frac{1}{2}+3B_{00}^{\langle 1,2\rangle}\left(p^2;M,0\right)\right], \tag{E.14}$$

E.2.3 Massive vector-scalar ($\boldsymbol{VS}$)

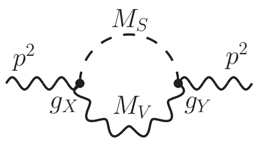

$$\frac{1}{g_X g_Y}\,G^T_{VS}(p^2;M_V,M_S)=$$

$$=-B_0\left(p^2;M_V,M_S\right)+\frac{1}{M_V^2}\left[B_{00}\left(p^2;M_V,M_S\right)-B_{00}\left(p^2;M_V\sqrt{\xi},M_S\right)\right], \tag{E.15}$$

$$\frac{1}{g_X g_Y}\,G^L_{VS}(p^2;M_V,M_S)=$$

$$=\frac{1-\xi}{2}-\xi B_0\left(p^2;M_V\sqrt{\xi},M_S\right)-\frac{3}{M_V^2}\left[B_{00}\left(p^2;M_V,M_S\right)-B_{00}\left(p^2;M_V\sqrt{\xi},M_S\right)\right]. \tag{E.16}$$

E.2.4 Massless vector-scalar ($\boldsymbol{SA}$)

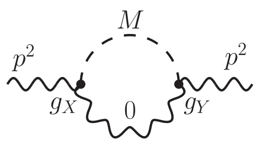

$$\frac{1}{g_X g_Y}\,G^T_{SA}(p^2;M)=-B_0\left(p^2;M_S,0\right)-(\xi_A-1)B_{00}^{\langle 1,2\rangle}\left(p^2;M,0\right), \tag{E.17}$$

$$\frac{1}{g_X g_Y}\,G^L_{SA}(p^2;M)=-B_0\left(p^2;M,0\right)-(\xi_A-1)\left\{\frac{1}{2}+\left(p^2+M^2\right)B_0^{\langle 1,2\rangle}\left(p^2;M,0\right)+\right.$$

$$\left.+\,2p^2B_1^{\langle 1,2\rangle}\left(p^2;M,0\right)-3\,B_{00}^{\langle 1,2\rangle}\left(p^2;M,0\right)\right\}. \tag{E.18}$$

E.2.5 Scalar-scalar (SS)

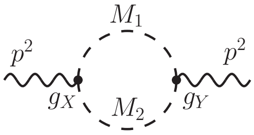

$$\frac{1}{g_X g_Y}\, G^T_{SS}(p^2; M_1, M_2) = 4B_{00}\left(p^2; M_1, M_2\right), \tag{E.19}$$

$$\frac{1}{g_X g_Y}\, G^L_{SS}(p^2; M_1, M_2) = 2A_0(M_2) + p^2 B_0\left(p^2; M_1, M_2\right) + 2\left(p^2 - M_1^2 + M_2^2\right) B_1\left(p^2; M_1, M_2\right). \tag{E.20}$$

E.2.6 Ghost-ghost (UU)

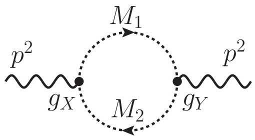

$$\frac{1}{g_X g_Y}\, G^T_{UU}(p^2; M_1, M_2) = -B_{00}\left(p^2; M_1, M_2\right), \tag{E.21}$$

$$\frac{1}{g_X g_Y}\, G^L_{UU}(p^2; M_1, M_2) = -\frac{1}{2}\left[A_0(M_2) + \left(p^2 - M_1^2 + M_2^2\right) B_1\left(p^2; M_1, M_2\right)\right]. \tag{E.22}$$

E.2.7 Fermions (ff)

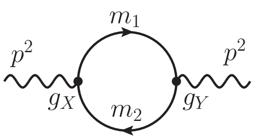

$$\begin{aligned} G^T_{ff}(p^2; m_1, m_2) &= \\ &= \sum_{\rho=\pm} \Bigg\{ -2\, g_X^{\rho} g_Y^{-\rho}\, m_1 m_2\, B_0\left(p^2; m_1, m_2\right) + \\ &\qquad + g_X^{\rho} g_Y^{\rho} \Big[2A_0(m_2) + 2m_1^2 B_0\left(p^2; m_1, m_2\right) + 2p^2 B_1\left(p^2; m_1, m_2\right) - 4B_{00}\left(p^2; m_1, m_2\right) \Big] \Bigg\}, \end{aligned} \tag{E.23}$$

$$\begin{aligned} G^L_{ff}(p^2; m_1, m_2) &= \\ &= \sum_{\rho=\pm} \Bigg\{ -2\, g_X^{\rho} g_Y^{-\rho}\, m_1 m_2\, B_0\left(p^2; m_1, m_2\right) + \\ &\qquad + g_X^{\rho} g_Y^{\rho} \Big[2m_1^2 B_0\left(p^2; m_1, m_2\right) + 2\left(m_1^2 - m_2^2\right) B_1\left(p^2; m_1, m_2\right) \Big] \Bigg\}. \end{aligned} \tag{E.24}$$

E.2.8 4-tadpoles

E.2.8.1 Vector (T_V)

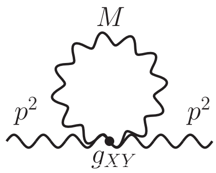

$$H_V(M) = \frac{g_{XY}}{3}\Big\{ - M^2\left(\xi^2 + 11\right) + 14\,A_0(M) + 4\xi A_0\left(M\sqrt{\xi}\right) - \frac{2}{M^2}\left[A_{00}(M) - A_{00}\left(M\sqrt{\xi}\right)\right]\Big\}. \tag{E.25}$$

E.2.8.2 Scalar (T_S)

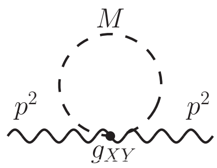

$$H_S(M) = -g_{XY}\,A_0(M). \tag{E.26}$$

E.3 Vertex diagrams

We encounter 2 diagram topologies in terms of fermion flow depicted schematically in fig. E.28. The first has the structure of a matrix element of a current $j^\mu_\rho = \bar{\psi}\gamma^\mu\omega_\rho\psi$, and we will call it *abelian* type. The second represents a *non-abelian* type. There are two types of abelian diagrams: scalar- and vector-exchange diagrams while the non-abelian class has 3, labelled by the virtual boson content: double-vector, scalar-vector and double-scalar diagrams. We furthermore have to distinguish between vertex diagrams with massive (final-state) and massless (initial-state) external fermions. Also, the W-diagrams of the final-state vertices have bottom quarks on internal lines (which we treat as massless), while Z-diagrams have virtual top quarks in the loop. These two cases also have to be treated separately (the naive limit $m_b \to 0$ cannot be taken anymore after the PV-tensor coefficients have been scalarized with the help of `Package-X`). We therefore also distinguish between *charged* and *neutral* diagrams with massless/massive virtual fermions respectively. In the initial-state case we only have the former case, as electrons are also treated as massless (neutrinos are by definition massless in the SM). To avoid confusion due to this nomenclature we provide schematic diagrams (drawn suggestively) where couplings and internal masses are indicated before each result.

The results are quoted in terms of (chiral) form factors obtained by applying the projection operators from sec. D. As usual we factor out ie of the various couplings g_i and (only here) also pull out a factor of $\frac{\alpha}{4\pi}$ of the form factors we quote. Specifically, we use the conventions

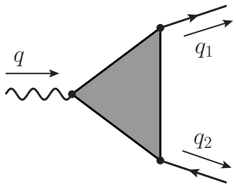

$$= ie\frac{\alpha}{4\pi}\,\bar{u}_t(q_1)\left[F_1^\rho\,\gamma^\mu\omega_\rho + F_2^\rho\,\frac{q_1^\mu - q_2^\mu}{m}\,\omega_\rho\right]v_t(q_2), \tag{E.27}$$

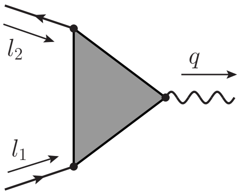

$$= ie\frac{\alpha}{4\pi}\,\bar{v}_e(l_2)\,[F_1^\kappa\,\gamma^\mu\omega_\kappa]\,u_e(l_1), \tag{E.28}$$

and similarly for the initial-state vertices. For diagrams with vector bosons we again split the results into Feynman-gauge $\xi = 1$ and additional gauge pieces,

$$F_i = F_i^{\xi=1} + \Delta F_i^{\xi}, \tag{E.29}$$

and give both parts separately.

E.3.1 Abelian vector

E.3.1.1 Charged massive $(ffV)_c$

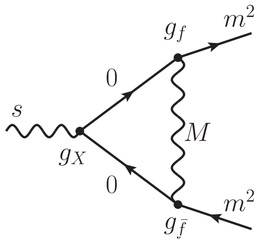

$$\begin{aligned}
F^{\rho,\xi=1}_{1,ffV} = g_X^\rho g_f^\rho g_{\bar{f}}^\rho \Bigg\{ &\frac{1}{\epsilon} + \ln\left(\frac{\mu^2}{M^2}\right) + \\
&+ \frac{1}{s-4m^2}\Bigg[-\left(-6m^2 + 2M^2 + 3s\right)\ln\left(\frac{M^2}{-s-i0^+}\right) + \\
&\qquad - \frac{2\left(m^2 - M^2\right)\left(5m^2 - M^2 - 2s\right)}{m^2}\ln\left(\frac{M^2}{M^2 - m^2 - i0^+}\right) + \\
&\qquad - 2\left(3m^4 - 4m^2\left(M^2+s\right) + \left(M^2+s\right)^2\right) C_0\left(m^2, m^2, s; 0, M, 0\right)\Bigg]\Bigg\} + \\
+ \frac{g_X^{-\rho} g_f^{-\rho} g_{\bar{f}}^{-\rho}}{s-4m^2}\Bigg\{ &4m^2 \ln\left(\frac{M^2}{-s-i0^+}\right) - 4\left(m^2 - M^2\right)\ln\left(\frac{M^2}{M^2-m^2-i0^+}\right) + \\
&- 2m^2\left(2m^2 - 2M^2 - s\right) C_0\left(m^2, m^2, s; 0, M, 0\right)\Bigg\},
\end{aligned} \tag{E.30}$$

$$\begin{aligned}
F^{\rho,\xi=1}_{2,ffV} = &\frac{g_X^\rho g_f^\rho g_{\bar{f}}^\rho + g_X^{-\rho} g_f^{-\rho} g_{\bar{f}}^{-\rho}}{\left(s-4m^2\right)^2} \times \\
\times \Bigg\{ &-\left(m^2 + M^2\right)\left(s - 4m^2\right) + m^2\left(14m^2 - 6M^2 - 5s\right)\ln\left(\frac{M^2}{-s-i0^+}\right) + \\
&- \frac{\left(m^2 - M^2\right)\left(14m^4 - 5m^2\left(2M^2 + s\right) + M^2 s\right)}{m^2}\ln\left(\frac{M^2}{M^2 - m^2 - i0^+}\right) +
\end{aligned}$$

$$
-2m^2\left(7m^4-5m^2\left(2M^2+s\right)+3M^4+4M^2s+s^2\right)C_0\left(m^2,m^2,s;0,M,0\right)\Bigg\}, \tag{E.31}
$$

$$
\begin{aligned}
\Delta F^{\rho;\xi}_{1,ffV} = g^{\rho}_X g^{\rho}_f g^{\rho}_{\bar{f}} \Bigg\{ & (\xi-1)\left(\frac{1}{\epsilon}+\ln\left(\frac{\mu^2}{M^2}\right)+2\right)+ \\
& +\frac{1}{s-4m^2}\Bigg[-\frac{2m^4-m^2\left(4M^2\xi+s\right)+M^2\xi s}{M^2}\ln(\xi)+ \\
& -\frac{\left(m^2-M^2\right)\left(2m^4-m^2\left(4M^2+s\right)+M^2s\right)}{m^2M^2}\ln\left(\frac{M^2}{M^2-m^2-i0^+}\right)+ \\
& +\frac{\left(m^2-M^2\xi\right)\left(2m^4-m^2\left(4M^2\xi+s\right)+M^2\xi s\right)}{m^2M^2}\ln\left(\frac{M^2\xi}{M^2\xi-m^2-i0^+}\right)+ \\
& -\frac{m^4\left(-2m^2+2M^2+s\right)}{M^2}C_0\left(m^2,m^2,s;0,M,0\right)+ \\
& -\frac{m^4\left(2m^2-2M^2\xi-s\right)}{M^2}C_0\left(m^2,m^2,s;0,M\sqrt{\xi},0\right)\Bigg]\Bigg\}+ \\
+\frac{g^{-\rho}_X g^{-\rho}_f g^{-\rho}_{\bar{f}}}{s-4m^2}\Bigg\{ & m^2(\xi-1)\log\left(\frac{M^2}{-s-i0^+}\right)-\frac{m^4-m^2M^2\xi}{M^2}\ln(\xi)+ \\
& -\frac{\left(m^2-M^2\right)^2}{M^2}\ln\left(\frac{M^2}{M^2-m^2-i0^+}\right)+ \\
& +\frac{\left(m^2-M^2\xi\right)^2}{M^2}\ln\left(\frac{M^2\xi}{M^2\xi-m^2-i0^+}\right)+ \\
& -\frac{m^2M^4-m^6}{M^2}C_0\left(m^2,m^2,s;0,M,0\right)+ \\
& -\frac{m^6-m^2M^4\xi^2}{M^2}C_0\left(m^2,m^2,s;0,M\sqrt{\xi},0\right)\Bigg\},
\end{aligned} \tag{E.32}
$$

$$
\begin{aligned}
\Delta F^{\rho;\xi}_{2,ffV} = & \frac{g^{\rho}_X g^{\rho}_f g^{\rho}_{\bar{f}}+g^{-\rho}_X g^{-\rho}_f g^{-\rho}_{\bar{f}}}{\left(s-4m^2\right)^2}\times \\
& \times\Bigg\{\frac{1}{2}m^2(\xi-1)\left(s-4m^2\right)+3m^4(\xi-1)\ln\left(\frac{M^2}{-s-i0^+}\right)+\frac{m^4\left(2m^2+6M^2\xi+s\right)}{2M^2}\ln(\xi)+ \\
& +\frac{\left(m^2-M^2\right)\left(2m^4+m^2\left(10M^2+s\right)-M^2s\right)}{2M^2}\ln\left(\frac{M^2}{M^2-m^2-i0^+}\right)+ \\
& -\frac{\left(m^2-M^2\xi\right)\left(2m^4+m^2\left(10M^2\xi+s\right)-M^2\xi s\right)}{2M^2}\ln\left(\frac{M^2\xi}{M^2\xi-m^2-i0^+}\right)+ \\
& +\frac{m^4\left(m^4+m^2\left(2M^2-s\right)-3M^4-2M^2s\right)}{M^2}C_0\left(m^2,m^2,s;0,M,0\right)+
\end{aligned}
$$

$$+\frac{m^4\left(-m^4+m^2\left(s-2M^2\xi\right)+M^2\xi\left(3M^2\xi+2s\right)\right)}{M^2}C_0\left(m^2,m^2,s;0,M\sqrt{\xi},0\right)\Bigg\} \tag{E.33}$$

E.3.1.2 Neutral massive $(ffV)_n$

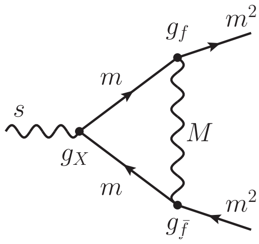

$$\begin{aligned}
F^{\rho,\xi=1}_{1,ffV} = g^{\rho}_X g^{\rho}_f g^{\rho}_{\bar{f}} \Bigg\{ &\frac{1}{\epsilon}+\ln\left(\frac{\mu^2}{M^2}\right)+\\
&+\frac{1}{s-4m^2}\Bigg[-\left(-8m^2+2M^2+3s\right)\Lambda(s;m,m)+\left(-12m^2+2M^2+4s\right)\Lambda\left(m^2;m,M\right)+\\
&-\frac{-4m^4+m^2\left(6M^2+s\right)-M^2\left(M^2+2s\right)}{m^2}\ln\left(\frac{m^2}{M^2}\right)+\\
&-2\left(8m^4-6m^2\left(M^2+s\right)+\left(M^2+s\right)^2\right)C_0\left(m^2,m^2,s;m,M,m\right)\Bigg]\Bigg\}+\\
&+\frac{g^{-\rho}_X g^{-\rho}_f g^{-\rho}_{\bar{f}}}{s-4m^2}\Bigg\{4m^2\Lambda(s;m,m)-4m^2\Lambda\left(m^2;m,M\right)-2M^2\ln\left(\frac{m^2}{M^2}\right)+\\
&-2m^2\left(4m^2-2M^2-s\right)C_0\left(m^2,m^2,s;m,M,m\right)\Bigg\}+\\
&-g^{-\rho}_X g^{\rho}_f g^{\rho}_{\bar{f}}\, 2m^2\, C_0\left(m^2,m^2,s;m,M,m\right),
\end{aligned} \tag{E.34}$$

$$\begin{aligned}
F^{\rho,\xi=1}_{2,ffV} = &\frac{g^{\rho}_X g^{\rho}_f g^{\rho}_{\bar{f}}+g^{-\rho}_X g^{-\rho}_f g^{-\rho}_{\bar{f}}}{\left(s-4m^2\right)^2}\times\\
&\times\Bigg\{-M^2\left(s-4m^2\right)+m^2\left(20m^2-6M^2-5s\right)\Lambda(s;m,m)+\\
&+\left(-24m^4+2m^2\left(5M^2+3s\right)-M^2s\right)\Lambda\left(m^2;m,M\right)+\\
&+\frac{M^2\left(-32m^4+2m^2\left(5M^2+4s\right)-M^2s\right)}{2m^2}\ln\left(\frac{m^2}{M^2}\right)+\\
&-2m^2\left(16m^4-8m^2\left(2M^2+s\right)+3M^4+4M^2s+s^2\right)C_0\left(m^2,m^2,s;m,M,m\right)\Bigg\}+\\
&+\frac{g^{\rho}_X g^{-\rho}_f g^{\rho}_{\bar{f}}+g^{-\rho}_X g^{-\rho}_f g^{\rho}_{\bar{f}}}{s-4m^2}\Bigg\{4m^2\Lambda(s;m,m)-4m^2\Lambda\left(m^2;m,M\right)-2M^2\ln\left(\frac{m^2}{M^2}\right)+
\end{aligned}$$

$$- 2m^2 \left(4m^2 - 2M^2 - s\right) C_0 \left(m^2, m^2, s; m, M, m\right) \Bigg\}, \tag{E.35}$$

$$\begin{aligned}
\Delta F^{\rho;\xi}_{1,ffV} = & \; g^{\rho}_X g^{\rho}_f g^{\rho}_{\bar{f}} \left\{ (\xi - 1) \left(\frac{1}{\epsilon} + \ln\left(\frac{\mu^2}{M^2}\right) + 1 \right) - \xi \ln(\xi) \right\} + \\
& + \frac{2 g^{\rho}_X g^{\rho}_f g^{\rho}_{\bar{f}} - g^{\rho}_X g^{-\rho}_f g^{\rho}_{\bar{f}} - g^{\rho}_X g^{\rho}_f g^{-\rho}_{\bar{f}}}{2} \times \\
& \times \left\{ \xi \Lambda\left(m^2; m, M\sqrt{\xi}\right) - \Lambda\left(m^2; m, M\right) + \xi \left(\frac{M^2 \xi}{2m^2} - 1 \right) \ln\left(\frac{m^2}{M^2 \xi}\right) + \right. \\
& \qquad \left. + \left(1 - \frac{M^2}{2m^2}\right) \ln\left(\frac{m^2}{M^2}\right) + \xi - 1 \right\} + \\
& + \frac{g^{-\rho}_X g^{-\rho}_f g^{-\rho}_{\bar{f}} + g^{-\rho}_X g^{\rho}_f g^{\rho}_{\bar{f}} - g^{-\rho}_X g^{-\rho}_f g^{\rho}_{\bar{f}} - g^{-\rho}_X g^{\rho}_f g^{-\rho}_{\bar{f}}}{s - 4m^2} \times \\
& \times \left\{ m^2 \Lambda\left(m^2; m, M\right) - m^2 \xi \Lambda\left(m^2; m, M\sqrt{\xi}\right) + \right. \\
& \qquad + m^2 (\xi - 1) \Lambda(s; m, m) + \frac{1}{2} M^2 \ln\left(\frac{m^2}{M^2}\right) - \frac{1}{2} M^2 \xi^2 \ln\left(\frac{m^2}{M^2 \xi}\right) + \\
& \qquad \left. - m^2 M^2 C_0\left(m^2, m^2, s; m, M, m\right) + m^2 M^2 \xi^2 C_0\left(m^2, m^2, s; m, M\sqrt{\xi}, m\right) \right\},
\end{aligned} \tag{E.36}$$

$$\begin{aligned}
\Delta F^{\rho;\xi}_{2,ffV} = & \; \frac{g^{\rho}_X g^{\rho}_f g^{\rho}_{\bar{f}} + g^{-\rho}_X g^{-\rho}_f g^{-\rho}_{\bar{f}} + g^{\rho}_X g^{-\rho}_f g^{-\rho}_{\bar{f}} + g^{-\rho}_X g^{\rho}_f g^{\rho}_{\bar{f}} - g^{\rho}_X g^{-\rho}_f g^{\rho}_{\bar{f}} - g^{\rho}_X g^{\rho}_f g^{-\rho}_{\bar{f}} - g^{-\rho}_X g^{-\rho}_f g^{\rho}_{\bar{f}} - g^{-\rho}_X g^{\rho}_f g^{-\rho}_{\bar{f}}}{\left(s - 4m^2\right)^2} \times \\
& \times \left\{ \frac{1}{2} m^2 (\xi - 1) \left(s - 4m^2\right) + 3m^4 (\xi - 1) \Lambda(s; m, m) + \right. \\
& \quad + \frac{1}{2} m^2 \xi \left(s - 10m^2\right) \Lambda\left(m^2; m, M\sqrt{\xi}\right) + \frac{1}{2} m^2 \left(10m^2 - s\right) \Lambda\left(m^2; m, M\right) + \\
& \quad - \frac{1}{4} \left(8m^4 - 2m^2 \left(5M^2 + s\right) + M^2 s\right) \ln\left(\frac{m^2}{M^2}\right) + \\
& \quad + \frac{1}{4} \left(8m^4 - 2m^2 \left(5M^2 \xi + s\right) + M^2 \xi s\right) \xi \ln\left(\frac{m^2}{M^2 \xi}\right) + \\
& \quad + m^4 \left(4m^2 - 3M^2 - s\right) C_0\left(m^2, m^2, s; m, M, m\right) + \\
& \quad \left. + m^4 \xi \left(-4m^2 + 3M^2 \xi + s\right) C_0\left(m^2, m^2, s; m, M\sqrt{\xi}, m\right) \right\}
\end{aligned} \tag{E.37}$$

E.3.1.3 Massless (llV)

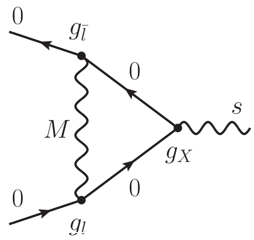

$$F_{1,llV}^{\kappa,\xi=1} = g_X^\kappa g_l^\kappa g_{\bar{l}}^\kappa \Bigg\{ \frac{1}{\epsilon} + \ln\left(\frac{\mu^2}{M^2}\right) - \left(\frac{2M^2}{s} + 3\right) \ln\left(\frac{M^2}{-s - i0^+}\right) - \frac{\left(M^2 + s\right)^2}{s^2} \ln^2\left(\frac{M^2}{-s - i0^+}\right) +$$
$$- \frac{\pi^2 M^4 + 6\left(M^2 + s\right)^2 \mathrm{Li}_2\left(1 + \frac{M^2}{s + i0^+}\right) + 2\left(3 + \pi^2\right) M^2 s + \left(12 + \pi^2\right) s^2}{3s^2} \Bigg\}, \quad \text{(E.38)}$$

$$\Delta F_{1,llV}^{\kappa,\xi} = g_X^\kappa g_l^\kappa g_{\bar{l}}^\kappa \left\{ (\xi - 1)\left(\frac{1}{\epsilon} + \ln\left(\frac{\mu^2}{M^2}\right) + 1\right) - \xi \ln(\xi) \right\}, \quad \text{(E.39)}$$

E.3.2 Abelian scalar

E.3.2.1 Charged $(ffS)_c$

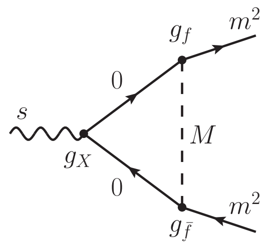

$$F_{1,ffS}^{\rho} = g_X^{-\rho} g_f^{-\rho} g_{\bar{f}}^{\rho} \Bigg\{ \frac{1}{2}\left(\frac{1}{\epsilon} + \ln\left(\frac{\mu^2}{M^2}\right) + 1\right) +$$
$$- \frac{1}{s - 4m^2} \Bigg[\frac{1}{2}\left(2m^2 + 2M^2 - s\right) \ln\left(\frac{M^2}{-s - i0^+}\right) +$$
$$+ \frac{\left(m^2 - M^2\right)^2}{m^2} \ln\left(\frac{M^2}{M^2 - m^2 - i0^+}\right) +$$
$$+ \left(M^4 - m^4\right) C_0\left(m^2, m^2, s; 0, M, 0\right) \Bigg] \Bigg\} +$$
$$+ \frac{g_X^\rho g_f^\rho g_{\bar{f}}^{-\rho}}{s - 4m^2} \Bigg\{ - 2m^2 \ln\left(\frac{M^2}{-s - i0^+}\right) + 2\left(m^2 - M^2\right) \ln\left(\frac{M^2}{M^2 - m^2 - i0^+}\right) +$$
$$- m^2\left(-2m^2 + 2M^2 + s\right) C_0\left(m^2, m^2, s; 0, M, 0\right) \Bigg\}, \quad \text{(E.40)}$$

$$
\begin{aligned}
F^{\rho}_{2,ffS} = \frac{g_X^{-\rho} g_f^{-\rho} g_{\bar{f}}^{\rho} + g_X^{\rho} g_f^{\rho} g_{\bar{f}}^{-\rho}}{\left(s-4m^2\right)^2} \Bigg\{ & -\frac{1}{2}\left(m^2+M^2\right)\left(s-4m^2\right) + \\
& -\frac{1}{2}\, m^2 \left(2m^2+6M^2+s\right) \ln\left(\frac{M^2}{-s-i0^+}\right) + \\
& + \frac{\left(m^2-M^2\right)\left(2m^4+m^2\left(10M^2+s\right)-M^2 s\right)}{2m^2} \ln\left(\frac{M^2}{M^2-m^2-i0^+}\right) + \\
& + m^2\left(m^4+m^2\left(2M^2-s\right)-3M^4-2M^2 s\right) C_0\left(m^2,m^2,s;0,M,0\right) \Bigg\}
\end{aligned}
\tag{E.41}
$$

E.3.2.2 Neutral $(ffS)_n$

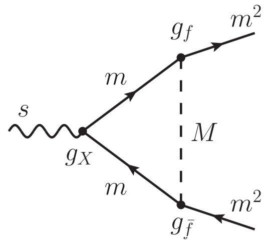

$$
\begin{aligned}
F^{\rho}_{1,ffS} = g_X^{-\rho} g_f^{-\rho} g_{\bar{f}}^{\rho} \Bigg\{ & \frac{1}{2}\left(\frac{1}{\epsilon}+\ln\left(\frac{\mu^2}{M^2}\right)+1\right) + \\
& + \frac{1}{s-4m^2}\Bigg[-\frac{1}{2}\left(2M^2-s\right)\Lambda(s;m,m) + \left(M^2-2m^2\right)\Lambda\left(m^2;m,M\right) + \\
& \qquad - \frac{-4m^4+m^2\left(2M^2+s\right)-M^4}{2m^2} \ln\left(\frac{m^2}{M^2}\right) + \\
& \qquad - M^2\left(M^2-2m^2\right) C_0\left(m^2,m^2,s;m,M,m\right) \Bigg]\Bigg\} + \\
& + \frac{g_X^{-\rho} g_f^{-\rho} g_{\bar{f}}^{-\rho} + g_X^{-\rho} g_f^{\rho} g_{\bar{f}}^{\rho} - g_X^{\rho} g_f^{-\rho} g_{\bar{f}}^{-\rho} - 2 g_X^{\rho} g_f^{\rho} g_{\bar{f}}^{-\rho} - g_X^{\rho} g_f^{\rho} g_{\bar{f}}^{\rho}}{s-4m^2} \times \\
& \times \Bigg\{ m^2 \Lambda(s;m,m) - m^2 \Lambda\left(m^2;m,M\right) - \frac{1}{2}\, M^2 \ln\left(\frac{m^2}{M^2}\right) + m^2 M^2 C_0\left(m^2,m^2,s;m,M,m\right) \Bigg\} + \\
& - \left(g_X^{\rho} g_f^{\rho} g_{\bar{f}}^{\rho} + g_X^{\rho} g_f^{-\rho} g_{\bar{f}}^{\rho} + g_X^{\rho} g_f^{\rho} g_{\bar{f}}^{-\rho} + g_X^{\rho} g_f^{-\rho} g_{\bar{f}}^{-\rho}\right) m^2\, C_0\left(m^2,m^2,s;m,M,m\right),
\end{aligned}
\tag{E.42}
$$

$$
\begin{aligned}
F^{\rho}_{2,ffS} = \frac{g_X^{-\rho} g_f^{-\rho} g_{\bar{f}}^{\rho} + g_X^{\rho} g_f^{\rho} g_{\bar{f}}^{-\rho}}{\left(s-4m^2\right)^2} \Bigg\{ & -\frac{1}{2}\, M^2\left(s-4m^2\right) + \frac{1}{2}\, m^2\left(4m^2-6M^2-s\right)\Lambda(s;m,m) + \\
& -\frac{1}{2}\left(8m^4-2m^2\left(5M^2+s\right)+M^2 s\right)\Lambda\left(m^2;m,M\right) + \\
& + \frac{M^2\left(-16m^4+2m^2\left(5M^2+2s\right)-M^2 s\right)}{4m^2} \ln\left(\frac{m^2}{M^2}\right) +
\end{aligned}
$$

$$+ m^2 M^2 \left(8m^2 - 3M^2 - 2s\right) C_0\left(m^2, m^2, s; m, M, m\right) \Bigg\} +$$

$$+ \frac{g_X^\rho g_f^\rho g_{\bar{f}}^\rho + g_X^{\bar{\rho}} g_f^\rho g_{\bar{f}}^\rho}{s - 4m^2} \Bigg\{ - m^2 \Lambda(s; m, m) + m^2 \Lambda\left(m^2; m, M\right) + \frac{1}{2} M^2 \ln\left(\frac{m^2}{M^2}\right) +$$

$$- m^2 M^2 C_0\left(m^2, m^2, s; m, M, m\right) \Bigg\}. \tag{E.43}$$

E.3.3 Non-abelian vector-vector

Comment: we only need to take the charged case (there are only a WW-diagrams for our purposes, no ZZ-diagrams). To make the results presentable, we restrict ourselves to the case $M_1 = M_2 = M$, which suffices for our purposes.

E.3.3.1 Charged massive $(fVV)_c$

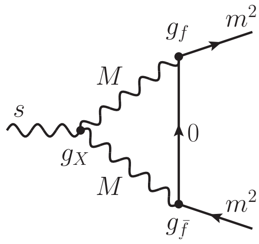

$$F_{1,fVV}^{\rho,\xi=1} = g_X g_f^\rho g_{\bar{f}}^\rho \Bigg\{ -3\left(\frac{1}{\epsilon} + \ln\left(\frac{\mu^2}{M^2}\right) + 2\right) +$$

$$+ \frac{1}{s - 4m^2}\Bigg[\left(2M^2 + s\right) \Lambda(s; M, M) +$$

$$+ \frac{2\left(m^2 - M^2\right)\left(6m^2 - M^2 - 2s\right)}{m^2} \ln\left(\frac{M^2}{M^2 - m^2 - i0^+}\right) +$$

$$- 2\left(m^2 - M^2\right)\left(6m^2 - M^2 - 2s\right) C_0\left(m^2, m^2, s; M, 0, M\right) \Bigg]\Bigg\} +$$

$$+ \frac{g_X g_f^{\bar{\rho}} g_{\bar{f}}^{\bar{\rho}}}{s - 4m^2} \Bigg\{ - 6m^2 \Lambda(s; M, M) + 6\left(m^2 - M^2\right) \ln\left(\frac{M^2}{M^2 - m^2 - i0^+}\right) +$$

$$- 6m^2\left(m^2 - M^2\right) C_0\left(m^2, m^2, s; M, 0, M\right) \Bigg\}, \tag{E.44}$$

$$F_{2,fVV}^{\rho,\xi=1} = \frac{g_X\left(g_f^\rho g_{\bar{f}}^\rho + g_f^{\bar{\rho}} g_{\bar{f}}^{\bar{\rho}}\right)}{\left(s - 4m^2\right)^2} \times$$

$$\times \Bigg\{ \left(M^2 - m^2\right)\left(s - 4m^2\right) + 2m^2\left(-7m^2 + 3M^2 + s\right) \Lambda(s; M, M) +$$

$$+ \frac{\left(m^2 - M^2\right)\left(14m^4 - 2m^2\left(5M^2 + s\right) + M^2 s\right)}{m^2} \ln\left(\frac{M^2}{M^2 - m^2 - i0^+}\right) +$$

$$- m^2\left(m^2-M^2\right)\left(10m^2-6M^2-s\right)C_0\left(m^2,m^2,s;M,0,M\right)\Bigg\}, \tag{E.45}$$

$$\begin{aligned}
\Delta F^{\rho,\xi}_{1,fVV} =&\, g_X g_f^\rho g_{\bar f}^\rho \times \\
&\times\Bigg\{-\frac{3}{2}\left(\xi-1\right)\left(\frac{1}{\epsilon}+\ln\left(\frac{\mu^2}{M^2}\right)\right)+\frac{\left(\xi-1\right)\left(\left(\xi-12\right)s-M^2(\xi-1)\right)}{6s}+ \\
&\quad+\frac{1}{s-4m^2}\times \\
&\quad\times\Bigg[-\frac{m^2\left(40M^4-48M^2s-4s^2\right)+s\left(-16M^4+18M^2s+s^2\right)}{12M^4}\Lambda(s;M,M)+ \\
&\qquad-\frac{\left(M^2-s\right)\left(s\left(M^4(\xi-1)^2-2M^2(\xi-5)s+s^2\right)-4m^2\left(M^4(\xi-1)^2+M^2(7-2\xi)s+s^2\right)\right)}{6M^4s}\times \\
&\qquad\qquad\times\Lambda\left(s;M,M\sqrt{\xi}\right)+ \\
&\qquad-\frac{s\left(s-4m^2\right)\left(s-4M^2\xi\right)}{12M^4}\Lambda\left(s;M\sqrt{\xi},M\sqrt{\xi}\right)+ \\
&\qquad-\frac{1}{12M^2s^2}\Big[4m^2\left(M^6(\xi-1)^3-M^4\left(\xi^3-6\xi+5\right)s+3M^2\left(\xi^2+4\xi+6\right)s^2-(3\xi+8)s^3\right)+ \\
&\qquad\qquad+s\left(-M^6(\xi-1)^3+M^4\left(\xi^3-9\xi+8\right)s-3M^2\left(\xi^2+3\xi+6\right)s^2+(3\xi+8)s^3\right)+ \\
&\qquad\qquad-48m^4M^2s\Big]\ln(\xi)+ \\
&\qquad+\frac{\left(m^2-M^2\right)\left(4m^4M^2+m^2s\left(s-6M^2\right)+M^2s^2\right)}{m^2M^2s}\ln\left(\frac{M^2}{M^2-m^2-i0^+}\right)+ \\
&\qquad-\frac{\left(m^2-M^2\xi\right)\left(4m^4M^2+m^2s\left(s-2M^2(2\xi+1)\right)+M^2\xi s^2\right)}{m^2M^2s}\ln\left(\frac{M^2\xi}{M^2\xi-m^2-i0^+}\right)+ \\
&\qquad+\frac{2m^2\left(m^2-M^2\right)\left(M^2-s\right)}{M^2}C_0\left(m^2,m^2,s;M,0,M\right)+ \\
&\qquad+\frac{2m^2\left(M^2-s\right)\left(m^2\left(2M^2(\xi-1)-s\right)+M^2s\right)}{M^2s}C_0\left(m^2,m^2,s;M\sqrt{\xi},0,M\right)\Bigg]\Bigg\}+ \\
&+\frac{g_X g_f^{-\rho} g_{\bar f}^{-\rho}}{s-4m^2}\times \\
&\times\Bigg\{\frac{m^2\left(m^2\left(4M^2-2s\right)-4M^4+4M^2s+s^2\right)}{4M^4}\Lambda(s;M,M)+ \\
&\qquad-\frac{m^2\left(M^2-s\right)\left(2m^2+M^2(\xi-3)-s\right)}{2M^4}\Lambda\left(s;M,M\sqrt{\xi}\right)+ \\
&\qquad-\frac{m^2s\left(2m^2+2M^2\xi-s\right)}{4M^4}\Lambda\left(s;M\sqrt{\xi},M\sqrt{\xi}\right)+ \\
&\qquad+\frac{m^2}{4M^2s}\Big[2m^2\left(M^2(3\xi+5)-3(\xi+1)s\right)+M^4\left(\xi^2-4\xi+3\right)+ \\
&\qquad\qquad-M^2\left(\xi^2-2\xi+5\right)s+(2\xi+1)s^2\Big]\ln(\xi)+
\end{aligned}$$

$$
\begin{aligned}
&- \frac{\left(M^2-m^2\right)\left(m^2\left(2M^2(\xi+3)-(2\xi+5)s\right)-M^2 s\right)}{2M^2 s} \ln\left(\frac{M^2}{M^2-m^2-i0^+}\right)+\\
&- \frac{\left(m^2-M^2\xi\right)\left(m^2\left(2M^2(\xi+3)-(2\xi+5)s\right)-M^2\xi s\right)}{2M^2 s} \ln\left(\frac{M^2\xi}{M^2\xi-m^2-i0^+}\right)+\\
&- \frac{m^2\left(m^4\left(2M^2-s\right)-2m^2M^2s-2M^6+3M^4s\right)}{2M^4} C_0\left(m^2,m^2,s;M,0,M\right)+\\
&- \frac{m^2}{M^4 s}\Big[m^4 s\left(s-M^2\right)-m^2M^2(\xi-1)\left(M^2-s\right)\left(M^2(\xi+3)-s\right)+\\
&\qquad + M^4\xi s\left(M^2-s\right)\Big] C_0\left(m^2,m^2,s;M\sqrt{\xi},0,M\right)+\\
&+ \frac{m^2 s\left(m^2-M^2\xi\right)^2}{2M^4} C_0\left(m^2,m^2,s;M\sqrt{\xi},0,M\sqrt{\xi}\right)\Bigg\},
\end{aligned}
\tag{E.46}
$$

$$
\begin{aligned}
\Delta F^{\rho,\xi}_{2,ffV} = &\frac{g_X\left(g^{\rho}_f g^{\rho}_{\bar f}+g^{-\rho}_f g^{-\rho}_{\bar f}\right)}{\left(s-4m^2\right)^2}\times\\
&\times\Bigg\{-\frac{1}{4}m^2(\xi-1)\left(s-4m^2\right)+\\
&+ \frac{m^2\left(m^4\left(2s-4M^2\right)+m^2\left(-4M^4+8M^2s+s^2\right)+4M^2s\left(M^2-s\right)\right)}{4M^4}\Lambda(s;M,M)+\\
&+ \frac{m^2\left(M^2-s\right)\left(2m^4+m^2\left(M^2(5-3\xi)+s\right)-2M^2s\right)}{2M^4}\Lambda\left(s;M,M\sqrt{\xi}\right)+\\
&+ \frac{m^4 s\left(2m^2-6M^2\xi+s\right)}{4M^4}\Lambda\left(s;M\sqrt{\xi},M\sqrt{\xi}\right)+\\
&- \frac{m^2\left(s-M^2\right)}{4M^2 s}\Big[2m^4(\xi+15)+2s\left(M^2(\xi-1)+s\right)+\\
&\qquad + m^2\left(M^2\left(3\xi^2-8\xi+5\right)-2(\xi+7)s\right)\Big]\ln(\xi)+\\
&+ \frac{m^2-M^2}{4M^2 s}\Big[m^2 s\left(2M^2(\xi-10)+(11-2\xi)s\right)+M^2s^2+\\
&\qquad + m^4\left(4M^2(\xi+7)-2(2\xi+13)s\right)\Big]\ln\left(\frac{M^2}{M^2-m^2-i0^+}\right)+\\
&- \frac{m^2-M^2\xi}{4M^2 s}\Big[m^4\left(4M^2(\xi+7)-2(2\xi+13)s\right)+M^2\xi s^2+\\
&\qquad - m^2 s\left(2M^2(4\xi+5)+(2\xi-11)s\right)\Big]\ln\left(\frac{M^2\xi}{M^2\xi-m^2-i0^+}\right)+\\
&+ \frac{m^2\left(m^2-M^2\right)\left(m^4\left(2M^2-s\right)+m^2\left(-2M^4+3M^2s+s^2\right)+2M^2s\left(M^2-s\right)\right)}{2M^4}\times\\
&\qquad\times C_0\left(m^2,m^2,s;M,0,M\right)+\\
&- \frac{m^2\left(s-M^2\right)}{2M^4 s}\Big[-2m^6s+m^2M^2s\left(M^2\left(\xi^2-8\xi+5\right)-(\xi+3)s\right)+2M^4\xi s^2+\\
&\qquad + 2m^4\left(M^4\left(\xi^2+6\xi-7\right)-M^2(\xi-3)s+s^2\right)\Big]\times
\end{aligned}
$$

$$\times C_0\left(m^2, m^2, s; M\sqrt{\xi}, 0, M\right) +$$

$$- \frac{m^4 s\left(m^2 - M^2\xi\right)\left(m^2 + 3M^2\xi - s\right)}{2M^4} C_0\left(m^2, m^2, s; M\sqrt{\xi}, 0, M\sqrt{\xi}\right)\Bigg\} \tag{E.47}$$

E.3.3.2 Massless (lVV)

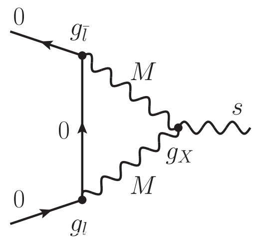

$$F^{\rho,\xi=1}_{1,lVV} = g_X g^\kappa_l g^\kappa_{\bar{l}} \Bigg\{ 3\left(\frac{1}{\epsilon} + \ln\left(\frac{\mu^2}{M^2}\right)\right) + 2 - \frac{2M^2}{s} - \left(\frac{2M^2}{s} + 1\right)\Lambda(s; M, M) +$$

$$+ 2M^2\left(\frac{M^2}{s} + 2\right) C_0(0, 0, s; M, 0, M)\Bigg\}, \tag{E.48}$$

$$\Delta F^{\kappa,\xi}_{1,lVV} = g_X g^\kappa_l g^\kappa_{\bar{l}} \Bigg\{ \frac{3}{2}(\xi - 1)\left(\frac{1}{\epsilon} + \ln\left(\frac{\mu^2}{M^2}\right)\right) + \frac{(\xi - 1)\left(M^2(\xi - 1) - (\xi - 6)s\right)}{6s} +$$

$$+ \frac{1}{12}\left(\frac{s^2}{M^4} + \frac{18s}{M^2} - 16\right)\Lambda(s; M, M) +$$

$$+ \frac{\left(M^2 - s\right)\left(M^4(\xi - 1)^2 - 2M^2(\xi - 5)s + s^2\right)}{6M^4 s}\Lambda\left(s; M, M\sqrt{\xi}\right) +$$

$$+ \frac{s\left(s - 4M^2\xi\right)}{12M^4}\Lambda\left(s; M\sqrt{\xi}, M\sqrt{\xi}\right) +$$

$$+ \frac{-M^6(\xi - 1)^3 + M^4\left(\xi^3 - 9\xi + 8\right)s - 3M^2\left(\xi^2 + 3\xi + 6\right)s^2 + (3\xi + 8)s^3}{12M^2 s^2}\ln(\xi)\Bigg\}. \tag{E.49}$$

E.3.4 Non-abelian vector-scalar

Comment: note that all the vector-scalar diagrams have a global VVS-coupling, which has mass dimension +1. By virtue of the EWSB-mechanism, it can only scale as $\sim v \sim \Lambda_{\text{EW}}$. Since we cannot set the masses equal (because there are for example the ZH-diagrams) the expressions are somewhat complicated.

E.3.4.1 Charged $(fVS)_c$

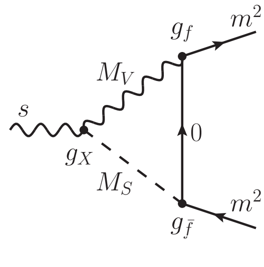

$$
\begin{aligned}
F^{\rho,\xi=1}_{1,fVS} = \frac{g_X g^{-\rho}_f g^{\rho}_{\bar{f}}\, m}{s-4m^2}\Bigg\{ & \Lambda(s; M_S, M_V) - \frac{-4m^2+M_S^2-M_V^2+s}{2s}\ln\left(\frac{M_S^2}{M_V^2}\right)+\\
& -\frac{2\left(m^2-M_S^2\right)}{s}\ln\left(\frac{M_S^2}{M_S^2-m^2-i0^+}\right)+\\
& +\frac{\left(2m^2-s\right)\left(m^2-M_V^2\right)}{m^2 s}\ln\left(\frac{M_V^2}{M_V^2-m^2-i0^+}\right)+\\
& -\frac{sM_S^2-m^2\left(2M_S^2-2M_V^2+s\right)}{s}C_0\left(m^2,m^2,s;M_V,0,M_S\right)\\
+\frac{g_X g^{\rho}_f g^{-\rho}_{\bar{f}}\, m}{s-4m^2}\Bigg\{ & -\Lambda\left(s;M_S,M_V\right)-\frac{-4m^2-M_S^2+M_V^2+s}{2s}\ln\left(\frac{M_S^2}{M_V^2}\right)+\\
& -\frac{\left(2m^2-s\right)\left(m^2-M_S^2\right)}{m^2 s}\ln\left(\frac{M_S^2}{M_S^2-m^2-i0^+}\right)+\\
& +\frac{2\left(m^2-M_V^2\right)}{s}\ln\left(\frac{M_V^2}{M_V^2-m^2-i0^+}\right)+\\
& -\frac{m^2\left(-2M_S^2+2M_V^2+s\right)-sM_V^2}{s}C_0\left(m^2,m^2,s;M_V,0,M_S\right)\Bigg\},
\end{aligned}
\tag{E.50}
$$

$$
\begin{aligned}
F^{\rho,\xi=1}_{2,fVS} = \frac{g_X g^{-\rho}_f g^{\rho}_{\bar{f}}\, m}{s-4m^2}\Bigg\{ & -\Lambda(s; M_S, M_V) - \frac{4m^2-M_S^2+M_V^2-s}{2s}\ln\left(\frac{M_S^2}{M_V^2}\right)+\\
& +\frac{2\left(m^2-M_S^2\right)}{s}\ln\left(\frac{M_S^2}{M_S^2-m^2-i0^+}\right)+\\
& -\frac{\left(2m^2-s\right)\left(m^2-M_V^2\right)}{m^2 s}\ln\left(\frac{M_V^2}{M_V^2-m^2-i0^+}\right)+\\
& -\frac{-sM_S^2+m^2\left(2M_S^2-2M_V^2+s\right)}{s}C_0\left(m^2,m^2,s;M_V,0,M_S\right)\Bigg\},
\end{aligned}
\tag{E.51}
$$

$$
\begin{aligned}
\Delta F^{\rho,\xi}_{1,fVS} = & \frac{g_X g^{-\rho}_f g^{\rho}_{\bar{f}}\, m}{s-4m^2}\times\\
& \times\Bigg\{-\frac{2m^2+M_S^2+M_V^2-s}{4M_V^2}\Lambda\left(s;M_S,M_V\right)+\\
& +\frac{2m^2+M_S^2+\xi M_V^2-s}{4M_V^2}\Lambda\left(s;M_S,M_V\sqrt{\xi}\right)+\\
& +\frac{m^2\left(6M_S^2-6\xi M_V^2-4s\right)-2sM_S^2+2\xi sM_V^2+M_S^4-\xi^2M_V^4+s^2}{8sM_V^2}\ln(\xi)+\\
& +\frac{(\xi-1)\left(6m^2+(\xi+1)M_V^2-2s\right)}{8s}\ln\left(\frac{M_S^2}{M_V^2}\right)+
\end{aligned}
$$

$$
\begin{aligned}
&- \frac{(\xi-1)\left(m^2-M_S^2\right)}{2s} \ln\left(\frac{M_S^2}{M_S^2-m^2-i0^+}\right) + \\
&- \frac{\left(m^2-M_V^2\right)\left(m^2\left(-2M_S^2+2M_V^2+s\right)-sM_V^2\right)}{4m^2sM_V^2} \ln\left(\frac{M_V^2}{M_V^2-m^2-i0^+}\right) + \\
&- \frac{\left(m^2-\xi M_V^2\right)\left(m^2\left(2M_S^2-2\xi M_V^2-s\right)+\xi sM_V^2\right)}{4m^2sM_V^2} \ln\left(\frac{M_V^2\xi}{M_V^2\xi-m^2-i0^+}\right) + \\
&+ \frac{m^4s+m^2\left(-M_S^2\left(2M_V^2+s\right)-sM_V^2+M_S^4+M_V^4\right)+sM_S^2M_V^2}{2sM_V^2} \times \\
&\qquad\qquad\qquad \times C_0\left(m^2,m^2,s;M_V,0,M_S\right) + \\
&- \frac{m^4s+m^2\left(-M_S^2\left(2\xi M_V^2+s\right)+\xi M_V^2\left(\xi M_V^2-s\right)+M_S^4\right)+\xi sM_S^2M_V^2}{2sM_V^2} \times \\
&\qquad\qquad\qquad \times C_0\left(m^2,m^2,s;M_V\sqrt{\xi},0,M_S\right) \Bigg\},
\end{aligned}
\tag{E.52}
$$

$$
\begin{aligned}
\Delta F_{2,fVS}^{\rho,\xi} = &\frac{g_X g_f^{-\rho} g_{\bar{f}}^{\rho}\, m}{\left(s-4m^2\right)^2} \times \\
\times \Bigg\{ &- \frac{(\xi-1)\left(2m^2-s\right)\left(s-4m^2\right)}{4s} + \\
&+ \frac{m^2\left(2m^2\left(4M_S^2-4M_V^2+s\right)+s\left(-5M_S^2-M_V^2+s\right)\right)}{4sM_V^2} \Lambda\left(s;M_S,M_V\right) + \\
&+ \frac{m^2\left(s\left(5M_S^2+\xi M_V^2-s\right)-2m^2\left(4M_S^2-4\xi M_V^2+s\right)\right)}{4sM_V^2} \Lambda\left(s;M_S,M_V\sqrt{\xi}\right) + \\
&- \frac{m^2}{8s^2M_V^2}\Big[16m^4s+2m^2\left(-M_S^2\left(8\xi M_V^2+s\right)+\xi sM_V^2+4M_S^4+4\xi^2M_V^4-4s^2\right) + \\
&\qquad + s\left(2M_S^2\left(2\xi M_V^2+s\right)+\left(s-\xi M_V^2\right)^2-5M_S^4\right)\Big] \ln(\xi) + \\
&+ \frac{m^2(\xi-1)\left(2m^2\left(-8M_S^2+4(\xi+1)M_V^2+s\right)+s\left(4M_S^2+(\xi+1)M_V^2-2s\right)\right)}{8s^2} \times \\
&\qquad\qquad\qquad \times \ln\left(\frac{M_S^2}{M_V^2}\right) + \\
&- \frac{3m^2(\xi-1)\left(m^2-M_S^2\right)}{2s} \ln\left(\frac{M_S^2}{M_S^2-m^2-i0^+}\right) + \\
&- \frac{\left(m^2-M_V^2\right)\left(8m^6+m^4\left(2M_S^2+6M_V^2-3s\right)+m^2s\left(-2M_S^2-7M_V^2+s\right)+s^2M_V^2\right)}{4m^2sM_V^2} \times \\
&\qquad\qquad\qquad \times \ln\left(\frac{M_V^2}{M_V^2-m^2-i0^+}\right) + \\
&+ \frac{\left(m^2-\xi M_V^2\right)\left(8m^6+m^4\left(2M_S^2+6\xi M_V^2-3s\right)+m^2s\left(-2M_S^2-7\xi M_V^2+s\right)+\xi s^2M_V^2\right)}{4m^2sM_V^2} \times
\end{aligned}
$$

$$\times \ln\left(\frac{M_V^2\xi}{M_V^2\xi - m^2 - i0^+}\right) +$$

$$+ \frac{m^2}{2sM_V^2}\Big[m^2\left(-2M_S^2\left(M_V^2 - s\right) - 4sM_V^2 - M_S^4 + 3M_V^4 + s^2\right) +$$

$$- m^4\left(4M_S^2 - 4M_V^2 + s\right) + sM_S^2\left(M_S^2 + 2M_V^2 - s\right)\Big]\times$$

$$\times C_0\left(m^2, m^2, s; M_V, 0, M_S\right) +$$

$$+ \frac{m^2}{2sM_V^2}\Big[m^2\left(-2M_S^2\left(s - \xi M_V^2\right) + 4\xi sM_V^2 + M_S^4 - 3\xi^2 M_V^4 - s^2\right) +$$

$$+ m^4\left(4M_S^2 - 4\xi M_V^2 + s\right) + sM_S^2\left(-M_S^2 - 2\xi M_V^2 + s\right)\Big]\times$$

$$\times C_0\left(m^2, m^2, s; M_V\sqrt{\xi}, 0, M_S\right)\Bigg\}+$$

$$+\frac{g_X g_f^\rho g_{\bar{f}}^{-\rho}\, m}{\left(s - 4m^2\right)^2}\times$$

$$\times\Bigg\{\frac{\left(\xi - 1\right) m^2\left(s - 4m^2\right)}{2s} +$$

$$+ \frac{m^2\left(m^2\left(-8M_S^2 + 8M_V^2 + 2s\right) + s\left(-M_S^2 - 5M_V^2 + s\right)\right)}{4M_V^2 s}\Lambda\left(s; M_S, M_V\right) +$$

$$+ \frac{m^2\left(m^2\left(8M_S^2 - 2\left(4M_V^2\xi + s\right)\right) + s\left(M_S^2 + 5M_V^2\xi - s\right)\right)}{4M_V^2 s}\Lambda\left(s; M_S, M_V\sqrt{\xi}\right) +$$

$$+ \frac{m^2}{8s^2M_V^2}\Big[16m^4 s + 2m^2\left(4M_S^4 + M_S^2\left(s - 8M_V^2\xi\right) + 4M_V^4\xi^2 - M_V^2\xi s - 4s^2\right) +$$

$$+ s\left(M_S^4 - 2M_S^2\left(s - 2M_V^2\xi\right) - 5M_V^4\xi^2 + 2M_V^2\xi s + s^2\right)\Big]\ \ln(\xi)+$$

$$+ \frac{m^2(\xi - 1)\left(2m^2\left(8M_S^2 - 4M_V^2(\xi + 1) + s\right) + s\left(-4M_S^2 + 5M_V^2(\xi + 1) - 2s\right)\right)}{8s^2}\times$$

$$\times \ln\left(\frac{M_S^2}{M_V^2}\right) +$$

$$+ \frac{\left(\xi - 1\right)\left(m^2 - M_S^2\right)\left(m^2 - s\right)}{2s}\ \ln\left(\frac{M_S^2}{M_S^2 - m^2 - i0^+}\right) +$$

$$+ \frac{\left(m^2 - M_V^2\right)\left(8m^4 + m^2\left(6M_S^2 + 2M_V^2 - 5s\right) + M_V^2 s\right)}{4M_V^2 s}\ \ln\left(\frac{M_V^2}{M_V^2 - m^2 - i0^+}\right) +$$

$$- \frac{\left(m^2 - M_V^2\xi\right)\left(8m^4 + m^2\left(6M_S^2 + 2M_V^2\xi - 5s\right) + M_V^2\xi s\right)}{4M_V^2 s}\ \ln\left(\frac{M_V^2\xi}{M_V^2\xi - m^2 - i0^+}\right) +$$

$$+ \frac{m^2}{2sM_V^2}\Big[m^2\left(3M_S^4 - 2M_S^2\left(M_V^2 + 2s\right) - M_V^4 + 2M_V^2 s + s^2\right) +$$

$$+ m^4\left(4M_S^2 - 4M_V^2 - s\right) + M_V^2 s\left(2M_S^2 + M_V^2 - s\right)\Big]\times$$

$$\times C_0\left(m^2, m^2, s; M_V, 0, M_S\right) +$$

$$
\begin{aligned}
&+\frac{m^2}{2sM_V^2}\Big[m^2\left(-3M_S^4+2M_S^2\left(M_V^2\xi+2s\right)+M_V^4\xi^2-2M_V^2\xi s-s^2\right)+\\
&\qquad+m^4\left(-4M_S^2+4M_V^2\xi+s\right)+M_V^2\xi s\left(-2M_S^2-M_V^2\xi+s\right)\Big]\times\\
&\qquad\qquad\times C_0\left(m^2,m^2,s;M_V\sqrt{\xi},0,M_S\right)\Bigg\}.
\end{aligned}
\tag{E.53}
$$

E.3.4.2 Neutral $(fVS)_n$

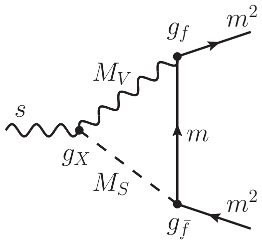

$$
\begin{aligned}
F_{1,fVS}^{\rho,\xi=1}=\;&\frac{g_X g_f^{-\rho} g_{\bar{f}}^{\rho}\, m}{s-4m^2}\Bigg\{\Lambda(s;M_S,M_V)+\left(\frac{M_V^2}{s}-\frac{M_V^2}{4m^2}\right)\ln\left(\frac{M_S^2}{M_V^2}\right)+\\
&+\left(\frac{-M_S^2+M_V^2+s}{s}-\frac{M_V^2}{2m^2}\right)\ln\left(\frac{m^2}{M_SM_V}\right)+\\
&-\frac{2m^2}{s}\Lambda\left(m^2;m,M_S\right)-\frac{s-2m^2}{s}\Lambda\left(m^2;m,M_V\right)+\\
&-\frac{M_S^2 s-2m^2\left(M_S^2-M_V^2+s\right)}{s}C_0\left(m^2,m^2,s;M_V,m,M_S\right)\Bigg\}+\\
&+\frac{g_X g_f^{\rho} g_{\bar{f}}^{-\rho}\, m}{s-4m^2}\Bigg\{-\Lambda\left(s;M_S,M_V\right)+\left(\frac{M_S^2}{s}-\frac{M_S^2}{4m^2}\right)\ln\left(\frac{M_S^2}{M_V^2}\right)+\\
&+\left(\frac{M_S^2}{2m^2}-\frac{M_S^2-M_V^2+s}{s}\right)\ln\left(\frac{m^2}{M_SM_V}\right)+\\
&+\frac{s-2m^2}{s}\Lambda\left(m^2;m,M_S\right)+\frac{2m^2}{s}\Lambda\left(m^2;m,M_V\right)+\\
&-\frac{2m^2\left(-M_S^2+M_V^2+s\right)-M_V^2 s}{s}C_0\left(m^2,m^2,s;M_V,m,M_S\right)\Bigg\}+\\
&+g_X g_f^{\rho} g_{\bar{f}}^{\rho}\, m\; C_0\left(m^2,m^2,s;M_V,m,M_S\right),
\end{aligned}
\tag{E.54}
$$

$$
\begin{aligned}
F_{2,fVS}^{\rho,\xi=1}=\;&\frac{g_X g_f^{-\rho} g_{\bar{f}}^{\rho}\, m}{s-4m^2}\Bigg\{-\Lambda\left(s;M_S,M_V\right)-\frac{M_S^2+M_V^2-s}{2s}\ln\left(\frac{M_S^2}{M_V^2}\right)+\\
&-\frac{2m^2\left(-M_S^2+M_V^2+s\right)-M_V^2 s}{2m^2 s}\ln\left(\frac{m^2}{M_V^2}\right)+\\
&+\frac{2m^2}{s}\Lambda\left(m^2;m,M_S\right)+\frac{s-2m^2}{s}\Lambda\left(m^2;m,M_V\right)+
\end{aligned}
$$

$$- \frac{2m^2\left(M_S^2 - M_V^2 + s\right) - M_S^2 s}{s} C_0\left(m^2, m^2, s; M_V, m, M_S\right) \Bigg\}, \tag{E.55}$$

$$\Delta F^{\rho,\xi}_{1,fVS} = \frac{g_X\left(g_f^{\rho} g_{\bar{f}}^{\rho} - g_f^{-\rho} g_{\bar{f}}^{\rho}\right) m}{s - 4m^2} \times$$
$$\times \Bigg\{ \frac{M_S^2 + M_V^2 - s}{4M_V^2} \Lambda\left(s; M_S, M_V\right) - \frac{M_S^2 + M_V^2\xi - s}{4M_V^2} \Lambda\left(s; M_S, M_V\sqrt{\xi}\right) +$$
$$- \frac{m^2\left(M_S^4 - 2M_S^2\left(s - M_V^2\xi\right) - 3M_V^4\xi^2 - 2M_V^2\xi s + s^2\right) + M_V^4\xi^2 s}{8m^2 M_V^2 s} \ln(\xi) +$$
$$- \frac{(\xi - 1)\left(2M_S^2 + M_V^2(\xi + 1) - 2s\right)}{8s} \ln\left(\frac{M_S^2}{M_V^2}\right) +$$
$$- \frac{(\xi - 1)\left(2m^2\left(-2M_S^2 + M_V^2(\xi + 1) + 2s\right) - M_V^2(\xi + 1)s\right)}{8m^2 s} \ln\left(\frac{m^2}{M_V^2}\right) +$$
$$+ \frac{(\xi - 1)m^2}{2s} \Lambda\left(m^2; m, M_S\right) +$$
$$- \frac{2m^2\left(M_S^2 - M_V^2 - s\right) + M_V^2 s}{4M_V^2 s} \Lambda\left(m^2; m, M_V\right) +$$
$$- \frac{2m^2\left(-M_S^2 + M_V^2\xi + s\right) - M_V^2\xi s}{4M_V^2 s} \Lambda\left(m^2; m, M_V\sqrt{\xi}\right) +$$
$$- \frac{m^2\left(M_S^4 - 2M_S^2\left(M_V^2 + s\right) + \left(M_V^2 - s\right)^2\right) + M_S^2 M_V^2 s}{2M_V^2 s} \times$$
$$\times C_0\left(m^2, m^2, s; M_V, m, M_S\right) +$$
$$+ \frac{m^2\left(M_S^4 - 2M_S^2\left(M_V^2\xi + s\right) + \left(s - M_V^2\xi\right)^2\right) + M_S^2 M_V^2\xi s}{2M_V^2 s} \times$$
$$\times C_0\left(m^2, m^2, s; M_V\sqrt{\xi}, m, M_S\right) \Bigg\}, \tag{E.56}$$

$$\Delta F^{\rho,\xi}_{2,fVS} = \frac{g_X\left(g_f^{\rho} g_{\bar{f}}^{\rho} - g_f^{-\rho} g_{\bar{f}}^{\rho}\right) m}{\left(s - 4m^2\right)^2} \times$$
$$\times \Bigg\{ \frac{(\xi - 1)\left(2m^2 - s\right)\left(s - 4m^2\right)}{4s} +$$
$$+ \frac{m^2\left(8m^2\left(-M_S^2 + M_V^2 + s\right) + s\left(5M_S^2 + M_V^2 - 5s\right)\right)}{4M_V^2 s} \Lambda\left(s; M_S, M_V\right) +$$
$$- \frac{m^2\left(8m^2\left(-M_S^2 + M_V^2\xi + s\right) + s\left(5M_S^2 + M_V^2\xi - 5s\right)\right)}{4M_V^2 s} \Lambda\left(s; M_S, M_V\sqrt{\xi}\right) +$$
$$+ \frac{1}{8s^2 m^2 M_V^2}\Big[8m^6\left(M_S^4 - 2M_S^2\left(M_V^2\xi + s\right) + M_V^4\xi^2 + s^2\right) - m^2 M_V^2\xi s^2\left(2M_S^2 + 7M_V^2\xi\right) +$$

$$+ M_V^4\xi^2 s^3 + m^4 s\left(-5M_S^4 + 2M_S^2\left(3M_V^2\xi + 5s\right) + 7M_V^4\xi^2 + 6M_V^2\xi s - 5s^2\right)\Big]\ \ln(\xi) +$$

$$- \frac{(\xi-1)\left(m^4\left(6\left(M_V^2(\xi+1)+2s\right)-4M_S^2\right)-m^2 s\left(2M_S^2+7M_V^2(\xi+1)\right)+M_V^2(\xi+1)s^2\right)}{8m^2 s}\times$$

$$\times \ln\left(\frac{m^2}{M_V^2}\right) +$$

$$- \frac{m^2(\xi-1)\left(8m^2\left(M_V^2(\xi+1)-2M_S^2\right)+s\left(10M_S^2+M_V^2(\xi+1)-6s\right)\right)}{8s^2}\times$$

$$\times \ln\left(\frac{M_S^2}{M_V^2}\right) +$$

$$+ \frac{3m^4(\xi-1)}{2s}\,\Lambda\left(m^2; m, M_S\right) +$$

$$+ \frac{\left(m^2-s\right)\left(2m^2\left(M_S^2+3M_V^2-s\right)-M_V^2 s\right)}{4M_V^2 s}\,\Lambda\left(m^2; m, M_V\right) +$$

$$+ \frac{\left(m^2-s\right)\left(M_V^2\xi s-2m^2\left(M_S^2+3M_V^2\xi-s\right)\right)}{4M_V^2 s}\,\Lambda\left(m^2; m, M_V\sqrt{\xi}\right) +$$

$$- \frac{m^2\left(8m^2\left(-M_S^2+M_V^2\xi+s\right)+s\left(5M_S^2+M_V^2\xi-5s\right)\right)}{4M_V^2 s}\,\Lambda\left(s; M_S, M_V\sqrt{\xi}\right) +$$

$$+ \frac{m^2}{2sM_V^2}\Big[m^2\left(M_S^4+2M_S^2\left(M_V^2-s\right)-3M_V^4+2M_V^2 s+s^2\right) +$$

$$- s\left(M_S^4+2M_S^2\left(M_V^2-s\right)+s\left(s-M_V^2\right)\right)\Big]\times$$

$$\times C_0\left(m^2, m^2, s; M_V, m, M_S\right) +$$

$$+ \frac{m^2}{2sM_V^2}\Big[-m^2\left(M_S^4-2M_S^2\left(s-M_V^2\xi\right)-3M_V^4\xi^2+2M_V^2\xi s+s^2\right) +$$

$$+ s\left(M_S^4-2M_S^2\left(s-M_V^2\xi\right)+s\left(s-M_V^2\xi\right)\right)\Big]\times$$

$$\times C_0\left(m^2, m^2, s; M_V\sqrt{\xi}, m, M_S\right)\Bigg\} +$$

$$+ \frac{g_X\left(g_f^{-\rho}g_{\bar f}^{-\rho}-g_f^{\rho}g_{\bar f}^{-\rho}\right)m}{\left(s-4m^2\right)^2}\times$$

$$\times\Bigg\{-\frac{m^2(\xi-1)\left(s-4m^2\right)}{2s} +$$

$$+ \frac{m^2\left(8m^2\left(M_S^2-M_V^2-s\right)+s\left(M_S^2+5M_V^2-s\right)\right)}{4M_V^2 s}\,\Lambda\left(s; M_S, M_V\right) +$$

$$+ \frac{m^2\left(8m^2\left(-M_S^2+M_V^2\xi+s\right)+s\left(-M_S^2-5M_V^2\xi+s\right)\right)}{4M_V^2 s}\,\Lambda\left(s; M_S, M_V\sqrt{\xi}\right) +$$

$$- \frac{1}{8s^2M_V^2}\Big[M_V^4\xi^2 s^2 + 8m^4\left(M_S^4-2M_S^2\left(M_V^2\xi+s\right)+M_V^4\xi^2+s^2\right) +$$

$$+ m^2 s \left(M_S^4 - 2M_S^2 \left(s - 5M_V^2\xi\right) - 3M_V^4\xi^2 - 6M_V^2\xi s + s^2\right) \Big] \ln(\xi) +$$

$$+ \frac{(\xi-1)\left(2m^2\left(2M_S^2 + M_V^2(\xi+1) - 6s\right) + s\left(2M_S^2 + M_V^2(\xi+1)\right)\right)}{8s} \times$$

$$\times \log\left(\frac{m^2}{M_V^2}\right) +$$

$$+ \frac{(\xi-1)\left(8m^4\left(M_V^2(\xi+1) - 2M_S^2\right) + m^2 s\left(6M_S^2 - 5M_V^2(\xi+1) + 6s\right) - 2M_S^2 s^2\right)}{8s^2} \times$$

$$\times \ln\left(\frac{M_S^2}{M_V^2}\right) +$$

$$- \frac{m^2(\xi-1)\left(m^2 - s\right)}{2s} \Lambda\left(m^2; m, M_S\right) +$$

$$- \frac{m^2\left(2m^2\left(3M_S^2 + M_V^2 - 3s\right) + M_V^2 s\right)}{4M_V^2 s} \Lambda\left(m^2; m, M_V\right) +$$

$$+ \frac{2m^4\left(3M_S^2 + M_V^2\xi - 3s\right) + m^2 M_V^2 \xi s}{4M_V^2 s} \Lambda\left(m^2; m, M_V\sqrt{\xi}\right) +$$

$$+ \frac{m^2}{2sM_V^2}\Big[m^2\left(-3M_S^4 + 2M_S^2\left(M_V^2 + 3s\right) + M_V^4 + 2M_V^2 s - 3s^2\right) +$$

$$+ M_V^2 s\left(-2M_S^2 - M_V^2 + s\right)\Big] C_0\left(m^2, m^2, s; M_V, m, M_S\right) +$$

$$+ \frac{m^2}{2sM_V^2}\Big[m^2\left(3M_S^4 - 2M_S^2\left(M_V^2\xi + 3s\right) - M_V^4\xi^2 - 2M_V^2\xi s + 3s^2\right) +$$

$$+ M_V^2\xi s\left(2M_S^2 + M_V^2\xi - s\right)\Big] C_0\left(m^2, m^2, s; M_V\sqrt{\xi}, m, M_S\right) \Bigg\}. \tag{E.57}$$

E.3.5 Non-abelian scalar-vector

Comment: expressions for the scalar-vector diagrams are identical to the vector-scalar ones except for the following replacements:

- $g_{\bar{f}}^{\pm\rho} \to g_{\bar{f}}^{\mp\rho}$ for $F_1^{\rho,\xi=1}$ and $\Delta F_1^{\rho,\xi}$,

- $g_f^{\pm\rho} \to g_f^{\mp\rho}$ for $F_2^{\rho,\xi=1}$ and $\Delta F_2^{\rho,\xi}$.

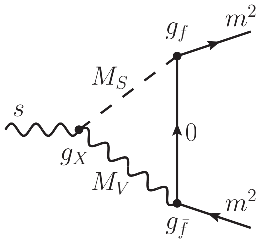

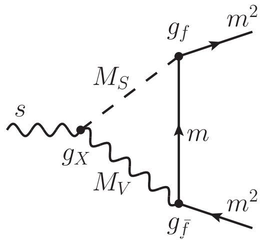

E.3.6 Non-abelian scalar-scalar

E.3.6.1 Charged $(fSS)_c$

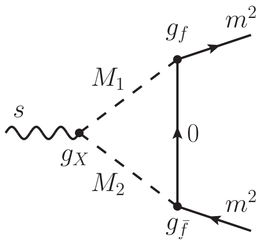

$$
\begin{aligned}
F^{\rho}_{1,fSS} = {} & g_X g_f^{-\rho} g_{\bar{f}}^{\rho} \times \\
& \times \Bigg\{ \frac{1}{2}\left(\frac{1}{\epsilon} + \ln\left(\frac{\mu^2}{M_1^2}\right) + 3\right) + \\
& + \frac{1}{s-4m^2}\Bigg[-\frac{1}{2}\left(2m^2 + M_1^2 + M_2^2 - s\right)\Lambda(s; M_1, M_2) + \\
& \qquad - \frac{m^2\left(-6M_1^2 + 6M_2^2 + 4s\right) - M_1^4 + 2M_1^2 s + M_2^4 - 2M_2^2 s - s^2}{4s} \ln\left(\frac{M_1^2}{M_2^2}\right) + \\
& \qquad - \frac{\left(m^2 - M_1^2\right)\left(m^2\left(2M_1^2 - 2M_2^2 + s\right) - M_1^2 s\right)}{2m^2 s} \ln\left(\frac{M_1^2}{M_1^2 - m^2 - i0^+}\right) + \\
& \qquad - \frac{\left(m^2 - M_2^2\right)\left(m^2\left(-2M_1^2 + 2M_2^2 + s\right) - M_2^2 s\right)}{2m^2 s} \ln\left(\frac{M_2^2}{M_2^2 - m^2 - i0^+}\right) + \\
& \qquad - \frac{-m^4 s + m^2\left(-M_1^4 + M_1^2\left(2M_2^2 + s\right) - M_2^4 + M_2^2 s\right) - M_1^2 M_2^2 s}{s} \times \\
& \qquad \qquad \times C_0\left(m^2, m^2, s; M_2, 0, M_1\right)\Bigg]\Bigg\}, \qquad \text{(E.58)}
\end{aligned}
$$

$$
\begin{aligned}
F^{\rho}_{2,fSS} = {} & \frac{g_X g_f^{\rho} g_{\bar{f}}^{-\rho}}{\left(s-4m^2\right)^2} \times \\
& \times \Bigg\{ - \frac{\left(s-4m^2\right)\left(m^2\left(2M_1^2 - 2M_2^2 - s\right) + M_2^2 s\right)}{2s} + \\
& \quad + \frac{m^2\left(2m^2\left(4M_1^2 - 4M_2^2 + s\right) + s\left(-5M_1^2 - M_2^2 + s\right)\right)}{2s} \Lambda(s; M_1, M_2) + \\
& \quad - \frac{m^2}{4s^2}\Big[16m^4 s + s\left(-5M_1^4 + 2M_1^2\left(2M_2^2 + s\right) + \left(M_2^2 - s\right)^2\right) + \\
& \qquad + 2m^2\left(4M_1^4 - M_1^2\left(8M_2^2 + s\right) + 4M_2^4 + M_2^2 s - 4s^2\right)\Big] \ln\left(\frac{M_1^2}{M_2^2}\right) + \\
& \quad + \frac{\left(m^2 - M_1^2\right)\left(8m^4 + m^2\left(2M_1^2 + 6M_2^2 - 5s\right) + M_1^2 s\right)}{2s} \ln\left(\frac{M_1^2}{M_1^2 - m^2 - i0^+}\right) + \\
& \quad - \frac{\left(m^2 - M_2^2\right)\left(8m^6 + m^4\left(2M_1^2 + 6M_2^2 - 3s\right) + m^2 s\left(-2M_1^2 - 7M_2^2 + s\right) + M_2^2 s^2\right)}{2m^2 s} \times
\end{aligned}
$$

$$\times \ln\left(\frac{M_2^2}{M_2^2-m^2-i0^+}\right)+$$

$$+\frac{m^2}{s}\Big[m^2\left(-M_1^4-2M_1^2\left(M_2^2-s\right)+3M_2^4-4M_2^2s+s^2\right)+$$

$$+M_1^2s\left(M_1^2+2M_2^2-s\right)-m^4\left(4M_1^2-4M_2^2+s\right)\Big]C_0\left(m^2,m^2,s;M_2,0,M_1\right)\Bigg\}+$$

$$+\frac{g_X g_f^{-\rho} g_{\bar{f}}^{\rho}}{\left(s-4m^2\right)^2}\times$$

$$\times\Bigg\{-\frac{\left(s-4m^2\right)\left(M_1^2s-m^2\left(2M_1^2-2M_2^2+s\right)\right)}{2s}+$$

$$+\frac{m^2\left(2m^2\left(-4M_1^2+4M_2^2+s\right)+s\left(-M_1^2-5M_2^2+s\right)\right)}{2s}\Lambda(s;M_1,M_2)+$$

$$+\frac{m^2}{4s^2}\Big[16m^4s+s\left(M_1^4+M_1^2\left(4M_2^2-2s\right)-5M_2^4+2M_2^2s+s^2\right)+$$

$$+2m^2\left(4M_1^4+M_1^2\left(s-8M_2^2\right)+4M_2^4-M_2^2s-4s^2\right)\Big]\ln\left(\frac{M_1^2}{M_2^2}\right)+$$

$$-\frac{\left(m^2-M_1^2\right)\left(8m^6+m^4\left(6M_1^2+2M_2^2-3s\right)+m^2s\left(-7M_1^2-2M_2^2+s\right)+M_1^2s^2\right)}{2m^2s}\times$$

$$\times \ln\left(\frac{M_1^2}{M_1^2-m^2-i0^+}\right)+$$

$$+\frac{\left(m^2-M_2^2\right)\left(8m^4+m^2\left(6M_1^2+2M_2^2-5s\right)+M_2^2s\right)}{2s}\ln\left(\frac{M_2^2}{M_2^2-m^2-i0^+}\right)+$$

$$+\frac{m^2}{s}\Big[m^2\left(3M_1^4-2M_1^2\left(M_2^2+2s\right)-M_2^4+2M_2^2s+s^2\right)+$$

$$+m^4\left(4M_1^2-4M_2^2-s\right)+M_2^2s\left(2M_1^2+M_2^2-s\right)\Big]C_0\left(m^2,m^2,s;M_2,0,M_1\right)\Bigg\}, \tag{E.59}$$

E.3.6.2 Neutral $(fSS)_n$

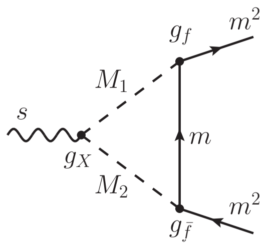

$$F_{1,fSS}^{\rho}=g_X g_f^{-\rho} g_{\bar{f}}^{\rho}\times$$

$$\times\Bigg\{\frac{1}{2}\left(\frac{1}{\epsilon}+\ln\left(\frac{\mu^2}{M_1^2}\right)+3\right)+$$

$$
\begin{aligned}
&+\frac{1}{s-4m^2}\Bigg[-\frac{1}{2}\left(M_1^2+M_2^2-s\right)\Lambda(s;M_1,M_2)+\\
&\qquad+\frac{m^2\left(M_1^4+2M_1^2\left(M_2^2-s\right)-3M_2^4-2M_2^2s+s^2\right)+M_2^4s}{4m^2s}\ln\left(\frac{M_1^2}{M_2^2}\right)+\\
&\qquad+\frac{8m^4s-2m^2\left(M_1^4-2M_1^2\left(M_2^2-s\right)+M_2^4+2M_2^2s\right)+s\left(M_1^4+M_2^4\right)}{4m^2s}\ln\left(\frac{m^2}{M_1^2}\right)+\\
&\qquad-\frac{2m^2\left(M_1^2-M_2^2+s\right)-M_1^2s}{2s}\Lambda\left(m^2;m,M_1\right)+\\
&\qquad-\frac{2m^2\left(-M_1^2+M_2^2+s\right)-M_2^2s}{2s}\Lambda\left(m^2;m,M_2\right)+\\
&\qquad+\frac{m^2\left(M_1^4-2M_1^2\left(M_2^2+s\right)+\left(M_2^2-s\right)^2\right)+M_1^2M_2^2s}{s}\times\\
&\qquad\qquad\times C_0\left(m^2,m^2,s;M_2,m,M_1\right)\Bigg]\Bigg\},
\end{aligned}
\tag{E.60}
$$

$$
\begin{aligned}
F^{\rho}_{2,fSS}=\frac{g_X g_f^{\rho} g_{\bar f}^{\rho}}{s-4m^2}\Bigg\{&-2m^2\Lambda(s;M_1,M_2)+\frac{1}{2}\left(-4m^2+M_1^2+M_2^2\right)\log\left(\frac{m^2}{M_1^2}\right)+\\
&-\frac{2m^2\left(-M_1^2+M_2^2+s\right)-M_2^2s}{2s}\ln\left(\frac{M_1^2}{M_2^2}\right)+\\
&+m^2\Lambda\left(m^2;m,M_1\right)+m^2\Lambda\left(m^2;m,M_2\right)+\\
&+m^2\left(M_1^2+M_2^2-s\right)C_0\left(m^2,m^2,s;M_2,m,M_1\right)\Bigg\}+
\end{aligned}
$$

$$
\begin{aligned}
&+\frac{g_X g_f^{\rho} g_{\bar f}^{-\rho}}{\left(s-4m^2\right)^2}\times\\
&\times\Bigg\{-\frac{\left(s-4m^2\right)\left(2m^2\left(M_1^2-M_2^2-s\right)+M_2^2s\right)}{2s}+\\
&\quad+\frac{m^2\left(8m^2\left(M_1^2-M_2^2+s\right)+s\left(-5M_1^2-M_2^2+s\right)\right)}{2s}\Lambda(s;M_1,M_2)+\\
&\quad+\frac{1}{4s^2m^2}\Big[-8m^6\left(M_1^4-2M_1^2M_2^2+M_2^4-2M_2^2s-s^2\right)+m^2M_2^2s^2\left(2M_1^2+7M_2^2+2s\right)+\\
&\qquad\qquad-M_2^4s^3+m^4s\left(5M_1^4-6M_1^2\left(M_2^2+s\right)-7M_2^4-18M_2^2s+s^2\right)\Big]\ln\left(\frac{M_1^2}{M_2^2}\right)+\\
&\quad+\frac{1}{4sm^2}\Big[16m^6s+m^2s\left(M_1^4+2M_1^2M_2^2+7M_2^4+2M_2^2s\right)-M_2^4s^2+\\
&\qquad\qquad+2m^4\left(M_1^4+2M_1^2\left(M_2^2-3s\right)-3M_2^4-10M_2^2s+s^2\right)\Big]\ln\left(\frac{m^2}{M_1^2}\right)+\\
&\quad+\frac{2m^4\left(M_1^2+3M_2^2-3s\right)+m^2M_1^2s}{2s}\Lambda\left(m^2;m,M_1\right)+
\end{aligned}
$$

$$+\frac{-2m^4\left(M_1^2+3\left(M_2^2+s\right)\right)+m^2s\left(2M_1^2+7M_2^2\right)-M_2^2s^2}{2s}\Lambda\left(m^2;m,M_2\right)+$$

$$-\frac{m^2\left(m^2\left(M_1^4+2M_1^2\left(M_2^2+s\right)-3\left(M_2^2-s\right)^2\right)+M_1^2s\left(-M_1^2-2M_2^2+s\right)\right)}{s}\times$$

$$\left.\times C_0\left(m^2,m^2,s;M_2,m,M_1\right)\right\}+$$

$$+\frac{g_X g_f^{-\rho}g_{\bar{f}}^{\rho}}{\left(s-4m^2\right)^2}\times$$

$$\times\left\{-\frac{\left(s-4m^2\right)\left(M_1^2s-2m^2\left(M_1^2-M_2^2+s\right)\right)}{2s}+\right.$$

$$+\frac{m^2\left(8m^2\left(-M_1^2+M_2^2+s\right)+s\left(-M_1^2-5M_2^2+s\right)\right)}{2s}\Lambda(s;M_1,M_2)+$$

$$+\frac{1}{4s^2}\Big[m^2s\left(M_1^4+2M_1^2\left(5M_2^2-s\right)-3M_2^4-6M_2^2s+s^2\right)+$$

$$+M_2^4s^2+8m^4\left(M_1^4-2M_1^2\left(M_2^2+s\right)+M_2^4+s^2\right)\Big]\ln\left(\frac{M_1^2}{M_2^2}\right)+$$

$$+\frac{1}{4sm^2}\Big[16m^6s+m^2s\left(7M_1^4+2M_1^2\left(M_2^2+s\right)+M_2^4\right)-M_1^4s^2+$$

$$+2m^4\left(-3M_1^4+2M_1^2\left(M_2^2-5s\right)+M_2^4-6M_2^2s+s^2\right)\Big]\ln\left(\frac{m^2}{M_1^2}\right)+$$

$$+\frac{-2m^4\left(3M_1^2+M_2^2+3s\right)+m^2s\left(7M_1^2+2M_2^2\right)-M_1^2s^2}{2s}\Lambda\left(m^2;m,M_1\right)+$$

$$+\frac{2m^4\left(3M_1^2+M_2^2-3s\right)+m^2M_2^2s}{2s}\Lambda\left(m^2;m,M_2\right)+$$

$$+\frac{m^2\left(m^2\left(3M_1^4-2M_1^2\left(M_2^2+3s\right)-M_2^4-2M_2^2s+3s^2\right)+M_2^2s\left(2M_1^2+M_2^2-s\right)\right)}{s}\times$$

$$\left.\times C_0\left(m^2,m^2,s;M_2,m,M_1\right)\right\}, \tag{E.61}$$

E.4 Box diagrams

There are 2 types of box diagrams we need to consider:

- **Charged box**: the internal lines are 2 massless fermions and 2 massive gauge bosons (with equal masses M and gauge parameters ξ). For this type we only need the *crossed type* (see below). The charged box type corresponds to the WW-box.

- **Neutral box**: the internal lines are 1 massless fermion, 1 massive fermion and 2 massive gauge bosons (with equal masses M and gauge parameters ξ). Both requires *crossed* and *direct type* are required (see below). The neutral box type corresponds to the ZZ-boxes.

For the boxes there is a distinction according to the relative orientation of the virtual fermion lines into crossed type (fermion lines point in opposite direction clockwise) and direct type (where the orientation of both fermion lines is (counter-)clockwise). The box results are quoted in terms of chiral form factors

(for the definition of the amplitude basis see main text)

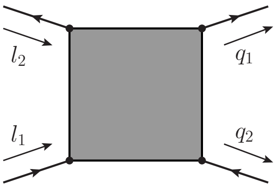

$$= i\frac{\alpha^2}{s}\left[F_1^{\rho\kappa}\,\bar{M}_1^{\rho\kappa} + F_2^{\rho\kappa}\,\bar{M}_2^{\rho\kappa}\right]. \tag{E.62}$$

Again we give Feynman-gauge results for the chiral form factors separately from the additional gauge parts (cf. eq. E.29).

E.4.1 Charged box

E.4.1.1 Crossed type

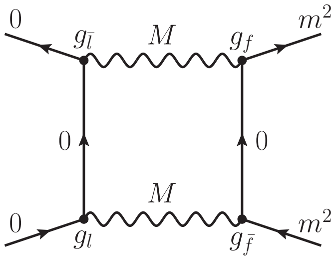

$$F_{1,c}^{\rho\kappa,\xi=1} = g_l^\kappa g_{\bar{l}}^\kappa g_f^\rho g_{\bar{f}}^\rho \times$$

$$\times\Bigg\{ -2s\,\delta_{\kappa,\rho}\Big(C_0(0,0,s;M,0,M) + C_0\left(m^2,m^2,s;M,0,M\right) +$$

$$- u\,D_0\left(0,0,m^2,m^2;s,u;M,0,M,0\right)\Big) +$$

$$+ \frac{su\,\delta_{\kappa,-\rho}}{m^4 - tu}\times$$

$$\times\Bigg[-2\Lambda(s;M,M) + \frac{4\left(m^2-M^2\right)}{m^2-u}\ln\left(\frac{M^2}{M^2-m^2-i0^+}\right) - \frac{2\left(m^2+u\right)}{m^2-u}\ln\left(\frac{M^2}{-u-i0^+}\right) +$$

$$- \frac{2m^6\left(M^2+u\right) - 2m^4u\left(2M^2+t\right) - 2m^2u^2\left(M^2+u\right) + u^2\left(2M^2(t+u)+t^2+u^2\right)}{u\left(m^4-tu\right)}\times$$

$$\times C_0(0,0,s;M,0,M) +$$

$$- \frac{2}{\left(m^2-u\right)\left(m^4-tu\right)}\Big(-2m^8 + 2m^6\left(2M^2+u\right) + m^4u\left(-2M^2+t+u\right) +$$

$$- 2m^2u\left(M^2(t+u)+u^2\right) + u^3\left(2M^2-t+u\right)\Big)\times$$

$$\times C_0\left(0,m^2,u;0,M,0\right) +$$

$$- \frac{1}{u\left(m^4-tu\right)}\Big(2m^8 - 2m^6\left(M^2-u\right) + 2m^2u^2\left(M^2-t\right) +$$

$$+ u^2\left(2M^2(t+u)+t^2+u^2\right) - 2m^4u\left(2M^2+t+u\right)\Big)\times$$

$$
\begin{aligned}
&\times C_0\left(m^2,m^2,s;M,0,M\right)+\\
&+\frac{1}{m^4-tu}\Big(2m^6\left(3M^2+u\right)-2m^4\left(3M^4+2M^2u+tu\right)-2m^2u\left(M^2(t+2u)+u^2\right)+\\
&+u\left(2M^4(t+2u)+4M^2u^2+u\left(t^2+u^2\right)\right)\Big)\times\\
&\times D_0\left(0,0,m^2,m^2;s,u;M,0,M,0\right)\Bigg]+
\end{aligned}
$$

$$
\begin{aligned}
&+\frac{g_l^{\kappa}g_{\bar{l}}^{\kappa}g_f^{-\rho}g_{\bar{f}}^{-\rho}\,\delta_{\kappa,\rho}\,m^2s}{m^4-tu}\times\\
&\times\Bigg\{-2\Lambda(s;M,M)+\frac{4\left(m^2-M^2\right)}{m^2-u}\ln\left(\frac{M^2}{M^2-m^2-i0^+}\right)-\frac{2\left(m^2+u\right)}{m^2-u}\ln\left(\frac{M^2}{-u-i0^+}\right)+\\
&+\frac{m^4\left(2M^2+t-u\right)-2m^2\left(M^2+u\right)(t-u)+u^2\left(-2M^2+t-u\right)}{m^4-tu}\times\\
&\times C_0(0,0,s;M,0,M)+\\
&+\frac{2}{\left(m^2-u\right)\left(m^4-tu\right)}\Big(m^8-2m^6M^2-2m^4u^2+2m^2u^2\left(M^2-t+u\right)+\\
&-u^2\left(u(u-2t)-2M^2(t-u)\right)\Big)C_0\left(0,m^2,u;0,M,0\right)\\
&-\frac{1}{m^4-tu}\Big(2m^6+m^4\left(-2M^2+t-u\right)-2m^2\left(M^2(t-u)+tu\right)+u^2\left(2M^2-t+u\right)\Big)+\\
&\times C_0\left(m^2,m^2,s;M,0,M\right)+\\
&+\frac{1}{s\left(m^4-tu\right)}\Big(4m^8M^2-2m^6\left(M^2+u\right)\left(2M^2+t-u\right)+\\
&-2m^2u\left(M^2+u\right)\left(2M^2(t-2u)+t^2+tu-2u^2\right)+\\
&+m^4\left(2M^4(t+u)+4M^2u(t-2u)+u\left(t^2+4tu-5u^2\right)\right)+\\
&-u\left(M^4\left(-2t^2+2tu+4u^2\right)+M^2\left(4u^3-4t^2u\right)-t^2u^2+u^4\right)\Big)\times\\
&\times D_0\left(0,0,m^2,m^2;s,u;M,0,M,0\right)\,,
\end{aligned}
\tag{E.63}
$$

$$
\begin{aligned}
F_{2,c}^{\rho\kappa,\xi=1}&=\frac{\left(g_l^{\kappa}g_{\bar{l}}^{\kappa}g_f^{\rho}g_{\bar{f}}^{\rho}\,\delta_{\kappa,-\rho}+g_l^{\kappa}g_{\bar{l}}^{\kappa}g_f^{-\rho}g_{\bar{f}}^{-\rho}\,\delta_{\kappa,\rho}\right)m^2su}{m^4-tu}\times\\
&\times\Bigg\{-\frac{2\left(m^2+u\right)}{u\left(s-4m^2\right)}\Lambda(s;M,M)+\frac{2}{m^2-u}\ln\left(\frac{M^2}{-u-i0^+}\right)+\\
&+\frac{2\left(m^2-M^2\right)\left(m^4+2m^2u+tu\right)}{m^2u\left(s-4m^2\right)\left(m^2-u\right)}\ln\left(\frac{M^2}{M^2-m^2-i0^+}\right)+\\
&-\frac{m^6-m^4\left(M^2+3u\right)+m^2u\left(2M^2+3u\right)-u\left(M^2(u-s)+u^2\right)}{u\left(m^4-tu\right)}C_0(0,0,s;M,0,M)+\\
&-\frac{2\left(2m^6-m^4\left(3M^2+4u\right)+m^2u\left(4M^2-t+3u\right)+u\left(M^2(t-2u)+u(t-u)\right)\right)}{\left(m^2-u\right)\left(m^4-tu\right)}\times
\end{aligned}
$$

$$\times C_0\left(0, m^2, u; 0, M, 0\right) +$$

$$- \frac{1}{u\left(s-4m^2\right)\left(m^4-tu\right)}\Big(4m^8 + m^6\left(-4M^2+t+u\right) - m^4\left(M^2(t+3u)+3u(t+u)\right) +$$

$$+ m^2u^2\left(4M^2-3t+u\right) + u\left(M^2\left(-t^2+3tu+2u^2\right)+u^2(t+u)\right)\Big)\times$$

$$\times C_0\left(m^2, m^2, s; M, 0, M\right) +$$

$$+ \frac{m^6 - m^4\left(5M^2+3u\right) + m^2\left(4M^4+10M^2u+3u^2\right) - u\left(4M^4+M^2(s+5u)+u^2\right)}{m^4-tu}\times$$

$$\times D_0\left(0, 0, m^2, m^2; s, u; M, 0, M, 0\right) \tag{E.64}$$

$$\Delta F_{1,c}^{\rho\kappa,\xi} = \frac{g_l^\kappa g_{\bar{l}}^\kappa g_f^\rho g_{\bar{f}}^\rho}{M^2\left(s-4m^2\right)}\times$$

$$\times\Bigg\{ - \frac{M^2\left(s-4m^2\right)}{6}(\xi-1)^2 + \frac{s\left(s\left(20M^2+s\right)-4m^2\left(14M^2+s\right)\right)}{12M^2}\Lambda(s;M,M)+$$

$$- \frac{s\left(M^4(\xi-1)^2-2M^2(\xi-5)s+s^2\right)-4m^2\left(M^4(\xi-1)^2+M^2(7-2\xi)s+s^2\right)}{6M^2}\times$$

$$\times\Lambda\left(s; M, M\sqrt{\xi}\right) +$$

$$+ \frac{s\left(s-4m^2\right)\left(s-4M^2\xi\right)}{12M^2}\Lambda\left(s; M\sqrt{\xi}, M\sqrt{\xi}\right) +$$

$$- 2\left(M^2-m^2\right)\left(2m^2-s\right)\ln\left(\frac{M^2}{M^2-m^2-i0^+}\right) +$$

$$- 2\left(2m^2-s\right)\left(m^2-M^2\xi\right)\ln\left(\frac{M^2\xi}{M^2\xi-m^2-i0^+}\right) +$$

$$- \frac{1}{12s}\Big(- 48m^4s + 4m^2\left(M^4(\xi-1)^3 - 3M^2\left(\xi^2-3\xi+2\right)s + 3(\xi+4)s^2\right) +$$

$$+ s\left(-M^4(\xi-1)^3 + 3M^2\left(\xi^2-4\xi+3\right)s - 3(\xi+3)s^2\right)\Big)\ln(\xi)+$$

$$+ 2m^2s\left(m^2-M^2\right)C_0\left(m^2, m^2, s; M, 0, M\right) +$$

$$- \left(m^4\left(2s-4M^2(\xi-1)\right) - 2m^2M^2s\right)C_0\left(m^2, m^2, s; M\sqrt{\xi}, 0, M\right) +$$

$$+ \frac{g_l^\kappa g_{\bar{l}}^\kappa g_f^{-\rho} g_{\bar{f}}^{-\rho}}{M^2\left(s-4m^2\right)}\times$$

$$\times\Bigg\{ \frac{m^2s\left(2m^2-6M^2-s\right)}{4M^2}\Lambda(s;M,M) - \frac{m^2s\left(2m^2+M^2(\xi-3)-s\right)}{2M^2}\Lambda\left(s; M, M\sqrt{\xi}\right) +$$

$$+ \frac{m^2s\left(2m^2+2M^2\xi-s\right)}{4M^2}\Lambda\left(s; M\sqrt{\xi}, M\sqrt{\xi}\right) +$$

$$+ m^2(\xi+3)\left(m^2-M^2\right)\ln\left(\frac{M^2}{M^2-m^2-i0^+}\right) +$$

$$
\begin{aligned}
&- m^2(\xi+3)\left(m^2-M^2\xi\right)\ln\left(\frac{M^2\xi}{M^2\xi-m^2-i0^+}\right)+\\
&+\frac{1}{4}m^2\left(2m^2(3\xi+5)+M^2\left(\xi^2-4\xi+3\right)-2(\xi+1)s\right)\ln(\xi)+\\
&-\frac{m^2s\left(m^2-M^2\right)\left(m^2+3M^2\right)}{2M^2}C_0\left(m^2,m^2,s;M,0,M\right)+\\
&-\frac{\left(-m^6s-m^4M^2(\xi-1)\left(M^2(\xi+3)-s\right)+m^2M^4\xi s\right)}{M^2}C_0\left(m^2,m^2,s;M\sqrt{\xi},0,M\right)+\\
&-\frac{m^2s\left(m^2-M^2\xi\right)^2}{2M^2}C_0\left(m^2,m^2,s;M\sqrt{\xi},0,M\sqrt{\xi}\right)\Bigg\},
\end{aligned}
\tag{E.65}
$$

$$
\begin{aligned}
\Delta F_{2,c}^{\rho\kappa,\xi} =& \frac{\left(g_l^\kappa g_{\bar{l}}^\kappa g_f^\rho g_{\bar{f}}^\rho + g_l^\kappa g_{\bar{l}}^\kappa g_f^{-\rho} g_{\bar{f}}^{-\rho}\right)}{2M^2\left(s-4m^2\right)^2}\times\\
&\times\Bigg\{-\frac{s\left(2m^6+m^4\left(10M^2+s\right)-4m^2M^2s\right)}{2M^2}\Lambda(s;M,M)+\\
&+\frac{s\left(2m^6+m^4\left(M^2(5-3\xi)+s\right)-2m^2M^2s\right)}{M^2}\Lambda\left(s;M,M\sqrt{\xi}\right)+\\
&-\frac{m^4s\left(2m^2-6M^2\xi+s\right)}{2M^2}\Lambda\left(s;M\sqrt{\xi},M\sqrt{\xi}\right)+\\
&+m^2\left(m^2-M^2\right)\left(2m^2(\xi+7)+(\xi-5)s\right)\ln\left(\frac{M^2}{M^2-m^2-i0^+}\right)+\\
&-m^2\left(m^2-M^2\xi\right)\left(2m^2(\xi+7)+(\xi-5)s\right)\ln\left(\frac{M^2\xi}{M^2\xi-m^2-i0^+}\right)+\\
&+\frac{1}{2}m^2\left(2m^4(\xi+15)+m^2\left(M^2\left(3\xi^2-8\xi+5\right)-2(\xi+7)s\right)+2s\left(M^2(\xi-1)+s\right)\right)\ln(\xi)+\\
&+\frac{s\left(m^2-M^2\right)\left(m^6-m^4\left(5M^2+s\right)+2m^2M^2s\right)}{M^2}C_0\left(m^2,m^2,s;M,0,M\right)+\\
&+\frac{1}{M^2}\Big(-2m^8s+2m^6\Big(M^4\left(\xi^2+6\xi-7\right)-M^2(\xi-3)s+s^2\Big)+\\
&\qquad+m^4M^2s\left(M^2\left(\xi^2-8\xi+5\right)-(\xi+3)s\right)+2m^2M^4\xi s^2\Big)C_0\left(m^2,m^2,s;M\sqrt{\xi},0,M\right)+\\
&+\frac{m^4s\left(m^2-M^2\xi\right)\left(m^2+3M^2\xi-s\right)}{M^2}C_0\left(m^2,m^2,s;M\sqrt{\xi},0,M\sqrt{\xi}\right)\Bigg\},
\end{aligned}
\tag{E.66}
$$

E.4.2 Neutral

E.4.2.1 Crossed type

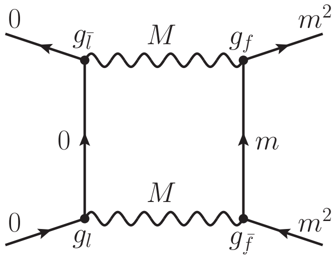

$$
\begin{aligned}
F_{1,c}^{\rho\kappa,\xi=1} = \delta_{\rho,\kappa}\Bigg\{ & -2s\, g_l^{\kappa} g_{\bar{l}}^{\kappa} g_f^{\rho} g_{\bar{f}}^{\rho}\Big[C_0\left(m^2,m^2,s;M,m,M\right)+C_0(0,0,s;M,0,M)+ \\
& \qquad +\left(m^2-u\right)D_0\left(0,0,m^2,m^2;s,u;M,0,M,m\right)\Big]+ \\
& +\frac{\left(g_l^{\kappa}g_{\bar{l}}^{\kappa}g_f^{\rho}g_{\bar{f}}^{-\rho}+g_l^{\kappa}g_{\bar{l}}^{\kappa}g_f^{-\rho}g_{\bar{f}}^{\rho}\right)m^2 s}{m^4-tu}\times \\
& \times\Big[\left(m^2-t\right)C_0(0,0,s;M,0,M)-2m^2C_0\left(0,m^2,u;0,M,m\right)+ \\
& +\left(m^2+t\right)C_0\left(m^2,m^2,s;M,m,M\right)+ \\
& +\left(m^4-m^2\left(2M^2+t+u\right)+tu\right)D_0\left(0,0,m^2,m^2;s,u;M,0,M,m\right)\Big]+ \\
& +\frac{g_l^{\kappa}g_{\bar{l}}^{\kappa}g_f^{-\rho}g_{\bar{f}}^{-\rho}\,m^2 s}{m^4-tu}\Bigg[-2\Lambda(s;M,M)+\frac{4m^2}{m^2-u}\,\Lambda\left(m^2;m,M\right)+ \\
& -\frac{2\left(m^2-M^2-u\right)}{m^2-u}\ln\left(\frac{m^2}{M^2}\right)+\frac{2\left(m^2+u\right)}{u}\ln\left(\frac{m^2}{m^2-u-i0^+}\right)+ \\
& +\frac{m^4\left(2M^2+3t-3u\right)-m^2(t-u)\left(2M^2+t+3u\right)+u^2\left(-2M^2+t-u\right)}{m^4-tu}\times \\
& \qquad\qquad \times C_0(0,0,s;M,0,M)+ \\
& +\frac{2}{\left(m^2-u\right)\left(m^4-tu\right)}\Big(m^8+m^6\left(-2M^2-t+u\right)+2m^4u(t-2u)+ \\
& \qquad +m^2u^2\left(2M^2-3t+3u\right)-u^2\left(u(u-2t)-2M^2(t-u)\right)\Big)\times \\
& \qquad\qquad \times C_0\left(0,m^2,u;0,M,m\right)+ \\
& -\frac{1}{m^4-tu}\Big(4m^6+m^4\left(-2M^2+t-u\right)+u^2\left(2M^2-t+u\right)+ \\
& \qquad -m^2\left(2M^2(t-u)+(t+u)^2\right)\Big)\times \\
& \qquad\qquad \times C_0\left(m^2,m^2,s;M,m,M\right)+ \\
& +\frac{1}{m^4-tu}\Big(m^6\left(4M^2+3t-3u\right)-m^4\left(2M^4+4M^2(t-u)+t^2+5tu-6u^2\right)+ \\
& \qquad +m^2u\left(4M^2(t-2u)+t^2+3tu-4u^2\right)+
\end{aligned}
$$

$$+ u\left(-2M^4(t-2u)+4M^2u(u-t)+u^2(u-t)\right)\Big)\times$$

$$\times D_0\left(0,0,m^2,m^2;s,u;M,0,M,m\right)\Bigg]\Bigg\}+$$

$$+ \delta_{-\rho,\kappa}\Bigg\{\frac{\left(g_l^\kappa g_{\bar{l}}^\kappa g_f^\rho g_{\bar{f}}^{-\rho}+g_l^\kappa g_{\bar{l}}^\kappa g_f^{-\rho} g_{\bar{f}}^{\rho}\right)m^2 s}{m^4-tu}\times$$

$$\times\Big[\left(u-m^2\right)C_0(0,0,s;M,0,M)-2uC_0\left(0,m^2,u;0,M,m\right)+$$

$$+\left(m^2+u\right)C_0\left(m^2,m^2,s;M,m,M\right)+$$

$$-\left(m^4-2m^2u+u\left(2M^2+u\right)\right)D_0\left(0,0,m^2,m^2;s,u;M,0,M,m\right)\Big]+$$

$$+\frac{g_l^\kappa g_{\bar{l}}^\kappa g_f^\rho g_{\bar{f}}^\rho s}{m^4-tu}\Bigg[-2u\,\Lambda(s;M,M)+\frac{4m^2u}{m^2-u}\Lambda\left(m^2;m,M\right)+$$

$$-\frac{2u\left(m^2-M^2-u\right)}{m^2-u}\ln\left(\frac{m^2}{M^2}\right)+2\left(m^2+u\right)\ln\left(\frac{m^2}{m^2-u-i0^+}\right)+$$

$$+\frac{1}{m^4-tu}\Big(2m^8-m^6\left(2M^2+t+3u\right)+2m^4u\left(2M^2+t-u\right)+$$

$$+m^2u^2\left(2M^2+t+3u\right)-u^2\left(2M^2(t+u)+t^2+u^2\right)\Big)\times$$

$$\times C_0(0,0,s;M,0,M)+$$

$$-\frac{2}{\left(m^2-u\right)\left(m^4-tu\right)}\Big(m^{10}-4m^8u+2m^6u\left(2M^2+u\right)+u^4\left(2M^2-t+u\right)+$$

$$+m^4u^2\left(-2M^2+t+3u\right)-m^2u^2\left(2M^2(t+u)+3u^2\right)\Big)\times$$

$$\times C_0\left(0,m^2,u;0,M,m\right)+$$

$$-\frac{1}{m^4-tu}\Big(2m^8-m^6\left(2M^2+t-5u\right)+m^2u^2\left(2M^2-3t-u\right)+$$

$$-2m^4u\left(2M^2+t+u\right)+u^2\left(2M^2(t+u)+t^2+u^2\right)\Big)\times$$

$$\times C_0\left(m^2,m^2,s;M,m,M\right)+$$

$$+\frac{1}{m^4-tu}\Big(2m^{10}-m^8\left(4M^2+t+5u\right)+m^6u\left(12M^2+3t+u\right)+$$

$$-m^2u^2\left(4M^2(t+2u)+t^2+tu+4u^2\right)-m^4u\left(6M^4+u(t-5u)\right)+$$

$$+u^2\left(2M^4(t+2u)+4M^2u^2+u\left(t^2+u^2\right)\right)\Big)\times$$

$$\times D_0\left(0,0,m^2,m^2;s,u;M,0,M,m\right)\Bigg]\Bigg\}, \tag{E.67}$$

$$F_{2,c}^{\rho\kappa,\xi=1}=\frac{g_l^\kappa g_{\bar{l}}^\kappa g_f^{-\rho} g_{\bar{f}}^\rho m^2 s}{m^4-tu}\Big[\left(m^2-u\right)C_0(0,0,s;M,0,M)+2u\,C_0\left(0,m^2,u;0,M,m\right)+$$

$$- \left(m^2+u\right) C_0\left(m^2,m^2,s;M,m,M\right)+$$

$$+\left(m^4-2m^2u+u\left(2M^2+u\right)\right) D_0\left(0,0,m^2,m^2;s,u;M,0,M,m\right)\Big]+$$

$$+\frac{\left(g_l^\kappa g_{\bar{l}}^\kappa g_f^\rho g_{\bar{f}}^\rho\,\delta_{\kappa,-\rho}+g_l^\kappa g_{\bar{l}}^\kappa g_f^{-\rho} g_{\bar{f}}^{-\rho}\,\delta_{\kappa,\rho}\right) m^2 s}{m^4-tu}\times$$

$$\times\Bigg\{-\frac{2\left(m^2+u\right)}{s-4m^2}\Lambda(s;M,M)+\frac{2\left(m^4+2m^2u+tu\right)}{\left(s-4m^2\right)\left(m^2-u\right)}\Lambda\left(m^2;m,M\right)+$$

$$-\frac{2m^6-m^4M^2-2m^2u\left(M^2+u\right)-M^2tu}{m^2\left(s-4m^2\right)\left(m^2-u\right)}\ln\left(\frac{m^2}{M^2}\right)-2\ln\left(\frac{m^2}{m^2-u-i0^+}\right)+$$

$$-\frac{m^6+m^4\left(-M^2+s-3u\right)+m^2u\left(2M^2-s+3u\right)-u\left(M^2(u-s)+u^2\right)}{m^4-tu}\times$$

$$\times C_0(0,0,s;M,0,M)+$$

$$+\frac{2\left(m^8-5m^6u+m^4u\left(3M^2+7u\right)+m^2u^2\left(-4M^2+t-4u\right)+u^2\left(u(u-t)-M^2(t-2u)\right)\right)}{\left(m^2-u\right)\left(m^4-tu\right)}\times$$

$$\times C_0\left(0,m^2,u;0,M,m\right)+$$

$$-\frac{1}{\left(s-4m^2\right)\left(m^4-tu\right)}\Big(6m^8-m^6\left(4M^2+t-5u\right)+m^2u\left(4M^2u+t^2-5tu\right)+$$

$$+u\left(M^2\left(-t^2+3tu+2u^2\right)+u^2(t+u)\right)+$$

$$-m^4\left(M^2(t+3u)+t^2+3tu+4u^2\right)\Big)\times$$

$$\times C_0\left(m^2,m^2,s;M,m,M\right)+$$

$$-\frac{1}{m^4-tu}\Big(m^8+m^6\left(-3M^2+s-4u\right)+m^4u\left(11M^2-2s+6u\right)+$$

$$+m^2u\left(-4M^4+M^2(s-13u)+u(s-4u)\right)+$$

$$+u^2\left(4M^4+M^2(s+5u)+u^2\right)\Big)D_0\left(0,0,m^2,m^2;s,u;M,0,M,m\right)\Bigg\}, \qquad \text{(E.68)}$$

$$\Delta F_{1,c}^{\rho\kappa,\xi}=\frac{g_l^\kappa g_{\bar{l}}^\kappa g_f^\rho g_{\bar{f}}^\rho}{s-4m^2}\times$$

$$\times\Bigg\{-\frac{s-4m^2}{6}(\xi-1)^2+\frac{s\left(s\left(20M^2+s\right)-m^2\left(50M^2+7s\right)\right)}{12M^4}\Lambda(s;M,M)+$$

$$-\frac{s\left(M^4(\xi-1)^2-2M^2(\xi-5)s+s^2\right)-m^2\left(4M^4(\xi-1)^2+M^2(25-11\xi)s+7s^2\right)}{6M^4}\times$$

$$\times\Lambda\left(s;M,M\sqrt{\xi}\right)$$

$$+\frac{s\left(m^2\left(22M^2\xi-7s\right)+s\left(s-4M^2\xi\right)\right)}{12M^4}\Lambda\left(s;M\sqrt{\xi},M\sqrt{\xi}\right)+$$

$$-\frac{1}{2}(\xi-1)\left(m^2(\xi+3)-2s\right)\ln\left(\frac{m^2}{M^2}\right)-\frac{2m^2s-m^4(\xi+3)}{M^2}\Lambda\left(m^2;m,M\right)+$$

$$-\frac{m^4(\xi+3)-2m^2s}{M^2}\Lambda\left(m^2;m,M\sqrt{\xi}\right)+$$

$$-\frac{1}{12M^2s}\Big(m^2\left(4M^4(\xi-1)^3-3M^2\left(7\xi^2-6\xi+7\right)s+18(\xi+1)s^2\right)+$$

$$+s\left(-M^4(\xi-1)^3+3M^2\left(\xi^2+3\right)s-3(\xi+3)s^2\right)\Big)\ln(\xi)+$$

$$-\frac{m^2s\left(m^2\left(4M^2+s\right)+5M^4-4M^2s\right)}{2M^4}C_0\left(m^2,m^2,s;M,m,M\right)+$$

$$+\frac{m^2\left(m^2\left(M^4\left(\xi^2+2\xi-3\right)-2M^2(\xi-1)s+s^2\right)+M^2s\left(M^2(\xi+2)-2s\right)\right)}{M^4}\times$$

$$\times C_0\left(m^2,m^2,s;M\sqrt{\xi},m,M\right)+$$

$$-\frac{m^2s\left(m^2\left(s-4M^2\xi\right)+M^4\xi^2\right)}{2M^4}C_0\left(m^2,m^2,s;M\sqrt{\xi},m,M\sqrt{\xi}\right)\Bigg\}+$$

$$+\frac{g_l^\kappa g_{\bar{l}}^\kappa g_f^{-\rho}g_{\bar{f}}^{-\rho}}{s-4m^2}\times$$

$$\times\Bigg\{-\frac{m^2s\left(6M^2+s\right)}{4M^4}\Lambda(s;M,M)+\frac{m^2s\left(s-M^2(\xi-3)\right)}{2M^4}\Lambda\left(s;M,M\sqrt{\xi}\right)+$$

$$-\frac{m^2s\left(s-2M^2\xi\right)}{4M^4}\Lambda\left(s;M\sqrt{\xi},M\sqrt{\xi}\right)-\frac{1}{2}m^2\left(\xi^2+2\xi-3\right)\ln\left(\frac{m^2}{M^2}\right)+$$

$$+\frac{m^4(\xi+3)}{M^2}\Lambda\left(m^2;m,M\right)-\frac{m^4(\xi+3)}{M^2}\Lambda\left(m^2;m,M\sqrt{\xi}\right)+$$

$$+\frac{m^2\left(M^2\left(3\xi^2+2\xi+3\right)-2(\xi+1)s\right)}{4M^2}\ln(\xi)+$$

$$-\frac{m^2s\left(m^2\left(4M^2+s\right)-3M^4\right)}{2M^4}C_0\left(m^2,m^2,s;M,m,M\right)+$$

$$-\frac{m^2M^4\xi s-m^4\left(M^4\left(\xi^2+2\xi-3\right)-2M^2(\xi-1)s+s^2\right)}{M^4}C_0\left(m^2,m^2,s;M\sqrt{\xi},m,M\right)+$$

$$-\frac{m^2s\left(m^2\left(s-4M^2\xi\right)+M^4\xi^2\right)}{2M^4}C_0\left(m^2,m^2,s;M\sqrt{\xi},m,M\sqrt{\xi}\right)\Bigg\}+$$

$$+\frac{\left(g_l^\kappa g_{\bar{l}}^\kappa g_f^\rho g_{\bar{f}}^{-\rho}+g_l^\kappa g_{\bar{l}}^\kappa g_f^{-\rho}g_{\bar{f}}^\rho\right)}{s-4m^2}\times$$

$$\times\Bigg\{\frac{m^2s\left(s-2M^2\right)}{4M^4}\Lambda(s;M,M)-\frac{m^2s\left(s-M^2(\xi+1)\right)}{2M^4}\Lambda\left(s;M,M\sqrt{\xi}\right)+$$

$$+\frac{m^2s\left(s-2M^2\xi\right)}{4M^4}\Lambda\left(s;M\sqrt{\xi},M\sqrt{\xi}\right)+\frac{1}{2}(\xi-1)\left(m^2(\xi+3)-s\right)\ln\left(\frac{m^2}{M^2}\right)+$$

$$-\frac{m^4(\xi+3)-m^2s}{M^2}\Lambda\left(m^2;m,M\right)-\frac{m^2s-m^4(\xi+3)}{M^2}\Lambda\left(m^2;m,M\sqrt{\xi}\right)+$$

$$-\frac{m^2\left(M^2\left(3\xi^2+6\xi-1\right)-2(\xi-1)s\right)-2M^2\xi s}{4M^2}\ln(\xi)+$$

$$+\frac{m^2 s\left(m^2\left(4M^2+s\right)+M^4-2M^2 s\right)}{2M^4}C_0\left(m^2,m^2,s;M,m,M\right)+$$

$$-\frac{m^2\left(m^2\left(M^4\left(\xi^2+2\xi-3\right)-2M^2(\xi-1)s+s^2\right)+M^2 s\left(M^2-s\right)\right)}{M^4}\times$$

$$\times C_0\left(m^2,m^2,s;M\sqrt{\xi},m,M\right)+$$

$$+\frac{m^2 s\left(m^2\left(s-4M^2\xi\right)+M^4\xi^2\right)}{2M^4}C_0\left(m^2,m^2,s;M\sqrt{\xi},m,M\sqrt{\xi}\right)\Bigg\}, \qquad \text{(E.69)}$$

$$\Delta F_{2,c}^{\rho\kappa,\xi}=\frac{g_l^\kappa g_{\bar{l}}^\kappa g_f^{-\rho} g_{\bar{f}}^\rho}{\left(s-4m^2\right)^2}\times$$

$$\times\Bigg\{\frac{s\left(m^4\left(10M^2+3s\right)-4m^2M^2 s\right)}{2M^4}\Lambda(s;M,M)+$$

$$+\frac{s\left(m^4\left(M^2(3\xi-5)-3s\right)+2m^2M^2 s\right)}{M^4}\Lambda\left(s;M,M\sqrt{\xi}\right)+$$

$$+\frac{3m^4 s\left(s-2M^2\xi\right)}{2M^4}\Lambda\left(s;M\sqrt{\xi},M\sqrt{\xi}\right)+$$

$$+\frac{1}{2}m^2(\xi-1)\left(2m^2(\xi+7)+(\xi-5)s\right)\ln\left(\frac{m^2}{M^2}\right)+$$

$$-\frac{m^4\left(2m^2(\xi+7)+(\xi-5)s\right)}{M^2}\Lambda\left(m^2;m,M\right)+$$

$$+\frac{m^4\left(2m^2(\xi+7)+(\xi-5)s\right)}{M^2}\Lambda\left(m^2;m,M\sqrt{\xi}\right)+$$

$$-\frac{m^2\left(m^2\left(M^2\left(5\xi^2+6\xi+5\right)-2(3\xi s+s)\right)+s\left(M^2\left(\xi^2-3\xi-2\right)+2s\right)\right)}{2M^2}\ln(\xi)+$$

$$+\frac{s\left(2m^6\left(12M^2+s\right)+m^4\left(-10M^4-12M^2 s+s^2\right)+4m^2M^4 s\right)}{2M^4}C_0\left(m^2,m^2,s;M,m,M\right)+$$

$$-\frac{m^2}{M^4}\Big(m^2 s\left(M^4\left(\xi^2-8\xi+5\right)-2M^2(\xi+3)s+s^2\right)+2M^4\xi s^2+$$

$$+2m^4\left(M^4\left(\xi^2+6\xi-7\right)-2M^2(\xi-3)s+s^2\right)\Big)C_0\left(m^2,m^2,s;M\sqrt{\xi},m,M\right)+$$

$$+\frac{m^4 s\left(2m^2\left(s-4M^2\xi\right)+6M^4\xi^2-4M^2\xi s+s^2\right)}{2M^4}C_0\left(m^2,m^2,s;M\sqrt{\xi},m,M\sqrt{\xi}\right)\Bigg\}+$$

$$+\frac{g_l^\kappa g_{\bar{l}}^\kappa g_f^\rho g_{\bar{f}}^{-\rho}}{\left(s-4m^2\right)^2}\times$$

$$\times\Bigg\{\frac{3m^4 s\left(s-2M^2\right)}{2M^4}\Lambda(s;M,M)+\frac{3m^4 s\left(M^2(\xi+1)-s\right)}{M^4}\Lambda\left(s;M,M\sqrt{\xi}\right)+$$

$$+\frac{3m^4 s\left(s-2M^2\xi\right)}{2M^4}\Lambda\left(s;M\sqrt{\xi},M\sqrt{\xi}\right)+\frac{1}{2}m^2(\xi-1)^2\left(2m^2+s\right)\ln\left(\frac{m^2}{M^2}\right)+$$

$$-\frac{m^4(\xi-1)\left(2m^2+s\right)}{M^2}\Lambda\left(m^2;m,M\right)+\frac{m^4(\xi-1)\left(2m^2+s\right)}{M^2}\Lambda\left(m^2;m,M\sqrt{\xi}\right)+$$

$$
\begin{aligned}
&- \frac{m^2(\xi-1)\left(m^2\left(M^2(5\xi+3)-6s\right)+M^2\xi s\right)}{2M^2}\ln(\xi)+ \\
&+ \frac{m^4 s\left(m^2\left(2s-8M^2\right)+6M^4-4M^2 s+s^2\right)}{2M^4} C_0\left(m^2,m^2,s;M,m,M\right)+ \\
&- \frac{m^4\left(2m^2\left(M^4(\xi-1)^2-2M^2(\xi+1)s+s^2\right)+s\left(M^4\left(\xi^2+4\xi+1\right)-2M^2(\xi+1)s+s^2\right)\right)}{M^4}\times \\
&\qquad\qquad\qquad \times C_0\left(m^2,m^2,s;M\sqrt{\xi},m,M\right)+ \\
&+ \frac{m^4 s\left(2m^2\left(s-4M^2\xi\right)+6M^4\xi^2-4M^2\xi s+s^2\right)}{2M^4} C_0\left(m^2,m^2,s;M\sqrt{\xi},m,M\sqrt{\xi}\right)\Bigg\}+ \\
&+ \frac{\left(g_l^\kappa g_{\bar{l}}^\kappa g_f^\rho g_{\bar{f}}^\rho + g_l^\kappa g_{\bar{l}}^\kappa g_f^{-\rho} g_{\bar{f}}^{-\rho}\right)}{\left(s-4m^2\right)^2}\times \\
&\times\Bigg\{ -\frac{s\left(m^4\left(2M^2+3s\right)-2m^2M^2 s\right)}{2M^4}\Lambda(s;M,M)+ \\
&+ \frac{s\left(m^4\left(M^2(1-3\xi)+3s\right)-m^2M^2 s\right)}{M^4}\Lambda\left(s;M,M\sqrt{\xi}\right)+ \\
&- \frac{3m^4 s\left(s-2M^2\xi\right)}{2M^4}\Lambda\left(s;M\sqrt{\xi},M\sqrt{\xi}\right)+ \\
&- \frac{1}{2}m^2(\xi-1)\left(2m^2(\xi+3)+(\xi-3)s\right)\ln\left(\frac{m^2}{M^2}\right)+ \\
&+ \frac{m^4\left(2m^2(\xi+3)+(\xi-3)s\right)}{M^2}\Lambda\left(m^2;m,M\right)+ \\
&- \frac{m^4\left(2m^2(\xi+3)+(\xi-3)s\right)}{M^2}\Lambda\left(m^2;m,M\sqrt{\xi}\right)+ \\
&+ \frac{m^2\left(m^2\left(M^2\left(5\xi^2+2\xi+1\right)-6\xi s+2s\right)+s\left(M^2\left(\xi^2-2\xi-1\right)+s\right)\right)}{2M^2}\ln(\xi)+ \\
&- \frac{s\left(2m^6\left(4M^2+s\right)+m^4\left(-2M^4-8M^2 s+s^2\right)+2m^2M^4 s\right)}{2M^4} C_0\left(m^2,m^2,s;M,m,M\right)+ \\
&+ \frac{1}{M^4}\Big(2m^6\left(M^4\left(\xi^2+2\xi-3\right)-2M^2(\xi-1)s+s^2\right)+m^2M^4\xi s^2+ \\
&\qquad + m^4 s\left(M^4\left(\xi^2-2\xi+3\right)-2M^2(\xi+2)s+s^2\right)\Big) C_0\left(m^2,m^2,s;M\sqrt{\xi},m,M\right)+ \\
&- \frac{m^4 s\left(2m^2\left(s-4M^2\xi\right)+6M^4\xi^2-4M^2\xi s+s^2\right)}{2M^4} C_0\left(m^2,m^2,s;M\sqrt{\xi},m,M\sqrt{\xi}\right)\Bigg\},
\end{aligned}
\tag{E.70}
$$

E.4.2.2 Direct type

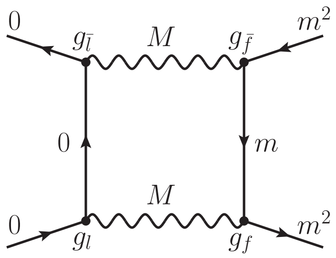

$$
\begin{aligned}
F_{1,d}^{\rho\kappa,\xi=1} = \delta_{-\rho,\kappa} \Bigg\{ & 2s g_l^\kappa g_{\bar{l}}^\kappa g_f^\rho g_{\bar{f}}^\rho \Big[C_0\left(m^2, m^2, s; M, m, M\right) + C_0(0,0,s;M,0,M) + \\
& \qquad + \left(m^2 - t\right) D_0\left(0,0,m^2,m^2;s,t;M,0,M,m\right) \Big] + \\
& + \frac{\left(g_l^\kappa g_{\bar{l}}^\kappa g_f^\rho g_{\bar{f}}^{-\rho} + g_l^\kappa g_{\bar{l}}^\kappa g_f^{-\rho} g_{\bar{f}}^\rho\right) m^2 s}{m^4 - tu} \times \\
& \times \Big[\left(u - m^2\right) C_0(0,0,s;M,0,M) + 2m^2 C_0\left(0,m^2,t;0,M,m\right) + \\
& - \left(m^2 + u\right) C_0\left(m^2,m^2,s;M,m,M\right) + \\
& - \left(m^4 - m^2\left(2M^2 + t + u\right) + tu\right) D_0\left(0,0,m^2,m^2;s,t;M,0,M,m\right) \Big] + \\
& + \frac{g_l^\kappa g_{\bar{l}}^\kappa g_f^{-\rho} g_{\bar{f}}^{-\rho} m^2 s}{m^4 - tu} \Big[2\Lambda(s;M,M) - \frac{4m^2}{m^2 - t} \Lambda\left(m^2; m, M\right) + \\
& + \frac{2\left(m^2 - M^2 - t\right)}{m^2 - t} \ln\left(\frac{m^2}{M^2}\right) - \frac{2\left(m^2 + t\right)}{t} \ln\left(\frac{m^2}{m^2 - t - i0^+}\right) + \\
& + \frac{m^4\left(-2M^2 + 3t - 3u\right) - m^2(t-u)\left(2M^2 + 3t + u\right) + t^2\left(2M^2 + t - u\right)}{m^4 - tu} \times \\
& \qquad \times C_0(0,0,s;M,0,M) + \\
& - \frac{2}{\left(m^2 - t\right)\left(m^4 - tu\right)} \Big(m^8 + m^6\left(-2M^2 + t - u\right) + 2m^4 t(u - 2t) + \\
& \qquad + m^2 t^2\left(2M^2 + 3t - 3u\right) - t^2\left(2M^2(t-u) + t(t - 2u)\right) \Big) \times \\
& \qquad \times C_0\left(0, m^2, t; 0, M, m\right) + \\
& + \frac{1}{m^4 - tu} \Big(4m^6 + m^4\left(-2M^2 - t + u\right) + t^2\left(2M^2 + t - u\right) + \\
& \qquad + m^2\left(2M^2(t-u) - (t+u)^2\right) \Big) C_0\left(m^2,m^2,s;M,m,M\right) + \\
& + \frac{1}{m^4 - tu} \Big(m^6\left(-4M^2 + 3t - 3u\right) + m^4\left(2M^4 - 4M^2(t-u) - 6t^2 + 5tu + u^2\right) + \\
& \qquad + m^2 t\left(M^2(8t - 4u) + 4t^2 - 3tu - u^2\right) + \\
& \qquad + t\left(M^4(2u - 4t) - 4M^2 t(t-u) + t^2(u-t)\right) \Big) \times
\end{aligned}
$$

$$
\left.\left.\times D_0\left(0,0,m^2,m^2;s,t;M,0,M,m\right)\right]\right\}+
$$

$$
+\delta_{\rho,\kappa}\left\{\frac{\left(g_l^\kappa g_{\bar{l}}^\kappa g_f^\rho g_{\bar{f}}^{-\rho}+g_l^\kappa g_{\bar{l}}^\kappa g_f^{-\rho} g_{\bar{f}}^\rho\right)m^2 s}{m^4-tu}\times\right.
$$

$$
\times\Big[\left(m^2-t\right)C_0(0,0,s;M,0,M)+2tC_0\left(0,m^2,t;0,M,m\right)+
$$

$$
-\left(m^2+t\right)C_0\left(m^2,m^2,s;M,m,M\right)+
$$

$$
+\left(m^4-2m^2t+t\left(2M^2+t\right)\right)D_0\left(0,0,m^2,m^2;s,t;M,0,M,m\right)\Big]+
$$

$$
+\frac{g_l^\kappa g_{\bar{l}}^\kappa g_f^\rho g_{\bar{f}}^\rho m^2 s}{m^4-tu}\left[2t\Lambda(s;M,M)-\frac{4m^2t}{m^2-t}\Lambda\left(m^2;m,M\right)+\right.
$$

$$
+\frac{2t\left(m^2-M^2-t\right)}{m^2-t}\ln\left(\frac{m^2}{M^2}\right)-2\left(m^2+t\right)\ln\left(\frac{m^2}{m^2-t-i0^+}\right)+
$$

$$
-\frac{1}{m^4-tu}\Big(2m^8-m^6\left(2M^2+3t+u\right)+2m^4t\left(2M^2-t+u\right)+
$$

$$
+m^2t^2\left(2M^2+3t+u\right)-t^2\left(2M^2(t+u)+t^2+u^2\right)\Big)\times
$$

$$
\times C_0(0,0,s;M,0,M)+
$$

$$
+\frac{2}{\left(m^2-t\right)\left(m^4-tu\right)}\Big(m^{10}-4m^8t+2m^6t\left(2M^2+t\right)+t^4\left(2M^2+t-u\right)+
$$

$$
+m^4t^2\left(-2M^2+3t+u\right)-m^2t^2\left(2M^2(t+u)+3t^2\right)\Big)\times
$$

$$
\times C_0\left(0,m^2,t;0,M,m\right)+
$$

$$
+\frac{1}{m^4-tu}\Big(2m^8-m^6\left(2M^2-5t+u\right)-2m^4t\left(2M^2+t+u\right)+
$$

$$
-m^2t^2\left(-2M^2+t+3u\right)+t^2\left(2M^2(t+u)+t^2+u^2\right)\Big)\times
$$

$$
\times C_0\left(m^2,m^2,s;M,m,M\right)+
$$

$$
+\frac{1}{m^4-tu}\Big(2m^{10}-m^8\left(4M^2+5t+u\right)+m^6t\left(12M^2+t+3u\right)+
$$

$$
-m^2t^2\left(4M^2(2t+u)+4t^2+tu+u^2\right)-m^4t\left(6M^4+t(u-5t)\right)+
$$

$$
+t^2\left(2M^4(2t+u)+4M^2t^2+t\left(t^2+u^2\right)\right)\Big)\times
$$

$$
\left.\left.\times D_0\left(0,0,m^2,m^2;s,t;M,0,M,m\right)\right]\right\},
\tag{E.71}
$$

$$
F_{2,d}^{\rho\kappa,\xi=1}=\frac{g_l^\kappa g_{\bar{l}}^\kappa g_f^{-\rho} g_{\bar{f}}^\rho m^2 s}{m^4-tu}\Big[\left(t-m^2\right)C_0(0,0,s;M,0,M)-2tC_0\left(0,m^2,t;0,M,m\right)+
$$

$$
+\left(m^2+t\right)C_0\left(m^2,m^2,s;M,m,M\right)+
$$

$$- \left(m^4 - 2m^2 t + t\left(2M^2 + t\right)\right) D_0\left(0,0,m^2,m^2;s,t;M,0,M,m\right) \Big] +$$

$$+ \frac{\left(g_l^\kappa g_{\bar{l}}^\kappa g_f^\rho g_{\bar{f}}^\rho \,\delta_{\kappa,\rho} + g_l^\kappa g_{\bar{l}}^\kappa g_f^{-\rho} g_{\bar{f}}^{-\rho}\,\delta_{\kappa,-\rho}\right) m^2 s}{m^4 - tu} \times$$

$$\times \Bigg\{ \frac{2\left(m^2+t\right)}{s-4m^2}\,\Lambda(s;M,M) - \frac{2\left(m^4+2m^2t+tu\right)}{\left(s-4m^2\right)\left(m^2-t\right)}\,\Lambda\left(m^2;m,M\right) +$$

$$+ 2\ln\left(\frac{m^2}{m^2-t-i0^+}\right) - \frac{-2m^6+m^4M^2+2m^2t\left(M^2+t\right)+M^2tu}{m^2\left(s-4m^2\right)\left(m^2-t\right)}\,\log\left(\frac{m^2}{M^2}\right) +$$

$$+ \frac{m^6+m^4\left(-M^2+s-3t\right)+m^2t\left(2M^2-s+3t\right)-t\left(M^2(t-s)+t^2\right)}{m^4-tu} \times$$

$$\times C_0(0,0,s;M,0,M) +$$

$$- \frac{2\left(m^8-5m^6t+m^4t\left(3M^2+7t\right)+m^2t^2\left(-4M^2-4t+u\right)+t^2\left(M^2(2t-u)+t(t-u)\right)\right)}{\left(m^2-t\right)\left(m^4-tu\right)} \times$$

$$\times C_0\left(0,m^2,t;0,M,m\right) +$$

$$+ \frac{1}{\left(s-4m^2\right)\left(m^4-tu\right)}\Big(6m^8 - m^6\left(4M^2-5t+u\right) - m^4\left(M^2(3t+u)+4t^2+3tu+u^2\right) +$$

$$+ m^2t\left(4M^2t+u(u-5t)\right) +$$

$$+ t\left(M^2\left(2t^2+3tu-u^2\right)+t^2(t+u)\right)\Big) C_0\left(m^2,m^2,s;M,m,M\right) +$$

$$+ \frac{1}{m^4-tu}\Big(m^8+m^6\left(-3M^2+s-4t\right)+m^4t\left(11M^2-2s+6t\right) +$$

$$+ m^2t\left(-4M^4+M^2(s-13t)+t(s-4t)\right)+t^2\left(4M^4+M^2(s+5t)+t^2\right)\Big) \times$$

$$\times D_0\left(0,0,m^2,m^2;s,t;M,0,M,m\right) \Bigg\}, \tag{E.72}$$

$$\Delta F_{1,d}^{\rho\kappa,\xi} = -\frac{g_l^\kappa g_{\bar{l}}^\kappa g_f^\rho g_{\bar{f}}^\rho}{s-4m^2} \times$$

$$\times \Bigg\{ -\frac{s-4m^2}{6}(\xi-1)^2 + \frac{s\left(s\left(20M^2+s\right)-m^2\left(50M^2+7s\right)\right)}{12M^4}\,\Lambda(s;M,M) +$$

$$- \frac{s\left(M^4(\xi-1)^2-2M^2(\xi-5)s+s^2\right)-m^2\left(4M^4(\xi-1)^2+M^2(25-11\xi)s+7s^2\right)}{6M^4} \times$$

$$\times \Lambda\left(s;M,M\sqrt{\xi}\right)$$

$$+ \frac{s\left(m^2\left(22M^2\xi-7s\right)+s\left(s-4M^2\xi\right)\right)}{12M^4}\,\Lambda\left(s;M\sqrt{\xi},M\sqrt{\xi}\right) +$$

$$- \frac{1}{2}(\xi-1)\left(m^2(\xi+3)-2s\right)\,\ln\left(\frac{m^2}{M^2}\right) - \frac{2m^2s-m^4(\xi+3)}{M^2}\,\Lambda\left(m^2;m,M\right) +$$

$$- \frac{m^4(\xi+3)-2m^2s}{M^2}\,\Lambda\left(m^2;m,M\sqrt{\xi}\right) +$$

$$
\begin{aligned}
&-\frac{1}{12M^2 s}\Big(m^2\left(4M^4(\xi-1)^3-3M^2\left(7\xi^2-6\xi+7\right)s+18(\xi+1)s^2\right)+\\
&\qquad\qquad +s\left(-M^4(\xi-1)^3+3M^2\left(\xi^2+3\right)s-3(\xi+3)s^2\right)\Big)\ln(\xi)+\\
&-\frac{m^2 s\left(m^2\left(4M^2+s\right)+5M^4-4M^2 s\right)}{2M^4}C_0\left(m^2,m^2,s;M,m,M\right)+\\
&+\frac{m^2\left(m^2\left(M^4\left(\xi^2+2\xi-3\right)-2M^2(\xi-1)s+s^2\right)+M^2 s\left(M^2(\xi+2)-2s\right)\right)}{M^4}\times\\
&\qquad\qquad\qquad\qquad\times C_0\left(m^2,m^2,s;M\sqrt{\xi},m,M\right)+\\
&-\frac{m^2 s\left(m^2\left(s-4M^2\xi\right)+M^4\xi^2\right)}{2M^4}C_0\left(m^2,m^2,s;M\sqrt{\xi},m,M\sqrt{\xi}\right)\Bigg\}+
\end{aligned}
$$

$$
\begin{aligned}
&-\frac{g_l^{\kappa}g_{\bar{l}}^{\kappa}g_f^{-\rho}g_{\bar{f}}^{-\rho}}{s-4m^2}\times\\
&\times\Bigg\{-\frac{m^2 s\left(6M^2+s\right)}{4M^4}\Lambda(s;M,M)+\frac{m^2 s\left(s-M^2(\xi-3)\right)}{2M^4}\Lambda\left(s;M,M\sqrt{\xi}\right)+\\
&-\frac{m^2 s\left(s-2M^2\xi\right)}{4M^4}\Lambda\left(s;M\sqrt{\xi},M\sqrt{\xi}\right)-\frac{1}{2}m^2\left(\xi^2+2\xi-3\right)\ln\left(\frac{m^2}{M^2}\right)+\\
&+\frac{m^4(\xi+3)}{M^2}\Lambda\left(m^2;m,M\right)-\frac{m^4(\xi+3)}{M^2}\Lambda\left(m^2;m,M\sqrt{\xi}\right)+\\
&+\frac{m^2\left(M^2\left(3\xi^2+2\xi+3\right)-2(\xi+1)s\right)}{4M^2}\ln(\xi)+\\
&-\frac{m^2 s\left(m^2\left(4M^2+s\right)-3M^4\right)}{2M^4}C_0\left(m^2,m^2,s;M,m,M\right)+\\
&-\frac{m^2M^4\xi s-m^4\left(M^4\left(\xi^2+2\xi-3\right)-2M^2(\xi-1)s+s^2\right)}{M^4}C_0\left(m^2,m^2,s;M\sqrt{\xi},m,M\right)+\\
&-\frac{m^2 s\left(m^2\left(s-4M^2\xi\right)+M^4\xi^2\right)}{2M^4}C_0\left(m^2,m^2,s;M\sqrt{\xi},m,M\sqrt{\xi}\right)\Bigg\}+
\end{aligned}
$$

$$
\begin{aligned}
&-\frac{\left(g_l^{\kappa}g_{\bar{l}}^{\kappa}g_f^{\rho}g_{\bar{f}}^{-\rho}+g_l^{\kappa}g_{\bar{l}}^{\kappa}g_f^{-\rho}g_{\bar{f}}^{\rho}\right)}{s-4m^2}\times\\
&\times\Bigg\{\frac{m^2 s\left(s-2M^2\right)}{4M^4}\Lambda(s;M,M)-\frac{m^2 s\left(s-M^2(\xi+1)\right)}{2M^4}\Lambda\left(s;M,M\sqrt{\xi}\right)+\\
&+\frac{m^2 s\left(s-2M^2\xi\right)}{4M^4}\Lambda\left(s;M\sqrt{\xi},M\sqrt{\xi}\right)+\frac{1}{2}(\xi-1)\left(m^2(\xi+3)-s\right)\ln\left(\frac{m^2}{M^2}\right)+\\
&-\frac{m^4(\xi+3)-m^2 s}{M^2}\Lambda\left(m^2;m,M\right)-\frac{m^2 s-m^4(\xi+3)}{M^2}\Lambda\left(m^2;m,M\sqrt{\xi}\right)+\\
&-\frac{m^2\left(M^2\left(3\xi^2+6\xi-1\right)-2(\xi-1)s\right)-2M^2\xi s}{4M^2}\ln(\xi)+\\
&+\frac{m^2 s\left(m^2\left(4M^2+s\right)+M^4-2M^2 s\right)}{2M^4}C_0\left(m^2,m^2,s;M,m,M\right)+
\end{aligned}
$$

$$- \frac{m^2 \left(m^2 \left(M^4 \left(\xi^2+2\xi-3\right)-2M^2(\xi-1)s+s^2\right)+M^2 s \left(M^2-s\right)\right)}{M^4} \times$$
$$\times C_0\left(m^2,m^2,s;M\sqrt{\xi},m,M\right)+$$
$$+ \frac{m^2 s \left(m^2 \left(s-4M^2\xi\right)+M^4\xi^2\right)}{2M^4} C_0\left(m^2,m^2,s;M\sqrt{\xi},m,M\sqrt{\xi}\right) \Bigg\}, \tag{E.73}$$

$$\Delta F_{2,d}^{\rho\kappa,\xi} = - \frac{g_l^\kappa g_{\bar{l}}^\kappa g_f^{-\rho} g_{\bar{f}}^\rho}{\left(s-4m^2\right)^2} \times$$
$$\times \Bigg\{ \frac{s \left(m^4 \left(10M^2+3s\right)-4m^2M^2 s\right)}{2M^4} \Lambda(s;M,M)+$$
$$+ \frac{s \left(m^4 \left(M^2(3\xi-5)-3s\right)+2m^2M^2 s\right)}{M^4} \Lambda\left(s;M,M\sqrt{\xi}\right)+$$
$$+ \frac{3m^4 s \left(s-2M^2\xi\right)}{2M^4} \Lambda\left(s;M\sqrt{\xi},M\sqrt{\xi}\right)+$$
$$+ \frac{1}{2} m^2(\xi-1)\left(2m^2(\xi+7)+(\xi-5)s\right) \ln\left(\frac{m^2}{M^2}\right)+$$
$$- \frac{m^4 \left(2m^2(\xi+7)+(\xi-5)s\right)}{M^2} \Lambda\left(m^2;m,M\right)+$$
$$+ \frac{m^4 \left(2m^2(\xi+7)+(\xi-5)s\right)}{M^2} \Lambda\left(m^2;m,M\sqrt{\xi}\right)+$$
$$- \frac{m^2 \left(m^2 \left(M^2 \left(5\xi^2+6\xi+5\right)-2(3\xi s+s)\right)+s\left(M^2\left(\xi^2-3\xi-2\right)+2s\right)\right)}{2M^2} \ln(\xi)+$$
$$+ \frac{s \left(2m^6 \left(12M^2+s\right)+m^4 \left(-10M^4-12M^2 s+s^2\right)+4m^2M^4 s\right)}{2M^4} C_0\left(m^2,m^2,s;M,m,M\right)+$$
$$- \frac{m^2}{M^4}\Big(m^2 s \left(M^4\left(\xi^2-8\xi+5\right)-2M^2(\xi+3)s+s^2\right)+2M^4\xi s^2+$$
$$+2m^4\left(M^4\left(\xi^2+6\xi-7\right)-2M^2(\xi-3)s+s^2\right)\Big) C_0\left(m^2,m^2,s;M\sqrt{\xi},m,M\right)+$$
$$+ \frac{m^4 s \left(2m^2\left(s-4M^2\xi\right)+6M^4\xi^2-4M^2\xi s+s^2\right)}{2M^4} C_0\left(m^2,m^2,s;M\sqrt{\xi},m,M\sqrt{\xi}\right) \Bigg\}+$$
$$- \frac{g_l^\kappa g_{\bar{l}}^\kappa g_f^\rho g_{\bar{f}}^{-\rho}}{\left(s-4m^2\right)^2} \times$$
$$\times \Bigg\{ \frac{3m^4 s \left(s-2M^2\right)}{2M^4} \Lambda(s;M,M) + \frac{3m^4 s \left(M^2(\xi+1)-s\right)}{M^4} \Lambda\left(s;M,M\sqrt{\xi}\right)+$$
$$+ \frac{3m^4 s \left(s-2M^2\xi\right)}{2M^4} \Lambda\left(s;M\sqrt{\xi},M\sqrt{\xi}\right) + \frac{1}{2} m^2(\xi-1)^2\left(2m^2+s\right) \ln\left(\frac{m^2}{M^2}\right)+$$
$$- \frac{m^4(\xi-1)\left(2m^2+s\right)}{M^2} \Lambda\left(m^2;m,M\right) + \frac{m^4(\xi-1)\left(2m^2+s\right)}{M^2} \Lambda\left(m^2;m,M\sqrt{\xi}\right)+$$
$$- \frac{m^2(\xi-1)\left(m^2\left(M^2(5\xi+3)-6s\right)+M^2\xi s\right)}{2M^2} \ln(\xi)+$$

$$
\begin{aligned}
&+\frac{m^4 s\left(m^2\left(2s-8M^2\right)+6M^4-4M^2s+s^2\right)}{2M^4}C_0\left(m^2,m^2,s;M,m,M\right)+\\
&-\frac{m^4\left(2m^2\left(M^4(\xi-1)^2-2M^2(\xi+1)s+s^2\right)+s\left(M^4\left(\xi^2+4\xi+1\right)-2M^2(\xi+1)s+s^2\right)\right)}{M^4}\times\\
&\qquad\qquad\qquad\qquad\times C_0\left(m^2,m^2,s;M\sqrt{\xi},m,M\right)+\\
&+\frac{m^4 s\left(2m^2\left(s-4M^2\xi\right)+6M^4\xi^2-4M^2\xi s+s^2\right)}{2M^4}C_0\left(m^2,m^2,s;M\sqrt{\xi},m,M\sqrt{\xi}\right)\Bigg\}+\\
&-\frac{\left(g_l^\kappa g_{\bar{l}}^\kappa g_f^\rho g_{\bar{f}}^\rho+g_l^\kappa g_{\bar{l}}^\kappa g_f^{-\rho} g_{\bar{f}}^{-\rho}\right)}{\left(s-4m^2\right)^2}\times\\
&\times\Bigg\{-\frac{s\left(m^4\left(2M^2+3s\right)-2m^2M^2s\right)}{2M^4}\Lambda(s;M,M)+\\
&+\frac{s\left(m^4\left(M^2(1-3\xi)+3s\right)-m^2M^2s\right)}{M^4}\Lambda\left(s;M,M\sqrt{\xi}\right)+\\
&-\frac{3m^4s\left(s-2M^2\xi\right)}{2M^4}\Lambda\left(s;M\sqrt{\xi},M\sqrt{\xi}\right)+\\
&-\frac{1}{2}m^2(\xi-1)\left(2m^2(\xi+3)+(\xi-3)s\right)\ln\left(\frac{m^2}{M^2}\right)+\\
&+\frac{m^4\left(2m^2(\xi+3)+(\xi-3)s\right)}{M^2}\Lambda\left(m^2;m,M\right)+\\
&-\frac{m^4\left(2m^2(\xi+3)+(\xi-3)s\right)}{M^2}\Lambda\left(m^2;m,M\sqrt{\xi}\right)+\\
&+\frac{m^2\left(m^2\left(M^2\left(5\xi^2+2\xi+1\right)-6\xi s+2s\right)+s\left(M^2\left(\xi^2-2\xi-1\right)+s\right)\right)}{2M^2}\ln(\xi)+\\
&-\frac{s\left(2m^6\left(4M^2+s\right)+m^4\left(-2M^4-8M^2s+s^2\right)+2m^2M^4s\right)}{2M^4}C_0\left(m^2,m^2,s;M,m,M\right)+\\
&+\frac{1}{M^4}\Big(2m^6\left(M^4\left(\xi^2+2\xi-3\right)-2M^2(\xi-1)s+s^2\right)+m^2M^4\xi s^2+\\
&\qquad+m^4s\left(M^4\left(\xi^2-2\xi+3\right)-2M^2(\xi+2)s+s^2\right)\Big)C_0\left(m^2,m^2,s;M\sqrt{\xi},m,M\right)+\\
&-\frac{m^4 s\left(2m^2\left(s-4M^2\xi\right)+6M^4\xi^2-4M^2\xi s+s^2\right)}{2M^4}C_0\left(m^2,m^2,s;M\sqrt{\xi},m,M\sqrt{\xi}\right)\Bigg\},
\end{aligned}
\tag{E.74}
$$

E.5 High-energy expansions

Below we give the high-energy expansions (i.e. neglecting power-corrections) of the various generic diagrams under the assumption

$$\{|s|,|t|,|u|\} \gg \{m^2, M^2\} \sim \Lambda_{\mathrm{EW}}^2, \tag{E.75}$$

derived by means of the results from the last sections in conjunction with the high-energy expanded scalar PV-functions from sec. B.2. For the bosonic loops of the bosonic XY-transitions we only give expansions of diagrams with massive internal bosons, as only ZZ-,ZA- and AA-transitions appear in the s-channel diagrams, but not the WW-self-energy. Tadpoles are independent of momentum, and the results of sec. E.2 remain the same in the boosted regime.

E.5.1 Massive vector-vector (VV)

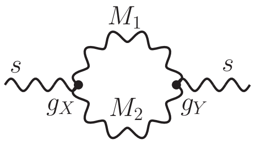

$$\frac{1}{s\,g_X g_Y}\,G^T_{VV}(p^2;M_1,M_2) = \frac{25-3(\xi_1+\xi_2)}{6}\left(\frac{1}{\epsilon}+\ln\left(\frac{\mu^2}{-s-i0^+}\right)\right) + \frac{9(\xi_1+\xi_2+\xi_1\xi_2)+89}{18}, \tag{E.76}$$

$$\frac{1}{s\,g_X g_Y}\,G^L_{VV}(p^2;M_1,M_2) = -\frac{1}{2}\left(\frac{1}{\epsilon}+\ln\left(\frac{\mu^2}{-s-i0^+}\right)+2\right). \tag{E.77}$$

E.5.2 Massive vector-scalar (VS)

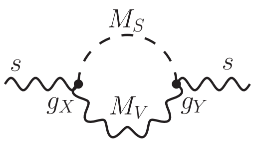

$$G^T_{VS}(p^2;M_1,M_2) = G^L_{VS}(p^2;M_1,M_2) = 0. \tag{E.78}$$

E.5.3 Scalar-scalar (SS)

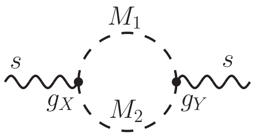

$$\frac{1}{s\,g_X g_Y}\,G^T_{SS}(p^2;M_1,M_2) = -\frac{1}{3}\left(\frac{1}{\epsilon}+\ln\left(\frac{\mu^2}{-s-i0^+}\right)+\frac{8}{3}\right), \tag{E.79}$$

$$\frac{1}{s\,g_X g_Y}\,G^L_{SS}(p^2;M_1,M_2) = 0. \tag{E.80}$$

E.5.4 Ghost-ghost (UU)

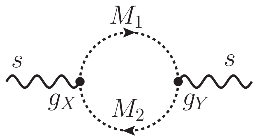

$$\frac{1}{s\, g_X g_Y}\, G^T_{UU}(p^2; M_1, M_2) = \frac{1}{12}\left(\frac{1}{\epsilon} + \ln\left(\frac{\mu^2}{-s - i0^+}\right) + \frac{8}{3}\right), \tag{E.81}$$

$$\frac{1}{s\, g_X g_Y}\, G^L_{UU}(p^2; M_1, M_2) = \frac{1}{4}\left(\frac{1}{\epsilon} + \ln\left(\frac{\mu^2}{-s - i0^+}\right) + 2\right). \tag{E.82}$$

E.5.5 Fermions

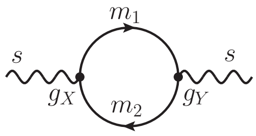

$$\frac{1}{s}\, G^T_{ff}(p^2; m_1, m_2) = -\frac{2}{3}\left(\frac{1}{\epsilon} + \ln\left(\frac{\mu^2}{-s - i0^+}\right) + \frac{5}{3}\right) \sum_{\rho=\pm} g^\rho_X g^\rho_Y, \tag{E.83}$$

$$\frac{1}{s}\, G^L_{ff}(p^2; m_1, m_2) = 0. \tag{E.84}$$

E.5.6 Abelian vector

E.5.6.1 Charged massive $(ffV)_c$

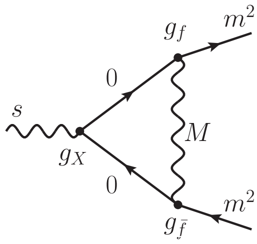

$$F^{\rho,\xi=1}_{1,ffV} = g^\rho_X g^\rho_f g^\rho_{\bar f}\Bigg\{\frac{1}{\epsilon} - \ln\left(\frac{M^2}{\mu^2}\right) - \ln^2\left(\frac{M^2}{-s - i0^+}\right) - 3\ln\left(\frac{M^2}{-s - i0^+}\right) + 2\ln^2\left(\frac{M^2}{-m^2 - i0^+}\right) + \\ + 4\left(1 - \frac{M^2}{m^2}\right)\ln\left(\frac{M^2}{M^2 - m^2 - i0^+}\right) + 4\,\mathrm{Li}_2\left(\frac{M^2}{m^2 - i0^+}\right)\Bigg\}, \tag{E.85}$$

$$F^{\rho,\xi=1}_{2,ffV} = 0, \tag{E.86}$$

$$\Delta F^{\rho,\xi}_{1,ffV} = g^\rho_X g^\rho_f g^\rho_{\bar f}\Bigg\{(\xi - 1)\left(\frac{1}{\epsilon} - \ln\left(\frac{M^2}{\mu^2}\right) + 2\right) + \left(\frac{m^2}{M^2} + \frac{M^2}{m^2} - 2\right)\ln\left(\frac{M^2}{M^2 - m^2 - i0^+}\right) + \\ - \frac{\left(m^2 - M^2\xi\right)^2}{m^2 M^2}\ln\left(\frac{M^2\xi}{M^2\xi - m^2 - i0^+}\right) + \left(\frac{m^2}{M^2} - \xi\right)\ln(\xi)\Bigg\}, \tag{E.87}$$

$$\Delta F_{2,ffV}^{\rho,\xi} = 0. \tag{E.88}$$

E.5.6.2 Neutral massive $(ffV)_n$

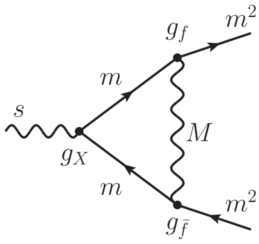

$$F_{1,ffV}^{\rho,\xi=1} = g_X^\rho g_f^\rho g_{\bar{f}}^\rho \Bigg\{ \frac{1}{\epsilon} - \ln\left(\frac{m^2}{\mu^2}\right) - \ln^2\left(\frac{M^2}{-s-i0^+}\right) - 3\ln\left(\frac{m^2}{-s-i0^+}\right) + \\ - \frac{2M^2}{m^2}\ln\left(\frac{M^2}{m^2}\right) + 4\Lambda\left(m^2; m, M\right) + \\ - 4\,\mathrm{Li}_2\left(\frac{2m^2}{M^2+\sqrt{M^2\left(M^2-4m^2\right)}}\right) - 4\,\mathrm{Li}_2\left(\frac{2m^2}{M^2-\sqrt{M^2\left(M^2-4m^2\right)}}\right) \Bigg\}, \tag{E.89}$$

$$F_{2,ffV}^{\rho,\xi=1} = 0, \tag{E.90}$$

$$\Delta F_{1,ffV}^{\rho,\xi} = g_X^\rho g_f^\rho g_{\bar{f}}^\rho \Bigg\{ (\xi-1)\left(\frac{1}{\epsilon} - \ln\left(\frac{m^2}{\mu^2}\right) - \frac{M^2(\xi+1)}{2m^2}\ln\left(\frac{M^2}{m^2}\right) + 2\right) + \\ - \Lambda\left(m^2; m, M\right) + \xi\Lambda\left(m^2; m, M\sqrt{\xi}\right) - \frac{M^2\xi^2}{2m^2}\ln(\xi) \Bigg\} + \\ + \frac{g_X^\rho\left(g_f^\rho g_{\bar{f}}^{-\rho} + g_f^{-\rho} g_{\bar{f}}^\rho\right)}{2} \Bigg\{ (\xi-1)\left[\left(\frac{M^2(\xi+1)}{2m^2} - 1\right)\ln\left(\frac{M^2}{m^2}\right) - 1\right] + \\ + \Lambda\left(m^2; m, M\right) - \xi\Lambda\left(m^2; m, M\sqrt{\xi}\right) + \xi\left(\frac{M^2\xi}{2m^2} - 1\right)\ln(\xi) \Bigg\} \tag{E.91}$$

$$\Delta F_{2,ffV}^{\rho,\xi} = 0. \tag{E.92}$$

E.5.6.3 Massless (llV)

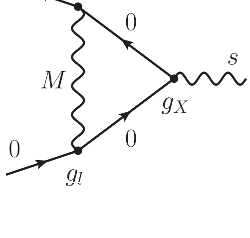

$$F_{1,llV}^{\kappa,\xi=1} = g_X^\kappa g_f^\kappa g_{\bar{f}}^\kappa \left\{ \frac{1}{\epsilon} - \ln\left(\frac{M^2}{\mu^2}\right) - \ln^2\left(\frac{M^2}{-s-i0^+}\right) - 3\ln\left(\frac{M^2}{-s-i0^+}\right) - 4 - \frac{2\pi^2}{3} \right\}, \tag{E.93}$$

$$\Delta F_{1,llV}^{\kappa,\xi} = g_X^\kappa g_f^\kappa g_{\bar{f}}^\kappa \left\{ (\xi-1)\left(\frac{1}{\epsilon} - \ln\left(\frac{M^2}{\mu^2}\right) + 1\right) - \xi\ln(\xi) \right\}. \tag{E.94}$$

E.5.7 Abelian scalar

Comment: the high-energy expressions of the scalar-exchange diagrams are independent of the masses of the virtual fermions, and therefore charged and neutral type are equal in this limit.

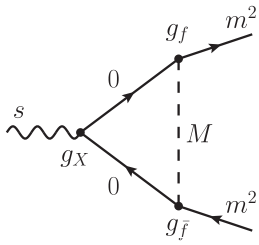

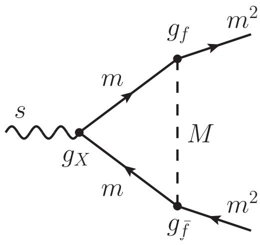

$$F_{1,ffS}^{\rho} = \frac{1}{2}\, g_X^{-\rho} g_f^{-\rho} g_{\bar{f}}^{\rho} \left\{ \frac{1}{\epsilon} + \ln\left(\frac{\mu^2}{-s-i0^+}\right) + 1 \right\}, \tag{E.95}$$

$$F_{2,ffS}^{\rho} = 0. \tag{E.96}$$

E.5.8 Non-abelian vector-vector

E.5.8.1 Charged massive $(fVV)_c$

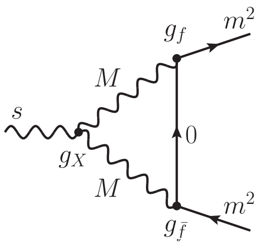

$$F_{1,fVV}^{\rho,\xi=1} = g_X g_f^\rho g_{\bar{f}}^\rho \left\{ -3\left(\frac{1}{\epsilon} - \ln\left(\frac{M^2}{\mu^2}\right) + 2\right) + \ln\left(\frac{M^2}{-s-i0^+}\right) + \right.$$
$$\left. + 4\left(\frac{M^2}{m^2} - 1\right)\ln\left(\frac{M^2}{M^2-m^2-i0^+}\right) \right\}, \tag{E.97}$$

$$F_{2,fVV}^{\rho,\xi=1} = 0, \tag{E.98}$$

$$\Delta F_{1,fVV}^{\rho,\xi} = g_X g_f^\rho g_{\bar{f}}^\rho \left\{ -\frac{3}{2}(\xi-1)\left(\frac{1}{\epsilon} + \frac{1-\xi}{3} + \ln\left(\frac{\mu^2}{-s-i0^+}\right)\right) + \right.$$

$$+\left(\frac{m^2}{M^2}-\frac{M^2}{m^2}\right)\ln\left(\frac{M^2}{M^2-m^2-i0^+}\right)+$$

$$\left.+\left(\frac{M^2\xi^2}{m^2}-\frac{m^2}{M^2}\right)\ln\left(\frac{M^2\xi}{M^2\xi-m^2-i0^+}\right)+\frac{m^2}{M^2}\ln(\xi)\right\}, \tag{E.99}$$

$$\Delta F^{\rho,\xi}_{2,fVV}=0. \tag{E.100}$$

E.5.8.2 Massless (lVV)

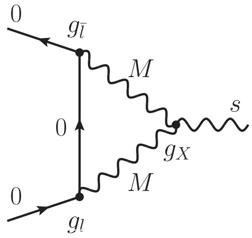

$$F^{\kappa,\xi=1}_{1,lVV}=g_X g^\kappa_l g^\kappa_{\bar{l}}\left\{3\left(\frac{1}{\epsilon}-\ln\left(\frac{M^2}{\mu^2}\right)\right)-\ln\left(\frac{M^2}{-s-i0^+}\right)+2\right\}, \tag{E.101}$$

$$\Delta F^{\kappa,\xi}_{1,lVV}=g_X g^\kappa_l g^\kappa_{\bar{l}}\frac{\xi-1}{2}\left\{3\left(\frac{1}{\epsilon}+\ln\left(\frac{\mu^2}{-s-i0^+}\right)\right)-1-\xi\right\}. \tag{E.102}$$

E.5.9 Non-abelian vector-scalar and scalar-vector

Comment: all vector-scalar and scalar-vector diagrams are power-supressed because the VVS-coupling is dimensionful (mass dimension = +1) and scales as $g_{VVS}\sim\mathcal{O}(\Lambda_{\mathrm{EW}})$.

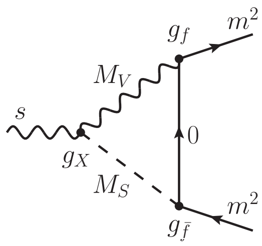

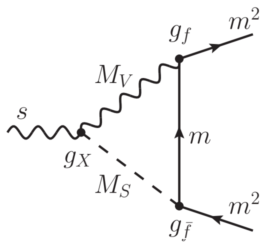

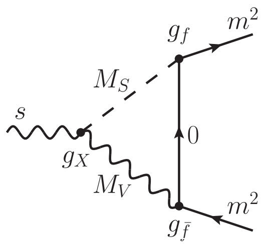

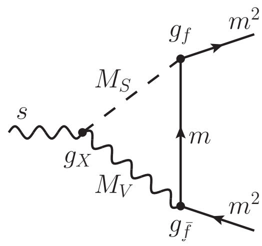

$$F^\rho_{1,fVS}=F^\rho_{1,fSV}=0, \tag{E.103}$$

$$F^\rho_{2,fVS}=F^\rho_{2,fSV}=0. \tag{E.104}$$

E.5.10 Non-abelian scalar-scalar

Comment: the high-energy expressions of the scalar-scalar diagrams are independent of the virtual fermions mass, and therefore charged and neutral type are equal in this limit.

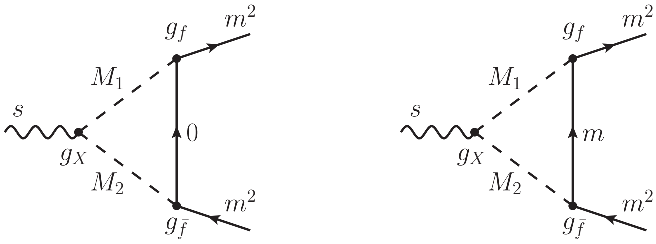

$$F^{\rho}_{1,fSS} = \frac{1}{2}\, g_X g_f^{-\rho} g_{\bar{f}}^{\rho} \left\{ \frac{1}{\epsilon} + \ln\left(\frac{\mu^2}{-s-i0^+}\right) + 3 \right\}, \tag{E.105}$$

$$F^{\rho}_{2,fSS} = 0. \tag{E.106}$$

E.5.11 Charged box

E.5.11.1 Crossed type

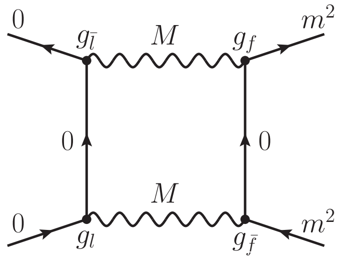

$$\begin{aligned} F^{\rho\kappa,\xi=1}_{1,c} = g_l^{\kappa} g_{\bar{l}}^{\kappa} g_f^{\rho} g_{\bar{f}}^{\rho} \Bigg\{ & 2\ln^2\left(\frac{M^2}{-s-i0^+}\right) - 4\ln\left(\frac{M^2}{-s-i0^+}\right)\ln\left(\frac{-u-i0^+}{-s-i0^+}\right) + \\ & - 2\ln^2\left(\frac{M^2}{-m^2-i0^+}\right) - 4\,\mathrm{Li}_2\left(\frac{M^2}{m^2+i0^+}\right) - \frac{4\pi^2}{3} + \\ & + \delta_{\kappa,-\rho}\left(\frac{t^2-u^2}{t^2}\left[\ln^2\left(\frac{-u-i0^+}{-s-i0^+}\right)+\pi^2\right] + \frac{2s}{t}\ln\left(\frac{-u-i0^+}{-s-i0^+}\right)\right) \Bigg\}, \end{aligned} \tag{E.107}$$

$$F^{\rho\kappa,\xi=1}_{2,c} = 0, \tag{E.108}$$

$$\begin{aligned} \Delta F^{\rho\kappa,\xi}_{1,c} = g_l^{\kappa} g_{\bar{l}}^{\kappa} g_f^{\rho} g_{\bar{f}}^{\rho} \Bigg\{ & 2(\xi-1)\ln\left(\frac{M^2}{-s-i0^+}\right) - 2\left(\frac{m^2}{M^2}-1\right)\ln\left(\frac{M^2}{M^2-m^2-i0^+}\right) + \\ & + 2\left(\frac{m^2}{M^2}-\xi\right)\ln\left(\frac{M^2}{M^2\xi-m^2-i0^+}\right) + \frac{1}{2}\left(-\xi^2-2\xi+3\right) \Bigg\}, \end{aligned} \tag{E.109}$$

$$\Delta F^{\rho\kappa,\xi}_{2,c} = 0. \tag{E.110}$$

E.5.12 Neutral box

E.5.12.1 Crossed type

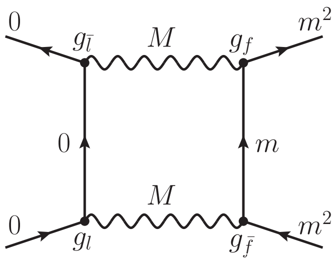

$$
\begin{aligned}
F_{1,c}^{\rho\kappa,\xi=1} = {} & g_l^\kappa g_{\bar{l}}^\kappa g_f^\rho g_{\bar{f}}^\rho \times \\
& \times \Bigg\{ 2\ln^2\left(\frac{M^2}{-s-i0^+}\right) - 4\ln\left(\frac{M^2}{-s-i0^+}\right)\ln\left(\frac{-u-i0^+}{-s-i0^+}\right) - \frac{4\pi^2}{3} + \\
& + 4\,\mathrm{Li}_2\left(\frac{2m^2}{M^2+\sqrt{M^2\left(M^2-4m^2\right)}}\right) + 4\,\mathrm{Li}_2\left(\frac{2m^2}{M^2-\sqrt{M^2\left(M^2-4m^2\right)}}\right) + \\
& + \delta_{\kappa,-\rho}\left(\frac{t^2-u^2}{t^2}\left[\ln^2\left(\frac{-u-i0^+}{-s-i0^+}\right)+\pi^2\right] + \frac{2s}{t}\ln\left(\frac{-u-i0^+}{-s-i0^+}\right)\right)\Bigg\},
\end{aligned}
\tag{E.111}
$$

$$
F_{2,c}^{\rho\kappa,\xi=1} = 0, \tag{E.112}
$$

$$
\begin{aligned}
\Delta F_{1,c}^{\rho\kappa,\xi} = {} & g_l^\kappa g_{\bar{l}}^\kappa g_f^\rho g_{\bar{f}}^\rho \left\{ 2(\xi-1)\ln\left(\frac{M^2}{-s-i0^+}\right) + \frac{1}{2}\left(-\xi^2-2\xi+3\right) + 2\xi\ln(\xi)\right\} + \\
& + g_l^\kappa g_{\bar{l}}^\kappa\left(g_f^\rho g_{\bar{f}}^\rho - \frac{g_f^\rho g_{\bar{f}}^{-\rho} + g_f^{-\rho} g_{\bar{f}}^\rho}{2}\right)\Bigg\{(\xi-1)\ln\left(\frac{m^2}{M^2}\right) - \xi\ln(\xi) + \\
& \qquad - 2\sqrt{1-\frac{4m^2}{M^2}}\ln\left(\frac{\sqrt{M^2\left(M^2-4m^2\right)}+M^2}{2mM}\right) + \\
& \qquad + 2\sqrt{\xi\left(\xi-\frac{4m^2}{M^2}\right)}\ln\left(\frac{\sqrt{M^2\xi\left(M^2\xi-4m^2\right)}+M^2\xi}{2mM\sqrt{\xi}}\right) + \\
& \qquad + \frac{2m^2}{M^2}\mathrm{Li}_2\left(\frac{2m^2}{2m^2-M^2+\sqrt{M^2\left(M^2-4m^2\right)}}\right) + \\
& \qquad + \frac{2m^2}{M^2}\mathrm{Li}_2\left(\frac{2m^2}{2m^2-M^2-\sqrt{M^2\left(M^2-4m^2\right)}}\right) + \\
& \qquad - \frac{2m^2}{M^2}\mathrm{Li}_2\left(\frac{2m^2}{2m^2-M^2\xi+\sqrt{M^2\xi\left(M^2\xi-4m^2\right)}}\right) + \\
& \qquad - \frac{2m^2}{M^2} + \mathrm{Li}_2\left(\frac{2m^2}{2m^2-M^2\xi-\sqrt{M^2\xi\left(M^2\xi-4m^2\right)}}\right)\Bigg\},
\end{aligned}
\tag{E.113}
$$

$$\Delta F_{2,c}^{\rho\kappa,\xi} = 0. \tag{E.114}$$

E.5.12.2 Direct type

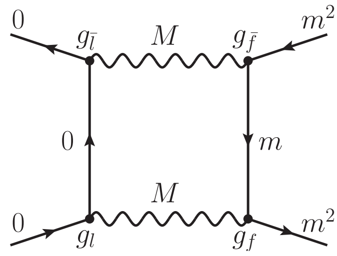

$$F_{1,d}^{\rho\kappa,\xi=1} = g_l^\kappa g_{\bar{l}}^\kappa g_f^\rho g_{\bar{f}}^\rho \times$$

$$\times \Bigg\{ -2\ln^2\left(\frac{M^2}{-s-i0^+}\right) + 4\ln\left(\frac{M^2}{-s-i0^+}\right)\ln\left(\frac{-t-i0^+}{-s-i0^+}\right) + \frac{4\pi^2}{3} +$$

$$-4\,\mathrm{Li}_2\left(\frac{2m^2}{M^2+\sqrt{M^2\left(M^2-4m^2\right)}}\right) - 4\,\mathrm{Li}_2\left(\frac{2m^2}{M^2-\sqrt{M^2\left(M^2-4m^2\right)}}\right) +$$

$$-\delta_{\kappa,\rho}\left(\frac{u^2-t^2}{u^2}\left[\ln^2\left(\frac{-t-i0^+}{-s-i0^+}\right)+\pi^2\right] + \frac{2s}{u}\ln\left(\frac{-t-i0^+}{-s-i0^+}\right)\right)\Bigg\}, \tag{E.115}$$

$$F_{2,d}^{\rho\kappa,\xi=1} = 0, \tag{E.116}$$

$$\Delta F_{1,d}^{\rho\kappa,\xi} = -g_l^\kappa g_{\bar{l}}^\kappa g_f^\rho g_{\bar{f}}^\rho \left\{ 2(\xi-1)\ln\left(\frac{M^2}{-s-i0^+}\right) + \frac{1}{2}\left(-\xi^2-2\xi+3\right) + 2\xi\ln(\xi)\right\} +$$

$$-g_l^\kappa g_{\bar{l}}^\kappa\left(g_f^\rho g_{\bar{f}}^\rho - \frac{g_f^\rho g_{\bar{f}}^{-\rho} + g_f^{-\rho} g_{\bar{f}}^\rho}{2}\right)\Bigg\{(\xi-1)\ln\left(\frac{m^2}{M^2}\right) - \xi\ln(\xi) +$$

$$-2\sqrt{1-\frac{4m^2}{M^2}}\ln\left(\frac{\sqrt{M^2\left(M^2-4m^2\right)}+M^2}{2mM}\right) +$$

$$+2\sqrt{\xi\left(\xi-\frac{4m^2}{M^2}\right)}\ln\left(\frac{\sqrt{M^2\xi\left(M^2\xi-4m^2\right)}+M^2\xi}{2mM\sqrt{\xi}}\right) +$$

$$+\frac{2m^2}{M^2}\mathrm{Li}_2\left(\frac{2m^2}{2m^2-M^2+\sqrt{M^2\left(M^2-4m^2\right)}}\right) +$$

$$+\frac{2m^2}{M^2}\mathrm{Li}_2\left(\frac{2m^2}{2m^2-M^2-\sqrt{M^2\left(M^2-4m^2\right)}}\right) +$$

$$-\frac{2m^2}{M^2}\mathrm{Li}_2\left(\frac{2m^2}{2m^2-M^2\xi+\sqrt{M^2\xi\left(M^2\xi-4m^2\right)}}\right) +$$

$$-\frac{2m^2}{M^2} + \mathrm{Li}_2\left(\frac{2m^2}{2m^2-M^2\xi-\sqrt{M^2\xi\left(M^2\xi-4m^2\right)}}\right)\Bigg\}, \tag{E.117}$$

$$\Delta F_{2,d}^{\rho\kappa,\xi} = 0. \tag{E.118}$$

Appendix F

Some details of fermion loop calculation

In this section we give some calculational details concerning the fermion loops in gauge boson self-energies $\Pi_{XY}^{\mu\nu}$. Throughout this section we will drop the superscript argument s, i.e. $\Pi_{XY}^{T}(s) \equiv \Pi_{XY}^{T}$. The fermionic loops can now be treated as massive or massless. When speaking of light fermion loops we usually understand the massive results expanded in some hard scale p^2 over the fermion mass m_f to leading order, but this agrees with the result for massless fermions. The generic expressions for both cases can be found in the section on generic diagrams, where the massless case coincides with the high-energy expanded results given there. For renormalization in this chapter we use the BHS-scheme.

F.1 Light fermions (light doublets)

We begin with the light fermion contributions, the top quark is covered in the next section. Starting with the AA-transition the bare diagrams (with off-shellness s) and the $\overline{\text{MS}}$-counterterm (for details on this choice see main text) for a single light (or massless) fermion f are given by

$$\begin{aligned}
\left(\Pi_{AA}^{T}\right)_f &= -\frac{\alpha}{3\pi}\, N_{c,f}\, Q_f^2\, s\left[\frac{1}{\epsilon} + \ln\left(\frac{\mu^2}{-s-i0^+}\right) + \frac{5}{3}\right], \\
\left(\delta Z_2^{\gamma}\right)_f^{\overline{\text{MS}}} &= -\frac{\alpha}{3\pi}\, N_{c,f}\, Q_f^2\, \frac{1}{\epsilon}, \\
\left(\hat{\Pi}_{AA}^{T}\right)_f &= \left(\Pi_{AA}^{T}\right)_f - \left(\delta Z_2^{\gamma}\right)_f^{\overline{\text{MS}}} = \\
&= -\frac{\alpha}{3\pi}\, N_{c,f}\, Q_f^2\, s\left[\ln\left(\frac{\mu^2}{-s-i0^+}\right) + \frac{5}{3}\right]. \qquad \text{(F.1)}
\end{aligned}$$

Due to $\overline{\text{MS}}$-subtraction there is now explicit μ-dependence, to be compensated by the running of $\alpha = \alpha(\mu)$. Every fermion charged under $U(1)_Q$ gives a contribution of this form, irrespectible of the multiplet structure of $SU(2)$ its left- and right-handed compontents are embedded in.

The ZA-transition is similiar, but due to the Z the renormalization procedure it is sensitive to the $SU(2)$-group-structure (via the renormalization constant δZ_c that also gets contributions from the WW-transition). We therefore give the results per light *doublet* D (or alternatively per light generation), containing fermions with isospin $\left(+\frac{1}{2}\right)$ and $\left(-\frac{1}{2}\right)$. The top-bottom doublet needs to be treated separately (see next section). Note that since $\delta Z_1^{\gamma Z} - \delta Z_2^{\gamma Z}$ does not get fermionic contributions, the counterterm simplifies as well as $\left(\delta Z_2^{\gamma}\right)_D = \left(\delta Z_1^{\gamma}\right)_D$. We emphasize that only $\left(\delta Z_2^{\gamma}\right)_D$ is constructed by minimal subtraction, the rest of the renormalization constants is defined in the OS-scheme. We obtain

$$\begin{aligned}
\left(\Pi_{ZA}^{T}\right)_D &= \frac{\alpha}{3\pi}\, N_{c,D}\Big(\sum_{f\in D} Q_f\, v_f\Big)\, s\left[\frac{1}{\epsilon} + \ln\left(\frac{\mu^2}{-s-i0^+}\right) + \frac{5}{3}\right], \\
\left(\delta Z_2^{\gamma Z}\right)_D^{\text{OS}} &= \frac{c_W s_W}{c_W^2 - s_W^2}\left[\left(\delta Z_2^{Z}\right)_D^{\text{OS}} - \left(\delta Z_2^{\gamma}\right)_D^{\overline{\text{MS}}}\right] \overset{(2.117)}{=}
\end{aligned}$$

$$= 2\underbrace{\left(\delta Z_1^{\gamma Z} - \delta Z_2^{\gamma Z}\right)_D^{\mathrm{OS}}}_{=0} - 2\frac{c_W}{s_W}\left(\delta Z_c\right)_D^{\mathrm{OS}} =$$

$$= -\frac{\alpha}{3\pi}\, N_{c,D}\Bigg\{\frac{1}{4s_W^2}\left[\frac{1}{\epsilon} + \ln\left(\frac{\mu^2}{M_W^2}\right) + \frac{5}{3}\right] +$$

$$- \Big(\sum_{f\in D} Q_f\, v_f\Big)\left[\frac{1}{\epsilon} + \ln\left(\frac{\mu^2}{M_Z^2}\right) + \frac{5}{3}\right]\Bigg\},$$

$$\left(\hat{\Pi}_{ZA}^T\right)_D = \left(\Pi_{ZA}^T\right)_D - \left(\delta Z_2^{\gamma Z}\right)_D^{\mathrm{OS}} - M_Z^2\underbrace{\left(\delta Z_1^{\gamma Z} - \delta Z_2^{\gamma Z}\right)_D^{\mathrm{OS}}}_{=0} =$$

$$= \frac{\alpha}{3\pi}\, N_{c,D}\, s\Bigg\{\underbrace{\Bigg(\Big(\sum_{f\in D} Q_f\, v_f\Big) - \frac{c_W}{4s_W^3} + \frac{c_W}{s_W}\Big(\sum_{f\in D}\left(v_f^2 + a_f^2\right)\Big)\Bigg)}_{=0}\left[\frac{1}{\epsilon} + \ln\left(\frac{\mu^2}{M_W^2}\right) + \frac{5}{3}\right] +$$

$$+ \Big(\sum_{f\in D} Q_f\, v_f\Big)\ \ln\left(\frac{M_W^2}{-s - i0^+}\right) + \frac{c_W}{s_W}\Big(\sum_{f\in D}\left(v_f^2 + a_f^2\right)\Big)\ \ln\left(\frac{M_W^2}{M_Z^2}\right)\Bigg\} =$$

$$= \frac{\alpha}{3\pi}\, N_{c,D}\, s\Bigg\{\Big(\sum_{f\in D} Q_f\, v_f\Big)\ \ln\left(\frac{M_W^2}{-s - i0^+}\right) + \frac{c_W}{s_W}\Big(\sum_{f\in D}\left(v_f^2 + a_f^2\right)\Big)\ \ln\left(\frac{M_W^2}{M_Z^2}\right)\Bigg\}. \tag{F.2}$$

Note that the explicit μ-dependence has cancelled. We rewrote everything in terms of sum of fermion $f \in D$ to emphasize that although the renormalization constants were sensitive to the doublet structure, the renormalized corrections of each light fermion decouple again. For this reason we wrote the total contribution as a sum over all (light) fermions rather than a sum over (light) doublets in eq. (3.47) in the main text.

Finally for the contribution of the light doublet D to the ZZ-transition we get

$$\left(\Pi_{ZZ}^T\right)_D = -\frac{\alpha}{3\pi}\Big(\sum_{f\in D} N_{c,f}\left(v_f^2 + a_f^2\right)\Big)\, s\left[\frac{1}{\epsilon} + \ln\left(\frac{\mu^2}{-s - i0^+}\right) + \frac{5}{3}\right],$$

$$\left(\delta Z_{M_Z}\right)_D^{\mathrm{OS}} = \frac{\alpha}{3\pi}\, N_{c,D}\Big(\sum_{f\in D}\left(v_f^2 + a_f^2\right)\Big)\, s\left[\frac{1}{\epsilon} + \ln\left(\frac{\mu^2}{M_Z^2}\right) + \frac{5}{3}\right] =$$

$$\left(\delta Z_2^Z\right)_D^{\mathrm{OS}} \overset{(2.117)}{=} \left(\delta Z_2^{\gamma}\right)_D^{\overline{\mathrm{MS}}} + 2\frac{c_W^2 - s_W^2}{c_W\, s_W}\Big[\underbrace{\left(\delta Z_1^{\gamma Z} - \delta Z_2^{\gamma Z}\right)_D^{\mathrm{OS}}}_{=0} - \frac{c_W}{s_W}\left(\delta Z_c\right)_D^{\mathrm{OS}}\Big] =$$

$$= -\frac{\alpha}{3\pi}\, N_{c,D}\Bigg\{\Big(\sum_{f\in D} Q_f^2\Big)\frac{1}{\epsilon} + \frac{c_W^2 - s_W^2}{s_W^2}\Bigg[\frac{1}{4s_W^2}\left[\frac{1}{\epsilon} + \ln\left(\frac{\mu^2}{M_W^2}\right) + \frac{5}{3}\right] +$$

$$- \Big(\sum_{f\in D} N_{c,f}(v_f^2 + a_f^2)\Big)\left[\frac{1}{\epsilon} + \ln\left(\frac{\mu^2}{M_Z^2}\right) + \frac{5}{3}\right]\Bigg]\Bigg\},$$

$$\left(\hat{\Pi}_{ZZ}^T\right)_D = \left(\Pi_{ZZ}^T\right)_D - (s - M_Z^2)\left(\delta Z_2^Z\right)_D^{\mathrm{OS}} + M_Z^2\left(\delta Z_{M_Z}\right)_D^{\mathrm{OS}} =$$

$$= -\frac{\alpha}{3\pi}\, N_{c,D}\Bigg\{(s - M_Z^2)\left[\frac{1}{\epsilon} + \ln\left(\frac{\mu^2}{M_W^2}\right) + \frac{5}{3}\right]\times$$

$$\times \Bigg(\underbrace{\Big(\sum_{f\in D} (v_f^2 + a_f^2) \Big) - \Big(\sum_{f\in D} Q_f^2 \Big) - \frac{c_W^2 - s_W^2}{c_W s_W} \left[\frac{1}{4s_W^2} - \Big(\sum_{f\in D} (v_f^2 + a_f^2) \Big) \right]}_{=0} \Bigg) +$$

$$+ \Big(\sum_{f\in D} (v_f^2 + a_f^2) \Big) \times$$

$$\times \left[s \ln\left(\frac{M_W^2}{-s - i0^+} \right) - M_Z^2 \ln\left(\frac{M_W^2}{M_Z^2} \right) + \frac{c_W^2 - s_W^2}{s_W^2} (s - M_Z^2) \ln\left(\frac{M_W^2}{M_Z^2} \right) \right] +$$

$$+ \Big(\sum_{f\in D} Q_f^2 \Big) (s - M_Z^2) \left[\ln\left(\frac{\mu^2}{M_W^2} \right) + \frac{5}{3} \right] \Bigg\} =$$

$$= -\frac{\alpha}{3\pi} \Bigg\{ \Big(\sum_{f\in D} (v_f^2 + a_f^2) \Big) \left[s \ln\left(\frac{M_Z^2}{-s - i0^+} \right) + \frac{c_W^2}{s_W^2} (s - M_Z^2) \ln\left(\frac{M_W^2}{M_Z^2} \right) \right] +$$

$$+ \Big(\sum_{f\in D} Q_f^2 \Big) (s - M_Z^2) \left[\ln\left(\frac{\mu^2}{M_W^2} \right) + \frac{5}{3} \right] \Bigg\}. \tag{F.3}$$

Once again the total contribution can be written as a sum over independent contributions of all light fermions, as done in sec. 3.4.2. The expressions (F.1), (F.2) and (F.3) are basically already identical to their high-energy exansions, only for $\big(\hat{\Pi}^T_{ZZ}\big)^{\mathrm{OS}}_D$ the explicit prefactors of M_Z^2 need to be dropped.

F.2 Top-bottom doublet

The full top contributions are a bit lengthy (especially for the ZZ-transition), and at the same time not that interesting. However, the high-energy limit looks a bit different than for the massless (light) doublets above, so we give some intermediate steps on the construction of the high-energy expression.

As the counterterm $\big(\delta Z_2^\gamma\big)^{\overline{\mathrm{MS}}}_f$ is defined in the $\overline{\mathrm{MS}}$-scheme, the top-bottom doublet contribution to $\big(\hat{\Pi}^T_{AA}\big)_{D_{tb}}$ in the high-energy regime looks identical to that of a light doublet D in eq. (F.1),

$$\big(\hat{\Pi}^T_{AA}\big)^{\mathrm{HE}}_{D_{tb}} = -\frac{\alpha}{3\pi} N_c \Big(Q_t^2 + Q_b^2 \Big)\, s \left[\frac{1}{\epsilon} + \ln\left(\frac{\mu^2}{-s - i0^+} \right) + \frac{5}{3} \right],$$

$$\big(\delta Z_2^\gamma\big)^{\overline{\mathrm{MS}}}_{D_{tb}} = -\frac{\alpha}{3\pi} N_c \Big(Q_t^2 + Q_b^2 \Big) \frac{1}{\epsilon},$$

$$\big(\hat{\Pi}^T_{AA}\big)_{D_{tb}} = \big(\Pi^T_{AA}\big)_{D_{tb}} - s\big(\delta Z_2^\gamma\big)^{\overline{\mathrm{MS}}}_{D_{tb}} = -\frac{\alpha}{3\pi} N_c \Big(Q_t^2 + Q_b^2 \Big)\, s \left[\ln\left(\frac{\mu^2}{-s - i0^+} \right) + \frac{5}{3} \right], \tag{F.4}$$

and this is already the high-energy value. The ZA- and ZZ-transitions are sensitive to the doublet structure however, so their contributions are a bit more involved. Using the notation $\delta\hat{Z}^{D_{tb}}_{M_W}$ and $\delta\hat{Z}^{D_{tb}}_{M_Z}$ to denote the UV-finite parts of the boson mass renormalization constants (cf. 2.5.2), we obtain

$$\big(\Pi^T_{ZA}\big)^{\mathrm{HE}}_{D_{tb}} = \frac{\alpha}{3\pi} N_c \left(Q_t\, v_t + Q_b\, v_b \right) \Big)\, s \left[\frac{1}{\epsilon} + \ln\left(\frac{\mu^2}{-s - i0^+} \right) + \frac{5}{3} \right],$$

$$\big(\delta Z_2^{\gamma Z}\big)^{\mathrm{OS}}_{D_{tb}} = 2 \underbrace{\big(\delta Z_1^{\gamma Z} - \delta Z_2^{\gamma Z}\big)^{\mathrm{OS}}_{D_{tb}}}_{=0} - 2\frac{c_W}{s_W} \big(\delta Z_c\big)^{\mathrm{OS}}_{D_{tb}} = -\frac{c_W}{s_W} \Big[\big(\delta Z_{M_W}\big)^{\mathrm{OS}}_{D_{tb}} - \big(\delta Z_{M_Z}\big)^{\mathrm{OS}}_{D_{tb}} \Big] =$$

$$= \frac{\alpha}{4\pi} \frac{N_c}{\epsilon} \Bigg\{ -\frac{c_W}{s_W} \left[\frac{2M_W^2 - 3m_t^2}{6 s_W^2 M_W^2} - \frac{4}{3}(v_t^2 + a_t^2 + v_b^2 + a_b^2) + \frac{8a_t^2}{M_Z^2} \right] \Bigg\} +$$

$$
-\frac{c_W^2-s_W^2}{s_W^2}\left[\left(\delta\hat{Z}_{M_W}\right)^{\text{OS}}_{D_{tb}}-\left(\delta\hat{Z}_{M_Z}\right)^{\text{OS}}_{D_{tb}}\right],
$$

$$
\begin{aligned}
\left(\hat{\Pi}^T_{ZA}\right)^{\text{HE}}_{D_{tb}} &= \left(\Pi^T_{ZA}\right)^{\text{HE}}_{D_{tb}} + s\left(\delta Z_2^{\gamma Z}\right)^{\text{OS}}_{D_{tb}} = \\
&= -\frac{\alpha}{3\pi}N_c\left(Q_t\,v_t+Q_b\,a_b\right)s\left[\ln\left(\frac{\mu^2}{-s-i0^+}\right)+\frac{5}{3}\right]+ \\
&\quad -\frac{c_W}{s_W}\left[\left(\delta\hat{Z}_{M_W}\right)^{\text{OS}}_{D_{tb}}-\left(\delta\hat{Z}_{M_Z}\right)^{\text{OS}}_{D_{tb}}\right].
\end{aligned}
\tag{F.5}
$$

For the ZZ-transition we note that in the high-energy limit we only need the renormalization constant $\left(\delta Z_2^Z\right)_{D_{tb}}$, as the part with δZ_{M_Z} is power-suppressed. We get

$$
\left(\Pi^T_{ZZ}\right)^{\text{HE}}_{D_{tb}} = -\frac{\alpha}{3\pi}N_c\left(v_t^2+a_t^2+v_b^2+a_b^2\right)\right)s\left[\frac{1}{\epsilon}+\ln\left(\frac{\mu^2}{-s-i0^+}\right)+\frac{5}{3}\right],
$$

$$
\begin{aligned}
\left(\delta Z_2^Z\right)^{\text{OS}}_{D_{tb}} &\overset{(2.117)}{=} \left(\delta Z_2^\gamma\right)^{\overline{\text{MS}}}_{D_{tb}} + 2\frac{c_W^2-s_W^2}{c_W\,s_W}\Big[\underbrace{\left(\delta Z_1^{\gamma Z}-\delta Z_2^{\gamma Z}\right)^{\text{OS}}_{D_{tb}}}_{=0}-\frac{c_W}{s_W}\left(\delta Z_c\right)^{\text{OS}}_{D_{tb}}\Big] = \\
&= \left(\delta Z_2^\gamma\right)^{\overline{\text{MS}}}_{D_{tb}} - \frac{c_W^2-s_W^2}{s_W^2}\left[\left(\delta Z_{M_W}\right)^{\text{OS}}_{D_{tb}}-\left(\delta Z_{M_Z}\right)^{\text{OS}}_{D_{tb}}\right] = \\
&= \frac{\alpha}{4\pi}\frac{N_c}{\epsilon}\left\{-\frac{4}{3}\left(Q_t^2+Q_b^2\right)-\frac{c_W^2-s_W^2}{s_W^2}\left[\frac{2M_W^2-3m_t^2}{6s_W^2M_W^2}-\frac{4}{3}(v_t^2+a_t^2+v_b^2+a_b^2)+\frac{8a_t^2m_t^2}{M_Z^2}\right]\right\}+ \\
&\quad -\frac{c_W^2-s_W^2}{s_W^2}\left[\left(\delta\hat{Z}_{M_W}\right)^{\text{OS}}_{D_{tb}}-\left(\delta\hat{Z}_{M_Z}\right)^{\text{OS}}_{D_{tb}}\right],
\end{aligned}
$$

$$
\begin{aligned}
\left(\hat{\Pi}^T_{ZZ}\right)^{\text{HE}}_{D_{tb}} &= \left(\Pi^T_{ZZ}\right)^{\text{HE}}_{D_{tb}} - s\left(\delta Z_2^{Z}\right)^{\text{OS}}_{D_{tb}} = \\
&= -\frac{\alpha}{3\pi}N_c\left(v_t^2+a_t^2+v_b^2+a_b^2\right)s\left[\ln\left(\frac{\mu^2}{-s-i0^+}\right)+\frac{5}{3}\right]+ \\
&\quad -\frac{c_W^2-s_W^2}{s_W^2}\left[\left(\delta\hat{Z}_{M_W}\right)^{\text{OS}}_{D_{tb}}-\left(\delta\hat{Z}_{M_Z}\right)^{\text{OS}}_{D_{tb}}\right].
\end{aligned}
\tag{F.6}
$$

F.3 Running of α over particle thresholds

The $\overline{\text{MS}}$-subtraction introduces an explicit μ-dependence into the expressions, that needs to be compensated by running of $\alpha(\mu)$. Differentiating the relation of bare to $\overline{\text{MS}}$-coupling

$$
\alpha_0 = \mu^{2\epsilon}Z_\alpha\,\alpha(\mu)
\tag{F.7}
$$

yields

$$
0 \overset{!}{=} \frac{d\alpha_0}{d\,\ln(\mu^2)} = \mu^{2\epsilon}\left(\epsilon\,Z_\alpha\,\alpha(\mu)+\alpha(\mu)\frac{dZ_\alpha}{d\,\ln(\mu^2)}+Z_\alpha\,\frac{d\alpha(\mu)}{d\,\ln(\mu^2)}\right).
\tag{F.8}
$$

Assuming $Z_\alpha = 1+\alpha(\mu)\,\frac{b}{\epsilon}+\mathcal{O}(\alpha^2)$, where b is some constant, we obtain

$$
\frac{dZ_\alpha}{d\,\ln(\mu^2)} = \frac{b}{\epsilon}\,\frac{d\alpha(\mu)}{d\,\ln(\mu^2)}.
\tag{F.9}
$$

Pluggin into eq. (F.8) and expanding to $\mathcal{O}(\alpha^2)$ yields

$$
\frac{d\alpha(\mu)}{d\,\ln(\mu^2)} = \beta_\epsilon\,\alpha(\mu)+\mathcal{O}(\alpha^2),
$$

$$\beta_\epsilon \equiv -\epsilon + b\,\alpha(\mu), \tag{F.10}$$

Sending $\epsilon \to 0$ and solving this ODE by separation of variables with some given initial condition $\alpha(\mu_0)$ yields

$$\alpha(\mu) = \frac{\alpha(\mu_0)}{1 - \alpha(\mu_0)\, b\, \ln\left(\frac{\mu^2}{\mu_0^2}\right)}. \tag{F.11}$$

Suppose now we have the value of the coupling $\alpha(m_1)$ at the mass scale m_1 of the lightest fermion (e.g. the electron mass m_e) as input. The theory above this threshold is a theory with one active fermion in the loop[1], and the running of α up to the scale m_2 of the next-to-lightest particles can be calculated with eq. (F.11)

$$\alpha^{(1)}(m_2) = \frac{\alpha^{(0)}(m_1)}{1 - \alpha^{(0)}(m_1)\, b^{(1)}\, \ln\left(\frac{m_2^2}{m_1^2}\right)}. \tag{F.12}$$

With the superscript on α and c we indicate how many active particles the theory had in which b was calculated. In the regime $\mu > m_2$ we now can solve the RGE again with 2 active particles in the theory (and in the loop), and the formal solution is analogous to eq. (F.11)

$$\alpha^{(2)}(\mu) = \frac{\alpha^{(1)}(m_2)}{1 - \alpha^{(1)}(m_2)\, b^{(2)}\, \ln\left(\frac{\mu^2}{m_2^2}\right)}, \tag{F.13}$$

where $b^{(2)}$ was now calculated in the theory with 2 active particles (with masses m_1, m_2). Inserting eq. (F.12) into (F.13) and multiplying out we get

$$\begin{aligned}\alpha^{(2)}(\mu) &= \frac{\alpha^{(0)}(m_1)}{1 - \alpha^{(0)}(m_1)\Big(b^{(1)}\, \ln\left(\frac{m_2^2}{m_1^2}\right) + b^{(2)}\, \ln\left(\frac{\mu^2}{m_2^2}\right)\Big)} = \\ &= \frac{\alpha^{(0)}(m_0)}{1 - \alpha^{(0)}(m_1)\Big(b^{(1)}\, \ln\left(\frac{\mu^2}{m_1^2}\right) + \left[b^{(2)} - b^{(1)}\right]\, \ln\left(\frac{\mu^2}{m_2^2}\right)\Big)}\end{aligned} \tag{F.14}$$

where we simply reordered the logarithms in the denominator. As the $\mathcal{O}(\alpha)$-corrections to Z_α and thus b are additive the quantity $b^{(2)} - b^{(1)}$ is just the 1-loop contribution of particle 2 to the β-function. This procedure can be iterated to cross more and more particle thresholds until one ends up in the desired energy regime. Writing the contribution to Z_α of the k-th individual particle as

$$\bar{b}^{(k)} \equiv b^{(k)} - \sum_{i=1}^{k-1} b^{(i)}, \tag{F.15}$$

then $\alpha^{(n)}(\mu)$ with $\mu > m_n$ for the theory with n active particles in the loop is given by

$$\alpha^{(n)}(\mu) = \frac{\alpha^{(0)}(m_1)}{1 - \alpha^{(0)}(m_1)\sum_{k=1}^{n} \bar{b}^{(k)} \ln\left(\frac{\mu^2}{m_k^2}\right)}. \tag{F.16}$$

In pure QED we only have fermions in the loop[2]. The result for the SM is given in the main text, eq. (3.45) in sec. 3.4.2.

[1]That the heavier particles decouple in the low energy regime is actually not visible in dimensional regularization, and the particles have to be taken out of the theory and added back by hand when the scales of the problem exceed the particles mass.

[2]In non-abelian theories there are also gauge bosons in the loop. However, in the EW-sector the weak gauge bosons are not included in the running for reasons of gauge-independence (see discussion in the main text).

Appendix G

Feynman rules of EW theory and complete Feynman diagram sets

G.1 Feynman rules of EW theory

In this section we give the complete EW Feynman rules in R_ξ-gauge (as introduced in the sec. 2.1.4), taken from [32]. All particles and momenta are treated as incoming.

G.1.1 Propagators

- **Vector (massive)**:

$$\begin{aligned}
&= \frac{-i}{k^2 - M_V^2 + i0^+}\left(g_{\mu\nu} + \frac{(\xi_V - 1)k_\mu k_\nu}{k^2 - M_V^2 \xi_V}\right) = \\
&= \frac{-i}{k^2 - M_V^2 + i0^+}\left(g_{\mu\nu} - \frac{k_\mu k_\nu}{k^2}\right) + \frac{-i\,\xi_V}{k^2 - M_V^2 \xi_V + i0^+}\frac{k_\mu k_\nu}{k^2} = \\
&= \frac{-i}{k^2 - M_V^2 + i0^+}\left(g_{\mu\nu} - \frac{k_\mu k_\nu}{M_V^2}\right) + \frac{-i}{k^2 - M_V^2 \xi_V + i0^+}\frac{k_\mu k_\nu}{M_V^2}.
\end{aligned} \tag{G.1}$$

- **Vector (massless)**:

$$= \frac{-i}{k^2 + i0^+}\left(g_{\mu\nu} + \frac{(\xi_V - 1)k_\mu k_\nu}{k^2}\right). \tag{G.2}$$

- **Scalar**:

$$= \frac{i}{k^2 - M_S^2 + i0^+}. \tag{G.3}$$

$\boldsymbol{S}$	H	χ	$\phi^\pm$
$\boldsymbol{M_S}$	M_H	$M_Z\sqrt{\xi_Z}$	$M_W\sqrt{\xi_W}$

- **Ghost**:

$$= \frac{i}{k^2 - M_u^2 + i0^+}. \tag{G.4}$$

$\boldsymbol{u}$	$\bar{u}^A, u^A$	$\bar{u}^Z, u^Z$	$\bar{u}^\pm, u^\pm$
$\boldsymbol{M_u}$	0	$M_Z\sqrt{\xi_Z}$	$M_W\sqrt{\xi_W}$

- **Fermion**:

$$= \frac{i(\not{k} + m_f)}{k^2 - m_f^2 + i0^+}. \tag{G.5}$$

G.1.2 Vertices

- $\boldsymbol{VVVV}$:

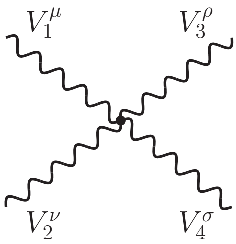

$$= \quad ie^2 C\Big[2g_{\mu\nu}g_{\rho\sigma} - g_{\mu\rho}g_{\nu\sigma} - g_{\mu\sigma}g_{\nu\rho}\Big] \tag{G.6}$$

$\boldsymbol{V_1V_2V_3V_4}$	$W^+W^+W^-W^-$	W^+W^-ZZ	W^+W^-AZ	$W^+W^-W^-AA$
$\boldsymbol{C}$	$\frac{1}{s_W^2}$	$-\frac{c_W^2}{s_W^2}$	$\frac{c_W}{s_W}$	-1

- $\boldsymbol{VVV}$:

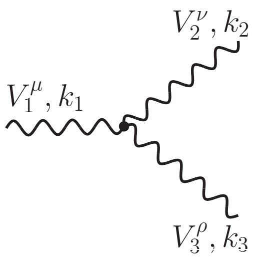

$$= \quad ie\, C\Big[g_{\mu\nu}(k_1 - k_2)_\rho + g_{\nu\rho}(k_2 - k_3)_\mu + g_{\mu\rho}(k_3 - k_1)_\nu\Big] \tag{G.7}$$

$\boldsymbol{V_1V_2V_3}$	AW^+W^-	ZW^+W^-
$\boldsymbol{C}$	1	$-\frac{c_W}{s_W}$

- $\boldsymbol{SSSS}$:

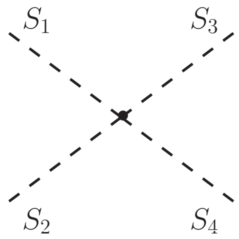

$$= \quad ie^2 C \tag{G.8}$$

$\boldsymbol{S_1S_2S_3S_4}$	$HHHH, \chi\chi\chi\chi$	$HH\chi\chi, HH\phi^+\phi^-, \chi\chi\phi^+\phi^-$	$\phi^+\phi^-\phi^+\phi^-$
$\boldsymbol{C}$	$-\frac{3}{4s_W^2}\frac{M_H^2}{M_W^2}$	$-\frac{1}{4s_W^2}\frac{M_H^2}{M_W^2}$	$-\frac{1}{2s_W^2}\frac{M_H^2}{M_W^2}$

- $\boldsymbol{SSS}$:

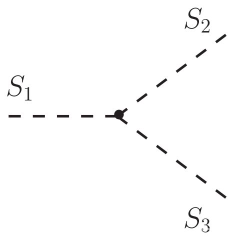

$$= \quad ie\, C \tag{G.9}$$

$\boldsymbol{S_1S_2S_3}$	HHH	$H\chi\chi, H\phi^+\phi^-$
$\boldsymbol{C}$	$-\frac{3}{2s_W}\frac{M_H^2}{M_W}$	$-\frac{1}{2s_W}\frac{M_H^2}{M_W}$

- $\boldsymbol{VVSS}$:

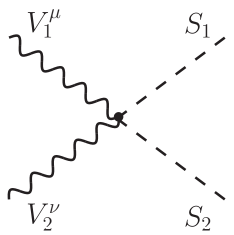

$$= \quad ie^2 C\, g_{\mu\nu} \tag{G.10}$$

$\boldsymbol{V_1V_2S_1S_2}$	$ZZHH, ZZ\chi\chi$	$W^+W^-HH, W^+W^-\chi\chi,$ $W^+W^-\phi^+\phi^-$	$AA\phi^+\phi^-$	$ZA\phi^+\phi^-$	$ZZ\phi^+\phi^-$
$\boldsymbol{C}$	$\frac{1}{2c_W^2 s_W^2}$	$\frac{1}{2s_W^2}$	2	$-\frac{c_W^2-s_W^2}{c_W s_W}$	$\frac{(c_W^2-s_W^2)^2}{2c_W^2 s_W^2}$

$\boldsymbol{V_1V_2S_1S_2}$	$W^\pm A\phi^\mp H$	$W^\pm A\phi^\mp\chi$	$W^\pm Z\phi^\mp H$	$W^\pm Z\phi^\mp\chi$
$\boldsymbol{C}$	$-\frac{1}{2s_W^2}$	$\mp\frac{i}{2s_W}$	$-\frac{1}{2c_W}$	$\mp\frac{i}{2c_W}$

- $\boldsymbol{VSS}$:

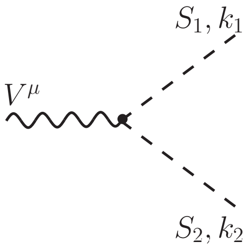

$$= \quad ie\,C(k_1 - k_2)_\mu \tag{G.11}$$

$\boldsymbol{VS_1S_2}$	$Z\chi\eta$	$A\phi^+\phi^-$	$Z\phi^+\phi^-$	$W^\pm\phi^\mp H$	$W^\pm\phi^\mp\chi$
$\boldsymbol{C}$	$-\frac{i}{2c_W s_W}$	-1	$\frac{c_W^2 - s_W^2}{2c_W s_W}$	$\mp\frac{1}{2s_W}$	$-\frac{i}{2s_W}$

- $\boldsymbol{SVV}$:

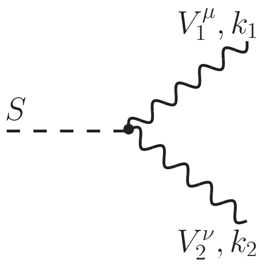

$$= \quad ie\,C\,g_{\mu\nu} \tag{G.12}$$

$S\boldsymbol{V_1V_2}$	HZZ	HW^+W^-	$\phi^\pm W^\mp A$	$\phi^\pm W^\mp Z$
$\boldsymbol{C}$	$\frac{1}{c_W^2 s_W}\,M_W$	$\frac{1}{s_W}\,M_W$	$-M_W$	$-\frac{s_W}{c_W}\,M_W$

- $\boldsymbol{Vff}$:

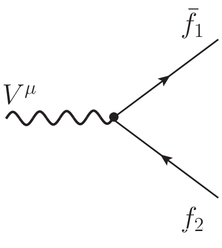

$$= \quad ie\,\gamma_\mu\left[C_{\mathrm{L}}\frac{1-\gamma_5}{2} + C_{\mathrm{R}}\frac{1-\gamma_5}{2}\right] \tag{G.13}$$

$\boldsymbol{V\bar{f}_1f_2}$	$A\bar{f}_i f_j$	$Z\bar{f}_i f_j$	$W^+\bar{u}_i d_j$	$W^-\bar{d}_j u_i$	$W^+\bar{\nu}_i l_j$	$W^-\bar{l}_j \nu_i$
$\boldsymbol{C_{\mathrm{L}}}$	$-Q_f\,\delta_{ij}$	$(v_f + a_f)\,\delta_{ij}$	$\frac{1}{\sqrt{2}s_W}\,V_{ij}$	$\frac{1}{\sqrt{2}s_W}\,V_{ji}^\dagger$	$\frac{1}{\sqrt{2}s_W}\,\delta_{ij}$	$\frac{1}{\sqrt{2}s_W}\,\delta_{ij}$
$\boldsymbol{C_{\mathrm{R}}}$	$-Q_f\,\delta_{ij}$	$(v_f - a_f)\,\delta_{ij}$	0	0	0	0

$$v_f = \frac{1}{2c_W s_W}\Big(T_3^f - 2Q_f s_W^2\Big), \qquad a_f = \frac{1}{2c_W s_W}\,T_3^f.$$

Note: in this work the CKM-matrix is set equal to the unit matrix: $V_{ij} = V_{ji}^\dagger = \delta_{ij}$. $T_3^f = \pm\frac{1}{2}$ is the isospin of fermion f.

- $\boldsymbol{Sff}$:

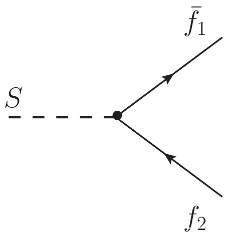

$$= \quad ie\left[C_{\mathrm{L}}\frac{1-\gamma_5}{2} + C_{\mathrm{R}}\frac{1-\gamma_5}{2}\right] \qquad \text{(G.14)}$$

$\boldsymbol{S\bar{f}_1 f_2}$	$H\bar{f}_i f_j$	$\chi\bar{f}_i f_j$	$\phi^+\bar{u}_i d_j$	$\phi^-\bar{d}_j u_i$	$\phi^+\bar{\nu}_i l_j$	$\phi^-\bar{l}_j \nu_i$
$\boldsymbol{C_{\mathrm{L}}}$	$\frac{-1}{2s_W}\frac{m_{f,i}}{M_W}\delta_{ij}$	$\frac{-i}{2s_W}2T_3^f\frac{m_{f,i}}{M_W}\delta_{ij}$	$\frac{1}{\sqrt{2}s_W}\frac{m_{u,i}}{M_W}V_{ij}$	$\frac{-1}{\sqrt{2}s_W}\frac{m_{d,j}}{M_W}V_{ji}^\dagger$	0	$\frac{-1}{\sqrt{2}s_W}\frac{m_{l,j}}{M_W}\delta_{ij}$
$\boldsymbol{C_{\mathrm{R}}}$	$\frac{-1}{2s_W}\frac{m_{f,i}}{M_W}\delta_{ij}$	$\frac{i}{2s_W}2T_3^f\frac{m_{f,i}}{M_W}\delta_{ij}$	$\frac{-1}{\sqrt{2}s_W}\frac{m_{d,j}}{M_W}V_{ij}$	$\frac{1}{\sqrt{2}s_W}\frac{m_{u,i}}{M_W}V_{ji}^\dagger$	$\frac{-1}{\sqrt{2}s_W}\frac{m_{l,j}}{M_W}\delta_{ij}$	0

Note: $T_3^f = \pm\frac{1}{2}$ is the isospin of fermion f.

- $\boldsymbol{Vuu}$:

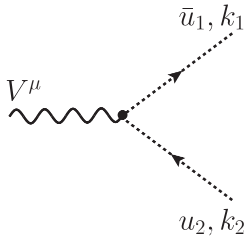

$$= \quad ie\,C\,k_{1,\mu} \qquad \text{(G.15)}$$

$\boldsymbol{V\bar{u}_1 u_2}$	$A\bar{u}^\pm u^\pm, W^\pm\bar{u}^A u^\mp, W^\mp\bar{u}^\mp u^A$	$Z\bar{u}^\pm u^\pm, W^\pm\bar{u}^Z u^\mp, W^\mp\bar{u}^\mp u^Z$
$\boldsymbol{C}$	± 1	$\mp\frac{c_W}{s_W}$

- $\boldsymbol{Suu}$:

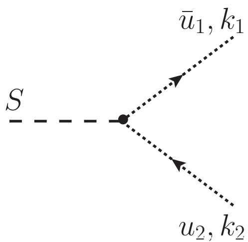

$$= \quad ie\,C \qquad \text{(G.16)}$$

$\boldsymbol{S\bar{u}_1 u_2}$	$H\bar{u}^Z u^Z$	$H\bar{u}^\pm u^\pm$	$\chi\bar{u}^\pm u^\pm$	$\phi^\pm\bar{u}^\pm u^A$	$\phi^\pm\bar{u}^\pm u^Z$	$\phi^\pm\bar{u}^Z u^\mp$
$\boldsymbol{C}$	$-\frac{\xi_Z}{2c_W^2 s_W}M_W$	$-\frac{\xi_W}{2s_W}M_W$	$\mp\frac{i\xi_W}{2s_W}M_W$	$\xi_W M_W$	$-\xi_W\frac{c_W^2-s_W^2}{2c_W s_W}M_W$	$\frac{\xi_Z}{2c_W s_W}M_W$

G.2 Complete Feynman diagram sets

All diagrams in this thesis were drawn with `JaxoDraw` [33]. Pure QED diagrams are not shown.

G.2.1 Fermionic 2-point

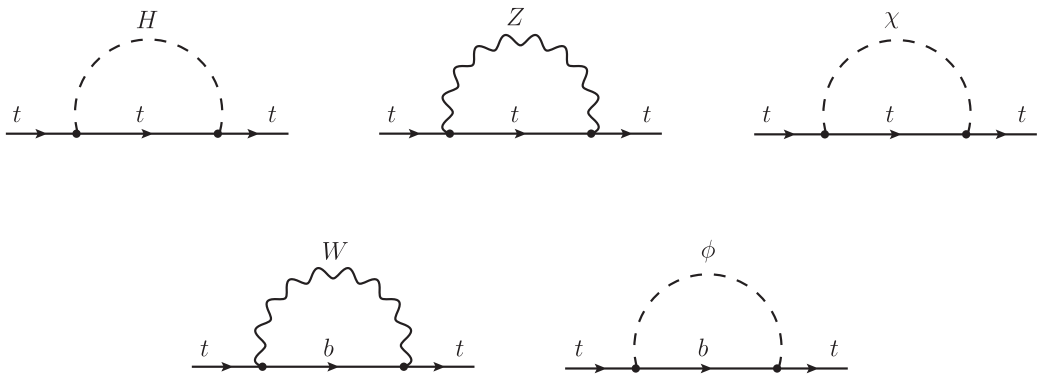

Figure G.1: EW contributons to the top quark self-energy.

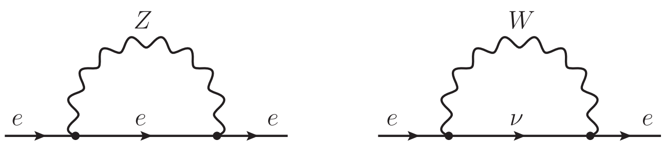

Figure G.2: EW contributons to the electron self-energy.

G.2.2 Bosonic 2-point

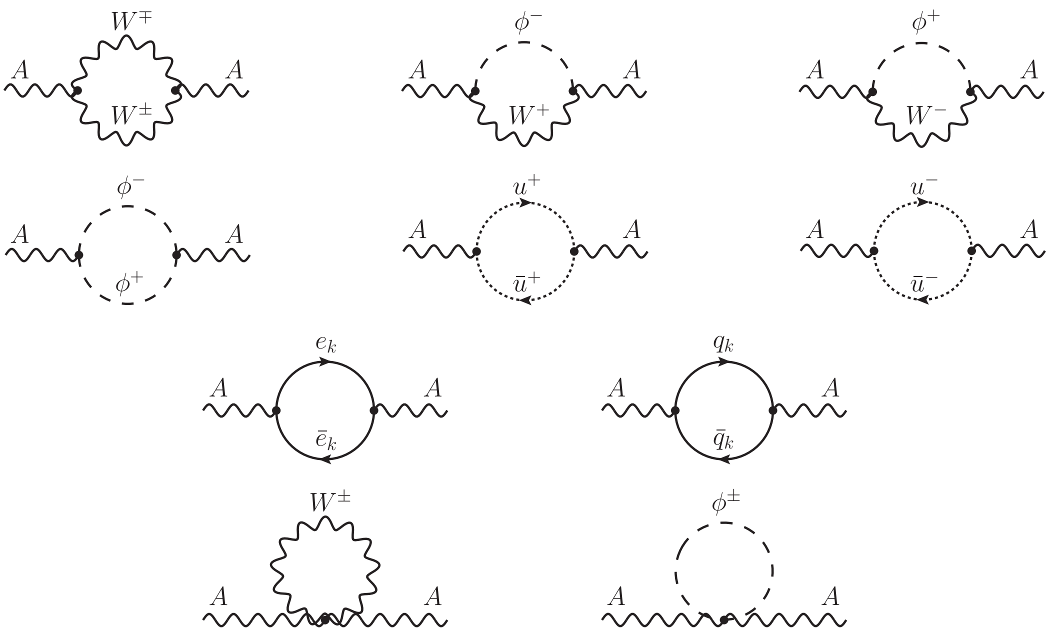

Figure G.3: EW contributons to the AA-transition.

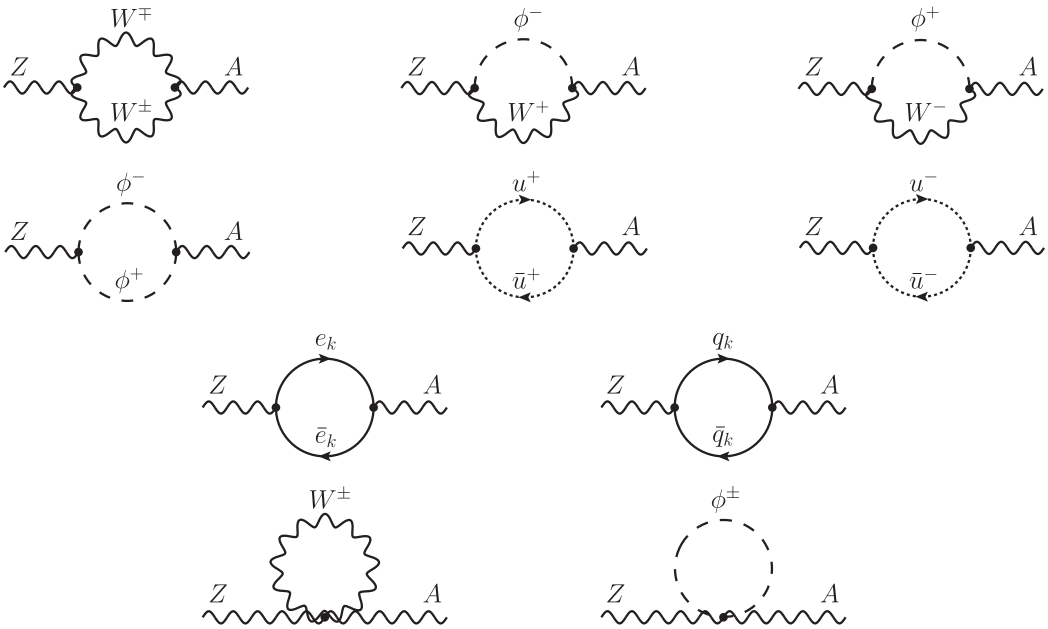

Figure G.4: EW contributons to the ZA-transition.

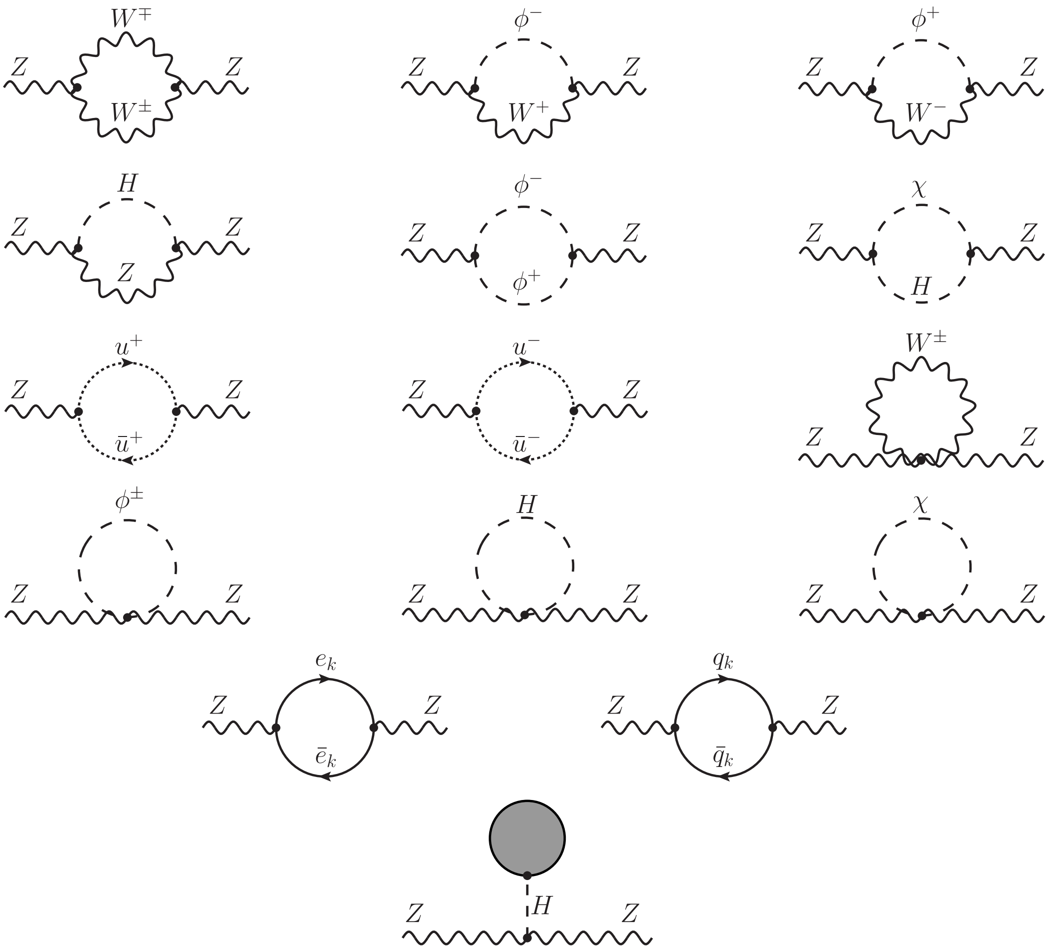

Figure G.5: EW contributons to the ZZ-transition.

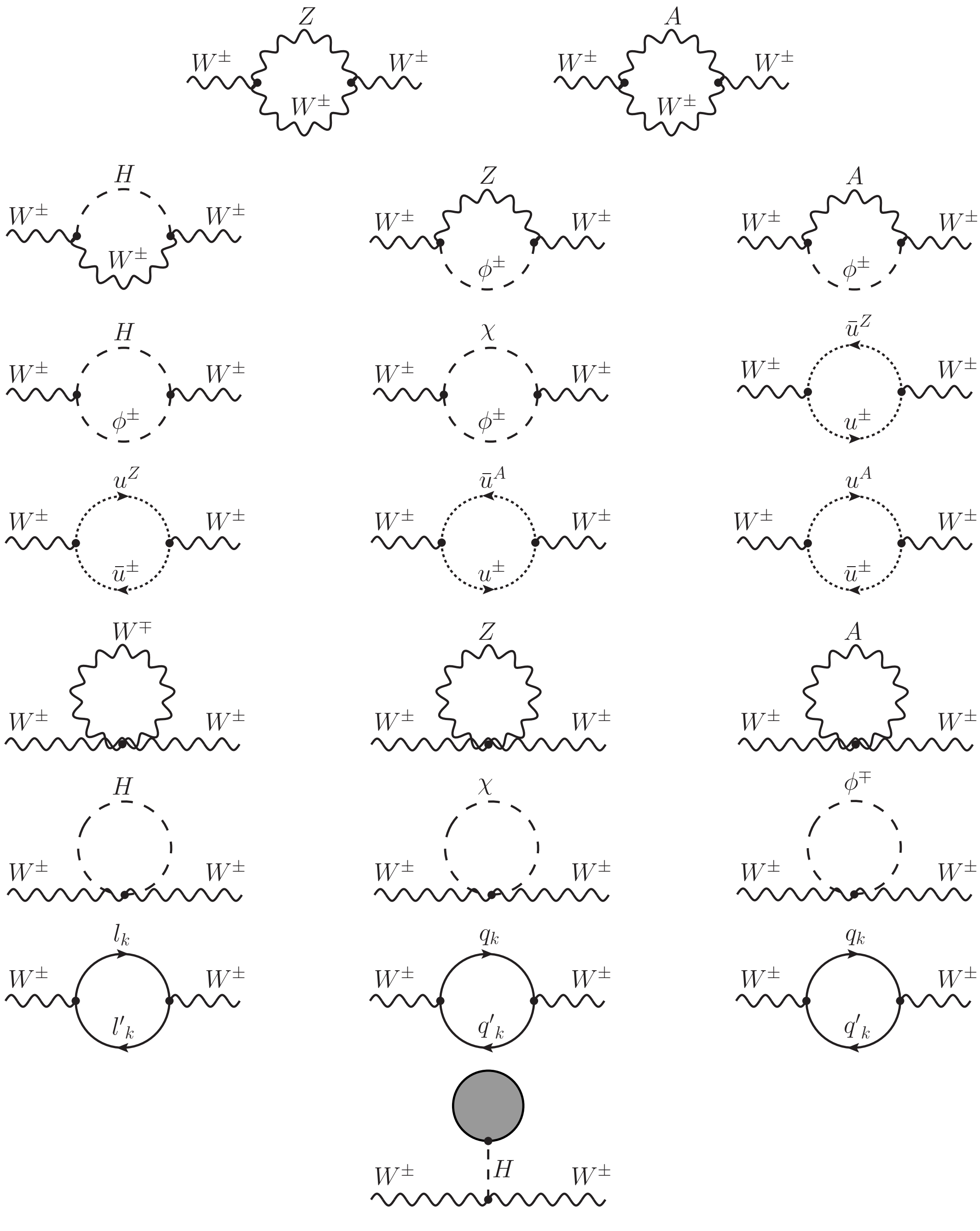

Figure G.6: EW contributons to the WW-transition.

G.2.3 Vertices

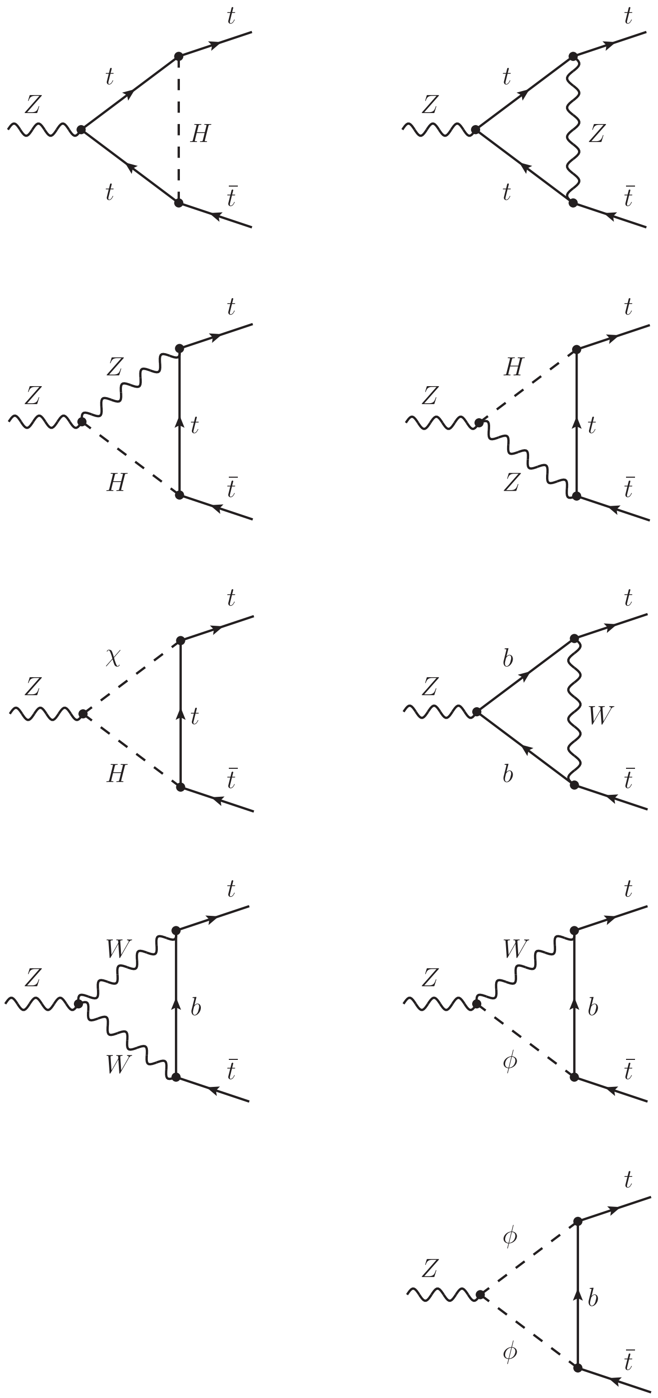

Figure G.7: EW contributons to the Ztt-vertex.

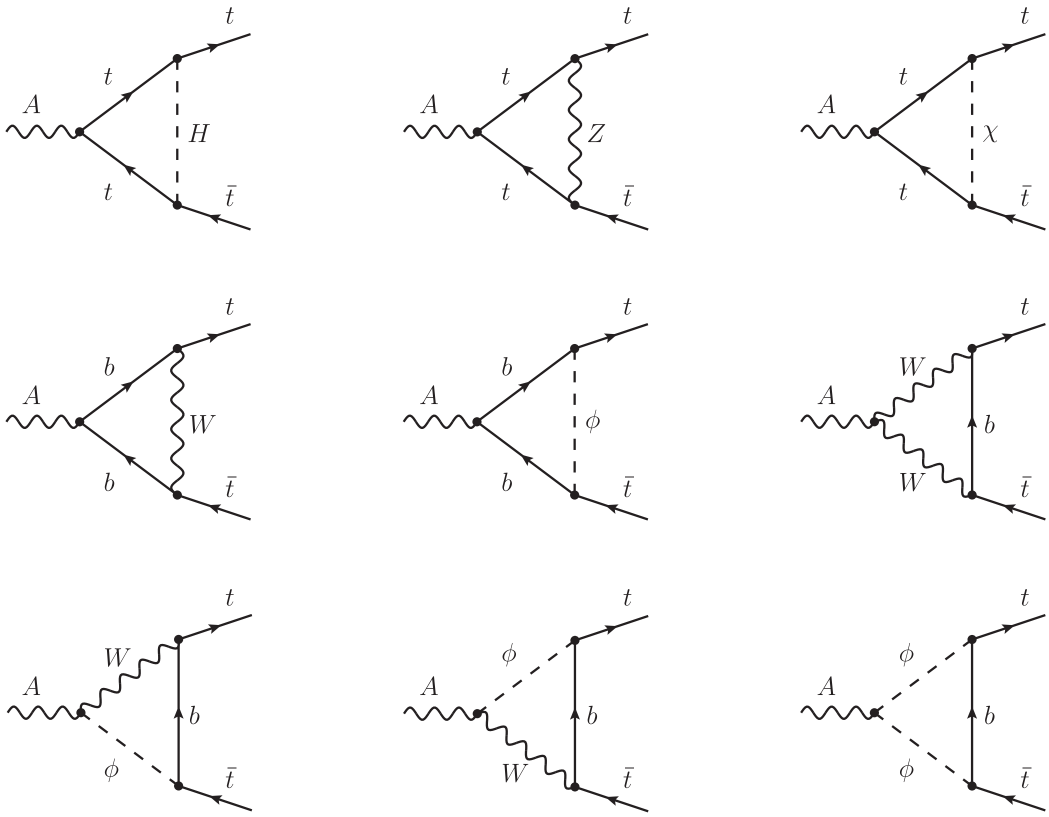

Figure G.8: EW contributons to the Att-vertex.

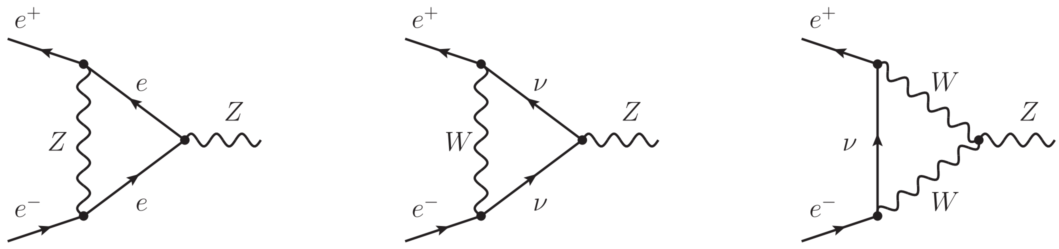

Figure G.9: EW contributons to the Zee-vertex.

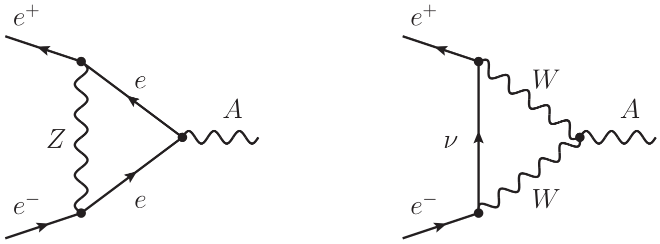

Figure G.10: EW contributons to the Aee-vertex.

G.2.4 Boxes

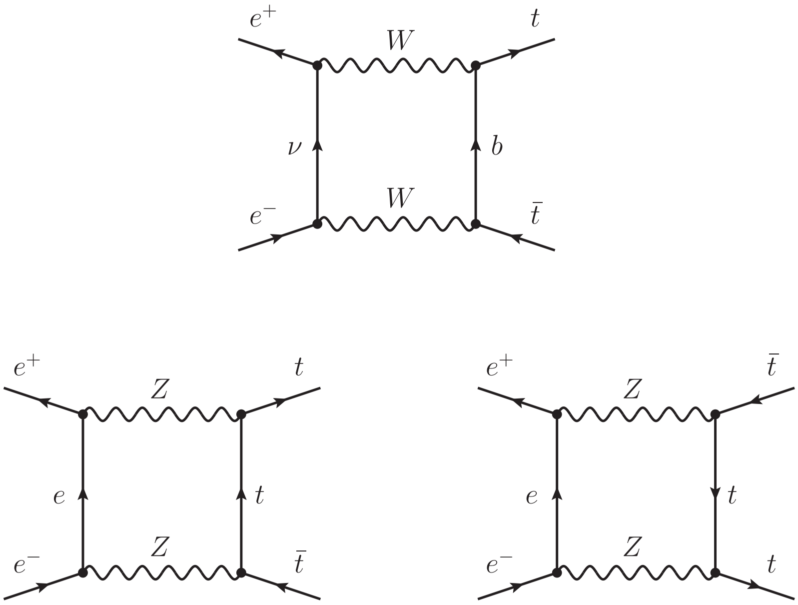

Figure G.11: EW box corrections.

Bibliography

[1] S. Fleming, A. H. Hoang, S. Mantry, and I. W. Stewart, "Jets from massive unstable particles: Top-mass determination," *Phys. Rev.* **D77** (2008) 074010, `arXiv:hep-ph/0703207 [hep-ph]`.

[2] S. Fleming, A. H. Hoang, S. Mantry, and I. W. Stewart, "Top Jets in the Peak Region: Factorization Analysis with NLL Resummation," *Phys. Rev.* **D77** (2008) 114003, `arXiv:0711.2079 [hep-ph]`.

[3] M. Boehm, H. Spiesberger, and W. Hollik, "On the 1-Loop Renormalization of the Electroweak Standard Model and its Application to Leptonic Processes," *Fortschritte der Physik* **34** no. 11, (1986) 687–751.

[4] W. F. L. Hollik, "Radiative Corrections in the Standard Model and Their Role for Precision Tests of the Electroweak Theory," *Fortschritte der Physik/Progress of Physics* **38** no. 3, (1990) 165–260.

[5] W. Beenakker, S. C. van der Marck, and W. Hollik, "e+ e- annihilation into heavy fermion pairs at high-energy colliders," *Nucl. Phys.* **B365** (1991) 24–78.

[6] A. Andonov, D. Bardin, S. Bondarenko, P. Christova, L. Kalinovskaya, and G. Nanava, "Update of one loop corrections for e+ e- $\to$ f anti-f, first run of CalcPHEP system," *Phys. Part. Nucl.* **34** (2003) 577–618, `arXiv:hep-ph/0207156 [hep-ph]`.

[7] J. Fleischer, A. Leike, T. Riemann, and A. Werthenbach, "Electroweak one loop corrections for e+ e- annihilation into t anti-top including hard bremsstrahlung," *Eur. Phys. J.* **C31** (2003) 37–56, `arXiv:hep-ph/0302259 [hep-ph]`.

[8] A. Denner, "Techniques for calculation of electroweak radiative corrections at the one loop level and results for W physics at LEP-200," *Fortsch. Phys.* **41** (1993) 307–420, `arXiv:0709.1075 [hep-ph]`.

[9] S. L. Glashow, "Partial-symmetries of weak interactions," *Nuclear Physics* **22** no. 4, (1961) 579 – 588.

[10] S. Weinberg, "A Model of Leptons," *Phys. Rev. Lett.* **19** (Nov, 1967) 1264–1266.

[11] A. Salam, "Weak and Electromagnetic Interactions," *Conf. Proc.* **C680519** (1968) 367–377.

[12] P. W. Higgs, "Broken Symmetries and the Masses of Gauge Bosons," *Phys. Rev. Lett.* **13** (Oct, 1964) 508–509.

[13] F. Englert and R. Brout, "Broken Symmetry and the Mass of Gauge Vector Mesons," *Phys. Rev. Lett.* **13** (Aug, 1964) 321–323.

[14] G. S. Guralnik, C. R. Hagen, and T. W. B. Kibble, "Global Conservation Laws and Massless Particles," *Phys. Rev. Lett.* **13** (Nov, 1964) 585–587.

[15] C. Reisser, *Finite Lifetime Effects in Top Quark Pair Production at Threshold*. Dissertation, Technische Universitaet Muenchen, Muenchen, 2008.

[16] M. Fox, W. Grimus, and M. Loeschner, "Renormalization and radiative corrections to masses in a general Yukawa model," `arXiv:1705.09589 [hep-ph]`.

[17] W. Hollik and M. Kollar, "NLO QED contributions to top-pair production at hadron collider," *Phys. Rev.* **D77** (2008) 014008, `arXiv:0708.1697 [hep-ph]`.

[18] A. Denner, L. Jenniches, J.-N. Lang, and C. Sturm, "Gauge-independent $\overline{MS}$ renormalization in the 2HDM," *JHEP* **09** (2016) 115, `arXiv:1607.07352 [hep-ph]`.

[19] B. A. Kniehl and O. L. Veretin, "Two-loop electroweak threshold corrections to the bottom and top Yukawa couplings," *Nucl. Phys.* **B885** (2014) 459–480, `arXiv:1401.1844 [hep-ph]`. [Erratum: Nucl. Phys.B894,56(2015)].

[20] H. H. Patel, "Package-X: A Mathematica package for the analytic calculation of one-loop integrals," *Comput. Phys. Commun.* **197** (2015) 276–290, `arXiv:1503.01469 [hep-ph]`.

[21] H. H. Patel, "Package-X 2.0: A Mathematica package for the analytic calculation of one-loop integrals," *Comput. Phys. Commun.* **218** (2017) 66–70, `arXiv:1612.00009 [hep-ph]`.

[22] T. Hahn, "Generating Feynman diagrams and amplitudes with FeynArts 3," *Comput. Phys. Commun.* **140** (2001) 418–431, `arXiv:hep-ph/0012260 [hep-ph]`.

[23] R. Mertig, M. Boehm, and A. Denner, "Feyn Calc - Computer-algebraic calculation of Feynman amplitudes," *Computer Physics Communications* **64** no. 3, (1991) 345 – 359.

[24] T. Hahn and M. Perez-Victoria, "Automatized one loop calculations in four-dimensions and D-dimensions," *Comput. Phys. Commun.* **118** (1999) 153–165, `arXiv:hep-ph/9807565 [hep-ph]`.

[25] J.-y. Chiu, F. Golf, R. Kelley, and A. V. Manohar, "Electroweak Corrections in High Energy Processes using Effective Field Theory," *Phys. Rev.* **D77** (2008) 053004, `arXiv:0712.0396 [hep-ph]`.

[26] J.-y. Chiu, R. Kelley, and A. V. Manohar, "Electroweak Corrections using Effective Field Theory: Applications to the LHC," *Phys. Rev.* **D78** (2008) 073006, `arXiv:0806.1240 [hep-ph]`.

[27] M. Roth and A. Denner, "High-energy approximation of one loop Feynman integrals," *Nucl. Phys.* **B479** (1996) 495–514, `arXiv:hep-ph/9605420 [hep-ph]`.

[28] M. Beccaria, G. J. Gounaris, J. Layssac, and F. M. Renard, "Subleading terms in asymptotic Passarino-Veltman functions," *Int. J. Mod. Phys.* **A23** (2008) 1839–1862, `arXiv:0711.1067 [hep-ph]`.

[29] M. Schwartz, *Quantum Field Theory and the Standard Model*. Quantum Field Theory and the Standard Model. Cambridge University Press, 2014.

[30] G. 't Hooft and M. J. G. Veltman, "Scalar One Loop Integrals," *Nucl. Phys.* **B153** (1979) 365–401.

[31] R. E. Cutkosky, "Singularities and Discontinuities of Feynman Amplitudes," *Journal of Mathematical Physics* **1** no. 5, (1960) 429–433.

[32] M. Boehm, A. Denner, and H. Joos, *Gauge Theories of the Strong and Electroweak Interaction*. Vieweg+Teubner Verlag, 2001.

[33] D. Binosi and L. Theussl, "JaxoDraw: A graphical user interface for drawing Feynman diagrams," *Computer Physics Communications* **161** no. 1, (2004) 76 – 86.